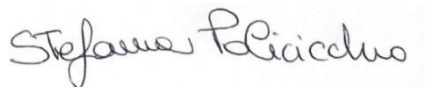# Examining epigenetic variation in the brain in mental illness

Submitted by

Stefania Policicchio

to the University of Exeter

as a thesis for the degree of

Doctor of Philosophy in Medical Studies

In December 2020

This thesis is available for the Library use on the understanding that it is copyright material and that no quotation from the thesis may be published without proper acknowledgement.

I certify that all material in this thesis which is not my own work has been identified and that this material has not previously been submitted and approved for the award of a degree by this or any other University.

Signature: ……………………………………………………………………..

Abstract

Mental health represents one of the most significant and increasing burdens to global public health. Depression and schizophrenia, among other mental illnesses, constitute strong risk factors for suicidality which results in over 800,000 deaths every year. The majority of suicides worldwide are indeed related to psychiatric diseases. A growing body of genetic, epigenetic and epidemiological evidence suggests that psychiatric disorders are highly complex phenotypes originating from the multilevel interplay between the strong genetic component and a range of environmental and psychosocial factors. Deeper understanding about the biology of the genome has led to increased interest for the role of non-sequence-based variation in the etiology of neuropsychiatric phenotypes, including suicidality. Epigenetic alterations and gene expression dysregulation have been repetitively reported in post-mortem brain of individuals who died by suicide. To date, however, studies characterizing disease-associated methylomic and transcriptomic variation in the brain have been limited by screening performed in bulk tissue and by the assessment of a single marker at a time. The main aim of this thesis was to investigate DNA methylation and miRNA expression differences in post-mortem brain associated with suicidality and unravel the complexity of epigenetic signals in a heterogeneous tissue like the human brain by developing a method to profile genomic variation at the resolution of individual neural cell types. The results here reported, provide further support for a suicide-specific epigenetic signature, independent from comorbidity with other psychiatric phenotypes, as well as confirming the strong bias perpetrated by bulk tissue studies hence the need to examine genomic variations in purified cell types. In summary, this thesis has identified a) a suicide-specific signal in two different epigenetic markers (DNA methylation and miRNA expression) and b) a protocol to simultaneously profile DNA methylation levels across three purified cell types in the healthy brain highlighting the utility of cell sorting for identifying cell type-driven epigenetic differences associated with etiological variation in complex psychiatric phenotypes.

Acknowledgements

Firstly, I would like to express my sincere, deep gratitude to both my two first supervisors. I got the luxury to get two instead of one and I could not have been luckier.

Thank you to Dr Therese Murphy, for her precious guidance, insightful comments and feedbacks, for her continuous availability and motivation. You have been not just my project supervisor but a mentor and a guide, an inspiration model in the first part of my journey when I most needed a direction. You have taught me so much, beyond the apparent, and gave me the support and confidence that at the time I lacked.

Thank you to Dr Emma Dempster, for her kindness, understanding and constant encouragement. For being my reference point and major supporter, particularly in the very last part of my PhD journey. I could not have made it through the end without your backing. Thank you for patiently dealing with my catastrophic outlook on experiment outcomes and life in general, as well as my unnecessarily long and detailed thesis's chapters. For being a great example of efficient multitasking, calm and positivity even during the most stressful times. Thank you for being an inspiring example of exceptional woman!

A huge thank you to Prof Jonathan Mill, a rare individual of outstanding brain capacity, deeply rooted passion and dedication to research, endless humbleness and of genuine inspiration for young researchers and the entire team. You are the living proof that excellence and success can coexist with truthfulness, good-heartedness and exhilarating humour.

To Dr Aaron Jeffries, a heartfelt thank you! For being a great guide in the lab since the very beginning of my PhD journey, and an amazing boss during the last year and a half. I have met very few people so skilled yet so approachable, kind and humble. I have learnt so much from you in the past four years. Thank you for being such a caring and supportive boss, particularly during the last couple of months while I was consumed by the thesis write up.

To Dr Joe Burrage, a special thank you for having shared with me the pain and joy of a protocol development which lasted 2 years. For having patiently showed and explained me the same things over and over and over, knowing I would have asked again. Thanks for all the "one question" answered. Thank you for your friendship while I was unable to be of any company as I could not take part in any conversation. Thanks for having taught me that Devon is actually an enjoyable place despite the weather, for all the amazing meals and walks in the nature.

To all my fellow lab mates in the Complex Disease Epigenetics Group, thanks to who have just joint and who has left (at least physically) leaving irremovable

memories (Dr Matthew Devall, Dr Ehsan Pishva, Dr Joana Viana, Giorgina, Aisha), thank you for being my family and my friends through these - at times- very tough years on my own in a foreign country. Thanks for being such a variegate group, always expanding, warmly welcoming, friendly, and so forgiving of my Italian temperament (as well as my English, pretty poor until not too long ago). But above everything else, thank you for being so rich in vibrant minds, priceless skills, it has been beyond words empowering and inspiring being part of it.

A special thanks to Dr Eilis Hannon whose statistical and analytical help and input has been essential and priceless. You so often made digestible and less scary to approach many scripts and R packages a little too inaccessible.

Extra special thanks to Szi Kay Leung, for being a great lab mate, for your empathy and genuine friendship. Thank you for the good time together, off work activities and group face calls.

Thanks to Gemma Shirby and Emma Walker for repetitively and gracefully offering me help with the analyses and coding troubleshooting during the most desperate times. I will never thank you enough and quantify my gratitude. Not just for the help and the time but for the kindness, patience and willingness to help. I have learnt so much through you, you are both genuinely brilliant and amazingly good at what you do!

Thank you to Dr Isabel Castanho, such a rich and kind soul. I hold fond memories of our private conversations. Thank you for taking my rants and complains at times, for your guidance and reassurance. You have been so often the glue of the whole student group, always asking intentional "how are you", checking in with everyone and being such a great example of outstanding student first and junior researcher more recently. On a side note, you have also such a good taste in fashion and style that has to be acknowledged. Last but definitely not least,

To my dad,
Thank you for passing on me your stubbornness and resilience.

To my mum,
Thank you for teaching me to always hold on hope and faith.

To myself,
Thanks for keeping your word and getting this done, you earnt my trust.

Table of Contents

List of Figures

List of Tables

Publications arising from this Thesis

Chapter 1 (published manuscript presented in Appendix A)

Policicchio S, Dempster EL, Murphy TM. Deciphering the Epigenetic Landscape of Suicidal Behaviour: A Review of Current Findings, Caveats and Future Directions. OBM Genetics 2018;2(4):039; doi:10.21926/obm.genet.1804039

Chapter 3 (published manuscript presented in Appendix B)

Policicchio S, Washer S, Viana J, Iatrou A, Burrage J, Hannon E, Turecki G, Kaminsky Z, Mill J, Dempster EL, Murphy TM (2020). Genome-wide DNA methylation meta-analysis in the brains of suicide completers. Transl Psychiatry. 2020:10(1):69.doi: 10.1038/s41398-020-0752-7.

Chapter 4 (published method presented in Appendix C)

Methods published on Protocols.io (online platform for sharing reproducible methods) (http://dx.doi.org/10.17504/protocols.io.bmh2k38e)

Policicchio S, Davies JP, Chioza B, Burrage J, Commin G, Hannon E, Schalkwyk LS, Mill J, Dempster EL. Mapping cell-type specific markers of genomic variation in the human brain. Nucleic Acid Research, manuscript in preparation

Declarations

The samples used in **Chapter 4 and 5** were obtained from the Edinburgh Brain and Tissue Banks (EBTB) at the University of Edinburgh and from the 5 Brains for Dementia Research (BDR) brain banks throughout the UK.

The Douglas-Bell Canada Brain Bank (DBCBB) provided the samples used in **Chapter 3 and 6** and this study was approved by the University of Exeter Medical School Research Ethics Board (REB).

All laboratory work was carried out by myself at the University of Exeter Medical school laboratories with the exception of the following:

- DNA methylation array and genotyping array processing of the prefrontal cortex samples from the EBTB and BDR presented in **chapters 4 and 5** which was carried out by Dr Joe Burrage at the University of Exeter Medical School (**Chapter 5**).

All bioinformatics and statistical analyses were performed by me with a few exceptions, where I had support from others:

- The TaqMan OpenArray data in **Chapter 6** were analysed by Dr Tyler J. Gorrie-Stone.

List of abbreviations

Abbreviation	Term
Δ	Corrected DNA methylation difference
450K array	Illumina Infinium 450K Methylation BeadChip Array
5caC	5-carboxylcytosine
5fC	5-formylcytosine
5hmC	5-hydroxymethlcytosine
5mC	5-methylcytosine
ACC	Anterior cingulate cortex
AD	Alzheimer's disease
ALS	Amyotrophic lateral sclerosis
APC	allophycocyanin
ASD	Autism-spectrum disorder
BA	Brodmann area
BBB	Blood Brain Barrier
BDR	Brains for Dementia Research
bp	Base pairs
BPD	Bipolar Disorder
BS	Bisulfite
cAMP	Cyclic Adenosine monophosphate
cDNA	complementary deoxyribonucleic acid
CER	Cerebellum
CETS	Cell epigenotype specific
CGIs	CpG islands
ChIP	Chromatin Immunoprecipitation
chr	Chromosome
CNS	Central Nervous System
CNV(s)	Copy number variation(s)
CpG	Cytosine-guanine dinucleotide
CSF	Cerebrospinal fluid
ct-DMP(s)	Cell-type (specific) differentially methylated position(s)
ct-DMR(s)	Cell-type (specific) differentially methylated regions(s)
CTR	Controls

DBCBB	Douglas-Bell Canada Brain Bank
DA	dopamine
DMP(s)	differentially methylated probe(s)
DMR(s)	differentially methylated region(s)
DNA	Deoxyribonucleic acid
DNMT(s)	DNA methyltransferase(s)
dNTP(s)	Deoxynucleotide(s)
EBTB	Edinburgh Brain and Tissue Banks
ELS	Early life stress
EPIC array	Illumina Infinium EPIC Methylation BeadChip Array
EWAS	Epigenome-wide association study
FACS	Fluorescence-activated cell sorting
FANS	Fluorescence-activated nuclei sorting
FDR	False discovery rate
FITC	Fluorescein isothiocyanate
FSC	Forward Scatter
GABA	gamma-Aminobutyric acid
GO	Gene ontology
GREAT	Genomic regions enrichment of annotations tool
GLU	Glutamate
GWAS	Genome-wide association studies
H3K27	Tri-methylation of lysine at positions 27 of histone 3
H3K4me3	Tri-methylation of lysine at positions 4 of histone 3
H3K9me3	Tri-methylation of lysine at positions 9 of histone 3
HLA	Human leukocyte antigen
hMeDIP-seq	Hydroxymethylated DNA immunoprecipitation Sequencing
hPSC(s)	Human Pluripotent stem cells
ICC	Immunocytochemistry
LC	Locus Coeruleus
LCM	Laser Capture microdissection
lncRNA	Long non-coding ribonucleic acid
LNDBB	London Neurodegenerative Diseases Brain Bank
LTP	Long-term potentiation
M	Methylated
MD	Medio-dorsal thalamus

MDS	Multidimensional scaling
MDD	Major Depressive Disorder
MECP2	Methyl-CpG binding protein 2
MHC	Major histocompatibility complex
miRNA(s)	Micro ribonucleic acid(s)
mQTL	Methylation quantitative trait loci
mRNA	Messenger ribonucleic acid
NCBI	National Center for Biotechnology Information
ncRNA	Non-coding ribonucleic acid
NGS	Next generation sequencing
NIH	National Institutes of Health
NMDA	N-methyl-D-aspartate
NPC(s)	Neural Progenitor Cell(s)
NTC	No template control
ONT	Oxford Nanopore Technologies
OPC(s)	Oligodendrocyte precursor cells
OR	Odds ratio
OxBS	Oxidative Bisulfite
PacBio	Pacific Biosciences
PBMCs	Peripheral blood mononuclear cells
PBS	Phosphate buffered saline
PC	Principal component
PCR	Polymerase chain reaction
PE	Phycoerythrin
PET	Positron Emission Tomography
PFC	Prefrontal cortex
PGC	Psychiatric Genetic Consortium
PPi	Pyrophosphate molecules
PRS	Polygenic Risk Score
PTSD	Post-Traumatic Stress Disorder
QC	Quality control
qPCR	Quantitative polymerase chain reaction
QQ	Quantile-quantile
REB	Research Ethics Board
RIN	Ribonucleic acid integrity number

RNA	Ribonucleic acid
RNA-seq	RNA sequencing
RRBS-seq	Reduced-representation bisulfite sequencing
rRNA	Ribosomal ribonucleic acid
RT	Room Temperature
RT-PCR	Real-time polymerase chain reaction
RT-qPCR	Real-time quantitative PCR
SA	Suicide Attempt
SB	Suicidal behaviour
SSC	Side Scatter
SCZ	Schizoprenia
scRNA-seq	Single cell RNA sequencing
SI	Suicidal Ideation
SNP	Single nucleotide polymorphism
snRNA	Small nuclear ribonucleic acid
SMRT	Single-molecule real-time sequencing
sSNV(s)	synonymous Single-nucleotide variant(s)
TET	Ten-Eleven Translocation
TF	Transcription Factor
TLDA	TaqMan low-density array
tRNA	Transporter ribonucleic acid
TSS	Transcription start sites
U	Unmethylated
WGBS	Whole-Genome Bisulfite Sequencing

Chapter 1 – General Introduction

1.1 Introduction to Epigenetics

The term Epigenetics ("on top of" genetic) refers to those modifications of the genome that do not change the DNA sequence, and are potentially heritable and reversible. These alterations allow the genome to adapt its transcriptional repertoire to the ever changing environmental conditions and/or to create different cell/tissue types in multi-cellular organisms (Abdolmaleky et al., 2015, Abdolmaleky et al., 2008). In fact, contrary to the genetic code which is fixed (with the exception of random mutations) and non-adaptive to the external conditions, epigenetic processes are flexible and responsive to environmental cues (Labonte and Turecki, 2010) by fine-tuning gene expression levels which remain dynamic throughout life (Labonte and Turecki, 2010, Autry and Monteggia, 2009, McGowan and Szyf, 2010). As such, they are critical for normal cellular development, tissue differentiation and the long-term regulation of gene function. For a glossary of key epigenetic terms used in this thesis see **Table 1.1.**

The most commonly studied epigenetic mechanisms that can influence gene expression are: molecular modifications of the DNA, post-translational histone modifications and non-coding RNA gene silencing, which are each described in detail in the following sections.

Term	Key reference	Definition
Chromatin	(Berger, 2007)	A DNA-protein complex that constitutes the chromosomes. The structure of chromatin can be altered through covalent modifications made to the DNA or the proteins associated with it (histones).
CpG island	(Deaton and Bird, 2011)	Typically defined as 200 to 500 base pairs (bp) in length with a cytosine (C) and guanine (G) content of more than 50% and an observed/expected C-G dinucleotide (CpG) ratio of 0.6.
CpG island shore	(Deaton and Bird, 2011)	Regions of DNA that lie at the outskirts of CpG islands (~2Kb from islands) rather than in the islands itself. > 75% of tissue-specific differentially methylated regions found in shores. Methylation in shores shows higher correlation with gene expression than CpG islands
CpG island shelf	(Visone et al., 2019)	Regions of DNA that lie at the outskirts of CpG islands (~4Kb from islands) rather than in the islands itself
CpG site	(Gerring et al., 2018)	A location within a DNA sequence in which a cytosine and guanine appear consecutively
DNA hydroxymethylation	(Shukla et al., 2015)	The oxidized product of active DNA demethylation produced by the action of ten-eleven translocation (TET) proteins. Highly abundant in the brain, suggesting a role in epigenetic control of neuronal function.
DNA methylation	(Moore et al., 2013)	The addition of a methyl group to carbon 5 of the cytosine pyrimidine ring. DNA methylation in certain CpG-rich promoter regions acts to repress gene expression by disrupting the binding of transcription factors and recruiting proteins associated with chromatin compaction.
Epigenetics	(Bird, 2007)	The study of mitotically heritable but reversible changes in gene expression that occur without a change in the genomic DNA sequence.
Epigenetic epidemiology	(Mill and Heijmans, 2013)	The integration of epigenetic analyses into population-based epidemiological research with the goal of identifying both the causes (that is, environmental, genetic or stochastic) and phenotypic consequences (that is, health and disease) of epigenomic variation.

Epigenetic inheritance	(Boskovic and Rando, 2018)	Epigenetic modifications are mitotically heritable and can therefore be maintained across cell division to contribute to cell line establishment. It is less clear (and controversial) whether epigenetic marks are inherited transgenerationally through meiosis in vertebrates.
Epigenome	(Campbell and Wood, 2019)	The collective combination of chemical modifications and proteins that interact with the human genome. The epigenome is dynamically regulated, serves as a signal-integration platform and is unique to each individual.
Histones	(Campbell and Wood, 2019)	Proteins upon which DNA is tightly wound and whose function is to condense and package DNA in the nucleus.
Histone modifications	(Berger, 2007)	Post-translational, covalent additions made to N-terminal histone tails that modulate chromatin structure. Modifications include acetylation, methylation and
Hypo/Hypermethylation	(Edwards et al., 2017)	An increase/decrease in normal methylation levels.
Genomic imprinting	(Davies et al., 2005)	Monoallelic expression of genes in a parent-of-origin specific manner, regulated by allele-specific epigenetic marks established in the germline. This process is fundamental to normal mammalian development.
Non-coding RNA (ncRNA)	(Kapranov et al., 2007)	RNA molecules that are not translated into protein which can have structural or regulatory consequences impacting directly upon gene transcription.
Long non-coding RNA (lncRNA)	(Kopp and Mendell, 2018)	Non-protein coding RNAs that are 200 base pairs or longer which are highly regulated, but many of their functions remain to be characterized
MicroRNA (miRNA)	(Tian et al., 2015)	Single-stranded, non-protein coding RNAs about 21-24 nucleotides in length expressed in plants and animals. They bind to their target gene's 3' untranslated region and block transcription or promote transcript degradation
Nucleosome	(Zhou et al., 2019b)	DNA-histone complex consisting of 147 base pairs of DNA wrapped around eight histone proteins.
Promoter	(Danino et al., 2015)	A regulatory DNA sequence, usually close to, and upstream from, the gene or genes it regulates. It serves as a binding site for transcription factors and for the protein complexes that initiate gene transcription, and it serves to identify the start site for transcription.

Table 1.1 **Glossary of key epigenetic terms used in this thesis**

1.1.1 DNA modifications

DNA methylation is the covalent modification at the C5 carbon of cytosine residues, occurring mainly at CG dinucleotides (CpG) (See **Figure 1.1**). In somatic cells, approximately 80% of CpGs are methylated (Tucker, 2001); the remaining unmethylated CpGs tend to be concentrated around gene promoters (CpG islands) (Labonte and Turecki, 2010). DNA methylation is one of the best-characterized epigenetic modifications and has been implicated in numerous biological processes, including transposable element silencing (Yoder et al., 1997), genomic imprinting (Morison et al., 2005) and X chromosome inactivation (Avner and Heard, 2001, Wu and Zhang, 2010). 5-methyl cytosine (5mC) is also central to the establishment of tissue-specific gene expression and cell differentiation (Gross et al., 2016). When found in promoter regions of genes, CpG methylation is generally associated with transcriptional repression or downregulation of RNA transcription (Siegmund et al., 2007). However, DNA methylation has also been described in other regions of the genome and the transcriptional effect in those areas is not consistent (Burns et al., 2018).
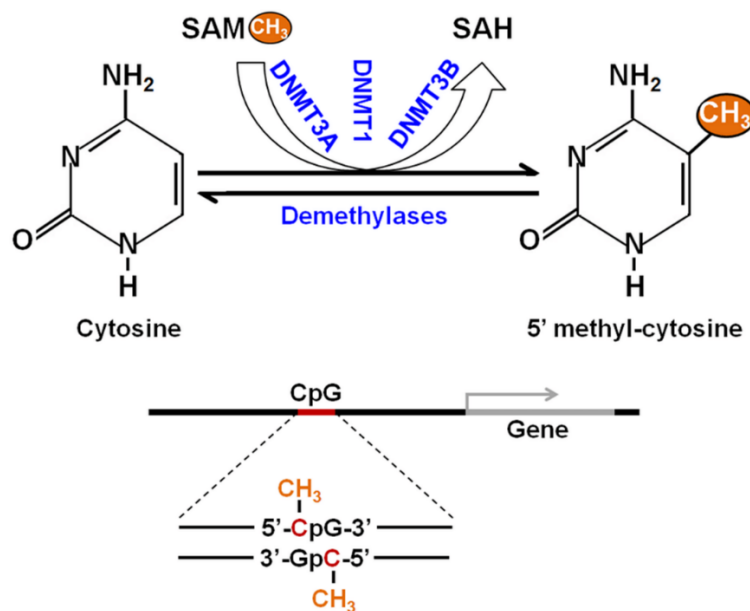
Figure 1.1 Schematic representation of DNA methylation.
The process starts with the covalent addition of a methyl group to form 5-methylcytosine (5mC). This process is catalysed by a family of DNA methyltransferases (DNMTs)— DNMT1, DNMT3A and DNMT3B. The majority of DNA methylation usually occurs at CpG sites and CpG islands nearby a gene to regulate related gene expression. DNA methylation is an epigenetic mechanism and required fine tuning for proper regulation. Figure taken from (Mandal et al., 2017).

Although DNA methylation used to be considered as a stable epigenetic mark, studies in the past decades have revealed that this modification is not as static as once thought. It is now widely accepted that DNA methylation can be both actively and passively removed from methylated cytosines (Tahiliani et al., 2009, Chen et al., 2003) and the specific mechanisms driving active DNA demethylation have now been characterized in detail. It has been shown that methyl groups can be removed by sequential oxidation of DNA methylation mediated by the ten-eleven translocation (TET) family of enzymes (Yong et al., 2016) via three intermediate modifications; 5-hydroxymethlcytosine (5hmC), 5-formylcytosine (5fC) and finally 5-carboxylcytosine (5caC) (He et al., 2011, Ito et al., 2011) which can then be removed by thymine DNA glycosylase (Zhang et al., 2012, Yu et al., 2012). **Figure 1.2** shows the proposed mechanisms of cytosine demethylation in the literature. Further research has now demonstrated that these other cytosine modifications, previously considered to only be transient intermediates, may also have functional roles in gene regulation (Inoue et al., 2011, Ito et al., 2011, Koh and Rao, 2013). Recent studies have also suggested that they may be epigenetic marks on their own (Kumar et al., 2018, Breiling and Lyko, 2015, Szulwach et al., 2011). Although considerably less abundant in the genome (Breiling and Lyko, 2015), these modifications have recently been shown to be more stable than previously thought (Bachman et al., 2015, Bachman et al., 2014). Furthermore, TET proteins have been implicated in meiosis, development, imprinting maintenance and stem-cell reprogramming (Yamaguchi et al., 2012, Gu et al., 2011b, Ficz et al., 2011, Dawlaty et al., 2013), suggesting wide-ranging functional roles for other products of active DNA demethylation. Hydroxymethylation in particular is a temporarily stable epigenetic modification of DNA (Globisch et al., 2010) highly dynamic during neurodevelopment (Wang et al., 2012, Spiers et al., 2017, Wang et al., 2017). Hydroxymethylated cytosines are enriched at the promoters and enhancers of developmental genes, and they correlate positively with gene expression during cell lineage commitment in early development. In addition, hydroxymethylation is present in gene bodies of actively transcribed genes (Colquitt et al., 2013, Tsagaratou et al., 2014, Nestor et al., 2016).The abundance of hydroxymethylation seems to be inversely correlated with the proliferation rate of a cell (Kriaucionis and Heintz, 2009, Bachman et al., 2014). Recent research has found that 5hmC in particular has a significantly higher abundance in the brain compared to other tissues (Lister et al., 2013,

Szwagierczak et al., 2010) and has been implicated in neurological disorders (Wang et al., 2017, Rustad et al., 2019, Condliffe et al., 2014, Lunnon et al., 2016, Cheng et al., 2018). The dynamic interplay between DNA methylation and hydroxymethylation is presumably important for maintaining normal gene expression patterns in a cell with recent studies demonstrating that 5hmC and 5mC have opposing effects on gene expression (Sherwani and Khan, 2015). However, the causes and consequences of the imbalance between these two DNA modifications are still to be understood.
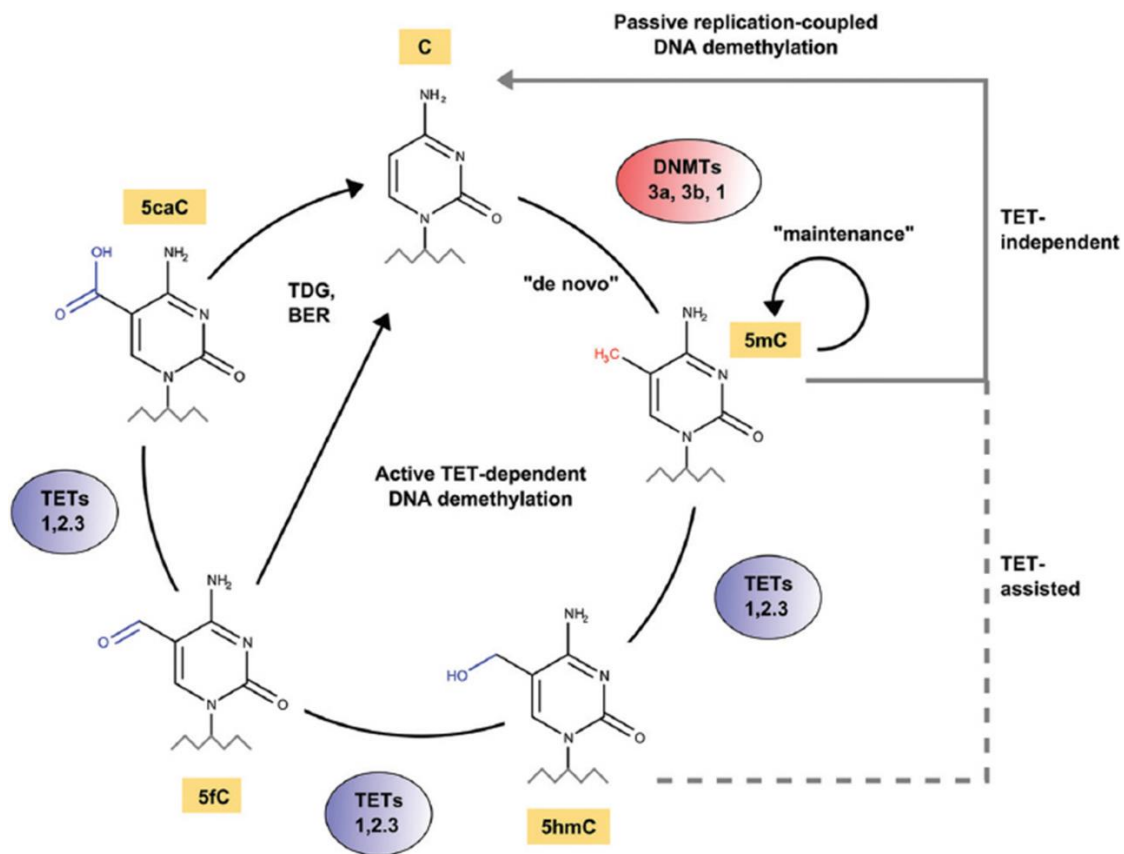
Figure 1.2 Pathways of active and passive DNA demethylation.

DNA methyltransferases (DNMTs) catalyze the methylation of cytosine by transferring a methyl group to the position C5. Ten-eleven translocation (TET) enzymes can catalyze the oxidation of 5-methylcytosine (5mC) to 5-hydroxymethylcytosine (5 hmC). Further TET-dependent oxidative reactions lead to the successive conversion of 5 hmC into 5-formylcytosine (5fC) and 5-carboxylcytosine (5caC). 5fC and 5caC are recognized and removed by thymine-DNA glycosylase (TDG), and the created abasic site is repaired by the base excision repair (BER) pathway, generating an unmodified cytosine. Dilution of modified cytosines, 5mC or 5 hmC, during DNA replication can also yield unmodified cytosine, through a mechanism termed passive DNA demethylation, which is either TET-independent or TET-assisted, respectively. Replication-coupled dilution of 5fC and 5caC by passive DNA demethylation are not depicted. Figure taken from (Meier and Recillas-Targa, 2017).

1.1.2 Histone modifications

In contrast to DNA methylation and hydroxymethylation, which are set de novo at early embryogenesis and maintained during DNA replication, histone modifications are post-translational changes. They act to remodel the chromatin structure and regulate gene expression through chromatin accessibility (Consortium, 2012, Cazaly et al., 2019). Chromatin indeed exists as two functional structures within the cell nucleus: euchromatin which is the "opened" state associated with gene transcription and heterochromatin which is the "closed" state associated with gene silencing. The nucleosome is the building unit of chromatin and is comprised of DNA wrapped around an octamer of globular proteins forming a 'spool'-like structure. The proteins packing the eukaryotic DNA into these structural units are called histones (H1, H2A, H2B, H3, and H4) (Elmallah and Micheau, 2019). These globular proteins, with a tail of amino-acids, can be covalently modified by the addition or the removal of chemical groups at specific residues on their N-terminus tails (See **Figure 1.3**) (Policicchio et al., 2018, Labonte and Turecki, 2010). Histone modifications are the largest category of chromatin modifications identified so far, with 15 known chemical modifications at more than 130 sites on five canonical histones and on around 30 histone variants (Cazaly et al., 2019). Although a number of post-translational covalent histone modifications have been described, the knowledge on their functional roles remain extremely limited. Histone acetylation/deacetylation and methylation are the two most widely studied (Labonte and Turecki, 2010). Specific histone modification patterns often correlate with known functional genomic elements. For example, H3K9me3 and H3K27me3 are associated with inactive promoters; while H3K4me3 and H3K27ac are shown to be enriched in active enhancers and promoters (Karlic et al., 2010, Zhou et al., 2011).
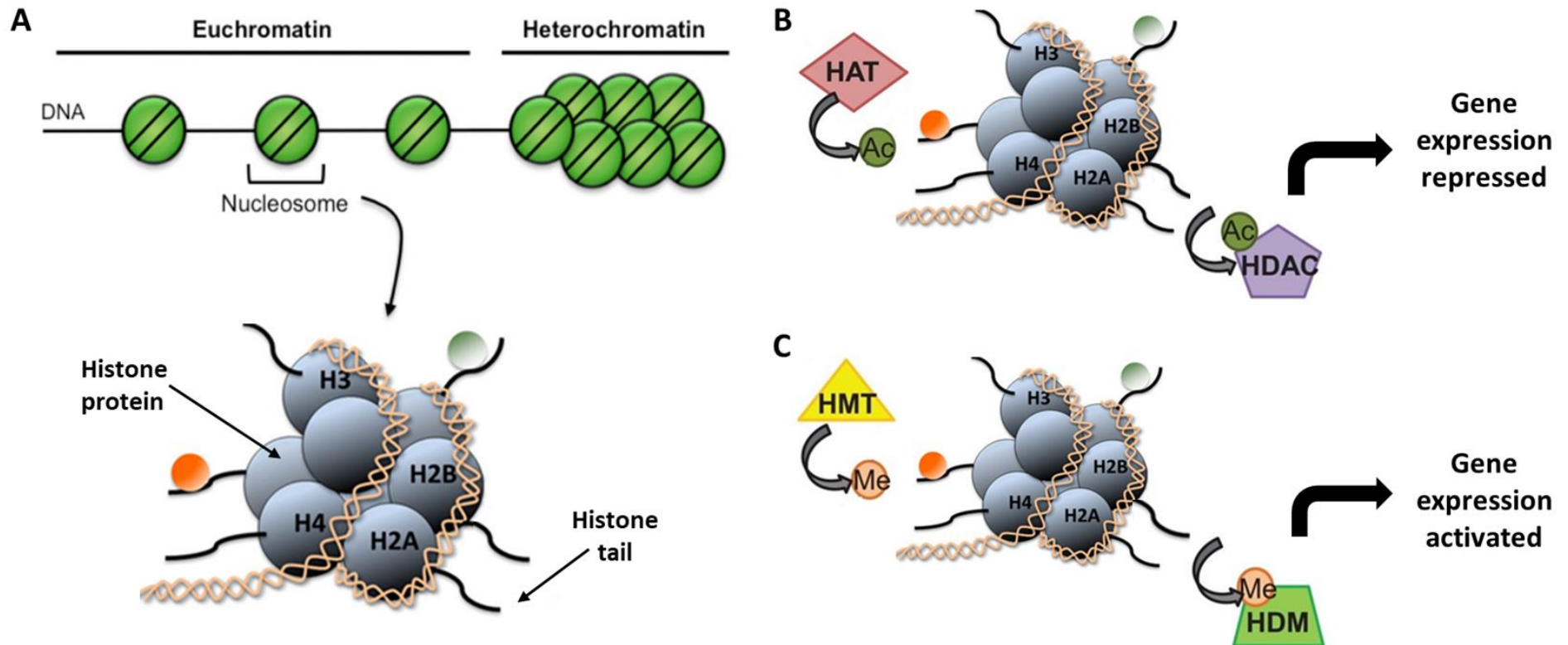
Figure 1.3 Illustration of histone core composition and simplified overview of two common histone modifications.
(A) Chromosomal DNA is packaged around histone proteins (H2, H4, H2A, H2B) to form nucleosomes. B) Nucleosome opening and accessibility to nuclear factors is regulated, in part, by post-translational modifications of histone tails that include among othes acetylation and methylation. Acetylation reactions on lysine (K) residues by histone acetyl-transferase (HAT) mask the positive charges of the aminoacidic side chains and thus allow chromatin to assume a less condensed conformation permissive for transcription. In contrast, deacetylation reactions by histone deacetylase (HDAC), increasing the chromatin packaging, prevent DNA transcription.C) Histone methyltransferases (HMT) add methyl groups to histones, generally associated with tightening wound DNA while histone demethylases (HDM) remove those methyl groups allowing the chromatin to assume a more open configuration which is associated to gene transcription activation. Ac, Acetyl group; Me, methyl group. Figure adapted from (Maddox et al., 2013).

1.1.3 Non-coding RNA

Another mechanism of epigenetic regulation of gene expression is mediated by non-coding RNAs (ncRNAs), functional RNA molecules that are transcribed from DNA but not translated into proteins (Policicchio S et al., 2018). These regulatory RNAs function to regulate gene expression at the transcriptional and post-transcriptional level. Several classes of ncRNAs have been identified and they are commonly distinguished in two major categories: small ncRNAs (<30 nts) and long non-coding RNAs (lncRNAs) (>200 nts) **Figure 1.4** schematically illustrates the identified mechanisms of action for both classes of molecules. Small ncRNAs can take several forms, namely small interfering RNAs (siRNA), small temporal RNAs (stRNA), small nuclear RNAs (snRNAs), small nucleolar RNAs (snoRNAs), piwi-interacting RNAs (piRNA) and microRNAs (miRNAs) (Barry, 2014, Mattick and Makunin, 2006). Small ncRNAs are present in all life kingdoms and play diverse roles in regulating gene expression, epigenetic processes (Smalheiser et al., 2014) and defence against viruses (Finnegan and Matzke, 2003). To date, miRNAs are the best characterised ncRNA group. They act as regulators of gene expression and protein translation in many tissues, including the brain, by binding to the target mRNA and contributing to its degradation through the RNA-induced silencing complex (RISC) or by directly inhibiting translation (Serafini et al., 2014). miRNAs are known to play a critical role in developmental processes, including neurodevelopment and synaptic plasticity and they have been implicated in the pathogenesis of various neuropsychiatric disorders like schizophrenia (SCZ), major depression (MDD) and bipolar disorder (BPD) (Smalheiser et al., 2014, Serafini et al., 2014, Xu et al., 2010, Miller and Wahlestedt, 2010). LncRNAs appeared later in evolution and are present in invertebrates, vertebrates and plants and are particularly enriched in the cell nucleus (Kung et al., 2013). LncRNA forms are highly specific to each cell type and maintain certain features seen in coding RNAs, like promoter regions and intron-exon boundaries (Barry, 2014). Enriched for expression in the brain (Derrien et al., 2012) and developmentally regulated (Aprea et al., 2013), the function of these long RNAs is still an area of intensive ongoing investigation, but they appear to play a role in chromatin regulation and shaping nuclear organization (Quinodoz et al., 2014) and they have been implicated in neuronal differentiation and brain development and evolution (Lv et al., 2015, Ng and Stanton, 2013, Qureshi and Mehler, 2012).
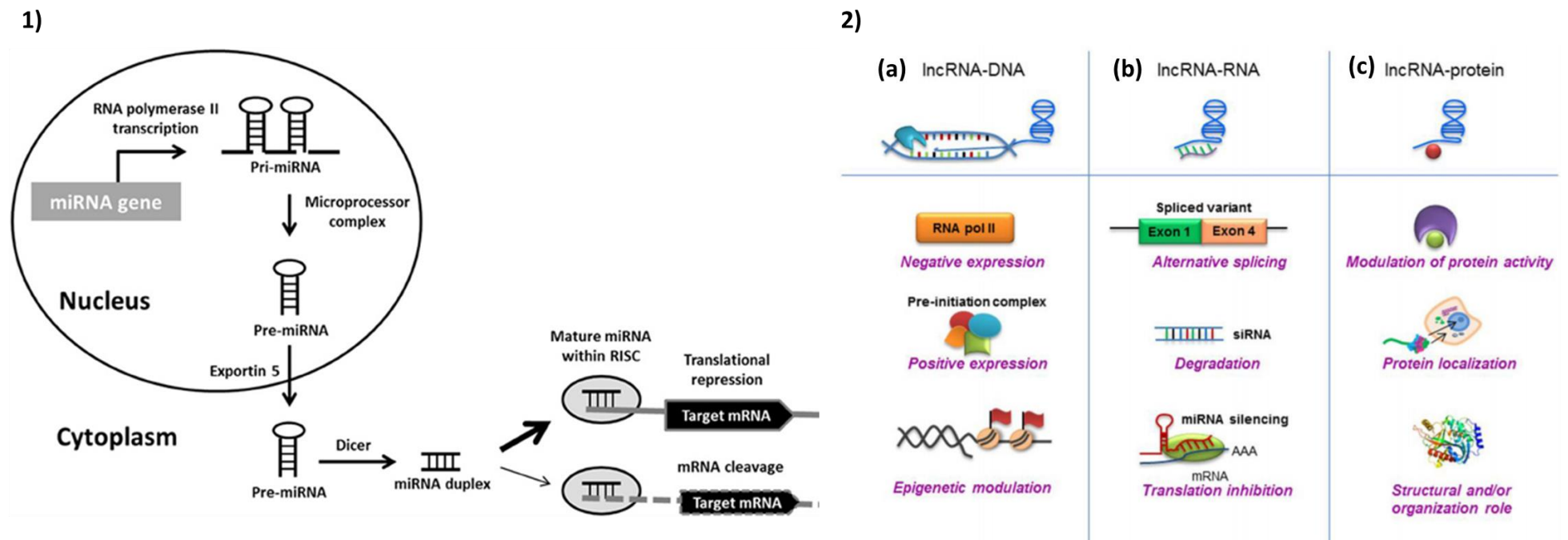
Figure 1.4 MicroRNA biogenesis pathway.
1) Primary miRNA (pri-miRNA) transcripts are transcribed by RNA polymerase II. Pri-miRNAs are processed by the microprocessor complex into precursor miRNA (pre-miRNA) hairpins. These are transported into the cytoplasm, where they are further processed by Dicer into miRNA duplexes. Following strand separation, the mature miRNAs are loaded into RNA-induced silencing complexes (RISCs) to guide the repression of protein synthesis or mRNA degradation. 2) LncRNA interactions and actions. (a) LncRNAs can target genomic DNA loci, and can modulate gene transcription by associating with RNA pol II or pre-initiation complexes, or through epigenetic modulation by guiding chromatin-modifying complexes to target genomic DNA loci. (b) LncRNA can contribute to RNA inhibition or degradation, by association with mRNAs and miRNAs to regulate splicing, or by binding with miRNAs as "endogenous sponges" to regulate gene expression (Lopez-Urrutia et al., 2019).(c) LncRNAs can modulate protein activity and localization by acting as molecular guides and scaffolds or as decoys for proteins such as transcription factors Figure adapted from (Goodall et al., 2013) and (Gori et al., 2015).

1.1.4 Epigenetic mechanisms of gene expression regulation

The epigenetic landscape of a given cell and the associated gene expression profile are established during development and maintained down the cell lineage through complex interactions that involve transcription factors, histone modifications, DNA modifications and ncRNA. Chromatin accessibility and nucleosome positioning have also been determined to serve as epigenetic mechanisms (Klemm et al., 2019). It is not uncommon to find elements that regulate gene expression (e.g. promoters, enhancers, insulators) in regions of the genome that are maintained as 'open' or accessible. These accessible regions can serve as binding sites for chromatin-modifying enzymes and other binding factors (Fingerman et al., 2013). These epigenetic mechanisms often act in concert for more complex levels of regulation. Examples of interaction between DNA methylation and histone modifications include recruitment of HDACs by DMNTs and methyl-CpG binding protein 2 *(MECP2)* (Saha and Pahan, 2006, Fuks et al., 2001, Bachman et al., 2001). Non-coding RNAs have also been found to interact with specific histone modifications (Ferreira and Esteller, 2018, Dinger et al., 2008, Yuan et al., 2011, Denis et al., 2011) and to serve as modular scaffolds for histone modifying enzymes (Tsai et al., 2010). It has been observed that enhancer elements, often found in regions where chromatin is maintained as accessible, can encode for small non-coding RNA molecules themselves (Ghildiyal and Zamore, 2009, Mattick et al., 2009, Zaratiegui et al., 2007, Kim et al., 2010). In addition, a role has emerged for ncRNAs in targeting mammalian DNMTs and controlling DNA methylation via regulation of DNA methyltransferases (Denis et al., 2011, Benetti et al., 2008). The discovery of more than 100 post-transcriptional modifications to ncRNA, such as methylated adenines and cytosines, is providing further insight into the interaction between these different epigenetic layers (Romano et al., 2018). Despite the increased understanding, the full extent of interactions between different epigenetic mechanisms to regulate gene expression in mammals remain widely unexplored (Bernstein et al., 2010). One of the reasons is because the different epigenetic modifications have been for long studied in isolation. However, recent international efforts have started to address this. The National Institutes of Health (NIH) launched the Roadmap Epigenomics Project in 2007 (Bernstein et al., 2010). One of the goals of this project was to combine whole genome epigenetic analysis with high throughput sequencing to create a series of publically available

reference epigenome maps. These maps encompass a wide array of cell lines, cell and human tissue types (over 100) from individuals at various developmental stages and health states. However, other large scale efforts to map epigenetic features and gene regulatory elements are currently ongoing. In 2011, the Epigenomics database at the National Center for Biotechnology Information (NCBI) was established to serve as a public resource for epigenomic data sets. Data were collected from both large scale studies such as the NIH Roadmap Epigenomics project, ENCODE and modENCODE as well as from smaller independent laboratory studies not involved in these project initiatives (Fingerman et al., 2011).

1.1.5 Profiling the methylome

Standard molecular biology approaches, including polymerase chain reaction (PCR), erase DNA modifications requiring therefore the exposure of the DNA to a methylation sensitive pre-treatment prior to DNA sequence analysis. Whole genome bisulfite sequencing (WGBS) is considered the gold standard technique to profile DNA methylation, allowing the coverage of ~28 million CpG sites across the human genome. However the high read depth required to quantify the small DNA methylation differences usually associated with complex disorders, make this method economically unfeasible for studies with large sample sizes (Ziller et al., 2015). Over the years, many proven high resolution methods of DNA methylation analysis platforms have been made available such as the Agilent Human CpG Island Microarray (27,800 CpG islands covering 21 MB) or the Agilent Human DNA Methylation Microarrays (27,627 expanded CpG islands and 5081 UMR regions) (Agilent Technologies, Santa Clara, CA, USA). The Illumina Infinium® Methylation arrays (Illumina, San Diego, CA, USA) have become the most popular tool for high-resolution screening compatible with large sample size. Illumina microarray technology (also known as BeadArray technology) uses silica microbeads housed in microwells and coated with multiple copies of two site-specific probes targeting chemically differentiated loci in the genome. The Infinium Methylation Assay detects cytosine methylation at CpG islands based on highly multiplexed genotyping of bisulfite-converted genomic DNA offering quantitative measurement of methylation at individual CpG sites (more details are provided in **Chapter 2**). The latest platform, the Infinium MethylationEPIC array

(EPIC array) interrogates over 850,000 CpG sites across the human genome (Dedeurwaerder et al., 2011, Needhamsen et al., 2017, Pidsley et al., 2016). Best compromise to date between coverage and cost, this approach enables DNA methylation quantification across the genome in a large number of samples. Although relatively simple and inexpensive, data have limited coverage and requires extensive within and between array normalization, pre-processing and integration across different microarray platforms (Fortin et al., 2017). However, many bioinformatics methods and pipelines specific for Illumina platforms and their integration have been developed (Fortin et al., 2017, Wilhelm-Benartzi et al., 2013), which has fostered their popularity and facilitated cross-study comparison of findings and meta-analyses. One limitation of standard bisulfite conversion-based approaches is the inability to distinguish between DNA methylation and other DNA modifications (Booth et al., 2012). More recently, new methods of quantifying 5mC, 5fC and 5hmC in one same sample have been described (Booth et al., 2012, Booth et al., 2013, Booth et al., 2014); however, for the chemical based method, the screening in parallel requires three times the amount of input DNA. Single, non-modified and non-amplified molecule sequencing methods proved to overcome some of the problems faced by bisulfite conversion and amplification-based methods of epigenetic marks profiling. Among the newer technologies, single molecule real-time (SMRT) sequencing by Pacific Biosciences (PacBio) (Eid et al., 2009) and Oxford Nanopore Technologies (ONT) (Clarke et al., 2009), offer the advantages of single molecule sequencing, including exceptionally long read lengths (>20 kb). These platforms permit deep sequencing/assembly through repetitive elements, direct variant phasing and direct RNA sequencing (no need for cDNA conversion) (Midha et al., 2019, Ardui et al., 2018, Jain et al., 2016). SMRT sequencing even allows the detection of different DNA modifications although these applications are still in development and further validation is required (Flusberg et al., 2010, Nakano et al., 2017). The PacBio sequencing-by-synthesis method distinguishes between the several modified nucleotides by reading the different duration of fluorescently labelled nucleotides incorporation. Nanopore sequencing, on the other hand, uses a voltage-based nanoscale pore in a membrane to measure the translocation of a linear, single-stranded (ss) DNA or RNA molecule through that pore. Nucleobase-by-nucleobase, measurements of changes in the current through the pore can then be decoded into a DNA sequence using an algorithm (Clarke et al., 2009,

Laszlo et al., 2013, Li et al., 2013). Sequencing also only lasts several hours, which is very appealing in a diagnostic setting. Although simple and low-cost nanopore based technologies (reviewed in (Jain et al., 2016, Deamer et al., 2016)) are catching on and likely represent future platforms, SMRT sequencing remains a more mature technology and therefore diagnostically applicable at this time (Ardui et al., 2018).

1.1.5.1 *Limitations in methylomic profiling*

DNA methylation studies require careful considerations for design as well as analysis: population and tissue selection, population stratification, cell heterogeneity, confounders, temporality, sample size, appropriate statistical analysis and validation of results are all factors impacting the robustness and trustworthiness of findings (Michels and Binder, 2018).

The recent technical advances such as WGBS, reduced-representation bisulfite sequencing (RRBS) and affordable epigenomic array-based technologies (e.g. Illumina EPIC array) have allowed researchers to measure epigenetic profiles of large cohorts at a genome-wide level, generating comprehensive high-dimensional datasets that may contain important information for disease development and treatment opportunities. However, partly due to the lack of appropriate and efficient computational methods, the majority of existing studies focus on a single epigenetic mark in isolation, although evidence of interactions of multiple markers have been described (see section 1.1.2 for more details). To facilitate the sharing of epigenomic data between different studies, the standardization of sample preparation and assay protocols becomes essential. While there are existing recommendations for reporting the minimal information to annotate omics studies (e.g. MIAME for gene expression data, MIAPE for proteomics data), the consensus for the annotation protocol for epigenetics data has yet to be achieved. This is partly due to the versatile techniques for various epigenetic features that require distinct experimental protocols for achieving optimal results. In order to address this issue, comparisons of the profiling techniques have been initiated by international consortia (e.g. the BLUEPRINT consortium (Blueprint consortium, 2016)).

Moreover, the epigenomic profile for a certain trait is the result of the complex interplay between multiple genetic and environmental factors, which poses an additional challenge to visualize and interpret these data. Besides that, due to

the dynamic nature of the epigenome, it is critical to determine causal relationships for the many associations reported (Relton and Davey Smith, 2012, Jhun et al., 2017). The focus, in more recent years, has become developing data analysis approaches for the identification of coordinated epigenetic changes and interpretation of their functional consequences in normal development and disease (Cazaly et al., 2019). An interdisciplinary research community is therefore needed to foster effective and robust data integration strategies for combining epigenetics data with other omics data.

Another major challenge that distinguishes epigenetic studies is the choice of tissue type. In contrast to genetic studies, epigenetic marks are by definition tissue- and cell-type specific, thus tissue choice for epigenetic studies of complex traits requires careful consideration (Mill and Heijmans, 2013). As almost all tissues consist of multiple epigenetically distinct cell types, a major concern in epigenetic epidemiology studies is that any apparent disease-associated epigenetic change may simply reflect differences in cellular composition (Policicchio S et al., 2018, Mendizabal et al., 2019). Furthermore, failure to account for this cellular heterogeneity could limit the power of epigenetic studies in complex phenotypes. A more comprehensive discussion about cellular heterogeneity, its implications in epigenome profiling and current approaches to address it are provided in **Chapter 4** and **5** of this thesis. A further aspect to consider is the sample selection. Common epigenetic study designs include case-control studies, cross-sectional or longitudinal cohort studies, and family or twin study designs. Without a careful selection of tissues and population samples, many EWAS associations may partly stem from the dynamic and complex nature of the interactions between the different epigenetic layers, or arise from the fact that epigenetic states differ spatially across tissues and cell types as well as during aging. A variety of data integration approaches, such as co-mapping and network analysis are currently employed to unravel the complexity of these various epigenetic layers and their interaction with other omics datasets (Hasin et al., 2017).

1.1.6 Epigenetic alterations and mental diseases

Major mental diseases such as BPD, SCZ, and MDD are brain disorders with complex aetiologies but all with a notable genetic contribution. Recurrent findings showed that the onset and development of these disorders cannot be well described by the "one-gene one-disease" approach. Instead, their clinical presentation is thought to result from the regulative interplay of a large number of genes (Alam et al., 2017). Up-regulation (or activation) or down-regulation (or silencing) of these genes by environmental factors plays a crucial role in contributing to the pathogenesis. Much of this interplay may be moderated by epigenetic changes. Similar to genetic mutations, epigenetic modifications such as DNA methylation, histone modifications, and RNA interference can influence gene expression and therefore may cause the behavioural and neural changes observed in mental disorders (Alam et al., 2017).

In the last decade, studies have shown hundreds of epigenetic alterations in blood and brain of psychiatric subjects as compared to corresponding tissues of normal controls (reviewed in (Abdolmaleky et al., 2015). For example, samples from individuals with autism have showed increased *DNMT1, 3A*, and *3B* expression in their cerebellum, which supports the findings of global increase in DNA methylation and hydroxymethylation in these individuals (Keil and Lein, 2016). Another study using human fetal cortex samples reported altered DNA methylation in key neurodevelopmental genes suggesting that epigenetic mechanisms mediate some of the effects observed in SCZ (Pidsley et al., 2014). Similar findings with respect to other mental disorders such as psychotic diseases have been also reported ad are reviewed elsewhere (Abdolmaleky et al., 2015).

The following sections provide a concise overview of the psychiatric phenotype which is the focus of this thesis: suicide.

1.2 Suicidal Behaviour

Suicide is a serious public health problem that can have lasting harmful effects on individuals, families, and communities (CDC Health Report, 2017). Globally, suicide is the second leading cause of death among 15–29 year olds and ranks amongst the top 20 leading causes of death across all ages (World Health Organization, 2017). Approximately 800,000 people die by suicide every year (World Health Organization, 2017) representing a significant global health burden and a major societal problem. Suicidal behaviour (SB) spans a spectrum ranging from suicide ideation (SI) to suicide attempt (SA) and completed suicide (Tsai et al., 2011, Preti, 2011). Up to one-third of individuals with SI have a SA within one year; individuals who have had a SA have 1.6% risk of suicide completion within the year (Nock et al., 2013). SAs are up to 30 times more common compared to completed suicides; they are however important predictors of repeated attempts as well as completed suicides (Bertolote et al., 2005, Bertolote et al., 2010). Differences arise between regions and countries with respect to the age, gender, and socioeconomic status of the individual as well as method of suicide, and access to health care (Bernal et al., 2007). Completed suicides are three times more common in males than females; for SAs, an inverse ratio can be found (Bachmann, 2018, Yildiz et al., 2019, Canetto, 2008). The most commonly used methods are hanging, self-poisoning with pesticides, and use of firearms (Ajdacic-Gross et al., 2008). The majority of suicides worldwide are related to psychiatric diseases (Bradvik, 2018); the number of suicides in individuals with mental illness are at least 10 times higher than in the general population. The reported percentage of completed suicides in this context ranges between 60% and 98% (Bertolote et al., 2004, Ferrari et al., 2014). Among those, depression, substance use, and psychosis constitute the most relevant risk factors, but also anxiety, personality-, eating- and trauma-related disorders significantly add to unnatural causes of death compared to the general population (Bertolote et al., 2004, Bertolote et al., 2003). A significant amount of underreporting is likely to be present too (Tollefsen et al., 2012). Overall, SB is proven to be a complex and multifactorial phenotype and despite the advancement of the field in unravelling the epidemiology of suicidal thoughts and behaviors, as well as in identifying environmental and psychological risk factors and novel biological correlates, crucial gaps in knowledge still remain to be uncovered. Acknowledging these gaps represents a critical first step to prompt innovative and promising directions

for future work. Suicides can indeed, at least partially, be prevented through early risk assessment and screening for molecular biomarkers as well as by restricting access to means of suicide, while training primary care physicians and health workers to identify people at risk (Bachmann, 2018).

1.2.1 The role of glia in Suicidal Behaviour

Glial cells account for at least 75% of brain cells, and are implicated in a range of psychiatric disorders, including suicide (Nagy et al., 2015b). In particular astrocytes, the most abundant type of glial cells in the CNS (Zhou et al., 2019a), is thought to play a crucial role as evidence of astrocytic dysfunction have been reported in depressive psychopathologies, including suicide (Rajkowska and Stockmeier, 2013). Astrocytes are multifaceted cells with numerous functions, including regulation of blood flow, synaptic communication and plasticity, immune regulation (Oberheim et al., 2012) and maintenance of neuronal functioning (Sidoryk-Wegrzynowicz et al., 2011). These - and other - physiological roles are likely impacted in depression and suicide given the evidence from post-mortem and animal studies showing altered astrocytic morphologies (Torres-Platas et al., 2011) and persistently decreased expression of astrocyte-specific genes (Ernst et al., 2011, Choudary et al., 2005, Bernard et al., 2011). Despite consistent reports, little is known about the underlying etiological mechanisms linking astrocytic dysfunction to depression and suicide. To this end, a recent study (Nagy et al., 2015b) characterized expression of astrocytic markers Glial Fibrillary Acidic Protein (*GFAP),* Aldehyde Dehydrogenase 1 Family Member L1 *(ALDH1L1),* Solute Carrier Family 1 Member 3 *(SLC1A3),* Gap Junction Protein Alpha 1 *(GJA1),* Gap Junction Protein Beta 6 *(GJB6),* Glutamate-Ammonia Ligase *(GLUL)* and SRY-Box Transcription Factor 9 *(SOX9)* in the dorsolateral prefrontal cortex (PFC) of 121 individuals who died by suicide (N=76) and sudden-death controls (N=45). All seven genes showed significantly decreased expression in suicide cases compared to controls (Nagy et al., 2015b). The same group also investigated genomic DNA methylation patterns that may contribute to astrocyte dysfunction in depression and suicide and found that the methylation differences correlated with the detected gene expression changes (Nagy et al., 2015b).

Recent findings regarding the correlation between suicide outcome and microglia based on post-mortem studies, positron Emission Tomography (PET), Cerebrospinal fluid (CSF), and serum/plasma analysis of human subjects, indicate microglial pathophysiology as a possible contributing factor in suicide and suicide-related behaviours. Neuroinflammation has been linked to suicide (Pandey et al., 2012, Pandey et al., 2018) and activated microglia have been suggested as one of the possible contributing factors to suicide and SBs via various mechanisms especially including the tryptophan-kynurenine pathway (Suzuki et al., 2019). Steiner et al. first suggested the possible link between suicide and microglial activation, analysing the morphological characteristics of microglia by immunohistochemistry in some regions of the brain of psychiatric patients including suicide victims (Steiner et al., 2006). Significant microgliosis (e.g. increased microglial density) was observed in the dorsolateral PFC, anterior cingulate cortex (ACC) and mediodorsal thalamus (MD) of suicide victims (Steiner et al., 2006, Steiner et al., 2008). Additionally, a case-control study with immunohistochemistry and gene expression analysis was conducted using post-mortem brains comparing suicide victims with MDD and control subjects without psychiatric disease who died of physical illnesses. Microglia were significantly increased in the brain of suicide victims with MDD and the proportion of blood vessels surrounded by a high density of macrophages was more than twice higher in suicide victims with MDD (Torres-Platas et al., 2014). In a more recent post-mortem study of psychiatric disorders, significant effects of suicide on activated microglia was reported in ventral prefrontal white matter in the suicide group but not in the control one (Schnieder et al., 2014). Finally, Brisch et al. showed that only the subgroup of patients with depression who were not suicide victims (i.e. sudden death by natural causes) were characterized by significantly decreased density of activated microglia suggesting reduced abnormal microglial activity (Brisch et al., 2017). One of the important biological impacts related to microglial activation is the altered regulation of the tryptophan-kynurenine pathway (Dantzer et al., 2011, Myint, 2012). An imbalance of neuroactive metabolites in this pathway mediated by microglia has been suggested as involved in the biological process of suicide by independent studies (Steiner et al., 2011, Busse et al., 2015, Clark et al., 2016, Bradley et al., 2015, Suzuki et al., 2019).

In a recent work, whole-exome sequencing (RNA-seq) of dorsolateral prefrontal cortex (BA9) was used to examine group differences in brain gene and miRNA expression between individuals with history of depression and suicide, individuals with history of depression but not suicide (cause of death was natural or unintentional), and sudden death non-psychiatric individuals (Pantazatos et al., 2017). Exploratory and hypothesis-driven GO functional pathway analyses revealed lower expression of genes involved in immune response, microglial and glial cell functions, regulation of glutamatergic neurotransmission, anti-apoptosis and neuroprotection in suicide cases with or without depression. These effects appeared to be driven primarily by depression, with the exception of DNA-dependent ATPase expression observed in suicide only (Pantazatos et al., 2017). Also worthy of mention, in a recent PET imaging study, which at present is regarded to be the only valid method to evaluate microglial activation in the brain of living human subjects (Suzuki et al., 2019), authors reported microglial activation during the presence of suicidal ideation in depression (Holmes et al., 2018). On the other hand, impaired gene expression of oligodendrocyte-specific connexins and key gap junction-related genes was observed in the ACC of depressed suicidal individuals, altogether suggesting impaired astrocyte-oligodendrocyte communication in the brain of depressed suicidal individuals (Tanti et al., 2019) which is in line with several post-mortem studies consistently reporting decreased expression of astrocytic connexins in frontal regions of suicidal individuals (Ernst et al., 2011, Nagy et al., 2017, Miguel-Hidalgo et al., 2014). These outcomes altogether have suggested a relationship between alteration of glia cells and suicide beyond the diagnostic classification of psychiatric disorders. Therefore, further larger studies including various psychiatric phenotypes are now needed in order to elucidate the relationship between glial cells, in particular microglia, and suicide beyond psychiatric comorbidities.

1.2.2 Genetics of Suicidal Behaviour

Genetic epidemiological studies have found evidence of family clustering of SB and have highlighted a clear genetic susceptibility to SB (Roy and Segal, 2001, Mullins et al., 2014) with heritability estimated to be about 43% (McGuffin et al.,

2010). A significant proportion of the heritability for SB and SA appears to be independent of diagnosed psychiatric diseases as when the heritability of SA is corrected for transmission of psychiatric disorders, specific heritability is between 17% and 36% (Fu et al., 2002, Brent et al., 1996, Brent et al., 2004, Kim et al., 2005, Anguelova et al., 2003, Brezo et al., 2008).

Pre-existing knowledge of biological systems likely to be associated with SB, such as serotonergic neurotransmission and neurotrophic factors, resulted in several candidate-gene association studies (Mullins et al., 2014, Anguelova et al., 2003, Brezo et al., 2008, Mann, 2013, Dwivedi, 2010) which have largely yielded inconsistent results. Most genome-wide association studies (GWASs) on this topic have provided evidence of association between SNPs and suicide (Coon et al., 2020, Erlangsen et al., 2020, Kimbrel et al., 2018, Levey et al., 2019). Candidate genes and GWAS designs have identified numerous loci associated with suicide attempts, including the serotonin receptor *5HTR2A* (rs1885884) (Brezo et al., 2010), a locus on 2p25 (rs300774) (Sokolowski et al., 2014, Willour et al., 2012); and the binding protein *ABI3BP* (rs2576377) (Perlis et al., 2010) among others (Sokolowski et al., 2015). However, most previous genome-wide significant findings have yet to be replicated sufficiently to confirm these associations (Li et al., 2017, Mirkovic et al., 2016) or have failed to identify robust associations (Schosser et al., 2011, Willour et al., 2012, Galfalvy et al., 2013) suggesting that the risk of SB is highly polygenic in nature and that individual gene variants are likely to account only for a very small proportion of the total phenotypic variability. Other factors, such as the environment, behavioural traits, lifestyle and coping mechanisms, are essential regulators of suicide risk and likely to account for more sizeable effects (Turecki and Brent, 2016). Furthermore, many molecular genetic studies, even combined ones, have been conducted on small sample sizes (sample < 8900; cases < 2810) (Sokolowski et al., 2014, Baldessarini and Hennen, 2004), implying that they potentially were underpowered and subject to false positives as well as false negatives. Additionally, studies have rarely adjusted for mental disorders or included a non-psychiatric, population-representative sample.

Mental disorders are strongly linked to suicidal behavior (Qin, 2011, Hawton and van Heeringen, 2009, Nordentoft et al., 2011). Indeed, often mental disorders and suicidality are seen as clinically related, e.g., suicidal ideation is considered as a

qualifying symptom for the diagnosis of depression. Given that liability for a wide range of mental disorders is associated with a set of genetic factors (Sullivan et al., 2000, Cross-Disorder Group of the Psychiatric Genomics, 2013), it is plausible that the effect of genes on suicidal behavior could be mediated through their impact on mental disorders (Sokolowski et al., 2014, McGirr et al., 2009). Although family studies have indicated support for a generic transmission of suicidal behavior independent of mental disorders (Agerbo et al., 2002, Runeson and Asberg, 2003, McGirr et al., 2009, Brent et al., 1996), this remains to be confirmed using molecular genetic data. This year a large population-based GWAS of young adults was undertaken to examine SA while accounting for the presence of mental disorders hereby, addressing the possible mediating role of mental disorders (Erlangsen et al., 2020). The authors conducting the GWAS, estimated SNP heritability for SA in a large sample of 6024 cases with history of suicide attempt and 44,240 controls with no record of a suicide attempt (Erlangsen et al., 2020). One of the lead SNP, rs6880062 on chromosome 5 with the closest gene being *FAM114A2* has not previously been associated with SB (Sokolowski et al., 2015) while another leading SNP identified on chromosome 20, rs4809706, was located nearby the *PREX1* gene which has been associated with depression and autism-like behavior (Li et al., 2015). Furthermore, all SNPs explained 4.6% of the variation in SA and controlling for mental disorders reduced the heritability estimate to 1.9% (Erlangsen et al., 2020); the reduction from 4.6 to 1.9% indicates that parts of the genetic transmission is likely explained through mental disorders.

In conclusion, the studies on the heritability of SB have shown a strong genetic component, highlighting how a large number of genetic variants appear to be involved in the emergence of SB each of which contributes a small modulation of risk. However, GWASs, useful for detecting small effects, have failed to clearly identify specific markers contributing to this genetic liability. The ability to identify significant associations and the relevance of such information to suicidality is linked both to the number of subjects in each group and to the method used to define the groups. Second, variations in the definition of SB in the studies on genetic association are considerable, a fact which would tend to render comparisons between the results obtained somewhat rash. Finally, multiple testing, the rates of false positives and statistical significance levels are important

issues in determining the strength of findings in genetic association studies (Mirkovic et al., 2016).

1.2.3 Epigenetics of Suicidal behavior

An important factor contributing to gene regulation that may bridge the gap between genetic variation and transcriptomic effects in suicide, and potentially mediate the translation of social stress into biological dysfunction, is the epigenetic control of gene expression. The epigenome is potentially malleable - changing with age (Bell et al., 2012) and in response to specific environmental (Feil and Fraga, 2012) and psychosocial factors (Burns et al., 2018) - providing a mechanism for the interaction between genotype and the environment (Mill and Heijmans, 2013). Particularly in more recent years, increased understanding of epigenetic processes that occur in the brain in health and disease has opened promising avenues in suicide research.

Ten epigenome-wide association studies (EWAS) have explored DNA methylation in suicide. Three studies compared global methylation levels in blood between suicidal subjects and non-suicidal controls. Despite the tissue-specific nature of DNA methylation, the inaccessibility of human brain samples necessitates the frequent use of surrogate tissues such as blood, in studies of associations between DNA methylation and brain function and health (Edgar et al., 2017, Walton et al., 2016). The first reported global hypermethylation levels in peripheral blood of 73 suicide attempters (SAs) with psychiatric illness compared to 70 psychiatric non-attempters (Murphy et al., 2013). Hypermethylation was also reported in postmortem ventral prefrontal cortex of suicide completers compared to non-psychiatric controls (N=25 and N=28 respectively) (Haghighi et al., 2014). The third study examined 6 suicide completers (5 of which were non-psychiatric) and 6 non-psychiatric sudden-death controls and significant global hypomethylation was found in the suicide group (Schneider et al., 2015). The opposite findings reported in these studies could be due in part to the differences in study populations (psychiatric vs. non-psychiatric subjects), suicide phenotypes (SA vs. suicide completers), methodologies for assaying DNA methylation (Methylflash for quantification of global 5-methylcytosine methylation vs. Methylation450K array for assaying methylation

levels at CpG sites across the genome) tissue types (peripheral blood vs. various postmortem brain regions) as well as differences in group size analysed. In addition to the analysis of global methylation levels, four studies conducted epigenome-wide comparisons of individual CpG sites between suicidal and non-suicidal controls. In the first study, the authors analyzed postmortem prefrontal cortical samples of MDD patients and found *SKA2, ATP8A1, LOC153328*, and *KCNAB2* to be differentially methylated between suicide cases and controls (Guintivano et al., 2014). Of these, only *SKA2* was differentially methylated in neuronal and glial fractions in both the discovery and replication samples (Guintivano et al., 2014). In addition, the authors were able to replicate the *SKA2* findings in two additional postmortem prefrontal cortical samples (Guintivano et al., 2014). In the second study, another research group compared peripheral blood DNA methylation levels between bipolar disorder patients with no suicidality and those with high suicidality (Jeremian et al., 2017) and identified DMRs within three genes that reached epigenome-wide significance: *MPP4*, *NUP133*, and *TBC1D16* (Jeremian et al., 2017). In the third epigenome study, the authors analysed methylation levels in neuronal fractions of postmortem orbitofrontal cortical samples (Kozlenkov et al., 2017). They identified 454 nominally differentially methylated CpG sites between suicide completers and non-suicide controls. Further differential analyses revealed that the hypermethylated sites were enriched for genes that were found to be also differentially expressed in glutamate neurons, whereas the hypomethylated sites were enriched for genes that were differentially expressed in GABA neurons (Kozlenkov et al., 2017). Most recently, another EWAS of SA in blood of SCZ patients yielded cg19647197 in the *CCDC53* gene as the top finding (Bani-Fatemi et al., 2018). In addition to the studies mentioned above, Labonte et al. found promoter hypermethylation of genes involved in cognitive pathways in postmortem hippocampal samples of suicide victims compared to those of non-psychiatric sudden-death controls (Labonte et al., 2013). In another study, Labonté et al. reported *ALS2* gene promoter to be hypermethylated in postmortem hippocampal samples of suicide victims with history of abuse compared to those of suicide victims without abuse and non-suicide controls (Labonte et al., 2012b). Taken together these findings, although requiring further replication, additional validation and more consistent study designs, suggest that global DNA methylation may be a biomarker of suicide risk in psychiatric patients.

If a robust body of evidence is available for DNA methylation, studies examining the role of histone modifications in SB remain limited to the study of candidate genes (Ernst et al., 2009a, Fiori et al., 2012) and genome-wide approaches have not yet been undertaken. Only three studies investigating histone modifications in relation to suicide stand out in the current literature. The first tested the *NTRK2* gene in postmortem brain samples of suicide completers and controls and found increased Histone 3 Lysine 27 (H3K27) methylation in suicide completers (Ernst et al., 2009a). The second study examined the polyamine stress response system, which has been associated with suicide (Fiori et al., 2011, Fiori et al., 2012, Gross et al., 2013). The authors focused particularly on five genes (i.e. *ARG2*, *SAM*, *AMD1*, and *OAZ1* and *OAZ2*) that are involved in polyamine metabolism (Fiori et al., 2012). They found increased Histone 3 Lysine 4 trimethylation (H3K4me3, an active promoter mark) in the upstream region of *OAZ1* in the prefrontal cortex of suicide completers compared to non-suicide controls (Fiori et al., 2012). The most recent paper investigated the Connexin genes *CX30* and *CX43*, which are important for communication between astrocytes through gap junctions, in suicide completers with low expression of astrocytic genes (Nagy et al., 2017). They found increased Histone 3 Lysine 9 trimethylation (H3K9me3, a repressive histone mark) for both CX30 and CX43 in the prefrontal cortex (Nagy et al., 2017).

1.2.4 Common neurobiological pathways epigenetically dysregulated in suicide

In the last decade, the investigation of epigenetic mechanisms in SB has implicated the role of key biological pathways, including hypothalamic pituitary adrenal (HPA) axis, stress response, polyamine system, neurotrophic signalling and lipid metabolism. A comprehensive list of studies reporting epigenetic dysregulation in association to suicide and SB can be found in **Table 1.2** (DNA methylation and histone modifications studies) **and Table 1.3** (Non-coding RNA studies) at the end of this chapter. Common pathways frequently targeted by epigenetic and miRNA dysregulation are illustrated in **Figure 1.5** and discussed in detail in the following sections.
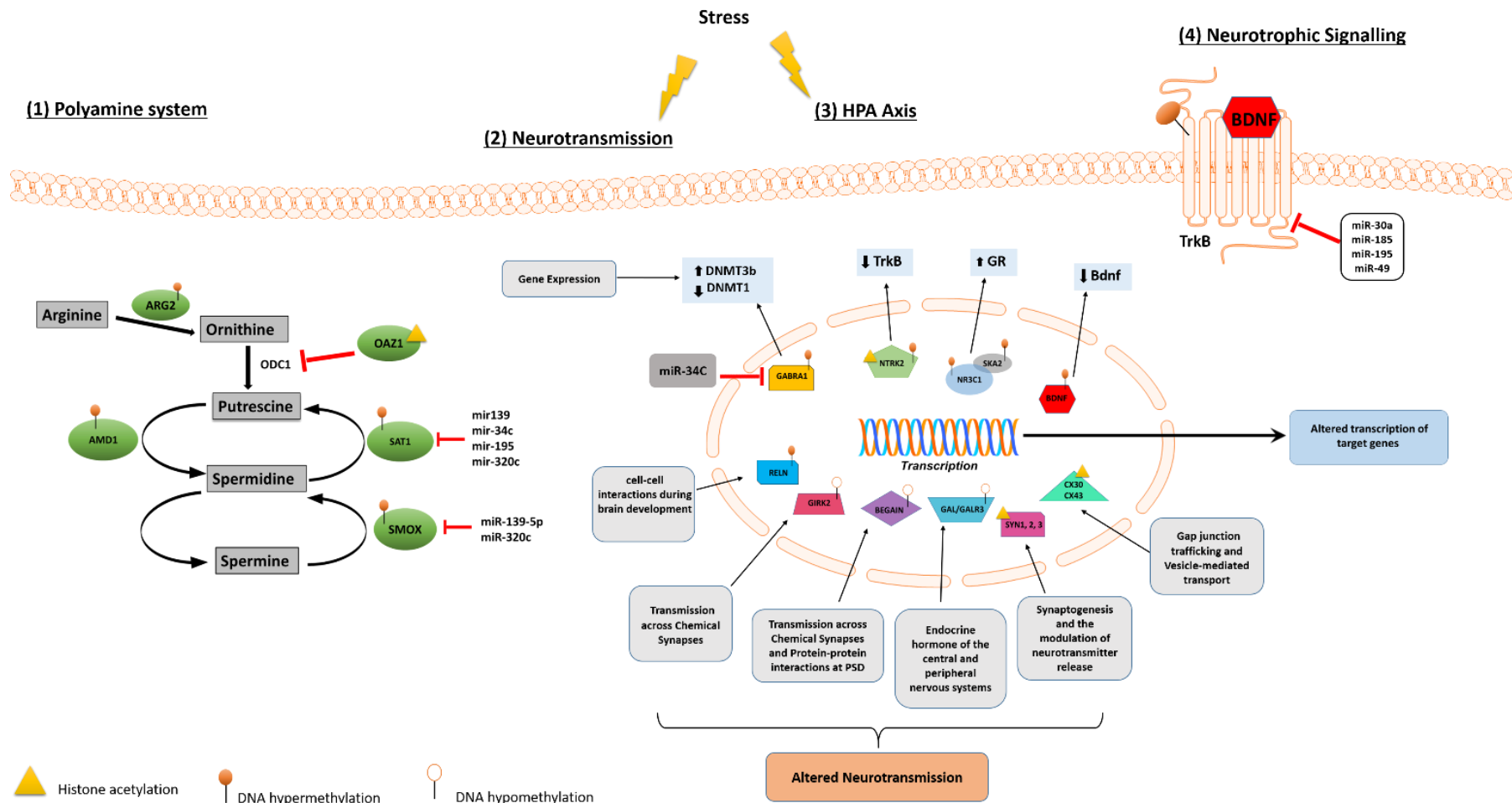
Figure 1.5 Molecular pathways involved in suicide behaviour.

(1) Polyamine system: several enzymes involved in the regulation of polyamine intracellular concentration exhibit epigenetic regulatory mechanisms in suicide through DNA methylation (AMD1, ARG2), histone methylation (OAZ1) and/or post-translational mechanisms (SAT1, SMOX) as miRNAs regulation. (2) Neurotransmission: many genes known to play a key role at chemical and/or electrical synapses have been reported as hypomethylated (BEGAIN, GIRK2, GALR3), hypermethylated (RELN) or histone methylated (SYN1-3, CX30, CX43) in suicide cases compared to non-psychiatric controls suggesting that neurotransmission may be compromised in suicide. (3) HPA axis: two genes differentially involved in cortisol release following stress (NR3C1, SKA2) have been found to be both significantly hypermethylated in suicide cases relative to controls supporting the hypothesis of suicide-associated HPA axis dysregulation. (4) Neurotrophic Signalling: several studies examining BDNF and TrkB in post-mortem suicide brains revealed distinct epigenetic regulation pattern for these two genes: the receptor TrkB seems to be regulated via miRNAs (miR-30a, miR-185, miR-195 and miR-49) and histone acetylation while the expression levels of the neurotrophin Bdnf correlate with DNA hypermethylation in the promoter region of the gene. Abbr: miR, microRNA; HPA, hypothalamic–pituitary–adrenal axis. For gene names refer to main text below. Figure taken from (Policicchio S et al., 2018).

1.2.4.1 HPA stress axis

It is well established that perturbations in the hypothalamic–pituitary–adrenal axis (HPA) axis are associated with the pathophysiology of suicide (Mann and Currier, 2010). The HPA axis is a neuroendocrine system, key regulator of cortisol release and the stress response (Raison and Miller, 2003). Research has shown that the HPA axis may be epigenetically programmed by the early-life environment (Turecki, 2014). Several HPA-axis coupled genes have been identified over the years: corticotropin releasing hormone (*CRH*), corticotropin releasing hormone binding protein (*CRHBP*), corticotropin releasing hormone receptor 1 (*CRHR1*), corticotropin releasing hormone receptor 2 (*CRHR2*), FK506-binding protein 51 (*FKBP5*) and the glucocorticoid receptor (*NR3C1*)(Roy et al., 2012)

More recently, a study aiming to identify DNA methylation shifts linked to severity of the SA in HPA-axis coupled genes was conducted in whole blood derived DNA. The authors reported reduced levels of DNA methylation at two loci within the *CRH* promoter in serious suicide attempters. The study did not investigate DNA methylation differences directly in brain tissue however, by using a bioinformatics comparison tool, authors were also able to assess whether the DNA methylation levels they observed in blood were present in brain. Interestingly, significant blood-brain correlations in DNA methylation were found suggesting that the alterations observed in blood may impact on expression profile of *CRH* in the brain (Jokinen et al., 2018).

1.2.4.2 Glucocorticoids

Glucocorticoids play a crucial role in the maintenance and survival of neurons and in synaptic plasticity (Myers et al., 2014). A study examining the DNA methylation status of *GR* exon 1F variant in individuals who died by suicide and were severely abused during childhood observed increased DNA methylation at the *GR* promoter compared to suicide victims with no childhood abuse or controls (McGowan et al., 2009). However, the same study reported that neither hippocampal GR expression nor the methylation status of the exon 1F NR3C1 promoter was altered in suicide victims with no history of abuse (McGowan et al., 2009) suggesting that variation in the methylation status is closely associated with a developmental history of familial adversity, in this case a history of

childhood abuse and not with suicide per se. Furthermore, *GR* methylation status appears to regulate the binding of the *NGFI-A* transcription factor associated with the *GR* expression (McGowan et al., 2009, Weaver et al., 2004). The disrupted GR function may result in inadequate control of the HPA axis, possibly leading to hyperactive cortisol secretion and development of anxiety traits (Herman et al., 2016). In turn, anxiety mediates the relationship between the exposure to early life adversity (ELA) and SB (Turecki, 2014, Wanner et al., 2012). These findings are also consistent with those from studies with rodent and non-human primates showing that persistent disruptions of mother-infant interactions are associated with increased hypothalamic corticotrophin-releasing hormone expression and increased HPA responses to stress (Meaney, 2001, Plotsky et al., 2005). Variations in maternal care in the rat influence hippocampal glucocorticoid receptor expression, as well as methylation of the rat fetal calf serum Nr3c1 promoter, the homolog of the human exon 1F NR3C1 promoter (Liu et al., 1997, Weaver et al., 2004).

Lastly, a study has suggested a role for dietary deficiencies in mediating the interaction between an altered GR system and SB (Weaver et al., 2005). DNA methyltransferases catalyse the transfer of a methyl group from the methyl donor, s-adenoslymethionine (SAM), onto the 5C position of the dinucleotide sequence CG. However, the synthesis of SAM is dependent on the availability of dietary foliates, vitamin B12 and choline, suggesting an alternative mechanism to altering the expression of the *GRII* exon 17 promoter (Bennett, 2011).

1.2.4.3 *SKA2 - Altered microtubule binding*

An exciting new candidate in the relationship between cortisol regulation and suicide is the spindle and kinetochore associated protein 2 (*SKA2*), a gene that has been implicated in GR signalling (Rice et al., 2008). This microtubule binding protein is thought to interact with the HPA axis by chaperoning the GR from the cytoplasm to the nucleus upon cortisol binding (Rice et al., 2008). Once in the nucleus, the GR can interact with genomic DNA and influence gene expression involved in negative feedback regulation of the HPA axis response. In 2014, a study identified site and allele-specific DNA methylation patterns in the *SKA2* gene, in particular increased *SKA2* 3′ untranslated region methylation and concomitantly decreased *SKA2* mRNA levels, were detected in the frontal cortex of MDD suicide completers relative to MDD non-suicide completers (Guintivano

et al., 2014). Further research found that *SKA2* DNA methylation predicted lifetime SA in saliva and blood in individuals suffering from post-traumatic stress disorder (PTSD) (Kaminsky et al., 2015). Higher DNA methylation at the same site and allele was also found to predict lower levels of miR-301a in the cortex of depressed suicide completers (Smalheiser et al., 2012). Since the expression of this miRNA is tied to *SKA2* expression, it was suggested as a proxy of suicide-associated *SKA2* decreases (Smalheiser et al., 2014, Kaminsky et al., 2015). Further support to these preliminary findings has been provided by more recent studies suggesting the influence of trauma exposure on *SKA2* DNA methylation as well as DNA methylation of the *SKA2* gene as a biomarker of suicide risk and stress-related psychopathology (Boks et al., 2016, Sadeh et al., 2016).

1.2.4.4 *Polyamine system and SAT1*

The polyamine system is another stress response pathway which has been extensively characterized in relation to suicide risk. Polyamines, aliphatic compounds with multiple amine groups, have been implicated in regulation of gene expression at transcriptional and posttranscriptional levels, regulating the function of several neuromodulators and acting as neurotransmitters themselves (Limon et al., 2016, Gilad and Gilad, 2003). Involvement of epigenetic modifications in the regulation of genes associated with polyamine biosynthesis has been implicated in SB (Gross et al., 2013).

SAT1 is an enzyme involved in polyamine catabolism and is arguably one of the most consistently downregulated gene in depressed suicide completers (Sequeira et al., 2006, Fiori et al., 2009, Guipponi et al., 2009, Fiori and Turecki, 2011, Fiori and Turecki, 2010, Le-Niculescu et al., 2013, Sequeira et al., 2007). A potential mechanism for *SAT1* downregulation is through epigenetic control, as studies have identified that *SAT1* promoter DNA methylation is inversely correlated with *SAT1* expression. Moreover, there is evidence for histone modifications affecting *SAT1* expression along with other key enzymes in polyamine synthesis (Fiori et al., 2012, Gross et al., 2013, Fiori and Turecki, 2011) and that miRNAs can target polyamine transcripts, including *SAT1* (Lopez et al., 2014). *SAT1* has therefore emerged as a potential biomarker for suicide, topping the lists of candidate genes in several studies (Le-Niculescu et al., 2013, Niculescu et al., 2015a, Niculescu et al., 2015b). However, it is still unknown

whether this gene is involved in major depressive disorder (MDD) independently of suicide, which isoforms are dysregulated and whether the gene undergoes differential splicing in suicide and depression (Pantazatos et al., 2015).

The expression of several other polyamine-associated enzymes were found altered in the cortex of post-mortem depressed suicide cases. The spermine oxidase (*SMOX*) gene, encoding for a catabolic enzyme, was found hypermethylated in the promoter region in the prefrontal cortex (PFC) of depressed suicide subjects relative to the depressed non-suicide group as well as the healthy control group. However, there was no correlation between aberrant promoter DNA hypermethylation and gene expression levels (Fiori and Turecki, 2010). Two studies have identified DNA hypomethylation at the promoter region of the arginase 2 (*ARG2*) and adenosylmethionine decarboxylase1 (*AMD1*) genes, which correlated with increased gene expression in suicide completers compared to controls (Fiori et al., 2012, Gross et al., 2013). A different epigenetic modification showed to regulate the Ornithine Decarboxylase Antizyme 1 (*OAZ1*) gene, also involved in the intracellular regulation of the polyamine levels. Increased H3K4me3 levels in the promoter region of *OAZ1* were found in suicide completers and appeared to correlate with the expression of *OAZ1* and *ARG2* in Brodmann area 44 (Fiori et al., 2012). Taken together this research provides support for the involvement of epigenetic modifications in the regulation of genes associated with polyamine biosynthesis, which may play an important role in SB.

1.2.4.5 *Neurotrophic pathways - BDNF and NTRK2*

Genome-wide DNA methylation studies in the brains of suicide completers indicates that suicide is associated with widespread changes in DNA methylation patterns of neurotrophic and neuroprotective factors in the hippocampus and PFC (Schneider et al., 2015, Labonte et al., 2013). Brain derived neurotrophic factor (BDNF) is a well-known receptor binding factor with growth factor activity; it is essential for the survival and plasticity of cortical and striatal neurons and it has been implicated in both stress response (Dwivedi, 2010) and mood disorders (Phillips, 2017). Increased *BDNF* promoter/exon 4 DNA methylation has been reported in suicide brains (Keller et al., 2010), a finding that is consistent with those observed in depressed patients with a history of SA, or with SI during treatment with antidepressants (Kang et al., 2013). Similarly, another study

focusing on the Wernicke area of suicide subjects, reported a remarkable increase of DNA methylation at the *BDNF* promoter IV in suicide subjects ($\Delta\beta=12\% \pm SD$) with respect to controls ($\Delta\beta =5\% \pm SD$) (Keller et al., 2011). Taken together this evidence suggest that *BDNF* DNA methylation status maybe a proxy marker for previous suicidal attempts and a clinical biomarker for poor treatment outcomes of SI in depression. However, larger studies are required to confirm these findings.

Interestingly, TrkB, main receptor of BDNF and encoded by the *NTRK2* gene, is also regulated through epigenetic changes that appear to have an impact on suicide risk. In brain tissue from individuals who died by suicide, mRNA expression of *Trk-BT1,* the astrocyte-enriched TrkB truncated variant, was found significantly decreased and correlated with increased DNA methylation at the *TrkB-T1* promoter suggesting that astrocytic dysfunction may occur in individuals who die by suicide (Ernst et al., 2009a, Ernst et al., 2009b, Maussion et al., 2014).

1.2.5 Non-coding RNAs and their role in SB

The specific dysregulation of ncRNA function in suicide has just began to be appreciated with a number of recent studies implicating a role for miRNA dysregulation in the pathogenesis of SB (see **Table 1.3** for full list of suicide-associated miRNAs). One hypothesis-free study examined post-mortem PFC samples of suicide completers and controls with SCZ, BPD or MDD (Smalheiser et al., 2014). Out of 232 miRNAs that showed strong association with expression, eight reached nominal significance, six of which were downregulated and two were upregulated. Overall, 70% of miRNAs showed downregulation in the suicide group; and this was consistent with the authors' previous finding of reduced global miRNA expression in depressed suicide cases compared to controls (Smalheiser et al., 2014). Another study screened the locus coeruleus for expression changes in 355 miRNAs between MDD suicide cases and non-psychiatric controls (Roy et al., 2017b). The authors found 10 miRNAs upregulated and three downregulated, with further analyses implicating neural transmission and plasticity. On the other hand, Pantazatos et al. found no difference in 1353 annotated miRNAs between MDD suicide cases and MDD controls from a different brain collection (Pantazatos et al., 2017). Interestingly, some of the suicide-associated genes

previously discussed as showing altered DNA methylation and/or histone modifications were found to be targets of differentially expressed miRNAs. For example, the expression levels of two genes involved in the polyamine metabolism (*SAT1* and *SMOX*) were found to be downregulated by overexpression of miRNAs (e.g. miR-139-5p, miR-34c-5p, miR-195, miR-320c) in suicide cases compared to controls (Lopez et al., 2014, Pantazatos et al., 2015). Similarly, a study comparing suicide completers and non-psychiatric controls with low post-mortem brain TrkB-T1 transcript expression found miR-185, which binds to 3′ untranslated region and is thought to regulate the *NTRK2* gene (TrkB receptor) to be upregulated in the frontal cortex of suicide completers (Maussion et al., 2012); this finding was also validated in an independent sample (Maussion et al., 2012). Furthermore, miR-185, together with miR-195 and miR-30a have been implicated in regulating the *BDNF* signalling pathway (Serafini et al., 2014, Maussion et al., 2012, Mellios et al., 2008), a pathway repetitively reported as involved in SB. Another study (Wang et al., 2018a) examined PFC levels of six potential regulators of the expression of tumor necrosis factor gene (*TNF-α*), a cytokine that have been associated with suicide, SA, and SI, (Lindqvist et al., 2009, Monfrim et al., 2014, Pandey et al., 2012). The level of miR-19a-3p was found to be upregulated in MDD suicide cases compared to healthy controls in samples obtained from two distinct brain collections (Wang et al., 2018a). Furthermore, Sun *et al*, implicated a role for notch signalling in SI in a study of miRNAs from peripheral blood leukocytes of MDD patients (Sun et al., 2016).The expression levels of two notch-associated miRNAs, miR-34b–5p and miR-369–3p, were found to be significantly lower in patients with SI relative to patients without SI (Sun et al., 2016). Consistent with these results, expression levels of these miRNAs have been previously shown to be reduced in PFC of depressive suicidal patients compared to normal controls (Smalheiser et al., 2012), highlighting the potential utility of examining differences in miRNA expression in peripheral tissue from individuals with SB. Taken together, these findings suggest a coordinated epigenetic and miRNA regulation of pathways potentially relevant to the aetiology of SB.

LncRNAs represent another interesting class as they are enriched for expression in the brain (Derrien et al., 2012) and are developmentally regulated (Aprea et al., 2013), but less evolutionarily conserved than other RNA species. Although

preclinical studies have begun to unravel how lncRNAs may contribute to emotional control (Spadaro et al., 2015) and affective disorders (Lin and Turecki, 2017), their role in SB, with the exception of few studies, remain mostly unexplored. Recently, our group suggested a role for DNA methylation at the *PSORS1C3* locus, a non-coding RNA, in the brains of suicide completers (Murphy et al., 2017). Although the function of the *PSORS1C3* gene product remains unknown, it is thought to potentially regulate nearby genes (for example, *POU5F1* and *HLA-C*), suggesting a role in immune system regulation. Moreover, *PSORS1C3* is a known psoriasis susceptibility gene further supporting a role in immune system regulation (Murphy et al., 2017). Furthermore, a recent study identified six lncRNAs (refer to **Table 1.3**) whose expression was downregulated in peripheral blood samples of MDD patients with SI (Cui et al., 2017) . Lastly, Punzi *et al* showed that the expression of an uncharacterized lncRNA, *LOC285758*, was significantly increased in violent suicide cases compared to non-violent suicide cases (Punzi et al., 2014). Interestingly, DNA methylation of an intragenic CpG island in the myristoylated alanine-rich protein kinase C substrate (*MARCKS*) gene, a locus previously reported as potential blood biomarker for suicidality (Le-Niculescu et al., 2013) was found to be associated with the expression of this lncRNA, suggesting that the previously reported *MARCKS* association with violent suicide may involve regulation by LOC285758 expression. In conclusion, profiling ncRNAs can substantially contribute to our understanding of how gene expression networks are reorganized in suicide.

The high miRNA diversity multiplied by the large number of individual miRNA targets generates a vast regulatory RNA network than enables flexible control of mRNA expression. The gene-regulatory capacity and diversity of miRNAs is particularly valuable in the brain, where functional specialization of neurons and persistent flow of information requires constant neuronal adaptation to environmental cues (O'Carroll and Schaefer, 2013). Furthermore, considering the relative lack of success of the analysis of variations in candidate protein coding genes and of GWAS to identify strong risk factors for common psychiatric phenotypes, miRNA genes are of particular interest for the field of psychiatric genetics as deregulation of the rate of transcription or translation of a normal gene may be phenotypically similar to disruption of the gene itself.

1.3 Limitations of current epigenetic research

One of the major challenges in studying epigenetic changes in neuropsychiatric disorders is the availability of samples from the primary target tissue (*i.e.*, the brain). Since it is not possible to perform *in vivo* epigenetic studies in the brain, only retrospective study designs using post-mortem brain samples are viable. These experiments are limited by access to high-quality, well-phenotyped samples. Post-mortem interval, storage time, pH, medication history, are all potential confounders that could influence epigenetic analyses of such samples (Pidsley and Mill, 2011). Considering the small absolute changes that are likely to be uncovered, the small number of brain samples available for neuropsychiatric epigenetic research is one of the major cause responsible for the limited power to detect significant associations.

The high dependence on epigenetic marks to delineate cell types and the cellular heterogeneity of many tissues compels scientists to refine their sampling procedures. Given the cell-specific differences identified in epigenetic gene regulation (Guintivano et al., 2013, Kozlenkov et al., 2014, Kozlenkov et al., 2016, Kundakovic et al., 2017, Mendizabal et al., 2019), the isolation of specific cell types (*e.g.*, neurons, glia, and astrocytes) from bulk tissue is crucial. Approaches such as laser capture microdissection (LCM) or fluorescence-activated cell sorting (FACS) have been recruited to detect disease-associated changes that manifest in only a small subset of cells, which may not be detectable in analyses of whole tissue (Steiner et al., 2012, Kim et al., 2015b, Policicchio S et al., 2018). It is indeed a major concern in epigenetic epidemiology studies that any apparent disease-associated epigenetic differences may simply reflect differences in cellular composition (Policicchio S et al., 2018, Barton et al., 2019, Mill and Heijmans, 2013) and failure to account for cellular heterogeneity could limit the power of epigenetic studies in complex phenotypes. Careful sample selection and high-sensitivity detection tools are therefore required in order to correctly understand the molecular implications of methylation at individual loci, either in development, or as a risk factor for mental illness (Cariaga-Martinez and Alelu-Paz, 2017). Lastly, epigenetic research applied to psychiatry currently only counts on fragmented information, focusing on DNA methylation or one histone modification as the main finding, with minimal interest in the interplay with other epigenetic mechanisms (Cariaga-Martinez and Alelu-Paz, 2017). Methylation itself (along with other DNA modifications) is not sufficient to fully understand the

putative role of epigenetics in the evolvement of mental disorders (Fullard et al., 2016). Given the present outlook and with the current lack of information, we are unable to get an adequate frame of knowledge of the actual epigenetic contribution to mental disorder development. To this end, neuroepigenomics represents an effort to unify the research available on the molecular pathology of mental diseases, which has been carried out through several approaches ranging from interrogating single DNA methylation events and hydroxymethylation patterns, to epigenome-wide association studies, as well as studying post-translational modifications of histones, or nucleosomal positioning and miRNA post-translational regulation (Cariaga-Martinez and Alelu-Paz, 2017).

1.4 General aims of my thesis

Despite the availability of cutting-edge technologies and the broader comprehension of the molecular pathology of severe mental illness, our knowledge about dysregulation of epigenomic mechanisms in the brain of individuals who died by suicide remain limited, largely based on studies conducted on small numbers of samples and/or studies performed on bulk brain tissue therefore overlooking the variation at the level of individual cell types. The general aim of this thesis was to further the knowledge on the extent of methylomic and transcriptomic variation in the brain of suicidal individuals as well as to develop an experimental approach which could enable us to address the cell heterogeneity issue in the context of profiling genomic variation in complex tissue like the human brain.

• In the first empirical chapter (**Chapter 3**) I aim to systematically investigate genome-wide methylomic variation associated with SB in the brain, by utilising previously published and unpublished methylomic datasets. In this study, genome-wide DNA methylation profiles were available from post-mortem brain samples of suicide completers and non-psychiatric, sudden-death controls. Methylomic data available for two different brain regions - Prefrontal cortex (PFC) and Cerebellum (CER), (PFC: 4 cohorts, n = 211; CER: 3 cohorts, n= 114) - were meta-analysed across the suicide cohorts for each brain region separately. I reported evidence for altered DNA methylation in suicide cases

compared to controls in both brain regions and found that suicide-associated DMPs were enriched among gene networks implicating biological processes relevant to neuropsychiatric phenotypes and suicidality, including nervous system development (PFC) and regulation of long term synaptic depression (CER). Finally, I examined the functional implications of a top-ranked PFC suicide-associated differentially methylated region (*PSORS1C3* DMR) on gene expression levels in that region and found no evidence of statistically robust correlation between DNA methylation status and gene expression of nearby genes.

• In the second empirical chapter (**Chapter 4**), by leveraging upon two different published protocols, I describe the optimisation of a method to purify discrete populations of nuclei derived from three neural cell types (neurons, oligodendrocytes and other glial cells) in the post-mortem human brain. These nuclei populations yield high quality genomic DNA and nuclear RNA which are suitable for parallel multi-omics assays. DNA methylation profiling and gene expression analysis are the two main applications I have chosen to focus on for the purpose of this thesis.

• In the third empirical chapter (**Chapter 5**) I investigate DNA methylation variation associated with cellular heterogeneity in the healthy human brain. I identified multiple cell type-specific differentially methylated positions (DMPs) and differentially methylated regions (DMRs) in the human PFC.This pilot study highlights the utility of disentangling the complexity of the bulk tissue at a cellular resolution to identify whether different epigenetic signatures are driven by distinct cell types helping therefore to better explain the phenotype variability observed in complex diseases.

• In the fourth empirical chapter (**Chapter 6**) I utilised post-mortem brain tissue to extract miRNAs from a cohort of depressed suicide completers and non-psychiatric controls in order to identify differentially expressed miRNAs using the TaqMan® OpenArray® Human microRNA Panel. Despite lacking strength of association, the preliminary findings of this screening provide suggestive evidence of differential expression of miRNA in suicide completers although requiring replication and validation in a larger independent cohort.

Table 1.2 Aberrant epigenetic changes associated with suicidal behaviour.

GENE SYMBOL	PROTEIN ENCODED	GENE FUNCTION (NCBI)	MOLECULAR FUNCTION (UniProt)	TISSUE	KEY FINDINGS	REFERENCES
DNA methylation						
Global DNA methylation	NA	NA	NA	PFC (BA47)	eight-fold increased DNA methylation in suicide group compared to controls	(Haghighi et al., 2014)*
Global DNA methylation	NA	NA	NA	Peripheral blood	Psychiatric patients with a history of SA had significantly higher levels of global DNA methylation compared with controls	(Murphy et al., 2013)*§
NR3C1	Glucocorticoid receptor	Maintenance and survival of neurons and in synaptic plasticity	Affects inflammatory responses, cellular proliferation and differentiation in target tissues. Involved in chromatin remodelling. Plays a role in rapid mRNA degradation	Hippocampus	Significant DNA hypermethylation at *GR* promoter in the hippocampus of suicide completers with history of abuse compared to controls	(McGowan et al., 2009)*§
				Hippocampus	DNA hypermethylation in the exon 1F of the *GR* gene in abused individuals who died by suicide compared to non-abused individuals	(Labonte et al., 2012a)*
RNR1	ribosomal RNA	Critical functions in the ribosome that allow protein synthesis to occur	NA	Hippocampus	Overall DNA hypermethylation of rRNA promoter in the hippocampus of suicide completers with history of abuse/childhood adversity	(McGowan et al., 2008)*

Gene	Protein	Function	Molecular function	Brain region	Findings	Reference
NTRK2	TrkB-T1 (astrocytic variant)	Receptors of neurotrophins. Role in neurotransmission, calcium release, synaptic plasticity, and cell survival. High affinity receptor of BDNF associated with mood disorders and SB	Development and the maturation of the central and the peripheral nervous system	PFC (BA 8/9)	Increased DNA methylation in two CpG sites within the promoter of TrkB-T1 accompanied by decreased mRNA expression in the PFC of suicide completers compared to controls	(Ernst et al., 2009b)
				PFC (BA 8/9)	DNA hypermethylation at four CpG sites in the TrkB-T1 3' UTR region in suicide cases compared to controls. Correlation between DNA methylation levels at these sites and TrkB-T1 expression	(Maussion et al., 2014)*
GABRA1	GABAA α1	Stabilizing or hyperpolarising the resting potential Inhibitory effect, reducing the activity of the neurons	Drug binding, GABA-A receptor activity, GABA-gated chloride ion channel activity	FPC	Increased DNA methylation detected in the *GABRA1* gene and negatively correlated with *DNMT3B* protein expression but positively with *DNMT1* mRNA in the FPC of suicide cases	(Poulter et al., 2008)
RELN	reelin, glutamic acid decarboxylase	Cell-cell interactions control, critical role in cell positioning and neuronal migration during brain development	Lipoprotein particle receptor binding, metal ion binding, protein kinase activity	Occipital cortex	DNA hypermethylation at the *RELN* promoter in SZ subjects who died by suicide compared to controls	(Grayson et al., 2005)
				Forebrain	Hypermethylation at 3 CpG sites within *RELN* promoter in SZ suicide cases compared to controls. DNA hypermethylation negatively correlated with reelin expression	(Tamura et al., 2007)

Gene	Name	Function	Activity	Tissue	Finding	Reference
SAT1	Diamine acetyltransferase 1	Enzyme in polyamine catabolism	Polyamine metabolism	PFC (BA 8/9)	DNA hypermethylation in suicide completers carrying the C allele at the rs6526342 SNP within the *SAT1* promoter region. CpG methylation at *SAT1* promoter negatively correlates with gene expression	(Fiori and Turecki, 2011)*
SMOX	spermine oxidase	Enzyme in polyamine catabolism	Role in the regulation of polyamine intracellular concentration	PFC	DNA hypermethylation in the promoter of *SMOX* in the brain of suicide subjects. No correlation with the gene expression levels	(Fiori and Turecki, 2010)[*]
BDNF	brain derived neurotrophic factor	Role in neuronal survival and plasticity, in the regulation of the stress response and in the biology of mood disorders	Growth factor activity, neurotrophin, TRKB receptor binding	Wernicke area	*BDNF* promoter IV hypermethylation in the suicide brains compared to controls. DNA hypermethylation levels correlates with significantly lower *BDNF*	(Keller et al., 2010)*[§]
				Peripheral blood	Increased *BDNF* methylation was significantly associated with SI and depression in female patients 1 year after breast surgery and this association was independent of previous depression, and *BDNF* genotype. No significant methylation–genotype interactions were found	(Kim et al., 2015a)*
				Peripheral blood	Higher *BDNF* DNA methylation levels significantly associated with previous SA, SI during antidepressant treatment, and SI at the last treatment session	(Kang et al., 2013)*[§]
				Peripheral blood	Higher DNA methylation at *BDNF* promoter is significantly associated with SI at baseline in a geriatric Korean population	(Kim et al., 2014)*[§]

ARG2	arginase 2	Suggested role in nitric oxide and polyamine metabolism	Role in the regulation of extra-urea cycle, arginine metabolism and down-regulation of nitric oxide synthesis	PFC (BA 44)	DNA methylation in the promoter region of *ARG2* showed a relationship to the respective levels of expression in suicides	(Fiori et al., 2012)*
				PFC (BA 44)	Increased expression of *ARG2* in suicide completers correlates with decreased DNA methylation levels of specific CpGs in the promoter region	(Gross et al., 2013)*
AMD1	S-adenosylmethionine decarboxylase	polyamine biosynthesis	Polyamines biosynthesis	PFC (BA 44)	Site-specific DNA methylation in the promoter region of *ADM1* was associated with *ADM1* gene expression in suicide cases compared to controls	(Fiori et al., 2012)*
				PFC (BA 44)	Increases in gene expression of *AMD1* in suicide completers correlate with decreases in methylation of specific CpGs in the promoter of this gene	(Gross et al., 2013)*
GRIK2	glutamate receptor ionotropic kainate 2	Regulation of circuit activity in neuronal cells, through G-protein coupled receptor stimulation	Ion channel, receptor activity	PFC (BA 8/9, BA10)	*GRIK2* is hypomethylated in suicide cases compared to controls. *GRIK2* showed higher levels of expression in cases	(Nagy et al., 2015b)*§
BEGAIN	brain-enriched guanylate kinase associated protein	Structural role in the postsynaptic density	Transmission across chemical synapses and protein-protein interactions at synapses	PFC (BA 8/9, BA10)	*BEGAIN* is hypomethylated in suicide cases compared to controls. *BEGAIN* showed higher levels of expression in cases relative to controls	(Nagy et al., 2015b)*§

SKA2	spindle and kinetochore associated complex subunit 2	Structural role, microtubule organization. Potential role in suppressing cortisol following stress	microtubule binding (Cell cycle, Cell division, Mitosis)	FC	DNA hypermethylation at C allele of rs7208505 predicted lower *SKA2* expression in suicide completers	(Guintivano et al., 2014)*§
				Blood and saliva	DNA methylation variation at *SKA2* gene mediates vulnerability to SB and PTSD through dysregulation of the HPA axis in response to stress	(Kaminsky et al., 2015)*§
ELOVL5	Elongation of very long chain fatty acids protein 5	Elongation of long-chain polyunsaturated fatty acids	Polyunsaturated fatty acid biosynthesis	Plasma	SA significantly associated with DNA methylation in *ELOVL5* gene regulatory regions	(Haghighi et al., 2015)*§
GAL, GALR3	amino acid neuropeptide galanin, galanin receptor 3	Mood regulation	Chemical synaptic transmission, inflammatory response, nervous system development	LC, DRN	Increased *GAL* and *GALR3* mRNA levels, in parallel with decreased DNA methylation suicide cases compared with controls	(Barde et al., 2016)*
				PFC (BA 8/9, BA 24)	*GAL* and *GALR3* transcript levels were decreased, *GALR1* was increased, and DNA methylation was increased in the DLPFC of male suicide cases compared to controls	(Barde et al., 2016)*
TNF-A	Tumor necrosis factor alfa	Cell signalling protein (cytokine)	Pro-inflammatory cytokine involved in inflammatory and immune responses, mediating neuronal death in injured brain	DLPFC	*TNF-A* promoter significantly hypomethylated in the suicide cases compared with the control group	(Wang et al., 2018a)
MARCKS	Protein Kinase C Substrate	Metabolism and Integration of energy metabolism	calmodulin binding and protein kinase C binding	DLPFC	DNA hypomethylation (cg24011531) in the *MARCKS* gene in violent suicide cases compared to controls	(Wang et al., 2018a)

Gene	Name	Function	Role	Region	Finding	Reference
PSORS1C3	Long non-coding RNA	Long non-coding RNA with a postulated role in immune system regulation	not reported	PFC (BA 11 and 25)	Significantly hypomethylated DMRs upstream of the *PSORS1C3* gene in both cortical regions in depressed suicide cases compared to controls	(Murphy et al., 2017)*§

Histone modifications

Gene	Name	Function	Role	Region	Finding	Reference
OAZ1	Ornithine antizym decarboxylase e 1	Role in cell growth and proliferation by regulating intracellular polyamine levels	intracellular polyamine biosynthesis and uptake	VLPFC (BA44)	Increased H3K4me3 levels in the promoter region of *OAZ1* in suicide completers correlated with the expression of *OAZ1* and *ARG2*	(Fiori et al., 2012)*
NTRK2	Neurotrophic Tyrosine Kinase Receptor Type 2	Receptors of neurotrophins	Role in neurotransmission, calcium release, synaptic plasticity, and cell survival	PFC (BA10)	Increased methylation at H3 Lysine 27 in suicide brains compared to controls. Significant correlation between increased H3 lysine 27 methylation and TrkB.T1 expression level	(Ernst et al., 2009a)
SYN1, SYN2 and SYN3	Neuronal phosphoproteins	Synaptogenesis, synaptic transmission and synaptic plasticity	Regulation of axonogenesis and synaptogenesis	PFC (BA10)	H3K4me3 promoter enrichment in psychiatric suicide cases relative to controls	(Cruceanu et al., 2013)*§
CX30, CX43	Connexin 30 and 43	Diffusion of ions and metabolites between the cytoplasm of adjacent cells	Gap junction channels	NEOCORTEX (BA4, BA17)	Enrichment of H3K9me3 for both *CX30* and *CX43* in the PFC of depressed suicide cases	(Nagy et al., 2017)

Abbreviations: PFC, Prefrontal cortex; FPC, frontopolar cortex; DLPFC, Dorsolateral Prefrontal cortex; LC, Locus Coeruleus; DRN, dorsal raphe nucleus; SZ, Schizophrenia *Study used age matched cases and controls and/or included age as a co-variate in their analysis. § Study used gender matched cases and controls and/or included gender as a co-variate in their analysis.

Table 1.3 Differentially expressed miRNAs associated with suicidal behaviour.

non-coding RNA	PUTATIVE / VALIDATED TARGET GENE	TARGET GENE FUNCTION (NCBI)	TISSUE	KEY FINDINGS	REFERENCES
MicroRNAs					
miR-152 miR-181a miR-330-3p miR-34a	NA	NA	PFC (BA10)	8 miRNAs were significantly altered (2 up, 6 down) in psychiatric suicide subjects	(Smalheiser et al., 2014)[¥§]
miR-34c-5p miR-320c	*SAT1*	Enzyme in polyamine catabolism	PFC (BA44)	miRNAs targeting the 3' UTR of *SAT1* upregulated in PFC of suicide cases and lower expression levels of *SAT1* gene in suicide cases vs controls	(Lopez et al., 2014)[*§]
miR-139-5p miR-320c	*SMOX*	Enzyme in polyamine catabolism (Roles in neurotransmission through the regulation of cell-surface receptor activity, involvement in intracellular signalling pathways)	PFC (BA44)	miRNAs targeting the 3' UTR of *SMOX* upregulated in PFC associated to a lower expression levels of *SMOX* gene in suicide cases	(Lopez et al., 2014)[*§]
miR-20b miR-20a miR-34a miR-34b miR-101	*BCL2* *DNMT3B* *MYCN* *VEGFA*	cellular growth and differentiation	PFC (BA9)	Globally downregulated expression pattern of miRNAs in the PFC of depressed suicide subjects compared to non-suicidal controls	(Smalheiser et al., 2012)

miRNA	Gene	Function	Tissue	Findings	Reference
miR-34b–5p miR-369–3p	NOTCH	neuronal plasticity (sequence-specific DNA binding transcriptional activator activity, RNA polymerase II transcription factor binding)	Peripheral blood	Expression levels of miR-34b–5p and miR-369–3p were significantly lower in leucocytes of Chinese MDD patients with suicide idea compared to MDD patients without suicide idea	(Sun et al., 2016)*§
miR-185 miR-491-3p	NTRK2	Receptors of neurotrophins Neurotransmission, calcium release, synaptic plasticity and cell survival	PFC (BA10)	The miRNA miR-185 found differentially expressed and inversely correlated with TrkB-T1 expression in the PFC of suicide completers	(Maussion et al., 2012)
miR-185 miR-195 miR-30a miR-49	DICER1 NTRK2	miRNA bio-synthesis (nucleic acid binding and hydrolase activity)	PFC	DICER1 expression level associated with SB in both MDD and BD samples; Polygenic profile scores negatively predicted SB in the BP sample for only 4 miRNA genes	(Pulay and Rethelyi, 2016)
miR-19a-3p	TNF-A	mediating neuronal death in injured brain	DLPFC	Specifically upregulated in individuals who died by suicide compared to normal controls	(Wang et al., 2018a)
miR-511	GFRA1	neurotrophic factor GDNF signalling	BLA	miR-511 overexpression is associated with downregulated expression levels of GFRα1a receptor in depressed suicidal individuals	(Maheu et al., 2015)

Long non-coding RNAs					
Global lncRNAs (differential lncRNA expression analysis)			ACC	Identified 23 differentially expressed lncRNAs in depressed suicide individuals	(Zhou et al., 2018)
LOC285758/ LINCO1268	MARCKS	Metabolism and Integration of energy metabolism (calmodulin binding and protein kinase C binding)	DLPFC	LOC285758 expression is significantly increased in violent suicides irrespective of MARCKS transcription levels but not the opposite	(Punzi et al., 2014)*§
			DLPFC	expression of LOC285758 was higher in the suicides by violent means group compared to both nonsuicides and suicides by nonviolent means	(Punzi et al., 2019)
TCONS_00019174 ENST00000566208 NONHSAG045500 ENST00000517573 NONHSAT034045 NONHSAT142707	NA	Protein complex biogenesis	PMBCs	Expression of 6 down-regulated lncRNAs had a negative association with suicide risk in MDD patients	(Cui et al., 2017)

Abbreviations: PFC, Prefrontal cortex; DLPFC, Dorsolateral Prefrontal cortex; LC, Locus Coeruleus; DRN, dorsal raphe nucleus; PBMCs, peripheral blood mononuclear cells; MDD, major depressive disorder; BD, bipolar disorder. *Study used age matched cases and controls and/or included age as a co-variate in their analysis. §Study used gender matched cases and controls and/or included gender as a co-variate in their analysis.

Chapter 2 – Materials and Methods

This chapter describes the generic materials and methods used throughout my thesis in multiple chapters. An in-depth description of individual sample cohorts and methods used for each analysis performed is given in the respective empirical chapters.

2.1   Human samples cohorts

Cryopreserved post-mortem tissue from the Edinburgh Brain and Tissue Banks (EBTB) and the Brains for Dementia Research (BDR) brain bank were used to study epigenomic variation associated with cell type in the healthy brain. The cohort comprised of prefrontal cortex tissue from non-psychiatric controls. The collection of brain tissue for banking by the Douglas Bell Canada Brain Bank (DBCBB) was used to profile non-coding RNAs expression in the brain of suicide completers. The cohort included brain tissue from two cortical regions (BA11 and BA25) obtained from major depressive disorder (MDD) suicide completers and non-psychiatric sudden death controls. The use of these samples for the research presented in my thesis was approved by the University of Exeter Medical School Research Ethics Committee (reference number Apr14/C/041Δ1). Additionally, raw DNA methylation data generated in house from cerebellum tissue collected from two distinct psychiatric cohorts (full details provided in **Chapter 3** of this thesis) were used to perform a genome-wide DNA methylation meta-analysis in the brains of suicide completers. Detailed information of each sample cohort specific to each study is given in the respective empirical chapters.

2.2   Investigating methods to tackle the issue of cellular heterogeneity in molecular studies of whole brain homogenates

The central nervous system (CNS) comprises complex cellular aggregates whose functional properties are dictated by the integration of multiple specialized cell types (Poulin et al., 2016). Due to the cellular heterogeneity of the brain tissue, a molecular description of each neural cell subtype is relatively difficult.

Epigenetic reprogramming is a tissue- and cell-type-specific process. Therefore examining mixed populations of cell types compromises epigenetic data and biases their interpretation (Deal and Henikoff, 2010, Reinius et al., 2012). Furthermore, brain cells are not easily accessible from living individuals while

archived human tissue is widely available and easier to obtain. To overcome these obstacles, different cell isolation protocols have been established over the years for frozen tissue samples most of which however yield low amounts of material (e.g. laser capture microdissection) or are too expensive to be applicable for large scale studies (e.g. single-cell technologies). One of the most promising methods remains flow cytometry.

In the following section I describe the basic principle and components of flow cytometry, the advantages of this approach as well as useful variation of the same application (e.g. FANS) to circumvent its intrinsic limitations.

2.2.1 Fluorescence-Activated Cell Sorting (FACS)

FACS is a specialized type of flow cytometry developed for detailed analysis of complex populations in a short period of time. It is a method for sorting heterogeneous mixture of fluorescent tagged cells one cell at a time, based on the specific fluorescent characteristics of each cell type (Maciorowski et al., 2017, Ibrahim and van den Engh, 2007). Its working depends on the light scattering features of the cells under investigation, which generally derives from dyes or monoclonal antibodies targeting either extracellular molecules located on the surface or intracellular molecules inside the cell (Adan et al., 2017). It is an efficient cell separation method that requires a single cell suspension for analysis and is performed by measuring multiple physical characteristics of a single cell such as size and granularity simultaneously as the cell flows in suspension through a measuring device (Rahmanian et al., 2017). While the fluid stream of cells/events passes through a laser beam, data corresponding to each cell/event are digitized and displayed in the form of graphs by the flow cytometer. The stream then breaks up into droplets, each containing a single cell/ event. The droplets, carrying the cells, are electronically charged and deflected, as a result of passage through an electric field, into separate collection tubes (Wilkerson, 2012). The amount of applied charge affects the degree of deflection, and hence multiple populations of cells can be separated simultaneously through applying charges of various voltages. There are different sorting modes allowing for a trade-off between sorting rate, purity, recovery, and yield depending on the aim of study.

75

The BD FACSAria III flow cytometer is a high-speed fixed-alignment benchtop cell sorter. It enables multicolour analysis of up to 18 fluorescent and two scatter options at a time (BD, FACSAria III User Guide) and contains the major components for all three subsystems: fluidics, optics, and electronics. The fluidics system is responsible for directing liquid containing particles to the focused light source. The excitation optic focuses the light source on the cells/particles while collection optics transmits the light scatter (fluorescent light of the particle) to an electronic network. The electronic network detects and converts the signals to a digital data that is proportional to light intensity; the computer is required to analyse the data (Wilkerson, 2012, Adan et al., 2017). **Figure 2.1** illustrates a schematic overview of the cell sorter used for the experiments performed in this thesis.
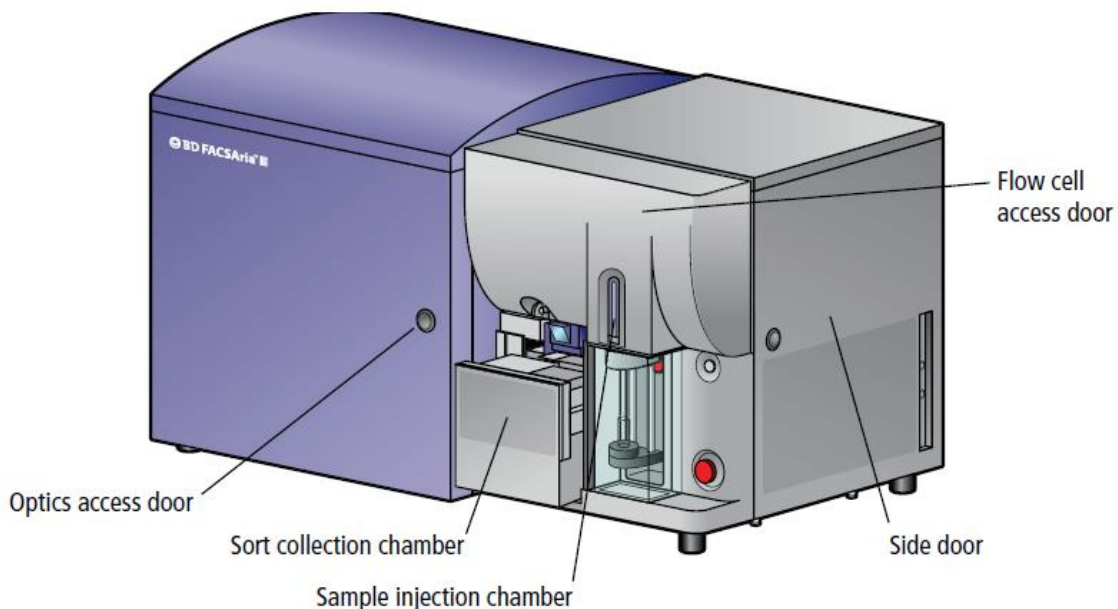
Figure 2.1 BD FACSAria III flow cytometer.
Figure showing the major components of the cytometer. Figure taken from (BD, FACSAria III User Guide).

2.2.1.1   Flow rate setting

When the fluidics system is activated, in the flow cell, pressurized sheath fluid surrounds the sample fluid to hydrodynamically focus the stream of suspended cells into the centre of the cuvette, where the particles are intercepted by the laser beam. The difference in pressure between the sheath fluid and the sample fluid

defines the diameter of the sample stream (see **Figure 2.2***)*. When the sample pressure is greater than the sheath fluid pressure, the cells align in a single file fashion through the laser beam. The injection rate of the cells into the laser beam can be manipulated by the flow cytometer based on the purpose of the analysis. The slow flow rate makes the size of the sample stream smaller while it increases the uniformity and accuracy of the illumination (Wilkerson, 2012, Adan et al., 2017). A higher flow rate is generally used for qualitative measurements such as immunophenotyping- the data is less resolved but is acquired more quickly. A lower flow rate is generally used in applications where greater resolution is critical (BD, FACSAria III User Guide). The precise definition of "low," "medium" and "high" flow rate will depend on the instrument and its configuration (Cossarizza et al., 2019). When cells are sensitive to the pressure applied pushing with higher pressure and higher flow rate may result in decreased recovery (Martin et al., 2017) therefore sorting of brain tissue is generally performed at lower flow rates ≤ 1,000 events/second (Rayaprolu et al., 2020). Another critical parameter for providing proper interception between particles and the laser beam is to ensure that fluidics system is free of air bubbles and debris and properly pressurized at all times.
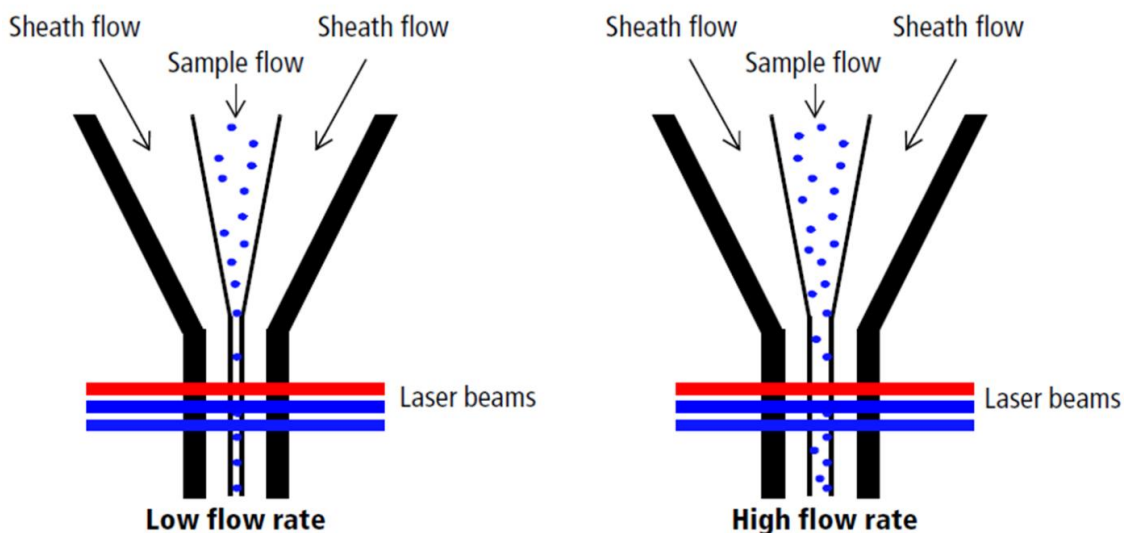
Figure 2.2 Hydrodynamic Focusing*.*
A lower difference in pressure between the sheath fluid and the sample fluid results in a relatively narrow core stream, while a higher difference results in a wider sample stream. Figure taken from (BD, FACSAria III User Guide).

2.2.1.2 Light scattering

A system of lenses are used to shape and focus the laser beam. Meanwhile, the laser produces light by energizing electrons to high energy orbitals. Light is deflected around the edges of the cell/ particle after the laser strikes it (light scattering). The factors affecting total light scatter include the membrane, nucleus, granularity of the cell, cell shape and surface topography. Two types of light scatter occur and they are named as forward scatter (FSC) and side scatters (SSC) (**Figure 2.3**). FSC is proportional to cell-surface area or size and suitable for detecting particles greater than a given size. On the other hand, SSC is proportional to cell granularity or internal complexity as important as the fluorescent light derived from fluorescent-labelled antibodies or dyes. In order to differentiate the cell types in a heterogeneous population correlated measurements of FCS and SSC are commonly used (Reggeti and Bienzle, 2011, Givan, 2011).

There is a variety of laser configurations in flow cytometers based on the type of fluorochromes being excited. The argon laser (excitation = 488 nm) is used to excite many synthetic dyes such as fluorescein isothiocyanate (FITC) resulting in the emission of light at a higher wavelength. Additional lasers used in most flow cytometers and sorters are the ultraviolet that excite UV (300–400 nm) sensitive fluorochromes or the red diode which excites fluorochromes of the far red (630 nm) range (Adan et al., 2017, Ibrahim and van den Engh, 2007, Telford, 2018).
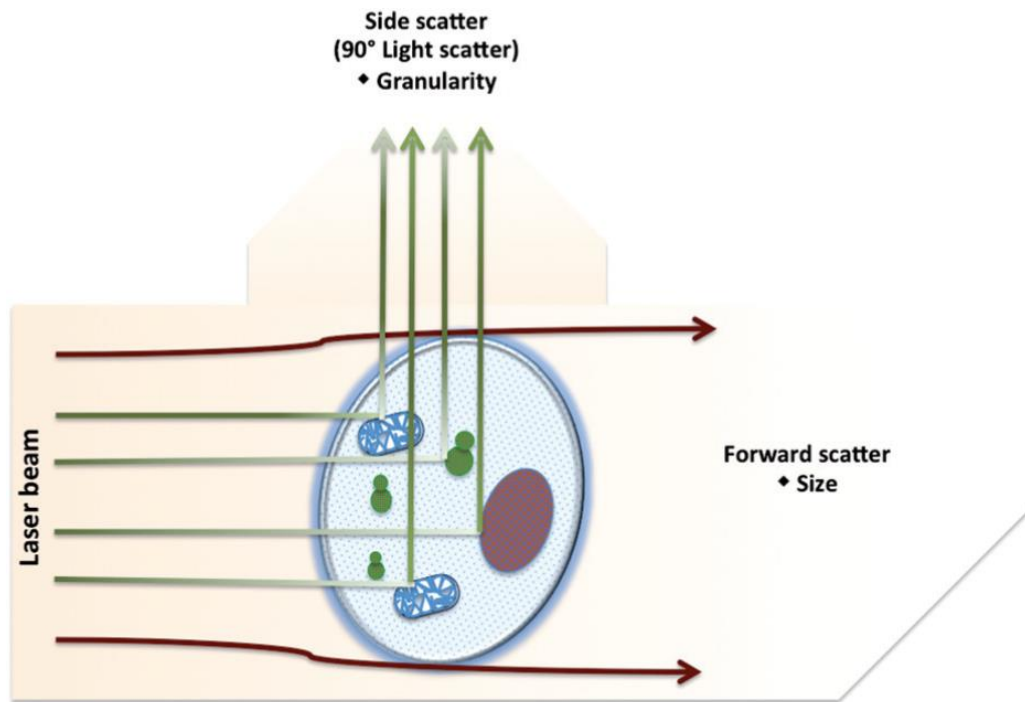
Figure 2.3 Light scattering.
FSC is proportional to size while SSC is proportional to cell granularity or internal complexity. Figure taken from (Adan et al., 2017)

2.2.1.3   *Fluorochromes - FITC, PE, APC*

Cellular and intracellular antigens are usually stained with fluorescent probes called fluorochromes that are able to show the presence of components that otherwise would not be visible. Fluorescent probes are used in a wide range of applications such as identification of different cell populations, cell surface receptors or intracellular organelles, cell sorting, immunophenotyping.

Each fluorochrome is characterized by an absorption spectrum at which a fluorescent compound can be excited and a range of emitted wavelengths (emission spectrum). The emission wavelength of any fluorochrome will always be longer than its excitation wavelength (Baumgarth and Roederer, 2000) (**Figure 2.4**). Since the colour of the exciting and emitting light is different, fluorochromes can be separated from one another by using optical filters. The total photons of light being absorbed by the fluorochrome are related to the wavelength of excitation. For example, FITC absorbs the light within the range of 400–550 nm, however, it gives maximum absorbance near 490 nm at which more photons are absorbed. Therefore, the fluorescence emission will be more intense (Shapiro, 2004).
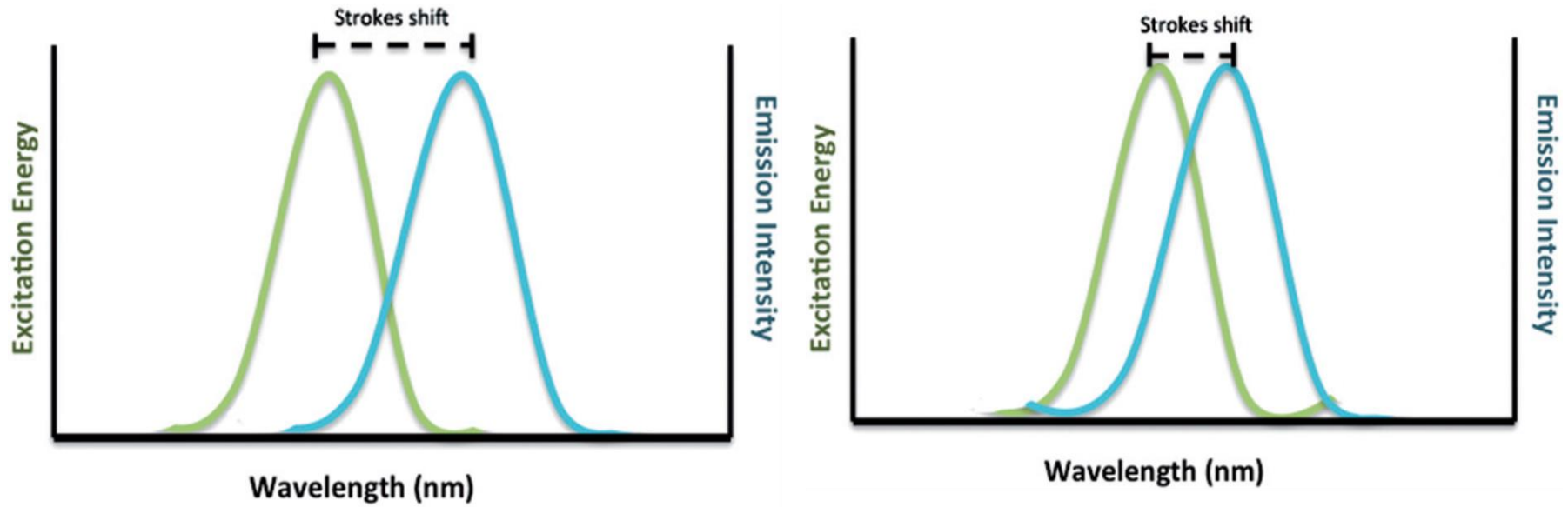
Figure 2.4 The absorption (green line) and emission (blue line) spectra of a fluorochrome.
The difference between the peak wavelengths of the absorption and emission spectra is known as the Stokes shift. The higher the Stoke's shift means the greater the separation between the exciting and the emitted light (top). Figure taken from (Adan et al., 2017).

The most widely used fluorochromes for labelling antibodies include FITC, phycoerythrin (PE) and allophycocyanin (APC) (Hawley et al., 2017). The selection of the most suitable fluorochrome is an important issue and depends on the laser to be used. FITC (excitation/emission maxima approximately 495/ 520 nm) is a good fluorochrome for single-color staining since its maximum absorbance is near 490 nm. On the other hand, its emission with longer wavelengths makes it inappropriate for multicolour applications. Moreover, its fluorescence is highly pH-sensitive and subjected to photobleaching with a high rate. For these reasons various FITC derivatives have been developed such as AlexaTM series allowing greater photostability and increased fluorescence (Adan et al., 2017). PE (excitation/emission maxima 495 565/578 nm) and APC (excitation/emission maxima 650/660 nm) are called phycobiliproteins, known components of photosynthetic systems. They have good light absorption and high fluorescence intensities. Cells labelled with phycobiliprotein antibodies have fluorescence intensities between five- and ten-fold greater than those labelled with FITC-labelled antibody. Although using an argon laser excites FITC and PE, the excitation of APC needs helium–neon laser due to its higher (650 nm) absorption maxima. The major drawback of using phycobiliproteins is related to their higher molecular weight, causing steric changes when conjugated to proteins. They can also give higher background stainings if the cells are not washed properly (Telford et al., 2015).

The development of tandem dyes, containing two fluorochromes, has increased the number of labelled proteins available for use. Examples include conjugates of PE and APC with various cyanine dyes (e.g. PE-Cy5 and APC-Cy7) (Hulspas et al., 2009a). In tandem dyes, when the first dye is excited and reaches its maximal absorbance, it transfers all its energy to the second dye located in close proximity. As a result, this second fluorochrome is activated and produces the fluorescence emission (Leavesley et al., 2013). Lastly, there are also UV-excited dyes such as Hoechst and DAPI that bind to AT-rich regions of DNA and therefore they can be used to imply where nuclei sits within the sample. Although they are membrane permeable dyes, dead cells can uptake them more easily (Telford, 2018).

Each fluorochrome has a wide emission spectrum resulting in some overlap between the fluorochromes when multiple ones are used. A good example of spectral overlap is given by FITC and PE. Their emission spectra are overlapped so that some of the light emitted by fluorescein will be pass through the filter used for PE. This spectral overlap is corrected by subtracting a fraction of the FITC signal from the PE signal or vice versa. This process is named as colour compensation, that also calculates how much interference (as a percent) a fluorochrome will have in a channel that was not assigned specifically to measure it (Roederer, 2001). In order to determine how much compensation should be applied to the dataset, some control readings must be performed first. Each of the two fluorochromes, should be read on itself and then the percent of its detectable total emission in the channel specific for the second fluorochrome should be determined (Tung et al., 2004).

2.2.1.4   Sorting

Electrostatic cell sorting is responsible for capturing and separation of the cells/nuclei with predefined features. The general principle of flow cell sorters is based on the electrostatic deflection of charged droplets, some of which contain cells/nuclei. In this method, the cells/nuclei are injected through a nozzle to form a stream of regular droplets by applying a vibration to the nozzle. Then, these droplets pass through one or more laser beams and are charged by a charging electrode at the same time. Droplets can be deflected from the mainstream based on their given charges. Positively charged droplets are deflected toward the negatively charged plate, negatively charged droplets are deflected toward the positively charged plate while uncharged droplets are collected into a waste container (**Figure 2.5**) (Maciorowski et al., 2017, Ibrahim and van den Engh, 2007).
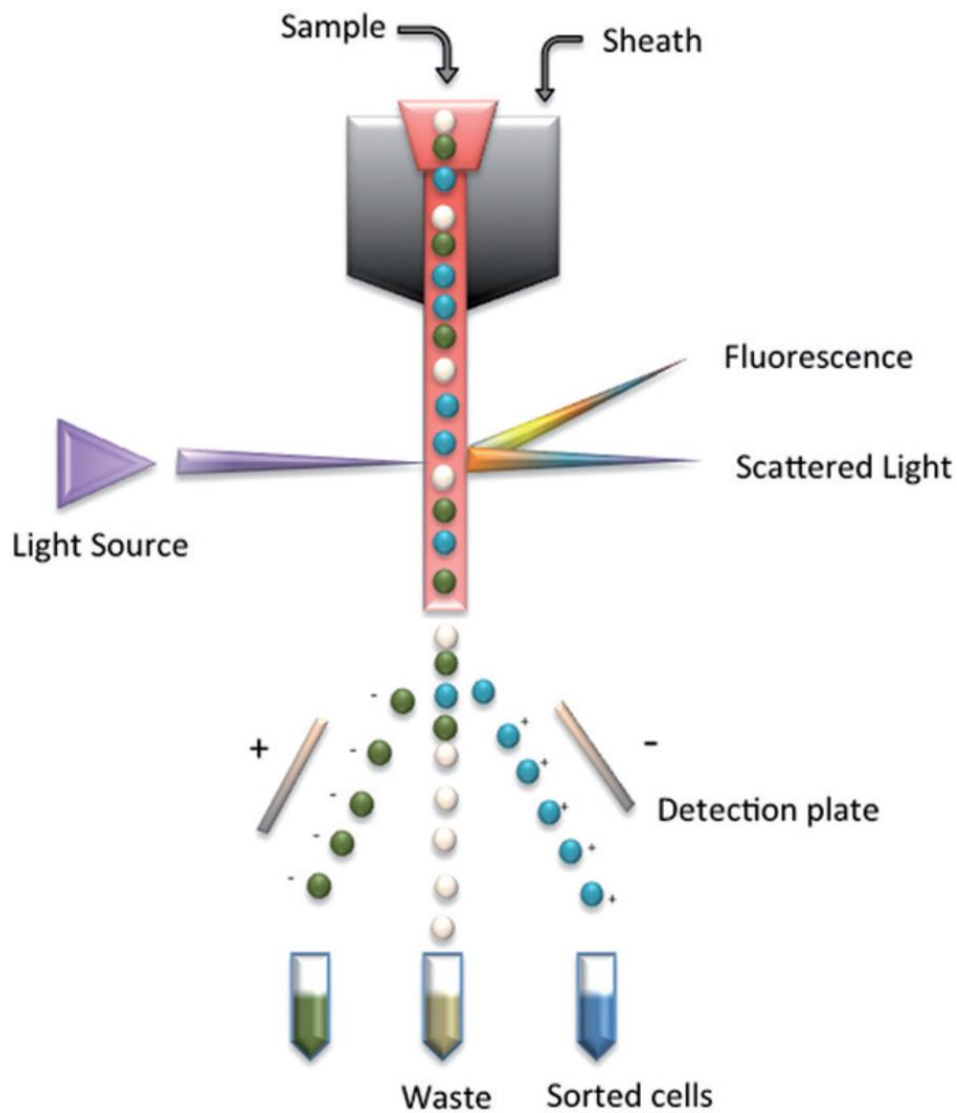
Figure 2.5 Schematic representation of sorting cells by droplet deflection.
Figure taken from (Adan et al., 2017).

2.2.1.5   Data analysis

Flow cytometry data analysis is the most critical parameter for biological experiments and aims to selectively show the cells of interest and to find out more about them. This method is called "gating" in flow cytometry. A set of points carefully selected by the user determine an area on a graph also called region. Several regions can be defined on the same graph. These parameters allow to exclude unwanted results from sample components or particles (e.g. dead cells and debris). Additionally, a gate is a numerical or graphical boundary that can be used to define the characteristics of particles for further analysis or to define a subset of data to which restrict your analysis.

The different physical characteristics of cell types within a certain heterogeneous tissue sample (e.g. blood, brain) allow them to be distinguished from each other. A subset of data can be defined by gating methods. FSC and SSC plots are commonly used as reference for gating strategy and initial discrimination of detected events. Based on FSC or cell size, a gate can be set on the FSC versus SSC plot for the analysis of a specific cell type or sample component. The resulting display would reflect the fluorescence properties of only that cellular population (Adan et al., 2017).

One method of data display are two parameter plots. These graphs display two measurement parameters, one on the x-axis and one on the y-axis and the cell count as a density (dot) plot or contour map. A dot plot provides a two-parameter display of data and each dot represents one or more events (particles) while density plot displays two parameters as a frequency distribution. The colour is used to code the different frequencies of events in density plot. In the contour plot the density of the cells is displayed as contour lines. A quadrant marker divides two-parameter plots into four sections to discriminate populations as negative, single positive or double positive. The upper-right quadrant of the plot indicates cells positive for both fluorescent marker (double positive). The lower-left quadrant displays events that are negative for both markers (double negative). The upper-left quadrant of the plot indicates cells only positive for the y-axis parameter. The lower-right quadrant contains events that are positive for the x-axis marker but negative for the y-axis fluorescent marker. **Figure 2.6** shows a representative example of data display using two parameter plots.
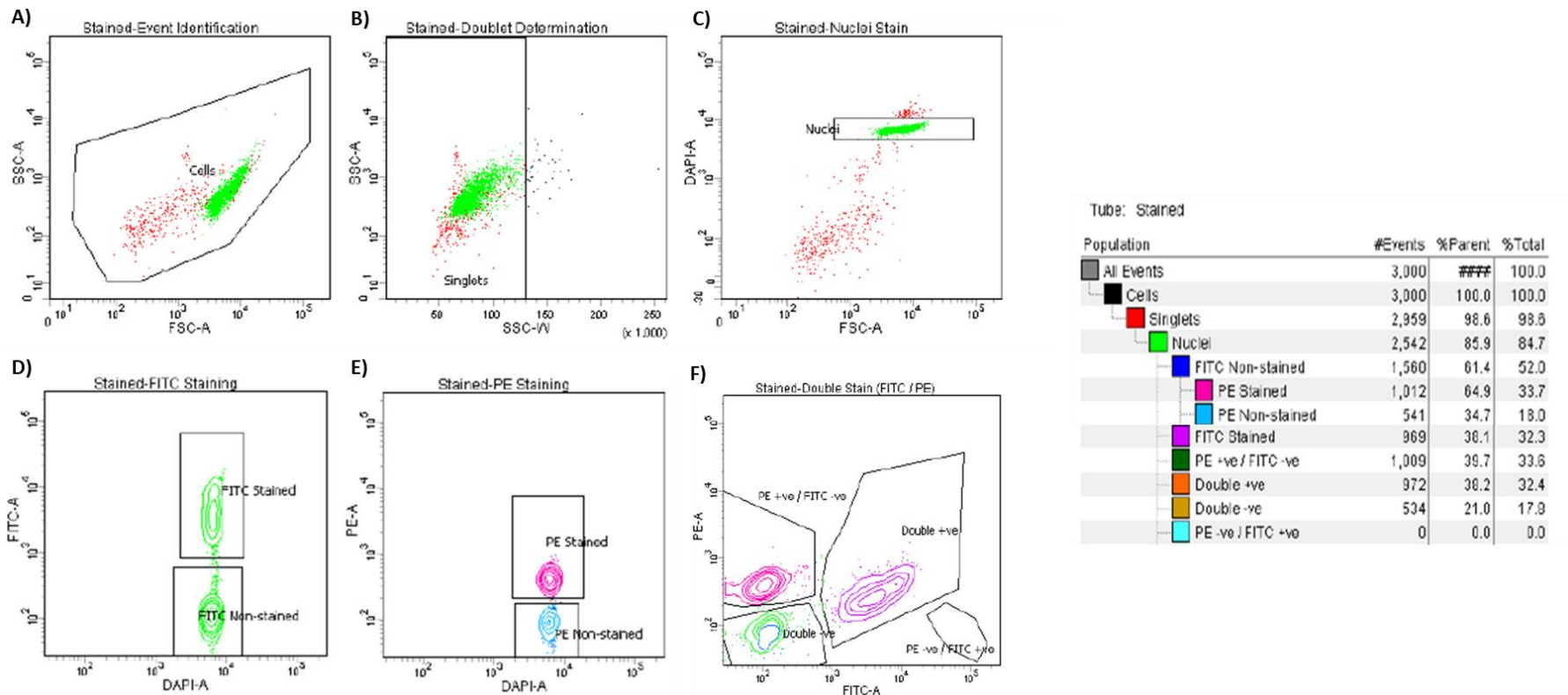
Figure 2.6. Example of data display using two parameter density plots.
Isolated human brain derived nuclei were labelled with two pre-conjugated antibodies (FITC- and PE-conjugated respectively) targeting two different antigens expressed by cell populations in a mutual exclusive manner. The immuno-labelled populations were analysed by flow cytometry. Events were gated on nuclei (green) (A-C). In the multichannel plot (F) the X-axis represents FITC-positive and the Y-axis represents PE-positive cells. Upper right quadrant shows FITC- and PE -double positive cells (cells expressing both antigens and therefore fluorescing in both channels). (D-E) The same data are displayed on single parameter density plots where the upper quadrant represents the cells positively stained for a given marker (FITC in D, PE in E) while the lower quadrant captures those cells which did not stain and therefore do not show an increase in the fluorescence signal intensity.

2.2.1.6 *Applications of flow cytometry*

Flow cytometry is a widespread technique used to identify, analyse, and separate complex mixtures of cells in suspension. This method is not suited for analysis of anatomical distribution, since the tissue is homogenized to generate a single-cell suspension. However, it allows to work with viable cells and it can be combined with cell-sorting for physical isolation of cells, opening the way for several downstream applications, ranging from establishment of primary cultures derived from pure cell populations, to gene-expression analyses and biochemical or functional assays on well-defined cell subtypes (Molina Estevez et al., 2019, Baumgarth and Roederer, 2000, Sykora and Reschke, 2019, Legroux et al., 2015). FACS takes advantage of the high throughput and multiplexing capabilities of flow cytometry to allow phenotypic characterization and quantification of different cell subtypes isolated from complex tissue based on expression of surface or intracellular antigens, but also functional measurements (e.g., rate of apoptosis, proliferation, cell cycle analysis, etc). Since specific antigens can be expressed on more than one cell type, immunophenotyping may require staining of a single cell type simultaneously with two or more antibodies. In general, the location of the antigen is what dictate the protocol and buffer system that will be used to get optimal staining of the protein of interest. FACS is especially useful when highly pure cells are desired (≥99% purity) and/or when the target cells are rare; in particular, this method has markedly improved the efficiency of isolation of rare cells (Johnson et al., 2007, Choudhery et al., 2013). FACS is also the preferable choice when dealing with a marker that exists at very low levels in the target cell or when two or more populations need to be purified based on the differential expression level of the same marker (Johnson et al., 2007, Basu et al., 2010).

Brain tissue is comprised of exceedingly diverse cell populations, and flow cytometry methods have the potential to facilitate the study of individual cell types found throughout the brain matrix. FACS of brain tissue was first used to segregate a small population of rat neurons based on intracellular markers three decades ago (Paden et al., 1986). Since that report, however, flow cytometry in neuroscience has been largely unexploited likely due to difficulties in achieving single cell suspensions from brain tissue. In recent years, a number of reports have been published that demonstrate the power of flow cytometry applied to

brain tissue for analysing a variety of neuronal and non-neuronal brain cell populations (Lobo et al., 2006, Finegersh and Homanics, 2016, Saxena et al., 2012, Krishnaswami et al., 2016).

2.2.2 Fluorescence activated nuclei sorting (FANS)

Although existing FACS methods for brain tissue are useful, they each differ in application and have certain limitations (Martin et al., 2017). They require cells genetically labelled with a fluorescent protein to achieve separation of specific populations (Lobo et al., 2006, Finegersh and Homanics, 2016, Saxena et al., 2012), they are not applicable to previously fixed tissue (Krishnaswami et al., 2016), or are not compatible with downstream mRNA analysis (Martin et al., 2017). While acknowledging some exceptions where cell-sorting has been used to recover specific neuronal or glial populations from brain tissue (Lobo et al., 2006, Guez-Barber et al., 2012) this approach remain limited by the difficulty and time required to dissociate adult brain, as well as cells rarely arriving intact to the end of the procedure with the risk of biochemical reactions altering observed responses. A more promising approach is the direct purification of nuclei (Marion-Poll et al., 2014).

In the last decade several reports have clearly demonstrated robust differences in DNA methylation and histone modification patterns between neuronal and non-neuronal cell populations in human and rodent brains (Guintivano et al., 2013, Kozlenkov et al., 2014, Kozlenkov et al., 2017, Tulloch et al., 2018).These cell type-specific epigenetic landscapes might ultimately determine the selective vulnerability to neurodevelopmental or environmental insults that could culminate in psychiatric or neurological conditions. Glial cells have generally been overshadowed by research on neurons in many brain related phenotypes, also due to the lack of isolating methods and markers. However, a growing body of evidence highlights the importance of glia in brain development, function and disease processes (Aguzzi et al., 2013, Ahmed et al., 2017, Laskaris et al., 2016). Thus, in order to characterize cell type-specific epigenetic signatures in the non-neuronal component of the brain I have implemented the existing NeuN-based FANS protocol to separate oligodendrocyte from other glial cells (predominantly

microglia and astrocytes).The need of working with nuclei samples is dictated by the difficulty in preserving cell structure when dissociating cryopreserved post-mortem brain samples into a single-cell suspension. Evidences have shown that the nuclei component is more robust and remains intact even after harsh procedures (Siegmund et al., 2007, Kozlenkov et al., 2017, Kozlenkov et al., 2014, Marion-Poll et al., 2014). **Figure 2.7** shows an overview of the optimised pipeline while **Appendix C** contains the latest version of the protocol which is published online.

Briefly, for each specimen, frozen dissected PFC tissue was ground in ice-cold lysis buffer (0.1% Triton, 0.32 M sucrose, 5 mM CaCl2, 3mM Mg(Ace)2, 10 mM Tris-HCl, 0.1 mM EDTA, 1mM DTT). The tissue homogenate was transferred in 12 mL capacity ultracentrifuge tubes (≤1mL homogenate per tube), prefilled with 8 mL of Sucrose Solution (1.8 M sucrose, 3mM Mg(Ace)2, 1mM DTT, 10mM Tris-HCl) and overlaid with 1mL more of lysis buffer. Samples were centrifuged for 45 minutes at 108,670 x g. The supernatant was removed and pellets were resuspended in staining buffer (5% BSA, 10x PBS, ddH20) and incubated for 15 minutes on ice (Blocking step to prevent unspecific staining). Pellets were centrifuged for 5 minutes at 0.8 x g (washing step), resuspended in ice-cold staining buffer and incubated simultaneously with the DNA dye Hoechst 33342 (Abcam, Cambridge, UK)(1:500), Alexa488-conjugated anti-NeuN antibody (EMD Millipore, Billerica, MA, USA) (1:1000 dilution) and NorthernLights™NL577-conjugated anti-Sox10 antibody (R&D systems, Minneapolis, USA) (1:10) for 1.5 hours at 4ºC in the dark. All tubes were then centrifuged for 5 minutes at 0.8 x g (washing step), resuspended in ice-cold staining buffer and kept on ice while waiting to be processed. The samples were subjected to the FANS procedure using BD FACSAria III (BD Biosciences, US) (refer to **Chapter 4** for details of method development). Finally, the sorted nuclear fractions were snap frozen and stored at −80◦C until DNA/RNA isolation. This protocol allows to routinely obtain well-separated NeuN+ve/Sox10+ve (neuronal enriched), NeuN−ve/Sox10+ve (oligodendrocytes enriched) and NeuN-ve/Sox10−ve nuclear fractions. Based upon the current understanding of cellular composition of the human brain (von Bartheld et al., 2016, von Bartheld, 2018). The double negative (NeuN-ve/Sox10−ve) fraction is assumed to be a mixed population consisting of astrocytes and microglia as well as endothelial cells. It is

now thought that endothelial cells in the whole human brain make up about 25% of all non-neuronal cells, with the rest (75%) of non-neuronal cells being glial cells, thus generating a ratio of about 5:3:1 for neurons, glia and endothelial cells in the human brain (Bahney and von Bartheld, 2018). To prevent the inclusion of false positives, aggregates, nuclei of dividing cells, and debris were excluded from sorting by performing event identification (FSC-A vs SSC-A plot) and doublet discrimination (SSC-W vs SSC-A plot). Confirmation of the cell-type specificity for the obtained neuronal and non-neuronal nuclei preparations was achieved by quantifying the enrichment for well-established neuronal or glial-specific transcripts in RNA samples extracted from the sorted neuronal, oligodendrocyte and other glial populations respectively (see **Chapter 4** section 4.3.6 and 4.4.3).
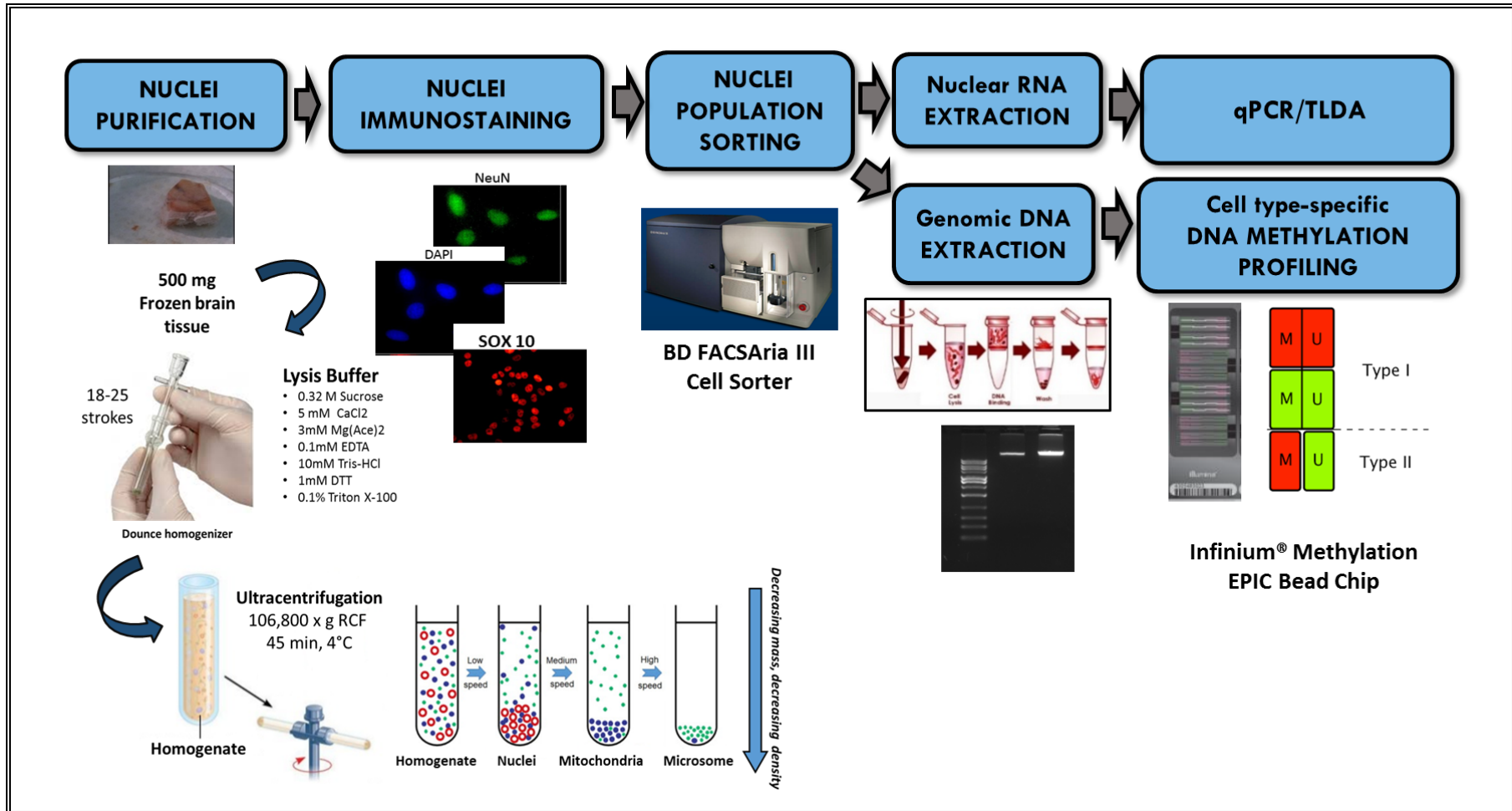
Figure 2.7 Fluorescence-activated nuclei sorting (FANS) protocol workflow.
Shown is a schematic overview of the main steps involved in the implemented FANS protocol.

2.3 Immunocytochemistry on human derived cell lines

Human neuroblastoma SH-SY5Y and immortalized Human Microglia - SV40 cell lines were used to assess the specificity of staining for the nuclear antibodies adopted in the FANS protocol (refer to section 2.2 for details). Cells were seeded and cultured on glass coverslips by keeping them in 12-well plate. Refer to **Appendix D** for details about reagents used and solution's recipes (solutions final concentrations provided).

2.3.1 Fixing cells

Performed prior to immunostaining, this step aims to preserve the cells in their current state as well as helping with the subsequent permeabilisation step. Without fixation, the intracellular structures would fall apart and diffuse away during the staining stage.

Fixation was performed at a confluence suitable to perform immunofluorescence staining (30,000 cells per coverslip). The cell coated coverslips were treated with paraformaldehyde to form cross-linkers and fix the cells in their current state. All the fixation steps were performed in the fume hood.

1. 4% PFA solution (5mL 40% PFA, with 45mL1x PBS) was freshly prepared

2. Media was aspirated from cells with a pipette

3. Cells were washed twice with 500 µL of 1x PBS

4. 500 µL of 4% PFA were added per well and cells were incubated at room temperature (RT) for 20 minutes

5. PFA solution was removed using a pipette and disposed in the waste bottle

6. Cells were washed 3 times with 500 µL of 1x PBS

At this stage cells can be stored in 500 µL of 1x PBS at 4°C for 1 week if unable to continue

2.3.2 Permeabilising

Permeabilising buffer (PB) was made fresh each time. See **Appendix D** for recipe.

1. Sufficient volume of PB was prepared according to the number of coverslips to be treated (0.2% Triton-X in 1x PBS/ well).

2. The buffer in which coverslips were left (1x PBS) was aspirated off

3. 500 µL of 0.2% Triton-X PBS was added in each well

Care was taken when adding the PB to each well. The volume was released to the side of the well, not directly on top of the coverslips to prevent washing away fixed cells.

4. Cells were incubated at RT for 20 minutes
5. Supernatant was aspirated from each well and cells were washed with 1x PBS three times (500µL, 30s each)

2.3.3 Blocking

Blocking buffer (BB) was made fresh each time. See **Appendix D** for recipe.

1. 500µL of BB (1% BSA 0.1% Tween-20 PBS solution) was added to each well
2. Cells were incubated for 1 hour at RT
3. Supernatant was aspirated. No washes required after blocking step

2.3.4   Immunostaining

1. Primary antibody was added at the required dilution (see **Chapter 4** for details and **Appendix D** for recipe) to the appropriate wells

2. Cells were incubated overnight (or 2 hours incubation) in the dark at 4˚C. NOTE- More than one incubation time has been adopted for testing purposes.

3. Cells were washed 3 times with 1x PBS (500µL per well, 10 minutes each). No further step are required when the antibody used is pre-conjugated.

4. 500 µL of secondary antibody (1:400 dilution) was added into each well

5. Cells were incubated for 1 hour at RT

6. Secondary antibody was aspirated off

7. Cells were washed 3 times with 1x PBS (500µL per well, 5 minutes each).

8. DAPI staining was diluted 1:5000 (2 mL DAPI + 8 mL 1x PBS if 1:1000 stock) and kept in the dark for the entire usage

9. 300 µL of DAPI staining were added in each well and incubated for 5 minutes

10. Supernatant was removed from each well and disposed in a separated waste bottle for safety purposes (because of its intercalating nature, DAPI dye is disposed of with dangerous substances).

11. Cells were washed 3 times with 1x PBS (500µL per well, 5 minutes each).

2.3.5 Mounting

1. Microscope glass slides were cleaned with 70% ethanol prior usage

2. Slides were appropriately labeled with relevant details about the mounted coverslips

3. A small drop (8-10 µL) of Fluorsave mounting media (Dako Omnis, Cat No: GM30411-2) was added in the middle of each slide. Care was taken not to shake or invert bottle of mounting medium to prevent bubbles from forming. The media was then allowed to spread gradually to the edges of the coverslip.

4. With the help of tweezers, coverslips were removed from the buffer and the excess solvent was blotted from the upper surface of the coverslip

4. Coverslips were carefully mounted onto the microscope slide with the cells facing towards the mounting media avoiding to create bubbles when lowering them into place.

5. Slides were stored in the dark to allow the media to dry completely before imaging.

6. Once dry, the surface of the coverslip was gently wiped with a tiny bit of ethanol on a lint free cloth to remove any PBS crystallization

7. The edges of each coverslip were sealed with clear nail varnish (optional, can be stored without sealing).

2.4 Genomic DNA isolation from sorted nuclei using phenol-chloroform

This section describes the isolation of genomic DNA from sorted nuclei suspensions derived from post-mortem human brain tissue. **Figure 2.8** shows an overview of the experimental procedure. Not all aliquots of nuclei collected were extracted as one-two tubes (200,000 nuclei/tube) per each nuclei population yielded the amount of genomic DNA ideally required to run the EPIC Array (300-500ng DNA in 20uL).
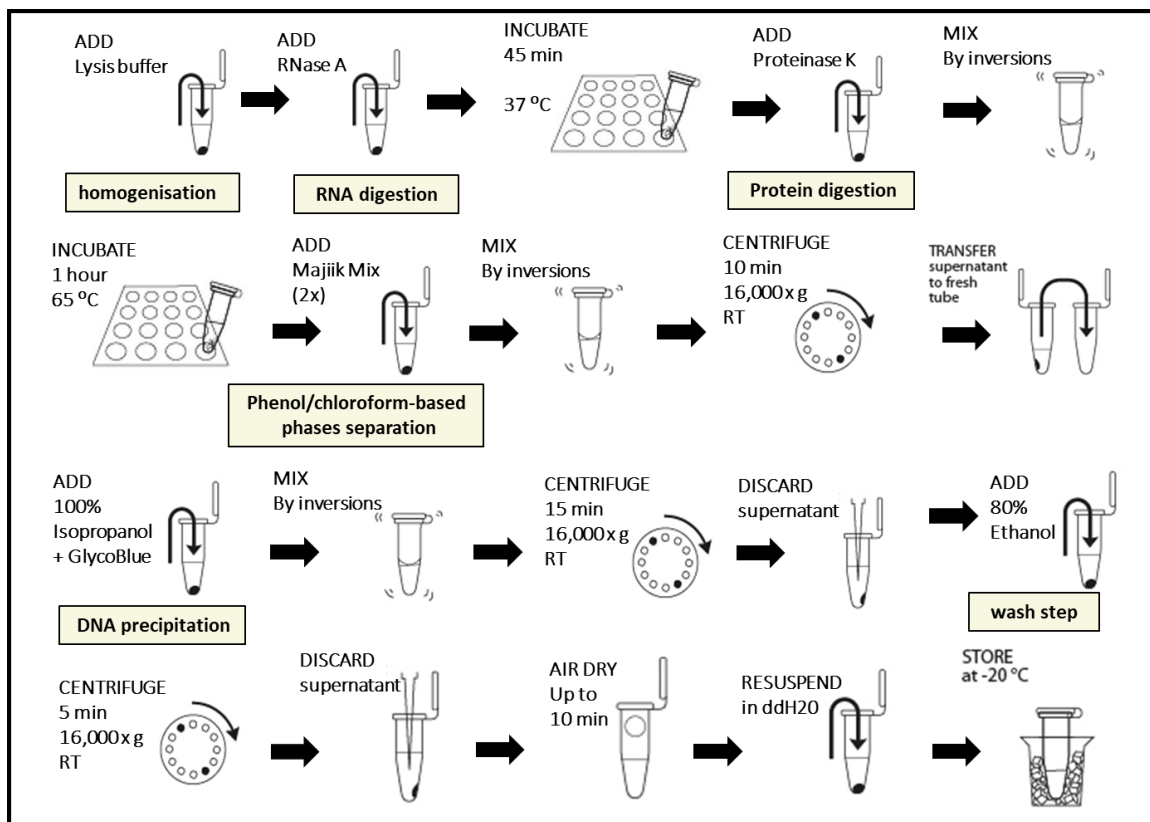
Figure 2.8 Schematic overview of the genomic DNA extraction experimental procedure.

Nuclei samples were defrosted on ice. 500uL of Slagboom buffer (SB) (5mL 10x STE buffer, 5mL 5% SDS, 40mL RNase-free DNase-free water) were added to each tube according to the number of nuclei collected by the FACS. Where nuclei were collected and stored in running buffer, the volume of 10x STE and 5% SDS to add to each sample was adjusted accordingly to keep the final concentration consistent. 1µl of DNase free RNase-A (10mg/ml) (Sigma Aldrich, UK) per 500ul SB was added and samples were incubated at 37ºC for 45 minutes (heat block). 5µl of proteinase K (20mg/ml) (Thermo Fisher Scientific, Waltham, MA, USA) was

added and samples were inverted at least 10 times. The samples were then transferred to a water bath at 65°C for 1 hour to deactivate the proteinase K, and then cooled to room temperature (RT) for 5 minutes. The samples were mixed by inverting the tubes ~10 times and centrifuged at 16,000 x g for 10 minutes. For each 500ul of SB initially used per sample 100 uL of "majiik mix" (a proprietary reagent made from 1:1 ratio yeast Reagent 3 (Autogen Bioclear, Wiltshire, UK) and 100% ethanol) was added (e.g. 200ul for 1 mL of SB). Majiik mix works as a substitute of the traditional phenol-chloroform mixture. The samples were mixed by vigorous inversions and centrifuged at 16,000 x g for 10 minutes at RT. For each sample the supernatant was carefully recovered and transferred to a new labelled tube (50ul was left at the bottom of each tube). Another 100ul of Majiik Mix were added to each tube and samples were first mixed by inverting ~10 times and then centrifuged at 16,000 x g for 10 minutes at RT. The supernatant of each sample was carefully recovered (making sure to leave 50ul at the bottom of the tube to prevent precipitates to be carried over) and transferred to a new appropriately labelled tube. Where exceeding 1mL total volume, supernatant was equally distributed into two new tubes.

An equal volume of 100% Isopropanol (Sigma Aldrich, UK) was added to each sample (e.g. 1mL supernatant + 1mL 100% Isopropanol) and slowly mixed by inversion to precipitate the DNA. At this stage, 0.5-0.8 ul GlycoBlue™ Co-precipitant (Invitrogen Ltd, Inchinnan, UK) was added to each sample. When a typical acetate/alcohol precipitation is done, the GlycoBlue™ Coprecipitant will precipitate with the nucleic acids, facilitating good DNA recovery while increasing the size and visibility of the pellet. Samples were then mixed by inverting the tubes ~10 times and centrifuged at 16,000 x g for 15 minutes at RT. For each tube the supernatant was carefully removed (care must be taken since the DNA pellet only weakly adheres to the side of the tube) and discarded.

500µl of 80% ethanol were added to each tube, samples were then mixed gently and centrifuged at 16,000 x g for 5 minutes. The supernatant was carefully removed and the pellets were left to air dry for 20 minutes or until dry. Each DNA pellet was resuspended in 15 µl of RNAse, DNase free water and left at 4ºC overnight to fully dissolve before quantification.

In order to determine the quality and quantity of the isolated gDNA samples:

1. A visual check was performed to make sure the DNA was well re-suspended before undertaking any downstream applications.

2. 1μL of the DNA sample was also loaded onto a Spectrometer (NanoDrop 2000) (Thermo Fisher, US) to determine the concentration and further check the quality of the DNA by assessing 260/280 and 230/280 ratios (above 1.8 and ~2 respectively for pure DNA).

3. A 0.9 % agarose gel was run for each sample to check for high molecular weight, not degraded DNA (see section 2.4.1 for details).

2.4.1   Agarose gel electrophoresis

The visualisation of DNA via gel electrophoresis was needed at various quality control stages in each empirical chapter: for checking the efficiency of BS conversion in empirical **Chapter 3 and 5** while in **Chapter 4** and **5** for checking the quality of the DNA extracted from FACS -sorted brain derived nuclei as described in Section 2.4.

Agarose gel electrophoresis enables the separation of DNA molecules based on their size. It is a three-dimensional matrix containing pores through which molecules can pass. The concentration of agarose influences the size of the pores in the matrix; therefore the concentration of agarose selected is dependent on the size of molecule to be separated. The gel is obtained by melting agarose powder (Sigma Aldrich, UK, Cat No. A9539) at a concentration ranging from 0.8 to 2%, in 1% tris-borate EDTA (TBE) buffer (Fisher Scientific, UK, Cat No 10031223). A small amount (10uL per 100 mL gel) of the Syto60 red Fluorescent (Fisher Scientific, UK, Cat No. 10194852) or ethidium bromide (Sigma Aldrich, UK) (0.5uL per 100ml gel) was added ubiquitously to the gel before cooling to allow DNA fragments to be observed after separation. The fluorescent Syto60/ ethidium bromide both intercalate into the DNA structure allowing it to be visualised after laser exposure. For example, the UV light is absorbed by the ethidium bromide and re-emitted as visible light (ethidium bromide, Excitation∕ Emission: 470/590 nm).

Once cooled, DNA samples were added to the gel matrix, an electrical charge was applied across it, causing the negatively charged DNA to migrate towards the positive anode, at a speed determined by the DNA fragment size. Smaller molecules move through the matrix faster, and therefore move further through the gel in the allocated time. In this thesis, 1.2% agarose gel was used for the

inspection of DNA extraction quality together with 1kb DNA Ladder (Thirteen Blunt-Ended Fragments of 250–10,000bp remixed with loading buffer) a convenient marker for determining the size of double-stranded DNA from 250 to 10,000 base pairs. On ethidium bromide-stained agarose gels, the 1,000 and 3,000 bp fragments have increased intensity relative to the other bands and serve as reference indicators. All fragments are blunt-ended. **Figure 2.9** shows an example of agarose gel used to inspect quality and integrity of four nuclei-derived gDNA samples.
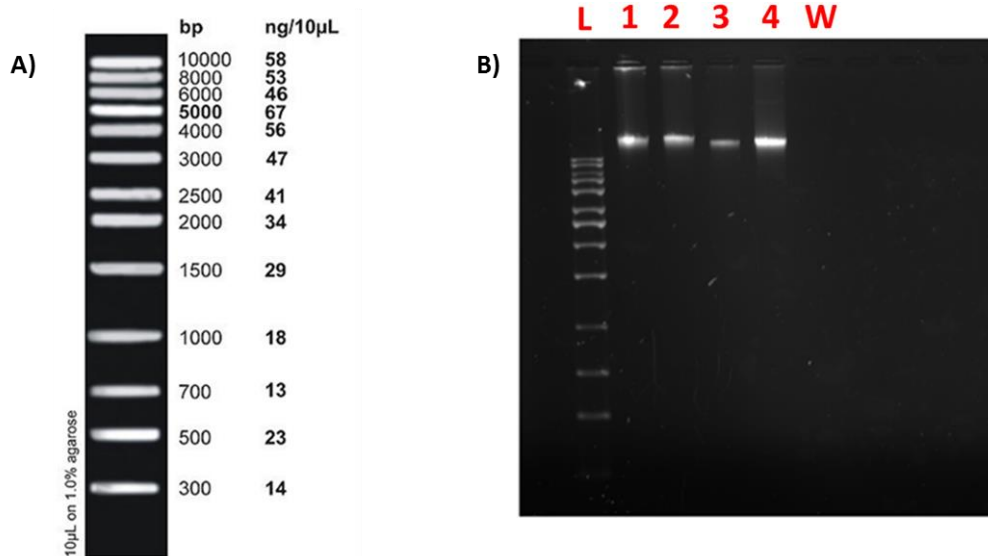
Figure 2.9 Example of an agarose gel used to inspect genomic DNA integrity*. A) Genomic DNA 1Kb ladder; containing 13 linear double-stranded DNA fragments it is commonly used as reference in DNA electrophoresis for size determination of double-stranded DNA from 250 bp to 10,000 bp. **B)** gel run example of four gDNA samples derived from four different nuclei fractions (1, NeuN+ve/Sox10+ve; 2, NeuN-ve/Sox10+ve; 3, NeuN-ve/Sox10-ve; 4, Total nuclei) purified from the same bulk brain sample. L, 1Kb ladder, W, water (negative control).*

2.5 RNA extraction from FACS-sorted nuclei

In order to extract nuclear RNA from the nuclei aliquots collected through FACS sorting, I used the Direct-zol RNA MicroPrep Kit (Zymo Research, Irvine, CA) which provides a streamlined method for the purification of high-quality RNA. No phase separation, precipitation, or post-purification steps are necessary (Zymo Research, Direct-zol™ RNA Microprep User Guide). The eluted RNA is suitable for subsequent molecular manipulation and analysis (including RT-PCR, transcription profiling) (See **Figure 2.10**).
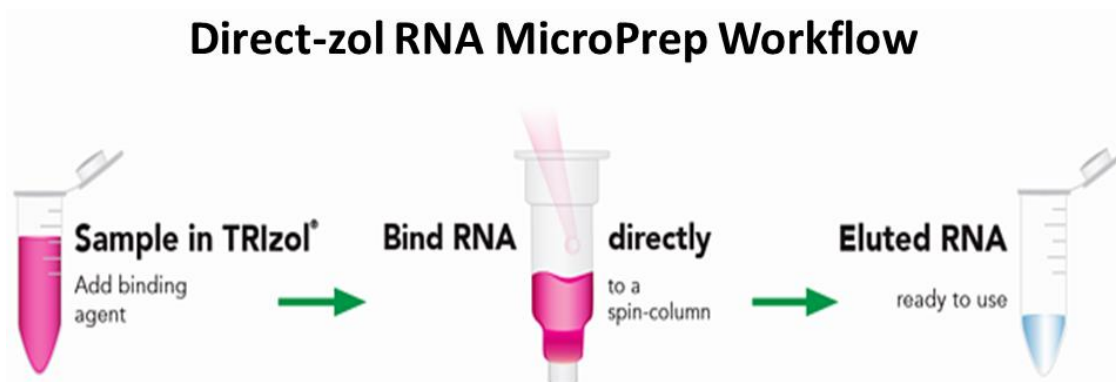
Figure 2.10 Direct-zol RNA MicroPrep Kit Workflow.
Streamlined method for the purification of high-quality RNA directly from samples in TRI Reagent® or similar. Total RNA, including small RNAs (17-200 nt), is effectively isolated from FACS-sorted brain derived nuclei. Figure taken from (Zymo Research, Direct-zol™ RNA Microprep User Guide).

The following guidelines are provided for processing various sample types stored and preserved in TRI Reagent®, TRIzol® or similar acid-guanidinium-phenol reagents. TRIzol Reagents inhibit RNase activity and inactivate viruses and other infectious agents, for these reasons it has been adopted as collecting buffer for our purified nuclei rather than a pH neutral salty solution (e.g. 1x PBS). RNA yield can vary with sample types, organism, quality and treatment of the starting material. Complete lysis and homogenization of the samples is also crucial to ensure to the best recovery.

This protocol consists of three parts: (I) Buffer Preparation (II) Sample Preparation and (III) RNA Purification.

2.5.1 Buffer Preparation

- Add 40 ml ethanol (100%) (Sigma Aldrich, UK) to the 160 ml Direct-zol™ RNA PreWash concentrate.
- Add 48 ml 100% ethanol to the 12 ml RNA Wash Buffer concentrate

2.5.2 RNA Purification

Perform all steps at RT and centrifugation at 14,000 x g for 30 seconds.

1. Add an equal volume of ethanol (100%) to a sample lysed in TRI Reagent® (Thermo Fisher Scientific, UK) or similar (TRIzol®, RNAzol® , QIAzol®,TriPure™ and all other acid-guanidinium-phenol reagents) and mix thoroughly.

2. Transfer the mixture into a Zymo-Spin™ IC Column in a collection tube and centrifuge. Transfer the column into a new collection tube and discard the flow-through.

NOTE-To process samples >700 uL, reload the column and repeat Step 2.

DNase I treatment (in-column).

Prior to use, reconstitute the lyophilized DNase I as indicated on the vial. Store frozen aliquots.

(D1) Add 400 µl RNA Wash Buffer to the column and centrifuge.

(D2) In an RNase-free tube, add 5 µl DNase I (6 U/µl), 35 µl DNA Digestion Buffer and mix by gentle inversion. Add the mix directly to the column matrix.

(D3) Incubate at room temperature (20-30°C) for 15 minutes. Proceed to step 3.

3. Add 400 µl Direct-zol™ RNA PreWash to the column and centrifuge. Discard the flow-through and repeat this step.

4. Add 700 µl RNA Wash Buffer to the column and centrifuge for 2 minutes to ensure complete removal of the wash buffer. Transfer the column carefully into an RNase-free tube.

5. To elute RNA, add 15 µl of DNase/RNase-Free Water directly to the column matrix and centrifuge. Alternatively, for highly concentrated RNA use ≥6µL elution. RNA samples can be used immediately or stored frozen at ≤-80°C.

2.6 cDNA synthesis from sorted nuclei derived nuclear RNA

Nuclear RNA from post-mortem brain tissue was reverse transcribed into complementary DNA (cDNA) using the Thermo Scientific Maxima Reverse Transcriptase (200U/1uL) (Thermo Scientific, UK). The enzyme possesses an RNA and DNA-dependent polymerase activity as well as RNase H activity (enhancing the melting of RNA-DNA duplex during the first cycles of PCR) which make it ideal for first strand cDNA synthesis for RT-PCR and RT-qPCR applications. The protocol was carried following manufacturer's instructions with some amendments in terms of reagents used and thermocycler settings. Pentadecamers (5'-NNN NNN NNN NNN NNN-3') (Integrated DNA Technologies, Leuven, Belgium) instead of random hexamers were used as primers. A number of reports (Stangegaard et al., 2006, Ross et al., 2008, Nardon et al., 2009) have shown an increased efficiency of priming and better coverage of the transcriptome when using pentadecamers (15-nucleotide-long random oligonucleotides) instead of random hexamers. Using the same amount of messenger RNA as starting material combined with random pentadecamer primers result in higher cDNA yield (at least 2-fold as much cDNA) and quality (Stangegaard et al., 2006).

2.6.1 Reaction setup

1µL Maxima Reverse Transcriptase (200U), 12µL nuclear RNA, 1µL pentadecamer primers, 1uL of dNTP mix (10 mM of each nucleotide), 4uL of 5x RT buffer and 1µL of nuclease-free water were combined for a 20uL total volume reaction per sample. The following temperature settings was used: 25°C for 10 minutes followed by 42°C for 1 hour, the reaction was terminated by heating at 85°C for 5 minutes (duration: 1 hour 15 minutes).

2.7 Quantitative PCR (qPCR) from sorted nuclei derived nuclear RNA

qPCR is a routinely used method for the detection and quantitation of gene expression in real time, it is a sensitive technique which uses specific probes to detect target sequences in the genome. Moreover, this technique is performed on an automated machine without the need of post PCR procedures, thus minimizing cross contamination between samples and simultaneously accelerating the analysis (Irshad et al., 2016). In **Chapter 4**, qPCR was used to examine expression levels of cell-type specific markers across different brain-derived nuclei populations. This step was performed as a quality control and validation step of the FANS procedure in order to verify the purity and enrichment of our nuclei fractions. Primers for three different markers were designed in house using the Primer3Plus software (Primer3Plus): two neuronal specific-markers (*NEUN, ENO2*), one glial-specific marker (*GFAP*) and 2 housekeeping genes (*GAPDH* and *POLR2A*) (**Table 2.1**). Primers were designed to be exon-exon junction spanning. This design reduces the risk of false positives from amplification of any contaminating genomic DNA, since the intron-containing genomic DNA sequence would not be amplified. It therefore bypasses the need for DNAse treatment preventing potential damage of the RNA samples. The comparative Quantitation Ct (ΔΔCt) method was applied to analyse relative gene expression levels.

Target name	Primer Sequences (5' to 3')	Position	Length (bp)	TM (°C)	GC content (%)
NeuN / RBFOX3	ACGTCTCCAACATCCCCTTC	F	20	56.8	55.0
	CCCCGCTCGTTAAAAATG	R	18	51.6	50.0
ENO2	TCACTGAAGCCATCCAAGC	F	19	55.3	52.6
	GGAAGTTATGTCCGGCAAAG	R	20	53.8	50.0
GFAP	CTGCGGCTCGATCAACTCA	F	19	57.6	57.9
	TCCAGCGACTCAATCTTCCTC	R	21	56.5	52.4
GAPDH	ACCACAGTCCATGCCATCAC	F	20	57.7	55.0
	TCCACCACCCTGTTGCTGTA	R	20	58.6	55.0
hPOLR2A	CCATCAAGAGAGTCCAGTTCG	F	21	55	52.4
	ACCCTCCGTCACAGACATTC	R	20	56.8	55.0

Table 2.1 Cell type specific qPCR primers sequences and specifications.

2.7.1 Reaction setup

For a 20 uL reaction volume, 4µL 5x HOT FIREPol® EvaGreen® qPCR Mix Plus (SolisBiodyne, Cat No: 08-24-00008), 3µL undiluted cDNA, 2µL forward and reverse primer sequences mix (2uM) (**Table 2.2**) and 11µL of H_2O were combined per sample replicate in 96 well plates. For each primer sets tested samples were loaded in duplicate and a non-template control (NTC) was also included as negative control.

Reagent	Function	Reagent Concentration	Volume (µL)
5x HOT FIREPol® EvaGreen® qPCR Mix	Complete master mix containing MgCl2, dNTPs, EvaGreen® dye, ROX dye and HOT FIREPol® DNA Polymerase	5x	4
PCR Primers	Short, single-stranded oligonucleotides complementary to target sequence	2 µM	2
cDNA template	nuclear RNA-derived cDNA	unknown	2
Ultra-pure water	Diluent ensures consistent reaction volume	Up to 20µL	12

Table 2.2 Sorted nuclei qPCR reagents and volumes.

2.7.2 StepOnePlus™ Instrument setup

The following qPCR programme was used: 95°C for 15 minutes, 45 cycles of: 95°C for 20 seconds, 60°C for 40 seconds, 72°C for 45 seconds followed by 95°C for 15 seconds (melt curve stage- step and hold). The dissociation stage was set at 60°C for 1 minute. Standard run mode (~2h to complete a run) was used to run each plate.

2.8 TaqMan low-density array (TLDA)

As further validation of the robustness and efficiency of the methodology developed, quantitative RT-PCR was performed in duplicate using the QuantStudio 12 K Flex (Applied Biosystems, CA, USA) in conjunction with the TaqMan low-density array (TLDA) platform (Life Technologies, Carlsbad, CA). TLDA is a microfluidic-technology format which provides a useful platform for multiple gene expression analyses and is based on singleplex qPCR assays that can be combined with various detection systems, including mass spectroscopy, bead sorting, dye-labelled probes, and microarray technology (Briese et al., 2005, Dominguez et al., 2008, Kodani et al., 2011). By using "off-the-shelf" pre-optimized assays I targeted (i) genes expressed in the major brain cell types to determine cell population specificity (*ENO2* for neurons, *OLIG2* for oligodendrocytes, *GFAP* for astrocytes, *CD68* for microglia, and *CD34* for endothelial cells), and (ii) five housekeeping genes (*ACTB, EIF4A2, GAPDH, SF3A1*, and *UBC*) identified as being the most stably expressed in the brain by two previous studies (Lunnon et al., 2014, Marzi et al., 2018). A full list of qPCR assays used is given in **Table 2.3** (from Supplementary Table 21(Marzi et al., 2018)).

Gene Symbol	Gene Name	TaqMan Assay ID
ACTB	actin beta	Hs99999903_m1
EIF4A2	eukaryotic translation initiation factor 4A2	Hs00756996_g1
GAPDH	glyceraldehyde-3-phosphate dehydrogenase	Hs99999905_m1
SF3A1	splicing factor 3a subunit 1	Hs01066327_m1
UBC	ubiquitin C	Hs00824723_m1
OLIG2	oligodendrocyte lineage transcription factor 2	Hs00377820_m1
ENO2	enolase 2	Hs00157360_m1
CD68	CD68 molecule	Hs00154355_m1
CD34	CD34 molecule	Hs02576480_m1
GFAP	glial fibrillary acidic protein	Hs00909233_m1

Table 2.3 Pre-optimized TaqMan assays for targeted gene expression analysis.

2.8.1 Sample prep and TaqMan Array Card filling

Each sample mix should contain 30 to 1000 ng (0.3 to 10 ng/µL) of total RNA converted to cDNA. The recommended amount of cDNA to add depends upon the expression level of the target genes of interest. In this specific case, the RNA input used for the amplification (PCR) reactions ranged between 100 ng (minimum) to 300 ng (optimal) per sample purely due to limited sample availability.

TaqMan® Universal PCR Master Mix (Applied Biosystems, Cheshire, UK) was used to prepare the reaction mix. For each sample, the total number of reservoirs to be filled was determined based on the format of the customized TaqMan Array card. The volume required for each reaction component was calculated as per manufacturer's instructions (total volume per reaction: 100uL).

Up to eight RNA samples can be run on each card (sorted nuclei fractions from 2 individuals) (see **Figure 2.11A**). Each sample was run in duplicate.
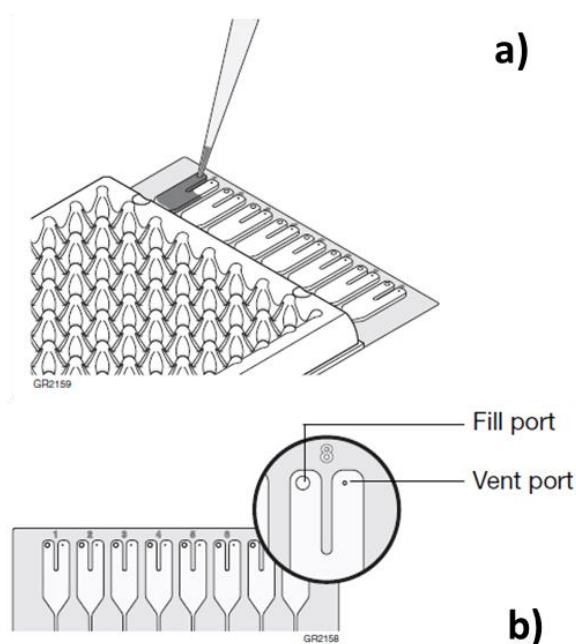
Figure 2.11 TaqMan® Array Micro Fluidic Card design.
A) Fill strip structure; each card provide spaces to fit in eight samples in duplicate. B) The fill port is located on the left arm of each fill reservoir; it is the larger of the two holes. Figure adapted from (TaqMan Array Micro Fluidic Cards User Guide).

Below is a brief description of the protocol used:

1. Frozen cDNA samples were thawed on ice and re-suspended by inverting the tubes, then gently vortexed. Master mix was mixed thoroughly by swirling the bottle.

2. The total volume required for each reaction component was calculated per the table below (**Table 2.4**): volume for one fill reservoir × the total number of fill reservoirs per sample. 10% excess volume was included in the calculations to compensate for the loss that occurs during pipetting.

Reaction Component	Volume (µL) for 1 Fill Reservoir
Diluted cDNA sample	50.0
TaqMan® Universal PCR Master Mix	50.0
Total Volume	**100.0**

Table 2.4 Sample prep for TaqMan Array Card - volume required for each reaction component.

3. For each sample, a 1.5-mL microcentrifuge tube was labelled, and the required components were added to the labelled tubes.

4. Once secured, tubes were gently vortexed to thoroughly mix the solution.

5. Tubes were then briefly centrifuged to spin down the contents and eliminate air bubbles.

6. The TaqMan Array card was thawed allowing it to reach RT (15 minutes minimum time required), then carefully removed from its packaging. Since prolonged exposure to indoor lighting can photo-degrade the fluorescent probes contained within the card the TaqMan Array card was kept on a lab bench, with the foil side down.

7. In order to fill the card, the micropipette tip was placed in the fill port (see Figure 10B for reference) and by holding the micropipette in an angled position, each fill reservoir was filled with sample-specific PCR mix made from a single cDNA sample (100 µL per fill reservoir ensure adequate filling. Volumes smaller than 100 µL may result in insufficiently filled cards). Care must be taken when pushing the micropipette plunger to expel the sample reaction mix from the tip. If a large

amount of air is released, it can push the reaction mix out of the fill reservoir or introduce bubbles into the fill reservoir.

8. The TaqMan Array card was centrifuged briefly to distribute the reaction mix to the reaction wells using a Sorvall® or Heraeus centrifuge (buckets and card holders are custom made for the TaqMan Array cards). The TaqMan Array card was then inserted into the card holder and the centrifuge was set as per manufacturer's instructions (see TaqMan Array Micro Fluidic Cards User Guide for details).

9. The TaqMan Array Card was sealed using a slow, steady, and deliberate motion of the sealer provided (see TaqMan Array Micro Fluidic Cards User Guide for details).

10. Using scissors, the fill strip was trimmed from the TaqMan Array card which was then placed in the instrument tray.

2.8.2 Run setup and data analysis

See 'Run the TaqMan® Array Micro Fluidic Card' section of user manual for instructions on how to set a run through the SDS software. PCR cycling conditions were 50 °C for 2 minutes, 94.5 °C for 10 minutes, and 45 cycles of 97 °C for 15 seconds and 60 °C for 1 minute. Stringent QC of raw qPCR data was undertaken, removing samples where there was high variability between duplicates (Ct > 0.5). The abundance of each test gene expressed was determined by the comparative Ct method (Pfaffl, 2001), relative to the geometric mean of the five housekeeping genes quantified in parallel. Data were log2-transformed to ensure normal distribution and presented as a fold-difference in expression.

2.9 DNA methylation profiling

Methods to profile DNA methylation have undergone significant improvements in the last decade due to the development of array- and sequencing-based technologies that have allowed the efficient quantification of DNA methylation at individual sites across the genome (Yong et al., 2016). The procedure adopted in this thesis uses the Illumina EPIC DNA methylation (Illumina Inc), which interrogates >850,000 DNA methylation sites across the genome (Moran et al., 2016).

2.9.1 Sodium bisulfite conversion

Many technologies have been developed to measure modifications in methylation with respect to biological processes, and the most common method, long considered a gold standard for identifying regions of methylation at a base-pair level sensitivity, is sodium bisulfite conversion (Leti et al., 2018). In this technique, genomic DNA is treated with sodium bisulfite, which reacts differently with unmethylated versus methylated cytosine, allowing therefore to quantify DNA methylation (Fouse et al., 2010). Sodium bisulfite promotes the conversion of unmethylated cytosine (C) to uracil (U), which is then replaced by thymine (T) by polymerase chain reaction (PCR) amplification (**Figure 2.12**). Methylated cytosines are unaffected by the bisulfite conversion, therefore remaining as cytosine in the DNA sequence after the bisulfite treatment reaction (Fouse et al., 2010, Yong et al., 2016).

Subsequent sequencing of the PCR clones derived from a single genomic DNA fragment allows to distinguish methylated cytosines, which are displayed as thymines in the resulting amplified sequence of the sense strand from 5-methylcytosines, which are displayed as cytosines in the resulting amplified sequence of the sense strand, at the single nucleotide level (Leti et al., 2018).

Bisulfite sequencing comes, however, with its challenges, particularly for studies in mammals: 1) repetitive elements (or repeated sequences), which occur in multiple copies throughout the genome and are usually highly methylated, make the alignment of short-read sequencing reads difficult; 2) the conversion of unmethylated cytosine to uracil/thymidine reduces genomic complexity to three bases in unmethylated regions, further complicating the alignment of sequencing reads; and 3) the costs associated with sequencing large genomes are relatively

high, making large studies unfeasible (Fouse et al., 2010). Another limitation of any method based on sodium bisulfte conversion is the inability to distinguish between 5-methycytosine (5mC, 'true methylation') and other DNA modifications such as 5hmC which is particularly enriched in the central nervous system (Lister et al., 2013). Lastly, bisulfite conversion causes DNA fragmentation, resulting in small sequences, typically smaller than 500 nucleotides (Tanaka and Okamoto, 2007). This is a result of the aggressive reaction condition of this conversion: pH 5 and temperatures up to 90°C (Holmes et al., 2014). Consequently, the analysis of the methylation of large CpG-islands is hampered (Ehrich et al., 2007). The treatment also causes DNA loss during clean-up with low recovery of bisulfite-converted DNA (Yi et al., 2017) which makes it unsuitable when several loci are to be interrogated (Mill and Petronis, 2009).

In the following section, the protocol used to perform sodium bisulfite conversion is described followed by the methods utilised to profile and analyse DNA methylation data in **Chapter 3, 4** and **5** of this thesis.
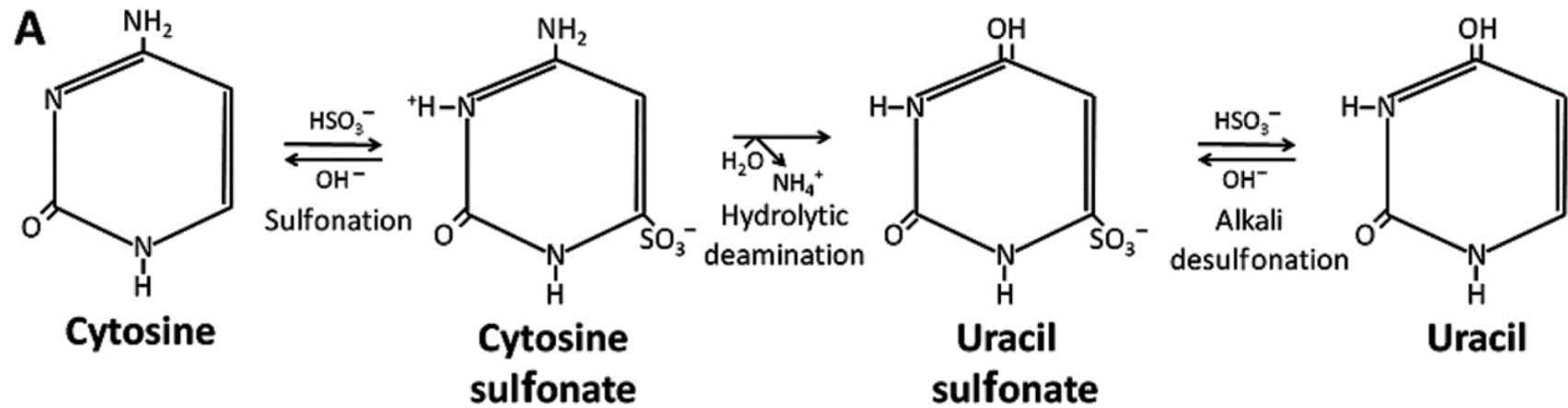
Figure 2.12. Sodium bisulfite treatment of genomic DNA.
(A)The procedure is based on the chemical reaction of single-stranded DNA with sodium bisulfite (HSO3−) at low pH and high temperatures.
The chemistry of each reaction step is as follows: sulfonation at the carbon-6 position of cytosine, irreversible hydrolytic deamination at the carbon-4 position to generate uracil sulfonate, and, finally, subsequent desulfonation under alkaline conditions to generate uracil. Methylation at the carbon-5 position impedes sulfonation at the carbon-6 position in the first reaction step. Although 5-methylcytosine can react with bisulfite, this reaction is extremely slow, and the equilibrium favors 5-methylcytosine rather than thymine (the deaminated product of 5-methylcytosine). Of note is that subsequent purification is necessary to remove bisulfite salts and other chemicals used in the procedure.
(B)The sodium bisulfite treatment converts unmethylated cytosines of the original DNA sequence to uracil, whereas methylated cytosines remain as cytosine. The CpG dinucleotide is the methylation target in human cells (bold). (Figure and legend taken from (Kristensen and Hansen, 2009).

Genomic human DNA was treated with sodium bisulfite using the EZ DNA Methylation-Gold Kit (Cambridge Bioscience, cat no.: D5007) which ideally requires 500ng high quality DNA in 20μL volume to provide sufficient BS-treated material for the profiling of cytosine modification using bead arrays or pyrosequencing. **Figure 2.13** shows an overview of the experimental procedure. The method below is an adaptation of the sodium BS treatment method developed by the manufacturer. Steps 14-17 deviate from the original protocol which is available from (EZ-96 DNA Methylation-Gold™ Kit Manual).

Input DNA

EZ DNA Methylation-Gold

Denature DNA with heat followed by CT – Conversion Reaction

Incubate

In-column desulphonation and clean-up

Elute Bisulfite-Converted DNA
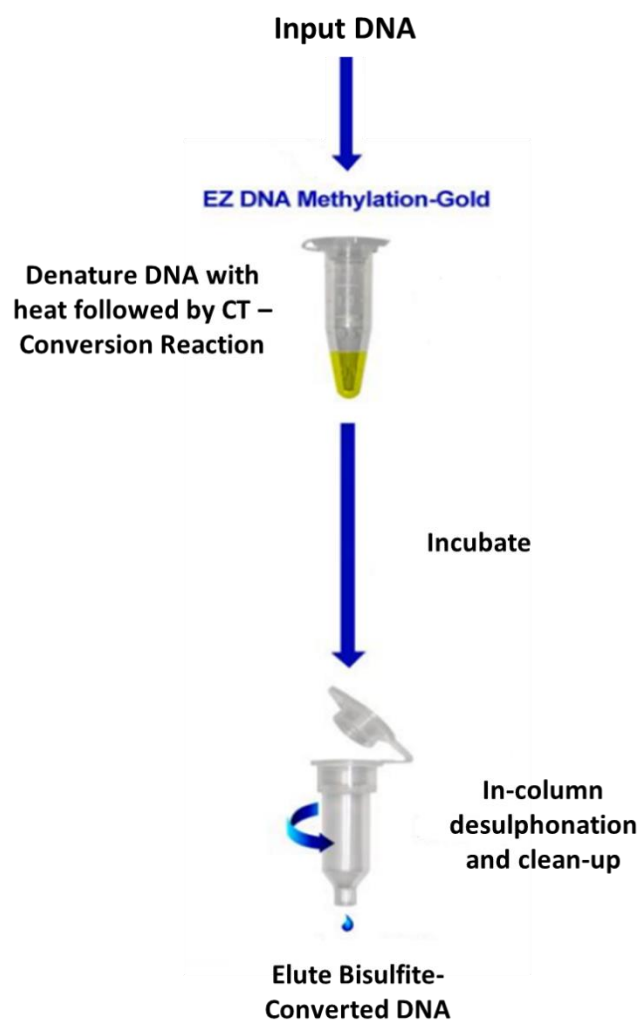
Figure 2.13 Outline of the EZ DNA Methylation-Gold™ Kit procedure.
Purified DNA is added directly to the CT-conversion reagent. Denaturation and bisulfite conversion are completed in a single-tube reaction. After desulphonation and purification in a spin-column, the purified bisulfite-converted DNA is ready for PCR. (Figure adapted from (EZ-96 DNA Methylation-Gold™ Kit Manual).

1. 500ng (25ng/µL in 20µL) of DNA was added to each well of a 96 well PCR plate

2. 130µL of the CT conversion reagent (**Table 2.5**) was added to each DNA sample in the conversion plate and mixed by pipetting

3. The plate was sealed with the provided film and transferred to a thermal cycler with the following steps performed:

        a. 98°C for 10 minutes

        b. 64°C for 2.5 hours

        c. 4°C storage for up to 20 hours

4. 400µL of M-Binding buffer was added to the wells of a Silicon-ATM binding plate mounted on a collection plate

5. The samples were transferred from the conversion plate (Step 2) to the corresponding wells of the Silicon-A™ binding plate (Step 3) and mixed by pipetting

6. The plate was centrifuged at 3,500 x g for 5 minutes then the flow-through was discarded

7. 400µL of M-Wash buffer (**Table 2.6**) was added to each well of the plate

8. The samples were centrifuged at 3,500 x g for 5 minutes

9. 200µL of M-Desulphonation buffer was added to each well and the plate was left to stand at room temperature (20-30°C) for 20 minutes

10. The plate was centrifuged at 3,500 x g for 5 minutes then the flow-through was discarded

11. 400µL of M-Wash buffer (**Table 2.6**) was added to each well of the plate

12. The plate was centrifuged at 3,500 x g for 5 minutes then the flow-through was discarded

13. 400µL of M-Wash buffer (**Table 2.6**) was added and centrifuged for 10 minutes

14. The Silicon-A™ binding plate was placed onto an elution plate

15. 15µL of M-Elution buffer was added directly to each well of the Silicon-A™ binding plate.

16. The plate was incubated for 5 minutes at RT

17. The plate was then centrifuged at 4,000 x g for 3 minutes to elute the DNA

18. Steps 15 to 17 were repeated

The eluted DNA was ready for immediate analysis or was stored at or below -20°C for later use in methylomic profiling. For long term storage, BS treated DNA was stored at -80°C.

BS conversion quality was assessed using BS-specific PCR amplification (Section 2.10) followed by gel electrophoresis (see Section 2.4.1). A single visible PCR band was taken as an indication of suitable BS conversion efficiency.

Reagent	Volume (mL)	Supplier
M-Dissolving Buffer	0.5	Zymo
M-Dilution Buffer	3	Zymo
CT Conversion Reagent	Bottle provided	Zymo
Ultra-pure H_2O	9	User

Table 2.5 CT Conversion Reagent required for BS conversion.
Using the Zymo EZ-96 DNA Methylation-GoldTM Kit (Cat No. D5007). The CT conversion reagent is supplied as a powder and must be dissolved prior to use and mixed at room temperature with frequent vortexing or shaking for 15 minutes.

Reagent	Volume (mL)	Supplier
M-Wash Buffer	36	Zymo
100% Ethanol	144	User

Table 2.6 Reagents required for the M-Wash Buffer for BS conversion.

2.9.2 Infinium Methylation EPIC array

The Illumina arrays have become one of the most popular methodologies to assess genome wide DNA methylation in mental illness and psychiatric conditions in recent years (Lunnon et al., 2014, Watson et al., 2016, Crawford et al., 2018, Murphy et al., 2017, Viana et al., 2017, Hannon et al., 2016) and as such it was selected for the EWAS presented in **Chapter 5** of this thesis.

Following sodium bisulfite conversion, the DNA samples included in this thesis were profiled using the Infinium Methylation EPIC array (EPIC array) and scanned on an iScan Microarray Scanner (Illumina, San Diego, CA, USA) according to the manufacturer's instructions.

The EPIC array, which is the updated version of the HumanMethylation450 BeadChip gives single-base methylation information for over 850,000 CpGs throughout the human genome. It contains more than 90% of the original Illumina HumanMethylation450K BeadChip (450K array) content but also provides unparalleled coverage of CpGs sites (outside of CpG islands), Non-CpG methylated sites identified in human stem cells (CHH sites), Reference Sequence database (RefSeq) genes, ENCODE open chromatin and FANTOM5 enhancers, DNase hypersensitive sites and miRNA promoter regions (Pidsley et al., 2016). The array uses two different types of chemistry to interrogate a single CpG locus, termed Infinium I and Infinium II probes. Infinium I has two probe types per CpG site with the same dye colour, one for the methylated (M) and the other for the unmethylated (U) state. The type I probe design assumes that the methylation status of CpG sites within 50bp are correlated with the target CpG (Infnium® HD Assay Methylation Protocol Guide).This could be a source of bias when CpGs underlying the probe are not co-methylated with the target site. The Infinium II probes use a single probe type with the 5mC state determined by a single base extension step after hybridisation by two different coloured dyes (green for methylated/modified sites and red for unmethylated/unmodified sites). This design includes the addition of a degenerate R [A/G] base at underlying CpG sites, and therefore is less influenced by nearby co-methylation patterns. Allele-specific single base extension of the probes incorporate a biotin nucleotide or a dinitrophenyl labelled nucleotide. Signal amplification of the incorporated label further improves the overall signal-to-noise ratio of the assay. A full description of this methodology, used in **Chapter 3, 4** and **5,** can be found on the Illumina website (Infinium MethylationEPIC Kit). **Figure 2.14** provides a detailed overview of the Infinium methylation probes design and its chemistry.
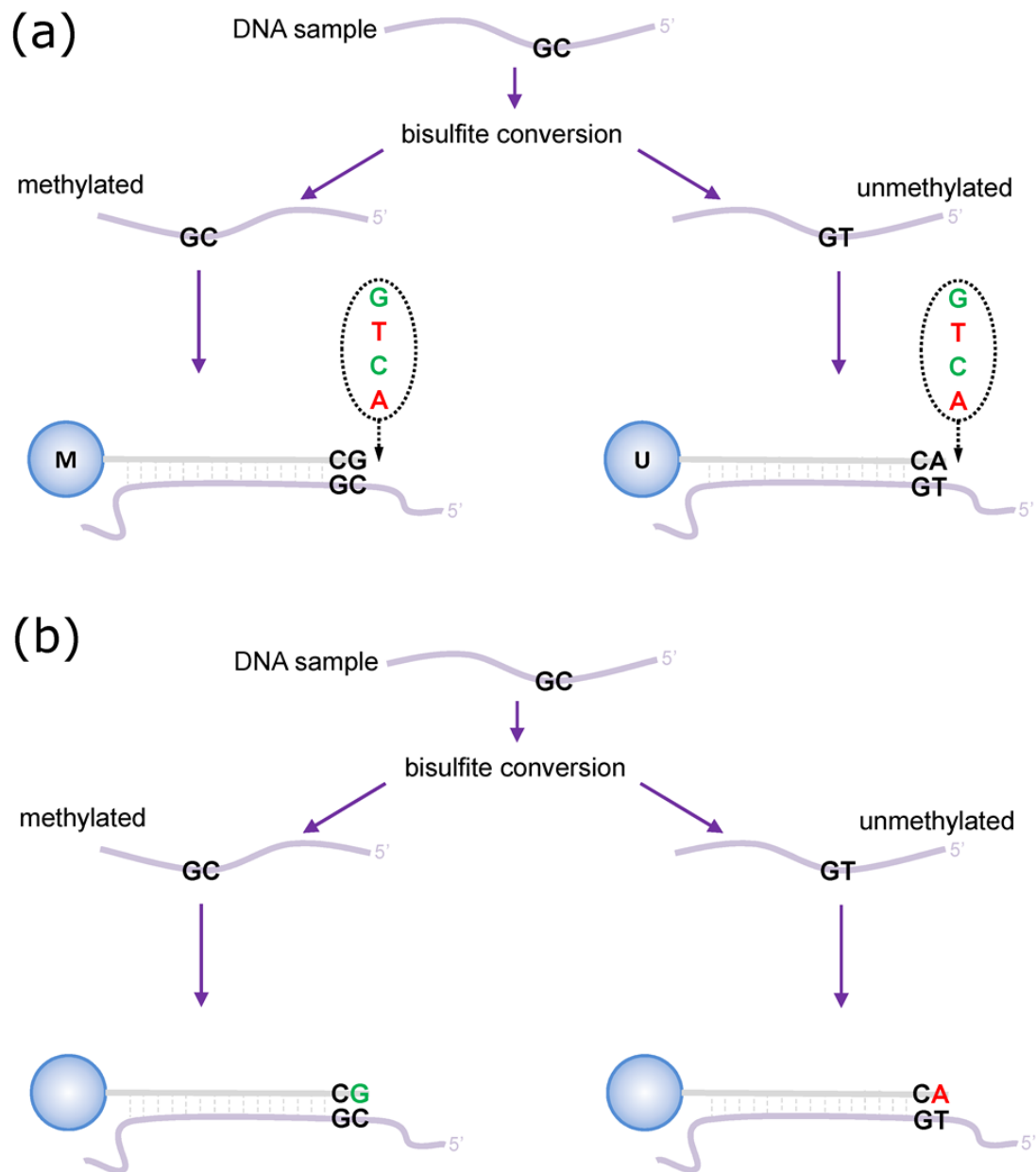
Figure 2.14 Illumina Infinium methylation probe design.
(a) Infinium I assay. Each individual CpG is interrogated using two bead types: methylated (M) and unmethylated (U). Both bead types will incorporate the same labeled nucleotide for the same target CpG, thereby producing the same color fluorescence. The nucleotide that is added is determined by the base downstream of the 'C' of the target CpG. The proportion of methylation can be calculated by comparing the intensities from the two different probes in the same color. (b) Infinium II assay. Each target CpG is interrogated using a single bead type. Methylation state is detected by single base extension at the position of the 'C' of the target CpG, which always results in the addition of a labeled 'G' or 'A' nucleotide, complementary to either the 'methylated' C or 'unmethylated' T, respectively. Each locus is detected in two colors, and methylation status is determined by comparing the two colors from the one position. Figure adapted from (Maksimovic et al., 2012).

Briefly, the first stage in the process included a denaturing and neutralisation stage before the bisulfite (BS)-treated DNA was whole-genome amplified. The denatured DNA was then isothermally amplified in an overnight step. The whole-genome amplification uniformly increases the amount of the DNA sample by several thousand fold without significant amplification bias (Mill and Petronis, 2009). A controlled enzymatic process was performed to fragment the amplified product. The process uses endpoint fragmentation to prevent over fragmentation. After an isopropanol precipitation, centrifugation at 4°C collected the fragmented DNA. The precipitated DNA was then suspended in Hybridisation buffer and dispensed onto EPIC arrays. Arrays were then incubated in an Illumina Hybridisation Oven to hybridise the samples onto the EPIC array surface. Eight samples were applied to each EPIC array, which were kept separate with an IntelliHyb seal. DNA samples annealed to locus-specific sites on the EPIC array. Un-hybridised and nonspecifically hybridised DNA was washed away and the EPIC array then underwent extension and staining in capillary flow-through chambers. Single-base extension of the oligonucleotides on the EPIC array, using the captured DNA as a template, allowed the incorporation of detectable labels on the EPIC array and determination of the 5mC/5hmC level at specific CpG sites. Finally, the EPIC array was imaged on the Illumina HiScan or iScan System (Illumina, San Diego, CA, USA), using a laser to excite the fluorophore of the single-base extension product on the beads. The scanner recorded high resolution images of the light emitted from the fluorophores. These in turn were used by the genome studio® software to produce a beta value (a measure of the levels of DNA modification) for each locus.

2.9.2.1 *Data normalisation and quality control*

The proportion of methylated bases in a sample was determined by calculating the ratio of the intensity of the fluorescent signal for M (modified) and U (unmodified), which gives a β (DNA modification) value for each site ranging from 0 (i.e. all cytosines at that site are unmodified) to 1 (i.e. all cytosines at that site are modified). The β value is calculated by the following equation:

$$\beta = \frac{Intensity\ M}{Intensity\ M + Intensity\ U + 100}$$

To avoid negative values after background adjustment, Illumina recommends adding a constant offset (+100) to the denominator to regularise β values when both methylated and unmethylated probe intensities are low (Du et al., 2010). Although this technology has been proven to be robust, it is not without its own limitations: for example, one disadvantage is the difference in performance between the two types of probe (Dedeurwaerder et al., 2011). Specifically, the β-values obtained from Infinium II probes have been shown to be less accurate and reproducible than those obtained from Infinium I probes (Dedeurwaerder et al., 2011). As a result, this has led to the development of several normalisation methods (Wang et al., 2015). Our research group has developed the wateRmelon package in R 3.3.2 (Pidsley et al., 2013), which offers a range of normalisation function and tools that were used to pre-process and normalise the DNA methylation data presented in this thesis.

An additional caveat, is the presence of SNP variation within close proximity of the query CpG site with the probe design on the array. The DNA methylation data at these sites could be confounded by the presence of nearby polymorphisms (Chen et al., 2013, Price et al., 2013). Therefore the DNA methylation levels detected by these probes could simply be a representation of the underlying genetic architecture. Additionally, 6-8% of the probes in the array have been found to cross-hybridise with other genomic locations and therefore do not accurately estimate the 5mC levels at the annotated site (Chen et al., 2013, McCartney et al., 2016). As a result of these issues, probes known to either cross-hybridise with another site (N=43,233 on 450K; N= 44,210 on EPIC) or contain common SNP variation (N= 19,224 on 450K; N=10,888 on EPIC) which can interfere with probe binding and confound measurement of DNA methylation were excluded prior to further analysis. The removal SNP probes was based on ancestry of the population, therefore probes with a common SNP (European population minor-allele frequency > 0.01) within 10 bp of the CpG site or a single base extension were excluded. Furthermore, control Illumina probes (rs) which assay highly-polymorphic SNPs rather than DNA methylation (N=65 on 450K array, N=59 on EPIC array) awere also removed. These are intentionally included on the array to allow sample quality control to check for relatedness between individuals and enable the detection of potential sample mix-ups (Daca-Roszak et al., 2015). The signal from these probes is expected to cluster into three distinct groups (representing the heterozygous and two homozygous groups). Although these are

not DNA methylation signals, they can be used to provide an indication of the degree of technical variance between samples (Chen et al., 2013).

Another major confounder in epigenetic studies is the variable cell composition of different tissues or different samples (Jaffe and Irizarry, 2014). Within the same brain region, different samples will have a different abundance of neurons and other brain cells. Recently, tools and new methodologies to control for such differences have become available. In 2013, an algorithm to estimate neuronal composition from Illumina 450k human brain data was developed (Guintivano et al., 2013). They identified cell epigenotype specific (CETS) markers based on DNA methylation differences between FACS neuronal and non-neuronal nuclei. Since the algorithm has been proven to be applicable to EPIC datasets too (Shireby G.L., 2020, Bettencourt et al., 2020), CETS was used to estimate neuronal to glia proportions in all the PFC datasets used in data **Chapter 3** of this thesis and these estimates were incorporated as covariates in subsequent analyses to control for cell composition differences across different samples. The algorithm was also used as a validation test of purity and enrichment of FACS-sorted nuclei fractions in **Chapter 4** and **5.**

2.10 Polymerase chain reaction (PCR)

PCR is a method used extensively to amplify a segment of DNA to generate numerous copies of the same fragment. Various components, including DNA, nucleotides, buffers, primers and polymerase are combined together and subjected to cycles of heating and cooling in a thermocycler. During the first stage of PCR the mix is heated to a high temperature to activate the heat sensitive polymerase taq. This is in turn followed by three steps:

1. A denaturation step, where the mix is heated to 95ºC to denature the double-stranded DNA

2. An annealing step where the mix is cooled to a primer-specific temperature (usually between 50ºC and 65ºC) to allow the primers to anneal with high specificity to the correct annealing sequence in the DNA

3. An extension step at 72ºC to allow the taq polymerase to synthesise the complementary strand of DNA using the deoxynucleotides (dNTPs)

These three steps are repeated for a specific number of cycles to allow the synthesis of an exponential number of DNA amplicons. A final step of 72ºC is added to allow a final extension.

The PCR in **Chapters 3** of this thesis was performed using BS-converted genomic DNA as the reaction template (see Section 2.9.1). This presents more of a challenge than using standard unconverted genomic DNA for several reasons. First, prolonged incubations using BS-treated DNA can lead to extensive damage to the DNA template. Second, BS treatment leads to reduced sequence complexity (the DNA largely comprises three bases rather than four), leading to a higher redundancy of the target sequence, and third, regions of interest often lie within CG-rich sequences, which become long stretches of Thymine following BS conversion, which can cause polymerase slippage. These reasons result in a higher chance of mispriming and non-specific PCR amplification. These issues were addressed in this thesis with careful primer design, using the following criteria which are widely reported to be optimal for successful BS-PCR:

1. Primers did not contain any CpG sites within their sequence to avoid discrimination between methylated or unmethylated DNA

2. Primers were not placed in a repetitive region

3. Primer length was at least 20 bases, to reduce non-specific amplification

4. Amplicon length was 177 bp as bisulfite treatment fragments DNA and it is difficult to amplify >400 bp regions (Masser et al., 2015).

The reagents used in a standard PCR reaction, together with their description and quantities are described in **Table 2.7** while **Table 2.8** reports the standard thermocycling conditions of a PCR reaction.

Reagent	Function	Concentration	Volume (µL)	Supplier	Cat. No
PCR Buffer B1	Maintains optimal pH	10X	2	Solis BioDyne	01-02-01000
Magnesium Chloride (MgCl2)	Required substrate for the Taq polymerase	1.5mM	1.2	Solis BioDyne	01-02- 01000
DNA nucleotides	DNA bases needed for the synthesis of new DNA	20mM	0.2	Fisher Scientific	1183-3933
Forward PCR primer	Short, single stranded oligonucleotides complementary to target sequence	10µM	0.2	IDT	
Reverse PCR primer			0.2		
Taq DNA Polymerase	Heat resistant enzyme that catalyses the PCR reaction	5U/µL	0.2	Solis BioDyne	01-02- 01000
DNA	Single stranded standard / BS treated DNA	10ng/µL	2		
Ultra-pure Water	Makes up reaction volume		14		

Table 2.7 Polymerase chain reaction (PCR) reagents and volumes used in this thesis.

Step	Temperature (ºC)	Time	N of Cycles
Hotstart/Initiation	95ºC	15 mins	1
Denaturation	95 ºC	30 secs	
Annealing	60 ºC	30 secs	40
Extension	72 ºC	1 min	
Final Extension	72 ºC	10 mins	1
End	15 ºC	∞	

Table 2.8 Standard Polymerase chain reaction (PCR) thermocycling conditions.

2.11 Bisulfite-PCR-Pyrosequencing

Bisulfite-PCR-pyrosequencing was used in this thesis to quantify DNA methylation across a specific genomic region (chr22:17,840,837-18,031,827) as a validation method for DNA methylation findings in empirical **Chapter 3.** The first step of this process is to treat the genomic DNA using sodium bisulfite (see section 2.9.1), followed by PCR (see section 2.10) to amplify specific target regions and pyrosequencing to quantify site-specific levels of DNA methylation. Pyrosequencing is a highly-sensitive 'sequencing-by-synthesis' technique often used to detect differences in DNA methylation levels at individual CpG sites in short DNA fragments (<200bp). The method works by monitoring the real-time incorporation of nucleotides via detection of the light signal resulting from the release of pyrophosphate molecules (PPi) during DNA elongation (Tost and Gut, 2007). DNA methylation analysis by pyrosequencing uses single-stranded, biotin-labelled bisulfite-PCR amplicons as a template.

The fundamental basis of pyrosequencing is that inorganic PPi is released when a deoxyribonucleotide triphosphate (dNTP) is added to the end of a growing strand of DNA. The PPi is then converted into ATP by ATP-sulfurylase and adenosine-5'-phosphosulfate. The newly formed ATP is then used for the conversion of luciferin into oxyluciferin by luciferase, which produces visible light. As a result of dNTPs being sequentially added to the reaction and because the light emitted is continuously detected by a charge coupled device camera, the DNA sequence and therefore the level of DNA modification at a specific genomic locations can be determined (23991743) (see **Figure 2.15** for details).

Biotinylated PCR primers (**Table 3.4**) were used to amplify a region of DNA for pyrosequencing. The incorporation of a biotin label into the primer indeed allows to capture single-strands of DNA. In addition, sequencing primers specific to the region of interest (approximately 200bp) were designed, these primers also had stringent design conditions as follows:

1. Sequencing primers did not contain any CpG sites within their sequence to avoid discrimination between methylated or unmethylated DNA

2. Sequencing primers were not placed in a repetitive region

3. Sequencing primers only contained non-CpG cytosines within their sequence to ensure exclusive amplification of BS-converted DNA

4. Sequencing primer length was no longer than 21 bases, to ensure efficient annealing

5. Sequencing primer annealing temperature was designed to be as close to 40°C as possible to be efficient within the pyrosequencer

All primers for PCR and pyrosequencing where designed using the PyroMark Assay Design software from Qiagen. CpG assay designs were created using the PyroMark Q24 software from Qiagen, using standard conditions. Two BS controls were used per assayed region to confirm BS conversion efficiency (i.e interrogation of the DNA sequence to check for BS conversion of a non-CpG cytosine by sequentially adding a C and T). At these positions a peak will only be present if the BS conversion is not efficient. These controls are built into the quality score for the data and the sites are different for every assay as they depend on the target sequence, (i.e. if the target region only includes CpG cytosines, no BS controls can be identified for that assay). Furthermore, commercially available fully methylated genomic DNA from Jurkat (human acute T-cell leukemia) cells enzymatically methylated with CpG Methyltransferase (M.SssI) (i.e. CpG Methylated Jurkat Genomic DNA, Cat. No SD1121) was used as fully methylated DNA standard (i.e 100% methylated control).

The following section details the process of pyrosequencing as per manufacturer's instructions on a targeted genomic region of BS treated DNA as used in this thesis. A full guide is also available from the manufacturer (PyroMark Q24 User Manual).

The cycling conditions, primer sequences (forward, reverse and sequencing) and PCR reagents used in this thesis for the pyrosequencing validation are reported in details in empirical **Chapter 3,** section 3.2.10.
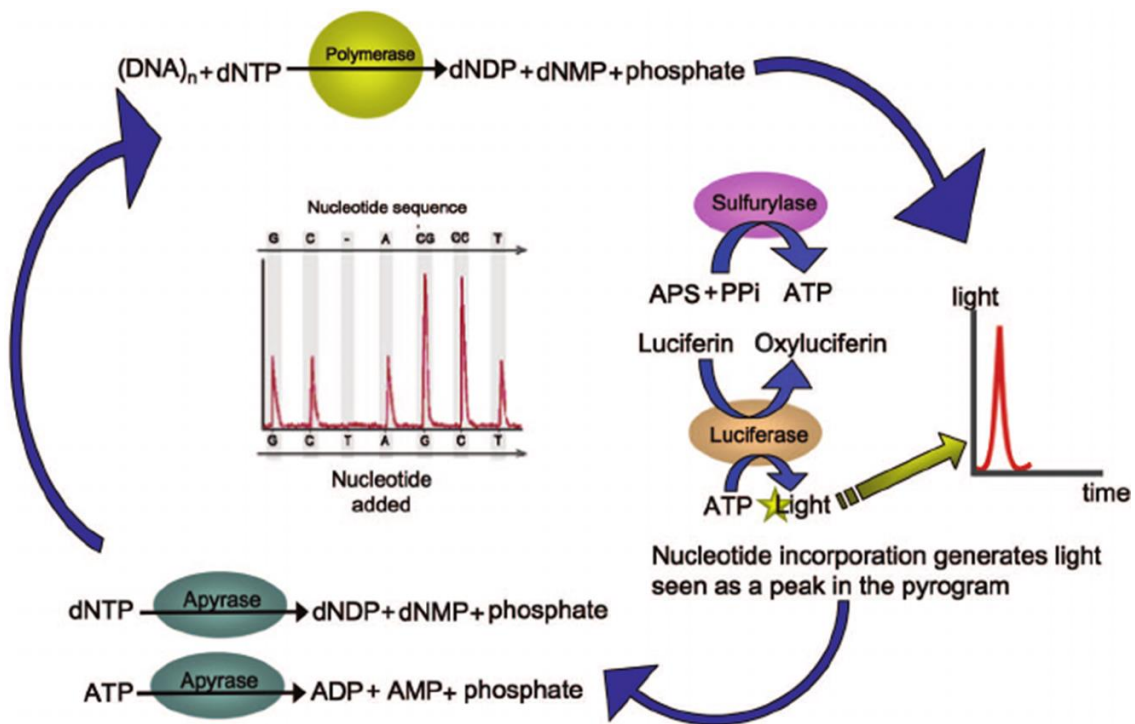
Figure 2.15 Pyrosequencing chemistry.
T*his figure shows the biochemical reactions and enzymes involved in the generation of light signals by DNA pyrosequencing. The pyrosequencing reaction takes place using a mixture of the single-stranded DNA template, the sequencing primer, and the enzymes DNA polymerase, ATP sulfurylase, luciferase, and apyrase. On the incorporation of complementary dNTPs by DNA polymerase, pyrophosphate (PPi) is released and is converted into ATP by ATP sulphurylase using adenosine 5'phosphosulfate. In the presence of ATP, luciferase converts luciferin into oxyluciferin that generates visible light. Each peak in the pyrograms represents a pulse of light detected in the instrument. Emitted light is proportional to the number of bases incorporated into the sequence. ATP, adenosine triphosphate; ADP, adenosine diphosphate; dNTP, deoxynucleoside triphosphate; dNDP, deoxynucleoside diphosphate; dNMP, deoxynucleoside monophosphate; PPi, pyrophosphate; APS, adenosine 5 J phosphosulfate. Figure taken from (Petrosino et al., 2009).*

2.11.1 Immobilising PCR product

1. Sepharose beads (Streptavidin Sepharose High Performance, GE Healthcare, Cat No: 11565015) were gently shaken to re-suspend

2. 2µL of beads (per sample) and Binding Buffer (Qiagen, Cat No: 979306) (40µL per sample) were combined in a 1.5mL centrifuge tube

3. Ultra-pure H2O was added to make a total volume of 60µL per sample

4. 60µL of the immobilising solution was pipetted into each well of a 24-well PCR plate

5. 20µL of biotinylated PCR product was added to each well of the PCR plate

6. The plate was then sealed and agitated for at least 10 minutes (200 x g).

2.11.2 Preparing the vacuum workstation

1. The appropriate troughs were filled with each reagent as follows:

      a. 50mL 70% Ethanol (Sigma Aldrich, Cat No: E7023)

      b. 50mL Denaturation Solution (0.2M Sodium Hydroxide (NaOH)) (Qiagen, Cat No: 979307)

      c. 70mL 1X Wash Buffer (Qiagen, Cat No: 979308)

      d. 70mL high-purity water

      e. 70mL high-purity water

2. The vacuum pump was switched on and filter probes were lowered into trough (e) (high purity water). All water was washed through the probes and the trough was re-filled.

3. The vacuum pump was turned off and returned to the "parking" position

2.11.3 Sequencing primer setup

1. The sequencing primer was diluted to 0.3µM in Annealing Buffer (Qiagen, Cat No: 979309); 25µL of the resulting solution was pipetted into each well of a Q24 well plate

2.11.4 Combining the Q24 plate

1. Once the PCR plate has finished its agitation it was moved to the Vacuum Workstation

2. The vacuum tool was turned on and the filter probes were immersed in the wells of the PCR pate

3. The vacuum tool with the DNA bound sepharose beads was then moved to the ethanol trough (a) and ethanol was aspirated for 5 seconds

4. The vacuum tool was then moved to the denaturation solution trough (b) and denaturation solution was aspirated for 5 seconds

5. The vacuum tool was then moved to the wash buffer trough (c) and wash buffer was aspirated for 10 seconds

6. The vacuum tool was then raised to 90° and the filter probes were left to dry for 20 seconds

7. The vacuum tool was then turned off and lowered into the waiting Q24 plate containing the sequencing primer

8. The vacuum tool was then agitated from side to side to dislodge the beads into the solution

9. The Q24 plate was then transferred to a heat block and incubated at 80°C for 2 minutes. It was then left to stand at room temperature for 5 minutes

2.11.5 Loading the pyrosequencer

1. For each assay performed, the sequencing cartridge was loaded using Pyromark Gold Q96 Reagents (Qiagen) (see **Figure 2.16***)* as described in the pre-run information produced by the Pyromark Q24 software.

2. The cartridge and plate were loaded into the sequencer; the appropriate run was loaded from an external memory drive and the run was initiated.
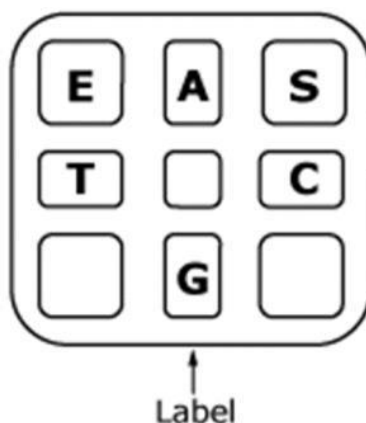
Figure 2.16 Schematic representation of the PyroMark Q24 cartridge.
Image taken from the PyroMark Q24 Cartridge Product Sheet (Qiagen, 2013). E, pyrosequencing enzyme; S, Pyrosequencing Substrate; A, dATP; C, dCTP; G, dGTP; T, dTTP.

2.11.6 Pyrosequencing data quality control

Analysis of the pyrogram was performed using the PyroMark Q24 software. BS conversion efficiency of less than 90% resulted in the exclusion of the affected samples. Using the inbuilt quality checker, traces were included or excluded from downstream analysis. DNA methylation values were reported as percentages of modifications at each CpG site profiled and these were taken forward for downstream analysis.

2.12 Total RNA extraction from bulk post-mortem human brain tissue

Total RNA was extracted using the miRNeasy Mini Kit (Qiagen, UK). **Figure 2.17** shows an overview of the experimental procedure (taken from the miRNeasy Mini Kit Handbook (Qiagen, 2014)). All the reagents were provided with the kit unless otherwise stated. Before starting, the lysophilised RNase-Free DNase I was prepared by adding 550µl of RNAse-free water, and 100% ethanol (Sigma Aldrich, UK) was added to the RPE and RWT buffers as indicated in the manufacturer instructions.

Approximately 30mg of frozen human brain tissue was excised from each sample using a sterile scalpel blade on a petri dish over dry ice and transferred into a sterile 1.5ml microcentrifuge tube. The tissue was homogenised in 350µl of QIAzol and using an RNase free, sterile plastic pestle. Another 350µl of QIAzol were added to each tube. The total 700µl of lysate were transferred into a QIAshredder column (Qiagen, UK) and centrifuged at 16,000 x g for 2 minutes. The samples were transferred to new microcentrifuge tubes and incubated at RT for 5 minutes. 140µl of chloroform (Sigma Aldrich, UK) was added and the samples mixed by shaking for 15 seconds. The samples were again incubated at RT for 2 minutes and centrifuged at 16,000 x g at 4ºC for 15 minutes. The upper layer of each sample was transferred to a new microcentrifuge tube and 525µl of 100% ethanol added and mixed by pipetting. The samples were transferred to RNeasy Mini spin columns, centrifuged at 9,000 x g for 15 seconds and the flow-through discarded. 350µl of RWT buffer were added to each column, the samples were centrifuged at 9,000 x g for 15 seconds and the flow-through discarded. For each sample, 10µl of DNase I solution was added to 70µl of RDD buffer I. 80µl of RDD buffer I was added to the centre of each column and the samples incubated at RT for 15 minutes. After incubation, 350µl of RWT buffer was added to each column, the samples were centrifuged at 9,000 x g for 15 seconds and the flow-through discarded. 500µl of RPE buffer was added to each column, the samples were centrifuged at 9,000 x g for 15 seconds and the flow- through discarded. Another 500µl of RPE buffer was added to each column, the samples were centrifuged at 9,000 x g for 2 minutes and the flow-through discarded. The columns were placed in new collection tubes and centrifuged at 16,000 x g for 1 minute to dry. The columns were placed into new microcentrifuge tubes and 15µl of RNAse-free water were added to the centre of each column and the samples

centrifuged at 9,000 x g for 1 minute to elute the RNA. Another 15µl of RNAse-free water were added to the centre of each column and the samples centrifuged at 9,000 x g for 1 minute to elute the remaining RNA.
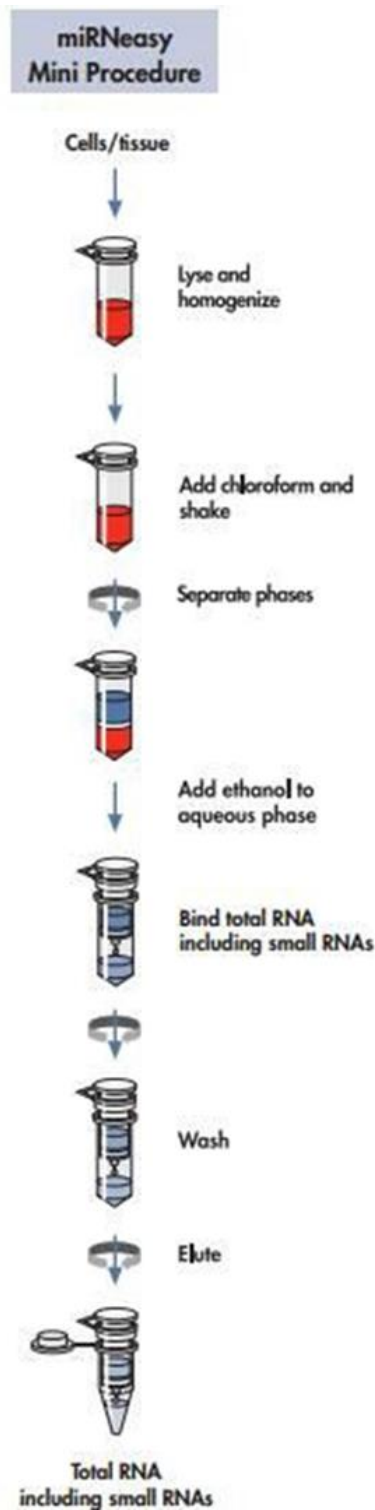
Figure 2.17 Overview of the total RNA extraction experimental procedure.
Figure taken from the miRNeasy Mini Kit Handbook (Qiagen, 2020).

2.12.1 Determining the quality and quantity of isolated nucleic acids

After extraction, DNA and RNA samples were quantified and checked for purity by spectrophotometry using a Nanodrop ND-8000 (Thermo Fisher Scientific, MA, US). Nucleic acids absorb UV light at a wavelength of 260nm, whereas proteins absorb UV light at a wavelength of 280nm and other compounds such as ethylenediamine tetraacetic acid (EDTA), carbohydrates and phenol, at a wavelength of ~230nm. Therefore, the absorbency rations of 260/280 and 260/230 indicate the presence of protein and other contaminants in the DNA and RNA samples. A 260/280 ratio of ~1.8 (for DNA) and ~2.0 (for RNA), and a 260/230 ratio between 1.8 and 2.2 is indicative of high purity sample. **Figure 2.18** shows an example of a typical RNA nanodrop profile.
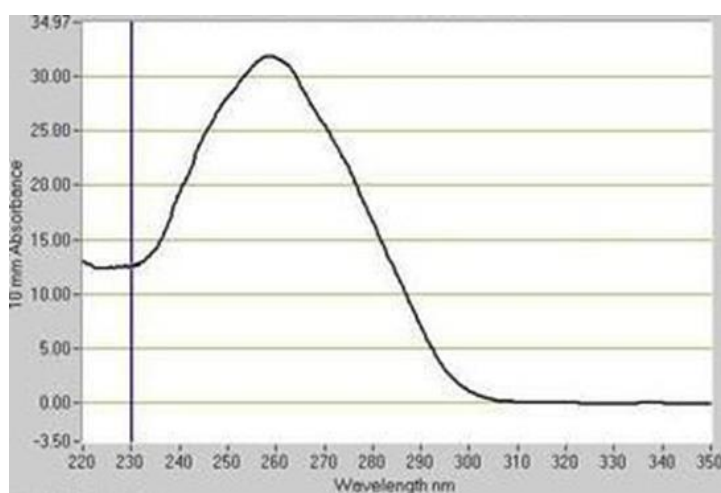
Figure 2.18 Typical nanodrop profile of a high quality, uncontaminated nucleic acid sample.

The purity and integrity of RNA samples was further assessed using an Agilent 2100 Bioanalyzer Instrument (Agilent Technologies, Santa Clara, CA, USA) in conjunction with the Agilent RNA 6000 Nano Kit (Agilent Technologies, CA, USA). The Bioanalyzer uses a fluorescent dye that binds to RNA on a gel electrophoresis chip. The Agilent Bioanalyzer software analyses the resulting electrophoresis gel and calculates an RNA integrity number (RIN) that can range between 1 (suggesting the RNA is highly degraded) and 10 (indicating the RNA has perfect integrity). **Figure 2.19A** shows an electropherogram detailing the regions that are indicative of RNA quality (taken from (Agilent Technologies, Standardization of RNA Quality Control)) and **Figure 2.19B** shows Bioanalyzer gel electrophoresis images of RNA sample degraded for varying times.
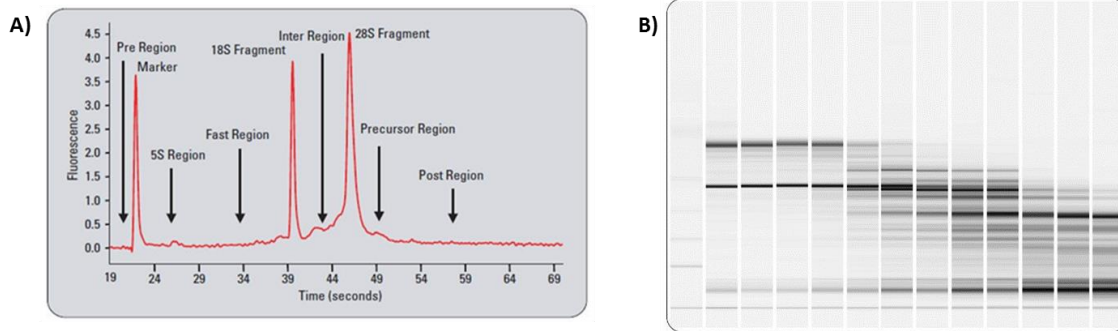
Figure 2.19 A) Electropherogram detailing the regions that are indicative of RNA quality.
B) Bioanalyzer gel electrophoresis images obtained from a total RNA sample degraded for varying times and analyzed on the Agilent 2100 Bioanalyzer System. A shift towards shorter fragment sizes (left to right) can be observed with progressing degradation. Both figures taken from(Agilent Technologies, Standardization of RNA Quality Control) .

All total RNA samples (N=71) used in empirical **Chapter 3** and **Chapter 6** were run on the Bioanalyzer and as expected, the samples were characterized by relatively low RIN numbers (ranging between 2.4 and 7.6) (see **Figure 2.20** for an example). Variable post-mortem interval before dissection and long-term storage (often several decades) which very often associate with several freeze-thaw cycles are two well-known factors affecting the quality of RNA when using post-mortem brain tissue (Pidsley and Mill, 2011). Despite the relatively low quality and high level of degradation of the total RNA, all samples were included in the study. Although the influence of RNA integrity on the performance of RT-qPCR and quantitative results is widely reported (Fleige et al., 2006, Nolan et al., 2006), common photometrical methods (e.g. Nanodrop) as well as standard lab-on-chip instruments (e.g. 2100 Bioanalyzer) for measuring the concentration of nucleic acids do not allow to discriminate between different fractions of RNAs (mRNA vs miRNAs). RIN is calculated as a ratio between 28S:18S ribosomal RNAs being an indication of RNA degradation (in the overall sense) thus with respect to integrity of miRNA, RIN is not a good factor to estimate miRNA degradation. Futhermore, due to their small length, miRNAs seem to be less susceptible to degradation because they show less binding sites for nucleases (Jung et al., 2010, Hall et al., 2012). Consequently, it can be assumed that the amplification of miRNA in qPCR might be less affected by a low RNA integrity compared to the longer mRNAs (Jung et al., 2010).

A   RIN = 7.6

B   RIN = 2.4
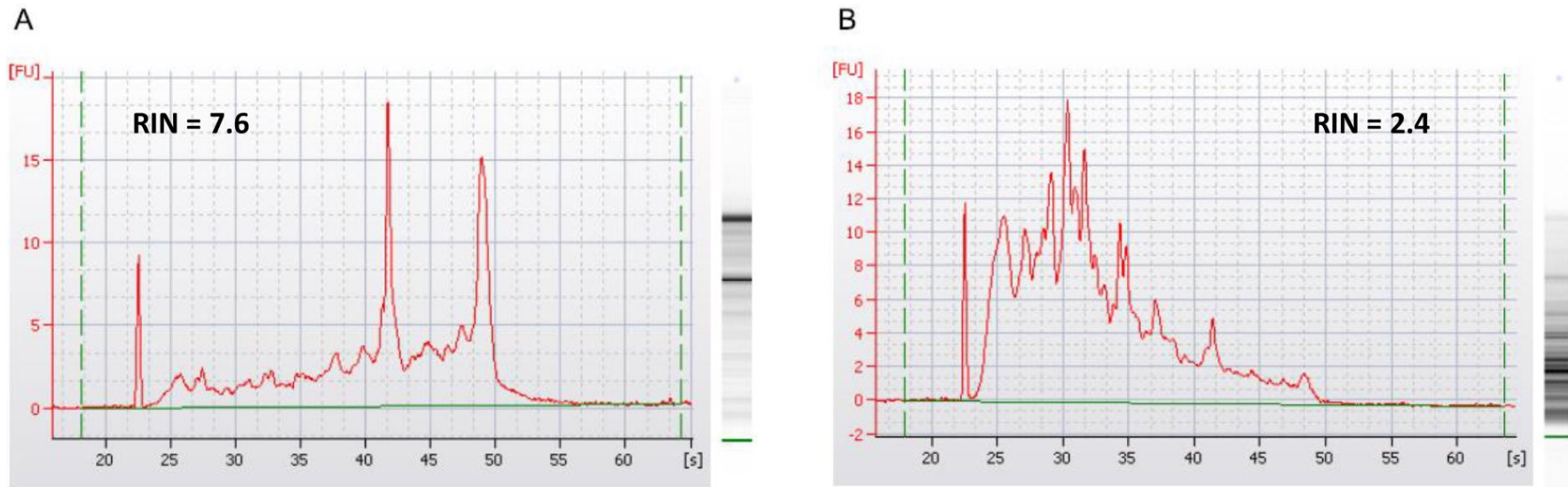
Figure 2.20 Bioanalyzer electropherograms and gel eleptrophoresis images from a good quality (A) and a degraded sample (B).
Shown are the bioanalyzer results for the prefrontal cortex sample s25_BA25 with a RIN=7.6 (A; good quality) and the prefrontal cortex sample s81_BA11 with a RIN=2.4 (B; highly degraded) both from the Douglas Bell-Canada Brain Bank (DBCBB).

2.13 cDNA synthesis from brain derived total RNA

Total RNA from post-mortem brain tissue was reverse transcribed into complementary DNA (cDNA) using the SuperScript™ VILO™ cDNA Synthesis Kit (Cat. No. 11754050) (Life Technologies Ltd, Paisley, UK) which contains SuperScript III Reverse Transcriptase (RT). The kit formulation allows to achieve superior cDNA yield and sensitivity even with suboptimal purity or scarce RNA templates. The protocol was carried out as per manufacturer's instructions. The reagents used in the cDNA synthesis, along with their quantities are outlined in **Table 2.9.**

Reagent	Volume (µL)
5x VILO Reaction MIx	4 uL
10x Super Script Enzyme Mix	2uL
Total RNA (up to 2.5 µg)	X uL (1000ng/sample)
DEPC-treated water	to 20uL

Table 2.9 First strand cDNA synthesis reagents and volumes.

RNA samples were diluted to a final concentration of 5 ng/uL. For each sample a total volume of 1ug of total RNA was used as template material for the reverse transcription reaction. Thermocycler conditions are outlined in **Table 2.10.**

Stage	Temperature	Time (min)
Primers annealing	25°C	10 mins
DNA polymerization	42°C	90 mins
Enzyme deactivation	85°C	5 mins

Table 2.10 Thermocycler programme temperatures and stages duration.

2.14 Quantitative PCR (qPCR) from brain derived total RNA

qPCR (for a comprehensive discussion on this technique see section 2.7) was used to examine expression levels of the suicide-associated non-coding RNA gene *PSORS1C3* and the nearby gene *POU5F1* in a subset of brain tissue samples (details in the section 2.1) to evaluate i) expression levels in the brain and ii) determine whether differences in DNA methylation levels affect expression of nearby genes.

Three housekeeping genes Ubiquitin Conjugating Enzyme E2 D2 (*UBE2D2*), Cytochrome C1 (*CYC1*), Ribosomal Protein L13 (*RPL13)* identified previously (Rydbirk et al., 2016) as being among the most stably expressed in the brain were selected to normalise the target gene expression. The protocol was carried as per manufacturer's instructions unless otherwise stated. The reagents used in the qPCR assay, along with their quantities are outlined in **Table 2.11**.

Reagent	Vol (1 rxn)
Taqman Fast Advanced Master Mix	10 ul
Taqman Gene Expression Assay	1 ul
Ultra pure water	5 ul
cDNA (1:5 diluted)	4 ul
Tot rxn volume	20 ul

Table 2.11 Gene expression assay – reagents and volume used.

Next, quantitative RT-PCR was performed in triplicate for each assay using the StepOnePlus Real-Time PCR machine (Applied Biosystems,CA, USA) and pre-optimized Taqman gene expression assays (Applied Biosystems, Cheshire, UK). A full list of the qPCR assays used is given in **Table 3.2 (Chapter 3).** Each plate included a qPCR and cDNA no template controls (NTCs). Thermocycler conditions were set as per manufacturer's recommendations and are outlined in **Table 2.12**.

	UNG incubation	Polymerase activation	PCR (40 cycles)	
Stage	Hold	Hold	Denature	Anneal / extend
Temperature	50°C	95°C	95°C	60°C
Duration	2 minutes	20 seconds	1 second	20 seconds

Table 2.12 qPCR run – programme setting.

Stringent QC of raw qPCR data was performed removing samples where there was high variability between triplicates (Ct > 0.5). The abundance of each test gene was determined by the comparative Ct method (Pfaffl, 2001), expressed relative to the geometric mean of the three housekeeping genes. Data were log2-transformed to ensure normal distribution and presented as a fold-difference in expression of suicide cases relative to controls using the $2^{-\Delta\Delta CT}$ method. Further info relating to the data analysis are provided in detail in **Chapter 3.**

2.15 TaqMan Open Array

OpenArray™ technology is an affordable real-time PCR–based solution for high-throughput gene expression analysis, genotyping, miRNA analysis, and digital PCR applications. This unique technology minimizes reagent use and helps streamline real-time PCR studies that use large numbers of samples, assays, or both (Applied Biosystems OpenArray® User Guide). It uses a microscope slide–sized microfluidic plate with 3072-well containing dehydrated TaqMan primers and probes. Each "through-hole" is treated with hydrophilic and hydrophobic coatings so that reagents are retained in the through-holes via surface tension. One OpenArray plate can hold as many samples as eight traditional 384-well plates.

The Standard Human TaqMan® OpenArray® Human MicroRNA Panel for miRNA analysis contains 754 human miRNA sequences from miRBase v14 (McCall et al., 2016) which have all been previously functionally validated with miRNA artificial templates (McCall et al., 2016). Although microarray- and sequencing-based platforms are preferable for most high-throughput applications, given the relative small number of common miRNAs, it is possible to use a qPCR-based platform (the gold standard for low-throughput measurement of gene expression) to measure the expression of all abundant

miRNAs in many tissues and cells (McCall et al., 2016).The primary advantage of qPCR-based technologies is the ability to simultaneously amplify and quantify a target transcript over sequential PCR cycles. The greater the initial amount of the target transcript present in a sample, the more rapidly the target will reach a threshold at which it can be detected by fluorescence (McCall et al., 2016). With TaqMan® Array, quantification of the gene expression levels is accomplished by loading the pre-amplified cDNA product onto the array for PCR amplification and real-time analysis. Gene expression is then measured using the comparative Ct (ΔΔCt) method of relative quantitation (Applied Biosystems OpenArray® User Guide).

TaqMan OpenArray℞ system was used in empirical **Chapter 6** of this thesis to identify differentially expressed miRNA relevant to suicide in a cohort of 70 post-mortem human brain samples. The following section describes procedures to prepare cDNA templates from total RNA followed by PCR amplification of the cDNA template for subsequent data analysis. First, mature miRNAs from total RNA are modified by 1) extending the 3' end of the mature transcript through poly(A) addition, then 2) lengthening the 5' end by adaptor ligation. The modified miRNAs then undergo universal reverse transcription followed by amplification to increase uniformly the amount of cDNA for all miRNAs (miRAmp reaction) (see **Figure 2.21**). The cDNA templates are then used with TaqMan® Advanced miRNA Assays for quantification of miRNA expression levels by qPCR analysis. TaqMan® Advanced miRNA Assays (Fisher Scientific, UK, Cat No. A25576) are pre-formulated primer and probe sets that are designed for analysis of miRNA expression levels. The assays can detect and quantify the mature form of the miRNA from 1–10 ng of total RNA from tissue (TaqMan® Advanced miRNA Assays User Guide). **Figure 2.22** provides a schematic overview of the TaqMan® Advanced miRNA Assays chemistry.
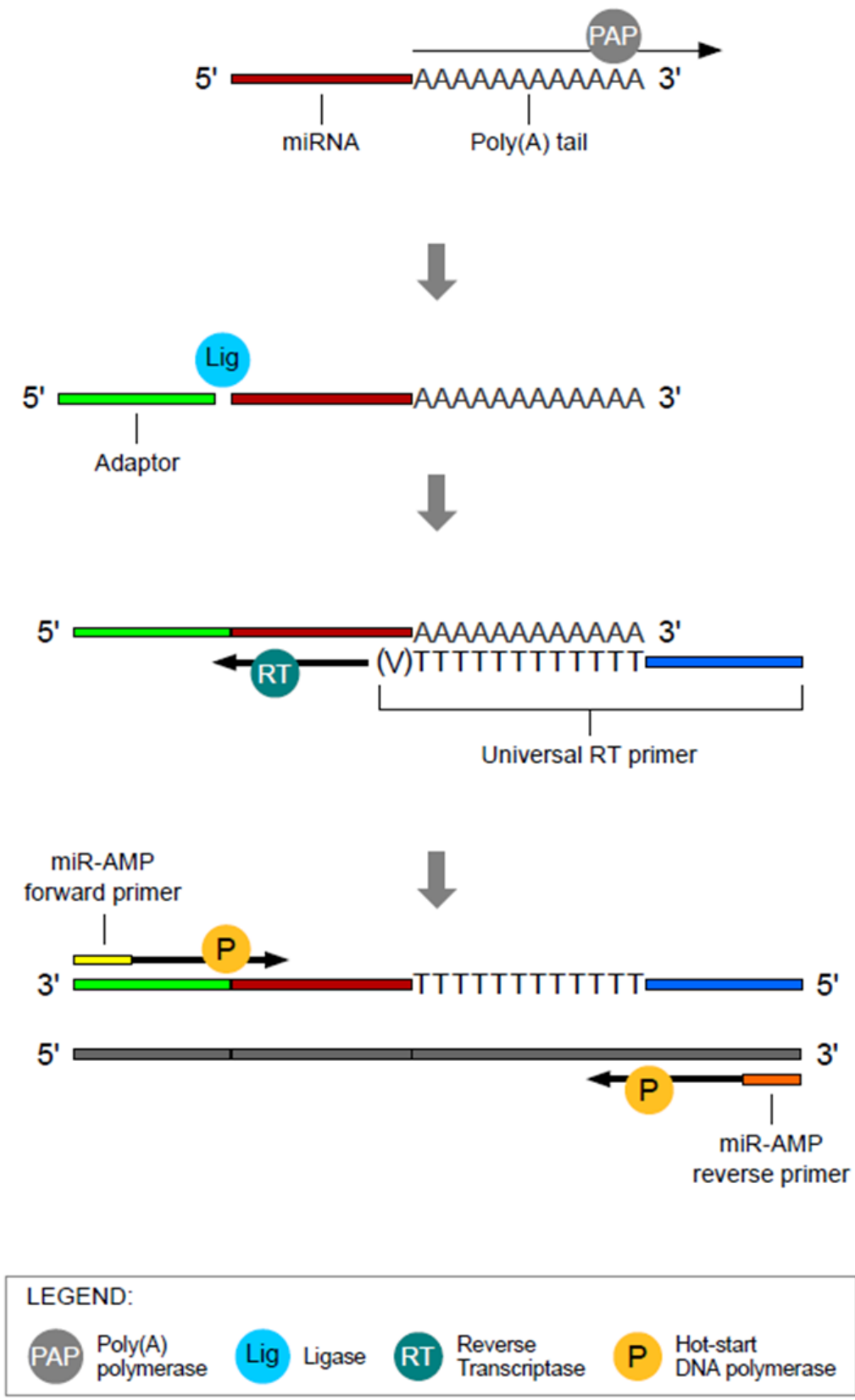
Figure 2.21 Overview of cDNA template preparation for quantification using TaqMan® Advanced miRNA Assays.
Figure taken from (TaqMan® Advanced miRNA Assays User Guide).
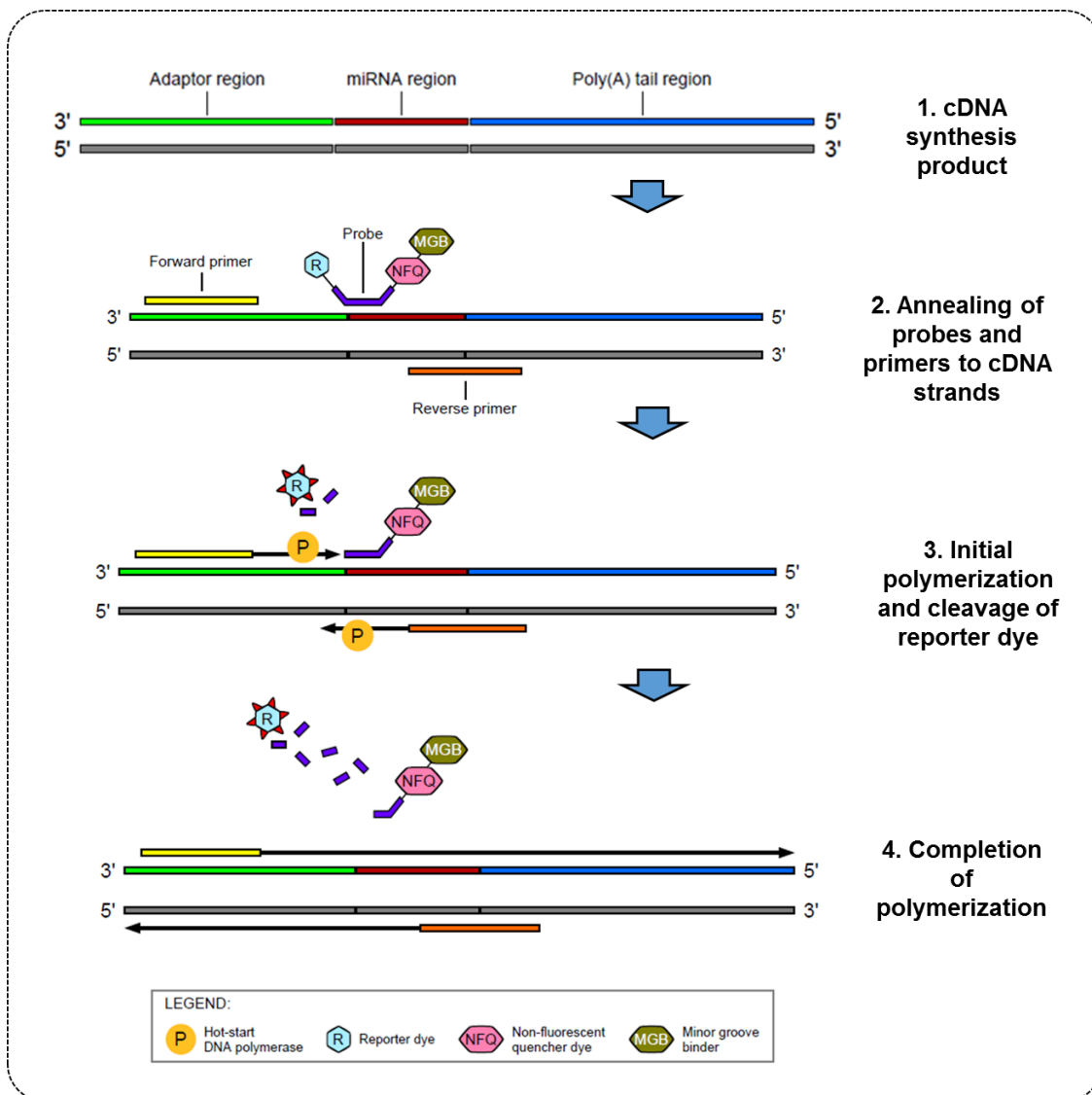
Figure 2.22 Overview of TaqMan® Advanced miRNA Assays chemistry.

Figure showing representation of real-time PCR with TaqMan® Advanced miRNA Assays. The 5' nuclease assay process takes place during PCR amplification. It occurs in every cycle and does not interfere with the exponential accumulation of product. During the PCR, the forward and reverse primers anneal to complementary sequences along the denatured cDNA template strands (stage 2). The primer binding sites vary depending on the target miRNA sequence and are designed to maximize specificity. Stage 2 shows an example representation in which the reverse primer is the primer that partially overlaps the miRNA region. The TaqMan® MGB probe (reporter dye: FAM™) anneals specifically to a complementary sequence between the forward and reverse primer sites (stage 2). When the probe is intact, the proximity of the reporter dye and quencher dye suppresses the reporter fluorescence. During polymerization, the DNA polymerase cleaves only probes that hybridize to the target sequence. Cleavage separates the reporter dye from the quencher dye resulting in increased fluorescence by the reporter dye (stage 3). This increase in fluorescence occurs only if the probe is complementary to the target sequence and if the target sequence is amplified during PCR avoiding therefore the detection of nonspecific amplification. Polymerization of the strand continues (Stage 4), but because the 3' end of the probe is blocked, no extension of the probe occurs during PCR. Figure adapted from (TaqMan® Advanced miRNA Assays User Guide).

2.15.1 cDNA synthesis

The TaqMan™ Advanced miRNA cDNA Synthesis Kit (Fisher Scientific, Loughborough, UK, Cat. No. A28007) was used to reverse transcribe total RNA into cDNA. The protocol was carried following the manufacturer's instructions. Strip tubes instead of plates were used to avoid cross contamination. In order to ensure consistency of the input material, RNA samples were diluted 1:10 aiming not to exceed 10 ng of total RNA per reaction. Briefly, the following steps were performed.

1. RNA samples were gradually thawed on ice. Temperature was controlled and kept constant in order to preserve the integrity of the RNA molecules.
2. cDNA kit reagents were defrosted and allowed to equilibrate at RT (with the exception of the enzymes which were kept on ice); reagent were mix thoroughly and briefly centrifuged
3. Water was added to each tube as per dilution calculation.
4. 2ul of RNA was added per well (5 ng/µL concentration)
5. The diluted RNA was vortexed and centrifuged briefly.

2.15.1.1 'PolyA' tailing

Sufficient Poly (A) Reaction Master mix (MM) was prepared for the required number of samples plus 10% overage (3µL/ sample) following the manufacturer's instructions (see **Table 2.13** for reference).

Component	1 Rxn
10X Poly(A) Buffer	0.5 µL
ATP	0.5 µL
Poly(A) Enzyme	0.3 µL
RNase-free water	1.7 µL
Total Poly(A) Reaction Mix volume	3.0 µL

Table 2.13 Reagents and volumes to prepare the Poly (A) Reaction Mix.

1. 2 µL of diluted RNA was transferred to new reaction tubes
2. 3 µL of MM were aliquoted per reaction tube (Final volume/reaction: 5uL)
3. Samples were briefly vortexed to mix and centrifuged to spin down

The thermocycler programme for the 'PolyA' tailing reaction followed manufacturer's recommendations and is reported in **Table 2.14.**

Step	Temperature	Time
Polyadenilation	37°C	45 mins
Stop reaction	65°C	10 mins
Hold	4°C	Hold

Table 2.14 Thermocycler programme for the 'PolyA' tailing reaction.

2.15.1.2 Adaptor ligation reaction

1. Reagents (yellow lid tubes) were vortexed and spun down before use, particular attention was taken when pipetting 50% PEG 8000 (very viscous reagent, tube requires to be vortexed at max speed to mix thoroughly and solution has to be aspirated and dispensed slowly).

2. Sufficient Ligation Reaction Master mix was prepared for the required number of samples plus 10% overage (10µL/sample) following the manufacturer's instructions (See **Table 2.15).**

Component	1 Rxn
5X DNA Ligase Buffer	3 µL
50% PEG 8000	4.5 µL
25X Ligation Adaptor	0.6 µL
RNA Ligase	1.5 µL
RNase-free water	0.4 µL
Total Ligation Reaction Mix volume	10 µL

Table 2.15 Reagents and volumes to prepare the Adaptor ligation Reaction Mix.

3. 10 µL of master mix were aliquoted to each reaction tube containing the poly (A) tailing reaction product (final volume: 15µL / tube).

4. Tubes were sealed, vortexed to mix properly (it does affect ligation efficiency) and the contents was spun down before to load tubes into the thermocycler. See **Table 2.16** for details.

Step	Temperature	Time
Ligation	16°C	60 mins
Hold	4°C	Hold

Table 2.16 Thermocycler programme for Adaptor ligation reaction stage.

2.15.1.3 *Reverse transcription (RT) reaction*

1. Reagents (green lid tubes) were vortexed and spun down before use

2. Sufficient RT Reaction Mix was prepared for the required number of samples plus 10% overage following the manufacturer's instructions (see **Table 2.17** for details). The mix was vortexed and spun down before dispensing.

3. 15uL of RT Master mix was aliquoted to each tube containing the adaptor ligation reaction product. Total volume per well should be 30uL at this stage.

4. Tubes were securely closed, vortexed to mix properly and the content spun down before loading tubes into the thermocycler. Programme settings as recommended by the manufacturers can be found in **Table 2.18**.

Component	1 Rxn
5X RT Buffer	6 µL
dNTPs Mix (25mM each)	1.2 µL
20X Universal RT Primer	1.5 µL
10X RT Enzyme Mix	3 µL
RNase-free water	3.3 µL
Total RT Reaction Mix volume	15 µL

Table 2.17 Reagents and volumes to prepare the RT Reaction Mix.

Step	Temperature	Time
Reverse Transcription	42°C	15 mins
Stop reaction	85°C	5 mins
Hold	4°C	Hold

Table 2.18 Thermocycler programme for RT reaction stage.

2.15.1.4 miR-Amp reaction

1. Reagents (clear lid tubes) were vortexed and spun down before use

2. Sufficient miR-Amp Reaction Mix was prepared for the required number of samples plus 10% overage following the manufacturer's instructions (see **Table 2.19** for details). The mix was vortexed briefly to mix and spun down.

3. In new strip tubes 45μL of miR-Amp Reaction Mix was aliquoted per well

4. 5μL of RT reaction product was distributed to each new tube (Total volume at this stage should be 50μL); remaining volume (25uL) can be stored at -20°C).

5. Tubes were securely closed, vortexed to mix properly and centrifuged to spin down the contents before to load tubes into the thermocycler. Programme settings as recommended by the manufacturers can be found in **Table 2.20**.

Component	1 Rxn
2X miR –Amp Master Mix	25 μL
20X miR- Amp Primer Mix	2.5 μL
RNase-free water	17.5 μL
Total miR-Amp Reaction Mix volume	45 μL

Table 2.19 Reagents and volumes to prepare the miR-Amp Reaction Mix.

Step	Temperature	Time	Cycles
Enzyme activation	95°C	5 mins	1
Denature	95°C	3 mins	20
Anneal/Extend	60°C	30 secs	
Stop reaction	99°C	10 mins	1
Hold	4°C	Hold	1

Table 2.20 Thermocycler programme for miR-Amp reaction stage.

2.15.2   Quality control of Real-time PCR

Quality of the cDNA samples (miR-Amp reaction product – see *section 2.15.1.4* for details) was assessed by performing real-time PCR for TaqMan® MicroRNA Assays. TaqMan™ Universal Master Mix II, no UNG (Cat No: 4440040) and two different TaqMan® Advanced microRNA Assays (478214_mir, 477863_mir, Cat No: A25576) were used. miR-Amp reaction product samples were diluted 1:10 (2uL undiluted miR-Amp product + 18uL of ddH20), briefly vortex and spin down. Reagents were thawed on ice, then mix thoroughly but gently. The PCR reaction mix was prepared by combining the following components (see **Table 2.21**):

Component	Volume per reaction (96-well plates)
TaqMan™ Universal Master Mix II, no UNG	5µL
TaqMan® Advanced miRNA Assay	0.5 µL
Nuclease-Free Water	2µL
miR-Amp reaction product	2.5µL
Total volume per reaction	10µL

Table 2.21 Real-time PCR reagents.

The PCR reaction mix was mixed thoroughly by vortexing, then centrifuged briefly to spin down the content and eliminate air bubbles. 5uL of PCR Reaction Mix was transferred to each well of a 96 well plate. 2.5µL of diluted miR-Amp reaction product were added to each reaction well for a total volume of 10uL per reaction. The plate was sealed with adhesive clear seal, vortexed briefly to thoroughly mix the contents and finally centrifuged (1500 x g, 1 minute) to spin down the content. Samples were loaded in duplicates together with 2 NTCs per each miRNA assay. **Table 2.22** reports the thermocycler conditions recommended in the user guide by the manufacturers to run the plate on the StepOnePlus PCR Instrument (Applied Biosystems, CA, USA). Fast cycling mode (duration: 90 minutes) was selected for loading.

Step	Temperature	Time	Cycles
Enzyme activation	95°C	20 secs	1
Denature	95°C	1 sec	40
Anneal/Extend	60°C	20 secs	

Table 2.22 StepOnePlus PCR Instrument thermal profiles.

2.15.3 Open Array plate loading

384-well plates were used to transfer the PreAmplification product and Master Mix into the OpenArray Plate using the OpenArray AccuFill Platform. The 384-well plate (24 columns, 16 rows) can be divided into eight regions, each containing 48 wells. Each 48-well region was used to fill one OpenArray Plate. Each sample well on the 384-well plate was used to load a subarray of 64 through-holes on the OpenArray Plate (**Figure 2.23**). For details see manufacturer's protocol (TaqMan® OpenArray® microRNA Panel).
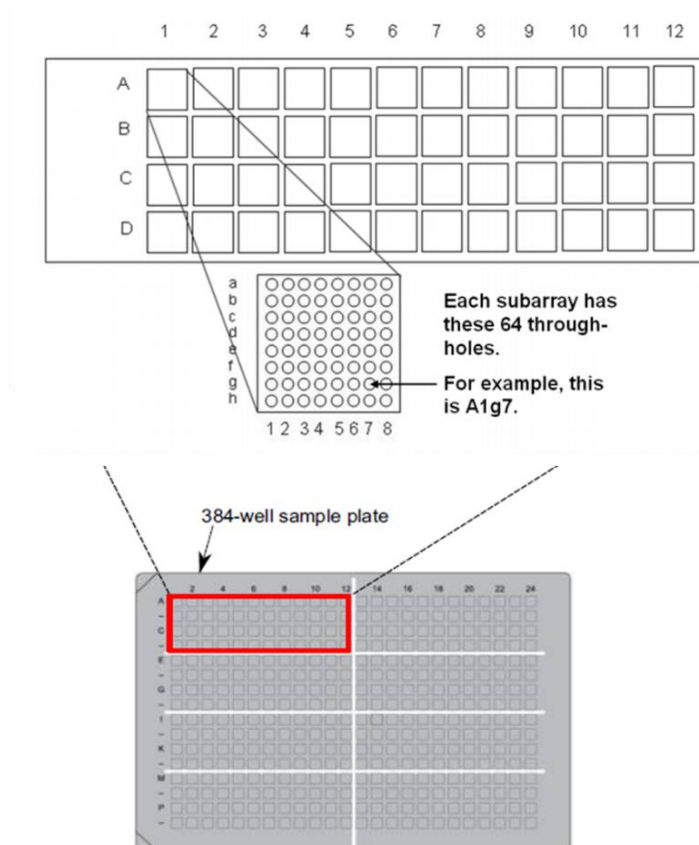
Figure 2.23 OpenArray 384-Well Reaction Plate.
The OpenArray Plate is divided into 48 subarrays; each subarray consists of 64 through-holes. Hydrophilic and hydrophobic coatings enable reagents to be held within the through-holes. An entire sub-array (64 throughholes) is loaded from each sample well in the 384-well sample plate using the AccuFill system. Figure adapted from (TaqMan® OpenArray® microRNA Panel).

1. The OpenArray plate was allowed to thaw to RT while still unopened as recommended by manufacturers.

2. The left over miR-AMP reaction product was diluted 1:20 (95 µL water + 5µL miR-AMP product) and diluted samples were mixed by vortexing and spun down

3. Reaction mix was prepared by combining the Taqman OpenArray Real-Time PCR Master Mix (Applied Biosystems, Cheshire, UK; Cat No. 4462164) (2.5µL) with the diluted miR-AMP product (2.5µL) as per manufacturer's instructions.

4. Strip tubes were used to load OpenArray plates in order to prevent cross contamination

5. 22.5 µL of Taqman OpenArray Real-Time PCR Master Mix was aliquoted in each well of a strip tube

6. 22.5 µL of diluted miR-AMP product were transferred to to each well previously loaded with master mix (final volume per well: 45µL)

7. Using the multichannel, 5µL of reaction mix were transferred to each well in the sets of 4x4 wells in the OpenArray 384-well sample plate (see **Figure 2.24A** for details about the plate layout). When strip tubes or plates are used, loading was started from one side of the plate and alternate wells were loaded to correspond to a 4x4 set of the array (see **Figure 2.24B**) as per manufacturer's recommendations.

① One full array
② One 4 × 4 set of an array (16 subarrays, 1 sample)
① Samples added to alternating tubes or wells
② 4 × 4 sets of an array
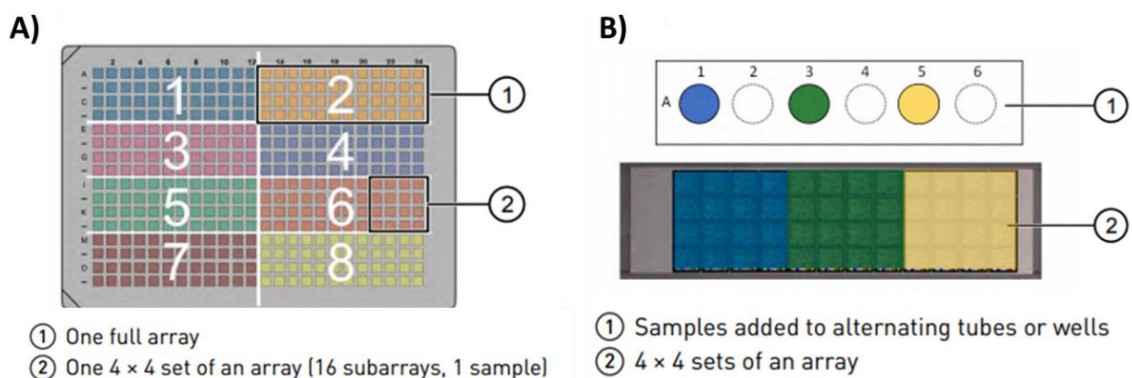
Figure 2.24 A) OpenArray 384-well sample plate layout. B) OpenArray Plate loading scheme.
Each OpenArray Plate is designed to accommodate three samples (or one sample in triplicate). One filled 384-well plate will load a total of eight OpenArray Plates.

8. Content of each well was mixed by pipetting up and down with the multichannel

9. Plates were sealed with adhesive foil seal, foil flap was removed and the edges of the filled areas was marked with a pen as reference when setting up the instrument

10. Plates were centrifuged to spin down (1 minute, 100 x g)

11. The manufacturer's Manual (TaqMan Array Micro Fluidic Cards User Guide) was followed to set up and load the Open Array AccuFill instrument (Applied Biosystems, Cheshire, UK) as well as to run the OpenArray plate(s) on the QuantStudio 12K Flex Instrument (Applied Biosystems, Cheshire, UK).

Chapter 3- Genome-Wide DNA Methylation Metaanalysis in the Brains of Suicide Completers

The work presented in this chapter is based on work published on Translational Psychiatry (Policicchio S et al et al., 2020). A copy of the published manuscript can be found in **Appendix B**.

3.1 Introduction

Suicide is a major public health problem worldwide, accounting for approximately one million deaths each year (Docherty et al., 2020) with 80% of suicides occurring in low- and middle-income countries (Naghavi and Global Burden of Disease Self-Harm, 2019). Throughout the world, suicide rates vary according to age and sex. Suicide is the foremost cause of death worldwide among peoples 15 to 24 years of age (Fazel and Runeson, 2020) with the highest rates occurring among men (15.6 suicides per 100,000 compared to 7.0 per 100,000 among women) (Fazel and Runeson, 2020). Despite major advances in recent years, gaps still remain in knowledge about risks and protective factors related to SB (Hawton and van Heeringen, 2009). While it is established that suicide is significantly heritable (Turecki and Brent, 2016), well-powered genomic research on the topic has been largely limited to the study of suicide-related behaviours rather than the ultimate phenotype of suicide death (Docherty et al., 2020) and although results from large-scale genome-wide association studies (GWASs) (Schosser et al., 2011, Willour et al., 2012, Galfalvy et al., 2013, Mullins et al., 2019) of SB have advanced our understanding of the process, they have failed to identify robust associations suggesting that the risk of SB is highly polygenic in nature and that individual gene variants are likely to account only for a very small proportion of the total phenotypic variability (Policicchio S et al., 2018). Other factors, such as the environment, behavioural traits, psychiatric diagnosis, life style and coping mechanisms, are essential regulators of suicide risk and likely to account for more sizeable effects (Turecki and Brent, 2016). Recently, increased understanding of epigenetic processes that occur in the brain has opened promising avenues in suicide research. The epigenome is potentially malleable—changing with age (Bell et al., 2012) and in response to specific environmental (Feil and Fraga, 2012) and psychosocial factors (Burns et al., 2018) —providing a mechanism for the interaction between genotype and the environment (Mill and Heijmans, 2013). Epigenetic processes, including DNA methylation, have recently been implicated in the etiology of numerous mental health disorders (Wong et al., 2014, Pidsley et al., 2014, Uddin et al., 2010, Fisher et al., 2015, Murphy et al., 2015, Dempster et al., 2014, Davies et al., 2014, Uddin et al., 2011) and SB (Murphy et al., 2017, Galfalvy et al., 2013).

In the last decade, research aiming to understand the contribution of epigenetic mechanisms to SB has implicated the role for key biological pathways, including hypothalamic pituitary adrenal (HPA) axis, stress response, polyamine system, neurotrophic signalling and lipid metabolism (Policicchio S et al., 2018). However, studies examining DNA methylation differences associated with SB have primarily focussed on candidate genes (Labonte et al., 2012b, Ernst et al., 2009a, Fiori et al., 2011, Keller et al., 2010) and few have examined genome-wide DNA methylation differences in the brains of suicide completers (Haghighi et al., 2014, Murphy et al., 2017). The availability of brain samples is a major challenge for neuropsychiatric research and many previous studies examining DNA methylation variation in suicide are performed on a limited number of post-mortem brain samples (Murphy et al., 2017, Fiori et al., 2012, Maussion et al., 2014). Such small studies have reduced statistical power to detect small changes in DNA methylation levels. The objective of this study was to identify suicide-associated DNA methylation differences in the human brain by utilising previously published and unpublished methylomic datasets.

3.2 Aims

Genome-wide DNA methylation profiles were available from post-mortem brain samples of suicide completers and non-psychiatric, sudden-death controls for a total of seven cohorts (PFC: four cohorts, n = 211; CER: three cohorts, n= 114). Methylomic data were meta-analysed for each brain region separately.

Main objectives of this study were:

1. To identify differentially methylated positions (DMPs) associated with SB in each brain region separately.

2. To identify differentially methylated regions (DMRs) associated with SB in each brain region separately.

3. To assess whether DNA methylation differences are significantly correlated between the two brains regions examined.

4. To investigate whether suicide-associated DMPs are enriched among functional pathways relevant to neuropsychiatric phenotypes and suicidality by performing gene ontology enrichment analysis in each brain region separately.

5. To examine whether DNA methylation within a PFC suicide-associated DMR (*PSORS1C3* DMR) is associated with expression of nearby genes, *PSORS1C3* and *POU5F1.*

3.3   Materials and Methods

3.3.1 Sample collection / data recruitment

For the PFC meta-analysis, I included four independent previously published studies (Kozlenkov et al., 2017, Guintivano et al., 2013, Murphy et al., 2017, Viana et al., 2017) aimed at profiling DNA methylation in human PFC in non-psychiatric controls and individuals with a diagnosed axis I psychiatric disorder According to the Diagnostic and Statistical Manual of Mental Disorders (DMS) edition IV, which provides a standardized classification system for the diagnosis of mental health disorders, Axis I includes any mental health conditions (other than personality disorders and mental retardation) and substance use disorders (American Psychiatric Association, 2000). Only data from individuals who died by suicide and non-psychiatric controls were included for the initial meta-analysis. In two of the four studies selected (Guintivano et al., 2013, Kozlenkov et al., 2017), DNA methylation was profiled from fluorescence-activated cell nuclei sorted (FANS) neurons, with the remaining two studies performed in bulk tissue (Murphy et al., 2017, Viana et al., 2017). Raw DNA methylation data for all four studies are deposited in the Gene Expression Omnibus (GEO) database (accession number: GSE89707, GSE88890, GSE98203, GSE41826) and full details of the sample cohort can be obtained from the original studies (Viana et al., 2017, Murphy et al., 2017, Kozlenkov et al., 2017, Guintivano et al., 2013). For the CER meta-analysis, three DNA methylation datasets were included two of which are currently unpublished (GSE137222 and GSE137223). Raw DNA methylation data for the CER published EWAS study (Viana et al., 2017) is deposited in GEO database (accession number: GSE89702). The unpublished studies were approved by the University of Exeter Medical School Research Ethics Board (REB). In all three CER cohorts DNA methylation profiles were derived from bulk brain tissue and cases were individuals who died by suicide (hanging, jumping from height, intentional poisoning, self-harm/bleeding). Cause and manner of death as well as joint presence of psychiatric diagnosis were determined by a forensic pathologist after evaluating autopsy results, circumstances of death, data from extensive toxicological testing, police reports, family interviews and medical records.

Controls were individuals who died suddenly (e.g. cardiac failure, viral infection, or accidents) and did not have evidence of axis I disorders. See **Table 3.1** for a complete description of sample selection and demographic characteristics of each cohort.

Table 3.1 Demographics summary of discovery cohorts

	Cohort	N	Age at death (yrs) Mean (SD)	Sex M	Sex F	PMI (hrs) Mean (SD)	Brain weight (g) Mean (SD)	pH Mean (SD)	Illumina Array Platform	Neuronal Comp. Mean (SD)
Prefrontal Cortex	***Viana J et al, 2016***									
	Suicide Cases	11	31.5 (9.3)	10	1	56.2 (33)	NA	13.1 (6.6)	450 K	0.3 (0.1)
	Non-Psychiatric Controls	24	43.6 (13.4)	20	4	41.6 (20)	NA	8.9 (6.8)		0.3 (0.1)
	Total	35								
	Guintivano J et al, 2013									
	Suicide Cases	22	27.4 (16.6)	12	10	19.3 (6.5)	NA	NA	450 K	Neuronal
	Non-Psychiatric Controls	35	35.2 (14.9)	16	19	15.9 (5.7)	NA	NA		Neuronal
	Total	57								
	Kozlenkov et al, 2017									
	Suicide Cases	21	31.5 (10.1)	16	6	4.1 (0.2)	NA	6.9 (0.1)	450 K	Neuronal
	Non-Psychiatric Controls	29	37.4 (13.7)	18	5	4 (1)	NA	6.7 (0.2)		Neuronal
	Total	50								
	Murphy et al, 2017									
	<u>**BA11**</u>									
	Suicide Cases	20	48.6 (20.8)	5	15	20 (15.6)	NA	6.6 (0.3)		0.45 (0.06)
	Non-Psychiatric Controls	20	39.4 (19.5)	4	16	26.1 (20.5)	NA	5.8 (3.5)		0.43 (0.11)
	Total	40							450 K	
	<u>**BA25**</u>									
	Suicide Cases	17	49.5 (22.4)	4	13	20.2 (16.9)	NA	6.5 (0.2)		0.33 (0.09)
	Non-Psychiatric Controls	18	41.2 (19.6)	4	14	23.4 (18.7)	NA	5.7(3.7)		0.33 (0.13)
	Total	35								
Cerebellum	***Viana e al, 2016***									
	Suicide Cases	7	32.6 (9.4)	6	1	55.9 (34.5)	NA	6.6 (0.4)	450 K	NA
	Non-Psychiatric Controls	16	44.1 (16.2)	13	3	32.2 (16.1)	NA	6.5 (0.3)		NA
	Total	23								
	Stanley Brain Bank 1									
	Suicide Cases	18	38.8 (10.9)	12	7	29.6 (16.2)	NA	6.2 (0.2)	450 K	NA
	Non-Psychiatric Controls	15	48.1 (10.6)	9	6	23.7 (9.9)	NA	6.3 (0.2)		NA
	Total	33								
	Stanley Brain Bank 2									
	Suicide Cases	21	42.8 (10.1)	10	11	37.6 (18.2)	1450.8 (121.5)	6.9 (0.1)	EPIC	NA
	Non-Psychiatric Controls	37	45.2 (9.3)	27	11	30.7 (15.1)	1435.2 (150.7)	6.6 (0.3)		NA
	Total	58								

Abbreviations: **Prefrontal Cortex, PFC; Cerebellum, CER; Post-mortem Interval, PMI; Broadmann Area 11, BA11; Broadmann Area 25, BA25.**

Table 3.1 Demographics summary of discovery cohorts*.*
DNA methylation profiles were available for 2 brain regions ((Prefrontal cortex (PFC) and Cerebellum (CER)) from post-mortem brain samples of suicide completers and non-psychiatric, sudden-death controls and were meta-analysed across 7 suicide cohorts (PFC, n = 211; CER, n= 114)). Information about age at death, gender, PMI, brain weight, pH were available for each cohort selected for this meta-analysis study. Also, neuronal cell proportion estimates (derived from DNA methylation data using CETS ((Guintivano et al., 2013)) were available for the PFC cohorts only.

3.3.2   DNA methylation analysis

DNA methylation was measured using the Illumina HumanMethylation450K BeadChip ("Illumina 450K array") or Infinium MethylationEPIC BeadChip ("Illumina EPIC array") platform (Illumina Inc., San Diego, CA, USA). To ensure consistency of the methodological approach, raw DNA methylation data (idat files) were recovered and each cohort was independently reanalysed, applying the same quality control (QC) and pre-processing pipelines. Briefly, QC checks, quantile normalization, and separate background adjustment of methylated and unmethylated intensities of type I and II probes were employed using the wateRmelon package in R (Pidsley et al., 2013). Probes on the X- and Y-chromosomes were used to confirm sample sex. Only samples which passed stringent QC measures (>1% of sites with a detection P value >0.05) were included. Probes were filtered to exclude those with a bead count < 3 or > 1% of samples with detection P value > 0.05 as well as non-specific probes, potentially cross-reactive probes or probes near SNPs (Price et al., 2013, Chen et al., 2013) were removed across all samples. Only probes common to both the 450K Array and EPIC array were included in downstream analyses for the CER (**Table 3.1** reports which study used which BeadChip array). For the annotation of probes, the University of California, Santa Cruz (UCSC) RefGene name from Illumina's annotation file were used and enhanced annotations to the UCSC Known Genes using publicly available catalogs such us GENCODE19 genes and CpG islands (https://www.gencodegenes.org/human/), ENCODE DNAse hypersensitivity sites (https://www.encodeproject.org/data/annotations/v4/), and FANTOM5 enhancers (https://slidebase.binf.ku.dk/human_enhancers/)   were also incorporated since accurate quantification of DNA methylation at more regulatory regions has been shown to be essential for the understanding of the role of DNA methylation in human development and disease (Pidsley et al., 2016). All annotations use the human February 2009 (GRCh37/hg19) assembly.

3.3.3   Estimating differential neuronal proportions

The R package (available at www.cran.r-project.org), Cell EpigenoType Specific (CETS) mapper, designed for the quantification and normalization of differing neuronal proportions in genome-wide DNA methylation datasets was used as

previously described (Guintivano et al., 2013) to estimate brain cellular heterogeneity in each of the four PFC cohorts. Similar estimates could not be obtained for the CER cohorts as the algorithm for the correction of brain cellular heterogeneity bias was developed using post-mortem frontal cortex data and NeuN is not expressed in CER Purkinje neurons (Guintivano et al., 2013) which are one of the most represented cell type in this region of the brain since constituting one of the three layers of the human cerebellar cortex (Cerminara et al., 2015).

3.3.4 Data analysis

Statistical analyses were performed using R statistical package (version 3.4.3). The β value is a ratio between methylated probe intensity and total probe intensities (sum of methylated and unmethylated probe intensities) and ranges from 0 to 1. Linear regression was used to examine differences in DNA methylation scores (reported as change in β value (Δβ)) between suicide cases and controls at each CpG site, controlling for potential confounders based upon the information available and design of each study included. Covariates included in the linear model of all seven cohorts were: age, sex and chip. For those cohorts where the information was available and represented a potential source of variation, ethnicity (Guintivano et al, 2013 for PFC and GSE137222 for CER) or brain bank (Viana et al., 2017 for PFC) were also included as covariates in the model. In the PFC cohorts only (all four), adjustment for estimated neuronal proportions was performed. For one study (Murphy et al., 2017), DNA methylation differences were investigated across individual matched cortical regions (Brodmann area 11(BA11), Brodmann area 25 (BA25)) by fitting a linear mixed-effect model using the lme4 R package (available at https://cran.r-project.org (Lattice, 2008)). Specifically, brain region and sample ID were included in the model as random effects ('within participants' factors) while diagnosis, age, sex, PH and cellular composition were included in the model as fixed effects.

3.3.5 Meta-analyses

3.3.5.1 Suicide completers versus non-psychiatric controls

The results obtained from the linear regression were then meta-analysed for each brain region independently. A fixed-effect model, using the 'metagen' function in the R package 'meta', was applied by providing the regression coefficients and standard errors from each individual cohort to calculate weighted pooled estimates and to test for significance. Experiment-wide significance (P <1E-07) (threshold estimated from permutation analysis in a larger dataset (n = 675 individuals) generated previously within my group for 450K array data (Hannon et al., 2016)) was chosen as multiple testing threshold to determine the strength of association between DNA methylation levels and suicide. Probes were ranked by P value, and Q-Q plots assessed to check for P-value inflation. QQ plots show the expected distribution of association test statistics (X-axis) across the probes compared to the observed values (Y-axis). Any deviation from the X=Y line implies a consistent difference between cases and controls across the whole genome (suggesting a bias or confounder). A perfect QQ plot should show a solid line matching X=Y until it sharply curves at the end (representing the small number – if there are any in fact - of true associations among thousands of un-associated probes).

3.3.5.2 Suicide completers versus non-suicide psychiatric controls

In order to assess whether the observed suicide-associated DNA methylation differencesidentified in my original meta-analysis were driven by the psychiatric disorder comorbidity rather than being suicide-specific differences, a second exploratory analysis was performed in additional samples obtained from the CER datasets only, which had additional non-suicide psychiatric samples with DNA methylation data available (not included in the primary analysis reported here). In the second meta-analysis, each CER cohort consisted of suicide cases (that were included in the original meta-analysis) and psychiatric controls, where individuals had a diagnosed axis I disorders (MDD, SCZ, BPD) but had no documented evidence of SB. In total, the secondary meta-analysis included 130 samples (case group, N =50; control group, N =80). Results obtained from the linear regression were then meta-analysed using a fixed-effect model as described previously.

3.3.6 Region based analysis

The results obtained from both the PFC and CER meta-analyses were used to perform a regional-based analysis using the Python module Comb-p (Pedersen et al., 2012), to identify suicide-associated DMRs. The Comb-p software groups spatially correlated DMPs (seed P value < 1E-03, minimum of three probes) at a maximum distance of 500 bp in each brain region. DMR P values were corrected for multiple testing using Šidák correction (Šidák, 1967) which corrects the combined P for n_a/n_r tests, where n_a is the total number of probes tested in the initial EWAS and n_r the number of probes in the given region.

3.3.7 Gene ontology term enrichment analysis

A previously described logistic regression approach (Lunnon et al., 2016) was used to test if genes (Illumina UCSC gene annotation) annotated to probes in the PFC and CER meta-analyses (DMPs with $P ≤ 1E-04$) predicted pathway membership, while controlling for the number of probes annotated to each gene. Briefly, pathways were downloaded from the Gene Ontology (GO) website (http://geneontology.org/) and all genes annotated to parent terms were also included. Genes containing at least one Illumina probe and annotated to at least one GO pathway were considered. Pathways were filtered to those containing between 10 and 2,000 genes and a list of significant (after correction for multiple testing- Bonferroni correction) pathways were identified as previously described (Lunnon et al., 2016).

3.3.8 Functional follow-up of significant DNA methylation findings

Tissue (n=71) from two regions of the cortex, BA11 (n=38) and BA25 (n=33), collected from 20 MDD suicide cases and 20 non-psychiatric sudden death controls was obtained from the Douglas Bell-Canada Brain Bank (DBCBB) (http://douglasbrainbank.ca/), further details are available in (Murphy et al., 2017). Previously, my group performed DNA methylation profiling in these samples (Murphy et al., 2017) and the results of that study were included in this meta-analysis study. To examine whether the identified suicide-associated DMR

(*PSORS1C3 DMR;* Chr6:31,148,370-31,148,553 (Hg19), 2694 bp downstream the TSS of *PSORS1C3* gene) is associated with the expression of nearby genes, expression levels of two nearby genes were measured in these brain tissue samples. Testing for association with gene expression was also performed firstly at the closest transcription start site (TSS) gene - the lncRNA gene*, PSORS1C3* - and then at the second closest gene*, POU5F1* (See **Figure 3.1** for details).

Thirty mg of frozen PFC tissue from each brain sample was homogenized with Qiazol Lysis Reagent (Qiagen, Valencia, CA, USA), as per the manufacturer's instructions, before running it through a QIAshredder (Qiagen, Valencia, CA, USA). Total RNA was extracted using the Qiagen miRNeasy Mini column-purification system and treated with DNase I as outlined by the manufacturer. The Agilent 2100 Bioanalyzer was used to check the quality and concentration of the extracted RNA samples. 1ug of total RNA was reverse transcribed into complementary DNA (cDNA) (20-μL reactions) according to the manufacturer's instructions using the Invitrogen VILO cDNA synthesis kit (Life Technologies Ltd, Paisley, UK). Three housekeeping genes Ubiquitin Conjugating Enzyme E2 D2 (*UBE2D2*), Cytochrome C1 (*CYC1*), Ribosomal Protein L13 (*RPL13)* identified previously (Rydbirk et al., 2016) as being among the most stably expressed in the brain were used to normalise the target gene expression. Next, quantitative RT-PCR was performed in triplicate for each assay using the StepOnePlus Real-Time PCR machine (Applied Biosystems, Cheshire, UK) and pre-optimized Taqman gene expression assays (Applied Biosystems, Cheshire, UK). A full list of the qPCR assays used is given in **Table 3.2**. PCR cycling conditions were as follow: 50°C for 2 minutes, 95°C for 20 seconds, and 40 cycles of 95°C for 10 seconds and 60°C for 20 seconds. A stringent QC of raw qPCR data was applied, removing samples where there was high variability between triplicates (Ct > 0.5). The abundance of each test gene was determined by the comparative Ct method (Pfaffl, 2001), expressed relative to the geometric mean of the three housekeeping genes. Data were log2-transformed to ensure normal distribution and presented as a fold-difference in expression of suicide cases relative to controls using the $2^{-\Delta\Delta CT}$ method. To assess whether *POU5F1* expression levels were associated with a history of suicide, a linear mixed-effect model (LMM) was adopted using the lme4 R package (available at https://cran.r-project.org) (Lattice, 2008) where ΔCt values of the target gene (*POU5F1*) was the response variable. Brain region and sample ID were included in the model as

random effects ('within participants' factors) while diagnosis, age, gender and neuronal proportion were included in the model as fixed effects. Finally, since 450K array data were available from the same individuals, the correlation between gene expression levels and mean DNA methylation levels at the DMR was investigated.
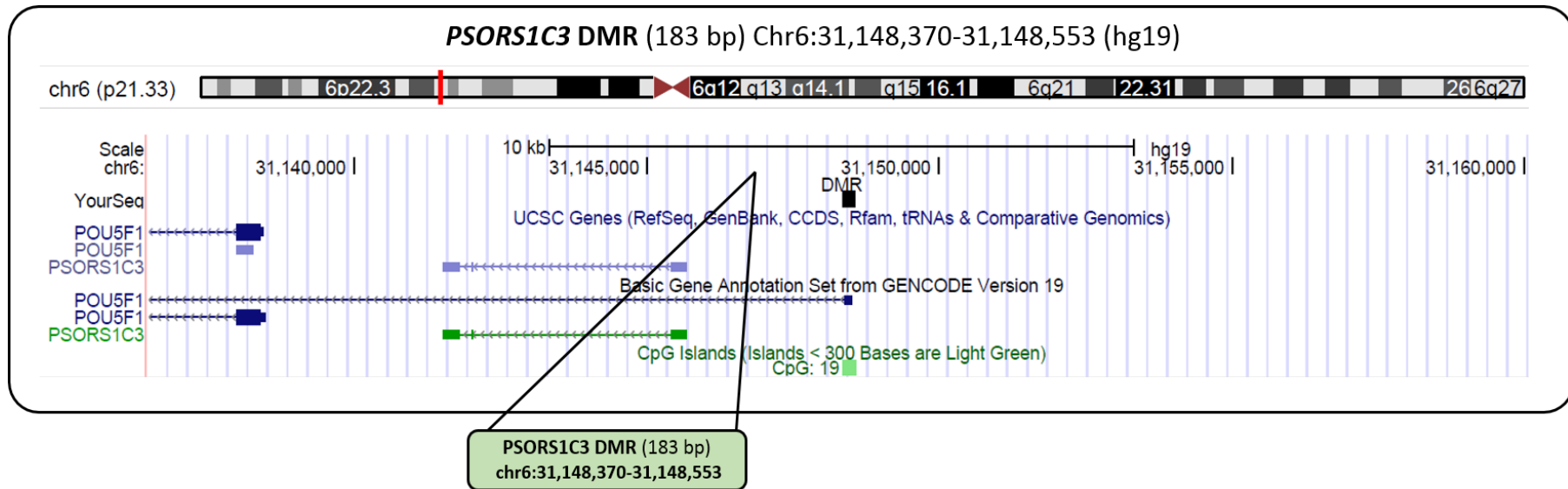
Figure 3.1 Figure showing the location within the human genome of the suicide-associated, PFC specific, PSORS1C3 DMR.
The two genes examined as part of the functional validation of the meta-analysis findings are also shown. Source: UCSC Genome Browser (hg19).

Target Gene Symbol	Target Gene Name	Catalog. number	Assay ID	Chromosome Location (GRCh37)	Assay Design	Exon boundary	Assay location	Amplicon Length
PSORS1C3	Psoriasis Susceptibility 1 Candidate 3	4351372	Hs05014866_m1	Chr.6: 31173735 - 31177899	Probe spans exons	1-2	294	83
POU5F1	POU Class 5 Homeobox 1	4331182	Hs04260367_gH	Chr.6: 31164337 - 31170693	Both primers and probe map within a single exon	5-5	1400	77
CYC1	Cytochrome C1	4331182	Hs00357717_m1	Chr.8: 144095035 – 144097527	Probe spans exons	5-6	832	73
RPL13	Ribosomal Protein L13	4331182	Hs00744303_s1	Chr.16: 89560657 - 89566829	Both primers and probe map within a single exon	6-6	866	137
UBE2D2	Ubiquitin Conjugating Enzyme E2 D2	4331182	Hs00366152_m1	Chr.5: 139561166 - 139628434	Probe spans exons	5-6	937	70

Abbreviations: GRCh37, Genome Reference Consortium Human genome build 37.

Table 3.2 Pre-optimized TaqMan ® Assays for targeted gene expression analysis.

3.3.9   Validation with bisulfite-PCR-pyrosequencing

Independent technical verification was performed using bisulfite PCR-pyrosequencing to assay the top-ranked CER DMR located within the *CERC2* gene which was found associated with suicide in the CER meta-analysis (see section 3.4.4.1 for details). BS pyrosequencing, as described in Section 2.11 of Methods, was used to quantify DNA methylation across four individual CpG sites (cg01010211, cg03408904, cg13762691, cg24074477) spanning from 17956453 to 17956561 within chromosome 22 (hg19). BS conversion was performed using the Bisulfite-Gold kit (Zymo research, USA). PCR amplification of a 177 bp amplicon was performed on sodium bisulfite treated DNA (see section 2.10) in duplicate. Subsequently, 10µl of each PCR duplicate were mixed to make a total of 20µl PCR product for each sample. The PCR products were incubated for 10 minutes with Streptavidin Sepharose beads (Qiagen, UK) to immobilise and capture the biotin-labelled DNA strands. This was followed by washes in 70% ethanol (Sigma-Aldrich Corporation, St. Louis, MO, USA), denaturation solution (0.2M NaOH), and Pyromark wash buffer (Qiagen, Venlo, Holland). Denatured PCR products were then sequenced using 0.3 µM sequencing primer and Qiagen Pyromark enzyme and substrate in a PyroMark Q24 Instument (Qiagen, UK). Fully methylated control samples and negative controls were included in all experiments. DNA methylation was quantified in a subset of pre-frontal cortex samples available (described in details in section 3.3.8) using the Pyromark Q24 system (Qiagen, UK) following the manufacturer's standard instructions and the Pyro Q24 CpG 2.0.6 software was used to retrieve DNA methylation values.

The assay cycling conditions, primer sequences and reagents used in this thesis for the *CERC2* PCR reactions, are described in **Table 3.3, Table 3.4** and **Table 3.5,** respectively.

Step	Temperature (ºC)	Time	N of Cycles
Hotstart	95ºC	15 mins	1
Denaturation	95 ºC	30 sec	35
Annealing	60 ºC	30 sec	
Extension	72 ºC	1 min	
Final Extension	72 ºC	10 mins	1
End	15 ºC	∞	

Table 3.3 CERC2 Polymerase chain reaction (PCR) thermocycling conditions.

	Length (nt)	Sequence	Position (5'-3')	GC (%)	Tm (ºC)
CERC2_Fwd PCR primer	23	[Btn]GGGAGGGAGTAGTGAGAGAAATA	458-480	47.8	60.9
CERC2_Rev PCR primer	25	TCTTAAAATACACACCCCTTCCTAC	634-610	40.0	60.7
CERC2_Seq Primer	20	ATCAACTCTACCCTTCCTTC	553-534	45.0	52.0

Table 3.4 CERC2 Polymerase chain reaction (PCR) and pyrosequencing primer sequences.

Reagent	Function	Concentration	Volume (µL)	Supplier	Cat. No
PCR Buffer B1	Maintains optimal pH	10X	2	Solis BioDyne	01-02-01000
Magnesium Chloride (MgCl2)	Required substrate for the Taq polymerase	3.0mM	1.2	Solis BioDyne	01-02- 01000
DNA nucleotides	DNA bases needed for the synthesis of new DNA	20mM	0.2	Fisher Scientific	1183-3933
Fwd PCR primer	Short, single stranded oligonucleotides complementary to target sequence	10µM	0.2	IDT	
Rev PCR primer			0.2		
Taq DNA Polymerase	Heat resistant enzyme that catalyses the PCR reaction	5U/µL	0.2	Solis BioDyne	01-02- 01000
DNA	Single stranded BS treated DNA	10ng/µL	2		
Ultra-pure Water	Makes up reaction volume		14		

Table 3.5 CERC2 Polymerase chain reaction (PCR) optimisation - reagents and volumes.

3.4 Results

An overview of the methodological approach used in this study is given in **Figure 3.2**. Briefly, genome-wide patterns of DNA methylation was assessed in two brain regions (PFC and CER) obtained from suicide completers (n=91 and n=46 respectively) and matched non-psychiatric, sudden-death controls (n=126 and n=68 respectively) profiled using the Illumina 450 K or EPIC array. Pre-processing, normalisation and stringent QC were performed as previously described (see Methods section for specific details). The initial analyses focused on identifying DMPs and DMRs associated to suicide assessing each brain region independently. In order to detect differences in DNA methylation levels specifically driven by suicide, an additional analysis was conducted excluding all the non-psychiatric controls from the CER cohorts originally included in the meta-analysis and a new meta-analysis was performed where individuals with documented Axis I psychiatric disorders (SCZ, MDD, BPD) and history of SB were compared to psychiatric cases without history of SB/suicide fatalities at the moment of death. Finally, functional evaluation of the second top-ranked suicide-associated DMR in the PFC (genomic location chr6:31148370-31148553) was performed using a subset of samples for which post-mortem brain tissue was available while for the top-ranked suicide-associated DMR in the CER (genomic location chr22:17956453-17956561) independent technical validation was attempted using gDNA from a subset of samples available from one of the three CER cohorts (Viana et al., 2017) included in the meta-analysis.
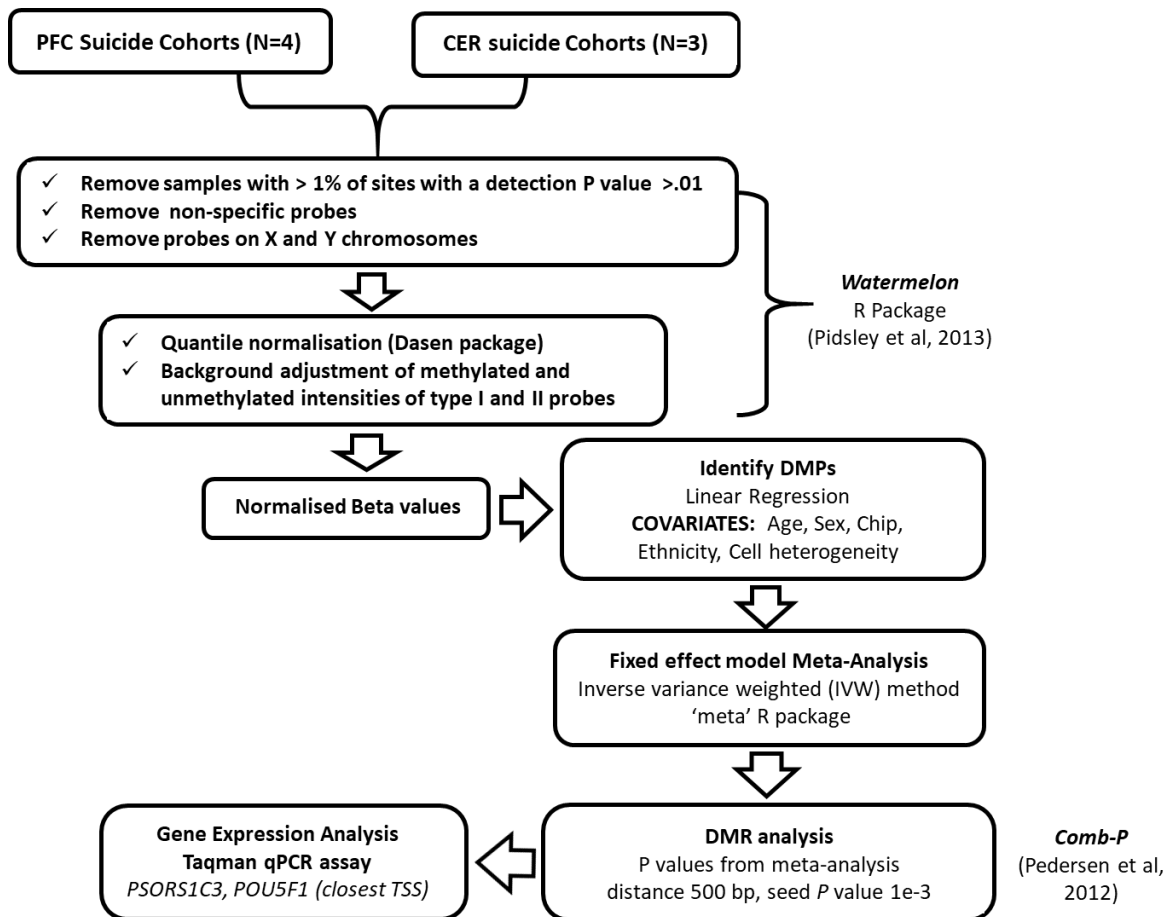
Figure 3.2 Methodological pipeline overview for DNA methylation analysis.
Flow chart describing the methodological meta-analysis approach used in this chapter. Data pre-processing, QC, normalisation and linear regression analysis were applied to each individual dataset selected for the study. The meta-analysis was performed across datasets but in each brain region separately. Initial quality control was performed on signal intensities for each probe and all samples underwent to further quality-control checks. Stringent quality control measures were employed. Non-specific probes and probes on the X and Y chromosomes were removed. Quantile normalisation and background adjustment of M and U intensities of probes were employed using Watermelon R package. Linear regression was used to examine differences in DNA methylation scores (reported as changes in beta values (Δβ) between suicide completers and CTRs at each CpGs site, controlling for potential confounders. The results from the linear model were then met-analysed for each brain region separately. A fixed effects meta-analysis of four PFC suicide cohorts was performed using the 'metagen' function in the R package 'meta'. The results obtained from both the PFC and CER meta-analysis were used to perform a regional-based analysis using the Python module Comb-p, to identify suicide-associated differentially methylated regions (DMRs). In addition, functional consequences of variable DNA methylation within a PFC suicide-associated differentially methylated region (PSORS1C3 DMR) were examined by assessing expression levels of nearby genes (real-time qPCR using pre-optimized Taqman assays). Abbreviations: Prefrontal Cortex, PFC; Cerebellum, CER.

3.4.1 Sample and cohort quality control

The raw DNA methylation data generated from the PFC (91 cases and 126 controls) and CER (46 cases and 68 controls) samples used in this chapter were pre-processed and normalised in each cohort separately as described in **Chapter 2** section 2.9.3. All computations and statistical analyses were performed using R 3.3.2 and Bioconductor 3.5 (Gentleman et al., 2004). Signal intensities for each probe were extracted using Illumina *GenomeStudio* software (Illumina, San Diego, CA, USA) and imported into R as a methylumi object. Initial QC checks were performed using functions in the *methylumi* and *minfi* packages (Aryee et al., 2014, Davis S et al., 2014).

3.4.1.1 Signal Intensities check

As robust indicator of sample quality, the median methylated signal intensity and unmethylated signal intensity for each sample was calculated and samples with signal intensities less than 2000 were removed (see **Figure 3.3** for an example). This threshold has been routinely applied within my group based upon experimental evidence observed in EWAS of blood samples (Hannon et al., 2018). Worth noting, this arbitrary cut-off has been recently revised and amended to 1500 since in brain samples the signal intensity distribution has been found to be generally lower compared to blood DNA samples. Prior data normalisation, further QC steps such as evaluation of the BS conversion efficiency, multi-dimensional scaling and DNA methylation tissue predictor (results reported in section 3.4.1.2 to 3.4.1.5), have been incorporated to exclude outliers and to ensure that only samples generating good quality data were considered at the stage of data normalisation.
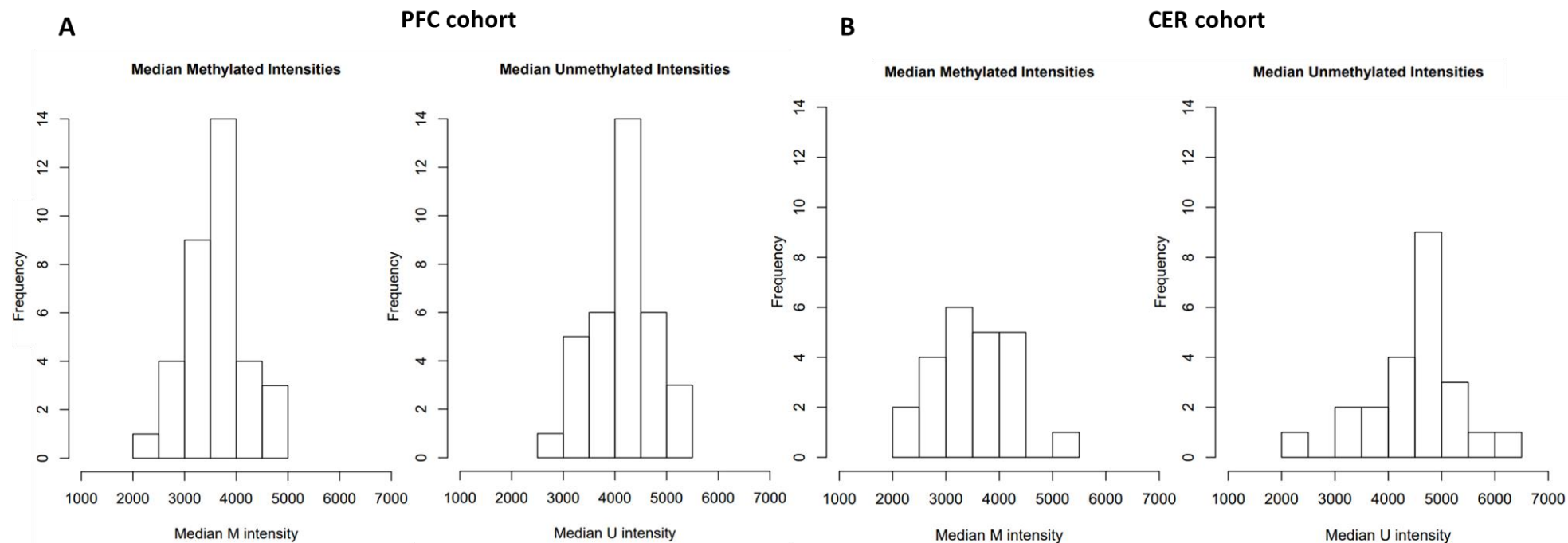
Figure 3.3 Example of raw signal intensities check as part of data quality control.
A) One of the PFC (GSE89707) and B) one of the CER cohorts (GSE137222) included in the suicide meta-analysis. The inspection of raw signal intensity across all samples is one way to identify poor performing samples (Wilhelm-Benartzi et al., 2013, Gujar et al., 2018). The median methylated signal intensity and unmethylated signal intensity for each sample was calculated per each individual cohort and samples which had signal intensities less than 1500 were excluded from further analysis.

3.4.1.2 Sodium bisulfite conversion rate

The ten sodium bisulfite conversion control probes on the array were used to calculate the efficiency of the conversion reaction and samples showing a score less than 90% were excluded from analysis (see **Figure 3.4**). No individual probes were discarded based on the BS conversion metrics.
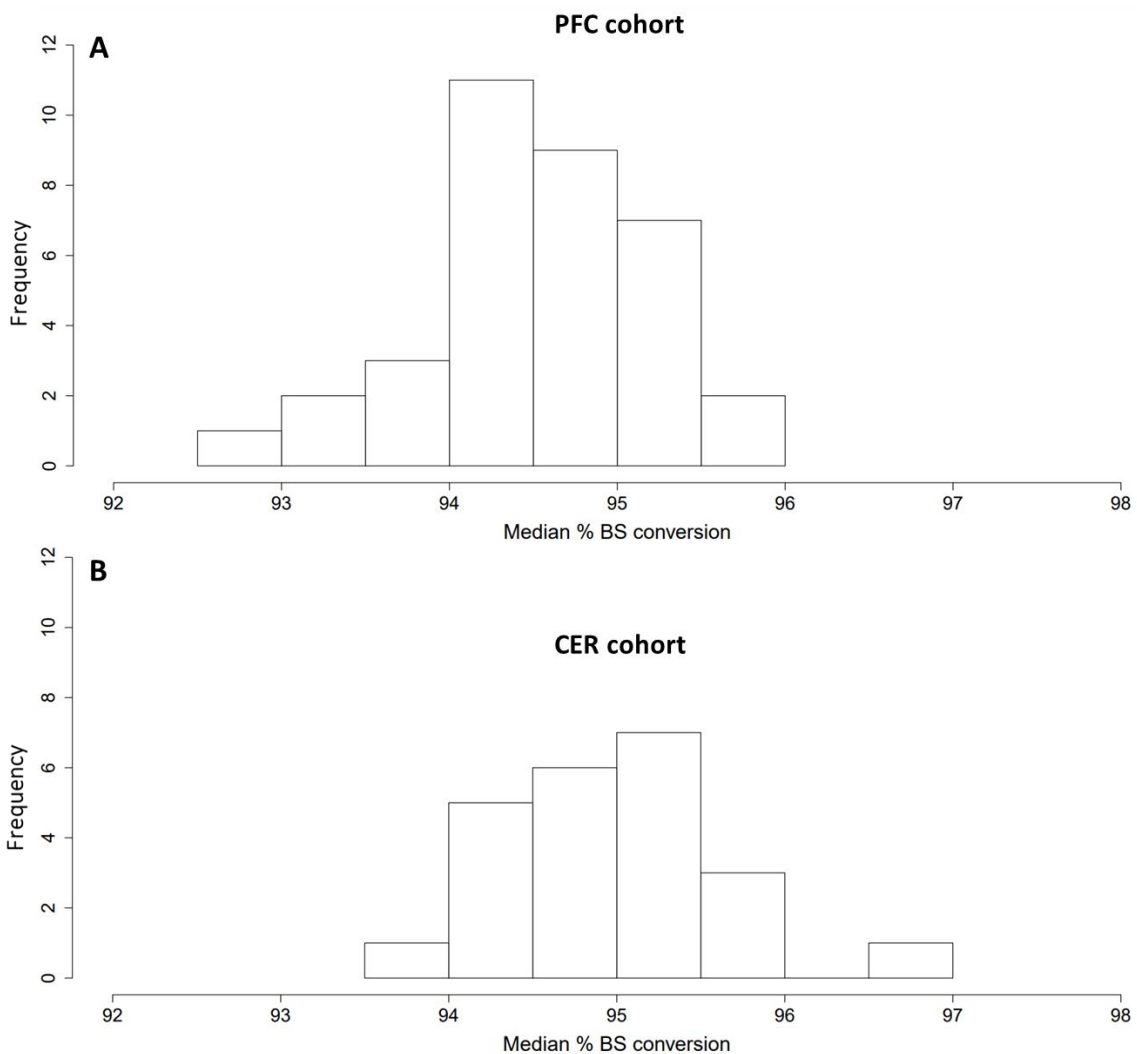
Figure 3.4 Histogram showing an example of the sodium bisulfite conversion rate.
A) One of the PFC (GSE89707) and B) one of the CER cohorts (GSE137223) included in the suicide meta-analysis. Only samples below the 90% bisulfite conversion threshold were excluded from further analysis.

3.4.1.3 Multi-dimensional scaling (MDS)

For each individual cohort, multi-dimensional scaling of both X and Y chromosomes were used to assess concordance between sex as recorded on post-mortem records and predicted sex using the 65 control SNPs (**Figure 3.5**).
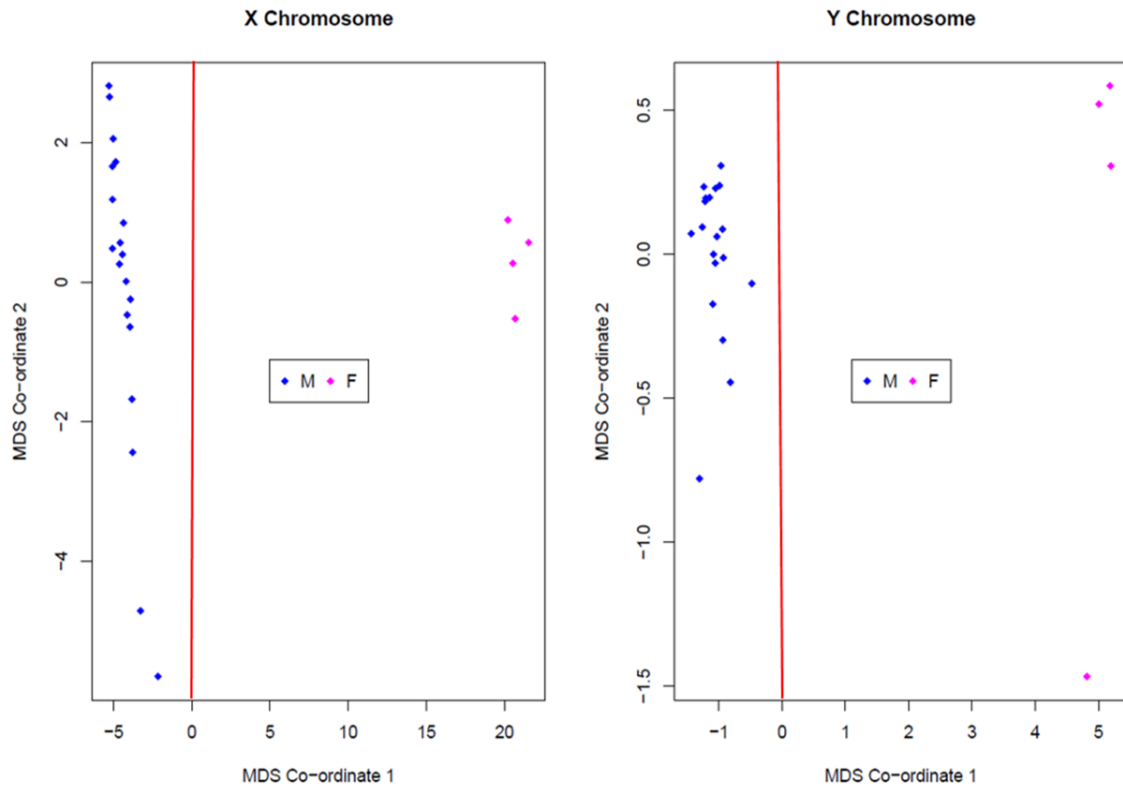
Figure 3.5 Example of Multi-dimensional scaling plot of sex chromosomes.
X-chromosome (A) and Y-chromosome (B) probes across all the samples of one of the CER cohort included for the meta-analysis (GSE137223). Reference line added, x-axis >0 =F, x-axis <0 =M. F, Female; M= Male. This was used to assess concordance between recorded and predicted sex in all samples in each individual PFC and CER cohorts included in the meta-analysis.

MDS plots of probes located on each of the autosomal chromosomes and for the thousand most variable probes across all samples were also used to check for group status (suicide/ctr) and batch effects related to microarray loading (see **Figure 3.6** for examples) in each individual cohort. Brain bank and ethnicity were also assessed as potential confounders in those PFC cohorts (GSE89707 and GSE41826 respectively) where these data were available and represented a potential source of bias (data not shown).
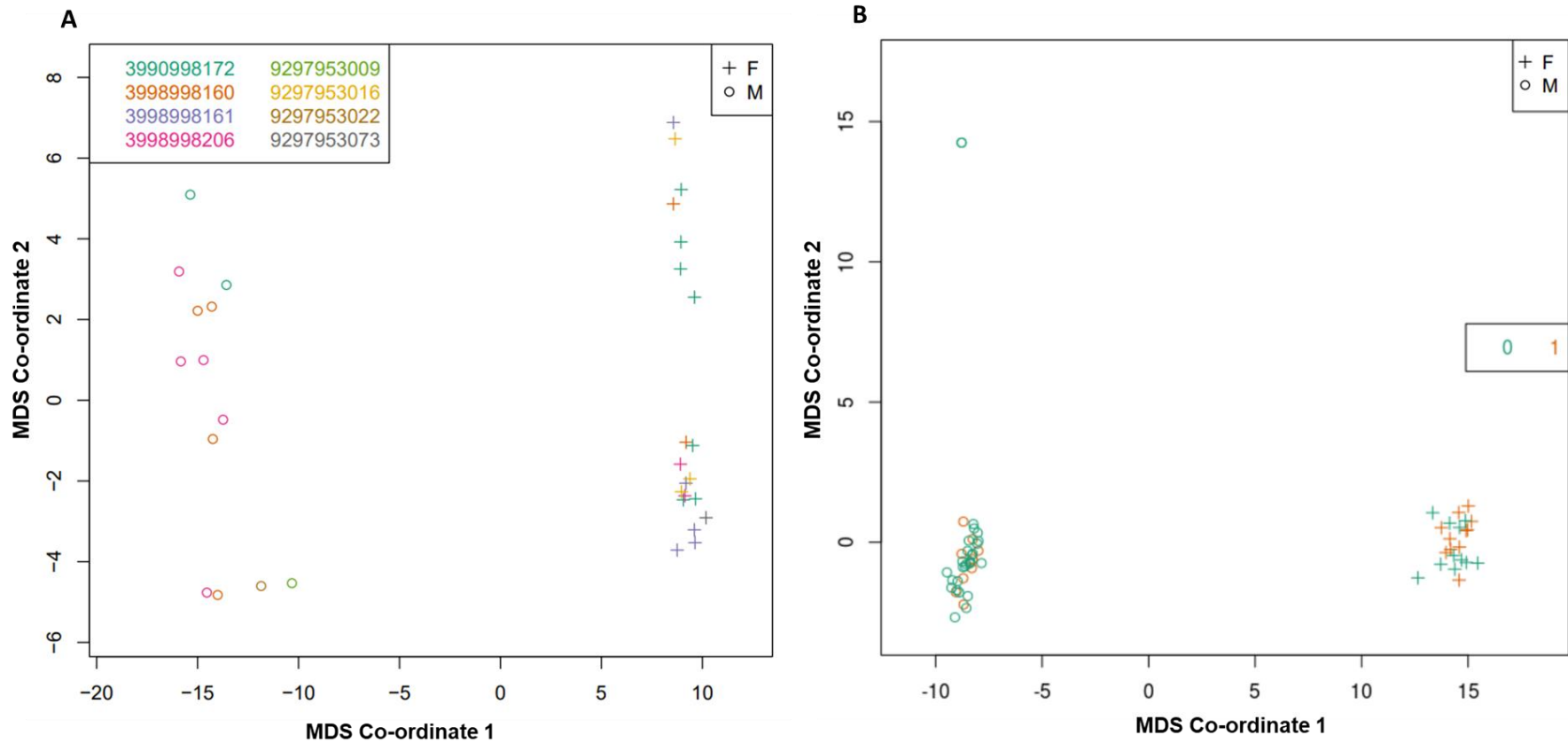
Figure 3.6 Examples of Multi-dimensional scaling (MDS) based data quality control revealing the existence of cohort substructures and sample relationships.

Plots were coloured by A) microarray chip, B) diagnosis (0= non-psychiatric control, 1= suicide) and different plot point styles were chosen to represent the sexes (Male, empty circle; Female, cross). In plot A is reported the data distribution for one of the PFC dataset (GSE88890). The samples do not show to cluster by microarray chip ID indicating that no obvious batch effect is associated with samples loading (technical variation) however samples do cluster by sex. Data shown in plot B belong to one of the CER cohorts (GSE137222) and similarly reveal samples clustering by sex but no by diagnosis.

3.4.1.4   *DNA methylation age calculation and tissue prediction*

The DNA methylation age online calculator (Horvath, 2013, Horvath, 2015) https://dnamage.genetics.ucla.edu/home) was used to estimate DNA methylation age for each sample. The DNA methylation age calculator was developed using 8,000 samples from a broad range of healthy tissues, cancer tissues and cell lines. The calculator allows the estimation of DNA methylation age from a complete 450K dataset, using weighted average data from 353 'clock CpGs', which is then transformed to DNA methylation age using a calibration function. Correlation coefficients between the chronological age and DNA methylation age was calculated for each sample from each cohort.

The tissue prediction feature within the online DNA methylation age calculator tool was used to predict the tissue of origin of each sample (Horvath, 2013) - https://dnamage.genetics.ucla.edu/home). This tool can be helpful in identifying mislabelled samples, although the author himself suggests caution in interpreting the predictions. All the samples that survived QC had matching reported tissue with the tissue predicted by the age calculator ("Brain prefCTX" and "Brain CRBLM" respectively). Moreover, the DNA Methylation age calculator (Horvath, 2013) also predicts sex from DNA methylation data. All the samples that passed QC had matching reported sex with the sex predicted by the age calculator (data not shown).

3.4.1.5   *Cell composition estimates*

The epigenetic profile of a cell contributes to its unique gene expression pattern and DNA methylation is known to be a marker of cell and tissue type (Roadmap Epigenomics et al., 2015, Rivera and Ren, 2013). Therefore using bulk tissue samples with a heterogeneous population of cells has obvious implications in EWAS which have made necessary the development of approaches to estimate cell type composition in different human tissues (Houseman et al., 2015, Guintivano et al., 2013).

In this study neuronal proportion was estimated for each sample using the Cell EpigenoType Specific (CETS) package in R (Guintivano et al., 2013) which estimates the cell type composition of a biological sample based on methylation data from Neun-sorted nuclei (Guintivano et al., 2013). One major limitation of this algorithm is that it has been developed and calibrated on DNA methylation

data from PFC samples which inevitably narrows its applicability on different brain regions given the considerable inter-tissue variability of DNA methylation (Byun et al., 2009). Moreover, age-related variation in the proportion of NeuN expressing (e.g. granule neurons) and non NeuN-expressing neurons (e.g. Purkinje neurons) has been reported in the CER proving CETS to be unsuitable for estimating cell composition in this brain region (Guintivano et al., 2013). For these reasons, the subsequent analyses on CER did not include neuronal proportion estimates as an independent variable.

3.4.1.6 *Data pre-processing and normalisation*

After these QC steps, remaining probes (≥400,000) in both PFC and CER were taken forward for analysis. Array data were normalised and the linear regression analysis was performed in each cohort individually and separately by brain region. **Table 3.6** at the end of this section reports the exact numbers of probes which remained after data normalisation and those included in the meta-analysis performed separately in each brain region.

3.4.1.6.1 *Removal of non-specific and polymorphic probes*

The 65 SNP probes, probes on sex chromosomes (Price et al., 2013, Chen et al., 2013) and probes with common (minor allele frequency (MAF) > 5%) SNPs in the CG or within 10 base pairs (bp) of single base extension position, as well as probes that are nonspecific or miss-mapped were flagged and discarded from the results (Chen et al., 2013).

3.4.1.6.2 *Sample and probe removal with pfilter*

The *pfilter* function of the wateRmelon package (Pidsley et al., 2013) was used to remove samples where 5% of sites had a detection p-value > 0.05. Specific sites were also removed if the beadcount was less than three in 5% of samples or if 1% of the samples had a detection p-value > 0.05 at that position. No samples were discarded at this stage of the analysis in any of the individual cohorts while between 2000 and 10000 sites were removed from the individuals PFC/CER cohorts. Plotting the mean raw β values density for all BS samples revealed a bimodal distribution (see **Figure 3.7** for an example).

3.4.1.6.3 Methylation beta densities

Data was pre-processed using the R package *wateRmelon* using the *dasen* function as previously described (Pidsley et al., 2013). DNA methylation (β) values were calculated from unmethylated (U) and methylated (M) signal [M/(U + M + 100)] and ranged from 0 to 1 (corresponding to 0 to 100% DNA methylation). **Figure 3.8** is representative of the distribution of the mean β values before (A) and after (B) quality control and normalisation steps for all probes.

Distribution of Beta Values
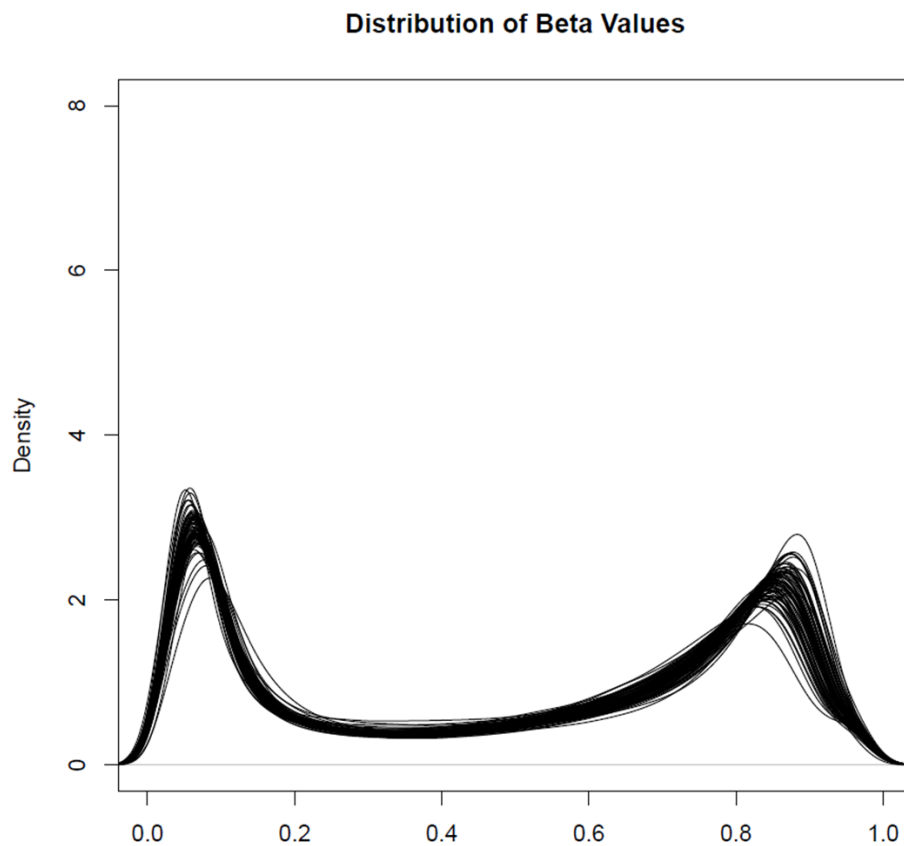
Figure 3.7 Density plot representative of the mean raw β values for all BS samples revealed a bimodal distribution.
Data shown for one of the CER cohort (GSE89702) included in the study.
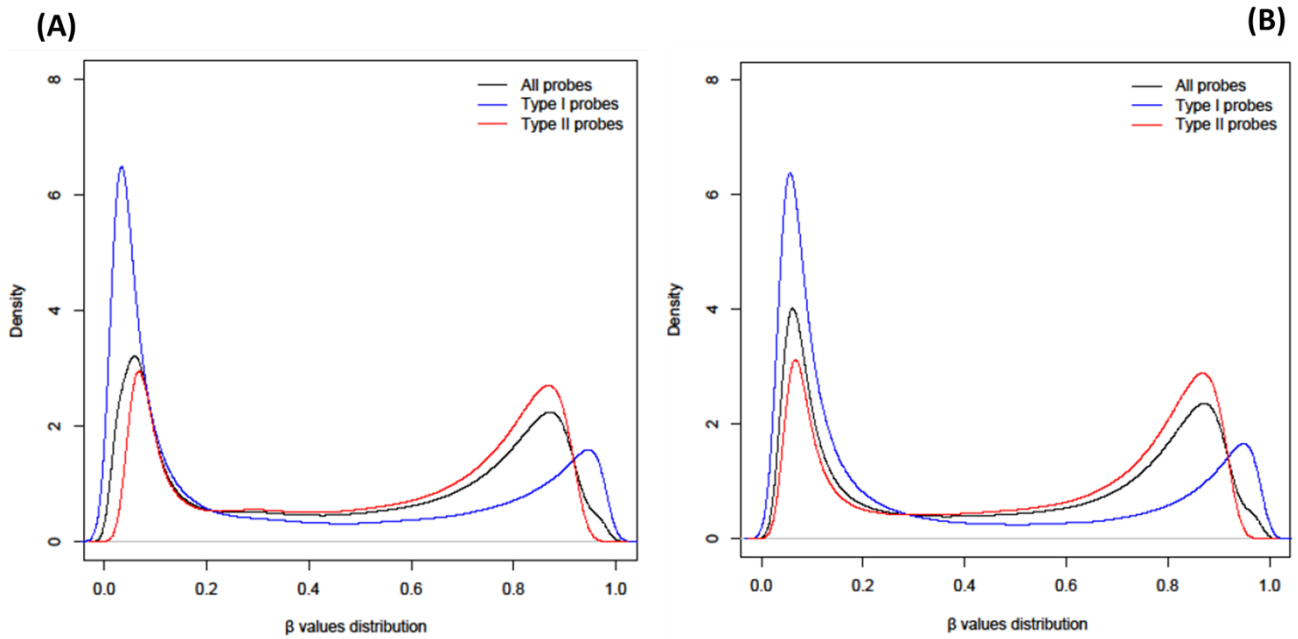
Figure 3.8 Density plots showing the β values distribution for one of the PFC cohort (GSE89707).
Shown are the β values distribution before (A) and after (B) quality control and normalisation steps for all probes (black), type I probes (blue) and type II probes (red).

Brain region	Cohort	No probes after Normalisation	No probes included for Meta-analysis
PFC	Viana J et al, 2017	428,152	407,457
	Guintivano J et al, 2013	425,815	
	Kozlenkov et al, 2017	423,164	
	Murphy et al, 2017	416,863	
CER	Viana e al, 2017	427,819	394,909
	Stanley Brain Bank 1	428,307	
	Stanley Brain Bank 2	804,351	

Table 3.6 Table summarising the N of probes which passed all steps of the QC and data normalisation as well as the actual number of probes taken forward for the brain region-specific meta-analysis.

3.4.1.6.4 Linear regression analysis

For the identification of differences in DNA methylation levels at individual probe specifically associated to SB, I performed a quantitative analysis in each brain region separately where samples were analysed using a linear regression model. The pre-processed and normalised DNA methylation (β) values of each cohort were included as the dependent variable and disease status, chronological age, sex and chip as independent variables. The bioinformatically derived CETS score was also included as a covariate and regressed out in the PFC analysis.

Other important phenotypical information (e.g. medication, smoking status) was not available and therefore these could not be included as independent variables. Although data have shown that ethnicity and smoking status can both be estimated from methylation data in peripheral tissue like blood tissue (Elliott et al., 2014) or placenta (Yuan et al., 2019), similar predictor tools have not been validated yet for brain tissue studies. Data were analysed separately for each brain region, probes were ranked by *P*-value, and Q-Q plots assessed to check for *P* value inflation (**Figure 3.9**).

The adjusted DNA methylation values for each probe and sample were calculated as follows:

a) Repeating the linear regression model for each brain region and cohort without including suicide status as an independent variable;

b) Calculating the sum of the regression residuals and intercept for each probe and sample.

A fixed effect meta-analysis on the adjusted mean DNA methylation values computed with inverse variance weights was performed for each probe using the *metacont* function from the *meta* package in R (Schwarzer G et al., 2015) (https://cran.r-project.org/web/packages/meta/meta.pdf). Only the probes that survived QC and were common to all the cohorts included in each brain region (see **Table 3.6** for exact numbers) were used in the meta-analysis.
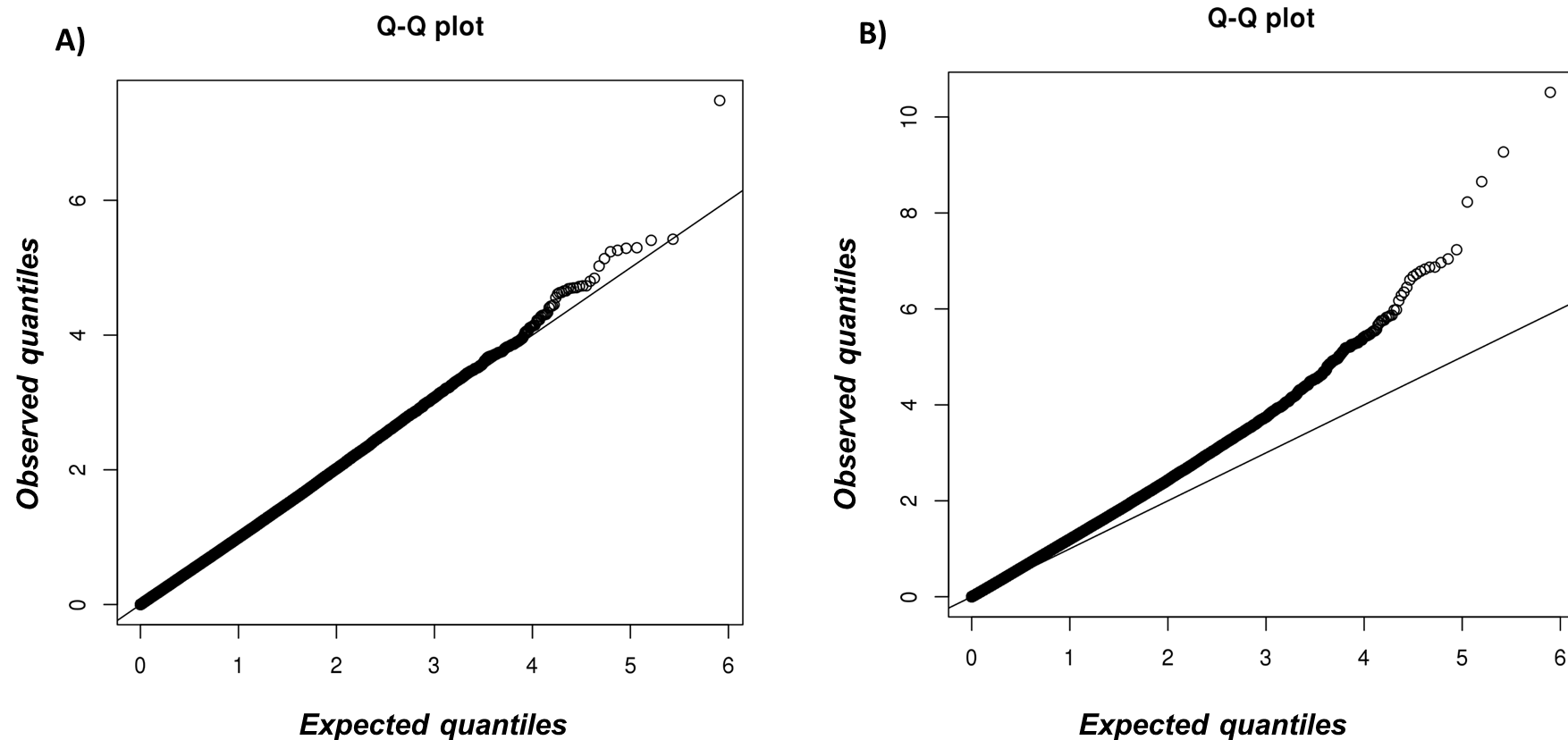
Figure 3.9 A) Quantile-quantile (Q-Q) plot Primary Meta-Analysis Pre-frontal Cortex.
Shown are the expected (x-axis) and observed (y-axis) quantiles in the meta-analysis of the PFC (four suicide cohorts included). QQ plot for the analysis in the human PFC highlights little evidence of systematic P-value inflation **B) Quantile-quantile (Q-Q) plot Primary Meta-Analysis Cerebellum**. *Shown are the expected (x-axis) and observed (y-axis) quantiles for the meta-analysis of the CER (three suicide cohorts included). The Q-Q plot for DNA methylation in the CER shows evidence of P value inflation in the analyses which could be explained by the impossibility to rule out the effect of cellular heterogeneity on DNA methylation quantification in CER cohorts. The CETS algorithm used to estimate neuronal proportions indeed, is not applicable to the CER and cannot inform about disease relevant DNA methylation differences in cell type proportions.*

3.4.2 Suicide-associated DMPs in human cortex

One DMP (cg00963169) which reached experiment-wide significance (P=3.30E-08 (**Figure 3.10**) was identified in the PFC. The effect size at this CpG site, located downstream of exon 1 of the neuron-specific protein coding gene, ELAV-like RNA binding protein 4 (*ELAVL4),* was largely consistent across all cohorts included (see **Figure 3.11**), showing hypomethylation in suicide cases relative to non-psychiatric controls. Interestingly, the 20 most significantly (P <5E-05) suicide-associated differentially methylated loci identified in the PFC, listed in **Table 3.7** include probes in the vicinity of several loci previously implicated in neuropsychiatric phenotypes. **Appendix E - Supplementary Figure 3.1** reports the heatmap showing the DNA methylation profile of the suicide-associated most variable DMPs across the PFC cohorts included in the meta-analysis study. Worth noting that probe cg20705321, which is located in proximity of the *C19orf38* locus on chromosome 19, reveals an opposite DNA methylation profile in the bulk cohorts (hypomethylation) compared to neuronal cohorts (hypermethylation) suggesting that DNA methylation differences can be driven by specific cell types.
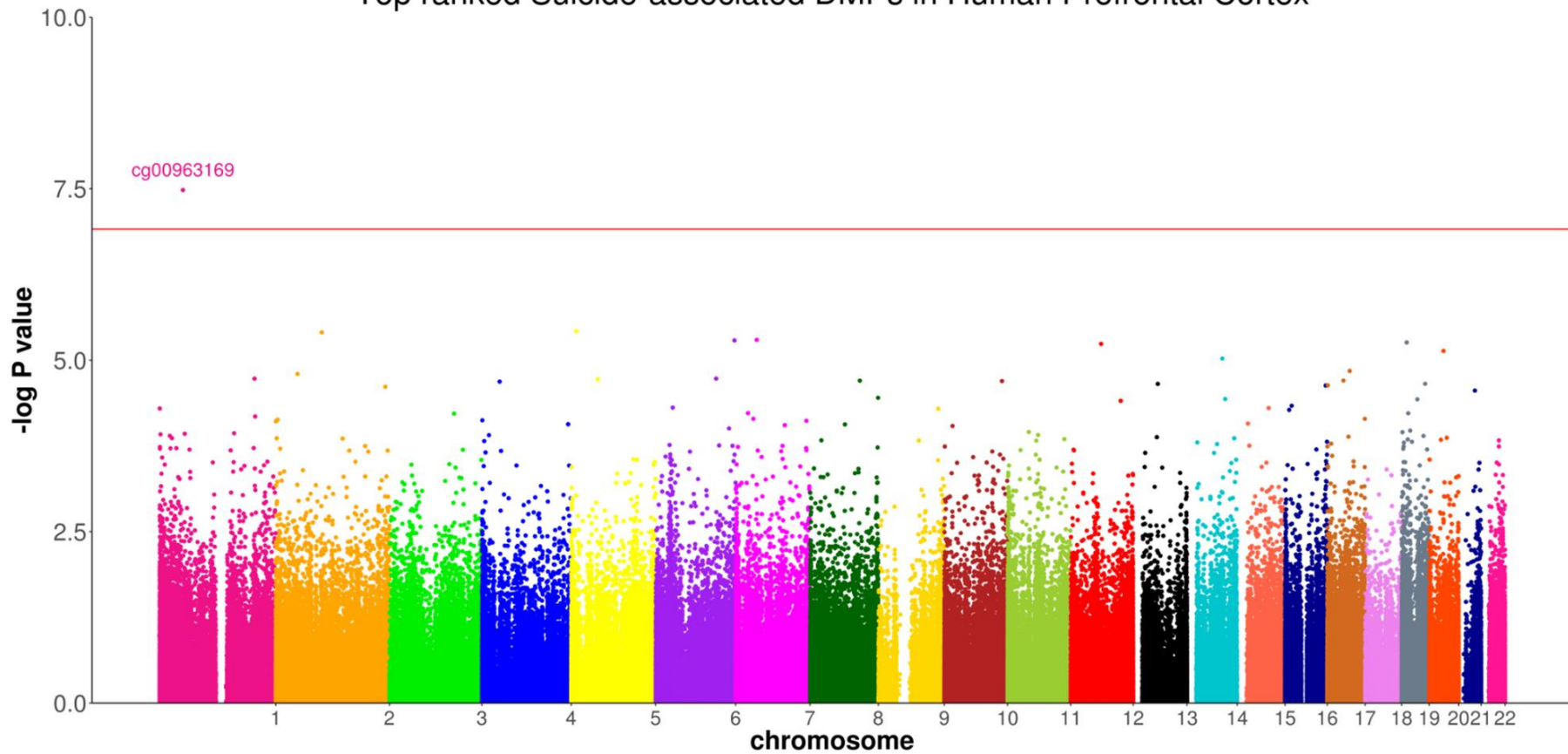
Figure 3.10 Manhattan plot of CpG associations with suicide in a meta-analysis of suicide cases and non psychiatric controls in human PFC.

Manhattan plot showing site-specific genome wide pattern of DNA methylation in the human Prefrontal Cortex (PFC). One CpG site (cg00963169) was identified as differentially methylated between suicide cases and non-psychiatric controls at experiment-wide significant (P=1E-07, indicated by the red line) in the PFC.

cg00963169 – ELAVL4

Cohort	DNAmΔ(%)	SE	95%-CI	Weight (fixed)	Weight (random)
cohort 1 (Bulk)	−0.19	0.2029	−0.19 [−0.58; 0.21]	15.2%	15.2%
cohort 2 (Bulk)	−0.67	0.4775	−0.67 [−1.61; 0.26]	2.7%	2.7%
cohort 3 (Neuronal)	−0.47	0.1126	−0.47 [−0.69; −0.25]	49.4%	49.4%
cohort 4 (Neuronal)	−0.49	0.1384	−0.49 [−0.76; −0.22]	32.7%	32.7%
Fixed effect model			−0.44 [−0.60; −0.29]	100.0%	--
Random effects model			−0.44 [−0.60; −0.29]	--	100.0%

Heterogeneity: $I^2 = 0\%$, $p = 0.57$

β effect size (% DNAmΔ)
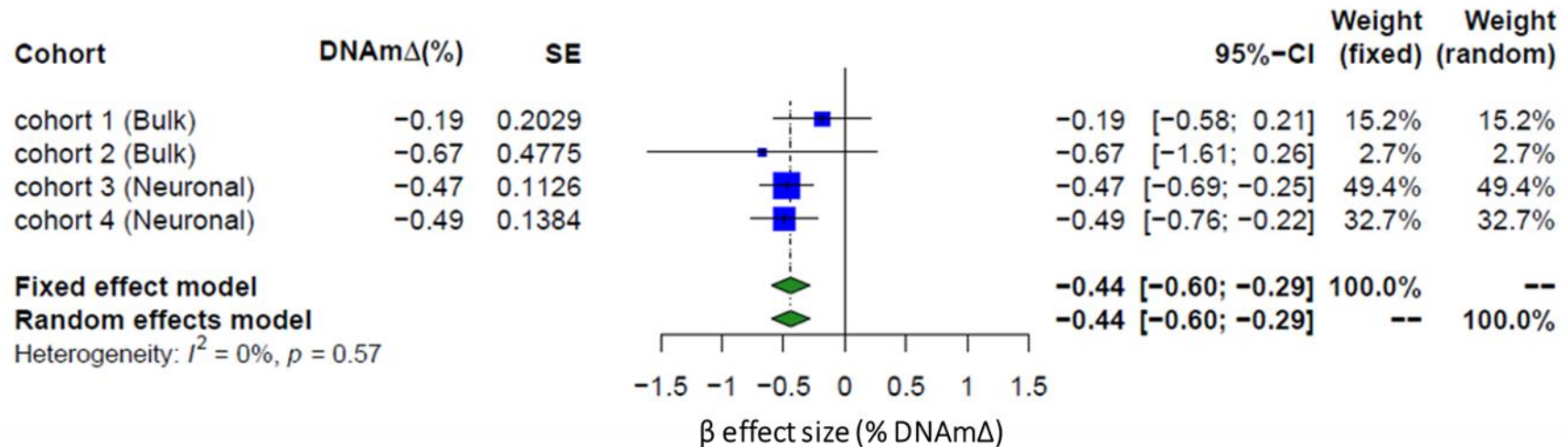
Figure 3.11 Top-ranked differentially methylated probe (DMP) in human Prefrontal Cortex (PFC).
Forest plot showing the effect size at the top ranked CpG site (cg00963169) which is largely consistent across all the independent studies included. Each square represents the point estimate of the effect for a single study, and its size is proportional to the weight of this included study.The horizontal line through the square represents the confidence interval (usually 95% CI) around the point estimate.The diamond at the bottom of the forest plot shows the result when all the individual studies are combined together and averaged, therefore the diamond represents the pooled effect estimate. The placement of centre of the diamond on the x-axis represents the point estimate, and the width of the diamond represents the 95% CI around this estimate. If the diamond shape does not touch the line of no effect (middle verticle line), the difference found between the two groups is statistically significant. DNAmΔ, DNA methylation changes (%); SE, standard errors; CI, confidence interval.

Probe ID	Mean Δβ (%)	P-value (Fixed Effect)	CHR	Hg19	Illumina Annotation (UCSC Ref Gene Name)	Probe Type	Gene annotation from GREAT (Distance from TSS)	SNP in Probe Sequence (>10bp from SBE)
cg00963169	-0.44	3.30E-08	1	Chr1:50513927	ELAVL4	I	ELAVL4 (-60666), AGBL4 (-24302)	
cg20963696	1.06	3.78E-06	5	Chr5:10679606	DAP	II	DAP (+81780), ROPN1L (+237633)	
cg15362194	-0.30	3.92E-06	2	Chr2:98262546	COX5B	I	COX5B (+26)	
cg18663341	-0.86	5.06E-06	7	Chr7:45148416	TBRG4	II	NACAD (-19924), TBRG4 (+2900)	
cg19477433	-1.08	5.15E-06	6	Chr6:168530427		II	FRMD1 (-50589), DACT2 (+189974)	
cg20705321	-1.07	5.52E-06	19	Chr19:10958970	C19orf38	I	C19orf38 (-135)	
cg07951810	0.57	5.79E-06	12	Chr12:65153561	GNS	II	GNS (-336)	
cg15570432	-0.86	7.33E-06	20	Chr20:30460881	TTLL9	II	DUSP15 (-2403), TTLL9 (+2377)	
cg08847533	-0.66	9.46E-06	14	Chr14:75593920	NEK9	I	NEK9 (-143)	rs12889309
cg00264958	-0.84	1.44E-05	17	Chr17:48023189		II	TAC4 (-97811), DLX4 (-23372)	rs12937307
cg00409434	-1.54	1.59E-05	2	Chr2:46414317	PRKCE	II	EPAS1 (-110223), PRKCE (+535275)	
cg26011314	-0.86	1.86E-05	6	Chr6:129255129	LAMA2	II	LAMA2 (+50844), ARHGAP18 (+776240)	
ch.1.3947147F	-2.62	1.86E-05	1	Chr1:203693763	ATP2B4	II	LAX1 (-40520), ATP2B4 (+97849)	
cg18392139	-1.20	1.89E-05	5	Chr5:56719150		II	ACTBL2 (+59485), GPBP1 (+209250)	
cg18100887	6.38	1.98E-05	17	Chr17:34611341		II	TBC1D3C (-19310), CCL3L1 (+14388)	
cg03976172	-1.76	1.99E-05	8	Chr8:106666746	ZFPM2	II	OXR1 (-793405), ZFPM2 (+335600)	
cg02522906	-1.12	2.02E-05	10	Chr10:123450196		II	FGFR2 (-92225), ATE1 (+237349)	rs2132902
cg19326874	-1.45	2.06E-05	4	Chr4:37903243	TBC1D1	II	PTTG2 (-58812), TBC1D1 (+10539)	
cg21712019	-0.39	2.21E-05	19	Chr19:50316342	FUZ	I	FUZ (+224)	
cg17872838	1.65	2.22E-05	13	Chr13:52607339	UTP14C	II	UTP14C (+4399), NEK5 (+95874)	

Abbreviations: PFC, Pre-frontal cortex; DMPs, differentially methylated positions; Hg19, Human Genome version 19; GREAT, Genomic Regions Enrichment of Annotations Tool; TSS, transcription start site; UCSC, University of California, Santa Cruz Genome Browser, SBE, Single binding extension.

Table 3.7 Top 20 suicide-associated DMPs in human PFC.

3.4.3 Suicide-associated DMPs in human cerebellum

In the CER, 6 probes (cg14392966, cg17855963, cg25590492, cg12284382, cg10757978, cg04525580) passed the experiment-wide significance threshold (P <1E-07) (**Figure 3.12**). Of interest is the top-ranked DMP, cg14392966 (P =3.06E-11) which is located within the coding region (exon1) of the *PUS3* gene on Chr11. This gene encodes a highly conserved enzyme responsible for posttranscriptional modification of tRNA and has been previously associated with intellectual disability (de Paiva et al., 2019) as well as severe neurodevelopmental disease (Abdelrahman et al., 2018). **Figure 3.13** shows that this DMP is hypomethylated in two of the three cohorts in suicide cases compared to non-psychiatric controls (Effect size = -0.79) showing that the direction of DNA methylation changes was not consistent across all three bulk studies assessed. Of interest, the sixth significant suicide-associated DMP found in the CER, *cg04525580 (*P = 9.08E-08*)* is located at the 5'-UTR of the interferon regulatory factor 2 (*IRF2)* gene. This locus plays an important role of transcriptional activation at promoters (Sun et al., 2018a) and regulate the expression of a variety of genes involved in immune responses in the brain (Drew et al., 1995). Finally, the top 20 suicide associated DMPs identified in this region, listed in **Table 3.8,** include probes in the vicinity of a number of loci previously implicated in the organogenesis of the CNS and cerebellum differentiation (e.g. *ZIC1*) or found to be crucial for the correct functioning of the brain (e.g. *RASD2*); furthermore, as shown in **Appendix E - Supplementary Figure 3.2** the DNA methylation profile at each reported DMP is mostly consistent across the cohorts included.
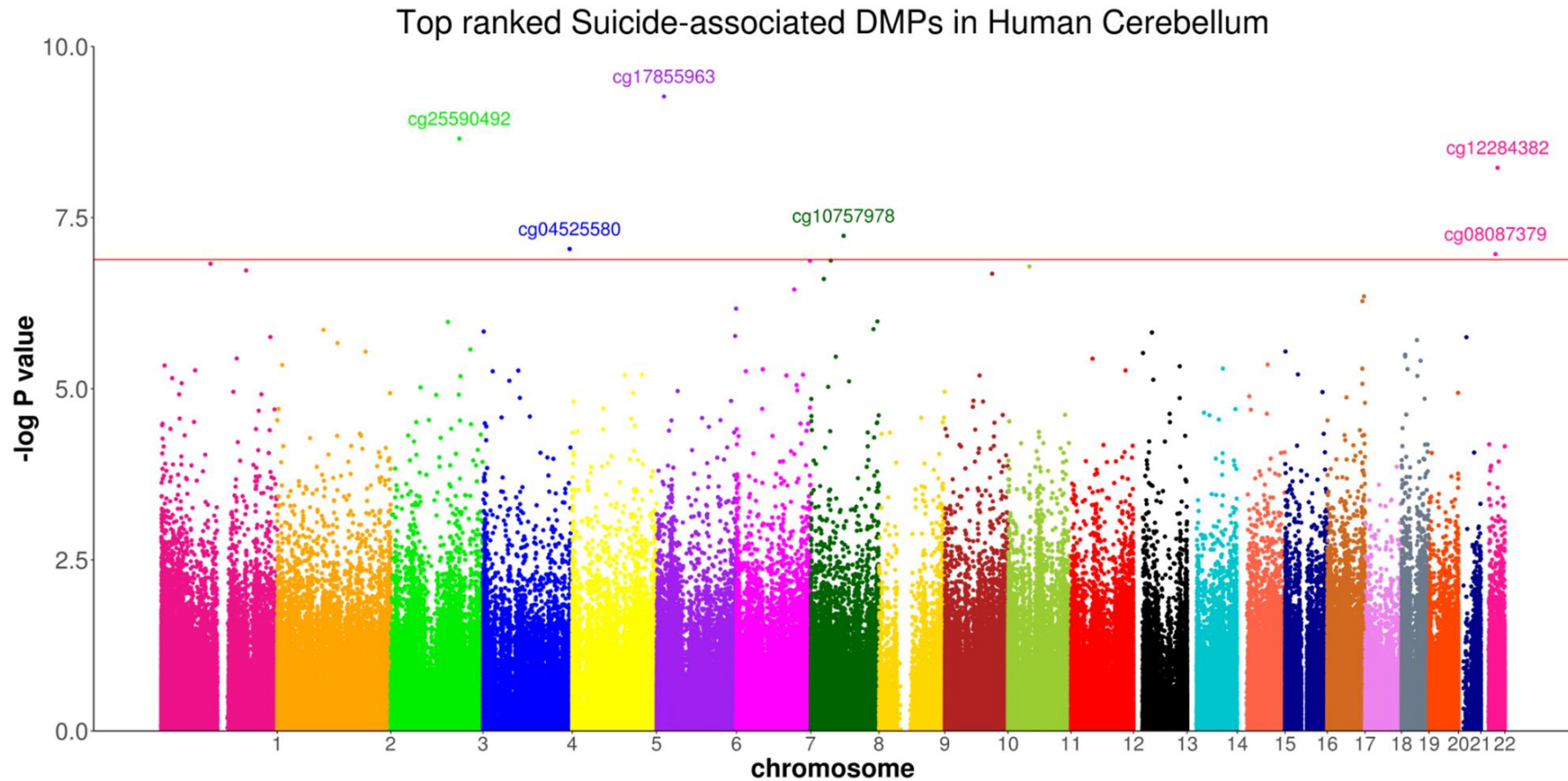
Figure 3.12 Manhattan plot of CpG associations with suicide in a meta-analysis of of suicide cases and non psychiatric controls in CER.
Manhattan plot showing site-specific genome wide pattern of DNA methylation in the human Cerebellum (CER). Six CpG sites were identified as differentially methylated between suicide cases and non-psychiatric controls at experiment-wide significant (P=1E-07, indicated by the red line) in the CER.
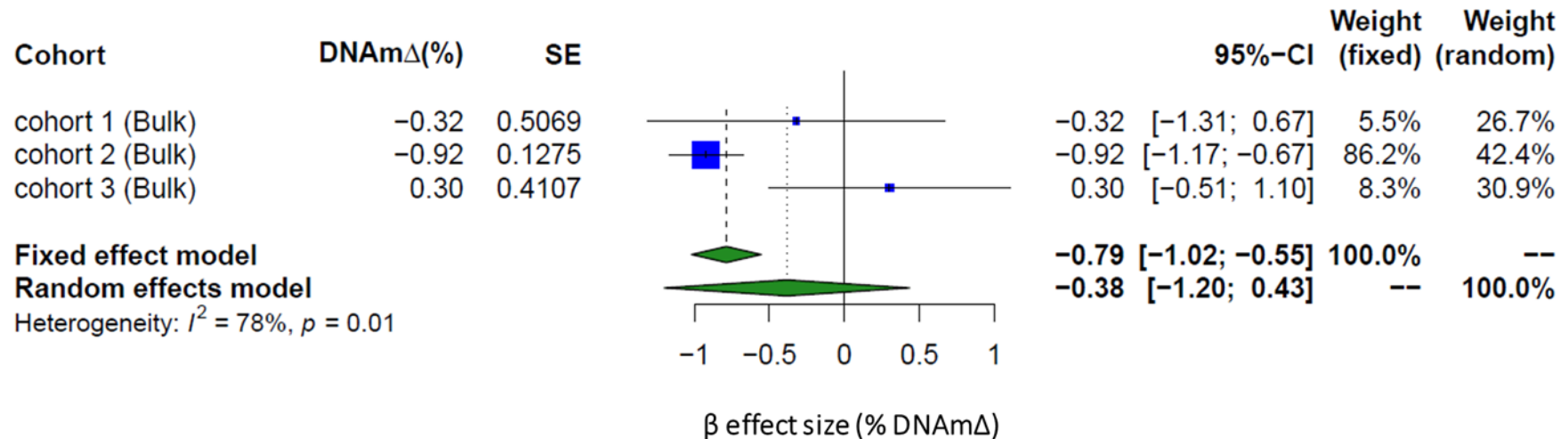
Figure 3.13 Top-ranked differentially methylated probe (DMP) in human Cerebellum (CER).
Forest plot showing the effect size at the top ranked CpG site (cg14392966) which shows inconsistent DNA methylation pattern across the independent studies included. This DMP, which was found hypomethylated in suicide cases compared to non-psychiatric controls in two of the three cohorts, is located in the promoter region of the pseudouridine synthase 3 (PUS3) gene encoding for a highly conserved enzyme responsible for posttranscriptional modification of tRNA. Each square represents the point estimate of the effect for a single study, and its size is proportional to the weight of this included study.The horizontal line through the square represents the confidence interval (usually 95% CI) around the point estimate.The diamond at the bottom of the forest plot shows the result when all the individual studies are combined together and averaged, therefore the diamond represents the pooled effect estimate. The placement of centre of the diamond on the x-axis represents the point estimate, and the width of the diamond represents the 95% CI around this estimate. If the diamond shape does not touch the line of no effect (middle verticle line), the difference found between the two groups is statistically significant. DNAmΔ, DNA methylation changes (%); SE, standard errors; CI, confidence interval.

Probe ID	Mean Δβ	P-value (Fixed Effect)	CHR	Hg19	Illumina annotation	Probe Type	Gene annotation from GREAT (Distance from TSS)	SNP in Probe Sequence (>10bp from SBE)
cg14392966	-0.786	3.06E-11	11	Chr11:125773125	DDX25;PUS3	I	DDX25 (-1146), PUS3 (-10)	
cg17855963	1.644	5.37E-10	6	Chr6:15873800		II	MYLIP (-255516), DTNBP1 (-210512)	
cg25590492	-1.504	2.22E-09	3	Chr3:147129952	ZIC1	II	ZIC1 (+2772)	
cg12284382	-2.662	5.92E-09	22	Chr22:35940438	RASD2	II	RASD2 (+3087), MB (+72945)	
cg10757978	3.261	5.84E-08	8	Chr8:70623125	SLCO5A1	II	SULF1 (+83119), SLCO5A1 (+124173)	rs2933044
cg04525580	1.156	9.08E-08	4	Chr4:185352181	IRF2	II	ENPP6 (-213068), IRF2 (+43544)	
cg08087379	4.569	1.08E-07	22	Chr22:31364274	TUG1;MORC2	II	MORC2 (-88)	
cg08982904	2.912	1.34E-07	8	Chr8:43127238		I	HGSNAT (+131647)	rs62516805
cg24197303	-1.704	1.35E-07	7	Chr7:157572599	PTPRN2	II	DNAJB6 (+442890), PTPRN2 (+807882)	
cg07419968	-1.686	1.49E-07	1	Chr1:106339081		II	NONE	
cg13702370	6.426	1.64E-07	11	Chr11:45844932		II	CRY2 (-24024), SLC35C1 (+19310)	
cg13606991	6.278	1.87E-07	1	Chr1:182556113	RNASEL	II	RNASEL (+2280), RGSL1 (+136858)	
cg17330203	1.708	2.09E-07	10	Chr10:101515599	CUTC	II	ABCC2 (-26863), COX15 (-23177)	
cg22230538	0.595	2.49E-07	8	Chr8:28258841		I	FZD3 (-92880), ZNF395 (-14865)	
cg24690692	-5.011	3.55E-07	7	Chr7:123842309		II	TMEM229A (-168787), GPR37 (+563371)	
cg01767927	1.855	4.47E-07	17	Chr17:78821024	RPTOR	II	CHMP6 (-144616), RPTOR (+302400)	
cg06791979	-7.151	5.25E-07	17	Chr17:75474070	SEPT9	II	TNRC6C (-526247), SEPT9 (+196579)	
cg03914925	1.712	6.75E-07	6	Chr6:170405976		II	DLL1 (+193720), C6orf70 (+254256)	
cg10548399	2.184	1.04E-06	8	Chr8:143009151		II	FLJ43860 (-491822), TSNARE1 (+475391)	
cg02464608	2.144	1.06E-06	3	Chr3:122631723	SEMA5B	II	SEMA5B (+114852), DIRC2 (+117823)	

Abbreviations: CER, cerebellum; DMPs, differentially methylated positions; Hg19, Human Genome version 19; GREAT, Genomic Regions Enrichment of Annotations Tool; TSS, transcription start site; UCSC, University of California Santa Cruz Genome Browser; SBE, Single binding extension.

Table 3.8 Top 20 suicide-associated DMPs in human CER.

3.4.4 Region-based analysis of altered DNA methylation in suicide completers

The python module, Comb-p (Pedersen et al., 2012) was used to identify DMRs in suicide cases compared to controls in each brain region. The regional analysis identified three and eight significant (Sidak-corrected P <0.05) DMRs in the PFC and CER, respectively (See **Table 3.9** for details). In the PFC, the top-ranked DMR was found within the *WRB* gene (Sidak-corrected P =5.11E-06) and was consistently hypomethylated across all five CpG sites in suicide cases relative to controls, in all four PFC methylomic studies (**Figure 3.14**). Of interest, the second top-ranked suicide-associated DMR in the PFC (Sidak-corrected P = 3.81E-05) was located upstream of the *PSORS1C3* non-coding gene, a DMR previously reported by my group as associated with MDD suicide completers (Murphy et al., 2017).

In the CER, the top-ranked suicide-associated DMR was identified on chromosome 22, distributed along the intronic region of the *CERC2* gene and spanning four CpG sites. The *CERC2*-associated DMR (**Figure 3.15**) showed significant hypermethylation (Sidak-corrected P =5.68E-07) across all four CpG sites within the region in suicide cases compared with controls. The direction of this change was found to be consistent across all three CER methylomic studies.

Table 3.9. **Comb-p differentially methylated region (DMR) analysis**

Brain region	Hg19	Annotated gene (UCSC)	No. Of probes	Slk *P*-value	Sidak *P*-value
PFC	chr21:40759534-40759695	*WRB*	5	2.02E-09	5.11E-06
	chr6:31148370-31148553	*PSORS1C3*	10	1.71E-08	3.81E-05
	chr22:38071168-38071189	*LGALS1*	3	3.37E-08	0.0006529
CER	chr22:17956453-17956561	*CECR2*	4	1.55E-10	5.68E-07
	chrX:79590789-79590956	*CHMP1B2P*	4	3.74E-09	8.84E-06
	chr13:99100506-99100587	*FARP1*	3	2.68E-09	1.31E-05
	chr6:31838402-31838529	*SLC44A4*	5	2.68E-08	8.32E-05
	chr3:149374761-149374915	*WWTR1*	3	7.56E-08	0.0001938
	chr12:116756805-116756949	*MED13L*	3	8.64E-08	0.0002369
	chr1:1846046-1846155	*CALML6*	3	9.40E-08	0.0003406
	chr11:2397486-2397686	*CD81-AS1*	4	2.10E-06	0.004138

Abbreviations: CER, Cerebellum; PFC, prefrontal cortex; Hg19,Human Genome version 19; UCSC, University of California, Santa Cruz Human Genome Browser. Stouffer-Liptak-Kechris correction (slk); one-step Sidak (1967) multiple-testing correction.

Table 3.9 Differentially methylated regions (DMRs) analysis.
Regional analysis was performed using the Python module Comb-p (Pedersen et al, 2012) to detect functionally relevant DNA methylation-suicide associations. Respectively, three and eight significant (Sidak corrected P < 0.05) DMRs were identified in the human PFC and CER.
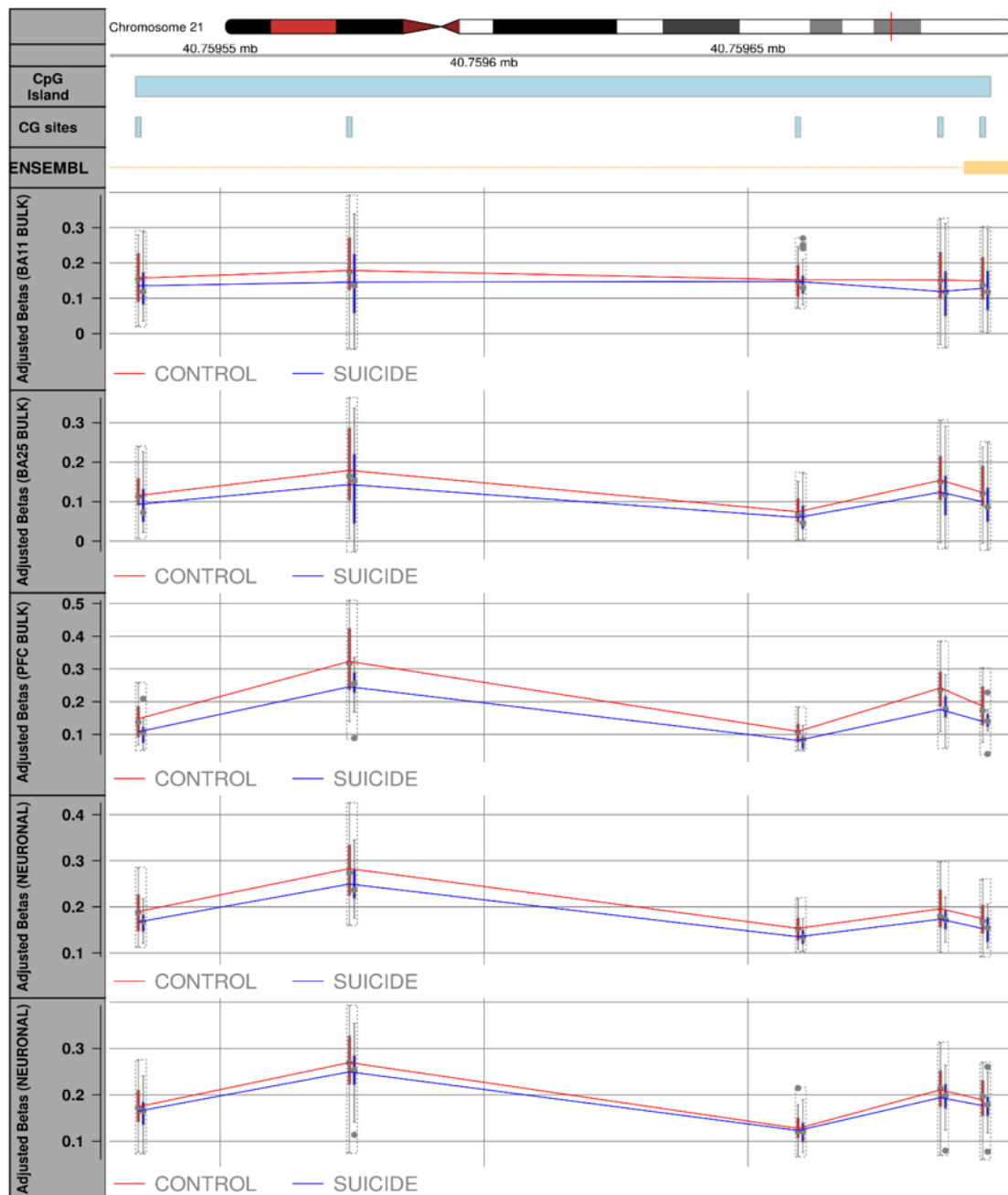
Figure 3.14 Suicide-associated differentially methylated region (DMR) in human Prefrontal cortex (PFC).
Plot showing the effect size for the top-ranked DMR in the PFC. This DMR, spanning five CpG sites and located in the promoter region of the WRB gene (Sidak corrected P = 5.11 E-6) was found consistently hypomethylated in suicide cases compared to non-psychiatric controls, across all four independent suicide brain cohorts included. The solid line is for illustration purposes and not indicative that the CpG sites between sites are also methylated.
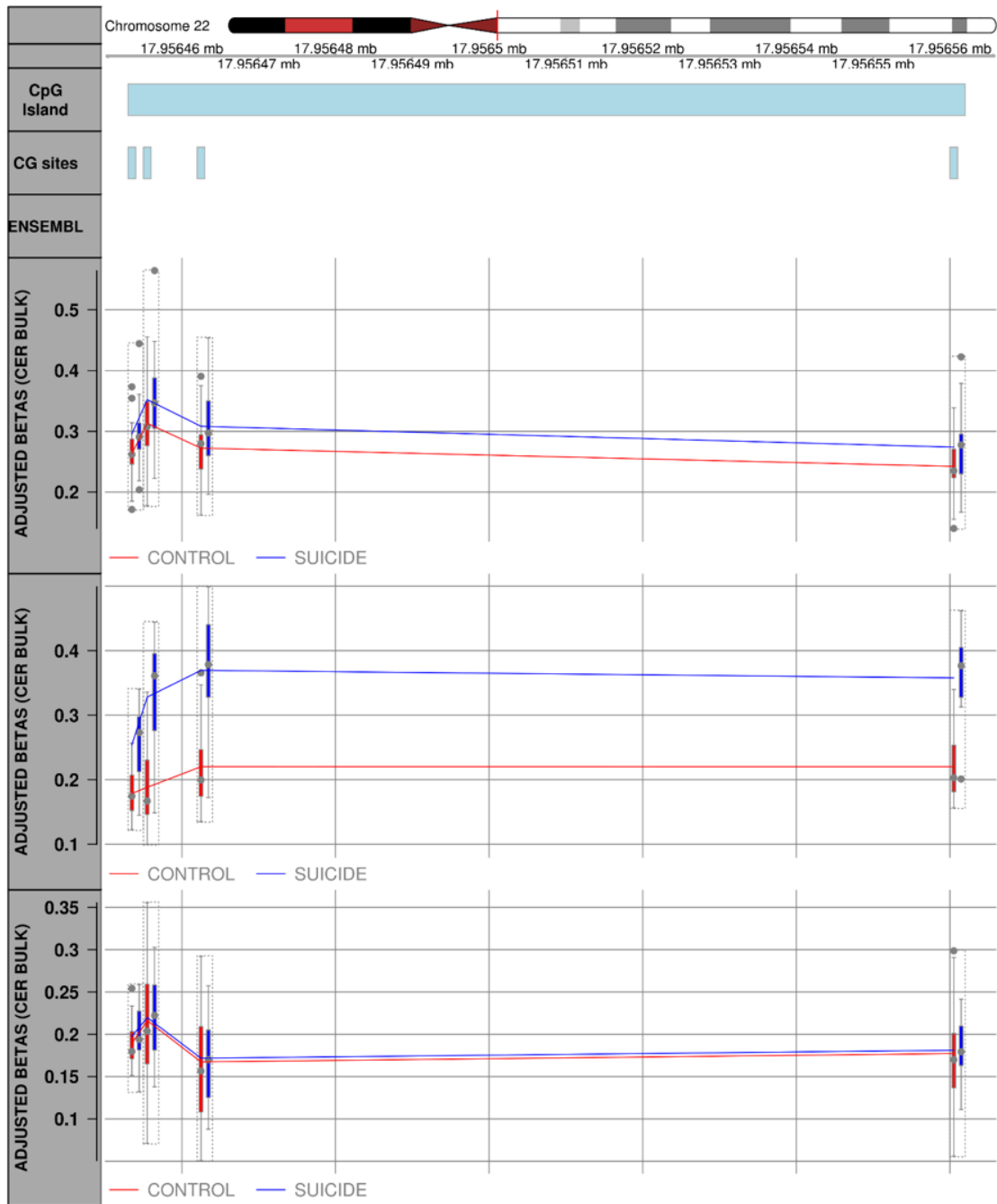
Figure 3.15 Suicide-associated differentially methylated region (DMR) in human Cerebellum (CER).

Plot showing the effect size for the top-ranked DMR in the CER. This DMR, spanning four CpG sites and located within the coding region of the CECR2 gene (Sidak corrected P = 5.68 E-7), was found consistently hypermethylated in suicide cases compared to non-psychiatric controls, across three independent suicide brain cohorts. The solid line is for illustration purposes and not indicative that the CpG sites between sites are also methylated.

187

3.4.4.1 *Technical validation of the top-ranked DMR in cerebellum samples*

To further confirm that *CERC2* epigenetic changes associated with suicide are driven by DNA hypermethylation, BS pyrosequencing was used to quantify DNA methylation across an extended region spanning four CpG sites (see section 3.3.9 for assay details). None of the four CpG sites assessed were characterised by significant ($P< 0.05$) suicide-associated hypermethylation (see **Appendix E - Supplementary Figure 3.3**) Due to time constraints additional pyrosequencing assays were not designed. However, the 450K assay data were previously validated within my group using bisulfite pyrosequencing in another study (Murphy et al., 2017).

3.4.5 *DNA methylation cross-region correlations*

To further investigate overlap between the two brain region-specific meta-analyses correlation was assessed between DNA methylation differences at the 500 top ranked (based upon *P* values) suicide-associated probes identified in the CER and the DNA methylation differences in the same probes in the PFC (**Figure 3.16A**) and vice versa (**Figure 3.16B***).* Comparison of the PFC versus CER DMPs suggest low correlation between two datasets therefore very little overlap (Pearson's R=0.09, *P*=0.043). In contrast, comparison of findings between the CER versus PFC DMPs showed a weak negative correlation (CER versus PFC: Pearson's R= -0.10, P= 0.028; PFC versus CER: Pearson's R= -0.09, P= 0.043).Taken together, these data appear to suggest limited overlap in suicide-associated DMPs across different brain regions. However, it is important to acknowledge that the two sets of probes (i.e top 500 based on *P* values ranking) selected to investigate potential cross-region correlations have very small effect size (<3% difference in DNA methylation for the majority of PFC probes) which makes difficult to draw definitive conclusion from this analysis.
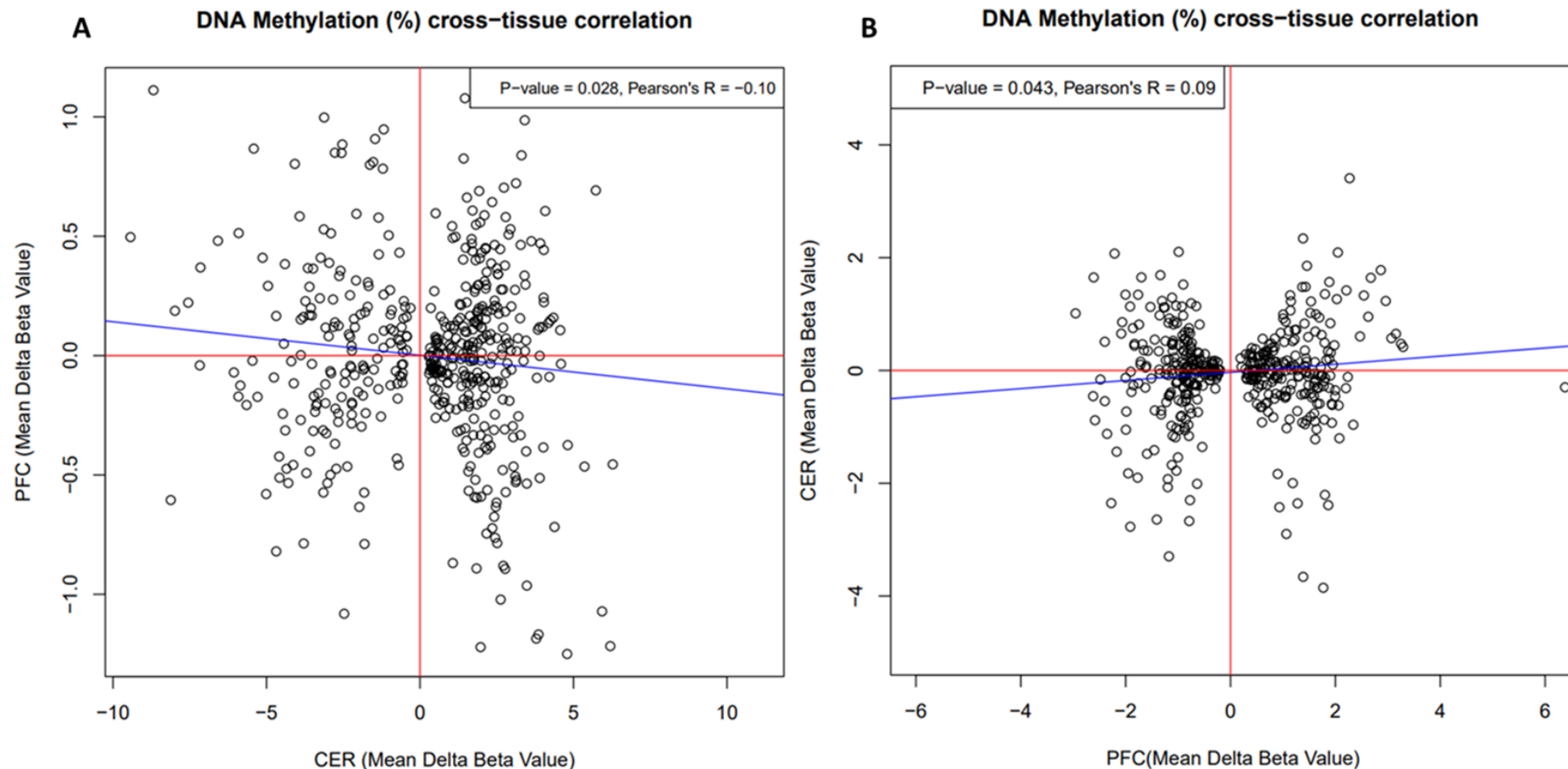
Figure 3.16 DNA methylation cross-tissue correlations.
*Correlation of effect sizes (mean adjusted beta difference) across the two brain regions, PFC and CER, of matched probes at **(A)** 500 top-ranked CER specific suicide-associated DMPs and **(B)** 500 top-ranked PFC specific suicide-associated DMPs. (CER versus PFC: Pearson's R= -0.10, P= 0.028; PFC versus CER: Pearson's R= -0.09, P= 0.043).The red lines in correspondence of y=0 and x=0 devides each plot in four quadrants which help to visualise how concordant the effect sizes are as those in the top right and bottom left quadrants have the same direction of effect. Relationships of effect sizes can be observed in all quadrants of **A** and **B** suggesting thay the effect sizes in CER are not significantly correlated with the effect sizes in PFC. Overall the effect sizes in PFC appear to be much lower than those in CER. PFC, Prefrontal cortex; CER, Cerebellum; DMP, differentially methylated position.*

3.4.6 Suicide-associated DNA methylation differences - Bulk versus neuronal

PFC bulk brain cohorts and FACS-sorted neuronal cohorts were meta-analysed separately in order to assess whether the results obtained in the primary meta-analysis (see section 3.4.2 for details) were driven by a specific cell type.

The site-specific genome wide DNA methylation analysis conducted in the neuronal datasets revealed that the association with suicide at the top-ranked PFC DMP (cg00963169) was largely driven by the neuronal cohorts (Effect size:-0.48) (**Figure 3.17**). Moreover, two additional DMPs in the neuronal cohorts showed suggestive evidence for association ($P < 5E{-}05$): cg20705321 located in proximity (TSS200) of *C19orf38 (P =4.75E-07)* and cg11017923 associated to the *ZBTB46* gene *(P = 7E-07) (*See **Figure 3.18***)*. Finally, no significant DMRs were identified when regional analysis was performed in the PFC neuronal cohorts.
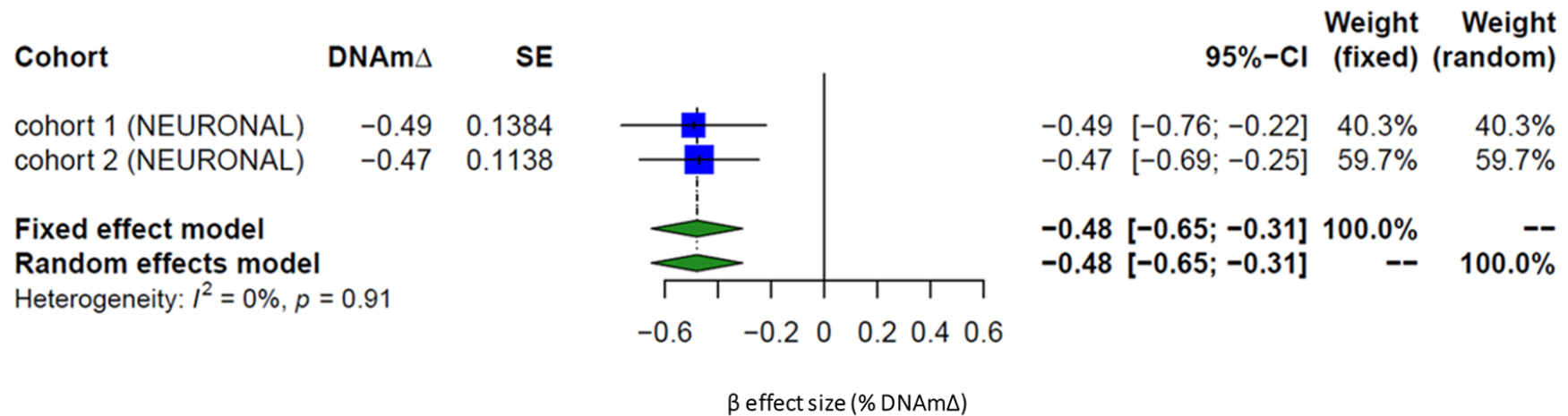
Figure 3.17 Neuronal PFC Meta-Analysis - Top-ranked differentially methylated probe (DMP).
Forest plot showing the effect size at the top ranked CpG site (cg00963169) when only the neuronal cohorts were included. Each square represents the point estimate of the effect for a single study, and its size is proportional to the weight of this included study.The horizontal line through the square represents the confidence interval (usually 95% CI) around the point estimate.The diamond at the bottom of the forest plot shows the result when all the individual studies are combined together and averaged, therefore the diamond represents the pooled effect estimate. The placement of centre of the diamond on the x-axis represents the point estimate, and the width of the diamond represents the 95% CI around this estimate. If the diamond shape does not touch the line of no effect (middle verticle line), the difference found between the two groups is statistically significant. DNAmΔ, DNA methylation changes (%); SE, standard errors; CI, confidence interval.

Figure 3.18 Neuronal PFC Meta-Analysis - Manhattan plot of CpG associations with suicide in a meta-analysis of suicide cases and non psychiatric controls.

The top-ranked PFC CpG site (cg00963169) confirmed to be the most variable probe even when only the neuronal cohorts were included for the analysis (P =1E-07) in the PFC. Interestingly, two additional suggestive significance probes (ZBTB46-associated cg1107923, P=7.03E-07; c19orf38-associated cg20705321 P=4.8E-07) were identified. Experiment wide P value cut-off of 1E-07 is indicated by the red line while the suggestive significance P value cut-off of 1E-06 is indicated by the blue line.

Analysis of the bulk tissue cohorts identified no differentially methylated probes that reached experiment wide statistical significance. However, two suggestive significance suicide-associated DMPs were identified (see **Figure 3.19**): cg18100887 located in proximity of the *D63785* gene (Closest TSS gene) and cg23563733 – located within the gene body of *LAMA2* locus. The top-ranked DMP cg18100887 (P=4E-07) showed consistent hypermethylation in suicide cases relative to non-psychiatric controls (effect size=8.45) while the second top-ranked DMP, cg23563733 (P=5.26E-07) was consistently hypomethylated in suicide cases relative to non-psychiatric controls (effect size= -3.83). Interestingly, the same locus, *LAMA2,* was also listed among the top 20 most variable DMPs (P = 1.86E-05) in the main PFC meta-analysis.

Finally, Comb-P regional analysis was performed including exclusively the PFC bulk cohorts (N=2) and seven suicide-associated DMRs survived the multiple testing correction (Sidak corrected P ≤ 2.38E-04) (see **Table 3.10** for details) among which the *PSORS1C3* DMR (Sidak P= 3.81E-05) already identified in the main PFC meta-analysis showing therefore that methylation level at this region is likely to be the result of cumulative changes happening across multiple cell types rather than driven by a specific neural cell type. Of interest is the top-ranked DMR (Sidak *P*= 8.55E-11) which is associated to the *CD2* locus, recently reported as involved in SCZ-related cognitive dysfunction in a mouse model (Grimm et al., 2018). Also noteworthy is the second top-ranked (*Sidak P*= 1.06E-07) PFC bulk DMR associated to the gene encoding the zinc finger protein 57 (*ZFP57*) on chr6 and spanning over 13 probes. Preferentially expressed early in development, *ZFP57* it is a transcriptional regulator, acting in the maintenance of imprinting (Zuo et al., 2012, Li et al., 2008b) and in DNA methylation (Quenneville et al., 2011, Plant et al., 2014). Methylomic changes (hypermethylation) at this locus have been reported in individuals with psychosis exposed in utero to endocrine disrupting compounds (Rivollier et al., 2017) and in a more recent study, *ZFP57* was found to be more methylated in cerebellar tissue of autistic female patients compared to female controls (Ladd-Acosta et al., 2014). Furthermore, SNPs in *ZFP57* have been associated with the immune response (Ovsyannikova et al., 2015) again reinforcing the hypothesis of the involvement of the immune system in SB. Lastly, in a study examining longitudinal changes of genome-wide blood DNA methylation profiles in relation to the development of post-traumatic stress disorder (PTSD) symptoms, decreased DNA methylation at the *ZFP57* DMR was

found to be associated with susceptibility to PTSD and broader expression of psychopathology in two independent samples, and by using two techniques for measuring DNA methylation levels (pyrosequencing-based DNA methylation results and the array-based results) (Rutten et al., 2018). Another locus of potential interest identified through the regional analysis is the TAP binding protein (*TAPBP*) (*Sidak P*=9.93E-07), component of the antigen processing machinery of the MHCI pathway. In a mouse study, increased expression of *TAPBP* was found to be associated to age-related hippocampal changes (deficits in spatial learning and memory) that may contribute to cognitive decline (VanGuilder Starkey et al., 2012). Finally, worth mentioning is the Ceramide Synthase 3 (*CERS3)*-associated DMR. Located on chr 15 and spanning over four CpG sites, this region remained nominally significant in the Bulk only analysis after multiple testing correction (Sidak P=2.38E-04). Ceramides are known to be important in embryogenesis (Rabionet et al., 2008, Park et al., 2010b) and this locus has been previously reported to be consistently differentially methylated in SCZ in a study investigating post-mortem PFC tissue in order to identify brain-specific epigenetic markers of SCZ (Wockner et al., 2015) further supporting the idea that this locus is a key epigenetic factor in the aetiology of SCZ and normal brain neurodevelopment.
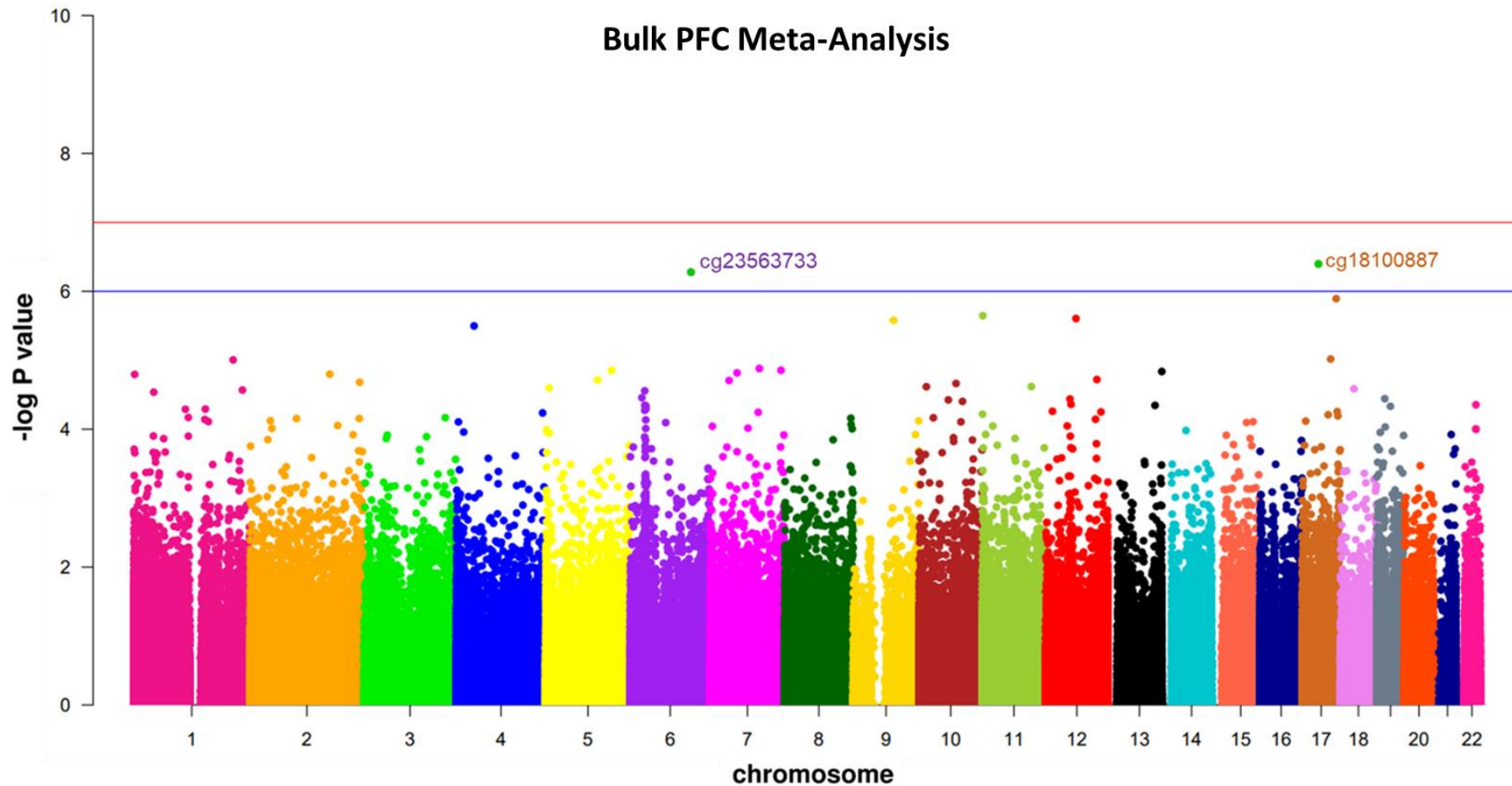
Figure 3.19 Bulk PFC Meta-Analysis - Manhattan plot of CpG associations with suicide in a meta-analysis of suicide cases and non-psychiatric controls.

No differentially methylated probes reached statistical significance when only bulk datasets were included in the Meta-Analysis. However, two suggestive significance probes (LAMA2-associated cg23563733, P=5.26E-07; cg18100887, P=4E-07) were identified. Experiment wide P value cut-off of 1E-07 is indicated by the red line while the suggestive significance P value cut-off of 1E-06 is indicated by the blue line.

Comb-p differentially methylated region (DMR) analysis in Human Prefrontal Cortex - Bulk Meta-Analysis

Brain region	Hg19	Annotated gene (UCSC)	No. Of probes	Slk P-value	Sidak P-value
PFC	chr1:117317838-117318233	*CD2*	6	8.15E-14	8.55E-11
	chr6:29648345-29648629	*ZFP57*	13	7.27E-11	1.06E-07
	chr6:33280390-33280519	*TAPBP*	9	3.09E-10	9.93E-07
	chr5:1841548-1841623	*LINC02116*	3	3.98E-09	2.20E-05
	chr12:54071090-54071195	*ATP5G2*	5	5.89E-09	2.33E-05
	chr6:31148370-31148553	*PSORS1C3*	10	8.36E-08	1.89E-04
	chr15:101084980-101085112	*CERS3*	4	7.58E-08	2.38E-04

Abbreviations: PFC, Prefrontal Cortex; Hg19, Human Genome version 19; UCSC, University of California, Santa Cruz Human Genome Browser. Stouffer-Liptak-Kechris correction (slk); one-step Siidak (1967) multiple-testing correction.

Table 3.10 Bulk PFC Meta-Analysis, differentially methylated region (DMR) Analysis.
Comb-p table reporting the details of the regional analysis. Seven DMRs identified in this meta-analysis survived the multiple testing correction (Sidak-corrected P ≤ 2.38E-04).

3.4.7 Suicide–associated DMPs identified in the CER are largely independent of comorbid psychiatric disorders.

In order to disentangle the relative contribution of psychopathology to DNA methylation levels specific to suicide, an additional meta-analysis was conducted in the CER whereby all the non-psychiatric controls initially included in the meta-analysis were excluded and individuals with documented Axis I psychiatric disorders (MDD, SZ, BD) and who died by suicide were compared to psychiatric cases without a documented history of SB /suicide fatalities (three cohorts, N=130, cases N=50, controls N=80). Comparison of the results (effect sizes at the top 500 (P < 0.05) DMPs) from the original CER meta-analysis and the secondary analysis revealed a strong positive correlation (P=2.2E-16; R=0.89) (**Figure 3.20**). Moreover, 2 of the 6 CER-associated DMPs (P <1 E-07) were nominally significant differentially methylated in suicide cases versus psychiatric controls analysis (cg10757978, P=1.19E-04; cg04525580, P=1.69E-02) and a similar direction of effect was observed for both analyses for the remaining four CER-associated DMPs (see **Table 3.11** for details). A similar analysis in the PFC could not be performed due to lack of samples from individuals with an axis-I diagnosis who did not die by suicide.
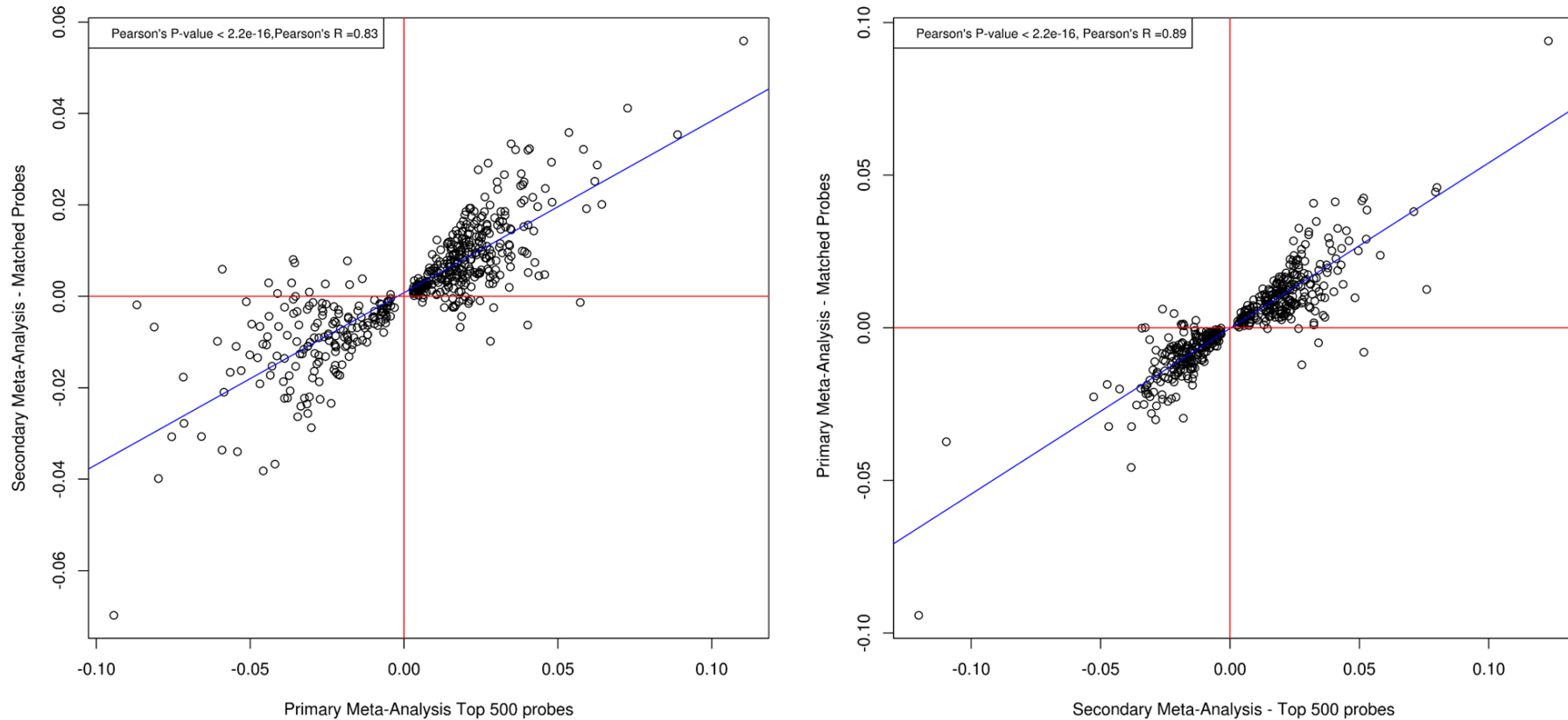
Figure 3.20 Secondary Meta-Analysis, suicide-specific DNA methylation differences in Human Cerebellum.

Correlation of effect sizes (adjusted beta difference) across the two suicide meta-analyses: a) Primary Meta-analysis (psychiatric suicide cases versus non-psychiatric controls) and (b) Secondary Meta-analysis (psychiatric suicide cases versus non-suicide psychiatric controls). Both plots showed a significant positive correlation between effect size at the most variable DMPs (Pearson's R=0.89, Pearson's R=0.83, respectively). The red lines in correspondence of y=0 and x=0 help visualise how concordant the effect sizes are as those in the top right and bottom left quadrants have the same direction of effect. The blue line indicate the correlation. PFC, Prefrontal cortex; CER, Cerebellum; DMP, differentially methylated position.

Probe ID	Illumina Annotation (UCSC RefGene Name)	CHR	Hg19	Probe Type	Gene annotation from GREAT (Distance from TSS)	Suicide *vs* Control (Mean Δβ)	Suicide *vs* Control (*P* value)	Suicide *vs* Psychiatric (Mean Δβ)	Suicide *vs* Psychiatric (*P* value)
cg14392966	*DDX25;PUS3*	11	Chr11:125773125	I	*DDX25* (-1146), *PUS3* (-10)	-0.79	3.06E-11	-0.16	3.24E-01
cg17855963		6	Chr6:15873800	II	*MYLIP* (-255516), *DTNBP1* (-210512)	1.64	5.37E-10	0.75	8.61E-02
cg25590492	*ZIC1*	3	Chr3:147129952	II	*ZIC1* (+2772)	-1.50	2.22E-09	-0.32	1.89E-01
cg12284382	*RASD2*	22	Chr22:35940438	II	*RASD2* (+3087), *MB* (+72945)	-2.66	5.92E-09	-0.27	5.44E-01
cg10757978	*SLCO5A1*	8	Chr8:70623125	II	*SULF1* (+83119), *SLCO5A1* (+124173)	3.26	5.84E-08	2.66	1.19E-04
cg04525580	*IRF2*	4	Chr4:185352181	II	*ENPP6* (-213068), *IRF2* (+43544)	1.16	9.08E-08	0.76	1.69E-02

Abbreviations: CER, cerebellum;Hg19, Human Genome version 19; GREAT, Genomic Regions Enrichment of Annotations Tool; TSS, transcription start site; UCSC, University of California Santa Cruz Genome Browser; DMPs, differentially methylated probes.

Table 3.11 Secondary Meta-Analysis in CER cohorts – Suicide-specific DMPs.

3.4.8 Pathway Analysis

The biological relevance of findings was investigated through gene ontology analysis on genes annotated to suicide-associated DMPs ($P \leq$1E-04). Results revealed an enrichment of DNA methylation alterations in genes involved in cognitive processes such as long term synaptic depression and brain development (See **Table 3.12** and **Table 3.13**). Given the hierarchical structure of the Gene Ontology annotations, many associated terms are not independent and are associated by virtue of their overlapping pathway membership. Those pathways labelled as "independent" represent independent associations for which the enrichment is not driven or shared with a more significant term while the "non-independent" pathways are terms where the significant enrichment is explained by the overlap with a more significant term.

Independent pathways									Non-independent pathways		
ID	Name	Type	nProbes inPathway	nGenes inPathway	nTestListProbesinPathway	nTestListGenesinPathway	P.GenesinTestList	GenesinTestListAndPathway	ID	Name	Type
GO:0009206	purine ribonucleoside triphosphate biosynthetic process	biological_process	1845	50	3	3	2.53E-09	COX5B|PRKAG2|TXNDC3	GO:0009145	purine nucleoside triphosphate biosynthetic process	Biological Process
									GO:0009201	ribonucleoside triphosphate biosynthetic process	Biological Process
									GO:0009142	nucleoside triphosphate biosynthetic process	Biological Process
									GO:0009152	purine ribonucleotide biosynthetic process	Biological Process
									GO:0006164	purine nucleotide biosynthetic process|	Biological Process
									GO:0009260	ribonucleotide biosynthetic process	Biological Process
GO:0030317	sperm motility	biological_process	1570	69	3	3	1.92E-08	ATP2B4|ING2|TXNDC3	GO:0097722	sperm motility	Biological Process
GO:0097228	sperm principal piece	cellular_component	937	21	2	2	3.96E-08	ATP2B4|TXNDC3			
GO:0035640	exploration behavior	biological_process	806	24	2	2	9.30E-08	ABAT|PRKCE			
GO:0021549	cerebellum development	biological_process	4045	87	3	3	3.49E-07	ABAT|HSPA5|RFX4	GO:0022037	metencephalon development	Biological Process
GO:0021587	cerebellum morphogenesis	biological_process	1601	34	2	2	9.09E-07	HSPA5|RFX4	GO:0021575	hindbrain morphogenesis	Biological Process
									GO:0021695	cerebellar cortex development	Biological Process
GO:0006754	ATP biosynthetic process	biological_process	1496	38	2	2	1.81E-06	COX5B|PRKAG2			
GO:0043279	response to alkaloid	biological_process	5140	110	3	3	2.32E-06	ABAT|HSPA5|PRKCE			
GO:0050806	positive regulation of synaptic transmission	biological_process	7420	124	3	3	5.91E-06	ABAT|LAMA2|PRKCE			
GO:0060359	response to ammonium ion	biological_process	6063	125	3	3	6.22E-06	ABAT|HSPA5|PRKCE			

Table 3.12 Gene Ontology PFC meta-analysis Suicide-associated DMPs (P-value= 1E-04).

201

			Independent pathways							Non-independent pathways		
ID	Name	Type	nProbesinPathway	nGenesinPathway	nTestListProbesinPathway	nTestListGenesinPathway	P.GenesinTestList	GenesinTestListAndPathway	ID	Name	Type
GO:1900452	regulation of long term synaptic depression	biological_process	415	12	3	3	1.46E-07	DGKI|SHANK3|SORCS3			
GO:0043548	phosphatidylinositol 3-kinase binding	molecular_function	1214	29	4	4	4.08E-07	CBL|FYN|PIK3AP1|RASD2			
GO:0046621	negative regulation of organ growth	biological_process	1554	28	4	4	5.54E-07	KCNK2|PTK2|TBX5|TP73	GO:0055022	negative regulation of cardiac muscle tissue growth	
									GO:0061117	negative regulation of heart growth	
GO:0060044	negative regulation of cardiac muscle cell proliferation	biological_process	966	13	3	3	6.05E-07	KCNK2|TBX5|TP73			
GO:0006555	methionine metabolic process	biological_process	654	20	3	3	3.90E-06	AHCYL2|CTH|MAT1A			
GO:0034236	protein kinase A catalytic subunit binding	molecular_function	1967	14	3	3	5.22E-06	KCNQ1|PRKAR1B|SOX9			

Table 3.13 Gene Ontology CER meta-analysis Suicide-associated DMPs (P-value= 1E-04).

3.4.9 Gene expression analysis of the PSORS1C3 DMR

Given the replication of a *PSORS1C3 DMR* in suicide (Murphy et al., 2017) I aimed to functionally evaluate its effect on the expression of nearby genes. Gene expression levels of nearby annotated genes (*PSORS1C3* and *POU5F1)* were quantified in a subset of sample for which brain tissue was available (two brain regions (BA11 and BA25, N=70; suicide cases (n=36), non-psychiatric controls (n=34)) and the correlation between expression levels of these selected target genes and mean DNA methylation at the suicide-associated DMR was examined. The analysis showed that in this sample set, *PSORS1C3* lncRNA was not expressed in the PFC (Ct Value >31 or undetermined) (see **Figure 3.21** for details). This result is consistent with findings in Genotype-Tissue Expression (GTEx) portal (Consortium, 2013) (https://www.gtexportal.org/home/gene/PSORS1C3), which shows little to no expression for this gene in brain samples examined (see **Figure 3.22** adapted from GTEX). Next, expression levels of the second closest gene (*POU5F1*) to the suicide-associated DMR were examined. A linear mixed-effect model was used to compare mean dCt values between suicide cases and non-psychiatric controls and the analysis showed no significant difference in gene expression levels between the two groups (*P* = 0.598; **Figure 3.23A**). Furthermore, no significant correlation was found between mean DNA methylation at the suicide-associated region *PSORS1C3* DMR and *POU5F1* gene expression levels (Pearson's R = -0.04, *P* =0.67; **Figure 3.23B**).
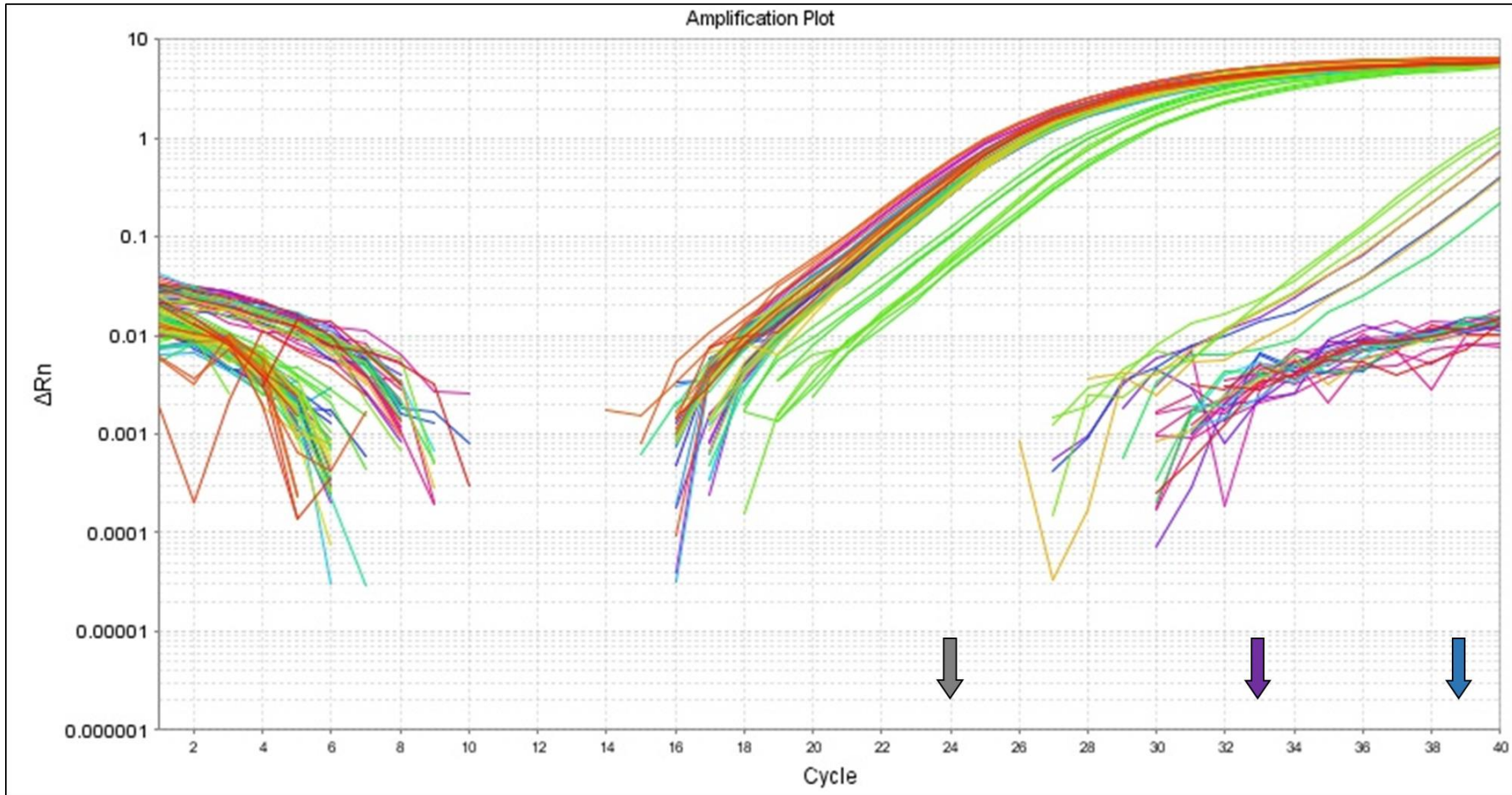
Figure 3.21 Targeted gene expression assay for PSORS1C3 gene – Amplification Plot.
Example of amplification plot and Ct values for eight samples (four cases, four CTRs). Each sample was run in triplicates per gene assay. Target gene: PSORS1C3; housekeeping genes: CYC2, UBED2, RPL13. Grey arrow, average Ct value for three housekeeping genes; Purple arrow, average Ct value for target gene PSORS1C3; blue arrow indicate Ct values for NTCs.

Figure 3.22 Gene expression for PSORS1C3 (ENSG00000204528.3).
Expression values are shown in TPM (transcript per million) calculated from a gene model with isoforms collapsed to a single gene. No other normalisation steps have been applied. Box plots are shown as median and 25th and 27th percentiles; points are displayed as outliers if they are above or below 1.5 times the interquartile range. Figure adapted from GTEx Analysis Release V8 (dbGaP Accession phs000424.v8.p2).
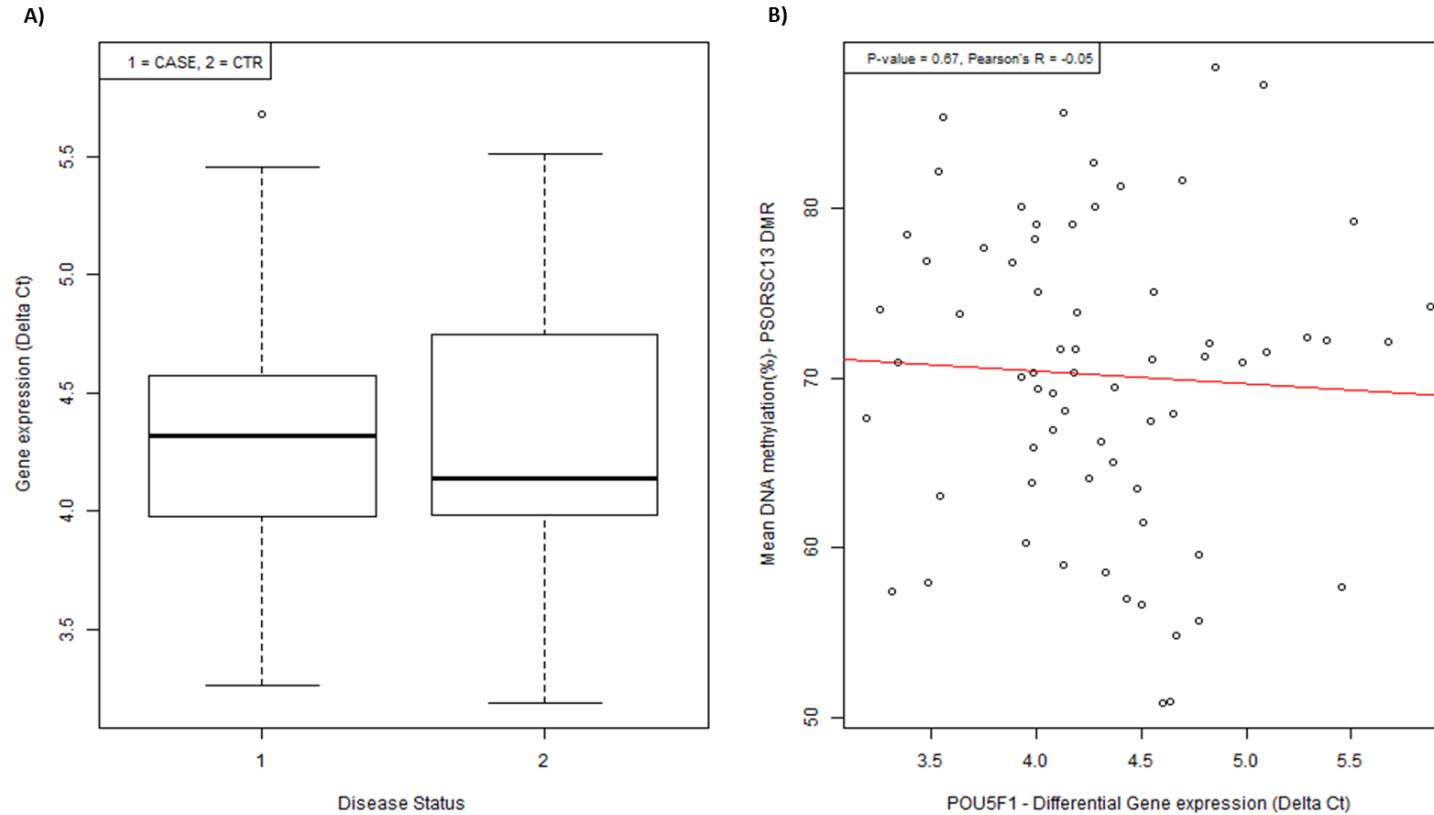
Figure 3.23 Gene expression levels of POUF15 gene in suicide cases and non-psychiatric controls.
A) The association between POU5F1 gene-expression and disease status was analysed using a linear mixed effects model. No statistically significant difference in POU5F1 expression was observed (P = 0.5). **B) Correlation between DNA methylation levels at PSORSC13 DMR and POU5F1 gene expression levels.** *As DNA methylation in a promoter region is often associated with down-regulated gene expression I tested whether a negative correlation was present between gene expression levels (Delta Ct) of the POU5F1 gene and mean DNA methylation (%) measured at the nearby suicide-associated PSORSC13 DMR. No significant correlation was found (cor test= -0.05).*

3.5   Discussion

3.5.1 Overview of results

In this study, previously published and unpublished methylomic datasets were utilised to perform a meta-analysis of variable DNA methylation in the brain of suicide completers. DNA methylation data were available for two different brain regions (PFC: four cohorts, n = 211; CER: three cohorts, n= 114) and data were meta-analysed across the suicide cohorts for each brain region separately. To my knowledge, this represents the most extensive methylomic study of suicide completers using post-mortem brain tissue to date. While several studies suggest the involvement of the PFC in SB (Schneider et al., 2015, Nagy et al., 2015b, Nagy et al., 2017, Murphy et al., 2017), suicide-associated epigenetic changes in the CER have not been investigated. However, the CER is known to play an important role in motor control, cognition, and emotional processing and is involved in a variety of psychiatric disorders, including MDD, BPD and SCZ (Phillips et al., 2015). SB in those with depression has been associated with a decreased cerebellar volume (Hwang et al., 2010) and low regional cerebral blood flow in the cerebellum(Amen et al., 2009). Moreover imaging studies have reported structural abnormalities associated to suicide attempt in MDD in cortical and subcortical regions, including cerebellum (Lee et al., 2016) and alterations in functional cerebellum networks were found in depressed patients with a suicide attempt history (Jung et al., 2019). Altogether these studies support the hypothesis of a potential involvement of CER in the psychopathology of attempted suicide in patients with MDD. I set out to further explore the role of DNA methylation and suicidality in this region as well as to determine if suicidality-associated DNA methylation differences are brain region specific.

3.5.2 Brain region specific suicide-associated DMPs

Firstly, site-specific genome-wide patterns of DNA methylation was examined in suicide cases compared with controls in the PFC and CER separately. One DMP (*cg00963169, P* = 3.30E-08) which reached experiment-wide significance was identified in the PFC. This probe, located in the intronic region of the *ELAVL4*

gene, shows consistent hypomethylation in suicide cases compared to controls. The *ELAVL4* gene has a known role in translation and stabilization of mRNA, especially in the brain, and acts as a negative regulator of proliferation, activity and differentiation in neural stem cells (Stawski et al., 2013, Akamatsu et al., 2005). Through their mRNA stabilizing activities, this family of proteins modulate neuronal development and maintenance, and their altered activity has been implicated in neurological conditions (Ince-Dunn et al., 2012) and disorders including AD (Talman et al., 2016) SCZ (Yamada et al., 2011) and ASD (Berto et al., 2016). Of interest, the association with suicide at this site was found to be largely driven by PFC cohorts derived from neuronal nuclei (see **Figure 3.18**). However, in these studies the neuronal fraction was identified through NeuN staining which is known for its broad specificity for most types of post-mitotic neuronal cells (Kim et al., 2009, Gusel'nikova and Korzhevskiy, 2015) which might explain the small change identified (DNAmΔ= -0.6). Thus, future replication of this finding in purified neuronal cells are required to confirm the neuronal-driven associations with suicide.

Six probes (cg14392966, cg17855963, cg25590492, cg12284382, cg10757978, cg04525580) at experiment-wide significance threshold (P < 1E-07) were identified in the CER. The top-ranked DMP, cg14392966 (P = 3.06E-11), is located in exon 1 of the *PUS3* gene. *PUS3* encodes a highly conserved enzyme responsible for post-transcriptional modification of tRNA and has previously been associated with intellectual disability (de Paiva et al., 2019) and severe neurodevelopmental disease (Abdelrahman et al., 2018). The remaining DMPs include probes in the vicinity of several loci previously implicated in pathways relevant to neuropsychiatric phenotypes. For example, *ZIC1* is thought to play an important role in neurogenesis and cerebellum differentiation (Yokota et al., 1996), whereas *RASD2* is known to modulate dopaminergic neurotransmission (Vitucci et al., 2016). Furthermore, the probe *cg04525580 (P* = 9.08E-08*),* is located at the 5'UTR of the interferon regulatory factor 2 (*IRF2)* gene. This locus plays an important role in transcriptional activation at promoters (Sun et al., 2018b) and regulates the expression of a variety of genes involved in immune responses in the brain (Drew et al., 1995), further supporting a role for immune-related pathways in suicide.

3.5.3 Region specific suicide-associated DMR identified in post-mortem human brain

To increase the power of the study to identify differences in DNA methylation levels between cases and controls and given that DNA methylation at adjacent probes is often correlated, the regional-based analysis, Comb-p, was employed to identify DMRs. My analysis identified three and eight significant (Sidak-corrected P <0.05) DMRs in the PFC and CER, respectively.

In the PFC, the top-ranked DMR, located in intron 1 of the *WRB* gene is consistently hypomethylated across all five CpG sites in suicide cases relative to controls, in all cohorts. Recent studies suggest a role for Wrb in photoreceptor synaptic transmission in zebrafish (Daniele et al., 2016) and the *WRB* locus was reported among the differentially expressed genes in a mouse model study looking at cognitive impairment and neuropathology in inidividuals affected by Down syndrome (Ling et al., 2014) further supporting the hypothesis of its involvement in the correct development and functioning of the CNS. The second top-ranked suicide-associated DMR in the PFC (Sidak-corrected P = 3.81E-05) was located upstream of the *PSORS1C3* non-coding gene, a DMR previously reported within my group as associated with MDD suicide completers (Murphy et al., 2017). Although the function of this gene product remains unclear, it is thought to be a potential regulator of nearby immune-related genes (Nair et al., 2006) and is a known risk gene for psoriasis (Chang et al., 2006, Wisniewski et al., 2018), supporting a role in immune system regulation. To gain further insight into the role of this suicide-associated *PSORS1C3* DMR on nearby gene expression a targeted gene expression assay was performed. No evidence of suicide-associated differential gene expression of nearby genes, *PSORS1C3* and *POU5F1* was found in the PFC. However, when the effect of this DMR on gene expression was examined using a dual luciferase assay as part of a collaboration within my group (Policicchio S et al et al., 2020), the methylated *PSORS1C3* DMR construct was found significantly associated with decreased expression of the reporter gene product, indicating that the methylation status of this DMR has the potential to modify promoter activity. This evidence strengthens the hypothesis that DNA methylation levels at this suicide-associated DMR are influencing expression in the region although the identity of the modified gene product remain unknown. It could be speculated that DNA methylation at this region is associated

with a different nearby gene or an unknown splice variant of either the *PSORS1C3* or *POU5F1* genes. Finally, an additional DMR was identified in the PFC; located on chromosome 22, in the promoter region of the *LGALS1* gene. This gene is thought to play a role in immune system functioning (Vitucci et al., 2016) and DNA methylation levels at this locus have been previously implicated in SCZ (Viana et al., 2017).

In the CER, the top-ranked suicide-associated DMR, located in the intronic region of the *CERC2* gene on chromosome 22, spans four CpG sites. This locus is known to be involved in the control of the periodic oscillation of cyclin E expression in proliferating cells likely through its histone deacetylase activity (Polanowska et al., 2001). The *CERC2*-associated DMR showed significant hypermethylation (Sidak-corrected P =5.68E-07) across all four CpG sites within the region in suicide cases compared with controls and the direction of this change was found to be consistent across all three independent CER methylomic studies. To the best of my knowledge, this gene has not been previously implicated in the pathology of SB. Seven additional suicide-associated DMRs were identified in the CER. Of interest is the DMR located in exon 10 of the *SLC44A4* gene; a gene recently implicated in a study looking at the role of the major histocompatibility complex region in SCZ susceptibility (Yamada et al., 2015). An additional suicide-associated DMR, worthy of further investigation, is located in exon 3 of the *WWTR1* gene, a transcriptional coactivator known for its role in preserving neuronal health (Pfleger, 2017). Furthermore, a missense variant in this gene was recently associated with lower cognitive ability in a GWAS study for infant mental and motor ability (Sun et al., 2018b). Finally, a suicide-associated DMR located upstream of *MED13L* gene was identified and genetic variants at this locus have been widely reported as associated with intellectual disability (Hamdan et al., 2014, Nizon et al., 2019) suggesting that this gene may play an important role in neurological development.

3.5.4 Additional analyses identified suicide diathesis-related DNA methylation differences in human cerebellum

Since SB is often a symptom of a psychiatric disorder, distinguishing suicide diathesis-related DNA methylation differencesfrom those associated with mood disorders and other psychiatric diseases remains a challenge. In order to unravel the relative contribution of psychopathologies from DNA methylation differences specific to suicide, an additional meta-analysis in the CER was performed whereby individuals with documented Axis I psychiatric disorders (MDD, SCZ, BPD) and who died by suicide were compared to psychiatric cases without a documented history of SB. Comparison of the results (effect size of the top 500 nominally significant ($P<0.05$) DMPs) from the original CER meta-analysis and the secondary analysis revealed a strong positive correlation (P=2.2E-16; R=0.89). Moreover, I replicated my findings for 2 of the 6 CER-associated DMPs, which reached multiple testing threshold in suicide cases versus psychiatric controls meta-analysis (cg10757978, P=1.19E-04; cg04525580, P=1.69E-02) and similar direction of effect was observed for the remaining loci. Taken together these findings suggest that suicide-associated DMPs identified in the CER by this study are largely independent of comorbid psychiatric disorders. Unfortunately, it has not been possible to perform the same analysis in the PFC due to the limited number of samples with no history of suicide while having an Axis-I diagnosis.

3.5.5 Limitations

Despite the power of the methodological approaches used in this study, there are several caveats. First, the modest number of studies included made this meta-analysis relatively underpowered to detect small differences in DNA methylation. Despite this I was able to identify several DMPs and DMRs in both brain regions strongly associated to suicide. Another major limitation is that bulk brain tissue was used in most of the studies included in the meta-analysis and cellular heterogeneity is a well-known confounder in DNA methylation studies. In order to address this issue, a previously reported *in silico* method was used to estimate the neuronal proportion in each sample in bulk PFC cohorts and included these estimates as covariates in the statistical models used (Guintivano et al., 2013). This method could not be applied to the analysis of the CER and thus it is plausible that cellular heterogeneity is confounding some of the CER results.

Third, recent research has implicated the importance of other DNA modifications (i.e., 5-hydroxymethyl cytosine) in the brain (Branco et al., 2011). DNA methylation measurements in this study cannot be distinguished from 5-hydroxymethyl cytosine (5hmC). Of interest, the presence of detectable 5hmC levels at statistical significant DMPs identified in this study in their respective brain regions was examined using the Hydroxymethylation Annotation in Brain Integrative Tool (HABIT) tool (http://epigenetics.iop.kcl.ac.uk/HMC/) (Lunnon et al., 2016). This tool identified detectable levels of 5hmC at various sites among which the suicide-associated DMPs cg00963169 (PFC) and cg17855963, cg04525580 (CER) suggesting that the majority of DMPs identified in this study are not confounded by 5hmC. However, future studies should attempt to examine the role of 5hmC in SB. Fourth, medication data, smoking information and method of suicide were not available for all individuals; thus, the possibility that the observed differences in DNA methylation levels are influenced by unaccounted confounders cannot be excluded. Fifth, I acknowledge the possibility that many of the associations reported (DMPs/DMRs) could be related to the severity and/or duration of the mental health disorder. From the secondary analysis in the cerebellum, I show that for certain top-ranked DMPs the association appears to be suicide-specific rather than driven by the underlying mental health disorder. Given the lack of information related to severity and/or duration of mental illness for samples included in this meta-analysis the contribution of the above mentioned confounders cannot be ruled out.

3.5.6 Future directions

Although this study presents evidence for novel DNA methylation differences associated with suicide, further replication using a larger sample size is required to support these results. Ongoing work in my group and others is focussing on using novel single cell approaches to examine cellular heterogeneity in complex tissues such as the brain and facilitate the identification of pathological changes in specific cells (and cell types). In addition, future studies could also examine the transcriptional consequences of the observed DNA methylation levels at the *PSORS1C3* DMR on additional nearby genes and/or novel splice variants in the region. There is considerable interest in using DNA methylation based

biomarkers as predictors for suicide risk and previous studies (Clive et al., 2016, Sadeh et al., 2016, Kaminsky et al., 2015, Lockwood et al., 2015, Maussion et al., 2014, Guintivano et al., 2014) have identified polymorphic CpGs that can act as a unique molecular signature for suicide prediction. The data from this study provide many more candidate regions as potential biomarkers for suicide risk and also identify genes/networks potentially dysregulated in the suicidal brain. Furthermore, future work focusing on identifying differentially expressed miRNA could provide a more comprehensive understanding of gene regulation at both the transcriptional and post-transcriptional level helping to disentangle its role on molecular processes associated with suicide. Finally, integrated omics analysis could be performed to identify suicide-associated DNA methylation differences proximal to miRNA genes which are having a functional effect on mRNA expression levels.

3.6   Conclusions

This study, which utilises several published and unpublished suicide cohorts, has identified DMPs and several DMRs associated with suicide in both the PFC and CER, including the previously identified DMR upstream of the *PSORS1C3* non-coding gene. When examining the functional implications of methylation status at the *PSORS1C3* DMR on gene expression levels in the region using a dual-luciferase reporter assay, DNA methylation of this DMR was found to decrease expression of firefly luciferase but was not associated with expression of nearby genes, *PSORS1C3* or *POU5F1* suggesting that this DMR has the potential to influence gene expression but its target gene yet has to be identified. All together these evidence support the hypothesis that changes in DNA methylation levels are associated with suicide and may offer novel insights into the molecular pathology associated with suicidality.

Chapter 4 - Fluorescence Activated Nuclei Sorting (FANS) Protocol Development

4.1 Introduction

The appearance and maintenance of multicellularity throughout evolution suggest that an advantage is conferred by multiple types of cells, each specialized in the execution of specific tasks (Arendt, 2008). This division of labour between distinct cell types is particularly prominent in the central nervous system (CNS), which is thought to contain thousands of neural cell types (Nelson et al., 2006, Bota and Swanson, 2007) that contribute to a variety of specialised functions. Even in a single brain region, individual neurons differ greatly in their morphology, connectivity and electrophysiological properties (Poulin et al., 2016). Differentiated cell phenotypes result from specific patterns of gene expression and long-lasting changes in cellular properties involve gene transcription regulation. In addition to the interplay of numerous transcription factors, epigenetic marks, including histone and DNA modifications, as well as non-coding RNAs, play a crucial role in transcription regulation (Borrelli et al., 2008, Meaney and Ferguson-Smith, 2010). Epigenetic marks are characteristic of cell types thus providing further traces of the cell history. In neurons, it has been proposed that epigenetic modifications contribute to long-lasting functional alterations reflecting environmental stimuli (Zhang and Meaney, 2010).

Numerous studies have reported consistent and robust alterations in DNA modifications in psychiatric and neurodegenerative disorders (Kouter et al., 2019, Policicchio S et al et al., 2020, Watson et al., 2016, Hannon et al., 2016, Jaffe et al., 2016). However, there are some caveats associated with many of the studies undertaken to date; one of the most apparent is that they are performed on bulk tissue and therefore confounded by cellular composition. Consequently, the downstream interpretation of these studies is compromised. This is particularly true in neurodegenerative conditions like Alzheimer's disease (AD) where alterations in the proportion of different cell types due to neuronal loss primarily, are well documented in AD brain (Andrade-Moraes et al., 2013, Smith et al., 2020).

The selective vulnerability of specific cell types in many neurodegenerative disorders is likely a result of the unique molecular properties of the affected cells. Furthermore, the latest SCZ GWAS findings have highlighted neurons as being the leading cell type involved in the pathogenicity (Ma et al., 2018, Yang et al., 2018, Xie et al., 2018). Thus, obtaining the gene regulatory profiles of specific

cell types that are known for being implicated in disease will provide valuable insights into disease mechanisms and could ultimately lead to therapeutic approaches to prevent or reduce selective neurodegeneration.

4.2   Neural cell diversity in the human cortex

The human brain, unlike any other organ in our body, is comprised of a heterogeneous mix of cell types that assemble into functional circuits that reflect a complex interaction between the unfolding genetic program and environmental interactions (Molnar et al., 2019). The cerebral cortex, in particular, is composed of a huge variety of highly specialised cell types which are generated largely during embryonic development. This includes numerous subtypes of neuronal cells and various different non-neuronal cells among which oligodendrocytes, microglia and astrocytes are the most abundant as well as the best characterized. **Figure 4.1** offers a schematic overview of the cell type differentiation in the brain during development while **Figure 4.2** shows the different cell types and how these relate to each other). The cerebral cortex, which constitutes more than half the volume of the human brain, shows considerable differences in the composition and proportions of these elements and these variations in cell composition are likely to reflect the different computational functions distinct cortical areas have to perform (Johnson and Walsh, 2017). The cerebral cortex is presumed to be responsible for the neuronal computations underlying complex phenomena such as perception, thought, language, attention, episodic memory and voluntary movement (Molnar et al., 2019) hence it does not surprise that it is involved in many human psychiatric and neurological conditions. Elucidating the cellular architecture of the human cerebral cortex is therefore central to understanding cognitive abilities and susceptibility to disease as well as for a better comprehension of the mechanistic underpinnings of neuropsychiatric disorders. In the following sections, a brief overview of the main roles attributed to each major neural cell types is provided.
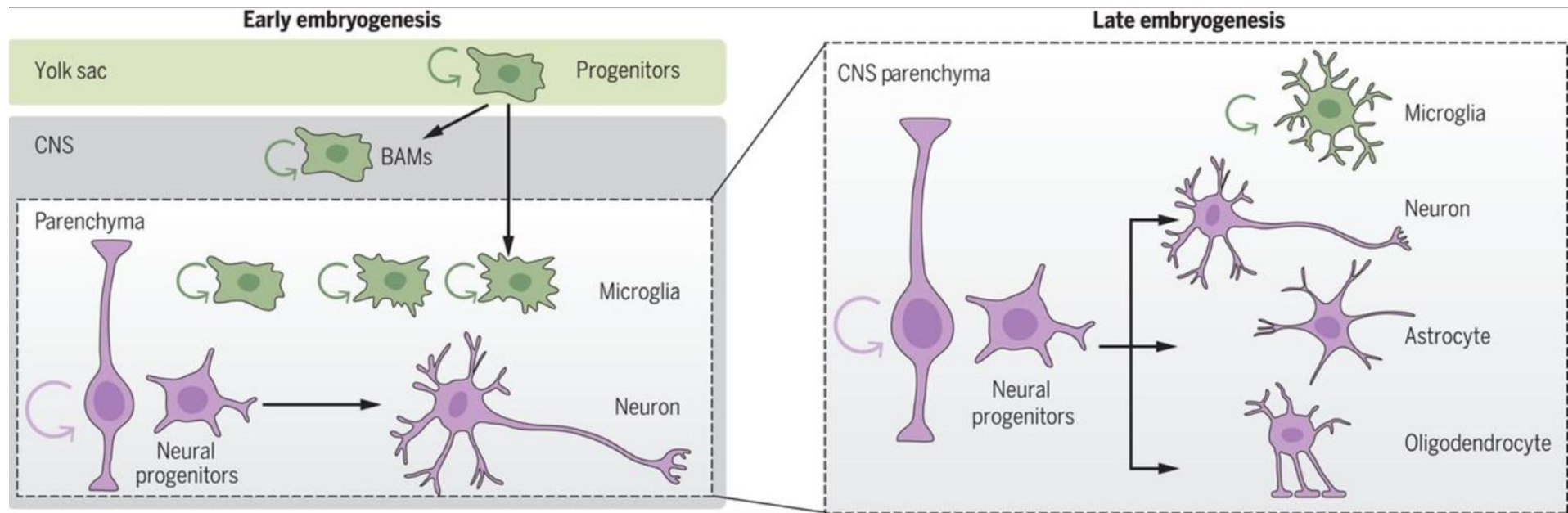
Figure 4.1 Schematic diagram of brain development and different cell types.
Parallel development of neural and immune cells of the CNS. Early CNS colonization by yolk sac -derived macrophages that give rise to microglia whereas neural progenitors generate neurons (left). At later embryonic stages (right), neural progenitors additionally produce oligodendrocytes and astrocytes in the parenchyma while the microglia undergo local differentiation. Figure adapted from (Thion et al., 2018).
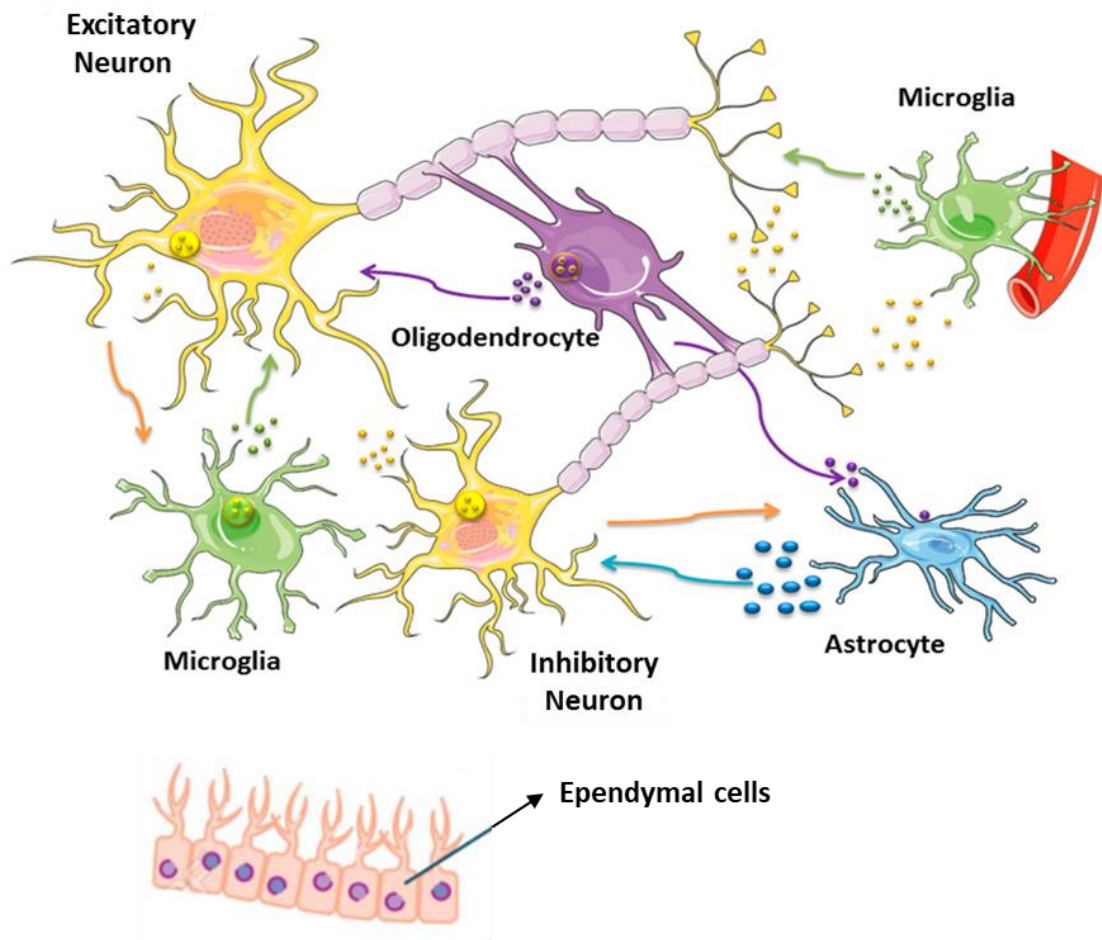
Figure 4.2 Schematic representation of the variety of neural cell types in the human brain and their reciprocal interactions.

4.2.1 Neurons

The mammalian neocortex is an extremely complex, highly organized, six-layered structure that contains hundreds of different neuronal cell types responsible for the highest levels of associative, cognitive and motor functions. In the cerebral cortex there are two broad classes of neurons both present in a plethora of different subtypes: inhibitory neurons (interneurons), which make local connections, and excitatory projection neurons, which extend axons to distant intracortical, subcortical and subcerebral targets (Lodato et al., 2015). Projection neurons are born from neural progenitors located in the developing proliferative zones of the dorsal telencephalon; they are glutamatergic and send long-distance axons to targets within and outside of the cortex (Molyneaux et al., 2007). Distinct populations of projection neurons are located in different cortical layers and areas, have unique morphological features, express different complements of transcription factors and ultimately serve different functions (Molyneaux et al., 2007). Inhibitory neurons have evolved as a highly heterogeneous collection of cell types that display a great diversity of molecular signatures, electrophysiological properties, connectivity and synaptic dynamics; they are GABAergic and connect locally within the cortical microcircuitry (Kepecs and Fishell, 2014). Current estimates suggest that up to 50 different types of GABAergic neurons may populate the cerebral cortex, all derived from progenitor cells in the subpallium, the ventral area of the embryonic telencephalon (Lim et al., 2018).The activity of projection neurons is finely modulated by cortical inhibitory neurons. The molecular classification of anatomically identified projection neuron classes is only beginning to be known. Several studies have purified and transcriptionally compared distinct projection neuron subtypes, providing the first sets of class-specific genes (Bernard et al., 2012, Molyneaux et al., 2009, Heiman et al., 2008). A few important lessons have emerged from these molecular studies. Firstly, that each and every one of these cell type gene expression markers present different degrees of restricted expression in any given projection neuronal class and thus that only the combinatorial use of multiple genes can identify, one projection neuronal population versus the others. Secondly, the combination of genes that distinguish one projection neuron class at a given point in time may not do so at another, indicating that signature profiles of gene expression for individual classes of projection neurons are temporally

dynamic. Finally, many of these new molecular markers label only subsets of the current classes of anatomically-defined neurons. This indicates that canonical classes of projection neurons are likely further subdivided into subclasses and that each neuronal population is per se heterogeneous. Single-cell transcriptional profiling of individual populations has the potential to clarify the diversity within each class of projection neurons and, further, define the functional meaning of intra-population diversification (Lodato et al., 2015).

4.2.2 Oligodendrocytes

Oligodendrocytes are the CNS glial cells responsible for axonal myelination which is essential for proper signal conduction along neuronal axons and for maintaining brain homeostasis (Simons and Nave, 2015). Oligodendrocytes indeed form and maintain the myelin sheaths that insulate axons and organize the distribution of axonal voltage-gated ion channels, a prerequisite for conduction of action potentials and trophic support of axons (Ehrlich et al., 2017). Defects in myelin production and/or maintenance are the predominant pathological feature of several diseases, including leukodystrophies and multiple sclerosis (Franklin et al., 2012). In addition to myelination, oligodendrocytes have a role in trophic and metabolic support of neurons, fuelling oxidative phosphorylation in the mitochondria of axons (Garcia-Leon et al., 2018). However, the complete role of oligodendrocytes is still only partially understood and vary depending on the CNS region wherein they reside (Marques et al., 2016). Lack of insight in human oligodendrocyte biology is in large part a consequence of the limited access to human oligodendrocytes (Chanoumidou et al., 2020) and difficulties in maintaining these cells *in vitro* (Monaco et al., 2012). Therefore, having access to human oligodendrocytes would represent a major step forward in studies aimed at understanding mechanisms that are deregulated in diseases with oligodendrocytes involvement.

The oligodendrocyte lineage originates from multi-potent neural progenitor cells (NPCs). First, NPCs become primitive oligodendrocyte progenitor cells expressing Olig1/2, then committed oligodendrocyte precursor cells (OPCs; also known as oligodendrocyte progenitor cells), which persist in the CNS throughout life (Dawson et al., 2003). OPCs can further proliferate and differentiate into

mature myelinating oligodendrocytes (Zuchero and Barres, 2013, Emery, 2010, Wegner, 2008). The transition into each of these stages requires the coordination of transcriptional regulatory events closely interconnected (Berry et al., 2020) as well as significant morphological changes by forming branching cell processes. OPCs differentiate into oligodendrocytes not only during the development of the CNS but also in cases of pathological demyelination in the mature CNS (Boulanger and Messier, 2014). Previous studies have shown that OPCs can differentiate into not only oligodendrocytes but also astrocytes and neurons, depending on the area of the brain and stages during CNS development. However, the majority of the OPC population differentiates to oligodendrocytes (Nishiyama et al., 2014). *In vitro*, OPCs differentiate to oligodendrocytes under serum-free culture conditions, while their differentiation can be directed towards astrocyte-lineage cells under high-serum culture conditions (Behar, 2001). Classically, these astrocytic cells derived from OPCs are called type II astrocytes, which are distinguished from type I astrocytes derived from glial precursor cells (Behar, 2001). However, the functional differences between type I and II astrocytes in physiological and/or pathological conditions have not yet been elucidated.

Deficits in the generation, proliferation, or differentiation of these cells or their maintenance have been linked to neurological disorders ranging from developmental disorders such as autism (Boddaert et al., 2009, Casanova, 2006, Deoni et al., 2015) as well as neurodegenerative diseases like Alzheimer's disease (Tse et al., 2018, Mathys et al., 2019). In addition, dysregulation of the processes controlling proliferation and differentiation in the oligodendrocyte lineage has been linked to the development of various brain cancers (Huse and Holland, 2010). Many of the key factors underlying these processes are epigenetic regulators that act by reprogramming gene expression in response to changes in the local microenvironment (Abdul et al., 2017). For example, activity can promote myelination of axons by newly formed oligodendrocytes. Critical periods exist during oligodendrocyte differentiation and myelination in development and postnatally (Makinodan et al., 2012, Liu et al., 2012, Barateiro et al., 2016) when oligodendrocytes are highly receptive and adaptive to neuronal activity (Purger et al., 2016). The plasticity of myelinating oligodendrocytes and adaptive myelination are important for normal neural circuit functioning and cognition (Monje, 2018).Epigenetic regulation is likely the mean through which

the effects of local stimuli are carried out (Samudyata et al., 2020). Indeed, epigenetic modifications are often reversible and provide the necessary plasticity for progenitor cells to respond to environmental cues (Berry et al., 2020).

4.2.3 Astrocytes

Glial cells account for at least 75% of brain cells (Nagy et al., 2015b), and are implicated in a range of psychiatric disorders, including SCZ (Bernstein et al., 2009), MDD (Rajkowska and Stockmeier, 2013) and suicide (Torres-Platas et al., 2011, Ernst et al., 2011). Astrocytes are multifaceted brain glial cells with numerous functions, including immune regulation (Oberheim et al., 2012) and maintenance of neuronal functioning (Sidoryk-Wegrzynowicz et al., 2011). Astrocytes provide structural and trophic support for neurons (Sidoryk-Wegrzynowicz et al., 2011), they maintain high rates of active oxidative glucose metabolism (Halford et al., 2017). They can regulate neuronal metabolic supply by adjusting local blood flow on demand because they enfold synapses as well as capillaries (Schousboe et al., 2014, Magistretti, 2006). The preferential storage of glycogen and glycoylsis in astrocytes has long been known (Hertz, 2004). Thus, astroglial metabolism is essential for maintaining neuro-metabolic coupling and brain energy homeostasis (Halford et al., 2017).

Interestingly, a transcriptomic study of FACS-isolated astrocytes from transgenic mice found astrocytes to be enriched in specific metabolic and lipid synthetic pathways, as well as phagocytic pathways suggesting that astrocytes are professional phagocytes (Cahoy et al., 2008). Moreover, mature astrocytes and oligodendrocytes seem not to share a large cohort of common "glial" genes suggesting that the notion of a molecularly defined glial cell type is largely misleading because all three mature cell types differ vastly based on the genes that they express (Cahoy et al., 2008). This cell type is also involved in the regulation of synaptogenesis and synaptic transmission, thereby contributing to neurological and psychiatric diseases (Cotter et al., 2001, Allen and Barres, 2005, Volterra and Meldolesi, 2005). Specifically, astrocytes are thought to play a key role in degrading glutamate to glutamine and in coupling synaptic activity and glucose utilization (Magistretti, 2006). Evidence of the ability of astrocytes to regulate synaptic formation (Christopherson et al., 2005) has been previously

reported and many astrocyte-enriched genes have been implicated in psychiatric diseases such as SCZ and BPD, including *GMR3* (Goudriaan et al., 2014) *Npas3* (Pieper et al., 2005), *MLC1* (found in distal astrocyte processes (Boor et al., 2005)), *LGI1/4* (Gu et al., 2004, Schulte et al., 2006) and *GPR56* (Mochida, 2005), providing clues to the potential ways that astrocytes may contribute to neurological and psychiatric diseases.

Astrocytes have in recent years become the focus of intense experimental interest, yet the development and function of astrocytes remain in many aspects uncharacterized. A central limitation in advancing our understanding of mature astrocyte development and function has been the lack of procedures that allow for their purification (Zhang et al., 2016). Moreover markers for their univocal identification remain both scarce and imperfect. Astrocytes have been traditionally identified immunohistochemically by antibodies that target cell-specific antigens in the cytoplasm or plasma membrane which do not permit such a high-resolution assignment of individual cell identity as they are often regulated developmentally and may be modulated functionally (Sun et al., 2017).

4.2.4   Microglia

Microglia are the tissue-resident macrophages of the brain, and as such, they serve both immune-related and glial functions by taking part in the immune surveillance, development and homeostasis of the organ (see **Figure 4.3** for a schematic overview). Microglia have a number of key features—including their long-range migration during development, their adaptation to the local environment, and their role in brain development (Casano and Peri, 2015). They account for a significant proportion of cells in the brain and their density remains stable throughout the lifespan due to constant turnover (Lopez-Atalaya et al., 2018, Casano and Peri, 2015) Although long debated, it is now clear that microglia have a mesodermal origin (Casano and Peri, 2015) and derive from a lineage that is distinct from that of hematopoietic stem cells (Gomez Perdiguero et al., 2015) (see **Figure 4.4**). For instance, in the absence of the myeloid transcription factor PU.1 in both mice and zebrafish no microglia are present in the brain (Beers et al., 2006, Schulz et al., 2012). Many groups have compared the chromatin landscape and the transcriptome of several tissue-resident

macrophage populations (Kohyama et al., 2009, Gautier et al., 2012, Lavin et al., 2014, Butovsky et al., 2014) in the attempt to establish how the environment impacts on tissue-resident macrophages. In particular, mapping enhancer histone modifications revealed that genes commonly found in all macrophages are differentially expressed within distinct populations, indicating that specific profiles and chromatin landscapes are likely to result from the crosstalk between the local microenvironment and the cell ontogeny (Lavin et al., 2014, Heinz et al., 2010, Gosselin et al., 2014).

Microglia have long been studied for their involvement in immunity and in many neurological disorders, such as AD and Parkinson's disease (for a review, see (Lehnardt, 2010). However, there is also mounting evidence for important roles played by these cells in the context of brain development and in the establishment of neuronal connectivity (Casano and Peri, 2015).
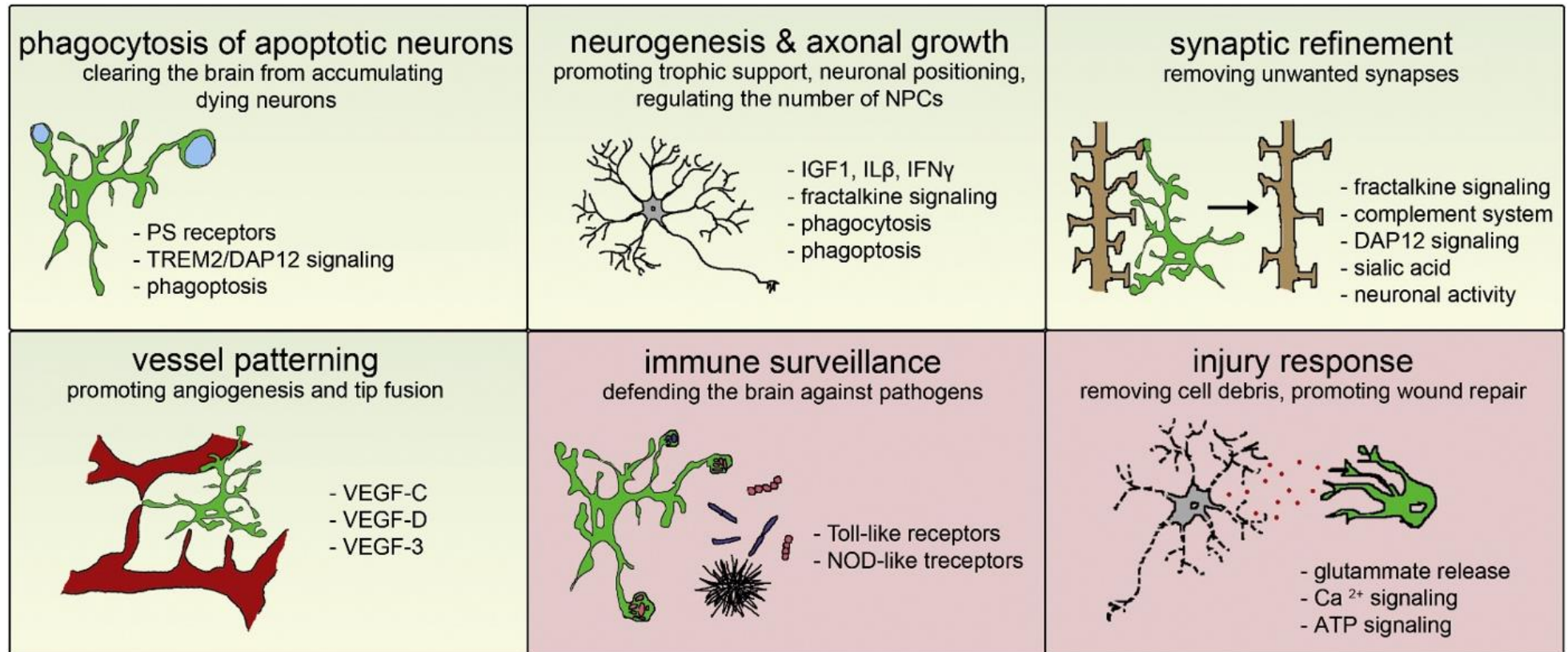
Figure 4.3 Schematic representation of microglial roles in the developing brain.
Yellow and pink boxes indicate microglial roles during developmental stages and general immune-related functions, respectively. <u>Abbreviations</u>: PS, phosphatidylserine; TREM2/DAP12, triggering receptor expressed on myeloid cells 2 (TREM2) and DNAX-activating protein of 12 kDa (DAP12) signalling; NPCs, Neural progenitor cells; IGF1, Insulin-like growth factor 1; ILβ, Interleukin 1 beta, IFNγ, interferon γ;mVEGF, vascular endothelial growth factor receptors; NOD-like, nucleotide-binding oligomerization domain like; Ca2+, calcium; ATP, Adenosine triphosphate. Figure taken from (Casano and Peri, 2015).
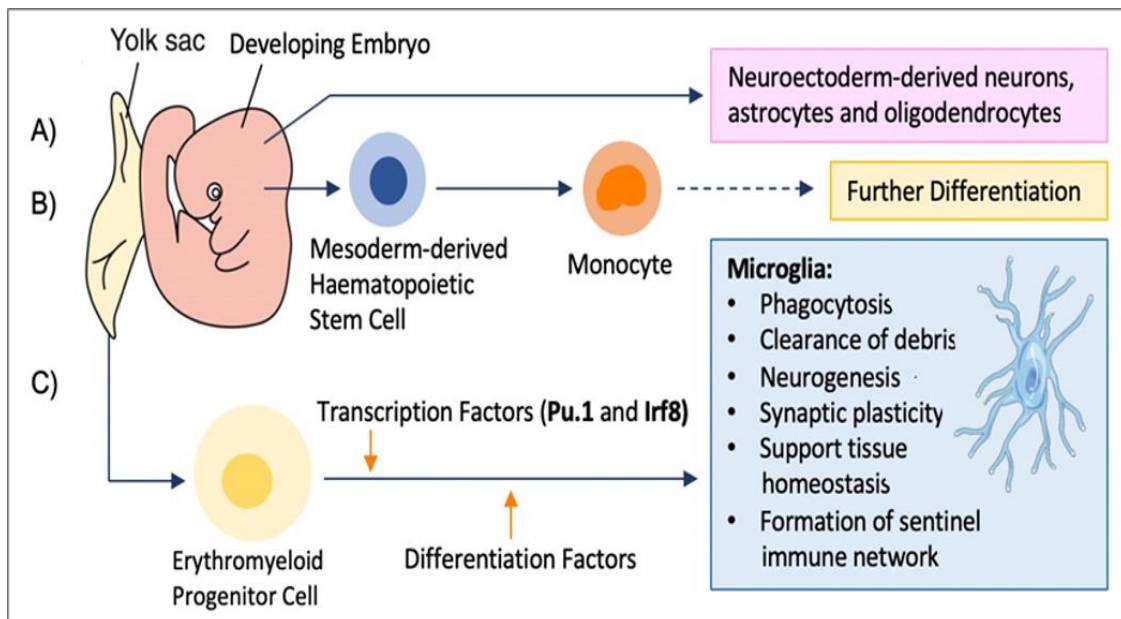
Figure 4.4 Monocyte and neural cell development during embryogenesis.
*Microglia development is distinct from the development of other monocytes and neural cells. **A)** Neurons, oligodendrocytes and astrocytes arise from the neuroectoderm (Prinz and Mildner, 2011) **B)** Monocytes arise from haematopoietic stem cells in the bone marrow (Ginhoux et al., 2010) **C)** Microglia arise from yolk sac-derived erythromyeloid progenitor cells via a Pu.1 and Irf8-dependent pathway (Ginhoux et al., 2010). After early entry into the CNS, microglia remain there and are independently maintained as the resident mononuclear phagocytes of the CNS with many different functions (Ajami et al., 2007).*

Microglia play a central role in removing apoptotic neurons, both during early CNS development and in the adult tissue (Caldero et al., 2009, Sierra et al., 2010). Recent work has shown that microglia have a high phagocytic index and that this remains constant not only during early adulthood but also in neuroinflammatory conditions (Sierra et al., 2010). *In vitro* studies have also suggested that the release of tumour necrosis factor alpha (TNF-α) by activated microglia could promote the microglial-mediated neuronal uptake and phagoptosis (Neniskyte et al., 2014) providing evidence for a role of microglia in promoting neuronal cell death.

The role of microglia in neurogenesis has mainly been addressed under pathological conditions; for example, during brain inflammation (Ekdahl et al., 2009). However, accumulating evidence from studies in rats has also highlighted the importance of microglia and microglial-mediated production of neurotrophic factors in modulating neurogenesis during embryogenesis and adulthood (Ueno et al., 2013, Shigemoto-Mogami et al., 2014, Rao et al., 2006).

Undoubtedly, one of the most intriguing roles of microglia in the brain is synaptic pruning which takes place in the mouse during early and late postnatal stages for the remodelling of neuronal connections (Wake et al., 2009) as well as in humans during development and, possibly, in disease (Sakai, 2020). Lack of pruning results in increased connectivity and redundant afferent synaptic inputs, causing impaired motor learning, associative memory and spatial memory (Paolicelli et al., 2011, Rogers et al., 2011). Interestingly, excessive synaptic pruning has been widely implicated in SCZ and other common neurological disorders (Sellgren et al., 2019, Prasad et al., 2016, Cardozo et al., 2019). Altogether, microglia related findings have shown that these cells are not just simply sentinels that survey the brain but are active multitasking specialists during development, adulthood, and senescence. Indeed, several studies have shown that a lack of microglia has detrimental effects on proper brain functionality, with consequent severe behavioural and learning deficits (Duarte et al., 2019, Nelson and Lenz, 2017, Torres et al., 2016).

It is interesting that microglia share some of their tasks with astrocytes, a cell type also involved in synapse elimination and apoptotic removal (Cahoy et al., 2008, Chung et al., 2013, Tasdemir-Yilmaz and Freeman, 2014). This redundancy highlights the importance of these processes, but it still remains to be established how these two cell types share these tasks.

4.2.5   The Glia/Neuron Ratio

The notion that the proportion of glial to neuronal cells in the brain increases with brain size, to the point that glial cells represent about 90% of all cells in the human brain has dominated the neuroscientific research literature for long time and only more recently proven to be incorrect (Herculano-Houzel and Dos Santos, 2018). Recent evidence have shown that the glia/neuron ratio is found to vary not with brain size, but most likely as a direct function of average neuronal size, with more glial cells per neuron as the latter become larger; however, this seems to happen due to simple mechanical limitations to glial cell proliferation during development in the face of a large variation in average neuronal size. (Herculano-Houzel, 2014). The emerging evidence that the glia/neuron ratio varies uniformly (the smaller the neuronal density, the larger the glia/neuron ratio) across the different

brain structures (Cahoy et al., 2008) highlights how fundamental for brain function must be the interaction between glial cells and neurons. In a recent mouse transcriptomic study gene profiles of astrocytes and oligodendrocytes were found to be as dissimilar to each other as they are to neurons (Cahoy et al., 2008).

Thus, the nature and role of neuron–glia interactions in controlling the development, function, and pathology of our brains remain among the greatest unsolved mysteries in neurobiology today. Arguably, the knowledge of the most highly expressed specific genes within a cell type should provide important clues as to the likely functions of that cell type. Identification of cell type specific markers however has long been problematic because of the great degree of regional and subtype heterogeneity.

4.2.6 Reviewing current methods to isolate neural cells/nuclei

The complex cellular heterogeneity of the CNS makes it relatively difficult to reliably obtain molecular descriptions with cell-type specificity and it makes the study of molecular signalling particularly challenging, as relevant changes occur only in a fraction of specific cells. A cell type is often defined as a group of cells that perform a similar function (Nelson et al., 2006, Bota and Swanson, 2007, Fishell and Heintz, 2013). However, the function of most cell types in the nervous system remain to date unknown or unclear. A given cell's function is rooted in its molecular composition and cell identity is generally thought to be defined by the expression of a combination of genes (Holmberg and Perlmann, 2012, McKenna and O'Malley, 2002). The three most widely employed methods for molecular characterization at the single-cell level are: immunolabelling, RNA in situ hybridization and transgenic approaches. One drawback of all these methods is that usually only one or two markers are examined simultaneously. Thus, concurrent profiling of the expression of many genes in a single cell has not been possible using these techniques, despite being considered crucial to assign cell type identity (Masland, 2004, Trapnell, 2015). In particular, comparative analysis of epigenetic regulation or molecular profiles is hampered by the lack of adequate methodology for selective purification of defined cell populations from CNS tissue (Okada et al., 2011). Indeed, comparative analysis of gene expression or molecular profiles has for long relied upon conventional histopathologic

examinations, including in situ hybridization, which provides only a small set of data with limited detection sensitivity and is not applicable to high throughput analysis.

In the endeavour to circumvent this, more recent studies have attempted to bioinformatically correct for cellular proportions in EWAS data by adopting methods that can estimate cell proportions, which can either be based on well-annotated reference data sets in separated cell populations (reference-based) (Houseman et al., 2012, Jaffe and Irizarry, 2014, Guintivano et al., 2013, Montano et al., 2013) or can be reference-free (Li and Wu, 2019, Houseman et al., 2016). Although these methods provide reassurance that loci nominated in the EWAS are not directly attributed to a shift in cell proportions, they are still unable to discriminate which cell type is driving a specific epigenetic signal, which greatly limits the interpretation of findings. Furthermore, the estimates provided by these approaches are often limited to the few most abundant cell types composing the tissue. Aside from this, if epigenetic changes in one cell type oppose the direction of the epigenetic changes in another cell type, then no total difference in epigenetic levels will be detected in bulk tissue, meaning that important disease-associated changes are likely to be missed when profiling heterogeneous tissue (Smith et al., 2020).

One of the reasons why purified cell populations of the CNS have been under-studied, is partly due to the difficulty of isolating intact whole cells. Thus, in recent years there have been numerous attempts to develop alternative methods for selective analysis of defined cell populations in CNS tissue (Kamme et al., 2003, Lobo et al., 2006, Doyle et al., 2008, Heiman et al., 2008, Sanz et al., 2009). Fluorescence-activated cell sorting (FACS) has been extensively used as method to purify functionally homogenous cell subpopulations or to enrich a particular cell type in suspension. In embryonic or neonatal organs, including CNS tissue in which the neural cell–cell adhesion is not very tight, the protocol is well established (Kawaguchi et al., 2001) and remain a very useful tool also for haematology and immunology research (Okada et al., 2011). In the adult CNS, however, this method has critical limitations and is not widely used for several reasons. First, the intertwined nature and tight cell–cell adhesions of neural cells make it difficult to separate cells without causing cellular damage. Enzymatic dissociation in the adult CNS often results in the loss of cells, including their type-specific transcripts, and induces reactive changes or cell death (Volovitz et al.,

2016, Mattei et al., 2020). Second, even when the cells are successfully isolated, the chances of the neuronal cells surviving is quite low, which is a major obstacle for the FACS procedure. Third, while conventional immunohistochemistry can be used to identify neural phenotypes with a large variety of cytoskeletal markers, such as neurofilaments, whereas there is a very limited number of adequate "cell surface antigens" that are useful for neural sorting (Okada et al., 2011).

Aside from FACS, laser capture microdissection (LCM) is another methodology that offers potential for identifying cell-type-specific epigenetic changes. This technique was developed to extract targeted cells from complex tissues to examine their gene expression or molecular profiles under microscopy. LCM provides quantitative information about the cells of interest and is a powerful technique, but very few cells can be analysed, which limits its use in amplification-based techniques such as microarray and quantitative PCR analysis. In addition, the procedure used for tissue adaptation and cellular isolation can lead to the loss or damage of tissue-specific molecules (Okada et al., 2011). LCM is more labour intensive than FACS, recovers only small amounts of brain tissue (Hackler et al., 2012, Merbs et al., 2012) and yields of DNA are usually lower, making this approach currently not suitable for large cohort studies exploring different cell types (Smith et al., 2020).

On the other hand, recent technological advancements have facilitated the quantitative analysis of a multitude of markers in a single cell, thereby enabling classification of neural cells. While analyses of gene expression in whole tissue using conventional real-time RT-PCR, DNA microarrays and RNA sequencing has provided insight into the state of cells in tissues under normal and pathological conditions.

Single-molecule fluorescence in situ hybridization (sm-FISH) has been the method of choice for single-cell gene expression analysis (Arrigucci et al., 2017). The power of microscopy-based sm-FISH lies in its ability to allow determination of integer counts of target mRNAs per cell and to provide information about the spatial distribution of RNAs (Tyagi, 2009). However, microscopy-based mRNA quantification is typically applied to small numbers of cells attached to a glass surface (usually ~100 cells) and is labour-intensive. The small sample size limits the ability to assess cell population behaviours and precludes identification of rare cell subsets displaying particular expression patterns. To overcome the limitations of the microscopy-based platform, a flow-cytometry-based protocol for

intracellular mRNA measurements in non-adherent mammalian cells using fluorescence in situ hybridization (FISH) probes has been recently developed (Arrigucci et al., 2017). Unlike microscopy, flow cytometry allows for high-throughput, multi-parametric analyses, therefore it is used to analyse complex cellular phenotypes for many cells at the same time (Chattopadhyay and Roederer, 2012). The method, named by the authors FISH-Flow, involves cell fixation, permeabilisation and hybridization with a set of fluorescently labelled oligonucleotide probes. In this protocol, surface and intracellular protein markers can also be stained with fluorescently labelled antibodies for simultaneous protein and mRNA measurement. With its ability to analyse thousands of cells simultaneously, FISH-Flow can be used to distinguish cells producing particular mRNAs (as few as ten molecules of mRNA per cell) from cells that do not (Arrigucci et al., 2017). FISH-Flow also offers several advantages over conventional, antibody-based flow cytometry. First, it allows concurrent detection of mRNA and cell surface markers, thereby adding a new dimension (gene expression) to the cell phenotyping obtained with conventional flow cytometry. Second, RNA flow cytometry can assay a much broader set of targets than antibody-based flow cytometry for the following reasons: (i) abundance of both coding and noncoding RNAs can be assessed; (ii) designing nucleic acid probes is more straightforward than obtaining suitable antibody probes for the analysis of protein targets; and (iii) nucleic acid probes can be readily designed to bind only under desired conditions (Arrigucci et al., 2017). Nevertheless, also this promising method comes with its drawbacks. One of the limitations of the FISH-Flow method is that fewer fluorochromes have been tested for nucleic acid probe conjugation than for antibody labelling. A second limitation is that the requirement for ~50 (at least 30) 17- to 20-nt-long probes per set limiting the selection of target mRNAs to those that are at least 500-nt long. Third, as mRNAs are typically present in lower copy numbers than the proteins they encode, the RNA-based assay yields signals having lower intensity than those associated with protein detection. Moreover, as with all fluorescence-based methods, the cell types that can be analysed by this method may be limited to those cells that exhibit low-level auto-fluorescence in the fluorescence channels that are used for the analysis (Grau-Exposito et al., 2017).

The emergence of single cell RNA sequencing (scRNA-Seq) technologies in the last decade has led to a rapid phase of discovery in complex tissue research.

Nonetheless, the application of this technology has practical limitations, perhaps the most important of which is the need for fresh tissue. Key output of single-cell transcriptomic experiments is a list of molecularly distinct cell types along with a set of genes expressed in each type. The list usually contains some previously identified and some new cell types, both revealed in unprecedented molecular detail (Poulin et al., 2016). Monitoring gene expression with single-cell resolution therefore offer a more accurate picture than the evaluation of changes in gene expression levels in bulk tissue, as variation in the expression of a given gene could otherwise be occluded by bulk measurements (Trapnell, 2015). However, single-cell transcriptomic relies on the reverse transcription of RNA to complementary DNA and subsequent amplification by PCR or in vitro transcription before deep sequencing, both procedures prone to losses or biases. The biases are exaggerated by the need for very high amplification from the small amounts of RNA found in an individual cell. Refinements to improve the signal-to-noise ratio even further by enhancing the efficiency of reverse transcription and PCR (Lein et al., 2007) or applying molecular barcoding strategies that control for amplification bias (Gong et al., 2003) remain essential. Moreover, expression of a gene that is reliably detected in a population may be anywhere from absent, to low, to high in a given cell because of random fluctuations (Poulin et al., 2016). Models have tried to explain such variability by describing transcription as occurring in discrete bursts driven by stochastic molecular processes (Eberwine et al., 1992). Single-cell transcriptome studies to date require cells in suspension (for example, dissociated tissues or cultures) so that the spatial organization of the population is often lost, unless cells had been picked from defined areas. Thus, despite fast advances in single cell technologies have enabled researchers to quantify transcriptomic variation in individual neural cells, this approach remain expensive, with several pitfalls to address and cannot be used to interrogate multiple genomic marks in parallel, limiting its utility for large studies of human brain disease.

A valid alternative approach has been the direct purification of identified nuclei from adult brain. The fluorescence-activated sorting of fixed nuclei (FAST-FIN) method proposed in 2014 allows immunolabelling and sorting of nuclei from fixed adult brain tissue for the preservation and study of dynamic and labile post-translational histone modifications (Marion-Poll et al., 2014). Although developed in mice striatum, authors have speculated about its applicability to other tissues

and species and to study DNA modifications (Marion-Poll et al., 2014). After many years of stagnation in the field of flow cytometry due to the lack of reliable technology, Jiang et al. in 2008 described a protocol to selectively collect immunolabelled neuronal nuclei from brain tissue with FACS for subsequent chromatin immunoprecipitation assays. They demonstrated that the chromatin structure in isolated nuclei remained unchanged even after a sucrose gradient ultracentrifugation (Jiang et al., 2008). Ever since, fluorescence-activated nuclei sorting (FANS) has been used in a growing number of studies to reduce the complexity of brain cell transcriptomes, epigenomes, and proteomes (Bilsland et al., 2006, Okada et al., 2011, Dammer et al., 2013). However, recent analyses of human brain cell nuclei demonstrated that the proteome and methylome of NeuN-positive (NeuN+ve) nuclei is quite distinct from that of NeuN-negative (NeuN-ve) nuclei (Dammer et al., 2013, Lister et al., 2013). By focusing on analysis of bulk tissue or purifying population exclusively based upon the neuronal marker NeuN, inevitably masks epigenomic changes that occur in other relevant (i.e microglia and astrocytes) or rarer cell types. These overlooked cell types are altered during disease and it is thought that they may play a major role in the development and progression of brain disorders (Wolf et al., 2017, Prinz et al., 2019). Particularly microglia represent approximately 5% of the total cell population in the brain and are challenging to detect using bulk approaches. Disease conditions can alter the proportional representation of particular cell types, which further complicates the interpretation of bulk tissue. For instance, an increased percentage of microglia due to a loss of neurons may incorrectly register as microgliosis by bulk RNA-seq. In light of these considerations it appears crucial the need for a wider range of cell type specific, nuclear antibodies to further disentangle the diversity of the NeuN-ve cellular component.

The scarcity of validated markers for this purpose is due, at least partially, to the difficulty in finding antibodies that meet all the requirements: the candidate marker has to detect nuclear proteins only expressed in a specific cell subtype and work efficiently in frozen post-mortem tissue as well as being compatible with flow cytometry applications. The number of criteria drastically narrows down the options suitable for testing. In consideration of this hurdle, immunocytochemistry assays using *in vitro* model of the cell type of interest have been performed for testing candidate antibodies as alternative approach to confirm the nuclear signal and therefore validate the efficiency of the tested marker.

4.3 Aims

The main aim of the work described in this chapter was to improve the existing FANS protocols enabling the isolation of nuclei populations from multiple neural cell types in order to perform multi-omics profiling from the same specimen. For this purpose, testing and optimisation work was needed in order to:

1. Evaluate and compare the performance of two different previously published FANS protocols (Krishnaswami et al., 2016, Kundakovic et al., 2017) for nuclei purification.

2. Identify novel cell type-specific nuclear markers to enable us to simultaneously immuno-label distinct neural cell types also using immunocystochemistry techniques to confirm their nuclear localisation

3. Extract from each purified nuclei population high quality nucleic acids in high yield suitable for high throughput downstream applications such as methlyomic profiling using the DNA methylation EPIC array, gene expression assay (qPCR), RNA-seq, ATAC-seq and ChIP-seq.

4. Confirm the robustness and reliability of the method developed through alternative technical validations (ICC, TLDA).

4.4 Material and Methods

FACS is an efficient cell separation method that is performed using a flow cytometer and requires a single cell suspension for analysis (Shapiro, 2003, Rahmanian et al., 2017). A fluid stream of cells passes through a laser beam and data corresponding to each cell are digitized and displayed in the form of graphs by the flow cytometer. The stream then breaks up into droplets, each containing a single cell. The droplets, carrying the cells, are electronically charged and deflected into separate collection tubes as a result of passage through an electric field. The amount of applied charge affects the degree of deflection, and hence multiple populations of cells can be separated simultaneously through applying charges of various voltages. There are different sorting modes allowing for a trade-off between sorting rate, purity, recovery, and yield depending on the aim of study. Here this technique was adopted to separate neural cells from post-mortem brain samples maximising the recovery of nuclear material and derived nucleic acids for a parallel multi-omics analysis. NeuN-based cell separation from human cortical post-mortem samples using FANS sorting has been proved to be a robust and reproducible approach, even across brain regions and cohorts by many studies (Gasparoni et al., 2018, Kozlenkov et al., 2017, Kozlenkov et al., 2016, Guintivano et al., 2013). However, one major limitation to this approach is that it is based on the expression of a single antigen, NeuN, and so it is not possible to determine whether the non-neuronal findings originated from microglia, astrocytes, oligodendrocytes or other cell types. In order to further discriminate the epigenetic signal within the non-neuronal component of the tissue, several cell-type specific nuclear antibodies have been tested for immunolabelling and those proved successful have been incorporated in the protocol for the purification of oligodendrocytes and microglia from the same brain specimen.

4.4.1 Published protocols testing for optimal nuclei purification

Two different previously published protocols were tested in order to identify the best method to isolate highly purified nuclei populations from bulk post-mortem tissue samples. Although aiming at different applications and tailored around different research questions, both protocols included a nuclei purification step by differential high-speed centrifugation. **Protocol 1** (Krishnaswami et al., 2016) was developed to perform single cell RNA-seq from brain tissue to capture the transcriptome of post-mortem neurons bypassing the alterations due to the cell dissociation stage; **Protocol 2** (Kundakovic et al., 2017) presented a ChIP-seq pipeline for mapping histone modifications in chromatin extracted from post-mortem brain samples in a cell-type specific manner. Both methods were performed as per author's instructions and their yield were compared in terms of nuclei recovery. Also, the integrity of the nucleic acids extracted from the nuclei was assessed by agarose gel electrophoresis prior testing downstream applications.

4.4.1.1 <u>Nuclei purification</u>

In order to isolate nuclei fractions from bulk post-mortem human brain a combined procedure of mechanical and chemical tissue dissociation was adopted in both tested protocols: the frozen sample was transferred in a lysing solution, which helps to digest the tissue, followed by repetitive strokes using ice pre-chilled glass pestles until solution becomes visually homogeneous. Given that nuclei can be isolated at 4°C from tissue homogenate with minimal damage (Krishnaswami et al., 2016), samples were kept on ice for the entire procedure in order to preserve the nuclei structure. For frozen human brain tissue, **protocol 1** recommended proceeding directly to FACS after filtering the homogenate using a cell strainer cap without further purification as nuclei have been subjected to freezing and additional purification steps can cause RNA damage. The filtering step is meant to remove major debris (larger than 35 µm) or undisrupted tissue; however, each purification step results in lower yields of nuclei. Differently, **protocol 2**, after tissue douncing included an ultracentrifugation clean-up (106,803 x g for 1 hour at 4°C) to extract nuclei via sucrose gradient when using frozen tissue.

4.4.1.2   *Nuclei Immunolabelling*

The nuclei recovered as pellets were then re-suspended in isotonic buffer and incubated with antibodies against cell-type specific markers. Both protocol used mouse monoclonal antibodies but different staining dilutions were adopted: the combination anti-NeuN unconjugated primary antibody + AlexaFluor 594 secondary antibody was proposed in **protocol 1** (1:5000 dilution, 30 minutes each, on a rotor, at 4°C) whereas **protocol 2** used an anti-NeuN antibody pre-conjugated to Alexa 488 (Cat No MAB377X) 1:500 dilution, 45-60 minutes on a rotor, at 4°C. Differently from **protocol 1, protocol 2** did not include gentle washing steps (400 x g for 5 minutes) after immunostaining but required filtering through a 35 µm cell strainer before sorting.

4.4.1.3   *Nuclei sorting*

As recommended in both protocols, nuclei suspensions were kept on ice while preparing for FACS and for downstream applications. As per **protocol 1**, the FACS droplet stream was optimized for timing delay, with any satellite droplets merged by the fifth drop after the droplet breakoff. Failure to optimize the droplet breakoff may result in a charge placed on the satellite droplet instead of the droplet of interest. FACS plots for doublet discrimination gating were set to prevent sorting of doublets and further groupings of attached nuclei (refer to **Methods** chapter - section 2.2.1.5 for detailed description of FACS gating criteria). A small amount of sample was initially loaded into the instrument to confirm gating and arrange gates on the FACS plots as needed. For immuno-stained samples, both positive and negative populations were collected. As recommended in **protocol 1,** the overall event rate for particles was set to be 200-2,000 events per second on the FACS instrument to prevent swamping of the detectors that may result in a poor sorting accuracy. Depending on the concentration of nuclei, dilution of the sample may be also required to preserve sorting efficiency. FACS-sorted nuclei were snap frozen on dry ice and stored at -20 °C for subsequent DNA and/or RNA extraction.

4.4.2 Genomic DNA isolation

Three different protocols were tested in order to isolate high quality genomic DNA from the purified nuclei populations: (1) an phenol/chloroform extraction method using Phase Lock Gel (PLG) tubes, (2) a column-based extraction technique using the Allprep DNA/RNA Mini Kit (Qiagen, UK) adapted to preserve the fragile nature of nuclei and (3) an isopropanol extraction method originally developed for tissue and cell extraction but adapted to sorted nuclei (see **Methods, section 2.4**). This last protocol variant was purely dictated by the nature of the samples. When the DNA concentration in the sample is low, isopropanol generally works better than ethanol for the extraction as DNA is less soluble in isopropanol so it precipitates faster even at low concentrations. Isopropanol is also preferable for precipitating DNA from large volumes as less alcohol is used. Collection/storage procedure of the nuclei after FACS sorting was also tested in order to optimise the input material and consequently the DNA yield after extraction; performance of DNA protocol 3 was indeed tested using frozen pelleted nuclei vs frozen nuclei suspension (nuclei collected in FACS running buffer).

DNA Protocol 1 is a commonly used liquid-liquid extraction technique to separate nucleic acids from proteins and lipids. The organic extraction solvent phenol/chloroform is added to promote the partitioning of proteins, lipids and cellular debris into the organic phase, leaving isolated DNA in the aqueous phase. Sodium acetate helps to neutralise the DNA charge by increasing of ionic strength so that DNA precipitation is facilitated when an alcohol is added. The PLG acts as a barrier between the organic and aqueous phases, allowing the nucleic-acid-containing phase to be easily recovered saving time while optimising the recovery of nucleic acids. Moreover, the use of PLG can result in an increase of 20 to 30% recovery of nucleic acids compared to traditional methods (Quantabio, 2007). Given that multiple extractions can be performed in the same tube as long as maximum sample volume is not exceeded, the extraction of both DNA and RNA from the same nuclei aliquot was attempted to maximise usage of sorted material and minimise the time consumption required for extraction procedures.

Briefly, for DNA protocol 1, PLG 2 mL heavy tubes were centrifuged at 14,000 x g for 30 seconds immediately prior usage to pellet down the gel matrix. To each sample (nuclei suspension) an equal volume of phenol/chloroform solvent (Fisher Scientific, Cat No BP1752-400) was added and the organic and aqueous phases were thoroughly mixed to form a transiently homogeneous suspension (do not

vortex). Tubes were centrifuged at 14,000 x g for 5 minutes to separate the phases. At this stage, if a second extraction is necessary, and maximum tube volume is not exceeded, more organic extraction solvent can be added to the same tube and the above step repeated. The aqueous upper phase (containing nucleic-acids) was carefully recovered and transferred to a new LoBind tube. 3M Sodium Acetate (NaAc) (1/10 of volume recovered) was added to each tube together with an equal volume of 100% Isopropanol to allow DNA precipitation. Tubes were then centrifuged at 14,000 x g for 5 minutes at RT and supernatant discarded. 1mL of 70% EtOH was added to each tube to remove some of the salt from the DNA pellet. Tubes were centrifuged at 14,000 x g for 5 minutes, supernatant was discarded and pellets were left to air dry before resuspension in a small volume of ddH20 (30µL/ DNA pellet). Ultra pure water was preferred over Tris EDTA (TE) buffer to solubilize the DNA as although it protects the nucleic acid from degrading by DNase or RNase it may interfere with downstream applications (for microarrays, it can inhibit cDNA synthesis (Illumina, 2016).

The AllPrep-DNA/RNA-Mini kit (**DNA protocol 2**) was initially tested with the aim of maximising yields of DNA and RNA from the same sample as well as streamlining the extraction procedure making it more time and labour effective. This kit allows the simultaneous purification of high-quality genomic DNA and RNA from the same biological sample. The protocol is divided in two parts and the purified DNA and RNA are eluted separately. A full guide is available from the manufacturer (Qiagen, 2005). The manufacturer's protocol (**Figure 4.5**), originally developed for tissue or single cells, required minor changes to be adapted to nuclei samples.

Briefly, 350µL to 600µL of RLT buffer (according to the initial number of nuclei per aliquot) were added to FACS sorted nuclei samples to help disrupt the nuclei; tubes were mixed through several inversions. The lysate samples were transferred to AllPrep DNA spin columns placed in the supplied 2 mL collection tubes. Tubes were centrifuged for 30 seconds at 9,000 x g. When necessary, centrifugation was repeated until all liquid passed through the membrane. Spin columns were placed in new 2 mL collection tubes. 500µL of Buffer AW1 were added to the AllPrep DNA spin columns and tubes were centrifuged for 20 seconds at 9,000 x g to wash the spin column membrane. The flow-through was discarded and 500 µL of Buffer AW2 were added to the AllPrep DNA spin column.

Tubes were then centrifuged for 2 minutes at full speed (≥18,000 x g) to wash the spin column membrane. The long centrifugation dries the spin column membrane, ensuring that no ethanol is carried over during DNA elution preventing interference with downstream reactions. After centrifugation, the AllPrep DNA spin columns were carefully removed from the collection tubes to prevent contact of the column with the flow-through. The AllPrep DNA spin columns were then placed in new 1.5 mL collection tube (supplied). 75 µL of elution buffer (EB) (preheated to 70°C) were subsequently added directly to the spin column membrane and tubes were incubated at RT (15–25°C) for 2 minutes, and then centrifuged for 1 minute at 9,000 x g to elute the DNA. The whole elution step was repeated twice to elute further DNA and to achieve a higher DNA concentration, elution volume was reduced to 20µL of EB per elution step. DNA samples were quantified and stored at -20°C until further processing.

For **DNA protocol 3**, which is the chosen extraction technique best suited for the FANS pipeline, full details are provided in **Methods, section 2.4.**
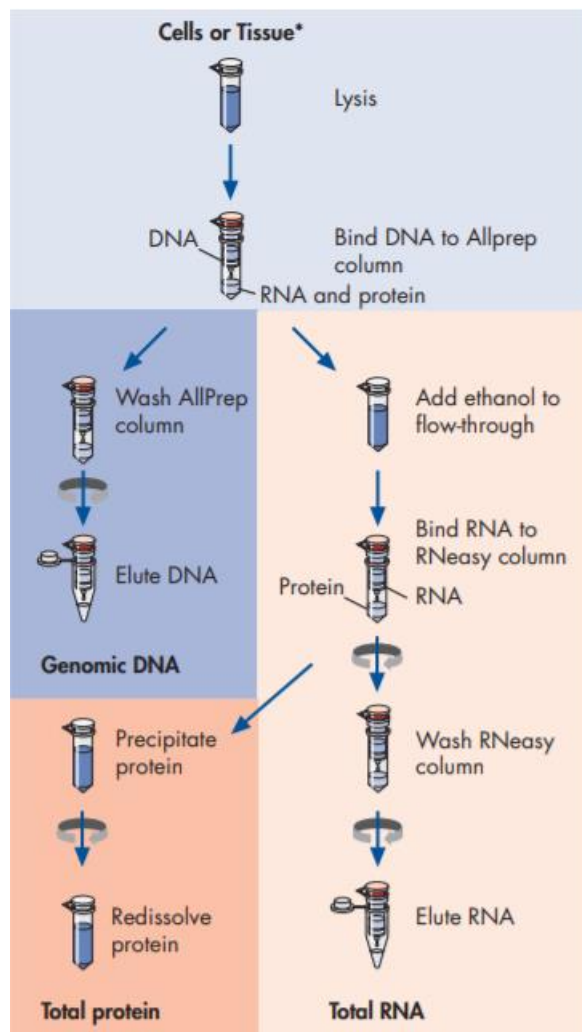
Figure 4.5 Schematic overview of the AllPrep DNA/RNA/Protein precipitation procedure.
Figure taken from manufacturer's manual. Extraction of genomic DNA extraction and RNA extraction do not happen in parallel, and require to follow two different sections of the protocol. Nuclei in solutions were used here as input material and protein extraction was not perform as beyond the scope of this work.

4.4.2.1   Genomic DNA quality assessment

In order to assess the integrity and overall quality of the extracted genomic DNA (gDNA), ethidium bromide-stained, 1% agarose gel electrophoresis was used to run few test samples for each nuclei population collected via FANS. 100 ng of gDNA per nuclei fraction were loaded in each well together with 1 µL of loading dye (5x Orange G) (Sigma-Aldrich, UK) for visual tracking of DNA migration. A molecular-weight size marker in the form of a 1kb DNA ladder (New England BioLabs, UK) was also used. Gels were run on low-medium voltage (100 mV) for 1 hour. Gel images were acquired using the Image Studio Lite Ver 5.2 software.

4.4.3 Nuclear RNA isolation

Several tests were also performed in order to isolate intact nuclear RNA from FANS purified nuclei aliquots. Three different approaches were explored and compared on performance:

(1) Qiagen AllPrep-DNA/RNA-Mini kit
(2) Trizol manual RNA extraction (regular eppendorfs vs heavy 2 mL PLG tubes)
(3) Directzol RNA MicroPrep

As previously mentioned in section 4.4.2, the Qiagen AllPrep-DNA/RNA-Mini kit (**RNA Protocol 1**) was tested in the attempt to maximise the RNA recovery and minimize alcohol and/or protein carry over as well as for time saving purposes. Extraction was conducted following the manufacturer's standard instructions (Qiagen, 2005). Differently, for the Trizol manual RNA extraction (**RNA protocol 2**), samples were defrosted at RT as sorted nuclei were collected in Trizol Reagent (Fisher Scientific, UK) and thawing on ice tends to enhance salts precipitation. However, every centrifugation step was performed at 4°C to preserve the RNA integrity. PLG 2 mL heavy tubes were spun down at 10,000 x g for 5 minutes immediately prior usage to pellet down the gel. After defrosting, nuclei suspensions were transferred to the PLG tubes. 100µL of chloroform (Sigma Aldrich, UK) were added per each 500 µL of sample (sorted nuclei collected in Trizol Reagent). Tubes were securely capped, mixed by inversions (5 times), incubated for 2-3 minutes at RT and centrifuged for 5 minutes at 10,000 x g. At this stage, three layers should be identifiable: a lower red phase (containing chloroform), an interphase, and a colourless upper aqueous phase. The aqueous phase containing the RNA was recovered by angling the tube at 45° and transferred to a new (regular), labelled 1.5 mL eppendorf. For every 500 µL of Trizol Reagent used for lysis, 250 µL of 100% Isopropanol (Sigma Aldrich, UK) were added. Each tube was gently mixed 3-5 times, incubated 10 minutes at RT and centrifuged for 10 minutes at 12,000 x g at the end of which precipitated RNA appeared as a white gel-like pellet at the bottom of the tube. Supernatant was discarded and RNA pellets were gently dislodged from the bottom of the tube and re-suspended in 500 µL of 75% ethanol (Fisher Scientific, UK). Tubes were then centrifuged for 5 minutes at 7,500 x g, supernatant was discarded from each

tube and RNA pellets were left to air dry at RT for 10 -15 minutes until they looked visually dry.

Care was taken to prevent pellets from over drying in order to ensure total solubilisation of the RNA when resuspended (partially dissolved RNA samples have a 260/230 ratio < 1.6). Each pellet was resuspended in 15 µL of RNAse free dH20 and stored at -80°C. **RNA protocol 3** was the chosen extraction technique best suited for the FANS pipeline, therefore full details are reported in **Methods, section 2.5.**

4.4.3.1   *RNA clean-up*

Two different clean-up procedures were tested in order to remove contaminants impurities or enzymatic inhibitors as well as to desalt nuclear RNA samples. Method 1 involved a second precipitation step using this time 100% ethanol instead of 100% isopropanol followed by a 75% ethanol wash aiming to remove salts precipitation, while method 2 used the RNeasy MinElute Cleanup kit (Qiagen, Cat No. 742040) which is designed to concentrate and purify RNA isolated by alcohol-precipitation and organic-extraction methods providing high quality samples suitable for use in high sensitivity assays.

Briefly, according to method 1, after the first 75% ethanol wash, supernatant was discarded and pellets were resuspended in 100 µL of dH20. Tubes were left on ice for 5 minutes to allow pellets to fully resuspend and then each suspension was transferred in new clean 1.5 mL tubes. 1/10 volume of Sodium Acetate (Fisher Scientific, UK) (10 µL if 100 µL starting volume) plus 3 volumes (300 µL if 100 µL starting volume) of 100 % ethanol were added to each sample and kept at -80°C overnight. Tubes were then centrifuged for 15 minutes at full speed, pellets were washed with 500 µL of 75% ethanol at 7,500 x g for 5 minutes. Supernatant was pipetted off from each tube followed by a pulse spin at 2,000 g max so that any residual volume left at the bottom of the tube could be removed. Each RNA pellet was left to air dry at RT for 10-15 minutes, resupended in 15uL of RNA-free water ready to be quantified and stored at -80°C until further usage. For method 2, the manufacturer's protocol was followed as per instructions. RPE and RLT buffers provided within the kit were modified as indicated to obtain the respective working solutions. Sample volumes were adjusted to 100 µL using RNase-free water. 350 µL of RLT buffer were added to each tube and mixed well

by pipetting. Then 250 μL of 100% ethanol were added to the diluted RNA samples and solutions were mixed well by pipetting. Immediately after, samples were transferred (700 μL) to an RNeasy MinElute spin column placed in a 2 mL collection tube. Tubes were securely capped and centrifuged for 15 seconds at 8,000 x g. Flow-through was then discarded. For samples >700 μL, the remaining sample (up to 700 μL) was transferred to the pre-used spin column and the centrifugation was repeated. The flow-through was discarded and the RNeasy MinElute spin columns were placed in new 2 mL collection tubes. 500 μL of RPE buffer were subsequently added to the spin column and tubes were centrifuged for 15 seconds at 8000 x g to wash the spin column membrane. Flow-through was discarded and collection tube reused for the subsequent step. 500 μL of 80% ethanol were added to the RNeasy MinElute spin column and tubes were secured and centrifuged for 2 minutes at 8,000 x g. After centrifugation, the RNeasy MinElute spin columns were carefully removed from the collection tubes avoiding the contact between the column and flow-through to prevent carryover of ethanol from occurring. RNeasy MinElute spin columns were placed in new 2 ml collection tubes and centrifuged at full speed for 5 minutes with the lids opened. Flow-through and collection tube were discarded. Care was taken to make sure the spin column membranes were completely dried since residual ethanol may interfere with downstream reactions. Centrifugation with the lids open ensures that no ethanol is carried over during RNA elution. RNeasy MinElute spin columns were then placed in new 1.5 mL collection tubes and 14 μL of RNase-free water was added directly to the centre of each spin column membrane and tubes were centrifuged for 1 minute at full speed to elute the RNA. Elution volumes should not be below 10 μL as the spin column membrane will not be sufficiently hydrated. Given that the dead volume of the RNeasy MinElute spin column is approximately 2 μL, for an elution volume of 14 μL, 12 μL of eluate are expected to be recovered.

4.4.3.2   *RNA quality control*

Quality check of the nuclear RNA was also performed to assess the integrity and purity of the extracted samples. NanoDrop 2000 spectrophotometer was used to measure the RNA concentration of each sample as well as to assess their purity estimated through the ratio scores: RNA absorbs at 260nm while proteins absorb at 280nm therefore the 260/280 ratio measures the concentration of RNA over

proteins in the sample; a score of ~2.0 is generally accepted as "pure" for RNA. The 260/230 ratio is a second measure for purity of the sample, as contaminants/impurities absorb at 230nm (i.e. EDTA, phenol, ethanol); values significantly lower than 2.2 generally indicate sample contamination.

Qubit fluorometer measurements were also performed to confirm sample concentration as the Nanodrop has limited sensitivity at quantifying <40ng/μL while the Qubit, as a fluorophore-based method, allows a very accurate determination of nucleic acid concentration (sub-nanogram concentrations detection). Furthermore, the Agilent Bioanalyzer 2100 RNA 6000 Nano kit (see **Methods**, **section 2.12.1** for details) was used as per manufacturers' instructions to assess the integrity of RNA samples and their level of fragmentation.

4.4.4   Immunostaining of nuclei – Optimization

Although over the past decades of research several robust antibodies have been identified and validated in brain tissue as unique marker of cell type identity, for the majority of cases, the antigen has surface or cytoplasmatic localisation. The field still lacks validated nuclear-targeting antibodies. Before assessing their performance on FANS, all the antibodies described below have been tested for immunocytochemistry (ICC) on *in vitro* human cell lines aiming at verifying the specificity of the chosen markers for distinct cell types and their selectivity in targeting the nucleus. Each antibody was added at a given concentration to the nuclei suspension simultaneously with the anti-NeuN antibody. Different antibody dilutions and incubation times were tested for each antibody in line with manufacturer's recommendations. **Table 4.1** provides full details about product specifications and tested dilutions for each tested antibody.

4.4.4.1   Oligodendrocyte-specific antibodies testing

I performed literature data mining and selected a set of transcription factors (TFs), which are enriched in oligodendrocytes compared with other neural lineages since required for oligodendroglial specification (Liu et al., 2007, Wang et al., 2014, Yang et al., 2013). Based upon previously published work, two different antibodies, anti-Olig2 and anti-Sox10 were tested using the FANS protocol in the attempt to identify and isolate the oligodendrocytes from the remaining cell types

constituting the bulk tissue. AlexaFluor555 anti-Olig-2 antibody (Millipore, Cat No AB9610-AF555) was tested at three different dilutions (1:50; 1:150 and 1:1000) and two different incubation time (1.5 hour vs 45 minutes, 4°C). Commercially available anti-Sox10 antibodies were acquired from two distinct suppliers (Santa Cruz Biotechnology and R&D Systems) in different formulations (pre-conjugated and/or unconjugated) each of which was tested at multiple dilutions for 1 hour at 4°C. Full details are provided in **Table 4.1.**

4.4.4.2 *Astrocyte-specific antibodies testing*

Similarly, a broad literature search was conducted to find previously reported nuclear markers for the astrocyte population. Three different antibodies were tested for FANS: anti-aldolase C antibody (Abcam, Cat No. ab87122) in both conjugated and unconjugated formulation at three different concentrations (1:200; 1:500, 1:1000), anti-Pax6 antibody pre-conjugated to AlexaFluor647 (Abcam, Cat No. ab215925) at two different dilutions (1:200, 1:1000) and anti-sox9 antibody (Santa Cruz Biotechnology, Cat No. Sc-166505) at 1:100 and 1:500 dilution. Full details about the antibodies tested are reported in **Table 4.1**. Aldolase C was also tested on SH-SY5Y neuroblastoma cells and human U373 astrocytoma cells (Weightman Potter et al., 2019) to assess the localisation of the staining within the cell while verifying its specificity for astrocytes.

4.4.4.3 *Microglia-specific antibodies testing*

Guided by preliminary findings in the literature, three candidate markers were selected for immunostaining testing on nuclei pellet. For Pu.1, two different antibodies were investigated: the AlexaFluor647 anti-Pu.1 (Santa Cruz Biotechnology, Cat No. sc-390405) and the unconjugated anti-Pu.1/Spi1 (R&D systems, Cat No. MAB5870) both tested at 1:50 and 1:500 dilution. The Anti-IRF8 antibody pre-conjugated to APC fluorochrome (Invitrogen, Cat No. 17-9852-82) was tested at three different concentrations (1:50, 1:250, 1:1000) while the anti-SALL1 antibody (Abcam, ab41974) was tested at a dilution of 1:100. For FANS, the chosen staining time for all three antibodies was 1.5 hour incubation at 4°C. *PU.1* and *SALL1* were also extensively screened in an ICC study on human cell lines. A detailed description of the study is provided in section 4.4.5 and 4.5.4 of this chapter.

4.4.4.4 *GABAergic neurons antibody testing*

Due to the heterogeneity of the neuronal population in the human brain I set out to further characterize the neuronal fraction by staining the purified nuclei suspension with a nuclear antibody previously published for being specific to human prefrontal cortex GABAergic interneurons (Kozlenkov et al., 2016). Since no details regarding the supplier were provided in the publication, the commercially available anti-Sox9 antibody (Santa Cruz Biotechnology, Cat No. Sc-166505) was selected and tested on nuclei samples at 1:50 and 1:400 dilution for 1.5 hour incubation.

Applic ation	Marker	Gene Name	Specificity	Molecular Target	Reference (PMID)	Supplier	Catalogue N.	Primary Ab	Specie raised	Dilution 1ry Ab	Secondary Ab	Dilution 2ry Ab
FANS	NeuN	*RBFOX3*	Neuronal nuclear marker	RNA-binding protein	24057217 18442397	Millipore	MAB377X	Pre-conjugated (Alexa Fluor 448)	mouse monoclonal	Titration 1:1000		
FANS	Sox9	*SRY-Box9*	GABA neuronal nuclei	Transcripti onal activator	26612861 17084361 19709629	Abcam	ab30455	Unconjugated	Rabbit polyclonal	1:200 1:500	Sc-45098 (PerCP)	1:200
FANS	Pax6	*PAX6*	Astrocyte nuclear marker	DNA binding protein	18448636 24114637	Abcam	ab215925	Pre-conjugated (AlexaFluor 647)	rabbit monoclonal	1:100		
ICC/ FANS	Aldolase C	*ALDOC*	Astrocyte marker	glycolytic enzyme	28816095 23688545 11487642	Abcam	ab87122	Unconjugated	Rabbit polyclonal	1:200 1:500 1:1000	A21236 (Alexa 647)	1:400
						Abcam	ab87122	Pre-conjugated (PE)	Rabbit polyclonal	1:200 1:500 1:1000		
FANS	Sox10	*SRY-Box10*	Mature oligodendr ocytes	Nucleo-cytoplasm ic shuttle protein	17084361	R&D Systems	AF2864	Unconjugated	Goat monoclonal	1:300 1:600	NL002 (NL637)	1:200
						R&D Systems	MAB2864	Unconjugated	mouse monoclonal	1:30	Sc-516141 (PE)	1:100
						Santa Cruz	Sc-365692	Pre-conjugated (PE)	Mouse monoclonal	1:50-1:500		

Assay	Marker	Gene	Description	Category	Publication IDs	Company	Catalogue	Conjugation	Host	Dilution	Secondary	Dilution
FANS	Olig-2	*OLIG2*	Oligodendroglial lineage marker	Transcription factor	17084361	R&D Systems	NL2864R	Pre-conjugated (NL577)	Mouse monoclonal	1:10-1:50		
					15198128 29922130 15790969	Millipore	AB9610-AF555	Pre-conjugated (AlexaFluor 555)	Rabbit polyclonal	1:150		
						Abcam	ab87122	Pre-conjugated (PE)	Rabbit polyclonal	1:200 1:500 1:1000		
ICC/ FANS	PU.1	*SPI1*	Microglia nuclear marker	Transcription factor	25574134 23483680	Santa Cruz Biotech	sc-390405	Pre-conjugated (AlexaFluor 647)	Mouse monoclonal	1:100 1:250		
						R&D Systems	MAB5870	Unconjugated	Mouse monoclonal	1:100 1:250 1:500	Sc-516141 (PE)	1:100
ICC/ FANS	SALL1	*SALL1*	Microglia nuclear marker	Transcription factor	27776109	Abcam	ab41974	Unconjugated	Mouse monoclonal	1:100	A21202 (FITC-Alexa 488)	1:200
ICC/ FANS	IRF8	*IRF8*	Microglia nuclear marker	Transcription factor	30867424 23166780 26002684	Invitrogen	17-9852-82	Pre-conjugated (APC)	Mouse monoclonal			

Table 4.1 Table reporting the full list of nuclear antibodies tested on FANS and/or ICC during the protocol optimisation.

4.4.5 Immunocytochemistry on human microglia cell line

Due to the difficulty in finding nuclear markers suitable for FANS applications, ICC was adopted as an alternative/ complementary approach to verify the nuclear specificity of the chosen candidate markers. Despite databases (e.g. https://www.proteinatlas.org/, https://www.ncbi.nlm.nih.gov/geo/) showing evidence of nuclear localisation indeed, the vast majority of the antibodies tested for nuclei immunolabelling were not detected by the cell sorter or showed generalised and non-specific staining. In particular, I focused on the microglia due to its relevance and involvement in brain related disorders (Zhan et al., 2014, Fakhoury, 2018, Salter and Stevens, 2017) as well as for the availability in house of a microglia cell line. Two of the three antibodies selected from the literature were extensively tested: *PU.1 and SALL1.* The other candidate marker, IRF8, since already proven to be suitable when tested on FANS and due to time constrains, was not tested further on microglia cell line.

4.4.5.1   *Human Lenti-SV40 immortalized microglia cell line*

Lenti simian virus-40 (SV40) immortalised human microglia cells, derived from human fetal brain tissue (AcceGen Biotech, Cat. No: ABITC4171) were cultured in microglial cell medium (AcceGen Biotech, Cat. No ABITM009). In order to increase surface adhesion, acid etching was performed on glass coverslips with 1M HCl at 65°C for 6 hours. Coverslips were washed five times with ultra-distilled water (dd.H20) followed by a 100% ethanol wash. After being placed in well plates, coverslips were then treated with diluted poly-D-lysine (PDL) (39ml ddH20 with 1mL PDL (Sigma-Aldrich, UK, Cat. No A-003-M)) and incubated for 3 hours at 37°C. After poly-D-lysine removal, they were washed in 1x phosphate-buffered saline (1x PBS). When cells in passage 4 reached 80% confluence, microglial medium was removed, and cells were washed with 1x PBS. In order to detach cells from the base of the container, the flask was incubated for 2 minutes at 37°C with 1x PBS and 0.05% trypsin-ethylenediaminetetraacetic acid ((EDTA) Sigma-Aldrich, UK, Cat. No T4174). Trypsin- EDTA was removed from the flask and the cell suspension was transferred into a 50mL falcon containing fresh microglial medium (5mL). The base of the flask was washed with trypsin neutraliser solution (Genlantis, CA, Cat.No. PR080100) which was added to the 50mL falcon. The

cell suspension was spun at 9,000 x g for 5 minutes and resuspended in fresh microglial medium. Cells were counted, imaged and plated out at 10,000 cells/dm^2.

4.4.5.2   *Immunofluorescence staining*

SV40 microglia-coated coverslips were treated with 4% paraformaldehyde (PFA) solution to encourage cross-link formation and fixing. Coverslips were incubated at RT for 20 minutes. PFA was removed and coverslips were washed three times with 1x PBS for 5 minutes. Cells were stored in 1mL of 1x PBS at 4°C to be used within one week of fixing. In order to optimise the antibody performance and immunostaining method, two different ICC protocols were tested to ensure that both reagents and techniques worked.

Pu.1 - Protocol 1: Cells were permeabilised with 0.2% Triton-X 100 (Sigma-Aldrich, St. Louis, MO) PBS solution for 20 minutes, followed by three 5-minutes 1x PBS washes. Cells were then incubated with blocking buffer (1x PBS with 1% BSA (Sigma-Aldrich, St. Louis, MO, Cat. No: 05470) and 0.1% Tween-20 (Sigma-Aldrich, St. Louis, MO, Cat. No: P1379)) for 1 hour at RT. Cells were stained with mouse monoclonal anti-Pu.1 IgG2B (1:100, 1:250, 1:500, 1:1000 dilutions, R&D Systems, Minneapolis, MN, Cat. No MAB5870, clone #732322) diluted in blocking buffer, and incubated overnight at 4°C. After 15 hours, cells had three 5-minutes 1x PBS washes. Cells were stained for 1 hour at RT with Alexa Fluor 488 donkey anti-mouse secondary antibody (1:400 dilution, Invitrogen, Carlsbad, CA, Cat. No A-21202) diluted in Dako antibody diluent (Agilent, Santa Clara, CA, Cat. No S080983-2). **Pu.1 - Protocol 2:** Cells were incubated with ADST buffer (1x PBS with 0.1M lysine, 10% donor calf serum, 0.02% sodium azide, 0.2% Triton-X 100) for 30 minutes at RT. This step simultaneously allowed cell membranes to be permeabilised and unspecific binding to be prevented. Cells were stained with the same mouse monoclonal anti-Pu.1 IgG2B (1:100, 1:250, 1:500, 1:1000 dilutions) diluted in antibody buffer, and incubated overnight at 4°C. After 15 hours, cells were incubated at RT for 2 hours, followed by three 5-minutes 1x PBS washes. Cells were stained for 1 hour at RT with Alexa Fluor 488 donkey anti-mouse secondary antibody (1:400 dilution, Invitrogen, Carlsbad, CA, Cat. #A-21202) diluted in Dako antibody buffer.

Sall1 - Protocol 1: Cells were permeabilised with 0.2% Triton-X 100 PBS solution for 20 minutes, followed by three 5-minutes 1x PBS washes. Cells were then incubated with blocking buffer (1x PBS with 1% BSA and 0.1% Tween-20) for 1 hour at RT. Cells were stained with mouse monoclonal anti-Sall1 [K9814] (1:100, 1:250, 1:500 and 1:1000 dilutions, Abcam, Cambridge, UK, Cat. No ab41974) diluted in blocking buffer. Cells were incubated overnight at 4°C. After 15 hours, cells were washed three times for 5 minutes with 1x PBS followed by staining for 1 hour at RT with Alexa Fluor 555 goat anti-mouse secondary antibody (1:400 dilution, Invitrogen, Carlsbad, CA, Cat. #A-21422) diluted in Dako antibody diluent. **Sall1 - Protocol 2:** Cells were incubated with ADST buffer (1x PBS with 0.1M lysine, 10% donor calf serum, 0.02% sodium azide, 0.2% Triton-X 100) for 30 minutes at RT in order to allow cellular membranes to be permeabilised and unspecific binding to be prevented. Cells were stained with the same mouse monoclonal anti-Sall1 (K9814) (1:10, 1:50, 1:100, 1:250 dilutions) diluted in blocking buffer and incubated overnight at 4°C in the dark. After 15 hours, cells were incubated at RT for 2 hours, followed by three 5-minutes 1x PBS washes. Cells were then stained for 1 hour at RT with Alexa Fluor 488 donkey anti-mouse secondary antibody (1:400 dilution, Invitrogen, Carlsbad, CA, Cat. No A-21202) diluted in Dako antibody diluent.

4.4.5.3   *Fluorescence imaging*

After staining, cells were washed three times for 5 minutes with 1x PBS. Cells were counterstained with 4',6- diamidino-2'-phenylindole dihydrochloride (DAPI) (1:5000 dilution, Sigma-Aldrich, St. Louis, MO, Cat. No: 10236276001) for 15 minutes at RT, followed by three 1 minute 1x PBS washes. Coverslips were placed on Dako fluorescence mounting medium (Agilent, Santa Clara, CA, Cat. No: S302380-2) on microscope slides and left to air dry overnight. Coverslips were imaged on the Leica DM4000 B LED Fluorescence Microscope (Leica Microsystems, Wetzlar, Germany).

4.4.6 Gene expression assay to validate nuclei fraction purity

300,000 nuclei were collected in 500µL of pre-chilled TRIzol™ LS Reagent (Invitrogen™, Cat No.11588616) and snap frozen on dry ice. Nuclear RNA was extracted from the separated nuclei suspension using the Direct-zol™ RNA MicroPrep column kit (Zymo Research, Cat No. R2060) following the manufacturer's instructions. Complementary DNA (cDNA) was obtained through reverse transcription using the Invitrogen VILO cDNA synthesis kit (Life Technologies, Cat No. 11754050) in 20µL reactions according to the manufacturer's instructions.

Quantitative RT-PCR was performed in duplicate using the QuantStudio 12K Flex (Applied Biosystems) in conjunction with the TaqMan low-density array (TLDA) platform using off-the-shelf pre-optimized assays targeting (i) genes highly expressed in the major brain cell types to control for cell type identity (*NEUN* and *ENO2* for neurons, *OLIG2* for oligodendrocytes, *GFAP* for astrocytes, *CD68* for microglia), and (ii) five housekeeping genes (*ACTB, EIF4A2, GAPDH, SF3A1*, and *UBC)* identified in previous studies (Marzi et al., 2018) as being the most stably expressed in the brain using GeNORM (Primer Design, Southampton, UK). PCR cycling conditions were 50°C for 2 minutes, 94.5°C for 10 minutes, and 45 cycles of 97°C for 15 seconds and 60°C for 1 minutes. Stringent QC of raw qPCR data was undertaken, removing samples where there was high variability between duplicates (Ct > 0.5). The abundance of each test gene was determined by the comparative Ct method (Pfaffl, 2001) expressed relative to the geometric mean of the five housekeeping genes quantified in parallel. Data were log2-transformed to ensure normal distribution and presented as a fold-difference in expression adopting the samples labelled as "total nuclei" (unsorted nuclei from the same sample) as baseline.

4.5   Results

An improved FANS protocol based on previously published methods was developed for the separation of cell-type specific nuclei populations using AlexaFluor488 anti-NeuN monoclonal antibody (Millipore Cat No. MAB377X) (whose antigen is specific for neuronal cells) and NL577-conjugated anti-Sox10 monoclonal antibody (R&D systems, Cat No. MAB5870) (whose antigen is specific for oligodendrocyte cells) (see **Figure 4.6** for a schematic overview of the different stages of the FANS method). Multiple extraction methods were tested and compared in performance in order to obtain high quality, high yield genomic DNA as well nuclear RNA from purified nuclei fractions to be used in sensitive downstream applications (DNA methylation profiling, gene expression assays, RNA-seq, Chip-seq, ATAC-seq) for multi-omics analysis. Gene expression levels of known cell-type specific marker genes were also assessed using Taqman targeted assays to validate the enrichment and purity of the sorted populations.
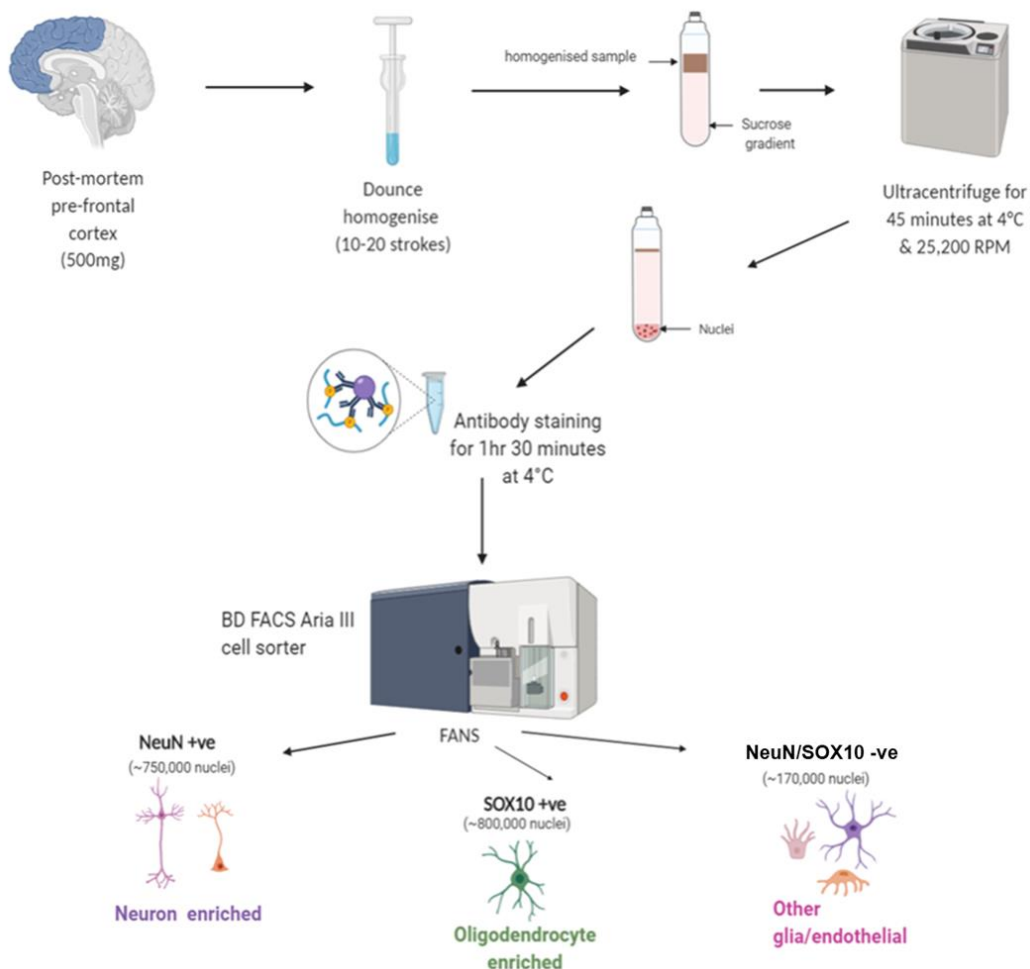
Figure 4.6. Schematic overview of the optimised FANS method.

4.5.1 High recovery of intact nuclei from frozen brain tissue using FANS

Two FANS protocols selected from the literature were independently tested using post-mortem human brain tissue and their performance was compared in terms of nuclei recovery, purity and time consumption. The protocol from Kundakovic et al. (Kundakovic et al., 2017) (i.e **protocol 2**) was the most robust and yielded the most nuclei however the DNA quality and integrity was suboptimal for the downstream processes required. I have since optimised this protocol to further maximise the nuclei recovery and obtain high quality, non degraded gDNA in order to interrogate multiple genomic marks in parallel (DNA methylation, chromatin accessibility and gene expression) from a small amount (500 mg) of cryopreserved human post-mortem brain tissue.

The optimised multistep procedure begins with the tissue disruption by Dounce homogenisation in the presence of a detergent (non-ionic surfactant Triton X-100) to lyse cellular membranes and release the nuclei. However, the detergent can also permeabilise and lyse the nuclear envelope if added in high amount and/or for an extended period of time (Krishnaswami et al., 2016) therefore using the appropriate concentration of detergent is crucial for an adequate cell lysis and ultimately higher nuclei yield. To reduce heat caused by friction, the Dounce homogenization was performed on ice with gentle strokes, and care was taken to avoid foaming. Pre-cooling the homogenisation buffer is also an important aid in heat reduction during homogenization. Differently from the authors' instructions, Doucing buffer was not utilised, instead tissue disruption was performed using the lysis buffer prepared as per published protocol. The number of Dounce strokes also required optimization and generally varied for each specimen: samples containing intracellular fibrous material or more fat tissue required more strokes. A complete/efficient homogenisation of the sample is indeed crucial to achieve optimal antibody staining and isolation by FACS without forming aggregates. However, although more homogenization (by increasing the number of strokes) released more nuclei, it also increased the number of damaged nuclei (Krishnaswami et al., 2016) therefore the number of strokes was kept at the minimum where possible stopping when solution looked visually uniform. Also, alternating loose with tight pestle proved to sensibly reduce the number of strokes required. Tissue douncing was followed by nuclei isolation via sucrose gradient ultracentrifugation as indicated in **protocol 2** although minor amendments were made.

The homogenate from each specimen was distributed in multiple ultracentrifuge tubes of bigger capacity (12mL instead of 10 mL) (Thermo Scientific, Cat No: 03699) making sure not to exceed 500 ul per tube as bigger volumes of sample per tube showed to impact the efficiency of the nuclei extraction (resulting in a nuclei pellet smaller in size with higher debris contamination). The tissue homogenate was slowly layered above 8 mL of sucrose buffer instead of 9 mL as recommended in **protocol 2.** The addition of further lysis buffer (2mL per tube) overlaid on the homogenate phase which was not included in the official protocol, was found to positively impact the nuclei extraction (bigger nuclei pellet). Furthermore, reducing the duration of the ultracentrifugation step from 1 hour to 45 minutes as well as slightly increasing the recommended spin speed from 106,803 x g to 108,670 x g was found to positively impact the intactness of the nuclei (i.e. reduced amount of debris and aggregates detected during FANS data acquisition) as well as the integrity of the gDNA isolated from them (as showed by the agarose gel images (see section 4.5.2.1). Implications on the gDNA are broadly discussed later in this chapter in section 4.5.2. Another relevant change from the original protocol was the adoption throughout the entire protocol of the same buffer solution containing a small percentage of BSA (10x PBS, 5% BSA, ddH20) utilised as resuspension, blocking and staining buffer for the nuclei samples and called for convenience staining buffer. This choice was dictated by the attempt to minimise the variation in pH and osmolarity to which the nuclei were exposed so to preserve their intactness. A brief and gentle washing step (5 minutes at 800 x g) was also introduced immediately after the resuspension of the nuclei pellets in order to remove any residual from the density gradient (e.g. sucrose) which otherwise could have interfered with the subsequent staining stage. Supernatant was discarded and each pellet was resuspended in fresh, ice-chilled staining buffer (500uL/pellet). Due to the initial choice of fractioning each specimen in multiple ultracentrifugation tubes, the resuspended nuclei aliquots derived from the same specimen were at this stage pulled together to keep the ratio nuclei/antibody molecules constant and minimize variation in staining efficiency among tubes. I found indeed, that by distributing the same specimen over multiple ultracentrifugation tubes after tissue douncing allowed to recover cleaner pellets ultimately improving nuclei recovery during sorting. Differently from the original **protocol 2**, DNA intercalating dye Hoechst 33342 (1.5 µL/1mL) was added to the pooled nuclei suspension prior staining with cell specific

antibodies to 1) assess whether the nuclei suspension contained encumbering amounts of non-nuclear material 2) to visualise nuclei during FACS. 150 µL of the nuclei suspension was then transferred into a separate tube so that for each specimen, two conditions were assessed: 1) stained (nuclei sample stained with Hoechst and nuclear markers) 2) unstained (Hoechst-only control). For both tubes a final volume of 2 mL was reached using ice-chilled staining buffer. To enable sorting of nuclei derived from different cell types, targeted immunostaining was achieved using 1) an Alexa488-conjugated antibody specific to NeuN, a nuclear membrane protein predominantly expressed by mature neurons and 2) a NL577-conjugated antibody specific to Sox10, a transcription factor critical for the terminal differentiation of oligodendrocytes. Therefore, into each stained tube, 2µL anti-NeuN (1:1000 dilution) and 150µL of anti-Sox10 (1:10 dilution) were added simultaneously. Both tubes, stained and unstained, were wrapped in aluminium foil and incubated for 1.5 hours (instead of 60 minutes as per protocol 2) at 4°C on a low speed rotor. The addition of the Sox10 antibody was the major novelty differentiating this method from the protocols here tested. To the best of my knowledge, at the time of testing no validated nuclear antibodies targeting human oligodendrocytes and suitable for FANS were available. The filtering step with a 35um cell strainer recommended in the original protocol was intentionally omitted as found to dramatically reduce the nuclear material in input. However, although not included in **protocol 2**, a second mild washing step was performed after the staining phase (5 minutes at 800 x g, RT) to remove the unbound antibody molecules with the purpose of limiting the background staining detected by FANS. Starting with the unstained sample (Hoechst-only stain) which was used as reference baseline, tubes were loaded into the FACS chamber. Data were acquired as per the pre-established gating parameters and sample performance was assessed for each specimen prior to proceed with nuclei collection. In line with both protocols' recommendations, appropriate gates were set and adjusted to capture most nuclei while avoiding unnecessary debris. **Figure 4.7** explains in detail the adopted gating strategy which, together with the abovementioned adjustments of the original protocol, has allowed to achieve the high enrichment in nuclei (≥70% of total events) observed across all samples processed (**Figure 4.8**). Gentle sort settings were recommended as they do not exert excessive mechanical force on the nuclei and keep collection volumes reasonable (Kundakovic et al., 2017). For these reasons, the 100µm nozzle was

adopted as it allows to achieve the less shearing force and the lower pre-set sheath fluid pressure (fixed parameter on our Aria III cell sorter). See **Methods** chapter for more details. For few test samples processed through the FANS pipeline, the collected aliquots of nuclei labelled as "NeuN+ve/Sox10+ve" (neuronal-enriched nuclei) and "NeuN-ve/Sox10+ve" (oligodendrocyte-enriched nuclei) were rerun through the cell sorter immediately after collection in order to confirm the validity of the gating strategy adopted. An intentionally strict cut off was applied by collecting the top and the bottom third of the events displayed during the sorting in order to prevent cross-contamination of purified populations. **Figure 4.9 i**llustrates the distribution of detected events for purified NeuN-stained nuclei populations when re-run through the cell sorter.

On average, every 500 mg of tissue yielded from 0.8 to 1.5 million neuronal and oligodendrocyte-enriched nuclei and up to 0.5 million double negative (other glia-enriched) nuclei with neurons/oligodendrocytes ratio close to 1.0:1.5 (prefrontal cortex, healthy brain). However, great variability in the abundance of each cell type was observed from specimen to specimen, going from samples missing completely the double negative fraction of nuclei to samples where the oligodendrocytes were less abundant than neurons (ratio 0.8:1.0). **Figure 4.10** captures the variability in cell proportions across samples, reporting the cell count data provided by the cell sorter for every specimen processed. The predicted cellular composition of FANS-processed bulk brain samples was estimated using a reference based deconvolution model based on FANS sorted human brain data and Houseman algorithm (ref to DNA methylation arrays as surrogate measures of cell mixture distribution (Houseman et al., 2012)). For the majority of the samples, neuronal derived (dark magenta) and oligodendrocyte derived (deep pink) nuclei were the most abundant populations, followed by other glia (orange) (see **Figure 4.11**) therefore supporting the experimental data recovered from the cell count. Interestingly, the other glia nuclei population (orange) was the one showing disparities when comparing collected data and predicitons. This could be explained by the high variability shown by the antibody staining across specimens and the minor adjustment of gating strategy consequently required.
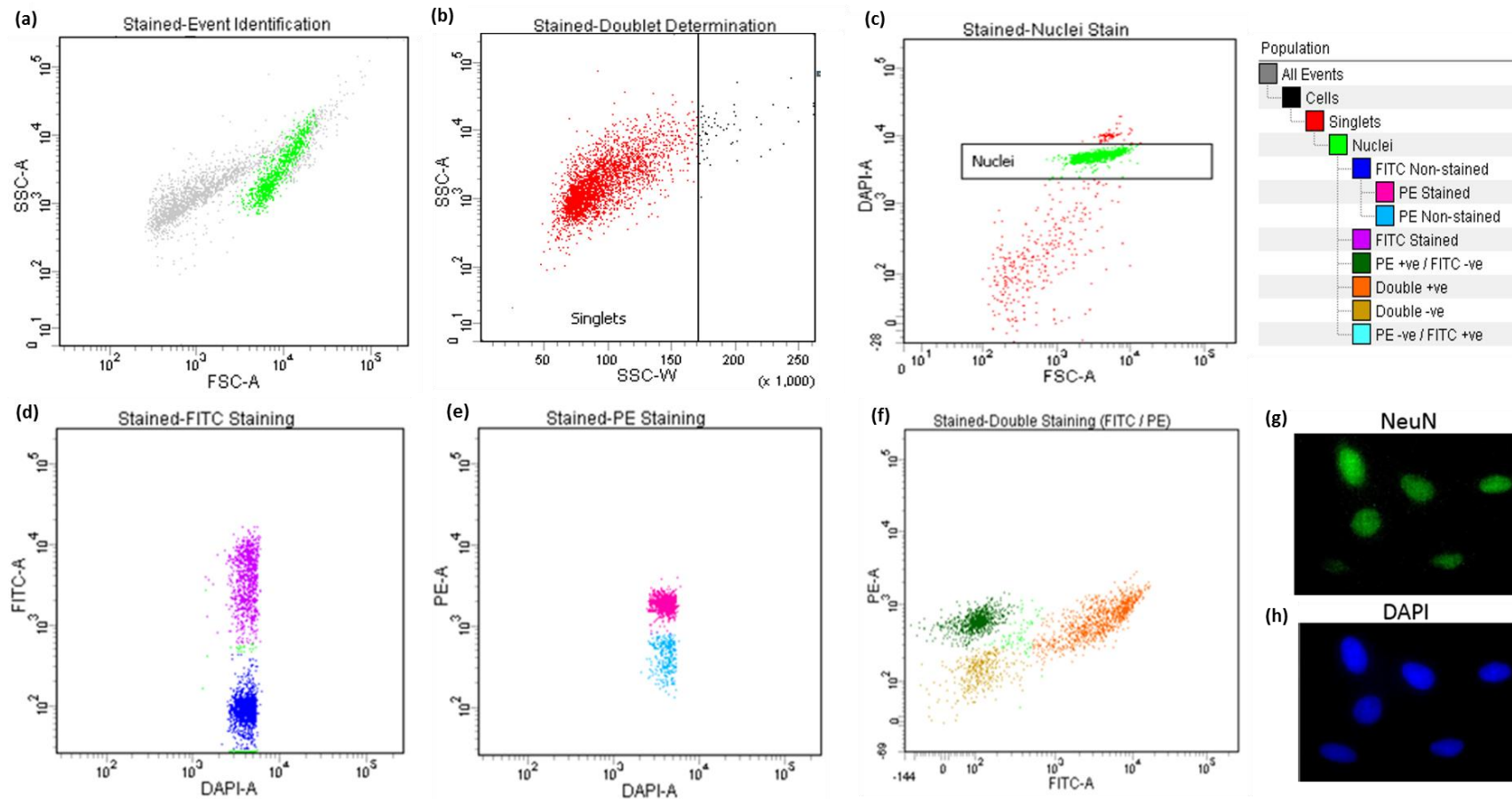
Figure 4.7 FANS gating strategy.
(a) Particles smaller than nuclei (grey dots) were eliminated with an area plot of forward scatter (FSC-A) versus side scatter (SSC-A). *(b)* Plots of area versus width in the side scatter channel were used for doublet discrimination with gating aiming at excluding aggregates of two or more nuclei and *(c)* intact nuclei were determined by subgating on Hoechst 33342.Subsequent density plots discerning *(d)* NeuN-Alexa Fluor488–conjugated antibody staining (magenta) *(e)* Sox10 NL577-antibody staining (deeppink) *(f)* the distribution of the three main nuclei subpopulations identified through double staining strategy (double+ve, neurons; double–ve, other glia; PE+ve/ FITC-ve, olygodendrocytes). The resultant hierarchical color key ensures that only nuclei that are positive or negative for staining with the NeuN and/or Sox10 antibody are passed through the subsequent gating condition. FACS gating of labeled nuclei was further confirmed via imaging on a microscope slide (data shown for NeuN staining only) *(g-h).*

259
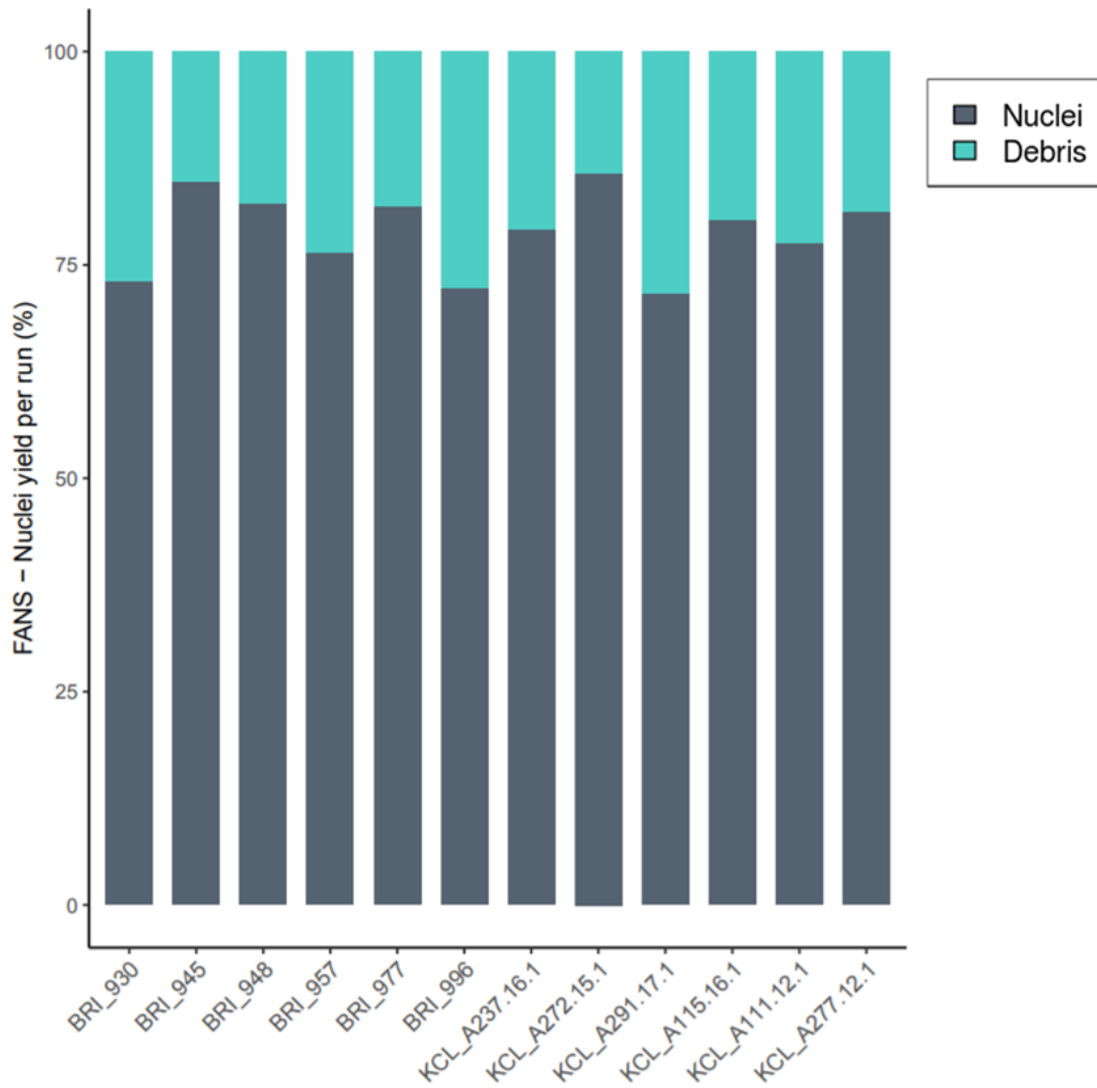
Figure 4.8 Nuclei purification QC.
The actual identity of the events detected by the cell sorter was assessed by recording for each individual experiment the percentage of nuclei (dark grey) relative to the total events detected (100%). The barplot here shows the high enrichment in nuclei (≥ 75% of the total events) and marginal carry-over of cellular debris (turquoise) across the 12 FANS samples confirming the efficacy of the density gradient centrifugation in obtaining highly purified nuclei suspensions. Data shown are those provided by the cell sorter for each individual experiment.
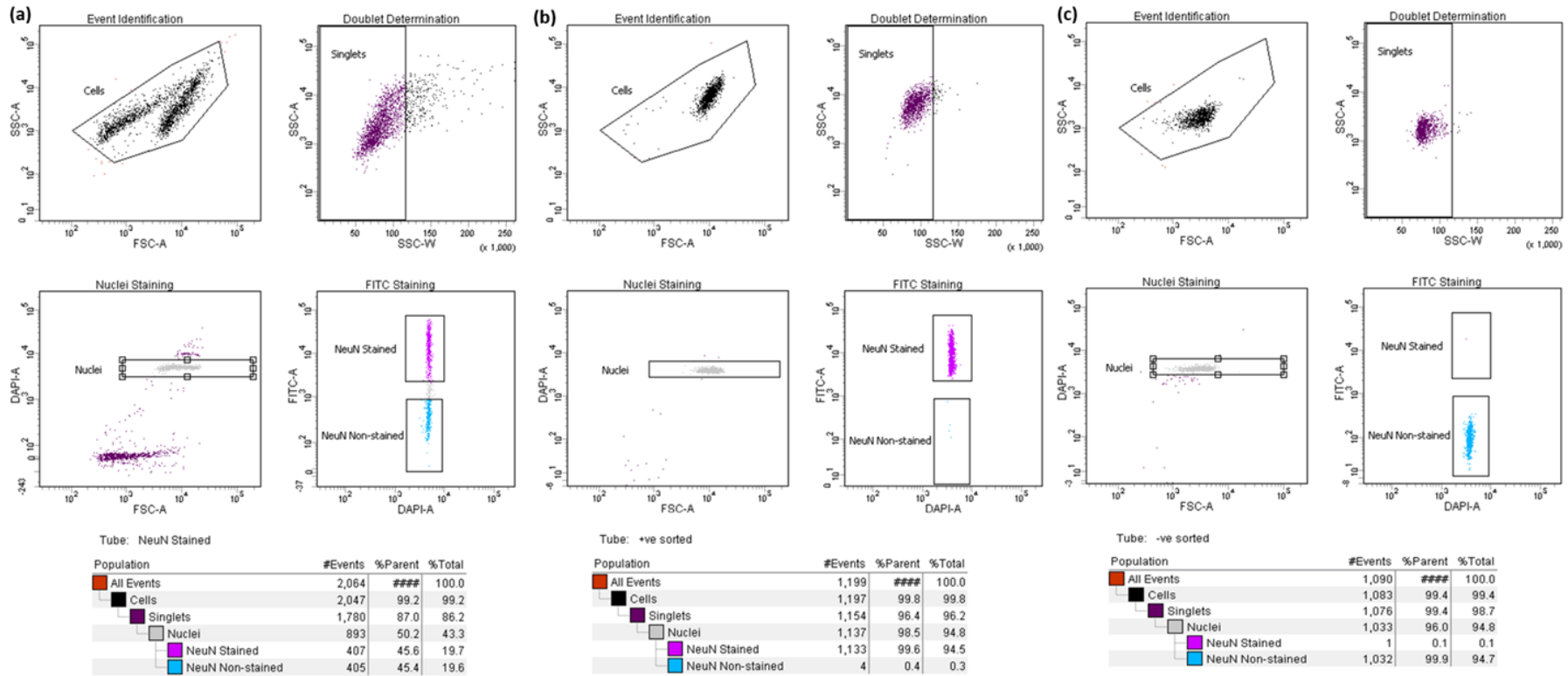
Figure 4.9 Sorting purity validation.

Nuclei underwent single staining with anti-NeuN antibody and were sorted using FANS. The collected aliquots of nuclei, labelled as "NeuN+ve"(neuronal nuclei) and "NeuN-ve" (non-neuronal nuclei), were run back through the cell sorter immediately after collection in order to confirm the validity of the gating strategy adopted for the NeuN staining. An intentionally strict cut off was applied by collecting only the top and the bottom third of the events displayed during the sorting in order to prevent cross-contamination of purified populations. (a) Shown is a representative example of brain specimen stained with NeuN-Alexa Fluor488–conjugated antibody and sorted through FANS; when purified fractions were re-acquired through the cell sorter, nuclei populations distribution ranged into the pre-established gates revealing an high degree of purity as shown in (b) for the NeuN+ve fraction and (c) for the NeuN-ve fraction.
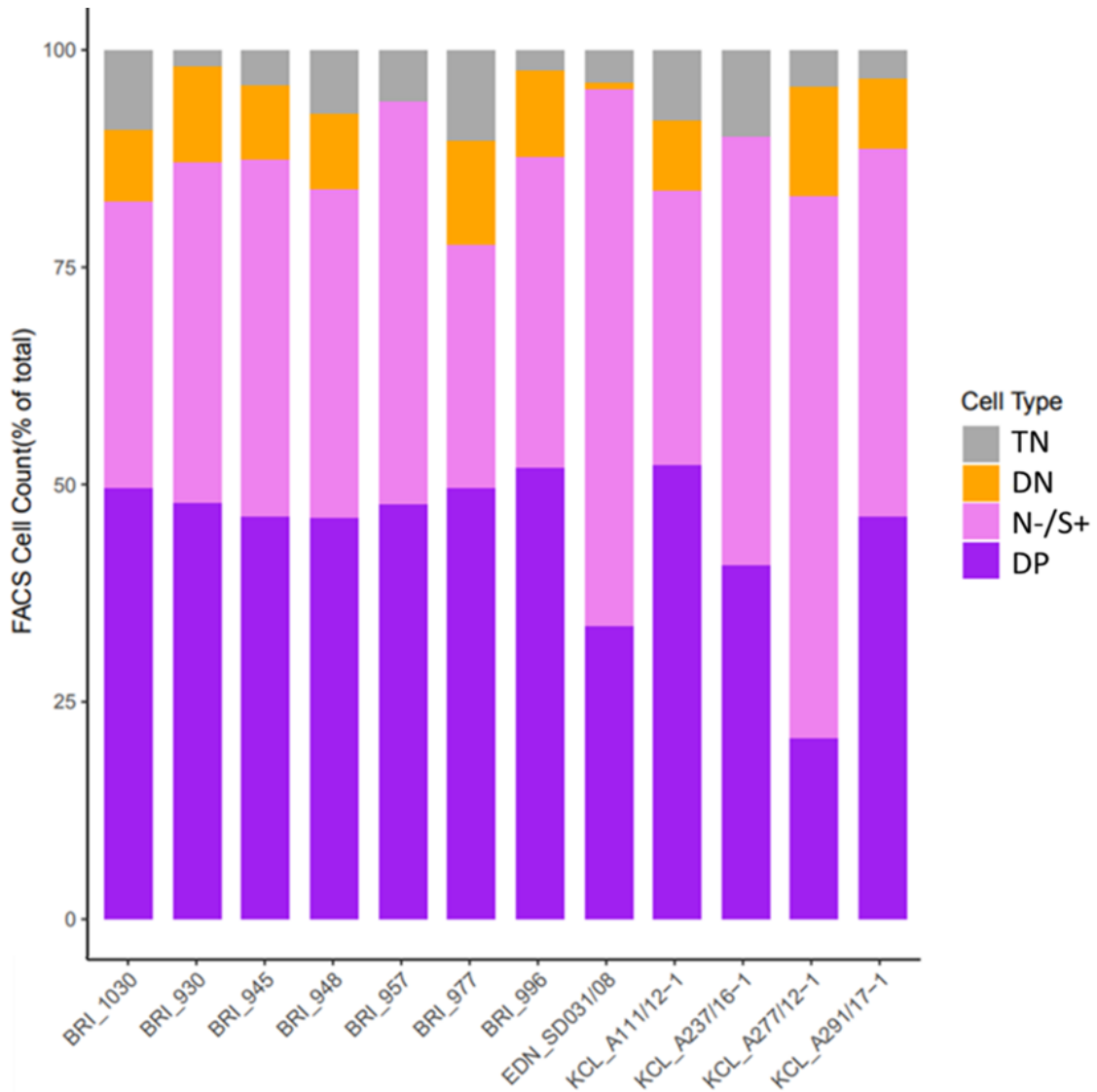
Figure 4.10 FACS Cell count.
Barplot displaying the actual cellular composition of the FANS-processed brain samples (N=12). Data shown are those provided by the cell sorter for each individual experiment. For the majority of the cases, neuronal derived nuclei (darkmagenta) represents the most abundant population, followed by oligodendrocytes (deep pink). The other glia population (orange) is the rarest population across all samples, in some not detected at all. FACS, fluorescence-activated cell sorter; TN, Total nuclei; DN, double negative (NeuN-ve/Sx10-ve); N-/S+ (NeuN-ve/Sox10+ve); DP, double positive (NeuN+ve/Sox10+ve).
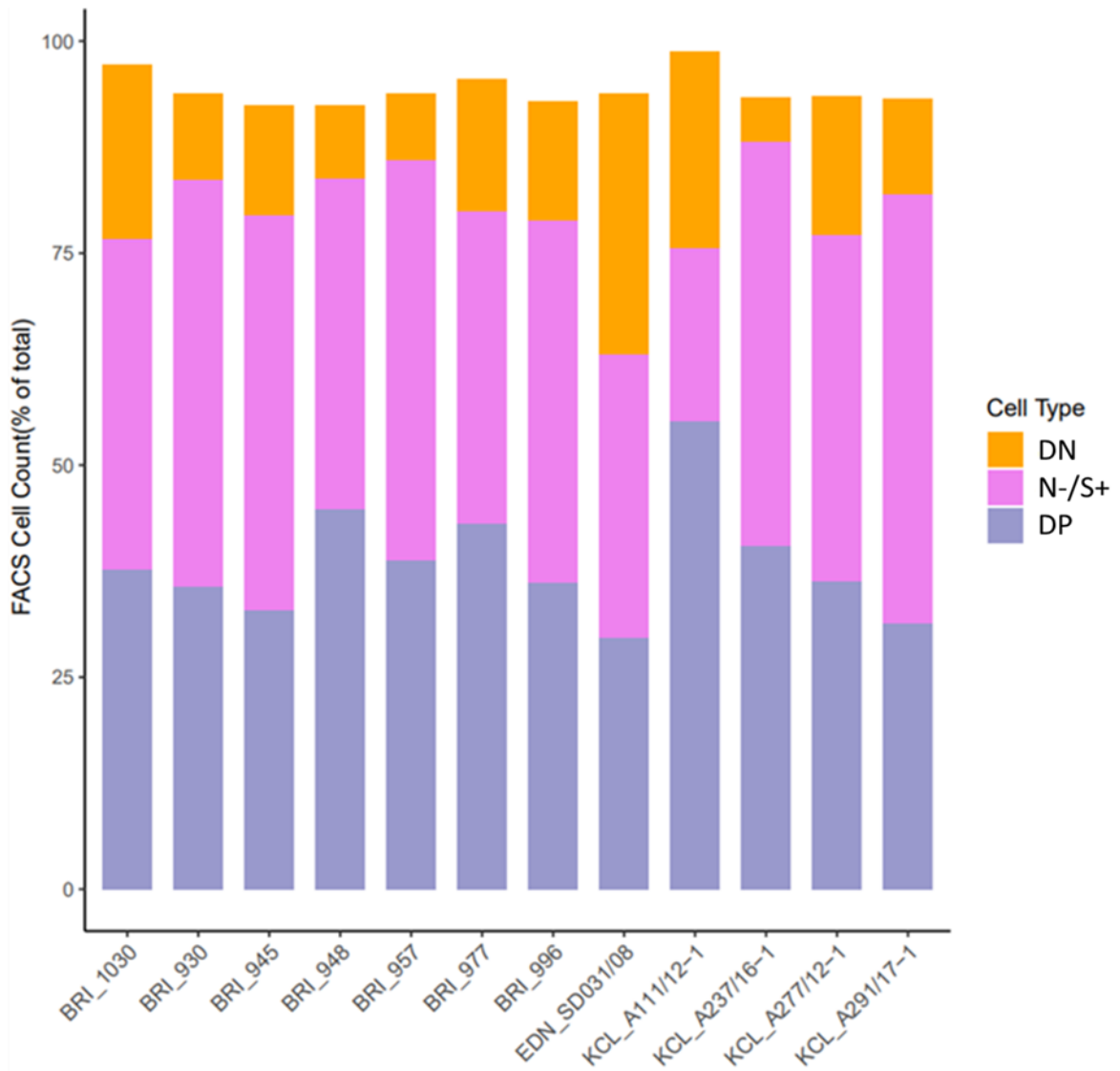
Figure 4.11 Cell composition prediction for bulk brain tissue.
Barplot displaying the predicted cellular composition of FANS-processed bulk brain samples using a reference based deconvolution model using FANS sorted brain and Houseman algorithm (ref to DNA methylation arrays as surrogate measures of cell mixture distribution (Houseman et al., 2012). For the majority of cases, neuronal derived nuclei (darkmagenta) and oligodendrocyte (deep pink) populations are the most abundant populations, followed by other glia (orange). FACS, fluorescence-activated cell sorter; DN, double negative (NeuN-ve/Sx10-ve); N-/S+ (NeuN-ve/Sox10+ve); DP, double positive (NeuN+ve/Sox10+ve).

4.5.2 High molecular weight genomic DNA can be obtained from sorted nuclei for high resolution downstream applications

Following testing and comparing the output of various extraction techniques, **DNA protocol 3** was adopted as standard method to isolate genomic DNA from purified nuclei populations due to the better performance displayed in terms of yield and purity. The table below reports the DNA measurements obtained with the Nanodrop 2000 (**Table 4.2**). On average, 200,000 nuclei (N events collected per aliquot) yielded ≥ 500 ng of gDNA. **Figure 4.12** showing representative absorbance profiles for DNA samples obtained from sorted nuclei confirm the successful recovery of DNA. However, the absorbance ratios revealed traces of organic contaminants (e.g. phenol, proteins) absorbing at 280 nm (260/280<1.8) and significant salt contamination (260/230 < 2.0). The addition of the co-precipitant GlycoBlue (Invitrogen Ltd, Inchinnan, UK) to help visualising DNA pellets might explain some sub-optimal ratios since the blue dye covalently linked to glycogen alone has absorbance peaks at both 230 and 260 nm therefore affecting the accuracy of the QC measurements. Despite this, the purified gDNA proved to be suitable for downstream applications and the lower purity did not seem to affect the results of the DNA methylation assay.

Sample Type	Brain Bank ID	My ID	Nuclei Population (enriched)	ng/µl	260/280	260/230
DNA	BRI_930	BRI1	Neurons	44	1.74	1.44
DNA	BRI_930	BRI1	Oligodendrocytes	40	1.69	1.58
DNA	BRI_930	BRI1	Other glia	62	1.71	1.54
DNA	BRI_930	BRI1	Total	89	1.69	1.53
DNA	BRI_945	BRI2	Neurons	63	1.67	1.56
DNA	BRI_945	BRI2	Oligodendrocytes	74	1.73	1.55
DNA	BRI_945	BRI2	Other glia	42	1.69	1.52
DNA	BRI_945	BRI2	Total	37	1.71	1.59
DNA	BRI_948	BRI3	Neurons	53	1.88	1.73
DNA	BRI_948	BRI3	Oligodendrocytes	62	1.84	1.77
DNA	BRI_948	BRI3	Other glia	38	1.81	1.71
DNA	BRI_948	BRI3	Total	38	1.86	1.76
DNA	BRI_957	BRI4	Neurons	64	1.67	1.68
DNA	BRI_957	BRI4	Oligodendrocytes	48	1.74	1.66
DNA	BRI_957	BRI4	Other glia	55	1.64	1.55
DNA	BRI_957	BRI4	Total	63	1.73	1.53
DNA	BRI_977	BRI5	Neurons	69	1.72	1.76
DNA	BRI_977	BRI5	Oligodendorcytes	55	1.76	1.78
DNA	BRI_977	BRI5	Other glia	57	1.66	1.73
DNA	BRI_977	BRI5	Total	57	1.77	1.69
DNA	BRI_996	BRI6	Neurons	27	1.73	1.42
DNA	BRI_996	BRI6	Oligodendrocytes	24	1.76	1.34
DNA	BRI_996	BRI6	Other glia	25	1.71	1.32
DNA	BRI_996	BRI6	Total	25	1.77	1.35
DNA	BRI_1030	BRI7	Neurons	25	1.8	1.3
DNA	BRI_1030	BRI7	Oligodendrocytes	23	1.7	1.27
DNA	BRI_1030	BRI7	Other glia	25	1.72	1.24
DNA	BRI_1030	BRI7	Total	24	1.73	1.29
DNA	KCL_A277/12-1	KCL1	Neurons	54	1.7	1.58
DNA	KCL_A277/12-1	KCL1	Oligodendrocytes	51	1.69	1.56
DNA	KCL_A277/12-1	KCL1	Other glia	57	1.71	1.54
DNA	KCL_A277/12-1	KCL1	Total	48	168	1.53
DNA	KCL_A237/16-1	KCL11	Neurons	48	1.79	1.48
DNA	KCL_A237/16-1	KCL11	Oligodendrocytes	38	1.77	1.49
DNA	KCL_A237/16-1	KCL11	Other glia	32	1.75	1.46
DNA	KCL_A237/16-1	KCL11	Total	43	1.77	1.51

DNA	KCL_A291/17-1	KCL13	Neurons	64	1.69	1.86
DNA	KCL_A291/17-1	KCL13	Oligodendrocytes	72	1.61	1.82
DNA	KCL_A291/17-1	KCL13	Other glia	56	1.65	1.83
DNA	KCL_A291/17-1	KCL13	Total	67	1.67	1.77
DNA	KCL_A111/12-1	KCL15	Neurons	29	1.68	1.55
DNA	KCL_A111/12-1	KCL15	Oligodendrocytes	21	1.77	1.42
DNA	KCL_A111/12-1	KCL15	Other glia	21	1.69	1.51
DNA	KCL_A111/12-1	KCL15	Total	20	1.79	1.37
DNA	SD031/08	EDN	Neurons	55	1.88	1.77
DNA	SD031/08	EDN	Oligodendrocytes	61	1.81	1.74
DNA	SD031/08	EDN	Other glia	44	1.79	1.7
DNA	SD031/08	EDN	Total	58	1.83	1.75

Table 4.2 Table of DNA yields.
For every individual (N=12), the DNA content of each nuclei population was measured using the Nanodrop 2000 spectrophotometer. Sample purity and presence of contaminants was also assessed by examining the ratio values. On average, 200,000 nuclei (N events collected per aliquot) yielded ≥ 500 ng of gDNA. However, the ratios reveal traces of organic contaminants (e.g. phenol, proteins) absorbing at 280 nm (260/280<1.8) and significant salt contamination (260/230 < 2.0). Neurons, NeuN+ve/Sox10+ve nuclei; Oligodendrocytes, NeuN-ve/Sox10+ve nuclei; other glia, NeuN-ve/Sox10-ve nuclei.
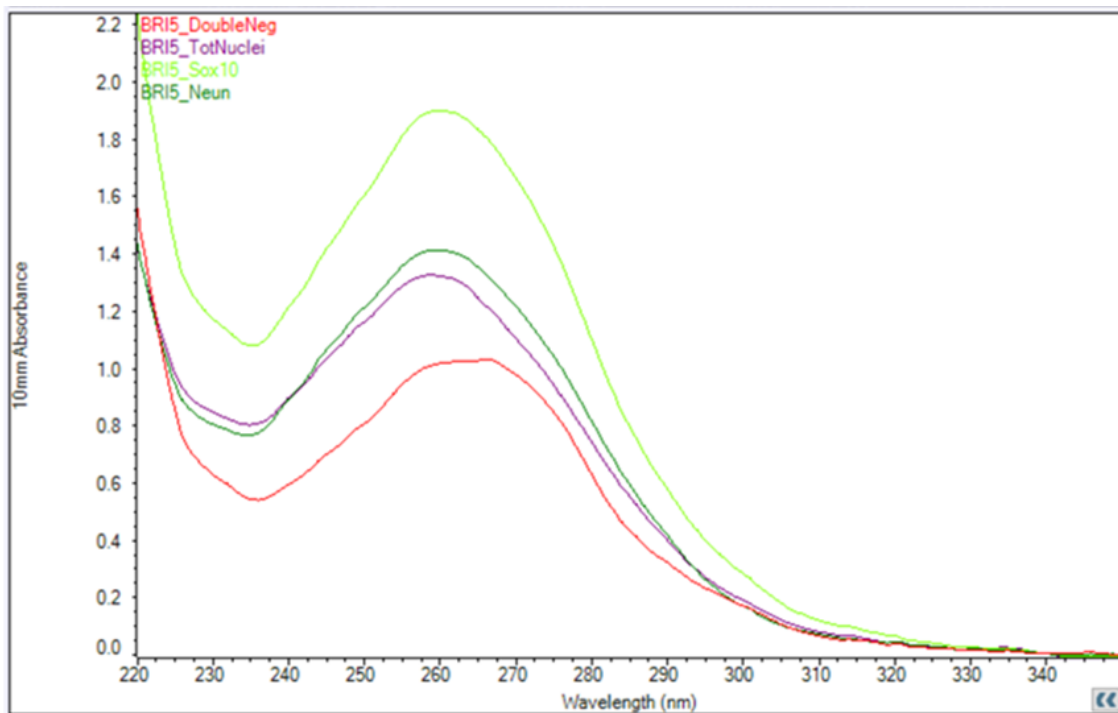
Sample Type	Sample ID	Nucleic Acid	Unit	260/280	260/230
DNA	BRI5_Neun	70.6	ng/µl	1.72	1.76
DNA	BRI5_Sox10	95.0	ng/µl	1.71	1.62
DNA	BRI5_TotNuclei	66.1	ng/µl	1.77	1.56
DNA	BRI5_DoubleNeg	50.7	ng/µl	1.60	1.61

Figure 4.12 Representative example of DNA profile for each nuclei fraction isolated from the same individual (BRI5).
Results here shown are taken from Nanodrop2000 readings. Neun, NeuN+ve/Sox10+ve nuclei; Sox10, NeuN-ve/Sox10+ve nuclei; DoubleNeg, NeuN-ve/Sox10-ve nuclei; TotNuclei, unsorted nuclei.

4.5.2.1   DNA quality assessment via agarose gel electrophoresis

Despite the recommendations of both tested protocols suggesting an ultracentrifugation step of 1 hour duration to separate the nuclei component from the remaining cell content, I found that by reducing the spin time to 45 minutes the integrity and molecular weight of the extracted DNA was better preserved (narrow, defined bands in the gel although faded due to minimal loading concentration- **Figure 4.13A**) while longer duration of this initial step would dramatically impact the quality of the DNA causing evident nucleic acid degradation (faded bands with extended smear **Figure 4.13B**).

267
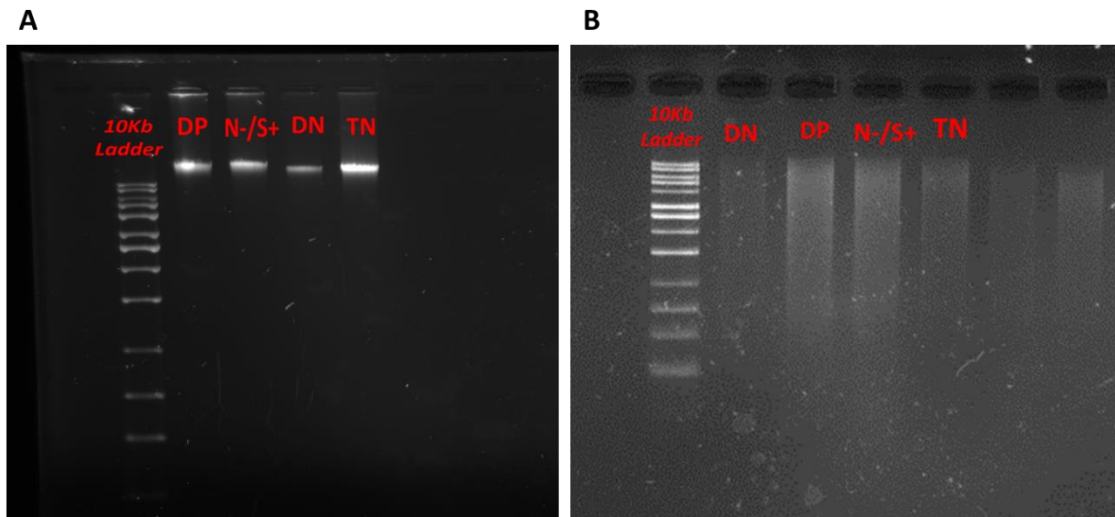
Figure 4.13 DNA quality check using 1% ethidium bromide agarose gel electrophoresis on test samples.
(A) *gDNA profile of four representative FANS-sorted nuclei fractions collected from the same specimen showing the integrity of the extracted nucleic acid when ultracentrifugation time was reduced to 45 minutes. **(B)** Representative gel picture showing the gDNA integrity for individual sorted nuclei fractions when ultracentrifugation step was performed for 1 hour as recommended in protocol 2. DNA quality was checked for all 12 sorted brain samples.*

4.5.3 Nuclear RNA can be obtained from sorted nuclei and is suitable for sensitive downstream applications.

Various extraction methods were tested for the purification of nuclear RNA from aliquots of FANS sorted nuclei (300,000 nuclei per aliquot). Manual extraction protocol (e.g. TRIZOL RNA Isolation) and column based ones (Qiagen AllPrep DNA/RNA Mini kit and RNeasy Mini Kit, Zymo Research Direct-zol™ RNA MicroPrep) were tested and compared in terms of yield, purity and quality in order to maximise the RNA recovery while preserving its integrity making it suitable for high sensitivity downstream applications such as RNA-seq.

RNA protocol 1 (Qiagen AllPrep DNA/RNA Mini kit) was tested on nuclei fractions from five different FANS sorted brain specimen. Despite the advantage of a quick, streamlined procedure, the extraction resulted in complete loss of RNA as revealed by the Nanodrop readings where the absorbance curve was flat and the concentration detected below 10 ng/ul (data not shown). Because of the low concentration, the purity of the samples could not be assessed by analyzing the A260/280 and A260/230 ratios as outside the lowest concentration the NanoDrop is designed to measure. More sensitive methods such as an Agilent Biolanalyzer or Qubit analysis were therefore explored. However, similar measurements were

obtained with both approach with Bioanalyzer RIN scores ranging between 3.0 and 4.0 (data not shown).

The RNA protocol 2 performed better than the RNA protocol 1 in regards of RNA recovery (30-40 ng/ul). However, the RNA extracted following this method was compromised in its purity showing out-of-range absorbance ratios when quantified on the Nanodrop. The use of PLG tubes instead of regular eppendorfs did not seem to have a relevant impact on the extraction outcome, although in the latter case extra care was required when recovering the aqueous phase in order to prevent Trizol carryover. The addition of Glycoblue co-precipitant (Thermo Fisher Scientific, Cat. No AM9515) (0.7 µL per sample) at the stage of RNA precipitation (immediately after adding 100 % Isopropanol) was also required as extra step to increase the visibility of RNA pellets otherwise it was too small to be detected by eye. Although this addition prevented from accidentally disrupting or discarding RNA pellets, it also interfered with the RNA concentration measurements especially when based exclusively on the Nanodrop spectrophotometer readings due to the blue dye covalently linked to the glycogen which has emission peaks at both 230 nm and 260 nm.

Post-extraction clean-up methods were also tested on nuclei-derived RNA samples in the attempt to improve the purity of RNA samples by removing contaminants and carryovers. Specifically, the RNeasy MinElute Cleanup kit (Qiagen, UK) was used as per manufacturer's instructions. This spin column-based kit is recommended for low RNA concentration thanks to small elution volumes as well as clean-up and desalting of RNA samples. Given the low input material, the clean-up process resulted in almost complete loss of the RNA along the process. Samples were quantified and checked for purity by spectrophotometry using the Nanodrop ND-2000 (Thermo Fisher Scientific, MA, US). Below is a representative example of Nanodrop report for the same RNA samples before and after spin-column based post-extraction clean-up (**Figure 4.14**).

Sample Type	Sample ID	Nucleic Acid	Unit	260/280	260/230
RNA	RNA_NeuN	453.3	ng/µl	1.69	0.30
RNA	RNA_Sox10	556.7	ng/µl	1.75	0.31
RNA	RNA_DoubleNeg	222.5	ng/µl	1.83	0.47
RNA	RNA_Total	260.7	ng/µl	1.89	0.45

Sample Type	Sample ID	Nucleic Acid	Unit	260/280	260/230
RNA	Total	5.7	ng/µl	1.18	0.41
RNA	DoubleNeg	4.7	ng/µl	1.20	0.18
RNA	Sox10	3.6	ng/µl	1.18	0.07
RNA	NeuN	3.0	ng/µl	1.26	0.09
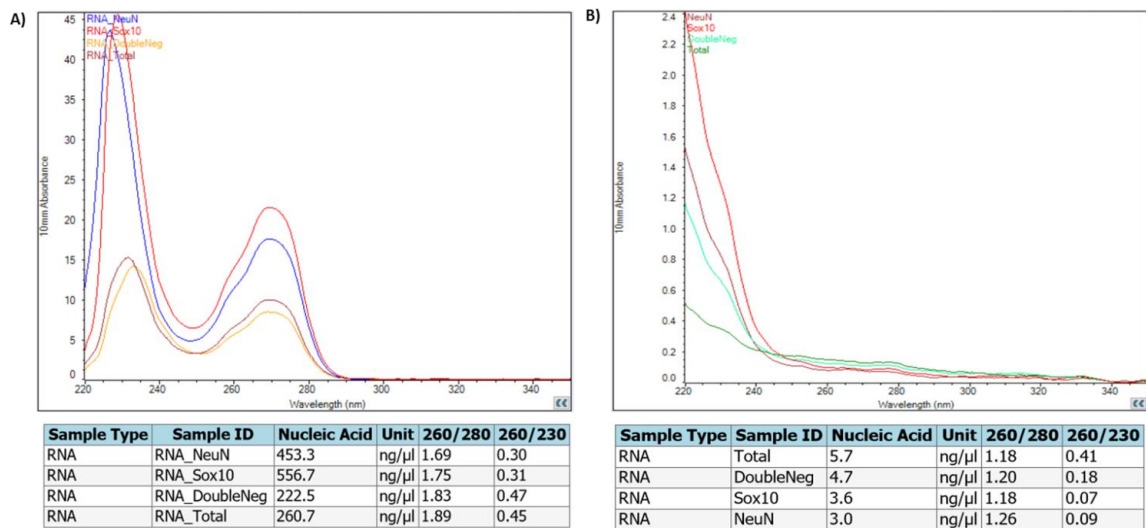
Figure 4.14 Nanodrop RNA profile for 4 nuclear RNA samples derived from the same brain specimen A) before and B) after clean-up.
The lack of bell-shaped profile in the absorbance plot on the right as well as the spectrophotometer reading reveals the loss of RNA sample together with only partial removal of contaminants absorbing UV light (260/230 ratio did not improve). NeuN, NeuN+ve/Sox10+ve nuclei; Sox10, NeuN-ve/Sox10+ve nuclei; DoubleNeg, NeuN-ve/Sox10-ve nuclei; Total, unsorted nuclei.

For these reasons, among the three methods tested, the Zymo Research extraction kit, Directzol RNA MicroPrep (Zymo Research, UK, Cat No. R2060) was chosen for the purification of high-quality, DNA-free, RNA directly from TRIzol bypassing traditional phase separation and precipitation procedures. This kit enabled a better purification of the RNA samples from contaminants as revealed by the improved 280/260 and 260/230 absorbance ratios. **Table 4.3** reports the nanodrop measurements for 35 RNA samples extracted using the Direct-zol™ RNA MicroPrep (Zymo Research, UK) and **Figure 4.15** shows an example of the typical RNA profile observed for nuclear RNA from sorted nuclei populations.

#	Sample ID	User name	Nucleic Acid	260/280	260/230	Sample Type
1	RNA_nuclei 1	PacBio Nanodrop PC	10.9	1.75	1.31	RNA
2	RNA_nuclei 2	PacBio Nanodrop PC	12.7	1.95	1.82	RNA
3	RNA_nuclei 3	PacBio Nanodrop PC	8.1	1.85	0.93	RNA
4	RNA_nuclei 4	PacBio Nanodrop PC	9.1	1.76	1.47	RNA
5	RNA_nuclei 5	PacBio Nanodrop PC	15.1	1.93	1.57	RNA
6	RNA_nuclei 6	PacBio Nanodrop PC	8.2	1.88	1.18	RNA
7	RNA_nuclei 6 rep	PacBio Nanodrop PC	8.0	1.71	1.54	RNA
8	RNA_nuclei 7	PacBio Nanodrop PC	9.9	1.85	1.21	RNA
9	RNA_nuclei 8	PacBio Nanodrop PC	10.7	1.90	0.71	RNA
10	RNA_nuclei 9	PacBio Nanodrop PC	9.1	1.75	1.30	RNA
11	RNA_nuclei 10	PacBio Nanodrop PC	9.1	1.78	1.50	RNA
12	RNA_nuclei 11	PacBio Nanodrop PC	11.5	1.83	1.92	RNA
13	RNA_nuclei 12	PacBio Nanodrop PC	13.2	1.82	1.49	RNA
14	RNA_nuclei 13	PacBio Nanodrop PC	7.1	1.85	1.07	RNA
15	RNA_nuclei 14	PacBio Nanodrop PC	11.7	1.87	2.12	RNA
16	RNA_nuclei 15	PacBio Nanodrop PC	9.5	1.81	1.18	RNA
17	RNA_nuclei 16	PacBio Nanodrop PC	11.3	1.77	1.63	RNA
18	RNA_nuclei 17	PacBio Nanodrop PC	8.4	1.84	1.50	RNA
19	RNA_nuclei 18	PacBio Nanodrop PC	7.7	1.83	1.66	RNA
20	RNA_nuclei 19	PacBio Nanodrop PC	9.6	1.86	1.82	RNA
21	RNA_nuclei 20	PacBio Nanodrop PC	12.6	1.79	1.33	RNA
22	RNA_nuclei 21	PacBio Nanodrop PC	7.8	1.95	1.70	RNA
23	RNA_nuclei 22	PacBio Nanodrop PC	12.5	1.88	1.36	RNA
24	RNA_nuclei 23	PacBio Nanodrop PC	11.2	1.93	0.47	RNA
25	RNA_nuclei 24	PacBio Nanodrop PC	6.9	1.87	1.10	RNA
26	RNA_nuclei 25	PacBio Nanodrop PC	8.7	1.84	1.91	RNA
27	RNA_nuclei 26	PacBio Nanodrop PC	6.4	1.89	1.23	RNA
28	RNA_nuclei 27	PacBio Nanodrop PC	8.9	1.63	0.56	RNA
29	RNA_nuclei 28	PacBio Nanodrop PC	6.4	1.70	1.22	RNA
30	RNA_nuclei 29	PacBio Nanodrop PC	12.1	1.90	1.92	RNA
31	RNA_nuclei 30	PacBio Nanodrop PC	9.5	1.83	1.66	RNA
32	RNA_nuclei 31	PacBio Nanodrop PC	14.0	1.82	1.59	RNA
33	RNA_nuclei 32	PacBio Nanodrop PC	7.2	1.79	2.13	RNA
34	RNA_nuclei 33	PacBio Nanodrop PC	7.1	1.79	1.78	RNA
35	RNA_nuclei 34	PacBio Nanodrop PC	6.4	1.65	1.87	RNA
36	RNA_nuclei 35	PacBio Nanodrop PC	7.3	1.86	2.09	RNA
37	RNA_nuclei 36	PacBio Nanodrop PC	7.5	1.96	2.10	RNA
38	RNA_nuclei 37	PacBio Nanodrop PC	13.0	1.78	2.21	RNA
39	RNA_nuclei 38	PacBio Nanodrop PC	14.8	1.76	1.52	RNA

Table 4.3 Table results of RNA samples quantification.
Data exported from the Nanodrop spectrophotometer showing concentration of nuclear RNA per ul (column labelled "Nucleic Acid") and purity measurements (260/280, 260/230 ratios) for each sample.
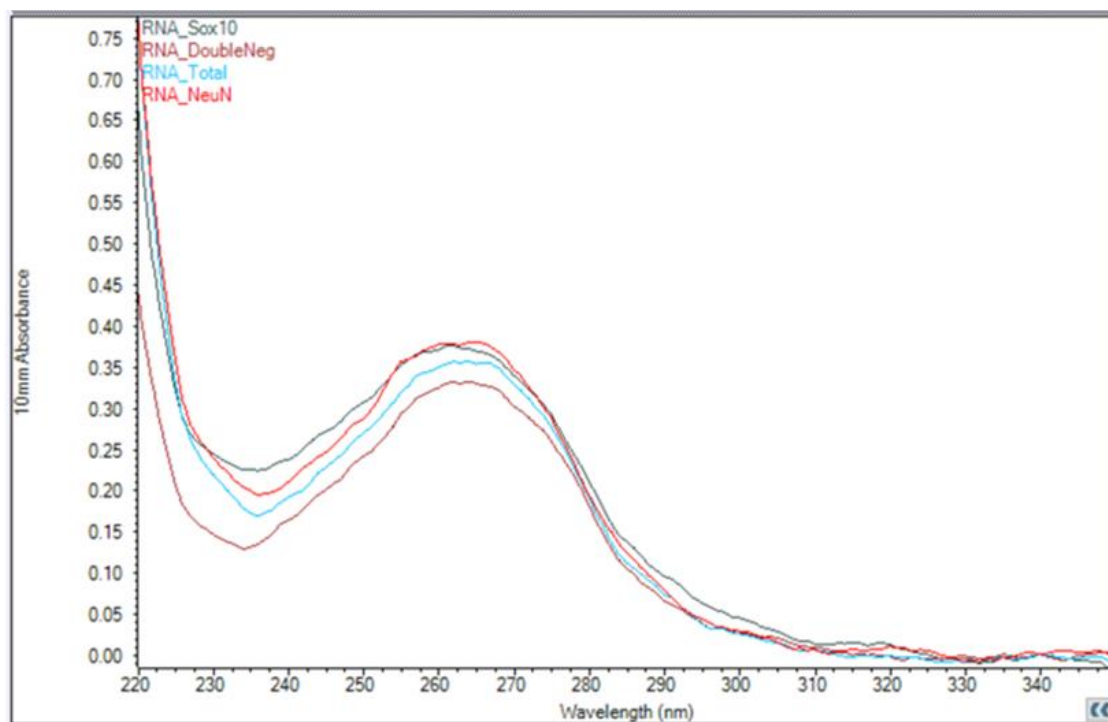
Sample Type	Sample ID	Nucleic Acid	Unit	260/280	260/230
RNA	RNA_NeuN	15.1	ng/µl	1.93	1.57
RNA	RNA_Total	14.0	ng/µl	1.82	1.59
RNA	RNA_DoubleNeg	13.0	ng/µl	1.78	2.21
RNA	RNA_Sox10	14.8	ng/µl	1.76	1.52

Figure 4.15 Representative example of RNA profile for each individual nuclei fraction sorted from the same individual.
NeuN, NeuN+ve/Sox10+ve (neuronal enriched-nuclei); Sox10 (NeuN-ve/Sox10+ve, (oligodendrocyte-enriched nuclei); DoubleNeg, NeuN-ve/Sox10-ve (other glia-enriched nuclei); Total, unsorted nuclei modelling bulk tissue.

As further quality check, randomly selected RNA samples were also run on the Agilent Bioanalyzer 2100 and on the Agilent Tape Station 2200 for purity and integrity assessment as well as to compare the yields with those provided by the Nanodrop. For both assays, the RNA Integrity Number (RIN), a widely accepted measure of RNA degradation, ranged between 3.0 and 4.5 revealing that the nuclei-derived RNA samples are not optimal for RNA sequencing or other high sensitivity gene expression assays which are known to require high quality input RNA (RIN ≥ 7.0). **Figure 4.16** illustrates a representative example of Tape Station data for nuclear RNA samples extracted from sorted nuclei using RNA protocol 2. It is worth noting however that both assays for RNA quality assessment are tailored to capture eukaryotic total RNA and therefore might not perform as expected when using nuclear RNA samples. Moreover, the RIN is calculated by looking at the ratio of the ribosomal RNAs which are found at lower amounts in

the nucleus than cytoplasm which again could explain the very low values showed by these RNA samples during the quality assessment. Furthermore, the RNA ScreenTape (Tape Station, Agilent Technologies, UK) and RNA 6000 Nano assay (BioAnalyzer, Agilent Technologies, UK) here utilised, despite being highly sensitive, might not be sufficient to detect very low amount of RNA when degraded or small size and the adoption of more sensitive assays could have been more informative. For example, high Sensitivity RNA ScreenTape assay provides efficient and reliable separation of total RNA samples of limited abundance down to 100 pg/µl, equivalent to the RNA 6000 Pico assay using the Agilent Bioanalyzer for the analysis of RNA samples of low abundance down to 50 pg/µL of total RNA. Lastly, the inconsistency of conventional methods for the evaluation of RNA quality has been widely discussed (Imbeaud et al., 2005, Alderman, 1988). Hence, despite failing the initial quality assessment, nuclei-derived RNA samples were used for reverse transcription and evaluated in their performance in qPCR assays.
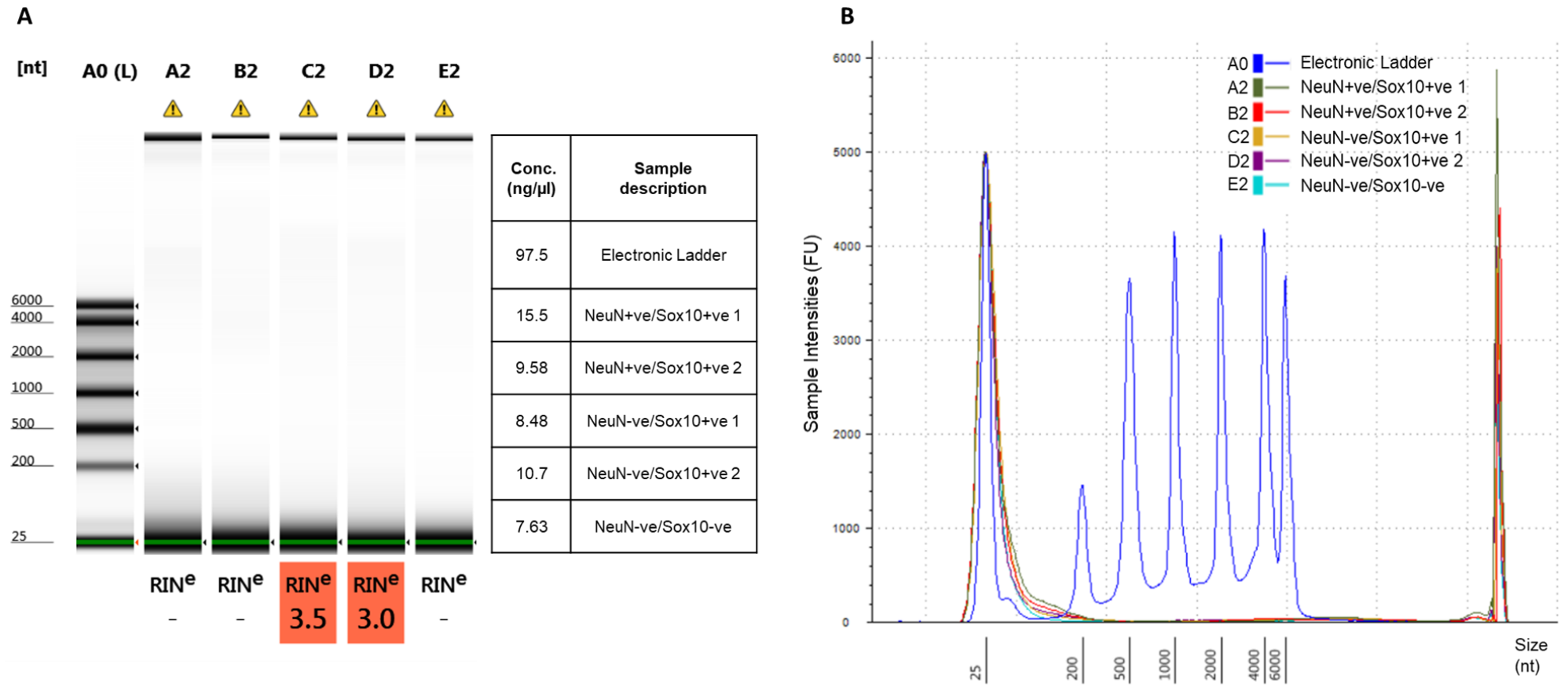
Figure 4.16 Eukaryotic RNA analysis using Agilent RNA ScreenTape assay.
Representative example of (A) gel electrophoresis image providing details about the RIN and RNA concentration per nuclei fraction; (B) Electropherogram showing the ladder profile in comparison with the profile of nuclear RNA from sorted nuclei. NeuN-ve/Sox10+ve (oligodendrocyte-enriched nuclei); NeuN-ve/Sox10-ve (other glia-enriched nuclei).

274

4.5.4 Immunostaining of cultured cell lines revealed the spatial expression pattern of candidate cell type-specific nuclear markers

Due to the difficulty in finding effective nuclear antibodies suitable for flow cytometry applications an alternative approach was utilised to verify the claims of literature and databases in regards to the specificity of these markers in targeting the nucleus. Macrophages have a tissue-specific identity determined by tight transcriptional regulation of uniquely expressed genes (Gosselin et al., 2014). Microglia, as cells derived from primitive macrophage progenitors (Ginhoux et al., 2010), express these unique signature genes (Wes et al., 2016). The scientific literature was enquired to identify microglia signature genes encoding for nuclear proteins, two of which (details in **Table 4.4**) have been tested using ICC on a SV40 immortalized microglia cell line.

Gene ID	Encoded protein	Biological Function	Cellular localisation & expression
Spi1	**Pu.1**	-Essential transcription factor for microgliogenesis -Essential lineage-determining transcription factor in primary macrophages	-Nuclear localisation (Smith et al., 2013, Heinz et al., 2010) -Microglia extracted from mixed glial cultures express Pu.1 (Rustenhoven et al., 2016) -Human induced microglia express Pu.1 in nucleus (Sellgren et al., 2017) -Pu.1 mRNA continuously expressed during microglial development (Kierdorf et al., 2013) -Spi1 -/- knockout mice were devoid of all microglia (Kierdorf et al., 2013)
SALL1	**Sall1**	-Transcriptional regulator (Buttgereit et al., 2016)) transcriptional repressor with unknown target genes (Koso et al., 2016) -Role in maintaining microglia identity in vivo (Buttgereit et al., 2016)(27776109) and microglia morphology during development (Koso et al., 2016)	-High expression levels in adult microglia (Gautier et al., 2012) -Microglia expression in healthy human CNS (Lavin et al., 2014) (although restricted to the haematopoietic compartment of the CNS (Buttgereit et al., 2016) - Not expressed by non-microglial mononuclear phagocytes (Buttgereit et al., 2016, Koso et al., 2016)

Table 4.4 Candidate microglia-specific nuclear markers.
Overview of the two candidate genes identified through literature search by Alexandra Sherrell, EH4 student in our group and tested by ICC on SV40 microglia cell line. Cellular localisation, specificity to microglia and biological function of the corresponding encoded proteins is provided.

4.5.4.1 Growth of SV40 immortalised primary human microglia

Human microglia derived from Primary Human Microglia Cells (>99% purity) (Accegen Biotech, Cat.No ABI-TC4171) immortalised used the Lenti-SV40 Lentivirus (SV40 cell line) was acquired and grown indefinitely in cell culture using the microglial Cell Medium Kit (AcceGen Biotech, Cat. No ABI-TM009). After growing and plating (30,000 cells per coverslip) the coverslips coated with SV40 immortalised microglia were imagined before staining using the EVOS XL Core Configured Microscope (Invitrogen, Carlsbad, CA) to confirm presence and identity of microglia (**Figure 4.17**).
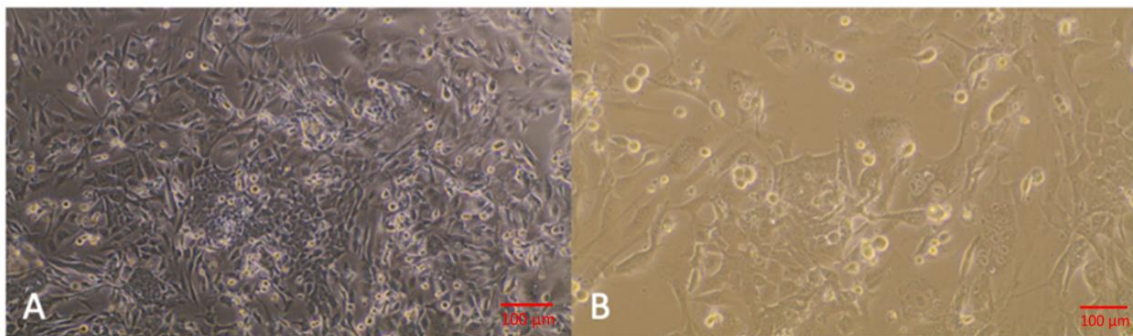
Figure 4.17 Confirmation of cell growth of SV40 immortalised microglia.
Immunocytochemistry images depicting SV40 microglia acquired at A) x 10 magnification and B) × 20 magnification. Both images were taken with the EVOS XL Core Cell Imaging System (Invitrogen, Carlsbad, CA). The scale bar represents 100 µm.

4.5.4.2 Anti-Pu.1 monoclonal antibody does not stain SV40 microglia nuclei

Previous immunocytochemical analyses have shown that the anti-PU.1 antibody stains the nuclei of microglia isolated from mixed glial cultures (Rustenhoven et al., 2016, Smith et al., 2013) and nuclei of human induced microglia (Sellgren et al., 2017). However, when SV40 microglia were stained with a mouse monoclonal anti-Pu.1 at 1:100, 1:250, 1:500 and 1:1000 dilutions, according to two different protocols, no evidence of a nuclear signal was found **(Figure 4.18).**
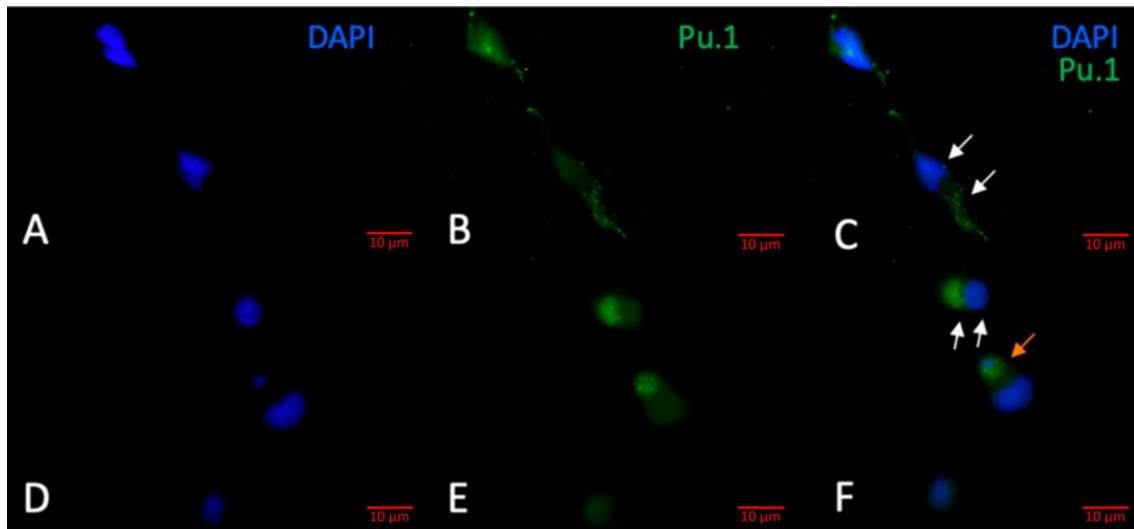
Figure 4.18 Anti Pu.1 monoclonal antibody does not stain SV40 microglia nuclei.
A representative example of confocal images of SV40 microglia acquired at × 40 magnification with a confocal laser scanning system depicting the staining of Pu.1 in SV40 microglia, where green is Pu.1. Nuclei were imaged using DAPI (blue). A-C: SV40 microglia stained with DAPI (1:5000) and mouse monoclonal anti-Pu.1 (1:250) according to Pu.1 Protocol 1. The same antibody showed stronger signal of fluorescence at 1:250 dilution. ***A)*** *DAPI (1:5000) staining microglia nuclei (blue).* ***B)*** *Anti-Pu.1 primary antibody (1:250) followed by anti-mouse Alexa Fluor488 secondary antibody staining (1:400) revealed weak extra-nucleic signal (green).* ***C)*** *Overlay of DAPI and Pu.1 staining showing that Pu.1 staining does not co-localise with DAPI staining. White arrows highlight distinct signals location for DAPI and Pu.1. D-F: SV40 microglia stained with DAPI (1:5000) and mouse monoclonal anti-Pu.1 (1:1000) according to Pu.1 protocol 2 instructions. 1:1000 anti-Pu.1 showed higher fluorescence intensity.* ***D)*** *DAPI (1:5000) staining of microglia nuclei.* ***E)*** *Anti-Pu.1 (1:1000) primary antibody + anti-mouse Alexa Fluor488 secondary antibody staining (1:400) revealed very green signal.* ***F)*** *Overlay of D and E confirming that Pu.1 signal does not overlap with DAPI signal and therefore suggesting that the Pu.1 staining is not localised within the nucleus area. Orange arrow showing potential overlap of DAPI and Pu.1 fluorescence in an individual cell. All images were taken on Leica DM4000 B LED Fluorescence Microscope (magnification 40 x; scale bar = 10 μm).*

Images from microglia stained following Pu.1 Protocol 1 showed a very weak signal under very high exposure (**Figure 4.18B**), not localised to microglia nuclei (**Figure 4.18C**). Microglia were also stained as per Pu.1 Protocol 2 which differ compared to Protocol 1 in the permeabilising and blocking step. This ensured that these stages were not responsible for the lack of nuclear signal and gave the cells a longer incubation period with the primary antibody, ensuring optimal staining conditions. Imaging of microglia stained according to Protocol 2 again showed a very weak signal under high exposure (**Figure 4.18E**). The overlay of

the DAPI with the Pu.1 signal revealed that the weak Pu.1 fluorescence was not localised to microglia nuclei (**Figure 4.18F**), except for one potential instance (orange arrow **in Figure 4.18F**).

The ICC analysis did not provide evidence that further optimisation could have enhanced signal intensity or detection of nuclear localisation; therefore, suggesting that Pu.1 was not an effective microglia-specific nuclear marker for SV40 immortalised primary human microglia.

4.5.4.3   *Anti-Sall1 monoclonal antibody stains SV40 microglia nuclei*

SV40 microglia were stained with a mouse monoclonal anti-Sall1 at 1:100, 1:250, 1:500 and 1:1000 dilutions as per Protocol 1 instructions. Fluorescence microscopy showed evidence of nuclear antibody binding and a weak Sall1 signal (**Figure 4.19**). Although the signal was weak, it had mostly nuclear localisation (**Figure 4.19C** and **4.19F**), indicating that the antibody had bound to Sall1 within SV40 microglia nuclei. However, Sall1 signal was detected outside the nucleus area (yellow arrow in **Figure 4.19F)** suggesting that its expression within the cell might not be exclusively intranuclear but also perinuclear.
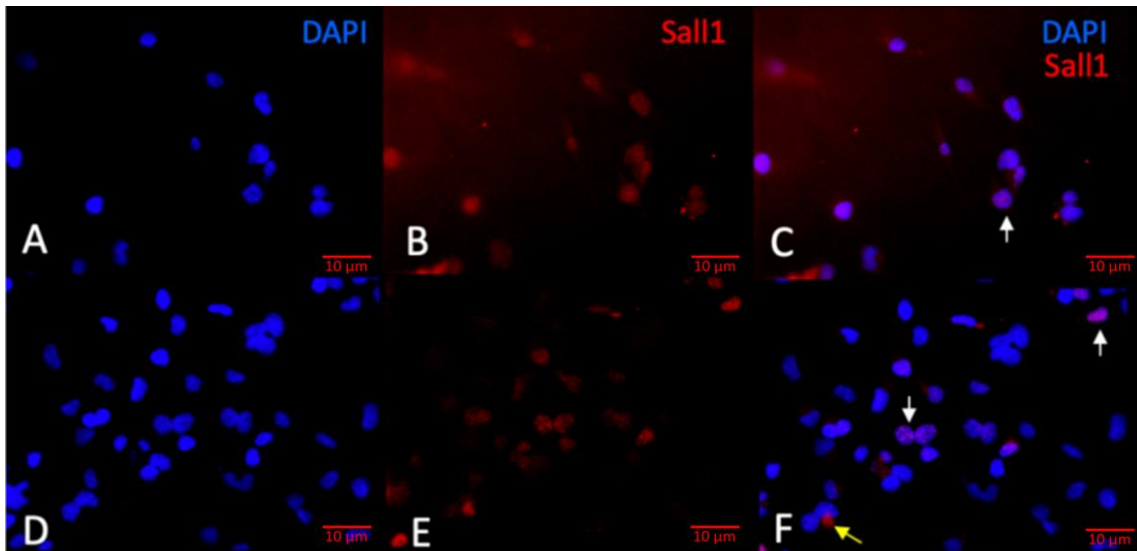
Figure 4.19 Anti-Sall1 monoclonal antibody stains SV40 microglia nuclei (Protocol1).

*A representative example of confocal images of SV40 microglia acquired at × 40 magnification with a confocal laser scanning system depicting the staining of Sall1 in SV40 microglia, where red is Sall1. Nuclei were imaged using DAPI (blue). **A-C**: SV40 microglia stained with DAPI (1:5000) and mouse monoclonal anti-Sall1 (1:100) according to Sall1 Protocol 1 guidelines**. A)** DAPI (1:5000) staining of microglia nuclei (Blue). **B)** Anti-Sall1 (1:100) primary with Alexa Fluor 555 secondary antibody (1:400) stains microglia nuclei (red) although the signal intensity is low. **C)** Overlay of A and B showing where Sall1 signal overlaps with DAPI signal; there is evidence of nuclear staining. **D-F:** SV40 microglia stained with DAPI (1:5000) and mouse monoclonal anti-Sall1 (1:500) following Sall1 Protocol 1.**D)** DAPI (1:5000) stains microglia nuclei (blue). **E)** Anti-Sall1 (1:500) primary with Alexa Fluor 555 secondary antibody (1:400) stains microglia nuclei (red). F) Overlay of A and B showing where Sall1 signal overlaps with DAPI signal; there is evidence of nuclear staining. White arrows highlight examples of staining co-localization. Yellow arrow indicates extra-nuclear Sall1 signal. All images were taken on Leica DM4000 B LED Fluorescence Microscope (magnification 40 x; scale bar = 10 µm).*

While the DAPI signal was strong in SV40 microglia nuclei, the nuclear signal detected for Sall1 was extremely weak. Therefore, the immunostaining protocol for Sall1 underwent minor adjustments in an attempt to optimise the staining conditions. Higher concentrations of the primary antibody (1:10, 1:50, 1:100 and 1:250 dilutions) and longer incubation period were tested (see Sall1- Protocol 2 for details). Alexa Fluor 488 was used as the secondary antibody rather than Alexa Fluor 555. When SV40 microglia were stained with the same mouse monoclonal anti-Sall1 following the protocol adjustments, a moderately stronger signal was detected with evidence of nuclear localisation (**Figure 4.20**).
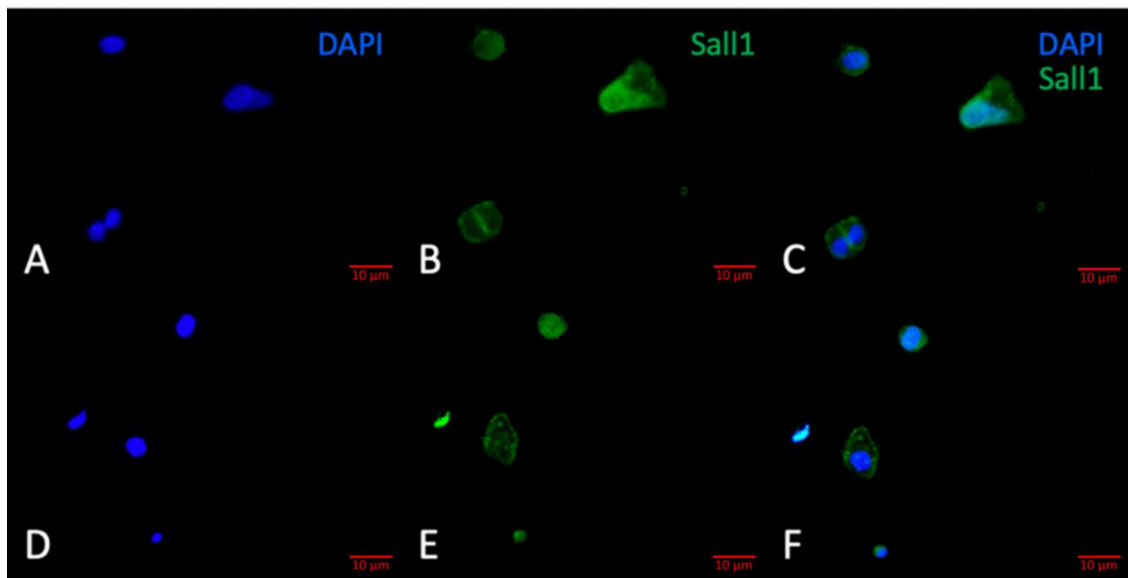
Figure 4.20 Anti-Sall1 monoclonal antibody stains SV40 microglia nuclei (Protocol2).
A representative example of confocal images of SV40 microglia acquired at × 40 magnification with a confocal laser scanning system depicting the staining of Sall1 in SV40 microglia, where green is Sall1. Nuclei were imaged using DAPI (blue). **A-C***: SV40 microglia stained with DAPI (1:5000) and mouse monoclonal anti-Sall1 (1:100) according to Sall1 Protocol 2 guidelines.* **A)** *DAPI (1:5000) stains microglia nuclei (Blue).* **B)** *Anti-Sall1 (1:100) primary with Alexa Fluor 488 secondary antibody (1:400) stains microglia nuclei (green).* **C)** *Overlay of A and B showing where Sall1 signal overlaps with DAPI signal; there is evidence of nuclear staining although the staining signal is beyond DAPI staining.* **D-F***: SV40 microglia stained with DAPI (1:5000) and mouse monoclonal anti-Sall1 (1:250) following Sall1 Protocol 2.* **D)** *DAPI (1:5000) stains microglia nuclei (blue).* **E)** *Anti-Sall1 (1:250) primary with Alexa Fluor 488 secondary antibody (1:400) stains microglia nuclei.* **F)** *Overlay of D and E showing where Sall1 signal overlaps with DAPI signal. All images were taken on Leica DM4000 B LED Fluorescence Microscope (magnification 40 x; scale bar = 10 μm).*

Although the Sall1 signal was localised to microglia nuclei, the antibody binding sites were not completely overlapping the DAPI binding sites; images from microglia stained according to Protocol 2 showed that anti-Sall1 stains beyond the edges of DAPI staining (**Figure 4.20C, F**). Nonetheless, the optimisation of anti-Sall1 immunostaining confirmed that the mouse monoclonal anti-Sall1 does in fact stain SV40 immortalised primary human microglia nuclei, generating a moderate immunofluorescence signal, suggesting therefore that the Sall1 transcription factor could be exploited as a microglia-specific nuclear marker.

4.5.5 *Testing of candidate antibodies for targeted immunostaining of nuclei suspensions revealed inconclusive results*

A broad literature search along with the investigation of gene expression databases (e.g. The Human Protein Atlas) was conducted to identify candidate markers for nuclei staining of neural cells. English-language, peer-reviewed publications published from January 1990 to June 2019, were located using PubMed, Medline, and ScienceDirect using various combinations of search terms: i) "nuclear antibody AND brain cells" ii) "nuclear marker AND human brain", iii) "nuclear marker AND human oligodendrocytes (or microglia or astrocytes)". Hand searching was also carried out and studies conducted in mouse model were also considered. Commercially available antibodies specific for the selected marker genes were tested on nuclei suspensions harvested through density gradient ultracentrifugation prior to sorting. The outcome of the testing is summarized in the table below (**Table 4.5**).

Target cell	Antibody tested	Supplier	Pre-conjugated	Comments
Oligodendrocytes	*SOX10*	Santa Cruz Biothechnology	PE	Failed to detect positively stained population at all concentration tested
		R&D Systems	X	Failed to detect positively stained population at all I concentration tested
		R&D Systems	X	Failed to detect positively stained population at all concentration tested
		R&D Systems	NL577	Positively stained population successfully detected at all concentration tested
	OLIG2	Millipore	AlexaFluor 555	Failed to detect positively stained population at all concentration tested
Astrocytes	*PAX6*	Abcam	AlexaFluor 647	Failed to detect positively stained population at all concentration tested
	SOX9	Santa Cruz Biothechnology	X	Failed to detect positively stained population at all concentration tested
	ALDOC	Abcam	X	Failed to detect positively stained population at all concentration tested
		Abcam	PE	Failed to detect positively stained population at all concentration tested
Microglia	*PU.1*	Santa Cruz Biothechnology	AlexaFluor 647	Failed to detect positively stained population at all concentration tested
		R&D Systems	X	Failed to detect positively stained population at all concentration tested
	SALL1	Abcam	X	Failed to detect positively stained population at all concentration tested
	IRF8	Invitrogen	APC	Positively stained population successfully detected at all concentration tested
GABA neurons	*SOX6*	Abcam	X	Failed to detect positively stained population at all concentration tested

Table 4.5 Table results summarising the outcome of the antibody testing for nuclear staining of different neural cell types.
*Each antibody has been tested at different concentrations and incubation times on purified nuclei suspensions obtained through FANS. For full details about each antibody see **Table 4.1**.*

To conclude, out of the nine tested, only two novel nuclear antibodies were successful for nuclei immunolabelling using FANS: Sox10, marking mature oligodendrocytes and Irf8 which is instead specific to human microglia. Both markers were therefore subjected to titration in order to determine the optimal antibody concentration and were stably integrated in the staining procedure of this optimised FANS protocol. **Figure 4.21** illustrates a representative example of data acquired during a FANS run where neural nuclei underwent triple staining.
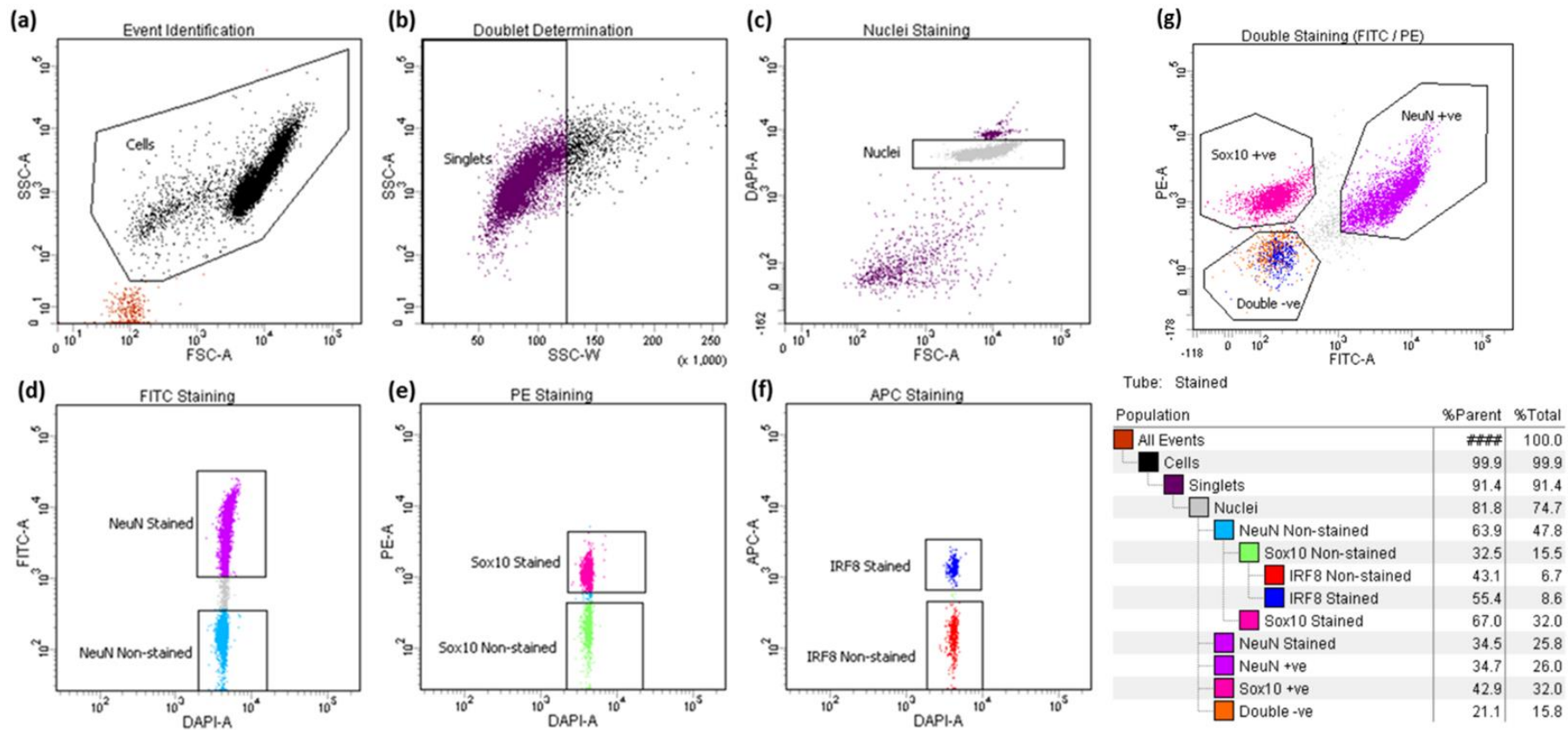
Figure 4.21 FANS triple-staining strategy.
a) Particles smaller than nuclei (black dots) were eliminated with an area plot of forward scatter (FSC-A) versus side scatter (SSC-A), with gating for nuclei-sized particles inside the gate (box). (b) Plots of height versus width in the side scatter channel are used for doublet discrimination with gating to exclude aggregates of two or more nuclei. (c) Doublet discrimination gating was used to visualise nuclei by subgating on Hoechst 33342 (d, f). Subsequent scatterplots discerning (d) NeuN-Alexa Fluor488–conjugated antibody staining (magenta) (e) Sox10 NL577-stained nuclei (darkpink) (f) IRF8-APC stained nuclei (darkblue). The resultant hierarchical colour key ensures that only nuclei that are positive or negative for staining with the NeuN and/or Sox10/Irf8 antibody are passed through the next gating condition. (g) The distribution of the three main nuclei subpopulations identified through triple staining strategy reveals how the IRF8+ve population (darkblue) sits within the double-ve fraction (orange) but does not fully overlap with it unveiling a fourth population (triple negative) likely to be constituted predominantly by astrocytes.

4.5.6 Targeted gene expression (TLDA) results confirmed enrichment of sorted nuclei for distinct cell type

Targeted gene expression analysis was performed on RNA extracted from two sorted brain specimen to confirm the identity of each purified nuclei population. Transcripts known to be enriched in major brain cell types (*NEUN* and *ENO2* (neurons), *OLIG2* (oligodendrocytes), *GFAP* (astrocytes) and *CD68* (microglia)) were quantified across the sorted nuclei populations. Expression levels of each cell-type marker gene were normalised to 5 reference genes (*ACTB, EIF4A2, GAPDH, SF3A1, UBC*) previously reported for being stably expressed in the human brain (Marzi et al., 2018). Expression of *NEUN* and *ENO2* transcripts, established markers of mature neurons, were enriched in the NeuN+ve/Sox10ve nuclei fraction, while showing lower expression levels in the remaining two sorted fractions (NeuN-ve/Sox10+ve and NeuN-ve/Sox10-ve) (**Figure 4.22 a, b**). In contrast, expression of *OLIG2* gene was found enriched in the NeuN-ve/Sox10+ve nuclei fraction while almost undetectable in the other two nuclei populations (**Figure 4.22 c**). Finally, both *GFAP*, a marker of astrocytes, and *CD68*, a microglia marker, showed higher expression levels in the double negative (NeuN-ve/Sox10-ve) nuclei population (**Figure 4.22 d, e**) compared to the other two populations supporting the hypothesis that the double negative fraction gathers the other two most abundant cell types in the brain: astrocytes and microglia.
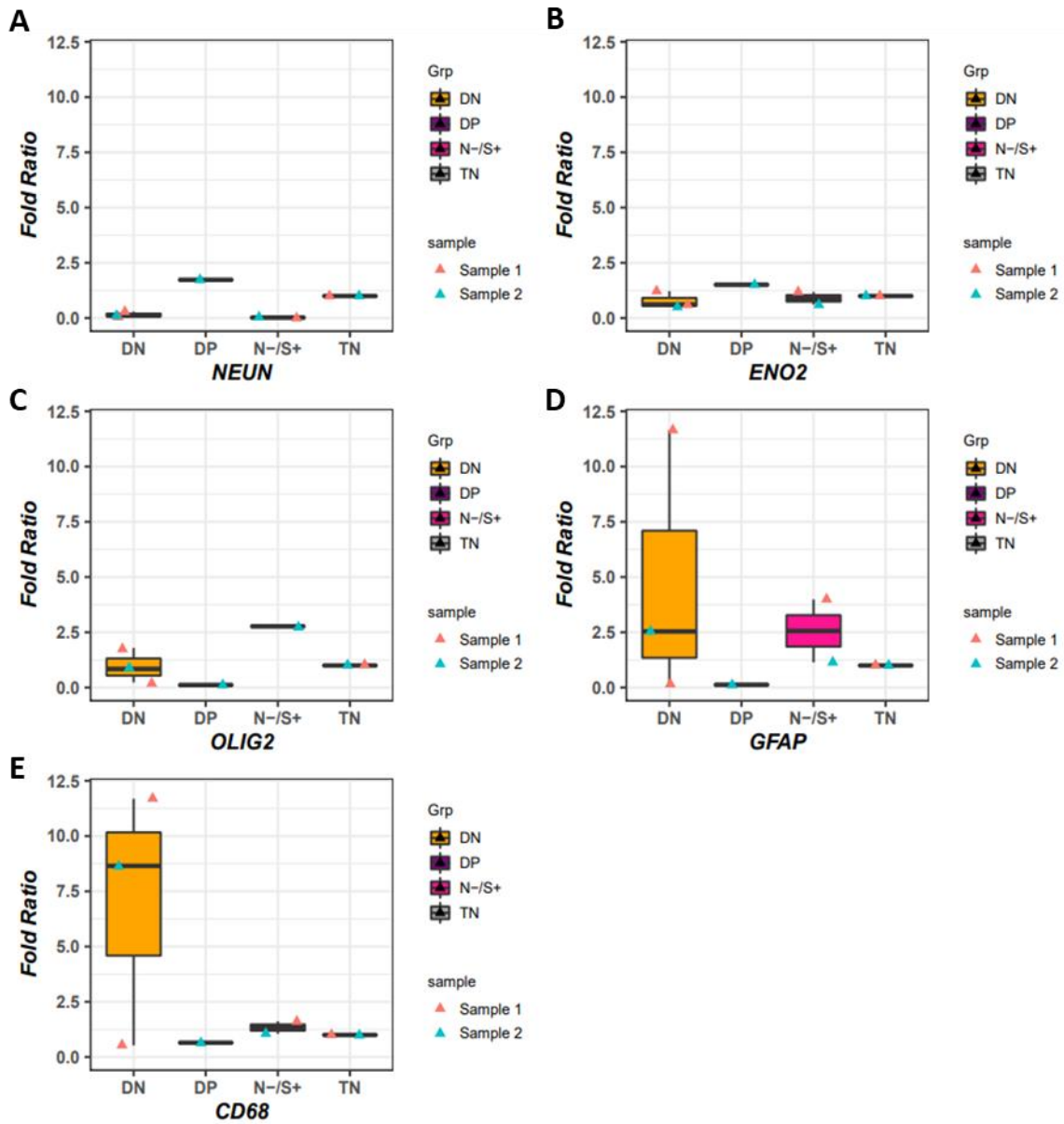
Figure 4.22 Relative gene expression analysis of cell markers in FANS sorted nuclei population.

NEUN and ENO2, neuronal markers; GFAP, astrocyte cell marker; OLIG2, oligodendrocyte cell marker; CD68, microglia cell marker. Results (fold ratio) for two distinct specimens are shown. Expression levels of each cell-type marker gene were normalised to 5 reference genes (ACTB, EIF4A2, GAPDH, SF3A1, UBC) knowing to be stably expressed in the human brain. Each gene assay was run in triplicates. Total fraction was set as baseline for comparisons. Abbreviations: DN, NeuN-ve/Sox10-ve; DP, NeuN+ve/Sox10+ve, N-/S+, NeuN-ve/Sox10+ve; TN, total nuclei.

4.6   Discussion

This work has optimised previous FANS protocols and its array of applications for use in post-mortem human brain allowing us to maximise and diversify the nature of data generated from each brain specimen. Leveraging upon existing techniques for FANS of post-mortem cortex, the yield and integrity of the isolated nuclei was significantly improved achieving minimal debris carry over (~20%) with nuclei recovery ranging from 70% to 80% therefore reducing the amount of valuable post-mortem tissue needed to solely 500 mg. The immunolabelling panel, originally limited to the characterisation of the NeuN staining (neuronal *vs* non-neuronal) was implemented with the anti-Sox10 antibody to collect populations enriched in neuronal cells (NeuN+ve/Sox10+ve) oligodendrocytes (NeuN-ve/Sox10+ve) and other glial cells (NeuN-ve/Sox10-ve).

The optimised protocol yields at least 500 ng of high molecular weight genomic DNA per nuclei fraction, which is ample for microarray-based epigenomic profiling. Genomic DNA samples from each nuclei population were run on Illumina EPIC array (Illumina, CA, USA) and QC checks as well as exploratory statistical analyses were undertaken (see **Chapter 5** for details). The procedure supplied sufficient nuclear material to also quantify chromatin accessibility (ATAC-seq) and histone modifications (Cut&Run-seq) (ongoing work, data not show here) enabling the quantification of multiple marks of gene regulation. Nuclear RNA was also extracted from these fractions and real-time qPCR performed using Taqman low-density array in order to provide an independent validation of specificity for the FACS-based nuclei purification (refer to section 4.5.6). Specifically, expression levels of cell type-specific phenotypic marker genes such as *GFAP* (astrocyte marker), *RBFOX3* and *ENO2* (neuronal markers), *CD68* (microglia markers) and *OLIG2* (oligodendrocyte marker) were assessed across sorted nuclei populations confirming the expected cell identity.

In order to further discriminate the composition of the nuclei fractions as well as validate the accuracy of the FANS approach, nine new candidate cell type-specific nuclear markers (see **Table 4.5** for a summary) were identified within the literature to immuno-label as many distinct populations as possible within the nuclei mixture. *IRF8*, a marker of microglia, proved to be successful in identifying the microglia population within the glial-enriched (NeuN-ve/Sox10-ve) fraction and was therefore stably implemented in the staining procedure (ongoing study).

However, given the difficulty in finding cell specific markers suitable for nuclei-based applications, immunocytochemistry techniques were adopted to confirm the nuclear localisation of those antibodies proposed by the literature as targeting the nucleus which however failed the immunolabelling when tested on FANS (for an example see Chapter 4- Appendix F) . Specifically, three candidate nuclear antibodies were tested on cultured human derived cell lines using ICC: *ALDOC1*, candidate astrocyte nuclear marker, was tested on SH-SY5Y neuroblastoma cells and U373 astrocytoma cells. *PU.1, and SALL1* (candidate microglia-specific markers) on SV40 microglia cells. For each antibody tested, different staining conditions, antibody dilutions and incubation times were examined. The ICC study offered valuable insights uncovering some of the reasons (e.g. peri-nuclear staining, different sensitivity, and variable antibody performance) which could explain the failed testing when the same antibodies (e.g. anti-SALL1) were used for FANS applications and therefore highlighting unforeseen limitations of this approach.

To the best of my knowledge, this is the first FANS protocol (publicly available on Protocols.io, dx.doi.org/10.17504/protocols.io.bmh2k38e) which allows to systematically separate and characterise on a multi-omics level three different cell types while utilising a small amount (~500mg) of cryopreserved human post-mortem brain tissue. Hence, this protocol has the potential to enhance the interpretation of previous findings derived from studies in bulk brain and elucidate whether the affected biological processes in the context of brain disease are driven by a specific cell type or whether reported differences simply reflect changes in cell-type proportions.

4.6.1 Optimization of nuclei extraction and purification

A number of adjustments were needed to maximise the nuclei yield as the main scope of this work was to perform multiple omics assays across multiple distinct neural cell populations (including neurons, oligodendrocytes and glial cells) from a small amount (~500mg) of cryopreserved human post-mortem brain tissue.

Due to loss of nuclei and damage to those recovered, any filtration step was omitted from this revised protocol. Centrifugation for a lengthy amount of time or at excessive speed although increases the yield of the nuclei, it also tends to promote contamination by non-nuclear material, as aggregates of cell debris

sediment faster than nuclei (Wu et al., 2014, Krishnaswami et al., 2016). For this reason, minor but substantial changes were made during the ultracentrifugation stage (e.g. spin length reduced to 45 min while speed was increased to 108,670 x g) since these were found to drastically impact the integrity and quality of the genomic DNA extracted from sorted nuclei. As already observed by the authors in protocol 1 (Krishnaswami et al., 2016), lack of nuclei within the specimen tissue as well as inadequate cell lysis to release nuclei or improper centrifugation were found to be the most frequent cause of low nuclei yield. Recovery was sensibly improved by keeping the number of freeze-thaw cycles at the lowest possible, by adjusting the number of Dounce strokes during homogenisation and by adapting the density gradient and the speed of centrifugation to the sample type.

4.6.2 Nuclear immunolabelling testing

There are several variables that need to be taken into consideration before selecting an isolation technique: purity, yield, intactness and frequency as well as isolation expense and time, and also availability of specific markers for isolation (Dainiak et al., 2007, Rahmanian et al., 2017). Although centrifugal sedimentation can be considered a simple, fast, and inexpensive cell fractionation method, this technique isolates cells based on the difference in size and/or density (Rahmanian et al., 2017) therefore high cell purity cannot be achieved unless adopting cell-type specific markers targeting the nucleus. Despite the panel of tested antibodies being broad and sourced from multiple robust studies, the majority of them failed to show evidence of immunolabelling when tried on human tissue derived nuclei samples. Various factors could help explaining these negative results. Firstly, the actual localisation of the antigens targeted by the antibodies. As observed thanks to the complementary ICC assays for Adolase C (astrocyte marker) (section 4.4 4.2) or Pu.1 (microglia marker) (section 4.4.5.2), the antigen to which the antibody bond is often located in the cytoplasmic space adjoining the nucleus (which is removed during the density gradient purification) or between the nuclear membrane layers which are likely to collapse during the FANS procedure due to the fragile nature of nuclei in suspension. Secondly, the different sensitivity between flow cytometry and immunocytochemistry in antigen detection is widely documented (Cordone et al., 2016, Balmaceda et al., 1995, Fine and Mayer, 1993). Immunophenotyping by flow cytometry is an objective

and quantitative method ideally suited to identify small populations of cells (Ward, 1999). Specificity and sensitivity of flow cytometry was found to be of 100% and 87.8%, respectively in a study comparing its performance to immunohistochemistry analysis for the detection of tumour cells (van der Meulen et al., 2018) suggesting specificity as the major strength of flow cytometry while being less accurate in detection. However, in another study similarly interested in the characterisation of cancer tissue, flow cytometry proved to be more sensitive than immunohistochemistry for the identification of selected markers, for antigen intensity quantification as well as for the evaluation of antigens co-expression on different cell populations (Cordone et al., 2016) highlighting the added value granted when performing flow cytometry.

Another important consideration when building multicolour panels is the titration of the chosen antibodies. Excess antibody will bind at low affinity and create background that will reduce the resolution and therefore mask the true signal. On the contrary, too little antibody may result in a false negative effect. Antibodies will preferentially bind to the high-affinity epitope they are raised to target (your target of interest). However, if there is an excessive amount of antibody around, and the primary targets are occupied, the antibody will bind to low-affinity targets (off-target effects). This is especially true in the case of intracellular targets (Telford et al., 2009). It is therefore important to determine the right concentration of antibody needed for a specific sample type. To be able to make accurate measurements of fluorescence, it is important to maximise the signal while reducing the noise. Some noise which comes from the cells (auto-fluorescence) and the inherent noise in the system is unavoidable (Maecker et al., 2004). Titration helps minimizing noise due to non-specific binding of the antibodies to low-affinity targets. For these reasons, for both working markers, NeuN and Sox10, a known amount of nuclei were stained with decreasing concentrations of antibody and fluorescence signals were analysed to determine the best signal-to-noise ratio using standard calculations. Despite antibody concentration being the critical factor, there are other variables influencing the titration: i) time of incubation, ii) temperature of incubation and iii) number of cells. The testing of candidate marker for FANS was performed consistently at 4°C and for 1.5 hours for a matter of practicality and time saving purposes. Further testing under different staining conditions might have yielded different results. Another common

factor which usually play an important role in antibody testing is the variation in performance often showed by different batches of the same antibody as well as the variation in performance of the same antibody when provided by different suppliers.

Although successfully adopted in a previous study for the purification of GABAergic neurons (Kozlenkov et al., 2016), the staining at two different concentrations (1:50, 1:400) and incubation time (45 minutes vs 2 hours) with a rabbit monoclonal primary antibody specific to Sox6 (see **Table 4.1** for details) followed by PerCP-conjugated secondary staining did not result in the distinctive labelling of the gabaergic neuronal subpopulation within the NeuN+ve fraction as expected in line with the data reported by Kozlenkov et al. (Kozlenkov et al., 2016). However, the antibody used by Kozlenkov et al. in their study was not commercially available and no other evidence suggesting anti-SOX6 as a nuclear marker suitable for FANS applications can be found in the literature at the present. Similarly, despite the numerous evidences found in literature suggesting *Olig2* as a candidate nuclear marker for human oligodendrocytes, a positively stained population was not identified when *Olig2* was added to the nuclei suspension (see **Appendix F- *Supplementary Figure 4.1***), whereas, *Sox10* proved to be effective in differentially staining bulk-derived nuclei allowing us to distinguish two different clusters of events along the fluorescence scale, a positively stained population (NeuN-ve/Sox10+ve) clearly distinct from the unstained one (NeuN-ve/Sox10-ve). However, *Olig2* is known to be highly expressed in OPCs (Douvaras and Fossati, 2015) which might explain the lack of staining in post-mortem tissue from elderly which is likely to contain primarily mature, fully differentiated oligodendrocytes.

When tested on purified nuclei, the Anti-Aldolase C antibody pre-conjugated to PE did not show evidence of staining at any of the concentrations examined (data not shown). Aldolase C antibody was also tested in its unconjugated form on a SHY5HY cell line as well as on the U373 astrocytoma cell line at various concentrations and for different incubation times (see **Table 4.1** for details). However, in all the conditions where a fluorescent signal was detectable the staining was predominately localised in the perinuclear region (cytoplasmic region just around the nucleus) and/or perinuclear space (see **Appendix F- *Supplementary Figure 4.2***). The observations gathered from the cell line assay appear to be in line with the flow cytometry assay: the expression of *ALDOC* in

the cytoplasmic area surrounding the nucleus which is removed during the nuclei purification step could explain the lack of staining observed in isolated nuclei samples. Even in the case of Aldolase C expression being localised along the nuclear membranes, the disruption and stress to which the nuclear envelope is subjected during the ultracentrifugation step might result in significant loss of antigen molecules.

Despite the evidence for its enrichment in astrocytes, a generalised, unspecific increase in fluorescence was observed during data acquisition preventing the identification of a Pax6-negatively stained population (data not shown).

Mouse monoclonal anti-Sox9 was tested on nuclei solutions derived from bulk brain tissue. Despite the striking body of evidence regarding its specificity for astrocytes, a generalised, unspecific increase in fluorescence was observed during data acquisition preventing the identification of a Sox9-negatively stained population (data not shown) revealing lack of specificity in staining neural nuclei. Mouse monoclonal anti-Irf8 antibody pre-conjugated to APC was tested on purified nuclei samples and found to be successful in staining a subpopulation within the NeuN-ve/ Sox10-ve fraction (**Figure 4.21**) although some variability in outcome was observed from brain specimen to specimen suggesting great heterogeneity in cell composition even in the healthy brain. The localisation of Irf8 antibody staining was not further validated on *in vitro* cell lines as per Sall1 and Pu1 markers due to time constraints. Nevertheless, Irf8 antibody has been successfully used for microglia nuclei purification and therefore stably incorporated in the FANS protocol here described (data not published).

4.6.3   Immunocytochemistry analyses

Several large-scale transcriptomic and genome sequencing studies have been conducted in order to identify microglia-specific signature genes and hundreds of candidates have been reported to be selectively expressed in microglia compared to other macrophages and neural cells; most of which, however, encoding cytoplasmic, transmembrane or receptor proteins (Gautier et al., 2012, Butovsky et al., 2014, Zhang et al., 2014, Hickman et al., 2013) Although not expressed exclusively in microglia (Rosenbauer and Tenen, 2007), *PU.1* is critical to microglia function and is expressed continuously throughout microglial

development (Kierdorf et al., 2013). It is the most differentially expressed transcription factor in human microglia (Butovsky et al., 2014) and has been used in previous studies binding anti-Pu.1 antibodies within the nucleus (Rustenhoven et al., 2016, Smith et al., 2013, Sellgren et al., 2017). The Pu.1 transcription factor is crucial for microglial development (Kierdorf et al., 2013); and recent research has uncovered Pu.1 as a critical regulator of microglial activation in neurodegeneration (Zhou et al., 2019c). Although Pu.1 is not specific for microglia alone, its expression increases the uniqueness of the microglial genetic profile and effectively distinguishes microglia from other myeloid cells (Geissmann et al., 2010). *SALL1* was also chosen as a candidate marker for this study: putative master regulator of microglial identity, fate and transcriptional signature, the expression of Sall1 is almost exclusive to microglia (Buttgereit et al., 2016). Sall1-deficient microglia show morphological defects proving that Sall1 is essential for microglia acquiring their typical ramified morphology after colonisation of the CNS (Barozzi et al., 2014, Gautier et al., 2012) which also explains why Sall1 is specifically expressed in microglia and not in macrophages.

Due to the difficulty experienced in finding markers successfully targeting the nucleus of their specific cell target and suitable for FANS, ICC was adopted 1) as complementary method to select candidate markers 2) to further investigate the failed immuno-tagging contrary to the expectations based upon previous findings. Immunocytochemical analyses revealed that the mouse monoclonal anti-Pu.1 did not bind to nuclei of SV40 immortalised human microglia, whilst the mouse monoclonal anti-Sall1 did appear to stain SV40 microglia nuclei.

4.6.3.1   *ICC antibody testing failed in confirming previous findings*

Three studies have used monoclonal anti-Pu.1 antibody as a microglia marker *in vitro* and demonstrated that Pu.1 can stain microglial nuclei (Rustenhoven et al., 2016, Smith et al., 2013, Sellgren et al., 2017). However, in my work, when SV40 immortalised human microglia were stained with a mouse monoclonal anti-Pu.1 according to two different protocols, only a very weak fluorescent signal was detected, and it was not localised to the cellular nucleus. There are some possible reasons why the findings here reported do not support previously published results. Firstly, it is known that monoclonal antibodies suffer from 'batch-to-batch variation' and therefore antibodies from different manufacturers can differ in

binding affinity and efficacy (Voskuil, 2017). Secondly, the immunostaining techniques and reagents here adopted might have affected the Pu.1 signal. Triton-X 100, a non-ionic detergent, is a widely used and well validated agent for permeabilising the cell membrane (Smith, 2017) but its efficacy as permeabilising agent may differ when it comes to nuclear protein immunostaining, rather than cytoplasmic. Incubation time is another variable which has potential to affect the staining intensity. Finally, the source of cell lines for these assays might have impacted findings. Rustenhoven et al. and Smith et al. isolated microglia samples from human adult brain tissue biopsies, whilst Sellgren et al. generated human microglia-like cells from peripheral blood mononuclear cells. For this work, an SV40 immortalised human microglia cell line was used. Immortalised microglia offer many advantages as these cell lines are easy to maintain and abundantly available. However, they are also susceptible to dedifferentiation and the immortalisation process can alter the microglial phenotype (Timmerman et al., 2018). Moreover, it has been demonstrated that microglial cell lines differ genetically and functionally from *ex vivo* microglia suggesting that gene expression differs significantly between isolated *ex vivo* cells and immortalised cell lines (Melief et al., 2016). As immortalised cell lines express different microglial signatures to isolated *ex vivo* microglia (Melief et al., 2016), Pu.1 could actually be an effective nuclear marker in *ex vivo* microglia (Rustenhoven et al., 2016). Future work, therefore, aiming to assess Pu.1 expression across multiple *in vitro* and *ex vivo* microglia models could help to establish whether Pu.1 is effectively a microglia-specific nuclear marker.

4.6.3.2 *Sall1 as a microglia-specific nuclear marker*

The ICC study undertaken as part of this thesis showed that mouse monoclonal anti-Sall1 antibody binds within SV40 human microglia nuclei; this is a significant and, to the best of my knowledge, novel development in the search for a microglia-specific nuclear marker. Interestingly, Kupffer cells and alveolar macrophages, which also originate from yolk sac-derived erythro-myeloid progenitors similarly to microglia (Gomez Perdiguero et al., 2015), do not express Sall1 (Gautier et al., 2012) showing that the microglia exclusive expression is not simply due to the yolk sac origin rather Sall1 expression is likely regulated by the local CNS microenvironment, meaning that cell line and *in vivo* Sall1 expression

may differ. As phenotypic and gene expression discrepancies between *ex vivo* human microglia and SV40 immortalised microglia are well-established (Melief et al., 2016), Sall1 requires replication and validation as a microglia-specific nuclear marker in *ex vivo* human microglia to determine the significance of the findings described here. SV40 immortalised microglia were stained with anti-Sall1 applying two different protocols. A stronger, more definite signal was observed under Protocol 2 compared to Protocol 1, therefore future work should seek to optimise further the staining procedure, ideally in an *ex vivo* microglial model to establish the significance of the findings here reported.

4.6.4 Optimisation of nucleic acids extractions

The main challenge encountered to obtain high quality, high yield nucleic acids was the need to tailor the extraction procedure to the sample type: although more robust than whole cells for FACS applications, nuclei are sensitive to harsh chemical treatments which, once disrupted the nuclear envelope, could affect the integrity of the nuclei acids as well as cause activation of enzymatic cleavage with subsequent fragmentation. This was particularly restrictive when dealing with RNA which is known for its extreme instability and fragility. Another obstacle was also represented by the different abundancy of individual cell types: the rarer populations provided insufficient yields, which forced the exclusion of all collected nuclei fractions deriving from the same specimen from downstream comparative assays.

4.6.5 Gene expression assays

Due to the abovementioned reasons, the targeted gene expression assay which demands high quality and abundant RNA needed additional caution particularly at the stage of RNA extraction and cDNA synthesis requiring reagents and assays specifically developed for very low input or fragmented RNA. As previously mentioned, the major limiting factor of working with nuclei-derived RNA is the inevitable loss of information encased in the cytoplasmic compartment. Nevertheless, the preliminary data here described show the applicability of this method to robustly detect gene expression signatures. Expression levels of well-

established markers of cellular identity were quantified in two different brain specimen in each nuclei fraction using RT-qPCR. Transcript levels of *NEUN* and *ENO2* (neuronal markers) were found enriched in the NeuN+ve/Sox10+ve fraction although expression levels of *ENO2* showed increased expression also in the NeuN-ve/Sox10+ve population suggesting a potential neuronal contamination of the oligodendrocyte-enriched fraction. *OLIG2* (marker of oligodendrocytes) was highly enriched predominantly in the Sox10+ve fraction while transcription levels for *GFAP* and *CD68* revealed a substantial increase in the NeuN-ve/Sox10-ve fraction which is presumed to be enriched in other glial cells. The targeted gene expression assay does not report data for the IRF8+ve nuclei population as performed prior testing and optimisation of the anti-irf8 antibody staining. Lastly, in line with its composition the total nuclei fraction (unsorted nuclei), included in the analysis as proxy for the bulk tissue, tends to sit in the middle of the expression fold change distribution lending support to the hypothesis that the expression profile captured by transcriptomic studies using bulk brain is likely tio mask the actual transcription rate in each individual cell types.

4.6.6 *Working with nuclei: advantages and strength*

The actual number of different cell types in the brain remains poorly understood. Cell 'type' implies stable characteristics, such as the synthesis of a particular neurotransmitter, and these cells have generally arisen by differentiation through developmental pathways. Identifying the abundance and functions of all the cell types in the brain is therefore essential and the use of nuclei bypasses the difficulties involved in obtaining undamaged whole cells. Through extensive comparisons of nuclear and cellular transcriptomes, studies have demonstrated that nuclei can substitute for whole cells (Grindberg et al., 2013) as for the majority of genes, nuclei yielded expression signatures that were very similar to those obtained from whole-cell controls (Grindberg et al., 2013). For most transcripts, the nuclear and whole-cell expression profiles were similar, and therefore nuclei can generally be substituted for whole cells to define cell lineage, state or type populations (Krishnaswami et al., 2016). For instance, the presence of the NeuN protein, a neuron-specific nuclear marker, based on antibody labelling during FACS of nuclei, was found to be consistent with the RNA-seq

detection of NeuN transcript in nuclei labelled with anti-NeuN antibody and none of the NeuN-negative nuclei (Krishnaswami et al., 2016). In cases in which the cell is positive for a protein marker based on FACS, but the transcript is not detected, it is possible that the protein is longer lived than the transcript. Transcription does not exactly reflect protein concentrations (Krishnaswami et al., 2016). Besides, gene expression values from nuclei can be used to identify cell types (Grindberg et al., 2013). Technical challenges including cell isolation and RNA quality which are known to profoundly alter gene expression can be overcome by using nuclei as well as including protease treatment to disperse whole cells (Huang et al., 2010). As the majority of accessible human brain specimen are obtained from frozen archives and collections, the use of nuclei may provide the best option that is currently available for RNA-seq from neural cells. The technical and biological variation is similar for whole cells and nuclei (Grindberg et al., 2013). This method could also allow investigation of biological features unique to nuclei, such as enrichment of certain transcripts and precursors of some noncoding RNAs in gene expression studies. Furthermore, studies of specific nuclear functions may be enhanced by directly accessing the nuclei - for example, studies investigating the regulatory processes controlling gene expression mediated by transcription factors, promoters, enhancers, epigenetic modifications and other mechanisms.

4.6.7 Working with nuclei: limitations and pitfalls

On the other hand, working with nuclei inevitably impose some limitations. Nuclei are generally fragile compared with whole cells, and some loss can be expected at each stage of the isolation procedure. However, for frozen brain tissue, whole cells tend to generate poor-quality cDNA (Krishnaswami et al., 2016).
Poor tissue quality can lead to high background fluorescence signal, or auto-fluorescence, which may be a consequence of increased oxidation of the tissue. Poor quality tissue is also the most common cause of lack of antibody staining. This is particularly problematic with long post-mortem intervals for autopsy samples or poor tissue handling during acquisition and freezing. Therefore, sample selection criteria should include low post-mortem intervals if possible. Ideally samples should be kept on ice immediately upon availability and should

be snap frozen as soon as possible, however this is not always possible and as post-mortem samples are a precious finite resource.

Gradual loss of antibody staining after repeated freeze-thaw cycles is another potential issue particularly with certain antigens as multiple freeze-thaw events lead to protein degeneration therefore the number of stained nuclei for a given population can be highly variable depending on tissue quality.

Use of nuclei inevitably results in loss of some information contained in cytoplasmic mRNA as cytoplasmic transcripts are not detectable, nor are small noncoding RNAs. Although low levels of mRNA is contained in the nucleus of the cell (Grindberg et al., 2013), harsh treatment have the tendency to perturb gene expression. Due to low amounts of RNA in the nucleus, 30 cycles were needed to amplify nuclear cDNA for the fraction purity validation (section 4.4.6) whereas only 21 cycles seemed satisfactory in another nuclei study (Krishnaswami et al., 2016); in both cases higher if compared with the 18 cycles sufficient when using whole cells (Krishnaswami et al., 2016). Nevertheless, some low-copy transcripts may still be difficult to detect in nuclei and increasing the cycle number (≥ 40) could introduce some amplification bias. Despite the abovementioned findings proving how nuclei well mirror the whole cell expression profile, nuclear and cytoplasmic transcriptomes are likely to differ in many ways, requiring therefore a more comprehensive analysis to determine the advantages and limitations of using nuclei for transcriptomic studies.

The considerable cellular heterogeneity of brain tissue poses another significant limitation, because typically various subpopulations of neurons are intermingled with different types of glia and other non-neuronal cells. Even within neuronal cells, NeuN does not capture the entire spectrum of subpopulations constitutive of the brain as several neuronal subtypes (e.g., cerebellar Purkinje cells and Golgi cells, olfactory Mitral cells, retinal photoreceptors, and gamma motor neurons) do not express NeuN (Mullen et al., 1992).

One possible solution would be to grow cell-type specific cultures, but most CNS cells, including neurons, are *ex vivo* sustainable for only a few weeks at best and thus they would provide an incomplete model for epigenetic mechanisms potentially operating across the full lifespan (Matevossian and Akbarian, 2008). The lack of validated antibodies specific to distinct neural cell subtypes which specifically target the nucleus and are also suitable for flow cytometry applications prevent us from furthering our understanding of the role played by

each subpopulation and their regulatory makeup particularly in the context of disease.

An additional weakness of this approach is that the cell-type specific markers used for FANS might capture heterogeneous cell populations as proven by preliminary data generated within my group using snRNA-seq (Policicchio S. et al, 2021). **Figure 4.23** reports an example of snRNA-Seq data obtained for total nuclei, Neuronal-enriched, and oligodendrocyte-enriched nuclei from human adult prefrontal cortex. The t-distributed stochastic neighbour embedding (t-SNE) plot in **Figure 4.23A** shows clustering of the total nuclei population based on similarity of individual "events" for the top ten expressed genes using the Seurat analysis pipeline (Stuart et al., 2019). Cells in total nuclei population that express NeuN (*RBFOX3*) (**Figure 4.23B**), are also identified as 'neuronal' using the expression other known neuronal markers. Similarly, cells in the total nuclei population expressing the oligodendrocyte marker *SOX10* (**Figure 4.23C**) are the same population identified as 'glial' using the expression of other known glial markers. Although in **Figure 4.23D**, the t-SNE plots show heterogeneity within the neuronal enriched (NeuN+ve/Sox10+ve) FANS-sorted population, cells whithin this population do not express the oligodendrocyte marker Sox10 (**Figure 4.23E**) suggesting that the heterogeneity observed in the NeuN+ve/Sox10+ve fraction is more likely to reflect the presence of multiple neuronal cell subtypes. Similarly, the t-SNE plot showing the cell clustering for the oligodendrocytes enriched (NeuN-ve/Sox10+ve) population (**Figure 4.23G**) (as determined by antibody staining and FACS sorting) confirms expression of Sox10 (**Figure 4.23H**) while contamination of NeuN expressing cells appears to be minimal (**Figure 4.23I**).
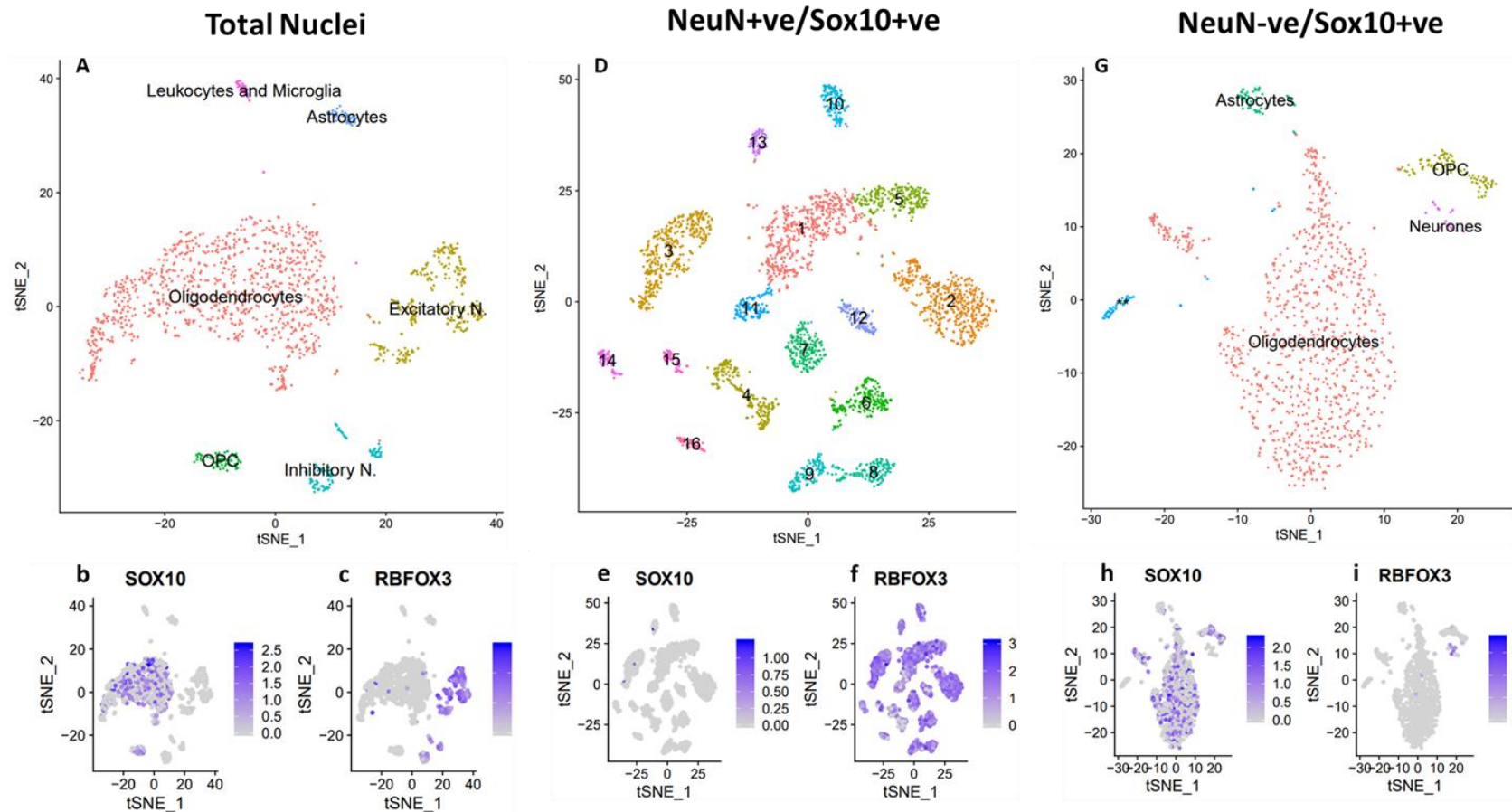
Figure 4.23 snRNA-Seq of total nuclei, neurons enriched, and oligodendrocytes enriched nuclei populations from FANS sorted human adult pre-frontal cortex.

A) T-distributed stochastic neighbour embedding (t-SNE) plot showing clustering of the total nuclei population based on similarity of individual "events" for the top ten expressed genes.Clusters are created using the Suerat analysis pipeline which groups the most closely related cells based on the PCA output. The colours are arbitrarily assigned to the clusters. Sox10 (b) and NeuN (c) are equally represented within the unsorted nuclei sample. D) t-SNE plot reveals heterogeneity of cell types (observed as distinct clusters of differentially coloured cells) constituting the NeuN+ve/Sox10+ve (neuronal enriched) FANS-sorted nuclei population. However, the expression of NeuN (f) is visibly higher than the expression levels for Sox10 (f) suggesting that the heterogeneity observed in the NeuN+ve/Sox10+ve fraction is more likely to reflect the presence of multiple neuronal cell subtypes. G) T-SNE plot showing how the NeuN-ve/Sox10+ve FANS-sorted nuclei population cosists of oligodendrocytes predominantly which find support in the expression levels detected for Sox10 (h) within this fraction Figure taken from (Policicchio S. et al, 2021).

Lastly, neurons, microglia, oligodendrocytes and astrocytes do not completely encapsulate all the major cell types in the brain. Additional cell types and cell states should be explored, potentially by incorporating combinations of multiple nuclear markers. These could include endothelial cells and pericytes of the blood brain barrier, which is compromised during degeneration (Nation et al., 2019, Sweeney et al., 2019); as well as the distinction between excitatory and inhibitory neuronal subtypes, only partially explored in the human brain (Kozlenkov et al., 2017). Cell states of interest could include homeostatic microglia and disease-associated macrophages, which have been identified as associated with amyloid plaques in AD (Keren-Shaul et al., 2017, Mathys et al., 2017, Mathys et al., 2019). Future testing of additional nuclear markers will allow to further discern cell-type populations and cell states associated with disease. Currently there remains a lack of usable antibodies for nuclear astrocytic markers. However, LIM/Homeobox 2 (*LHX2*) has been shown to be highly expressed in astrocytes and moderately expressed in neurons (Subramanian et al., 2011, Morel et al., 2017). Thus, astrocyte nuclei could be isolated using a combinatorial flow cytometry gating strategy of NeuN-negative and LHX2-positive nuclei (Nott et al., 2021).

One of the most fundamental questions asked in flow cytometry experiments is whether a subset of immunofluorescently stained cells is positive or negative, or what proportion of cells are positive or negative for a given marker. Answering this question accurately requires careful instrument setup and use of controls. Despite being the most widely used staining control, isotype controlswere not adopted for testing the validity of the staining procedure of this FANS method. Whether the more commonly used, but less rigorously selected, isotype controls are sufficient to determine non-specific binding has been under debate for over two decades (Keeney et al., 1998, O'Gorman and Thomas, 1999). The ideal isotype control should "match" the specific antibody not only in heavy chain (IgA, IgG, IgD, IgE, or IgM), subclass and light chain (kappa, lambda) class but also in fluorochrome type and number of fluorochrome molecules per immunoglobulin (F/P ratio). It should also have been derived by the same manufacturing process as the specific conjugate under investigation (Hulspas et al., 2009b). The variability of isotype controls regarding background binding can be also attributed to the isotype not exactly matching the tested antibody concentration. Even when each single antibody and matching isotype control is titrated, it is still necessary

302

to define the cytometer parameters in a two-colour setting (Trummer et al., 2008); this demands correct compensation of the two fluorescence channels which again requires distinct positive controls. In a panel with several surface markers this can be very laborious and costly (Trummer et al., 2008). The potentially different non-specific binding characteristics of an isotype antibody, the possible pitfalls in the interpretation of the data (Hulspas et al., 2009b) and the notion that it is virtually impossible to manufacture the perfectly matched isotype antibody, have lead to the reconsideration of earlier recommendations (Landay and Muirhead, 1989, McCoy et al., 1990).

Over the last decade or so, it has become more widely accepted that isotype controls are of little value in distinguishing positive from negative (Maecker and Trotter, 2006, Baumgarth and Roederer, 2000, Makinodan et al., 2012) and should therefore not be used to set positive gating regions for test antibodies (Hulspas et al., 2009b). Isotype controls are of limited use in determining the threshold of positivity/level of background fluorescence since isotype controls are by nature different reagents than the staining antibody, with a different amino acid composition in the variable region, different numbers of fluorochromes bound to the antibody and different concentrations, and, thus, have different "unspecific" binding properties. Therefore, a negative staining with the isotype control does not infer that the staining one observes with the experimental antibody is specific (Cossarizza et al., 2019). Furthermore, it has been suggested that not in all circumstances gating controls are actually needed. Certainly, some gates can be drawn unambiguously, without reference to any control sample (Maecker and Trotter, 2006). For example, any marker that has clearly bimodal expression, with no overlap of positive and negative populations, does not require a control for accurate determination of positive and negative populations. Gating controls become important when there is no clear division between positive and negative populations. Controls needs to be run for every marker in an experiment, but only for those markers where determination of a positive/negative boundary is otherwise ambiguous (Maecker and Trotter, 2006). Lastly, isotype control antibodies are optimally developed for cell surface staining protocols where they help assess the level of background staining inherent in cell-antibody binding assays. Many times the isotype control does not perform as expected in an intracellular staining experiment, with either extremely low or high levels of non-specific fluorescence (Koester and Bolton, 2000).

In order to circumvent all the above mentioned limitations intrinsic to the use of Isotype controls and since a clear division between positive and negative populations was consistently observed across all processed samples, the accuracy of the gating strategy was independently validated post-sorting with gene expression data obtained from the aliquots collected.

Furthermore, ongoing work is aiming to perform snRNA-seq on FANS purified nuclei using the 10X Chromium in order to confirm the immunolabelling-based enrichment of the nuclei populations. Preliminary data gathered within our group have shown that these 'purified' nuclei populations are actually a heterogeneous mix of different neural cell types and a large range of smaller cell populations can be identified alongside the ones selectively enriched (data not published). For instance, within the neuronal-enriched population, there are distinct sub-populations of neuronal cells which could represent neuronal precursors, excitatory, and inhibitory neurons. FANS sorting helps excluding these various other cell types by enriching for the selected cell types of interest. The considerable heterogeneity identified within each purified sub-fraction has important implications for the interpretation of genomic work undertaken on human post-mortem brain tissue.

One of the most apparent caveats of this method is the limited number of samples included in this pilot study which undoubtedly has limited the ability of exploring the inter-individual variability. For the same reason, focusing on pre-frontal cortex tissue only has allowed to disentangle the divergence across cell types specific to this area of the brain which is likely to differ when shifting the focus on a different brain region. The heterogeneity of source (two different brain collections) for the specimens used alongside the fact that samples were not matched in age and sex inevitably represent factors potentially confounding the results the extent of which cannot be ruled out without new studies replicating this approach on a wider, more homogeneous cohort.

4.6.8 Future directions

The rapid development of scRNA-seq promises to reveal new insights into the transitions that establish neuronal identity during development, differentiation, activity, and disease. Comparing single neuron data to reference atlases constructed from hundreds of thousands of single-cell transcriptomes will be

critical to understanding these transitions and the molecular mechanisms that drive them (Johnson and Walsh, 2017).

In the next few years, innovative approaches that can provide single-cell transcriptomic or highly multiplexed gene expression information in situ will be transformative. They will circumvent the need for tissue dissociation allowing the profiling of individual cells in accurate proportions while preserving spatial information (Crosetto et al., 2015, Ke et al., 2013). For instance, highly multiplexed single molecule fluorescence ISH (Chen et al., 2015, Lubeck et al., 2014) or in situ RNA sequencing (Ke et al., 2013, Lee et al., 2014) have been used to assess the expression of up to several thousands of genes while preserving spatial information. Another approach could be to exploit nanopore-based sequencing devices to directly sequence DNA or RNA molecules from a tissue section (Crosetto et al., 2015) theoretically preserving cellular resolution while providing a high-throughput single-cell molecular characterization. Together, these advances will move us closer to the goal of providing a complete catalogue of cell types in the nervous system.

The measurement of gene expression in single cells will revolutionize our understanding of gene regulation and resolve many longstanding debates in biology. Since cells tend to cluster by cell type or developmental state when grouped according to their expression profiles (Fishell and Heintz, 2013, Holmberg and Perlmann, 2012, Deneris and Hobert, 2014), expression-based clustering allows for the unbiased reconstruction of cell types in any population or tissue after sequencing enough individual cells. If the sampling of cells is extensive and sufficiently free from biases, such clustering can reveal all cell types present, including new ones. All cells in a cluster can also be used to derive robust cell-type expression profiles, again in a data-driven manner and without previous knowledge of which marker genes define a tissue or cell type. Single-cell profiling of RNAs is therefore a promising method that could lay a foundation for a quantitative, data-driven classification of cell types.

4.7 Conclusions

In this chapter I describe the optimisation of a protocol to enable the successful separation of three distinct neural groups that yields sufficient material for methylomic and transcriptomic profiling.

Although NeuN immunolabelling followed by FACS separation is a well establish method in literature (Iwamoto et al., 2011, Jiang et al., 2008, Matevossian and Akbarian, 2008, Lister et al., 2013), onlyin more recent time, advancement in research has enabled the identification of a robust nuclei marker specific to oligodendrocytes (Lutz et al., 2017b, Kozlenkov et al., 2018) and to microglia (van der Poel et al., 2019, Romani et al., 1988) allowing therefore to better discriminate among neural cell types and further characterise them. Leveraging upon existing data, I have expanded FANS applications further and better characterized the NeuN-negative subpopulation of nuclei. I have tested and optimised candidate nuclear antibodies for fluorescence-assisted nuclear sorting to successfully isolate neurons (NeuN+ve/Sox10+ve) oligodendrocytes (NeuN-ve/Sox10+ve) and microglia (NeuN-ve/Sox10-ve/Irf8+ve) from adult post mortem human brain. Despite the positive staining for the oligodendrocyte marker Sox10, the neuronal enrichment of the NeuN+ve/Sox10+ve fraction has been confirmed by PCR and single nuclei gene expression data.This protocol can be utilised to define gene regulatory elements of neurons, oligodendrocytes and microglia from adult human cortical tissue. This protocol will be informative to investigators interested in rare cell types that may be missed through analysis of bulk tissue. The ability to isolate nuclei of microglial origin is a major advance, as it enables interrogation of until recently overlooked non-neuronal component of brain-related disorders. Thus, the investigation of nuclei from specific cell types will provide an invaluable tool for researchers in the field of brain disorders.

The implemented protocol described here is particularly useful for studies focused on epigenetic changes of DNA methylation profile at the level of individual cell type and, more broadly, on the molecular phenotype of the nucleus in each cell type. Although calibrated on control samples, the same approach can be equally adopted to investigate the brain at various stages: normal development as well as aging, in neurological or psychiatric disease. The method is advantageous when the cellular heterogeneity of brain tissue, including potential shifts in neuron-to-glia ratio during the course of aging or due to disease, are a concern (Siegmund et al., 2007, Matevossian and Akbarian, 2008). Cell-

type-specific profiling may be critical for the discovery of disease-relevant epigenomic alterations. Insight into the mechanisms governing epigenetic regulation in the brain is necessary for a more complete understanding of complex behaviours and psychopathology, which will lead to novel therapeutic and diagnostic approaches in the future. Particularly, applying this method to clinical brain samples will enable to gain insight into the complexity of the brain and the role of genomic variation in individual neural cell types in neuropsychiatric and neurodegenerative disease making an important contribution to the field of psychiatric genomics. Further work is now needed to profile cell type specific DNA methylation in larger post-mortem brain datasets of a disease phenotype and to integrate other omics assays (DNA hydroxymethylation, chromatin accessibility, and RNA-seq) for a multi-level analysis across the three cell types (neurons, oligodendrocytes, microglia). Finally, further testing should be performed to identify novel nuclear antibodies targeting different neural subtypes and to expand the array of validated markers to implement in FANS applications to undertake multi-level omics profiling on as many cell types as possible in parallel.

Chapter 5 – Cell type-specific methylomic signature in the human prefrontal cortex

5.1 Introduction

In the last decade, a substantial body of evidence has surfaced, suggesting that several neurodevelopmental, neurodegenerative and neuropsychiatric disorders are in part caused by aberrant epigenetic modifications (see **Chapter 3**, (Urdinguio et al., 2009, Peter and Akbarian, 2011, Jakovcevski and Akbarian, 2012). Therefore, a thorough characterization of the epigenetic status of the brain is critical for understanding the molecular basis of its function in health and disease.

DNA methylation is a stable mostly repressive epigenetic modification that is extremely important both for the establishment of cell-type–specific identities in the nervous system (Takizawa et al., 2001) and in mediating environmentally induced changes in the adult brain (Kozlenkov et al., 2017). It is known to be a critical component of various processes and conditions including memory formation, stress responses, depression and drug addiction (Feng et al., 2010, LaPlant et al., 2010, Labonte et al., 2012a, Suderman et al., 2012). Despite its importance, the DNA methylation profile of the brain, especially in humans (owing to the obvious experimental difficulties), has not been sufficiently explored, and, for multiple decades when examined, was studied mostly using bulk (cellular heterogeneous) brain tissues (Varley et al., 2013, Numata et al., 2012, Davies et al., 2012, Zhang et al., 2010, Xin et al., 2011). Also refer to **Chapter 3** for an example. These studies have revealed that DNA methylation significantly varies between different brain regions as well as between white and grey matter of the same region (Ladd-Acosta et al., 2007, Davies et al., 2012, Gibbs et al., 2010, Ghosh et al., 2010).The brain, however, is characterized by multifaceted complexity, including heterogeneity of cell types, such as neurons and glia, as well as subpopulations within these cell types. **Figure 5.1** which provides a schematic representation of the main/most abundant cell types of the human brain is far from being comprehensive of the all cellular subtypes characterized to date. These cell types are differentially distributed among brain regions that themselves are heterogeneous in cytoarchitecture, connectivity and function. Hence, to achieve meaningful insight into the epigenetic landscape of the brain, the epigenetic marks should be studied within individual cell types that are captured from specific brain regions.
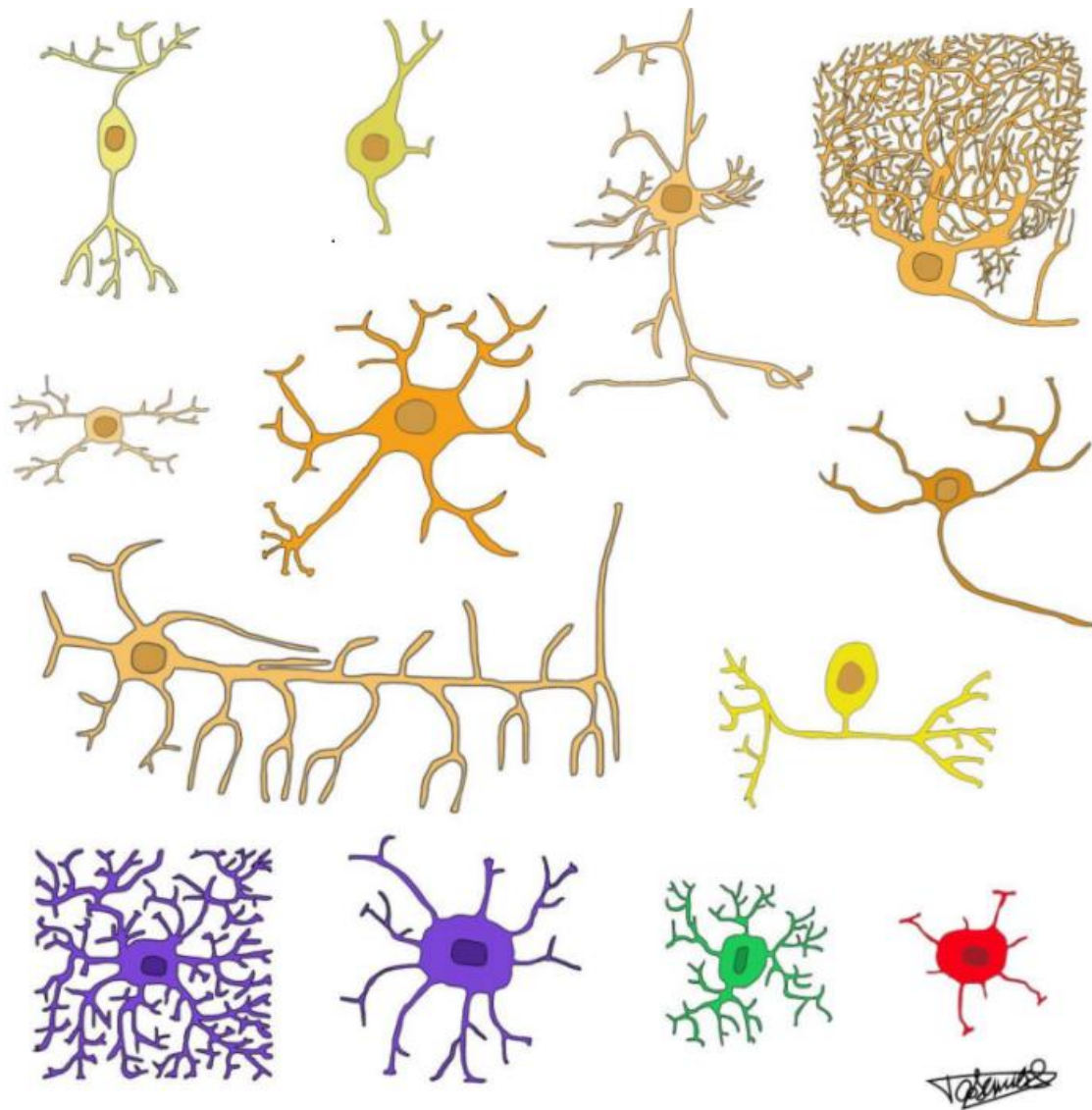
Figure 5.1 Schematic representation of the variety of neural cell types in the human brain.
Morphological neuronal cell types are more numerous than morphological glial cell types. Non- exhaustive representations of neuronal cell types in shade of yellow-orange (top three rows) and glial cells (bottom row) in purple, green and red. First row, left to right: bipolar cell, short axon cell, pyramidal cell, Purkinje cell. Second row, left to right: amacrine (anaxonic) cell, multipolar/motor cell, granule cell. Third row, left to right: basket cell, unipolar cell. Bottom row, left to right: protoplasmic astrocyte, like those found in grey matter; fibrous astrocyte, like those found in white matter; microglia; oligodendrocyte. Figure taken from (Herculano-Houzel and Dos Santos, 2018).

Recent reports have indeed demonstrated robust differences in DNA methylation and histone modification patterns between neuronal and non-neuronal cells in human and rodent brains (Iwamoto et al., 2011, Guintivano et al., 2013, Lister et al., 2013, Kozlenkov et al., 2014) suggesting that the previously reported epigenetic variation among brain regions could be largely owing to differences in neuron to glia ratios (Guintivano et al., 2013). These cell type-specific epigenetic

landscapes might ultimately determine the selective vulnerability to neurodevelopmental or environmental insults highlighting the need for more detailed studies on discrete cellular populations from post-mortem tissue. The essential role of frontal cortex in behaviour and cognition requires the coordinated interaction, via electrical and chemical signalling, of multiple neuronal cell types and a diverse population of glial cells (Lister et al., 2013). Individual brain cells have unique roles within circuits that are defined by their location and pattern of connections as well as by their molecular identity. Recent findings of the ENCODE and REMC projects revealed exquisite cell -type specificity of noncoding regulatory elements in neuronal and non-neuronal cells (Zhu et al., 2013, Consortium, 2012). Thus, a major challenge for genomic research is to characterize cell-type epigenetic signatures that mark these functional regions, especially in tissues containing heterogeneous cell populations. This task is particularly daunting in the case of the brain, where various cell types are differentially distributed among anatomically and functionally diverse brain regions and the fact that the brain is an inaccessible organ.

To date, the large majority of cell type-specific epigenome mappings in human brain are focused on comparisons between the neuronal and non-neuronal populations (Kozlenkov et al., 2014, Kozlenkov et al., 2016, Kundakovic et al., 2017, Price et al., 2019, Tansey and Hill, 2018) in the cortex predominantly. Very little is known about the epigenetic landscape of glial cells (e.g. astrocytes, oligodendrocytes, microglia), mostly due to the lack of effective methods for their isolation.

Glial cells have generally been overshadowed by research on neurons in many brain related phenotypes, but there is a growing body of evidence that highlights the importance of glia in brain development, function and disease processes (Valles et al., 2019, Allen and Barres, 2009, Barros et al., 2018, Stogsdill and Eroglu, 2017). Oligodendrocytes constitute the large majority of glial cells in the human cortical grey matter (Pelvig et al., 2008) producing the myelin sheath that insulates neuronal axons, increasing axonal conduction velocity and neural processing speed (Simons and Nave, 2015). Myelination predominantly occurs postnatally and extends into adulthood. Recently alterations in transcriptional and protein levels of oligodendrocytes and their precursors have been implicated in AD, MDD and SCZ (Nasrabady et al., 2018, Vostrikov and Uranova, 2018, Bernstein et al., 2019, Cai and Xiao, 2016). An explosion of findings driven by

new powerful technologies has expanded our understanding of microglia and the roles that these cells play in the neuropathology of a diverse array of disorders. Microglia activation has been noted in all types of psychiatric disorder (Mondelli et al., 2017, Hammond et al., 2018, Prinz et al., 2019) although the cause of the neuroinflammation in these diagnostic categories and its implications are still unclear. The contribution of microglia to CNS diseases may relate to their function as professional phagocytes of the CNS which is vital for development of the CNS and maintenance of brain homeostasis (Prinz et al., 2019). Increased microglial activation was reported in post-mortem brain samples from people with depression who died by suicide (Torres-Platas et al., 2014). Neuroinflammation is suggested to be linked to suicide (Pandey et al., 2012, Pandey et al., 2018) and microglia are regarded to play crucial roles in neuroinflammation via releasing inflammatory mediators (Suzuki et al., 2019). Microglial abnormalities might play a role in the etiology and pathophysiology of SCZ (Inta et al., 2017, Notter and Meyer, 2017). A prevalent hypothesis is that the functional disruption of these brain-resident immune cells may alter the normal course of brain development and maturation, (Coughlin et al., 2016) for example, by means of interfering with synaptic pruning (Hannestad et al., 2012). Moreover, it has been postulated that aberrant activation of microglia in SCZ may influence the clinical course of the disease and affect the severity of symptoms in patients (Liu et al., 2017). Very recently, differential expression levels were found in astrocyte and microglia genes in the PFC sub-regions in relation to SCZ and suicide, indicating possible disturbances of glia homeostasis in these brain conditions (Zhang et al., 2020).

Since the epigenome is highly variable across different cell-types, correlations between the phenotype of interest and the cell-type composition lead to a large number of false discoveries (Jaffe and Irizarry, 2014, Houseman et al., 2012). Several bioinformatics approaches have been developed to assess the effects of cell mixture on the measurement of DNA methylation (Houseman et al., 2012, Houseman et al., 2014, Guintivano et al., 2013, Newman et al., 2015, Rahmani et al., 2016). However, there is an ongoing dispute concerning their effectiveness (Rahmani et al., 2017, Zheng et al., 2017).

A comparison of cell sorting and bulk tissue-based screens elsewhere has revealed that cell-type purification efficiently reduces confounding noise generated by variable cell composition and enhances the detection of disease-

related changes (Gasparoni et al., 2018). By allowing assignment of identified signals to cell-type origin, cell sorting revealed that next to neurons also non neuronal cells experience strong epigenetic alterations (Gasparoni et al., 2018). In the attempt to address this challenge, in the present study I focused on characterising DNA methylation in three major brain cells (NeuN-expressing neurons, oligodendrocyte and other glial cells) which were obtained from a discrete area of the human PFC and separated by FANS.

5.2   Aims

The main objective of this chapter was to profile epigenetic changes (differences in DNA methylation levels primarily) at the resolution of individual cellular types to a) further the understanding of epigenetic regulation in heterogeneous tissues like the brain b) to verify the reproducibility and applicability of the method optimised in **Chapter 4** of this thesis in order to generate high quality data suitable for epigenomic profiling.

5.3 Materials and Methods

5.3.1 Subjects and samples

For BS Illumina EPIC profiling PFC brain samples from 12 healthy individuals archived in the Brains for Dementia Research (BDR) collection were used. These samples have been utilised in a recent EWAS study from my group as pilot training data for the development of a refined cell composition algorithm (paper in preparation). All samples were dissected by trained specialists, snap-frozen and stored at -80°C. Further information about all samples is provided in **Table 5.1**. Nuclei were extracted from ~500mg of post-mortem brain tissue following the FANS pipeline outlined in detail in section 5.3.2. Genomic DNA was isolated from each collected nuclei fraction using an adapted phenol-chloroform extraction method and tested for degradation and purity prior to analysis as described in section 5.3.3. Nuclear RNA was also extracted from each sorted sample using the Direct-zol RNA micro-prep kit as described in **Methods**, section 2.5.

Sample	Patient ID	Centre	Post-mortem diagnosis	Age at death	Sex	PMI (h)	Experiment	Included in final analysis
1	930	Bristol	Control	94	F	29.5	FANS for DNA methylation profiling	Yes
2	945	Bristol	Control	80	M	50	FANS for DNA methylation profiling	Yes
3	948	Bristol	Control	82	F	36	FANS for DNA methylation profiling	Yes
4	957	Bristol	Control	86	M	44.25	FANS for DNA methylation profiling	Yes
5	977	Bristol	Control	91	F	40.75	FANS for DNA methylation profiling	Yes
6	996	Bristol	Control	95	F	59.25	FANS for DNA methylation profiling; Targeted Gene Expression	Yes
7	1030	Bristol	Control	72	M	16.25	FANS for DNA methylation profiling	Yes
8	A237/16-1	KCL	Control	80	M	58	FANS for DNA methylation profiling	Yes
9	A272/15-1	KCL	Control	90	F	10	FANS for DNA methylation profiling	No (DN missing)
10	A291/17-1	KCL	Control	90	F	22	FANS for DNA methylation profiling	Yes
11	A115/16-1	KCL	Control	80	F	28.5	FANS for DNA methylation profiling	No (DN missing)
12	A111/12-1	KCL	Control	70	M	20	FANS for DNA methylation profiling	Yes
13	A277/12-1	KCL	Control	79	M	20	FANS for DNA methylation profiling	Yes
14	SD031/08	Edinburgh	Control	55	M	31	FANS for DNA methylation profiling	Yes
15	AN02646-1	Harvard	Control	52	M	19.55	FANS for DNA methylation profiling	No (AB not working)
16	AN17142-1	Harvard	Control	83	F	18.5	FANS for DNA methylation profiling	No (AB not working)
Sample1	AN05203-1	Harvard	Control	76	M	18.25	Targeted Gene Expression	No (low RNA yield)
Sample2	AN10547-1	Harvard	Control	88	M	16.32	Targeted Gene Expression	No (Poor quality RNA)
Sample3	1030	Bristol	Control	72	M	16.25	Targeted Gene Expression	No (low RNA yield)
Sample4	874	Bristol	Control	78	M	56	Targeted Gene Expression	yes
Sample5	A160/11-1	KCL	Control	89	F	53	Targeted Gene Expression	No (poor quality RNA)

Table 5.1 Phenotypic information across all samples processed for this study.
Samples where the double negative (DN) nuclei population could not be detected were excluded from the analysis as well as those samples where the Sox10 antibody (AB) did not work. DN, double negative (i.e NeuN-ve/Sox10-ve) nuclei population; AB, antibody; KCL, King's College London; FANS, Fluorescence-activated nuclei sorting.

5.3.2 Separation of neuronal and glia nuclei

Human post-mortem prefrontal cortex neuronal, oligodendrocyte and other glial origin nuclei were separated by fluorescence-assisted sorting of immunolabeled samples using a NeuN- (*RBFOX3*-) specific antibody and SOX10-specific antibody following the optimised FANS protocol profusely described in **Chapter 4**. Each brain specimen yielded four nuclei populations: 1) a double positive population (NeuN+ve/Sox10+ve) presumably enriched in NeuN-expressing neuronal nuclei 2) a single positive population (NeuN-ve/Sox10+ve) enriched in oligodendrocytic nuclei 3) a double negative population (NeuN−ve/Sox10-ve) and 4) a population of unsorted nuclei (total nuclei) serving as proxy for the bulk tissue. Since the double negative fraction is likely to consist of astrocytes and microglia predominantly, as well as a small population of endothelial cells, the decision to conveniently label this third population as 'other glia'-derived nuclei was made. Nuclei suspensions were assessed for the presence of debris by adjusting appropriately the gating strategy before proceeding with nuclei capture. Purity of nuclear fractions was > 98% as checked by repeating FACS on the separated populations. The 100µM nozzle was used and the event rate during data acquisition and sample collection was kept ≤ 3000 events/sec. On average, for each sorted population, 200,000 nuclei were collected for extraction of genomic DNA and 300,000 for nuclear RNA extraction.

5.3.3 Genomic DNA extraction from sorted nuclei fractions

DNA extraction was performed using an ethanol-isopropanol extraction protocol adapted for nuclei samples (for more details see **Methods**, section 2.4). Each DNA pellet was resuspended in 15 µL of RNAse, DNase-free water and left at 4ºC overnight to fully dissolve before quantification.

5.3.4 Infinium 850k bead chip methylomic profiling

500ng of genomic DNA from each nuclei fraction was treated with sodium BS using the Zymo EZ-96 DNA Methylation-Gold TM Kit (Cambridge Bioscience, UK) according to the manufacturer's standard protocol, as described in **Methods**, section 2.9. To assess DNA methylation signatures of over 850,000 CpG sites,

Illumina HumanMethylationEPIC BeadChip (EPIC 850K array) (Illumina, CA, USA) was used according to the manufacturer's instructions, with minor amendments and quantified using an Illumina HiScan System (Illumina, CA, USA). Individuals were randomised across plates and sorted nuclei fractions (N=4) from the same individual were randomised within the chip (random loading position). Illumina Genome Studio software was used to extract the raw signal intensities of each probe (without background correction or normalisation).

5.3.5   DNAm data preprocessing and quality control

All computations and statistical analyses were performed using R 3.5.2 (R Development Core Team 2018) and Bioconductor 3.5 (Gentleman et al., 2004). Signal intensities were imported as a methylumi object into R using the methylumi package (Wang et al., 2018b).

Raw signal intensity data were processed from idat files through a standard pipeline using the *Bigmelon* (Gorrie-Stone et al., 2019) and *Watermelon* (Pidsley et al., 2013) packages in R. A number of quality control steps were performed on these data prior to normalization. First, outlier samples were identified using principal component analysis, second, successful bisulphite conversion was confirmed using control probes, third the ages of the samples were estimated using the Horvath Epigenetic Clock algorithm (Horvath, 2013) and compared to reported age at sampling. Fourth, unaccounted variation was assessed through visualisation of principal components. The *pfilter* function was used to remove samples that were either dramatically altered as a result of normalisation or samples where >1% of sites had a detection p-value > 0.05. DNA methylation sites were also filtered to exclude those with a bead count < 3 or > 1% of samples with detection p-value > 0.05 as previously described (Mansell et al., 2019). Two samples and 18,279 sites were removed at this stage of the analysis. These data were then normalized using the dasen method previously described (Pidsley et al., 2013) which performs background adjustment and between-sample quantile normalization of methylated (M) and unmethylated (U) intensities separately for Type I and Type II probes. Prior to data analysis, SNP probes, probes with non-specific binding, probes affected by common (minor allele frequency (MAF) > 5%) SNPs (McCartney et al., 2016), and 65 probes annotated

to the Y chromosome were additionally removed. The final dataset contained 46 samples (12 individuals, three nuclei fractions + total per individual) and 848,122 DNAm sites.

5.3.6 Data analysis

All probes which passed the QC, were used to perform exploratory analyses in order to investigate whether any of the DNA methylation differences detected were driven by or associated to a particular cell type rather than shared across cell populations.

5.3.6.1   ANOVA Analysis of variance

In order to detect cell type differences at individual positions (DMPs) an analysis of variance (ANOVA) was performed as appropriate, and statistical significance was defined as $P< 0.05$. Anova examines the effect of one or more categorical independent variables, known as 'factors', (i.e. DNA methylation), on a dependent variable, (i.e. cell type). The total fraction (proxy for bulk tissue) was excluded from comparisons. Cell type specific P-values and F statistics were extracted and Student's t-test was performed by comparing each individual fraction to the two remaining fractions combined. Due to the high number of nominally significant ($P<0.05$) DMPs ($N= 550,733$), results were further filtered by applying a more stringent cut-off ($P=9E-08$, experiment-wide significance threshold for EPIC array DNA methylation studies (Mansell et al., 2019). Only the DMPs passing this cut-off were considered for subsequent analysis. The direction of change in DNA methylation at individual sites was also explored in each cell type separately by running a Sign test on the significant (P<9E-08) DMPs and investigating whether an enrichment of hypo- or hypo-methylated DMPs could be detected in any of the three nuclei fractions assessed.

5.3.6.2   MiAge

The MiAge Calculator is designed to estimate mitotic age of any tissue types using DNA methylation data from a panel of 268 selected "mitotic clock" CpGs by exploiting the stochastic replication errors accumulated in the epigenetic

inheritance process during cell divisions. Although the MiAge Calculator was built using the 450K data, it can be readily applied to methylation measures from the MethylationEPIC array as 241 sites out of the 268 selected mitotic clock CpGs are also on the EPIC array (Youn and Wang, 2018).Originally developed for cancer applications, the MiAge Calculator, it is readily applicable to aging studies using DNA methylation measures (Youn and Wang, 2018). Here the tool was used to calculate mitotic ages of the input samples to assess whether accelerated mitotic age was detectable in any specific cell type. Welch Two Sample t-test was also performed to test for correlation between mitotic age and gender.

5.3.6.3   Cell-type specific region calling using Comb-P

Results for every probe were converted into a BED file (containing genomic locations and t-test cell-type specific P-values) and run through the comb-p (Pedersen et al., 2012) pipeline to group ≥ 3 spatially correlated CpGs with a seed of P = 9x10-8 and distance parameter set to 500 bp. Briefly, comb-p generates DMRs by (1) calculating the autocorrelation between probes to adjust the input DMP P-values using the Stouffer–Liptak–Kechris correction, (2) running a peak finding algorithm over these adjusted P values to identify enriched regions around a seed signal, (3) calculating the region P value using the Stouffer– Liptak correction, and (4) correcting for multiple testing with the one-step Šidák correction. Significant regions were identified as those with at least three probes and a corrected P value < 0.05. Moreover, for each cell type, results were filtered by statistical significance (P= 9E-08) as well as UCSC gene name (only annotated probes were considered) in order to characterise the DNA methylation status at genomic regions within genes specific to each cell type of interest.

5.3.6.4   Pathway analysis

Pathway analysis of cell-type-specific methylation sites (ct-DMPs) reaching the EPIC array significance threshold (P< 9.0E-08) (Mansell et al., 2019) was performed using the *missmethyl 1.10.0* package from Bioconductor (Phipson et al., 2016). This P value threshold was used to limit the number of associated genes included, in an attempt to prevent the inclusion of false positive pathways.

Pathways were included if they met the following criteria: (1) the number of genes in the gene list was greater than one and less than 2000, (2) more than one gene from the analysis was present in the pathway and (3) the *P* value for the association was smaller than 9.0E-08. Furthermore, for each cell type, the list of significant GO terms (*P-value* cut off = 9E-08) was submitted to the web server Revigo (http://revigo.irb.hr/) developed in 2011 (Supek et al., 2011) which summarises long, unintelligible lists of GO terms by finding a representative subset of relevant terms using a simple clustering algorithm that relies on semantic similarity measures. The tool has been developed to remove redundant GO terms and assist in the interpretation of enriched gene functional categories defined by the GO (Supek et al., 2011).

5.3.6.5   *Enrichment analysis of regulatory regions in ct-DMPs and ct-DMRs distribution across genomic features*

To investigate whether ct-DMPs were enriched at specific gene features, a two-sided Fisher's exact 2×2 test was used to test for enrichment of significant differentially methylated loci ($P < 9E-08$) compared to all nominally significant DMPs ($P < 0.05$) at any particular gene feature as described by Zhou et al (Zhou et al., 2017). As this is exploratory work all DMPs with $P < 0.05$ were considered to ensure all biological differences could be captured. Statistical significance with respect to concrete genomic region was determined by two-sided Fisher's tests (significance level $p < 0.05$), and ORs were used as a measure of the association with respect to a particular feature. For statistical purposes, since background included all the probes interrogated by the EPIC array, appropriate adjustments were used in each of the comparisons. Furthermore, the genomic features distribution was also investigated in relation to ct-DMRs using the *Chipseeker* package which annotates the location of each given DMR in terms of genomic features. Genomic region positions were assigned using the R/Bioconductor packages   TxDb.Hsapiens.UCSC.hg19.knownGene   (version   3.2.2)   and ChIPseeker version 1.12.1 (Yu et al., 2015a).

5.4 Results

Nuclei immunolabelling followed by FACS separation was performed to obtain neuronal (NeuN+ve/Sox10+ve, referred to as neurons), oligodendrocytic (NeuN-ve/Sox10+ve, referred to as oligodendrocytes) and double negative nuclei (NeuN-ve/Sox10-ve, referred to as other glia) from 12 human post-mortem pre-frontal cortex samples. From this, 48 epigenome-wide cell-type specific profiles were generated on the Illumina EPIC 850k methylation array platform (for general work flow, processing and quality checks see "Methods" section and **Figure 5.2**).

Data quality control (QC)
- Intensity of M & U
- Fully methylated control
- Bisulfite conversion
- Samples from same person are genetically identical (using 59 SNP probes on EPIC array)
- Sex prediction from X & Y chromosome
- Correlation with SNP chip data
- Compare with predicted cell type (internal algorithm based on PCA)
- Site level filtering
- Dasen normalisation

ct-DMPs Detection
- One-way Anova
- student t-test

Regional Analysis
- Comb-P

Pathway Analysis
- GO term enrichment analysis

Enrichment Genomic Feature
- Fisher's exact test

Figure 5.2 Schematic flow chart summarising the analysis pipeline applied to the DNA methylation data generate in this chapter.

5.4.1 Samples quality control

A series of quality control (QC) metrics have been calculated for all samples and the most relevant were reported below. Exclusion thresholds were applied as per QC pipeline to identify poorly performing samples. For some QC metrics the provided technical and biological variables were used to identify any patterns or reasons behind sample failures.

Previous experience has shown that intensity level indicates sample quality and likelihood of passing the QC process. This is summarised for each sample by calculating the median of the methylated signal intensity and unmethylated signal intensity (**Figure 5.3**). Samples with really low intensity values (< 1500) are usually dropped at this stage. In this study two samples only showed relatively low intensities: KCL11_DN (M.median, 988; U.median, 1070) and BRI7_N (M.median, 2094; U.median, 1403). Both samples were kept at this stage to further assess their performance on different QC metrics.
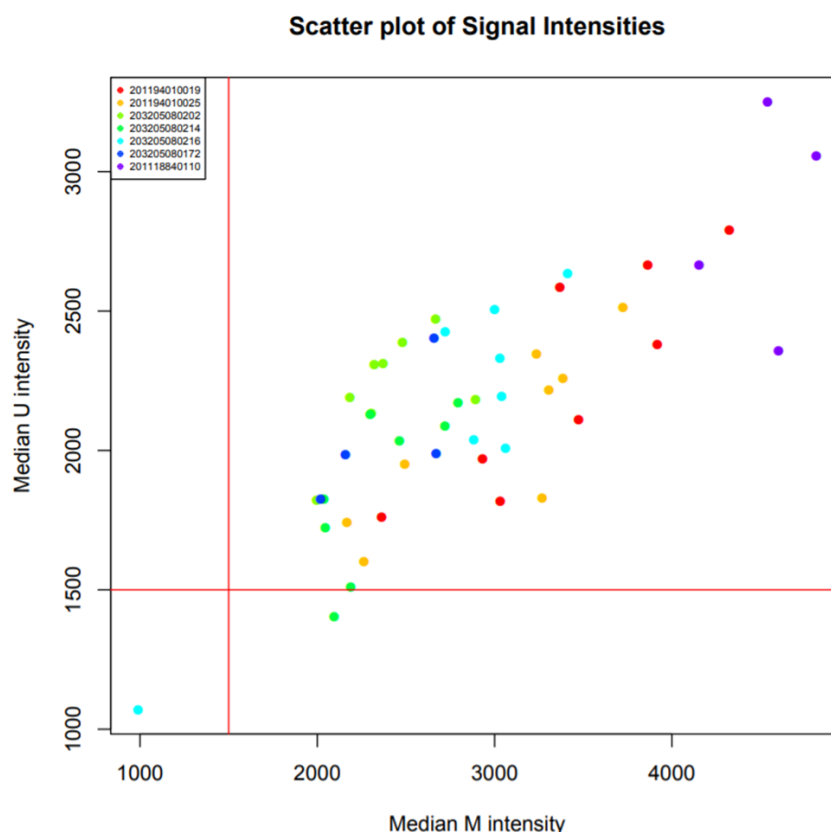
Figure 5.3 Methylated (M) and Unmethylated (U) intensities.
The intensity check is the best indicator of sample quality. The median methylated signal intensity and unmethylated signal intensity for each sample was calculated according to the QC pipeline. Two samples failed this step (M.median < 1500 | U.median < 1500) but they were kept until the end of the QC pipeline to check overall performance.

For each sample a bisulfite conversion statistic was calculated using the control probes present on the array as the median value across 100% fully methylated control probes. A threshold of 80% was applied excluding samples below this cut off. In this dataset one sample fell below this metrics (**Figure 5.4**) with a score of 60%: KCL11_DN.

Histogram of Bisulphite Converstion Statistics
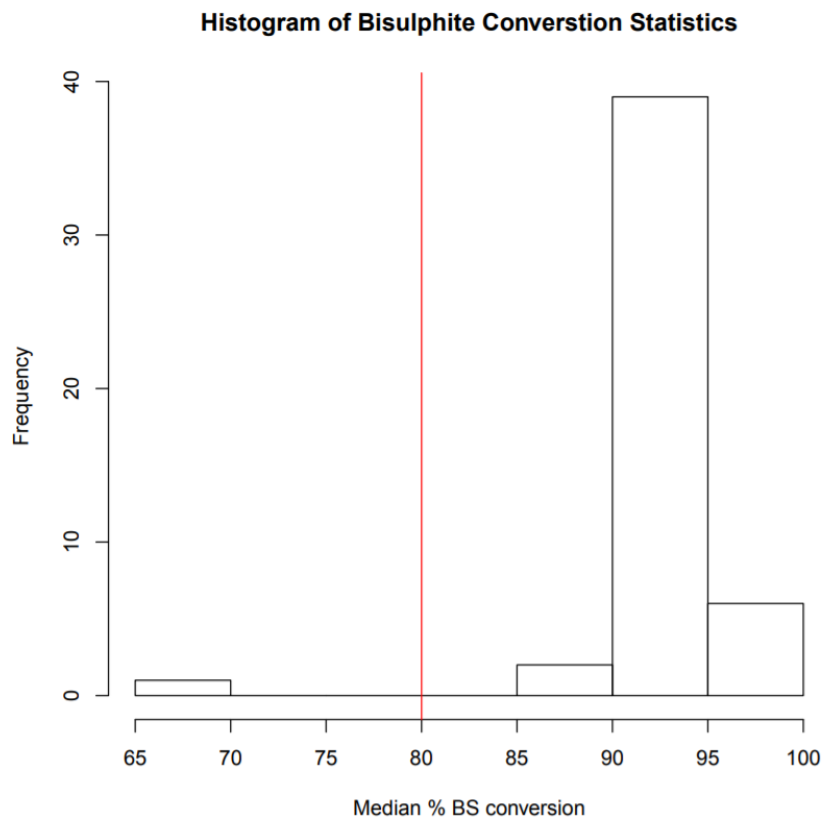
Figure 5.4 Bisulfite conversion rate.
Bisulphite conversion statistic for each sample was calculated, and a histogram of the results plotted. This shows the conversion statistics were generally high except for one sample. Samples with a conversion < 80% fail the QC and are removed at a later stage.

Detection *P*-values provides a measure of the accuracy of the DNA methylation detected at a given probe for a specific sample net of the background noise. Probe-level filtering was conducted after exclusion of poor performing samples. For each sample, the number of sites where the signal was not detectable above the background was calculated. Samples with a high percentage of these sites were excluded. In this dataset, one sample was recommended for removal (KCL11_DN) and therefore excluded from subsequent analyses.

The goal of normalisation was to convert data for each sample into a common distribution and minimise effects of technical variation. Outlier samples usually

need a high level of manipulation to be transformed and make them look more similar to the rest of the samples. To identify samples that were dramatically altered as a result of normalization the difference between the normalized and raw data was quantified at each probe for each sample calculating the root mean square. Furthermore, density plots of the beta values were plotted for each sample before and after normalisation separately for type I and type II probes (**Figure 5.5**).
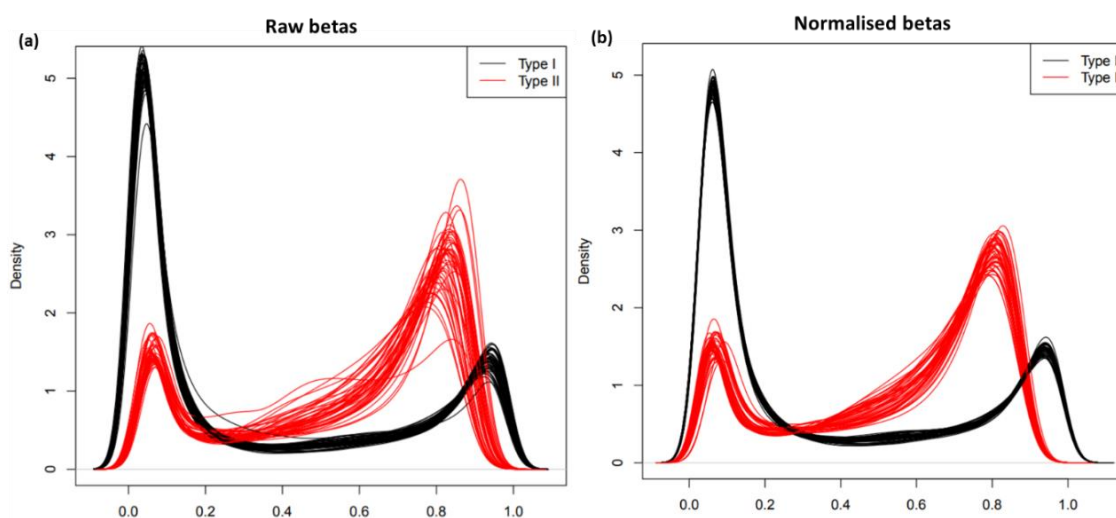
Figure 5.5 Density plots showing the β values distribution across samples.
Shown are the β values distribution before (a) and after (b) quality control and normalisation steps for type I probes (black) and type II probes (red).

Figure 5.6 reports the correlation between chronological age and predicted cortical DNA methylation age calculated separately for each FANS sorted cell type using a published algorithm (Shireby et al., 2020) while **Figure 5.7** and **Figure 5.8** shows respectively cell type specific and sex driven differences in mitotic age acceleration across sorted nuclei populations. Lastly, neuronal proportion was estimated for each FANS sorted brain samples by applying and comparing the output of two publicly available tools like the CETS algorithm and the Horvath DNA Methylation Age Calculator tool (see Methods for details)**.** Interestingly, neurons account for 25% or more of the cells in the double negative (NeuN-ve/Sox10-ve) fraction classified as "other glia" supporting the idea that neuronal subtypes are likely to be missed by the NeuN staining (see **Figure 5.9**).
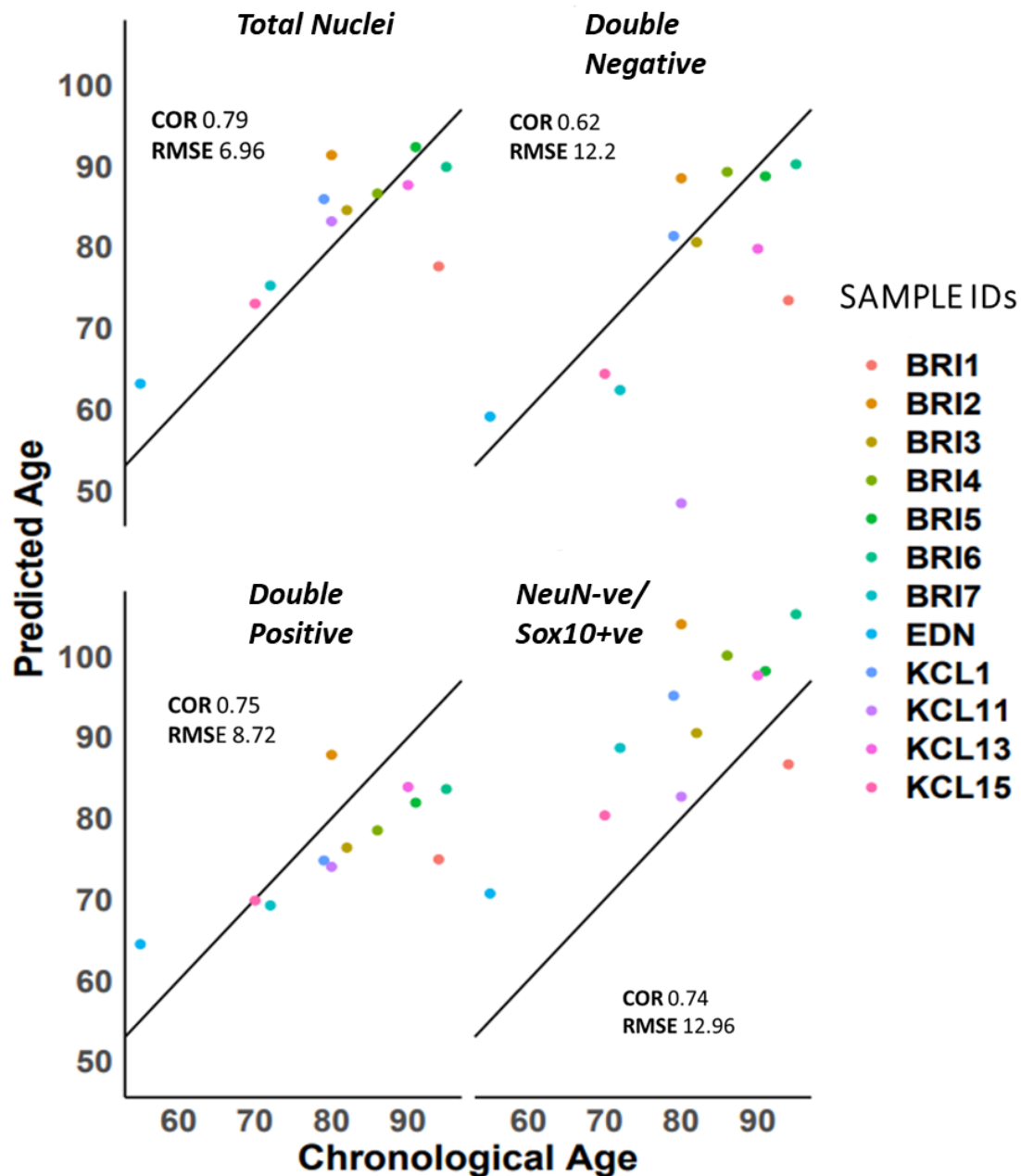
Figure 5.6 Correlation between chronological age and predicted Cortical DNAm Age.
Shown is the correlation between chronological age (x-axis) and predicted age (y-axis) calculated separately for each FANS sorted cell type for all 12 samples using the Cortical Clock from (Shireby et al., 2020). Interestingly, the total fraction (Total Nuclei) which mimics the bulk tissue and upon which the clock has been trained, distributes along the y=x line showing the highest correlation. Neuronal nuclei (NeuN+ve/Sox10+ve) display younger DNAm age while oligodendrocytes (NeuN-ve/Sox10-ve) slightly older DNAm Age compared to the chronological one. The other glial cells (NeuN-ve/Sox10-ve) shows the most deviant correlation.

325
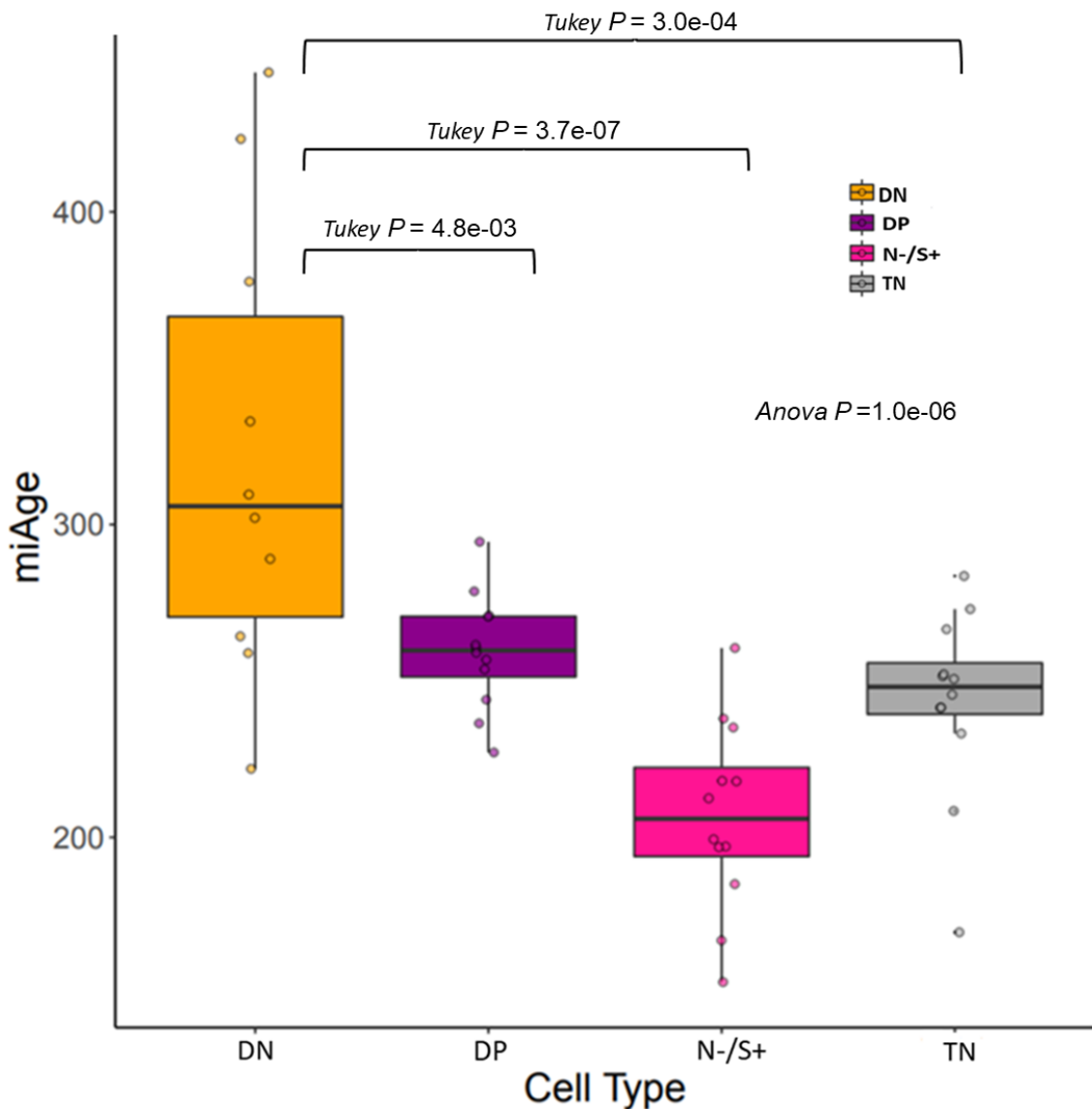
Figure 5.7 Mitotic age calculated for each nuclei fraction across all samples using miAge.

An Anova was run to compare all four groups against each other at once followed by a Tukey HSD post-hoc test which corrects for multiple comparisons. The Anova P value represents the level of significance that at least one of the group means is significantly different from the other. Mean differences between the groups compared were all suggesting significance (Tukey P<0.05) with the other glia-enriched nuclei population (NeuN-ve/Sox10-ve, orange) showing the greatest acceleration in the number of cell divisions among the four groups compared (Mean difference DN vs N-/S+= 115.7, Tukey P = 3.7e-07).Darkmagenta, Neuronal-enriched population; darkpink, oligodendrocytes-enriched population, orange, glial-enriched population; dark-grey,Total (unsorted) nuclei. DN, Double Negative (NeuN-ve/Sox10-ve); Double Positive (NeuN+ve/Sox10+ve); N-/S+ (NeuN-ve/Sox10+ve); TN (Total Nuclei).

326
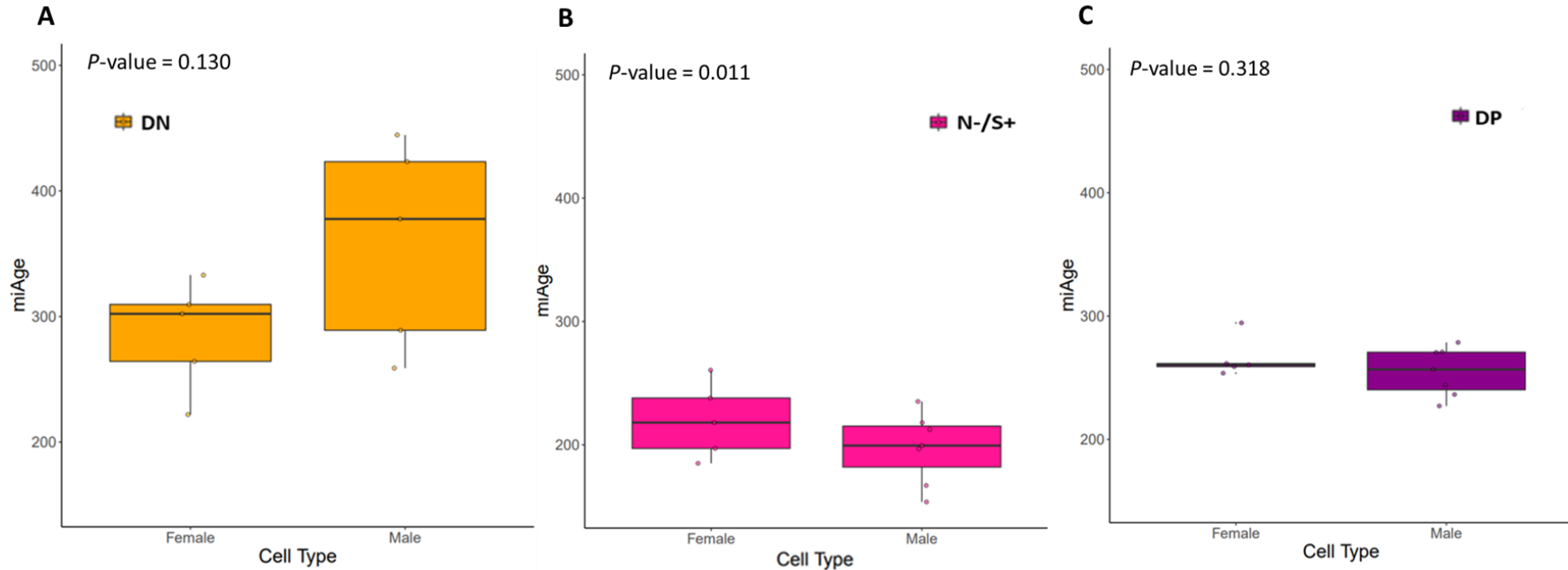
Figure 5.8 Sex differences in mitotic age acceleration across cell types.
(A) The other glia-enriched nuclei population (DN; NeuN-ve/Sox10-ve) showed the largest means difference in cell division rate between female and male (Mean F= 286.2, Mean M=358.7), however t-test P value was not significant (P>0.05) to support the hypothesis of true differences.This is likely to be due to the really large variance characterising the M group (B) The oligodendrocyte-enriched population (N-/S+; NeuN-ve/Sox10+ve) showed a less pronounced mean difference between sex (Mean F=184.8, Mean M=199.1) but significant (P<0.05). (C) The neuronal-enriched population (DP; Neun+ve/Sox10+ve) showed an even smaller mean difference between groups (Mean F= 265.8, Mean M=254.9) as well as non significant P value (P>0.05).
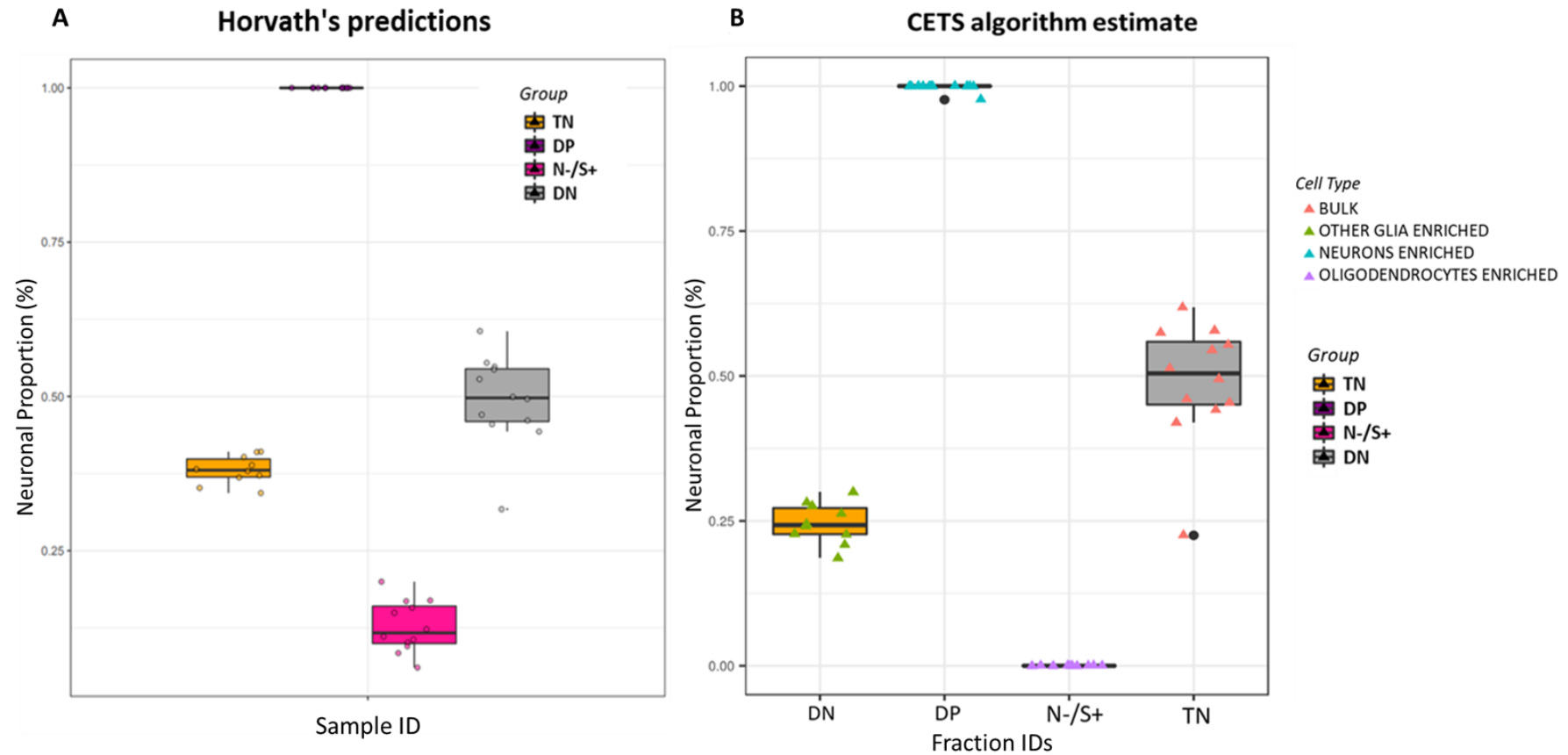
Figure 5.9 Neuronal proportion estimate in FANS sorted brain samples.
A) Boxplot showing the neuronal proportion contained in each of the four nuclei fractions (DP, NeuN+ve/Sox10+ve, neurons enriched fraction; N-/S+, NeuN-ve/Sox10+ve (oligodendrocyte enriched fraction); DN, NeuN-ve/Sox10-ve (other glia-enriched fraction); TN, Total (pool of unsorted nuclei). Proportion of neurons per fraction was estimated using Horvath DNA Methylation Age Calculator tool. B) Neuronal proportion estimate in FANS sorted brain samples using CETS algorithm. Boxplots are a standardized way of displaying the distribution of data based on a five number summary: minimum, maximum, median, first quartile, and third quartile. Each box extends from the first quartile to the third quartile (IQR). A line goes through the box at the median (mid-point of the data and is shown by the line that divides the box into two parts). The whisker lines go from each quartile to the minimum (1st quartile – 1.5 x IQR) or maximum (3rd quartile + 1.5 x IQR).

Taken together these data confirm a successful and clear separation of neuronal derived nuclei and oligodendrocyte derived nuclei from other glial origin nuclei in post-mortem frozen brain tissue.

5.4.2 FANS –purified nuclei fractions differ in DNA methylation profiles

The microarray data confirmed the strong enrichment of the nuclei fractions for specific cell type (neurons, oligodendrocytes and other glial cells) in agreement with the gene expression assays (qPCR and sn-RNAseq).

To systematically define cell-type-specific methylation sites (ct-DMPs), neurons, oligodendrocytes and other glia nuclei populations were compared by performing a one-sided Anova analysis followed by t-test and filtering for methylation differences significant at P value < 9E-08. For the NeuN+ve/Sox10+ve fraction, were identified 145,936 significant ct-DMPs (approx. 17% of all sites and 50% of ANOVA significant sites) distributed across 18,693 genes many of which known to be differentially expressed in neurons compared to oligodendrocytes and other glia cells such as *SYNPO* (Mundel et al., 1997, Gasparoni et al., 2018) (cg16264911, p=1.30E-30), *FOXP1* (Tamura et al., 2003, Gasparoni et al., 2018, Bacon et al., 2015) (cg03040208, p=9.42E-22) and *GRIN2B* (Hu et al., 2016a, Bell et al., 2018) (cg16862319, p=1.08E-31).

For the NeuN-ve/Sox10+ve fraction, in total 83,354 significant ct-DMPs (approx. 9% of all sites and 31% of ANOVA significant sites) distributed across 14,423 genes were identified. Many of these genes are known to be differentially expressed in oligodendrocytes or OPCs compared to neurons or other glia cells such as *PLP1* (Bozzola et al., 1991, Hamdan et al., 2015) (cg24974356, p= 1.10E-20), *MOG* (Ramanathan et al., 2016, Peschl et al., 2017) (cg00151089, p= 5.73E-24) and *OPALIN* (Aruga et al., 2007, Yoshikawa et al., 2008) (cg03285073, p= 3.26E-21).

For the NeuN-ve/Sox10-ve fraction, 42,559 ct-DMPs (approx. 5% of all sites and 16% of ANOVA significant sites) were found to be significant and distributed across 10,680 genes many of which are known to be differentially expressed in astrocyte (e.g. *SLC4A4* (Del-Aguila et al., 2019) (cg23726831, p= 1.72E-12); *NDRG2* (Li et al., 2020b, Flugge et al., 2014) (cg23288563, p= 3.47E-11); *ALDH1L1* (cg21532590, p= 1.30E-12) (Chen et al., 2016, O'Leary et al., 2020) or

microglia (e.g. CD74 (Thrupp et al., 2020, Peferoen et al., 2015), (cg01601628, 7.14E-15); *C1QB* (Walker et al., 1995), (cg04097715, p=4.88E-15); *CX3CR1* (Galatro et al., 2017, Gyoneva et al., 2019) (cg03296370, p=1.65E-15), compared to oligodendrocyte and/or neuronal cells.

When examining the methylation status of significant (P<9E-08) ct-DMPs across the three cell types a slightly larger proportion of DMPs were found to be hypomethylated in oligodendrocytes (53,6% hypomethylated, 46,4% hypermethylated, *P*<2.2E-16) while an higher proportion of DMPs was hyopermethylated in other glial cells (45,5% hypomethylated, 55,5% hypermethylated, *P*<2.6E-16). No significant differences were found for the neurons-specific DMPs (50,2% hypomethylated, 49,8% hypermethylated, *P*=0.15) (**Figure 5.10**). As showed by the Sign Test *P*-values reported, the difference in percentage between hypo- and hyper-methylated DMPs for both oligodendrocytes and other glial cells were statistically significant.

Interestingly, each isolated nuclei population revealed a distinct DNA methylation profile when compared with one another as well as relative to the total fraction (proxy of bulk tissue) as shown in **Figure 5.11**. These prominent differences that are completely masked in the bulk tissue prove the relevance of cell sorting to uncover within-tissue divergency of epigenetic signal.

Furthermore, when plotting individual differentially methylated sites, a consistent pattern of methylation became apparent: oligodendrocytes and other glial cells showed similar methylation levels (hypermethylation) while neurons were consistently hypomethylated at the same CpG sites relative to oligodendrocytes and glial cells. Worthy of note, the total fraction (unsorted nuclei) persistently exhibited 40 to 60% methylation levels for the same probes lending support to the hypothesis that changes captured in the bulk tissue could be influenced by fluctuations in cell composition in particular of the neuronal fraction. **Figure 5.12** displays an example of this, by reporting the DNA methylation levels across the four fractions for 10 of the top ranked probes
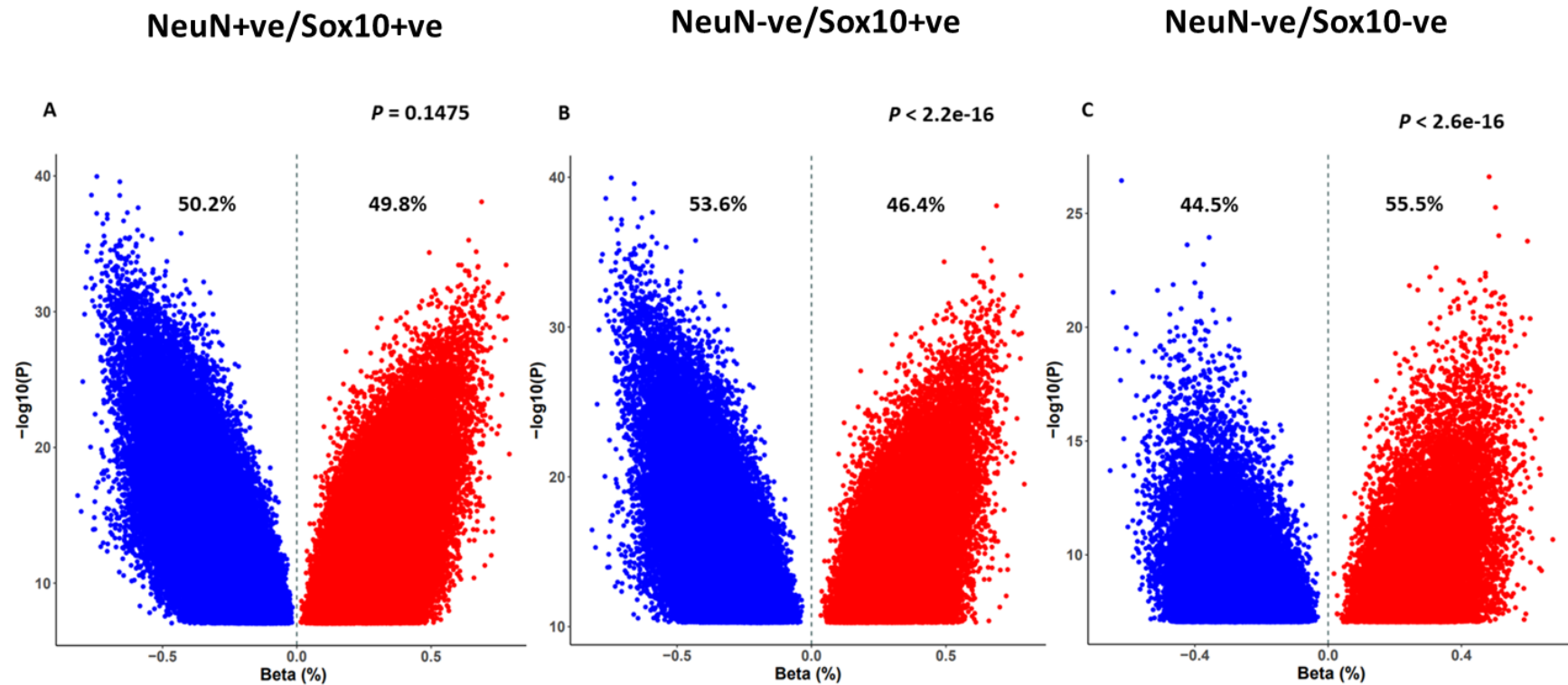
Figure 5.10 Volcano plots showing the methylation status of the most significant ct-DMPs across the three cell types profiled. *The reference group for the X-axis is the difference between the plotted cell type and the remaining two cell types combined.* **A)** *No significant difference in proportion was detected between hyper/hypo-methylated DMPs in neuronal enriched population (i.e.NeuN+ve/Sox10-ve) (50.2% vs 49.8%) meanwhile* **(B)** *the oligodendrocyte enriched population (i.e.NeuN+ve/Sox10-ve) showed a modest enrichment in hypomethylated DMPs (53.6%).* **(C)** *The nuclei population enriched in other glia (NeuN-ve/Sox10-ve) reported an enrichment of hypermethylated DMPs (55.5%). On the X-axis, Beta % is the DNA methylation difference (%). Blue (hypomethylated), red (hypermethylated).*
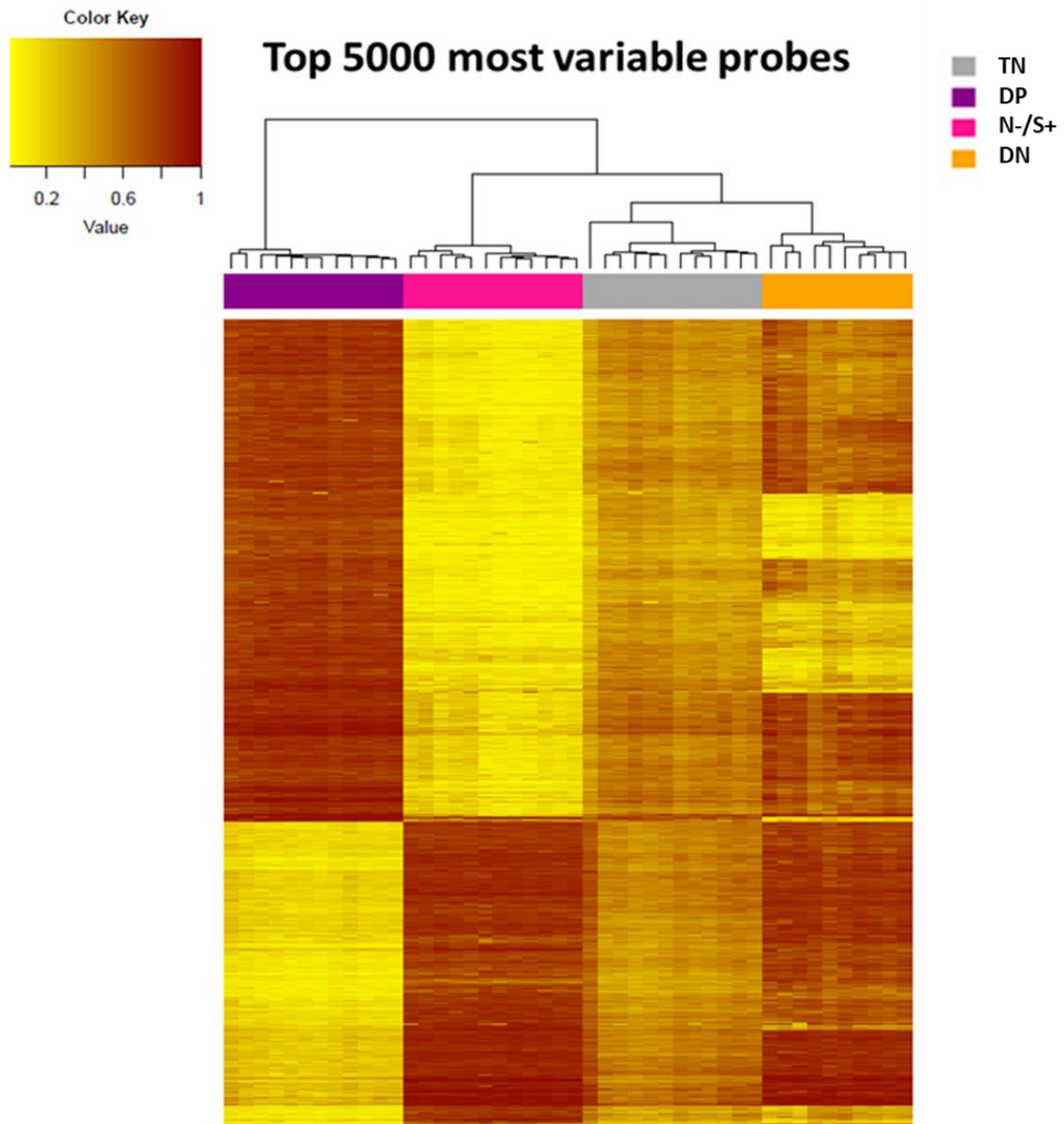
Figure 5.11 Hierarchical clustering of the 5000 most variably methylated probes across all samples.
Heatmap showing significant differentially methylated sites (DMPs) discriminating between nuclei fractions. DNA methylation was measured in the three separate neural nuclei fractions along with total nuclei using the Illumina EPIC array. T-statistics were calculated for each fraction compared to the remaining fractions combined to identify differentially methylated positions (DMPs) that are unique to each nuclei fraction. Standard deviation (sigma) at each site was calculated and plotted as measurement of variability. Each individual fraction showed a distinct pattern of methylation across the same 5000 most variable DMPs. Darkmagenta, DP (Neuronal-enriched population); deeppink, N-/S+ (oligodendrocytes-enriched population), orange, DN (glial-enriched population); dark-grey, TN (unsorted nuclei). DP, double positive; N+/S+, NeuN+ve/Sox10-ve; DN, double negative; TN, total nuclei.

Figure 5.12 Top 10 most variable DMPs across cell types.
Boxplots showing the DNA methylation levels (%) at different CpG sites which ranked among the most variable positions after the one-way ANOVA analysis. Interestingly, a consistent pattern in the distribution of the nuclei fractions can be identified along the methylation scale: the neuronal enriched (2, dark magenta) fraction is consistently hypomethylated compare to the oligodendrocyte (3, deep pink) and other glia enriched (4, orange) nuclei fractions which show higher DNA methylation levels (≥ 80%). DP (NeuN+ve/Sox10+ve), Neuronal-enriched nuclei; S-/N+ (NeuN-ve/Sox10+ve), oligodendrocyte enriched nuclei; DN, NeuN-ve/Sox10-ve, glial enriched fraction; TN, total nuclei. Boxplots are a standardized way of displaying the distribution of data. Each box extends from the first quartile to the third quartile (IQR). A line goes through the box at the median (mid-point of the data and is shown by the line that divides the box into two parts). The whisker lines go from each quartile to the minimum (1st quartile – 1.5 x IQR) or maximum (3rd quartile + 1.5 x IQR).

333

5.4.2.1   *Neuronal-specific DMPs across purified nuclei populations*

In order to further investigate the enrichment of the sorted nuclei fractions, DMPs located within or in proximity of known marker genes specific for different neural cell types were examined to compare DNA methylation levels across fractions. **Figure 5.13** shows the DNA methylation profile for eight representative neuronal marker genes recovered from the literature: *UCHL1, GRIN2B, RBFOX3, VSNL1, STMN2, GAD1, SCG2 and RTN1* (Del-Aguila et al., 2019, Grubman et al., 2019, Velmeshev et al., 2019). Interestingly, in genes which are highly expressed in neurons, the associated CpGs showed substantial loss of DNA methylation in the neuronal-enriched fraction compared to the other nuclei populations.
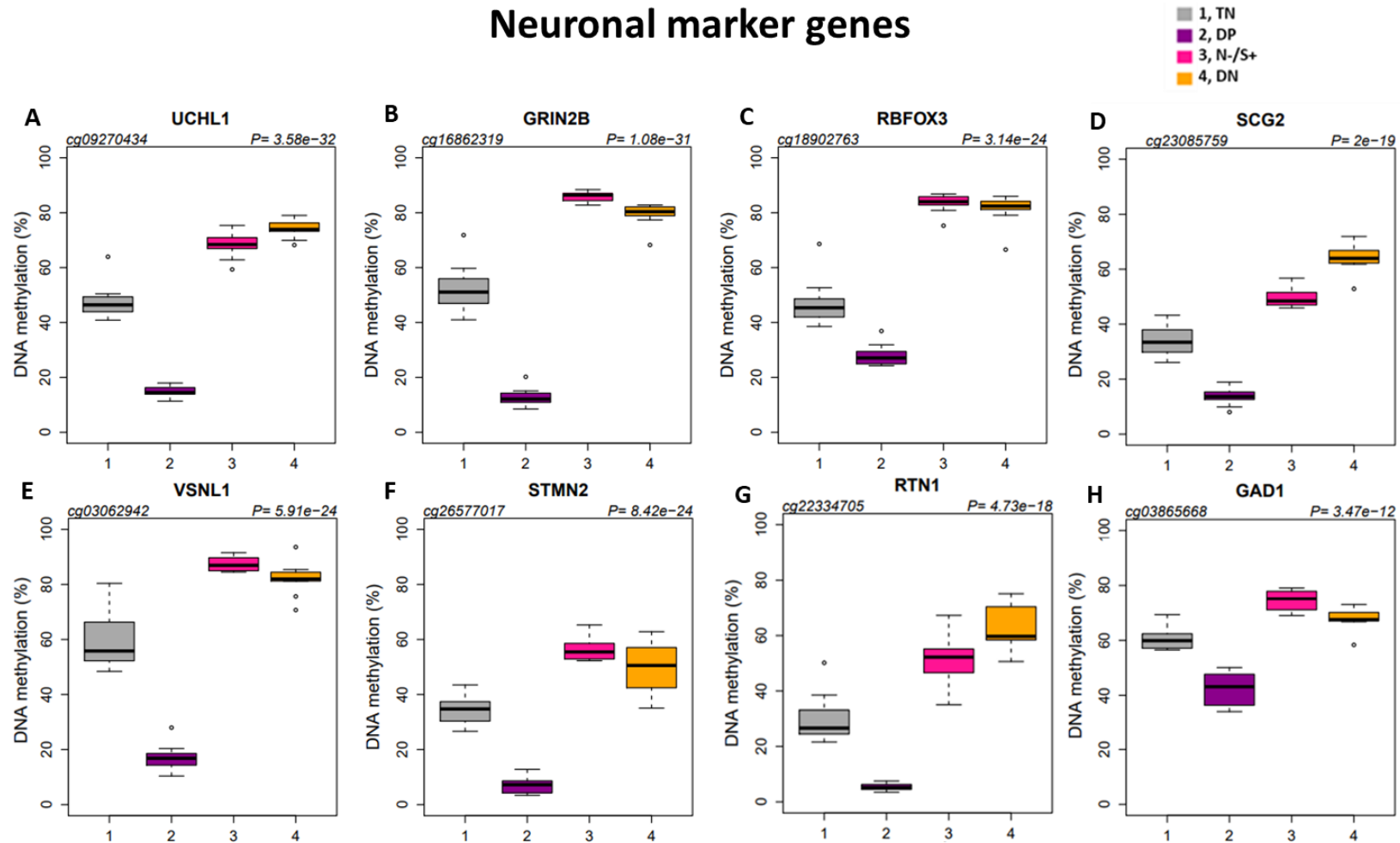
Figure 5.13 Neuronal-specific differentially methylated positions (DMPs).
Boxplots showing representative examples of CpG sites within known neuronal marker genes differentially methylated (t-test P< 9E-08) across nuclei fractions.The neuronal enriched (DP, NeuN+ve/Sox10+ve) population reveals a distinct DNA methylation pattern being significantly hypomethylated when compared to the other three fractions. To be noted, the total fraction which is a mixture of all nuclei, neuronal included, sits consistently in the middle of the distribution. Boxplots are a standardized way of displaying the distribution of data. Each box extends from the first quartile to the third quartile (IQR). A line goes through the box at the median (mid-point of the data and is shown by the line that divides the box into two parts). The whisker lines go from each quartile to the minimum (1st quartile – 1.5 x IQR) or maximum (3rd quartile + 1.5 x IQR). S-/N+ (NeuN-ve/Sox10+ve), oligodendrocyte enriched nuclei; DN, NeuN-ve/Sox10-ve, glial enriched fraction; TN, total nuclei.

5.4.2.2 *Oligodendrocyte-specific DMPs across purified nuclei populations*

Similarly, three gene signatures of oligodendrocyte precursor cells such as *TNR* (Czopka et al., 2009, Pesheva et al., 1997), *PTGDS* (Sakry et al., 2015) *and PDGFRA* (Dang et al., 2019) together with eight marker genes for mature oligodendrocytes *(TMEM144* (McKenzie et al., 2018), *OLIG1* (Dietz et al., 2016)*,* PLP1 (Werner et al., 2007), *UGT8* (Yang et al., 2019, Aston et al., 2005), *TF* (Aberg et al., 2006), *CNP* (Othman et al., 2011), *SCD* (Arion et al., 2006) *and PIP4K2A* (Noch et al., 2020)),were examined to assess the DNA methylation status at DMPs located in these marker genes. These CpGs showed a strong loss of DNA methylation in the Sox10+ve population except for the *TMEM144* oligodendrocyte marker which was found to be hypermethylated in the Sox10+ve nuclei compared to other glial cells and neuronal cells (see **Figure 5.14** and **Figure 5.15 for** details).
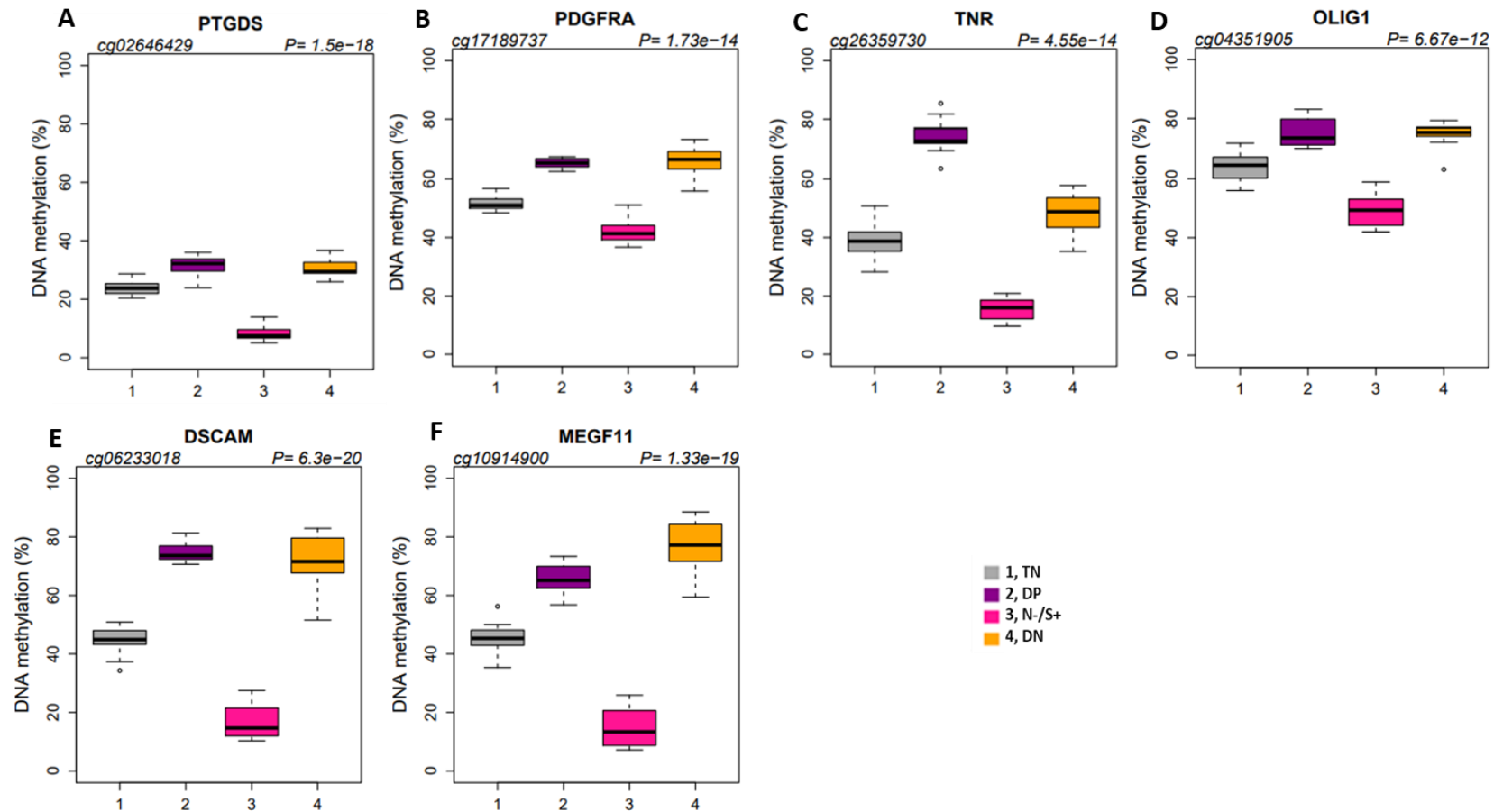
Figure 5.14 OPC-specific differentially methylated positions (DMPs).
Boxplots showing representative examples of CpG sites whithin known OPC marker genes differentially methylated (t-test P<9E-08) across nuclei fractions.The oligodendrocyte enriched (N-/S+, NeuN-ve/Sox10+ve) population reveals a distinct DNA methylation pattern being consistently hypomethiyated when compared to the other three fractions. To be noted, the total fraction which is a mixture of all nuclei, oligodendrocytic included, sits consistently in the middle of the distribution. Boxplots are a standardized way of displaying the distribution of data. Each box extends from the first quartile to the third quartile (IQR). A line goes through the box at the median (mid-point of the data and is shown by the line that divides the box into two parts). The whisker lines go from each quartile to the minimum (1st quartile – 1.5 x IQR) or maximum (3rd quartile + 1.5 x IQR). DP (NeuN+ve/Sox10+ve), Neuronal-enriched nuclei; DN,NeuN-ve/Sox10-ve, glial enriched fraction; TN, total nuclei.

Figure 5.15 Oligodendrocyte-specific differentially methylated positions (DMPs).
Boxplots showing representative examples of CpG sites whithin known marker genes of mature oligodendrocytes which are differentially methylated (t-test P<9E-08) across nuclei fractions.The oligodendrocyte enriched (N-/S+, NeuN-ve/Sox10+ve) population reveals a distinct DNA methylation pattern being hypomethylated (A-G) or hypermethylated (H) when compared to the other three fractions. To be noted, the total fraction which is a mixture of all nuclei, oligodendrocytic included, sits consistently in the middle of the distribution. Boxplots are a standardized way of displaying the distribution of data. Each box extends from the first quartile to the third quartile (IQR). A line goes through the box at the median (mid-point of the data and is shown by the line that divides the box into two parts). The whisker lines go from each quartile to the minimum (1st quartile – 1.5 x IQR) or maximum (3rd quartile + 1.5 x IQR). DP (NeuN+ve/Sox10+ve), Neuronal-enriched nuclei; DN,NeuN-ve/Sox10-ve, glial enriched fraction; TN, total nuclei.

5.4.2.3   *Other glial-specific DMPs across purified nuclei populations*

With a similar intent, the ANOVA results were screened to determine the DNA methylation status at CpGs located in markers of cell identity within the double negative nuclei fractions. Specifically, microglia marker genes such as *C1QB* (Byrnes et al., 2006), *C1QA* (Hartmann et al., 2019), *CSF1R* (Konno et al., 2018), *TMEM119* (Satoh et al., 2016), *MRC1* (Lecca et al., 2018), *SALL1* (Li et al., 2018), *MEF2C* (Deczkowska et al., 2017, Holtman et al., 2017) and *IRF8* (Masuda et al., 2012) and well documented astrocyte-specific genes (e.g. *CPE* (Klein and Fricker, 1993), *GPR37L1* (Nguyen et al., 2020, Liu et al., 2019b), *ALDH1L1* (Chen et al., 2016), *PAX6* (Sakurai and Osumi, 2008), and *GFAP* (Hol and Pekny, 2015)) were found to be significantly differentially methylated when compared to the remaining cell types suggesting the distinct identity of this population. CpGs at these genes showed a strong loss of DNA methylation in the double negative fraction for the majority of the genes assessed (see **Figure 5.15** and **Figure 5.16**) with few exceptions: the microglia marker *IRF8* (DNA methylation >75%) and *SALL1* (DNA methylation >60%) as well as the astrocyte marker *CPE* (DNA methylation > 60%). Interestingly, at this same locus, both the Neu+ve and Sox10+ve fractions were significantly unmethylated. Also worth mentioning, for the astrocyte-specific gene *PAX6* very low DNA methylation levels were observed not only in the double negative fraction but in the Sox10+ve fraction too suggesting that high gene expression levels at this locus characterize both astrocytes and oligodendrocytes (**Figure 5.15**). More in general, less consistent DNA methylation patterns were dispayed by each cell type when markers of other glial cells were examined. This should not surprise since the double negative fraction is the most heterogenous group of all where microglia and astrocytes are likely to be the most represented yet not the only cell type captured. Furthermore, the pre-designed probes coverage offered by the EPIC array might also explain the discrepancy of results. Such cases nicely illustrate the complexity of DNA methylation across cell-types and the advantage of cell sorting over bulk tissue.
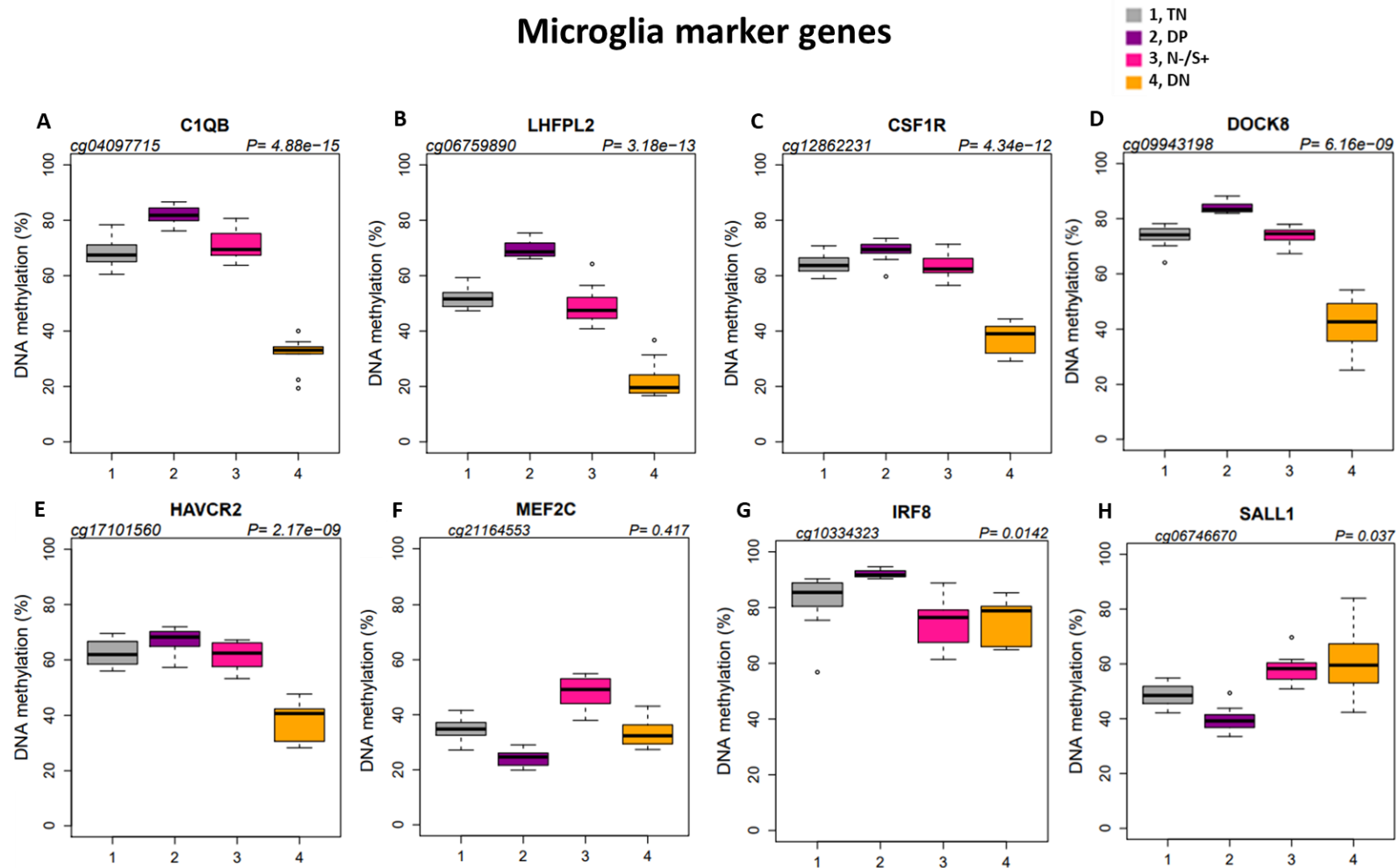
Figure 5.16 Microglia-specific differentially methylated positions (DMPs).
Boxplots showing representative examples of CpG sites within known marker genes of microglia which are differentially methylated (t-test P<9E-08) across nuclei fractions. The DN (NeuN-ve/Sox10-ve) population, presumably enriched in microglia and astrocytes, reveals a variable DNA methylation pattern being significantly hypomethilated at the majority of the sites investigated (A-E) when compared to the other three fractions. To be noted, the total fraction which is a mixture of all nuclei, glial included, here shows a methylation profile more similar to the neuronal and oligodendrocyte enriched fractions. Boxplots are a standardized way of displaying the distribution of data. Each box extends from the first quartile to the third quartile (IQR). A line goes through the box at the median (mid-point of the data and is shown by the line that divides the box into two parts). The whisker lines go from each quartile to the minimum (1st quartile – 1.5 x IQR) or maximum (3rd quartile + 1.5 x IQR). DP (NeuN+ve/Sox10+ve), neuronal-enriched population; N-/S+ (NeuN-ve/Sox10+ve) oligodendrocyte enriched population; TN, total nuclei.

Astrocyte marker genes
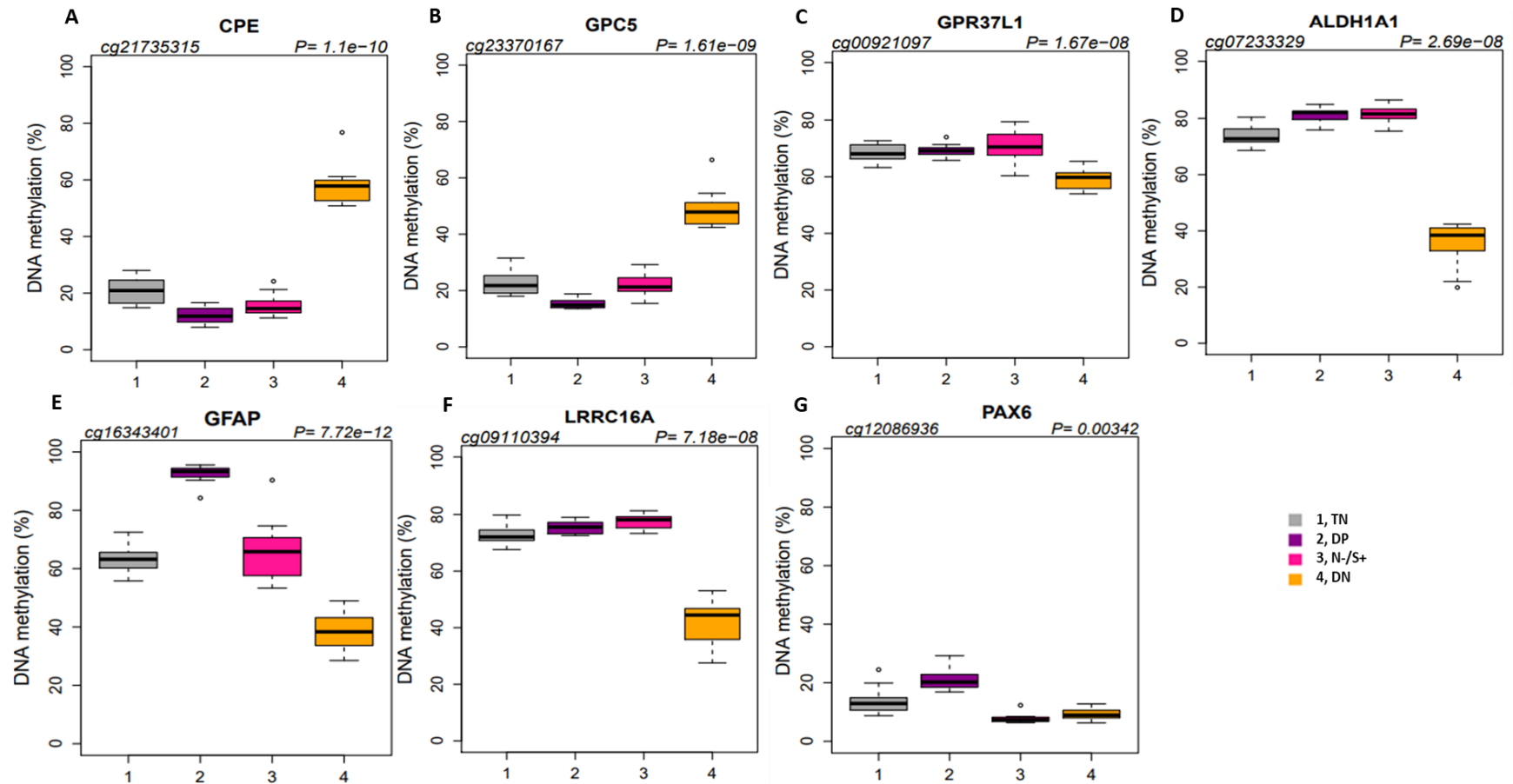
Figure 5.17 Astrocyte-specific differentially methylated positions (DMPs).
Boxplots showing representative examples of CpG sites within known marker genes of astrocytes which are differentially methylated (t-test P<9E-08) across nuclei fractions. The DN (NeuN-ve/Sox10-ve) population, presumably enriched in microglia and astrocytes, reveals a variable DNA methylation pattern being significantly hypermethilated (A-B) or Hypomethylated (C-F) when compared to the other three fractions. To be noted, the total fraction which is a mixture of all nuclei, glial included, here shows a methylation profile more similar to the neuronal and oligodendrocyte enriched fractions. Boxplots are a standardized way of displaying the distribution of data. Each box extends from the first quartile to the third quartile (IQR). A line goes through the box at the median (mid-point of the data and is shown by the line that divides the box into two parts). The whisker lines go from each quartile to the minimum (1st quartile – 1.5 x IQR) or maximum (3rd quartile + 1.5 x IQR). DP (NeuN+ve/Sox10+ve), neuronal-enriched population; N-/S+ (NeuN-ve/Sox10+ve) oligodendrocyte enriched population; TN, total nuclei.

5.4.3 Differentially methylated region analysis identified cell type specific DMRs with consistent DNA methylation pattern within cell type

The regional analysis conducted on sorted nuclei populations allowed to pinpoint several regions in the genome uniquely differentially methylated in each of the investigated cell type. As further measure of cell identity, the available literature was screened to recover well established cell type marker genes and examine whether those genes were significantly differentially methylated when comparing the three groups. Nine DMRs (P-value<9E-08) were detected in neuronal-specific genes (see **Table 5.2** for full details), three in astrocyte-specific genes (see **Table 5.3** for full details), six in microglia signature genes (see **Table 5.4** for full details) and eight in oligodendrocytes marker genes (see **Table 5.5** for full details). The following GVIZ plots (**Figure 5.18** to **Figure 5.32**) illustate the direction of the DNA methylation changes (hypo/hyper-methyation) across the CpG sites constituting the DMRs while comparing the three cell types, neurons (NeuN+ve/Sox10+ve nuclei), oligodendrocytes (NeuN-ve/Sox10+ve nuclei) and other glia (NeuN-ve/Sox10-ve nuclei). For each DMR reported in this result section, prior to the respective GVIZ plot, a brief review of the evidence justifying the selection of the explored gene as marker of cell type is provided.

CHR	DMR (Hg19)	N° of probes	Smallest *P*-value	RefGene Name (UCSC)	RefGene Group (UCSC)	CpG Islands Name (UCSC)	Relation to UCSC CpG Island
2	chr2:17720458-17837235	12	4.57E-09	*VSNL1*	TSS1500/ 5'UTR/ Body	chr2:17720155-17720417	S Shore
						chr2:17721537-17722021	S Shelf
2	chr2:224462651-224464760	3	3.00E-16	*SCG2*	Body/ 5'UTR		
3	chr3:63263752-63372516	5	2.32E-09	*SYNPR*	TSS200/ Body	chr3:63263989-63264205	N Shore
4	chr4:41258560-41270335	5	3.49E-09	*UCHL1*	TSS1500/ Body	chr4:41258759-41259867	N Shore
7	chr7:146072558-148111040	18	4.52E-08	*CNTNAP2*	Body		
8	chr8:80523191-80525764	6	1.62E-08	*STMN2*	TSS200/ Body	chr8:80523975-80525765	N Shore
12	chr12:13716374-14133168	16	5.28E-10	*GRIN2B*	Body/ 5'UTR	chr12:13715849-13717034	Island
14	chr14:60174988-60278381	5	1.69E-09	*RTN1*	Body	chr14:60193831-60194302	N Shelf
17	chr17:77142379-77474046	39	5.20E-08	*RBFOX3*	5'UTR	chr17:77460245-77460646	N Shore

Abbreviations: DMR, differentially methylated region; Chr, chromosome ; Hg19,Human Genome version 19; UCSC, University of California, Santa Cruz Human Genome Browser; TSS, transcriptional start site; UTR, untranslated region.

Table 5.2 Neuronal-specific differentially methylated regions identified in neuronal enriched (NeuN+ve/Sox10+ve) nuclei samples.

5.4.3.1   *Neuronal DMRs*

Synaptoporin (*SYNPR*) is a protein coding gene known for being expressed in mature neurons (Wilcox et al., 2011, Takagi et al., 2014). Its expression in the brain displays a distribution restricted to telencephalic structures, hippocampus, olfactory bulb and retina (Singec et al., 2002, Bergmann et al., 1993) and whithin these area, only in selected neuronal populations (Sun et al., 2006). However, the functional role of synaptoporin in the secretion of synaptic vesicles remains poorly understood (Sun et al., 2006). This neuron-related gene, elsewhere showed altered gene expression (downregulated) in association to human brain arteriovenous malformations indicating the loss of neurons associated with this condition (Takagi et al., 2014). Synaptoporin is the first synaptic vesicle protein that has been found to be up-regulated in primary sensory neurons after peripheral nerve injury. Thus, changes in its expression have been linked to the regulation of synaptic transmission in sensory afferent terminals under both physiological and pathological pain states (Sun et al., 2006). Despite its role in synaptic transmission, no evidence of its involvment in brain disorders has been reported to date.

SYNPR − PAN NEURONAL specific DMR
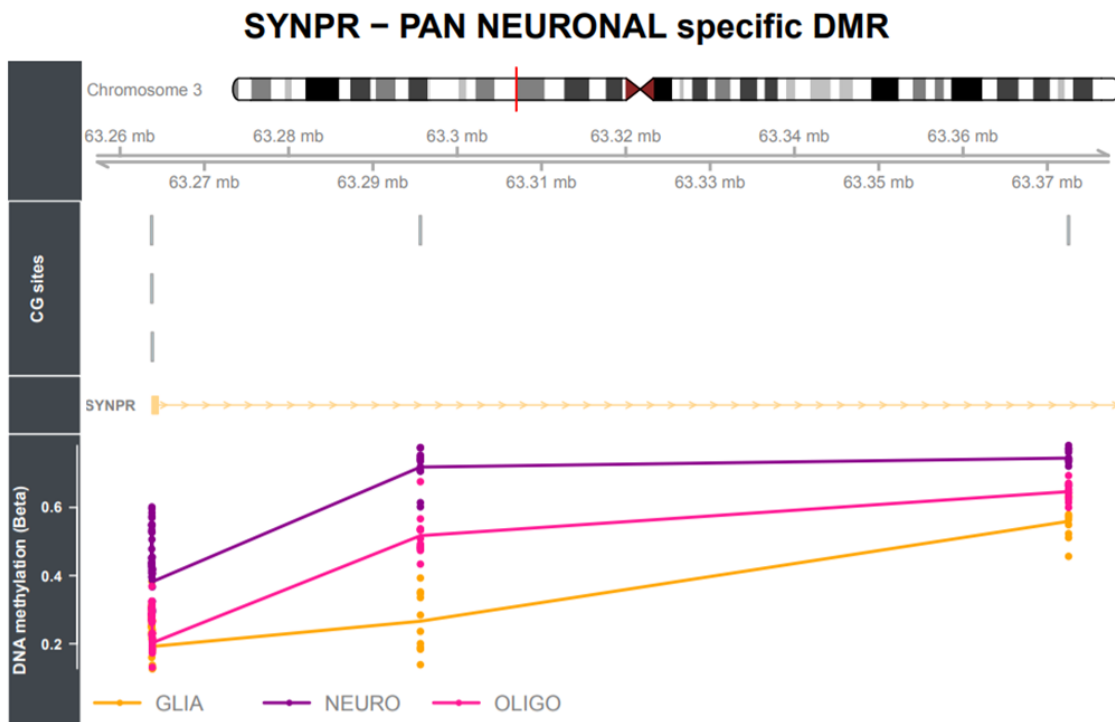
Figure 5.18 Neuron-specific differentially methylated region (DMR) in FANS sorted nuclei from human prefrontal cortex.
This DMR, spanning five CpG sites and located along the gene body of the neuronal marker SYNPR gene (P <9E-08), was found consistently hypermethylated in the neuronal fraction (dark magenta line) compared to oligodendrocyte (deep pink) and glial (orange)-enriched fractions. The solid line is for illustration purposes and not indicative that the CpG sites between sites are also methylated.

The (visinin-like 1) *VSNL1* gene product, Visinin-like-protein-1 (VILIP-1), is a member of the neuronal Ca^{2+}-sensor protein family (Braunewell, 2005, Burgoyne, 2007) Neuronal calcium sensor proteins are key players in different neuronal signalling pathways (Burgoyne, 2007, Cai et al., 2001) and have been implicated in numerous pathological processes of central nervous system disorders (Braunewell, 2005). In the nervous system, VILIP-1 is consistently expressed in hippocampal neurons, cerebellar granular cells, interneurons, cortical pyramidal cells, as well as in other neurons (Bernstein et al., 1999). VILIP-1 influences cytosolic cyclic adenosine mono phosphate (cAMP) levels and the activity of neurotransmitter receptors and ion channels, which are related to learning and memory processes (Spilker et al., 2002, Braunewell et al., 2003) Different lines of evidence have accumulated indicating that neuronal calcium sensor proteins, such as VILIP-1, are associated with SCZ . *VSNL1* has been correlated with cytoarchitectural abnormalities in SCZ and bipolar depression, with differentiated gene expression found in the frontal cortex thus proposing *VSNL1* as a potential

345

novel susceptibility factor (Kim and Webster, 2011). These results have been confirmed by independent microarray and proteomic studies (Miklos and Maleszka, 2004, Vercauteren et al., 2007). More recently, increased expression of miRNAs (e.g, miR-181b) was discovered in SCZ and was found to negatively regulate VILIP-1 expression in the brain of individuals affected by SCZ and in human dopaminergic SH-SY5Y neurons (Beveridge et al., 2008), further adding to the evidence implicating a role for VILIP-1 in SCZ. Furthermore, an association of SNPs in the *VSNL1* gene with SCZ and frontal cortical functions was reported (Braunewell et al., 2011). Similar to other potential SCZ susceptibility genes, *VSNL1* was found to affect cAMP signalling for differentiation and neurite outgrowth in rat neurons as well as human SH-SY5Y neuronal cells (Braunewell et al., 2011). Indeed, cAMP is a well-known promoter of neurite plasticity and branching (Cai et al., 2001, Baptiste and Fehlings, 2006). Lastly, VILIP-1 was also identified as a cerebrospinal fluid biomarker of neuronal/synaptic injury in AD (Braunewell, 2012, Sutphen et al., 2018, Lee et al., 2008, Gomez Ravetti et al., 2010). Although VILIP-1 was originally identified in the brain, its expression can be detected in peripheral tissues and organs such as heart, lung, liver, and testis (Gierke et al., 2004), suggesting a potential role in maintaining normal tissue homeostasis in both nervous tissue and non-neural tissues (Fu et al., 2009). Despite the recent reports highlighting the role of VILIP-1 in physiological and pathological processes, the molecular mechanisms controlling its expression remain unknown (Fu et al., 2009, Braunewell et al., 2011).

Figure 5.19 Neuron-specific differentially methylated region (DMR) in FANS sorted nuclei from human prefrontal cortex.
This DMR, spanning 15 CpG sites and located in the gene body of the neuronal marker VSNL1 gene (P <9E-08), was found consistently hypomethylated in the neuronal fraction (dark magenta line) compared to oligodendrocyte (deep pink) and glial (orange)-enriched fractions. The solid line is for illustration purposes and not indicative that the CpG sites between sites are also methylated.

Ubiquitin C-terminal hydrolase L1 (*UCHL1*) is a unique brain and neuron-specific protein (Day and Thompson, 2010) essential for axonal function (Larsen et al., 1996). *UCHL1* closely interacts with proteins of the neuronal cytoskeleton and may play an important role in axonal transport and maintaining axonal integrity (Bheda et al., 2010, Pukass and Richter-Landsberg, 2015, Liu et al., 2015). This deubiquitinating enzyme also regulates synaptic function and long-term potentiation (LTP) and may be involved in memory function (Sakurai et al., 2008, Gong et al., 2006). Mutations in *UCHL1* result in axonal pathology and extensive deficits in motor function (Liu et al., 2019a). *UCHL1* activity has showed to protect neurons from hypoxic injury by removal of abnormal proteins via the ubiquitin–proteasome pathway (UPP) and autophagy therefore preserving axonal conductance and synaptic function (Liu et al., 2019a).

Furthermore, mutations and aberrant function of *UCHL1* have been linked with neurodegeneration in Parkinson's (Liu et al., 2002, Bilguvar et al., 2013), Alzheimer's (Choi et al., 2004) and Huntington's disease (Naze et al., 2002). It remains unclear however, whether the link between low *UCHL1* function and neuronal death is a consequence of downregulation of protein turnover or whether levels of *UCHL1* activity affects other cell functions (Lombardino et al., 2005).

UCHL1 − PAN NEURONAL specific DMR

Figure 5.20 Neuron-specific differentially methylated region (DMR) in FANS sorted nuclei from human prefrontal cortex.
This DMR, spanning five CpG sites and located in the gene body of the neuronal marker UCHL1 gene (P <1E-07), was found consistently hypomethylated in the neuronal fraction (dark magenta line) compared to oligodendrocyte (deep pink) and glial (orange)-enriched fractions. The solid line is for illustration purposes and not indicative that the CpG sites between sites are also methylated.

Secretogranin II (*SCG2*) is a protein widely distributed in nervous and endocrine tissues, and abundant in neuroendocrine granules (Li et al., 2008a). *SCG2* is the precursor of a 33 amino-acid peptide secretoneurin, which modulates neurotransmission and inflammatory responses and may be involved in neuronal differentiation (Wiedermann, 2000, Taupenot et al., 2003). Secretoneurin promotes neurite outgrowth of immature cerebellar granule cells and also aids in the growth and repair of neuronal tissue, although the precise mechanisms underlying the promotion of brain tissue neuroprotection and plasticity by this

neuropeptide are not understood (Shyu et al., 2008). Notably, the highest degree of processing of *SCG2* (>90%) occurs in the brain, producing functional secretoneurin at concentrations comparable to other established neuropeptides (Li et al., 2008a). Progressive structural brain changes in individuals with BPD have been associated with defects in the secretion of neurotrophic factors and Secretogranin II has been suggested to be a biological marker of the regulatory secretory pathway in the brain (Jakobsson et al., 2013). Concentrations of secretogranin II were found significantly lower in CSF from patients with BPD type I than in healthy controls (Jakobsson et al., 2013). Since Secretogranin II may act as a neuroprotective peptide and is coreleased with neurotrophins, these findings support the hypothesis that defects in neurotrophin signalling are involved in the pathophysiology of severe BPD and that CSF marker secretogranin II might act as a biological marker for the disorder (Jakobsson et al., 2013).
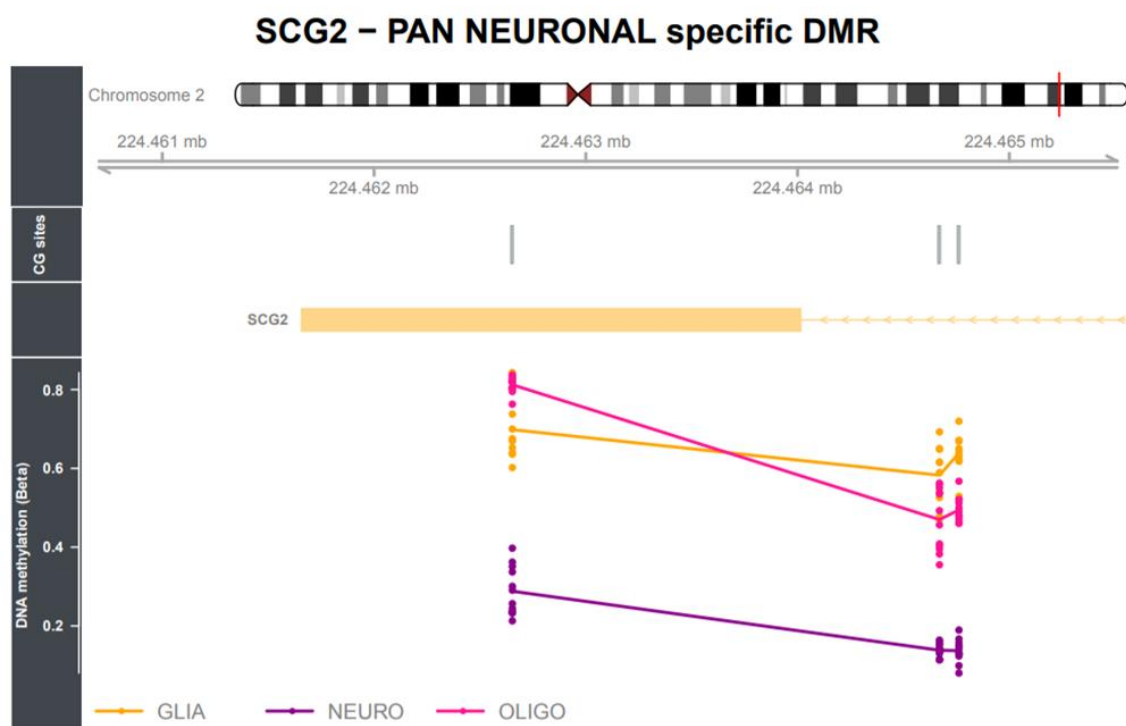
Figure 5.21 Neuron-specific differentially methylated region (DMR) in FANS sorted nuclei from human prefrontal cortex.
This DMR, spanning 3 CpG sites and located in the gene body of the neuronal marker SCG2 gene (P <1E-07), was found consistently hypomethylated in the neuronal fraction (dark magenta line) compared to oligodendrocyte (deep pink) and glial (orange)-enriched fractions. The solid line is for illustration purposes and not indicative that the CpG sites between sites are also methylated.

Astrocyte-specific differentially methylated regions identified in double negative nuclei populations

Hg19	Chr	No of probes	Slk P-value	Sidak P-value	Annotated gene (UCSC)	refGene feature	CpG Island Ext name	CpG Island Ext feature
chr9: 75612497-75612612	9	3	4.44E-13	3.20E-09	ALDH1A1	intergenic	CpG: 177	NA
chr17: 42988784-42989148	17	5	4.71E-18	1.07E-14	GFAP	intron+cds	CpG: 41	island
chr17: 70112050-70112308	17	4	1.03E-14	3.32E-11	SOX9	nc_intron	CpG: 26	island

Abbreviations: Hg19, Human Genome version 19; UCSC, University of California, Santa Cruz Human Genome Browser. Stouffer-Liptak-Kechris correction (slk); one-step Siidak (1967) multiple-testing correction.

Table 5.3 Astrocyte-specific differentially methylated regions identified in double negative nuclei populations using Comb-P.

5.4.3.2   Astrocyte-specific DMRs

Astrocytes have in recent years become the focus of intense experimental interest, yet markers for their definitive identification remain both scarce and imperfect (Sun et al., 2017). Astrocytes have been traditionally identified immunohistochemically by antibodies that target cell-specific antigens in the cytosol or plasma membrane including glial fibrillary acidic protein (*GFAP*), S100 calcium-binding protein B (*S100β*), glutamate transporter 1 (*GLT1*) (Rothstein et al., 1994), aquaporin-4 (*AQP4*), connexin-43 (*Cx43*), connexin-30 (*Cx30*) (Nagy et al., 1999), and, more recently, aldehyde dehydrogenase 1 family member L1 (*ALDH1L1*) (Cahoy et al., 2008). Several recent transcriptome analyses of astrocytic genes have suggested that **SRY-Box Transcription Factor 9 (*SOX9)*** is highly enriched in astrocytes (Lovatt et al., 2007, Barnabe-Heider et al., 2010, Molofsky et al., 2013, Zhang et al., 2014, Farmer et al., 2016). *SOX9* is a member of a highly conserved family of transcription factors defined by their similarity to the high-mobility group DNA-binding domain of SRY (sex-determining region Y). Studies have documented that *SOX9* plays important roles during the development of nervous system and especially in glial fate specification (Sun et al., 2017). *SOX9* may also regulate extracellular matrix production in astrocytes, which in turn modulate synaptic plasticity under physiological conditions (Faissner et al., 2010). A recent study assessing differential RNA expression in FACS-purified adult astrocytes showed that both *SOX9* mRNA and protein are expressed almost exclusively by astrocytes in the adult murine brain (Sun et al., 2017) and transcriptome comparisons of SOX9+ cells with GLT1+ cells revealed that the two populations of cells exhibit largely overlapping gene expression profile (Sun et al., 2017).The authors therefore have proposed *SOX9* as an astrocyte-specific nuclear marker in all major areas of the CNS outside of the neurogenic regions the adult murine brain (Sun et al., 2017). Interestingly, *SOX9* has been found downregulated in the dorsal lateral prefrontal cortex of individuals who died after suicide compared with sudden death controls (Ernst et al., 2011, Nagy et al., 2015b). Additionally, a study investigated genome-wide DNA methylation associated with astrocytic markers in depression and found *SOX9* expression significantly decreased in cases compared to controls (Nagy et al., 2015b) suggesting a role of *SOX9* and thereby of astrocytes in psychiatric disease. Furthermore, in a previous study, *SOX9* was found to affect the

expression of astrocyte connexin Cx30 in the dorsolateral PFC of suicide completers (Ernst et al., 2011) further implicating astrocytes in the suicide process (Rajkowska and Miguel-Hidalgo, 2007).
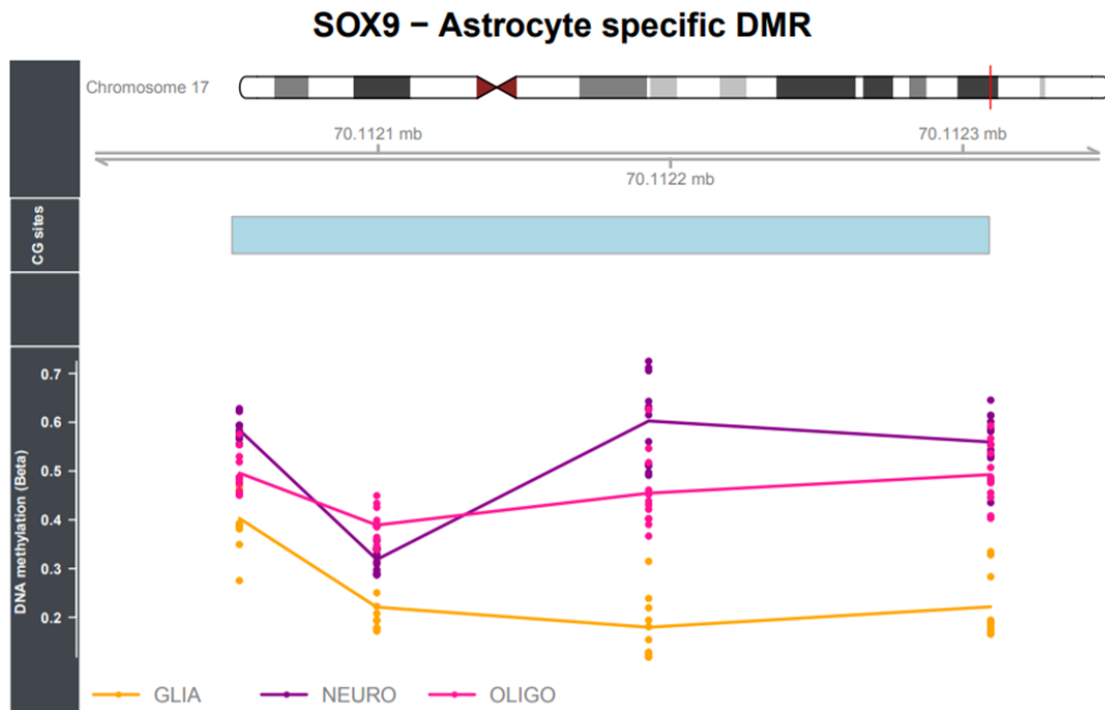
Figure 5.22 Astrocyte-specific differentially methylated region (DMR) in FANS sorted nuclei from human prefrontal cortex.
This DMR, spanning four CpG sites and located upstream of the astrocyte marker SOX9 gene (P <9E-08), was found consistently hypomethylated in the glial fraction (orange line) compared to neuronal (darkmagenta) and oligodendrocyte (deep-pink)-enriched fractions. The solid line is for illustration purposes and not indicative that the CpG sites between sites are also methylated.

Glial fibrillary acidic protein (*GFAP*) is the main intermediate filament protein in mature astrocytes, but also an important component of the cytoskeleton in astrocytes during development (Middeldorp and Hol, 2011). *GFAP* is thought to provide mechanical support for the plasma membrane where it comes into contact with other cells or with the extracellular matrix. In astrocytes, it is thought to help maintain mechanical strength, as well as the shape of cells (Middeldorp and Hol, 2011). Despite the huge number of studies using *GFAP* as a marker for astrocytes, the exact function of this gene remains an enigma. Classically *GFAP* is a marker for astrocytes, known to be induced upon brain damage or during CNS degeneration, and to be more highly expressed in the aged brain due to an increase of its transcription (Morgan et al., 1999, Nichols et al., 1993). In the past

decade, new methods have been developed which revealed more details on the morphology of astrocytes allowing the imaging of astrocytes in living brain slices (Nolte et al., 2001, Suzuki et al., 2003). Although traditional immunohistochemistry has shown that *GFAP* expression is predominantly cytoplasmic, high magnification images of these astrocytes revealed that *GFAP* immunoreactivity was mainly present in the perinuclear region and in the thick processes (Suzuki et al., 2003) suggesting its potential application as nuclear marker. The structural role of *GFAP* in astrocytes has been known for a long time, but over the years, *GFAP* has also been shown to be involved in astrocyte functions, which are important during regeneration, synaptic plasticity and reactive gliosis (Middeldorp and Hol, 2011). Increased *GFAP* expression due to astrogliosis was found to significantly correlate with compact neuritic plaques in the AD brain (Simpson et al., 2010) and a different study (Ingelsson et al., 2004) showed that the elevated *GFAP* levels in AD increased with tangle burden and disease duration. There is also evidence that *GFAP* correlates inversely with cognitive function, independently of AD pathology (Kashon et al., 2004). In addition to these neurodegenerative diseases, a decrease in *GFAP* expression in different brain areas has been correlated to depression (Johnston-Wilson et al., 2000, Si et al., 2004) whereas increased *GFAP* levels were found in relation to autism (Laurence and Fatemi, 2005). Lastly, levels of established astrocyte markers (*GFAP, S100B*) were found increased unevenly in patients with SCZ (Kashon et al., 2004, Kim et al., 2018) and reactive astrogliosis was found in approximately 70% of patients with SCZ (Mallya and Deutch, 2018, Schnieder and Dwork, 2011). Although associations between *GFAP* and symptoms have not been found yet, there are several evidences that astrocytes may play a major role in etiology and pathogenesis of SCZ (Tarasov et al., 2019).
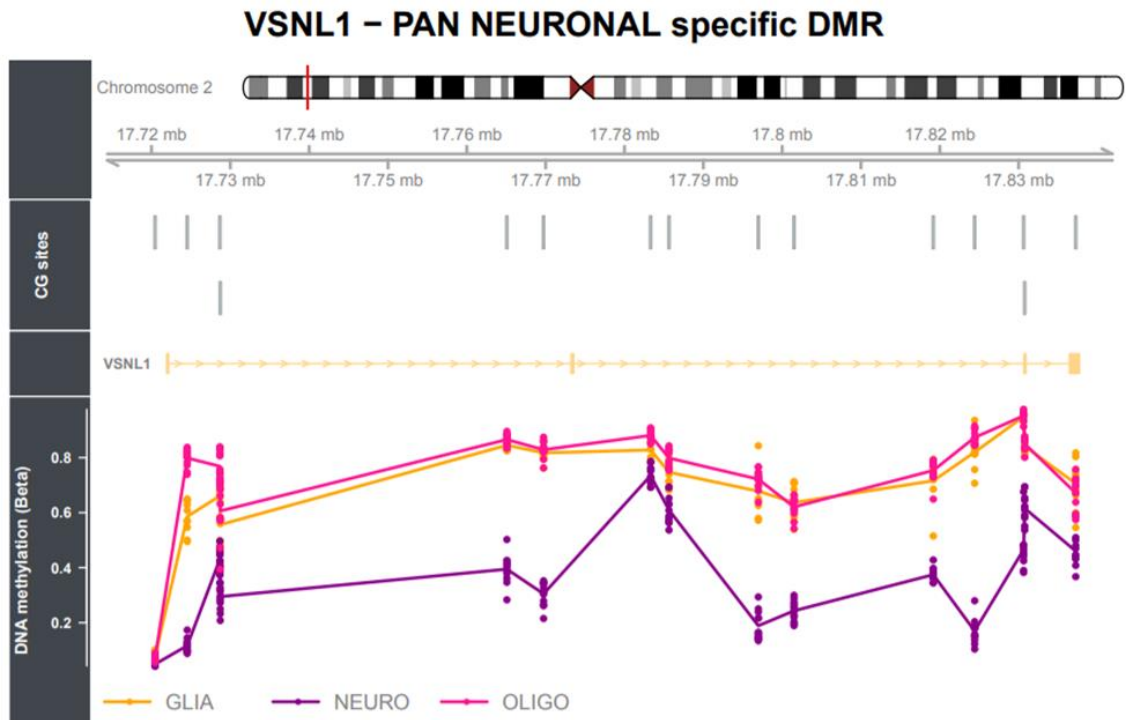
Figure 5.23 Astrocyte-specific differentially methylated region (DMR) in FANS sorted nuclei from human prefrontal cortex.
This DMR, spanning five CpG sites and located in the gene body of the astrocyte marker GFAP gene (P <1E-05), was found consistently hypomethylated in the glial fraction (orange line) compared to neuronal (darkmagenta) and oligodendrocyte (deeppink)-enriched fractions. The solid line is for illustration purposes and not indicative that the CpG sites between sites are also methylated.

Past studies on astroglial gene expression profiles have started to characterise the molecular identity of astrocytes *in vivo* (Lovatt et al., 2007) and identified **aldehyde dehydrogenase 1 family, member L1 (*ALDH1L1*)** as the new astroglial marker that also selectively labels cortical astrocytes *in vivo* (Cahoy et al., 2008). *ALDH1L1*, is a key enzyme in folate metabolism which is important in nucleotide biosynthesis and cell division and growth (Krupenko, 2009). Unique functions of *ALDH1L1* in the CNS have not been reported so far except a potential link to neural tube defects during early CNS development (Anthony and Heintz, 2007). *ALDH1L1* is currently recognized as a highly specific antigenic marker for astrocytes (Cahoy et al., 2008, Yang et al., 2011). Together with *GFAP, ALDH1L1* figured as astrocyte-associated gene in a study assessing cell type specific gene expression across brain disorders (SCZ, MDD, BP) (Barley et al., 2009) where higher mean expression levels were observed in astrocytes across regions in all psychiatric groups relative to controls (Barley et al., 2009). Similarly, *ALDH1L1* was examined as astrocyte-specific protein in a study investigating the role of

354

astrocytes in peripheral nerve injury and found to be upregulated during synaptogenesis induced by deafferentation (Lo et al., 2011). Strong *ALDH1A1* expression was observed in mature astrocytes co-expressing *GFAP* and *S100* providing further evidence for *ALDH1A1* as a marker of astrocytic differentiation during brain development (Adam et al., 2012). Remarkably, expression of *ALDH1A1* was restricted to differentiated astroglia and was not detectable in neurons, neuronal precursors or other progenitor populations suggesting that *ALDH1A1* protein expression is associated with advanced differentiation of astroglia (Adam et al., 2012). Furthermore, a study performing a comparative analysis of two unique astroglial reporters *in vivo* supported *ALDH1L1* as a general CNS astroglial marker (Yang et al., 2011). Finally, a transcriptomic study of FACS-isolated astrocytes from transgenic mice confirmed *ALDH1L1* gene being a highly specific antigenic marker for astrocytes with a substantially broader pattern of expression than the traditional astrocyte marker GFAP (Cahoy et al., 2008).

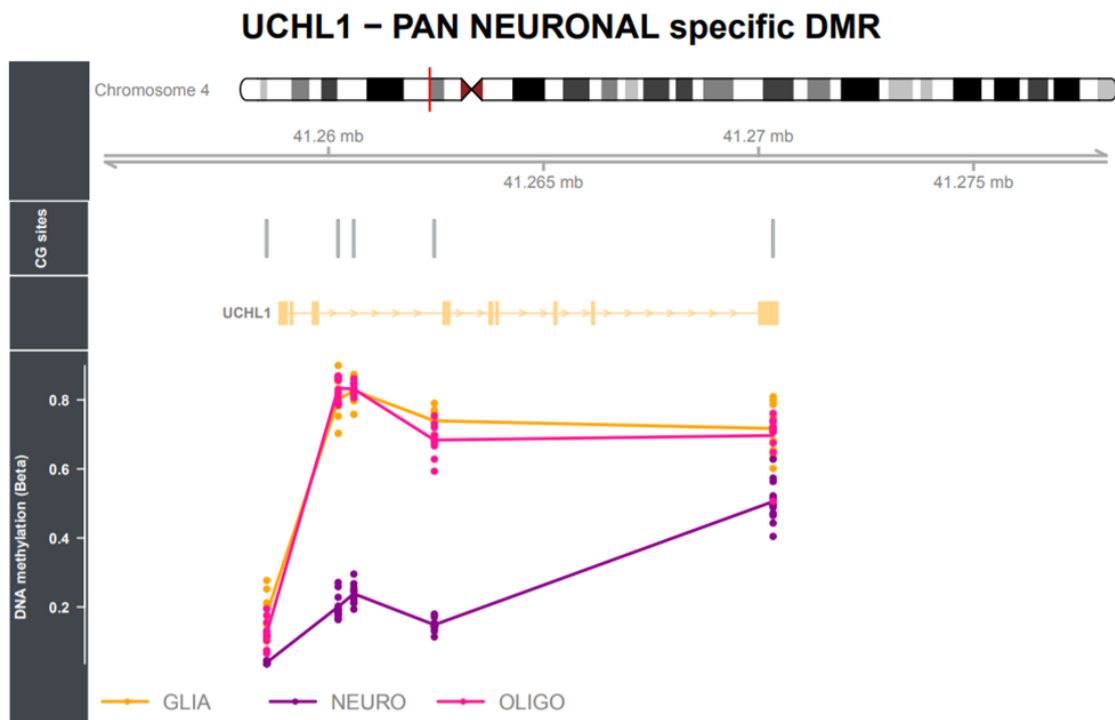***Figure 5.24 Astrocyte-specific differentially methylated region (DMR) in FANS sorted nuclei from human prefrontal cortex.***
This DMR, spanning three CpG sites and located downstream the astrocyte marker ALDH1A1 gene (P <1E-05), was found consistently hypomethylated in the glial fraction (orange line) compared to neuronal (darkmagenta) and oligodendrocyte (deeppink)-enriched fractions. The solid line is for illustration purposes and not indicative that the CpG sites between sites are also methylated.

CHR	DMR(Hg19)	N° of probes	*Smallest P*-value	RefGene Name (UCSC)	RefGene Group (UCSC)	CpG Islands Name (UCSC)	Relation to UCSC CpG Island
1	chr1:22978556-22979546	6	1.89E-08	*C1QB*	TSS1500/ TSS200		
5	chr5:77806538-77936665	12	5.82E-08	*LHFPL2*	5'UTR	chr5:77805753-77806313	S_Shore
5	chr5:149466091-149493099	5	6.00E-09	*CSF1R*	5'UTR/ TSS200		
12	chr12:108990874-108992148	3	5.04E-09	*TMEM119*	5'UTR/ TSS1500		
13	chr13:46745046-46757637	5	6.93E-08	*LCP1*	5'UTR/ TSS1500		
19	chr19:6719342-6721027	4	4.46E-09	*C3*	Body/ TSS1500		

Abbreviations: DMR, differentially methylated region; Chr, chromosome ; Hg19,Human Genome version 19; UCSC, University of California, Santa Cruz Human Genome Browser; TSS, transcriptional start site; UTR, untranslated region.

Table 5.4 Microglia-specific differentially methylated regions identified in glia-enriched (NeuN-ve/Sox10-ve) nuclei samples.

5.4.3.3   *Microglia-specific DMRs*

Transmembrane protein 119 (*TMEM119*) is a transmembrane protein of unknown function, which is a developmentally regulated and highly specific cell-surface marker of microglia not expressed by macrophages or other immune or neural cell types (Bennett et al., 2016). By comparative analysis of five comprehensive microglial transcriptome datasets, the evolutionarily conserved protein Tmem119 was identified as the most promising candidate of human microglial markers to discriminate resident microglia from blood-derived macrophages in the human brain (Satoh et al., 2016). Recent advances in RNA sequencing and other cell profiling technologies have enabled the discovery of cell-type-specific signature genes (Butovsky et al., 2014). Among these, *TMEM119* was confirmed to be highly and exclusively expressed in microglia in the brains of mice and humans (Satoh et al., 2016) where it has been used as antibody to isolate pure microglia and perform RNA-seq profiling (Bennett et al., 2016). A later study targeted the recently discovered microglia-specific Tmem119 gene to successfully generate knock-in mice for the identification and manipulation of microglia (Kaiser and Feng, 2019). Interestingly, in a study investigating the innate immune response in the brain of subjects with multiple sclerosis, *TMEM119* was used to differentiate microglia from recruited monocytes and revealed the contribution of resident microglia in multiple sclerosis lesions (Zrzavy et al., 2017).
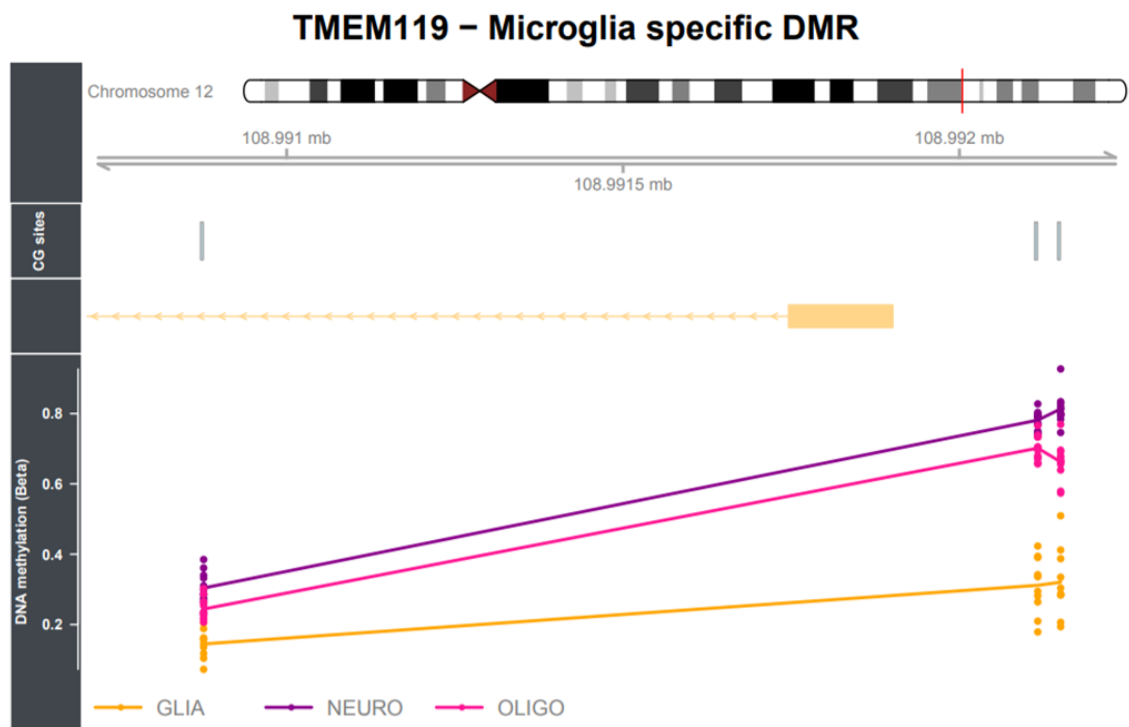
Figure 5.25 Microglia-specific differentially methylated region (DMR) in FANS sorted nuclei from human prefrontal cortex.
This DMR, spanning three CpG sites and located upstream the microglia marker TMEM119 gene (P <1E-07), was found consistently hypomethylated in the glial fraction (orange line) compared to neuronal (darkmagenta) and oligodendrocyte (deeppink)-enriched fractions. The solid line is for illustration purposes and not indicative that the CpG sites between sites are also methylated.

Colony-stimulating factor 1 receptor (*CSF1R*) is a receptor tyrosine kinase required for the development, maintenance, and proliferation of microglia (Easley-Neal et al., 2019). Microglia arise very early in mouse embryonic development and its survival depend upon *CSF1R* signaling (Ginhoux et al., 2010, Jin et al., 2017, Elmore et al., 2014). Compromised Csf1r transcription has been associated with lack of brain microglia in mice (Rojo et al., 2019) which was similarly observed in Csf1r−/− rat brains (Pridans et al., 2018). Furthermore, previous work showed that injection of a blocking antibody against *Csf1r* at the developmental stage depletes yolk sac macrophages, which are precursors to CNS microglia, and leads to a near complete loss of microglia in the developing mouse brain (Squarzoni et al., 2014). While much has been learned about the role of *CSF1R* in the regulation CNS microglial development, the localization and developmental roles of this receptor and its ligands in the brain remain poorly understood (Nandi et al., 2012). A study in 2012 suggested novel roles for *CSF1R* in the regulation of corticogenesis (Easley-Neal et al., 2019). Recent work in

humans, demonstrated several structural brain anomalies and almost complete absence of microglia in individuals with homozygous *CSF1R* mutations suggesting that *CSF1R* is required for human brain development (Oosterhof et al., 2019). Neuroinflammation and microglial activation are significant processes in AD pathology (Edison et al., 2008). Recent studies strongly supported the potential for inhibition of *CSF1R* as a target for the treatment of AD and other tau-mediated neurodegenerative diseases (Mancuso et al., 2019, Sosna et al., 2018).

CSF1R − Microglia specific DMR

Figure 5.26 Microglia-specific differentially methylated region (DMR) in FANS sorted nuclei from human prefrontal cortex.
This DMR, spanning five CpG sites and located upstream the microglia marker CSF1R gene (P <1E-07), was found consistently hypomethylated in the glial fraction (orange line) compared to neuronal (darkmagenta) and oligodendrocyte (deeppink)-enriched fractions. The solid line is for illustration purposes and not indicative that the CpG sites between sites are also methylated.

Complement components are important effectors of humoral immunity and inflammation in peripheral tissues but have not been considered as normally present in brain for long time until data suggested their involvement in acute responses to lesions that include activation of microglia and astrocytes during the removal of debris and the onset of synaptic remodelling (Fagan and Gage, 1990). Subsequently, immunocytochemistry and in situ hybridization techniques have detected C1qB mRNA in the cortex from AD brains and the increased C1qB mRNA was in part associated with microglia (Johnson et al., 1992). It is now stably recognized that microglia are a major site of induced complement C1q mRNA after brain injury (Dietzschold et al., 1995, Haga et al., 1996). TGF-β1, which can have anti-inflammatory actions, was found to decrease complement **C1qB** mRNA in microglia cell lines (Morgan et al., 2000). Several complement components including **C3** may be produced by glia surrounding plaques in AD brain (Stoltzner et al., 2000, Tenner, 2001), as Aβ peptides upregulate C3 production by microglia in vitro (Haga et al., 1993). Complement can recruit and activate microglia around fibrillary Aβ deposits (Eikelenboom and Veerhuis, 1996) and mediates, in part, the uptake and clearance of Aβ by the interaction of complement with its receptor on the surface of microglia (Fu et al., 2012). Furthermore, C3 has been found to be critical in microglia-mediated synaptic pruning during development (Stevens et al., 2007). Chronic stress upregulates the expression of C3 and its microglial receptors in PFC (Pan et al., 2014, Crider et al., 2018). Altogether, these evidence support the hypothesis of complement cascade components as marker of activated microglia.
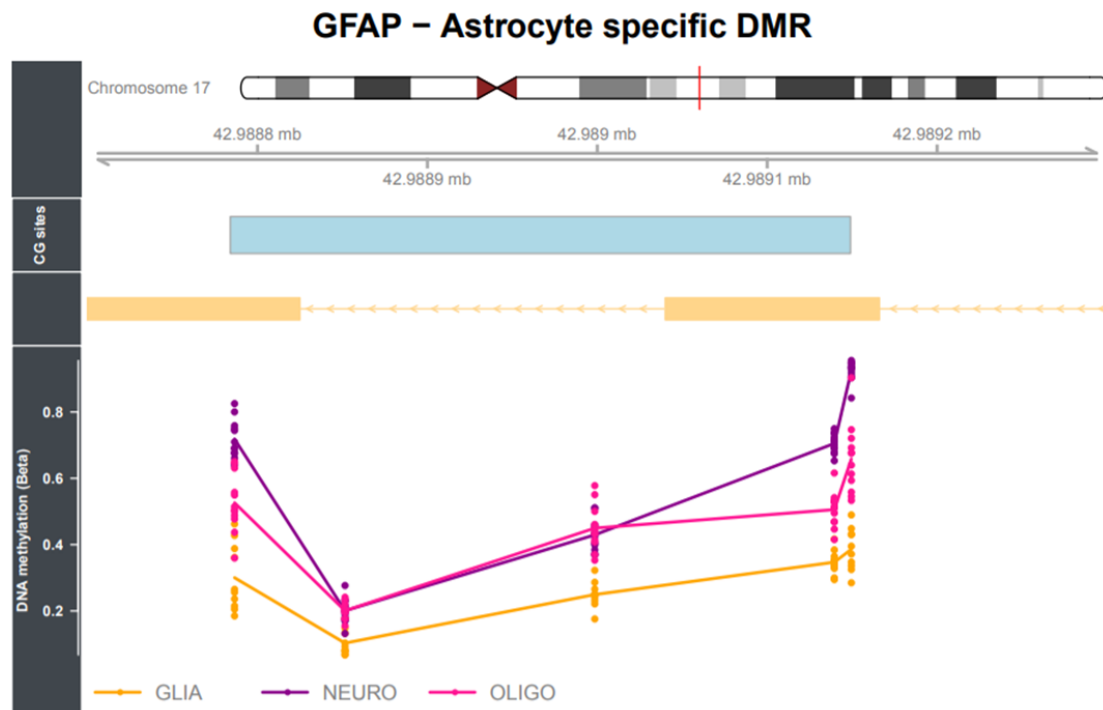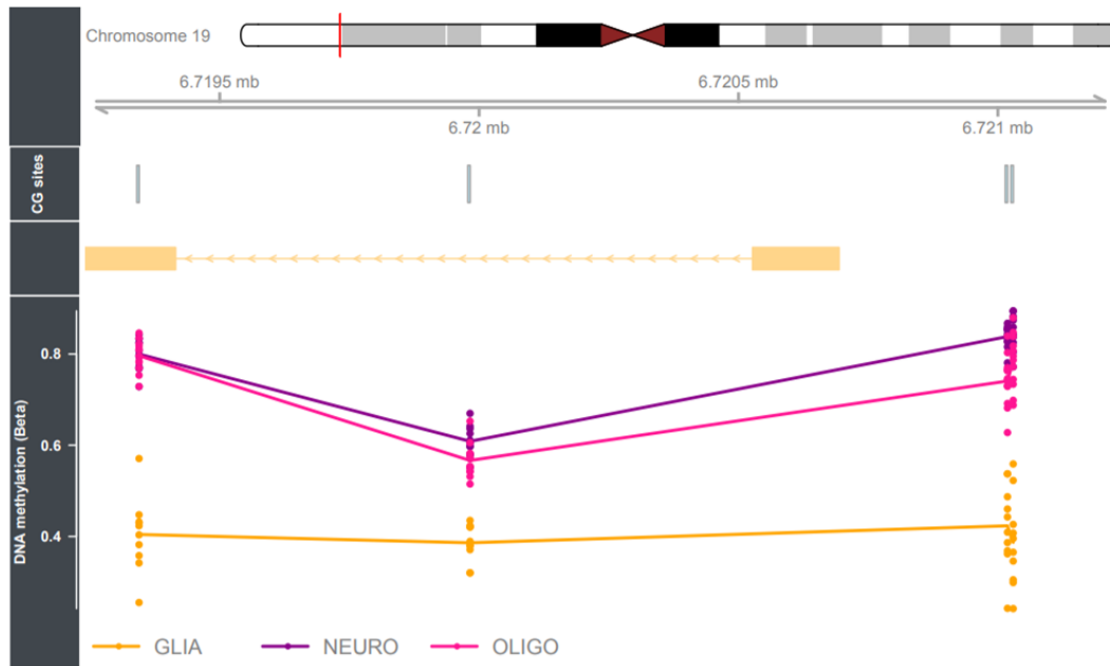
Figure 5.27 Microglia-specific differentially methylated region (DMR) in FANS sorted nuclei from human prefrontal cortex.

This DMR, spanning four CpG sites and located along the gene body of the microglia marker C3 gene (P <1E-07), was found consistently hypomethylated in the glial fraction (orange line) compared to neuronal (darkmagenta) and oligodendrocyte (deeppink)-enriched fractions.
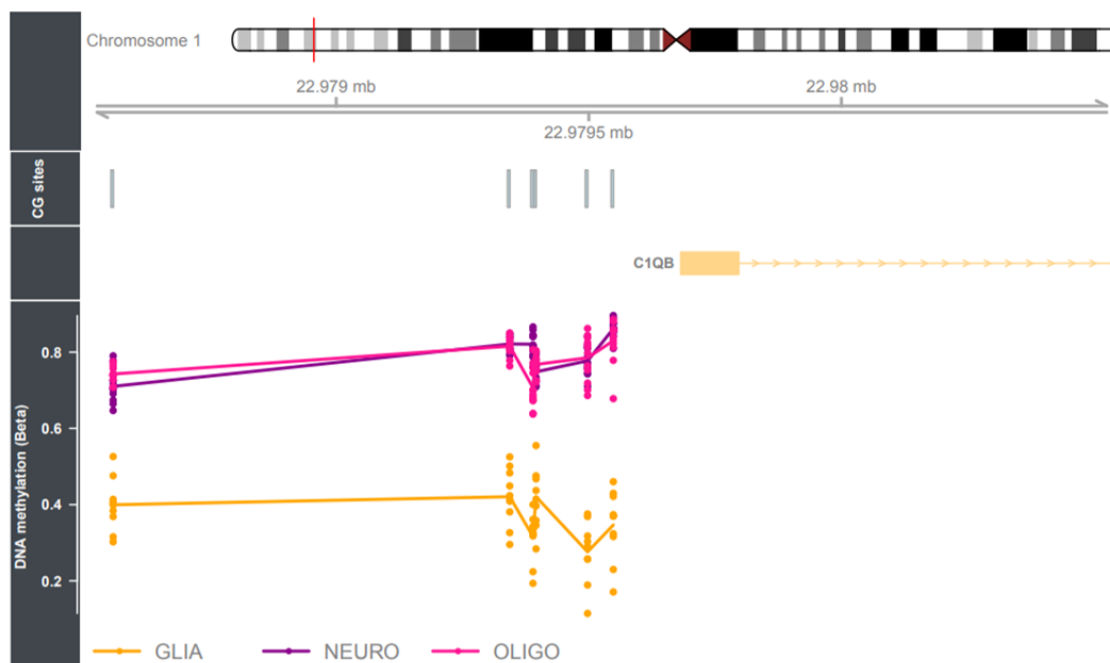
Figure 5.28 Microglia-specific differentially methylated region (DMR) in FANS sorted nuclei from human prefrontal cortex.

This DMR, spanning six CpG sites and located upstream of the microglia marker C1QB gene (P <1E-07), was found consistently hypomethylated in the glial fraction (orange line) compared to neuronal (darkmagenta) and oligodendrocyte (deeppink)-enriched fractions.

361

CHR	DMR (Hg19)	N° of probes	Smallest P-value	RefGene Name (UCSC)	RefGene Group (UCSC)	CpG Islands Name (UCSC)	Relation to UCSC CpG Island
Mature Oligodendrocytes							
1	chr1:84409003-84419549	3	3.40E-10	TTLL7	Body/ 5'UTR	chr1:84464223-84465232	N Shelf
3	chr3:133464047-133476947	17	1.35E-09	_TF_	TSS1500/ TSS200/ Body	chr3:133464949-133465420	N Shore/ S Shore
4	chr4:17490309-17513646	3	5.38E-08	_QDPR_	Body	chr4:17513309-17513981	Island
4	chr4:115518802-115536913	8	6.98E-09	_UGT8_	TSS1500/ 5'UTR	chr4:115519422-115520932	N Shore
10	chr10:22824354-22992381	41	4.87E-08	_PIP4K2A_	3'UTR/ Body		
17	chr17:40119847-40127892	12	5.63E-08	_CNP_	Body/ 3'UTR	chr17:40119811-40120047 chr17:40120233-40120471 chr17:40118605-40119301	Island Island S Shore
18	chr18:72201504-72212692	10	2.64E-08	_CNDP1_	TSS200/ Body		
22	chr22: 38368323- 38381626	7	2.23E-22	_SOX10_	Body/ TSS1500	chr22:38379093-38379964	Island/ S Shore
Oligodendrocyte precursor cell (OPC)							
1	chr1:175332749-175683971	13	3.13E-08	_TNR_	Body/ 5'UTR	chr1:175568376-175568808	N Shore
4	chr4:55104084-55143269	7	9.29E-08	_PDGFRA_	5'UTR/ Body	chr4:55096185-55100331	S Shelf
9	chr9:139871030-139875200	8	4.87E-08	_PTGDS_	TSS1500/ Body	chr9:139872237-139873143	N Shore
15	chr15:66195869-66547044	18	7.04E-08	_MEGF11_	Body / 5'UTR/ TSS1500	chr15:66274583-66274838 chr15:66332090-66332353 chr15:66544432-66546134	N Shelf N Shelf S Shore
21	chr21:41552656-41990060	4	9.88E-09		Body	chr21:41554618-41554959	N Shore

Abbreviations: DMR, differentially methylated region; Chr, chromosome ; Hg19,Human Genome version 19; UCSC, University of California, Santa Cruz Human Genome Browser; TSS, transcriptional start site; UTR, untranslated region.

Table 5.5 Oligodendrocyte-specific differentially methylated regions identified in oligodendrocyte-enriched (NeuN-ve/Sox10+ve) nuclei samples.

5.4.3.4   Oligodendrocyte-specific DMRs

SOX10, a high-mobility-group transcriptional regulator, is considered as the main Sox TF regulating oligodendrocyte specification and maturation, with also epigenetic functions (Weider et al., 2013, Vogl et al., 2013, Lopez-Anido et al., 2015). Sox10 is required for myelin gene expression (Stolt et al., 2002). In the CNS, Sox10 expression is elevated during differentiation of glial precursor cells into OPCs, and remains persistent throughout oligodendrocyte differentiation and maturation (Stolt et al., 2002). A recent study has demonstrated that overexpression of *SOX10* is sufficient to generate from human pluripotent stem cells (hPSCs) oligodendrocytes resembling primary human oligodendrocytes at the transcriptome level and which can myelinate neurons *in vivo* (Garcia-Leon et al., 2018). In line with an earlier study, in which overexpression of *SOX10* alone was found to be sufficient to induce oligodendroglial commitment in neural progenitors derived from the human fetal brain (Wang et al., 2014), a later study showed that *SOX10* was the only TF inducing expression of *O4+* (a highly specific marker of late-stage OPCs) in iPSC-derived neural progenitors, demonstrating that *SOX10* is a key TF to induce oligodendroglial lineage commitment. However, combination of *SOX10* with *OLIG2* and *NKX6.2* further enhanced the commitment into the oligodendroglial lineage, resulting in a significantly higher percentage of O4$^+$ cells having a global gene-expression profile comparable to primary human OL (Ehrlich et al., 2017). Additionally, it has been shown that mouse fibroblasts can be directly converted into OPC by the forced expression of SOX10 in combination with other oligodendroglial lineage markers (Yang et al., 2013, Najm et al., 2013).
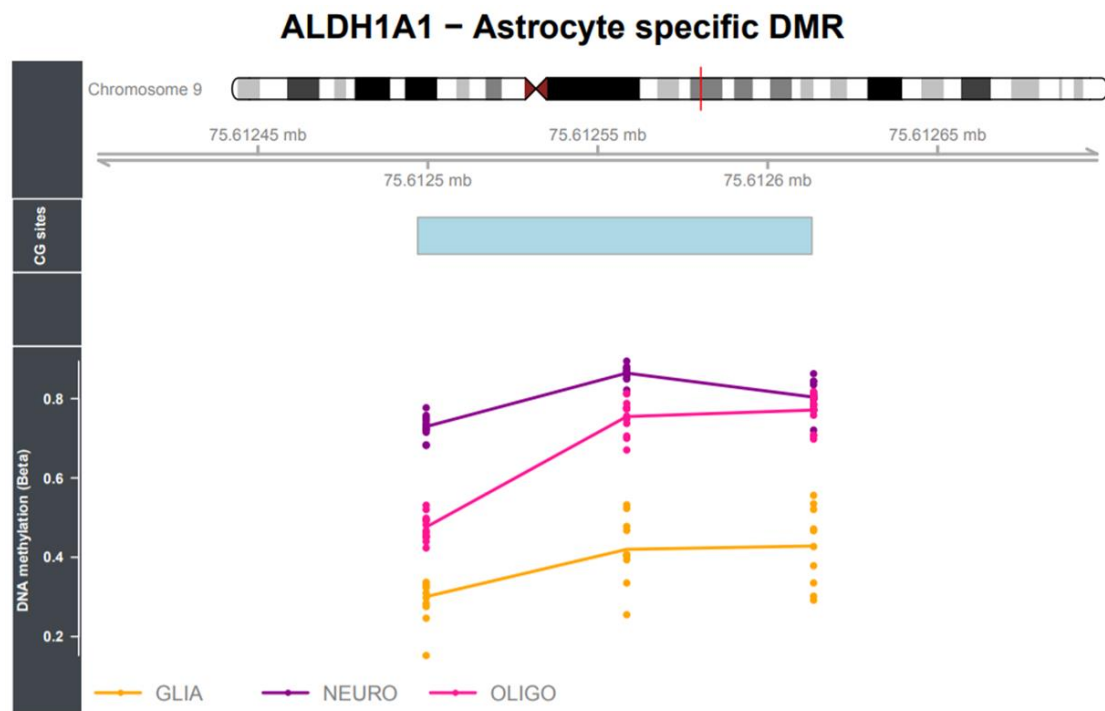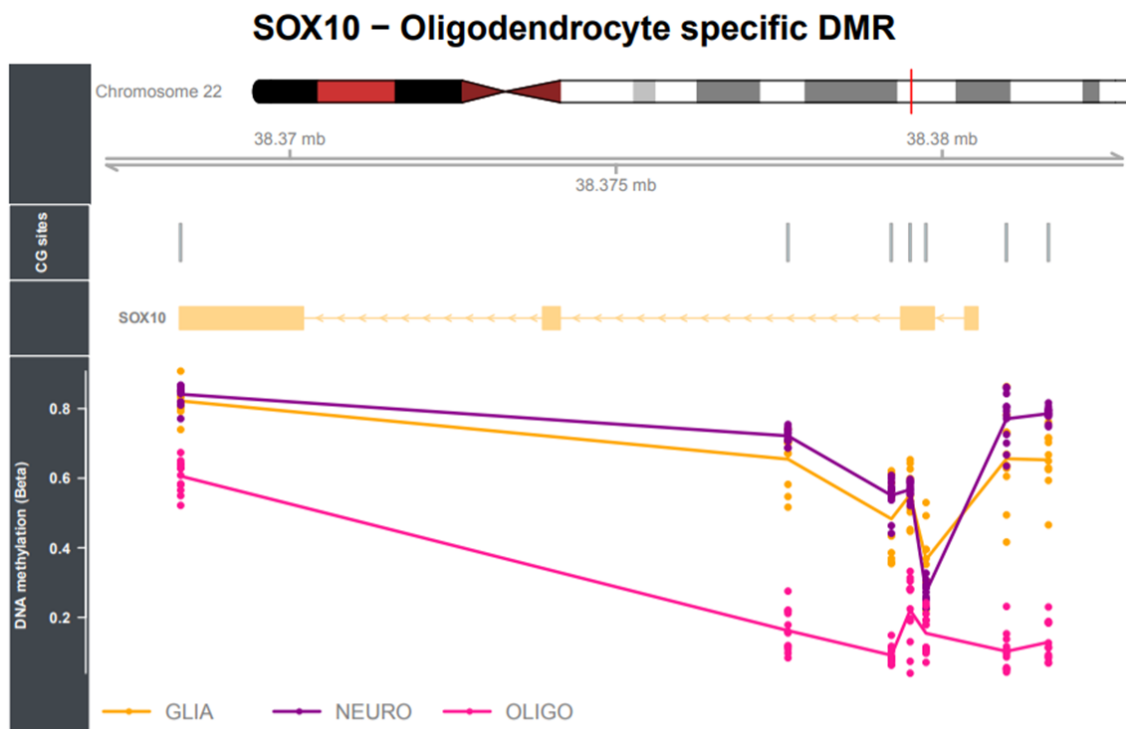
Figure 5.29 Oligodendrocyte-specific differentially methylated region (DMR) in FANS sorted nuclei from human prefrontal cortex.
This DMR, spanning seven CpG sites and distributed predominately along the gene body of the oligodendrocytic marker SOX10 gene (P<1E-05), was found consistently hypomethylated in the oligo fraction (deep pink line) compared to neuronal (darkmagenta) and glial (orange)-enriched fractions. The solid line is for illustration purposes and not indicative that the CpG sites between sites are also methylated

UDP glycosyltransferase 8 (*UGT8*) gene encodes cerebroside synthetase, a key enzyme involved in the synthesis of myelin constituents (Bosio et al., 1996). Highly expressed in brain oligodendrocytes (Yang et al., 2019) and linked to oligodendrocyte differentiation in previous reports (Baumann and Pham-Dinh, 2001, Dugas et al., 2006), *UGT8* was reported as one of the five top-scoring candidate biomarkers for low mood in a study investigating blood biomarkers for mood disorders using convergent functional genomics (Le-Niculescu et al., 2009). *UGT8* expression was found significantly decreased in patients with MDD indicating that MDD may share common oligodendroglial abnormalities with SCZ and BPD (Aston et al., 2005). Similarly, significant decrease in expression for *UGT8* was detected in the prefrontal cortex (BA46) of schizophrenic subjects providing further evidence for disruption of sphingolipid metabolism in SCZ (Narayan et al., 2009). Furthermore, transcriptomic analysis of brain tissue isolated from mice with a genetic ablation of the key oligodendrocyte-associated myelin gene *UGT8*, recapitulated dysregulation in gene pathways related to myelination already seen in human AD brains (McKenzie et al., 2017) supporting

previous findings suggesting that AD may be associated with dysmyelination and a breakdown of oligodendrocyte-axon communication (Braak and Del Tredici, 2015, Zhang et al., 2013a).
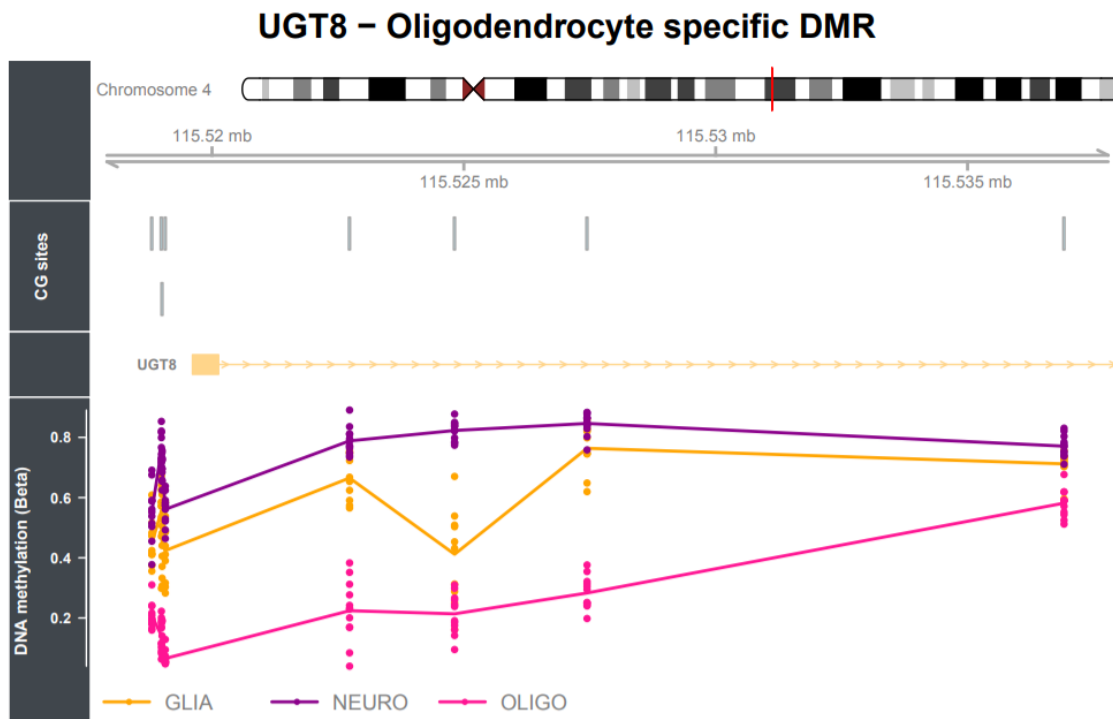
Figure 5.30 Oligodendrocyte-specific differentially methylated region (DMR) in FANS sorted nuclei from human prefrontal cortex.
This DMR, spanning eight CpG sites and located along the gene body of the oligodendrocytic marker UGT8 gene (P<9E-08), was found consistently hypomethylated in the oligo fraction (deep pink line) compared to neuronal (darkmagenta) and glial (orange)-enriched fractions. The solid line is for illustration purposes and not indicative that the CpG sites between sites are also methylated

The oligodendrocyte marker **2', 3'-cyclic nucleotide phosphodiesterase (*CNP*)** encodes for a structural protein of the myelin sheath (Janova et al., 2018). Recent data reported alterations of oligodendrocytes after experimental cerebral ischemic stroke in mice (Mages et al., 2019) where the absence of *CNP* was found to be associated with impaired cellular transport in the axonal compartment (Mages et al., 2019). *CNP* has been also suggested to promote microtubule assembly and to be firmly associated with tubulins, indicating it is functionally linked to the cytoskeleton (Bifulco et al., 2002, Esposito et al., 2008). Mice with genetic ablations of *Cnp* mimicked aspects of myelin and mitochondrial gene expression dysregulation seen in brain samples from patients with AD (McKenzie et al., 2017). Interestingly, in humans and mice, reduced expression of the

structural myelin protein *CNP* was associated with catatonic signs in SCZ cohorts, pointing to the involvement of myelin-producing oligodendrocytes in this "psychomotor" syndrome frequently observed across neuropsychiatric diseases (Janova et al., 2018).
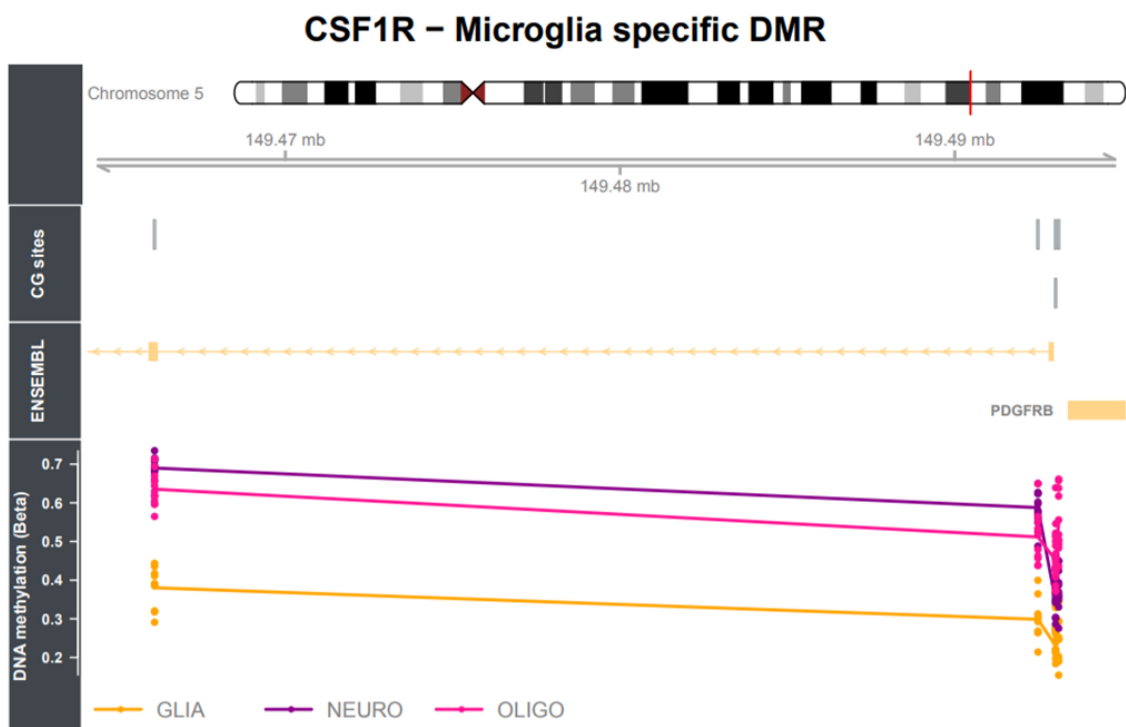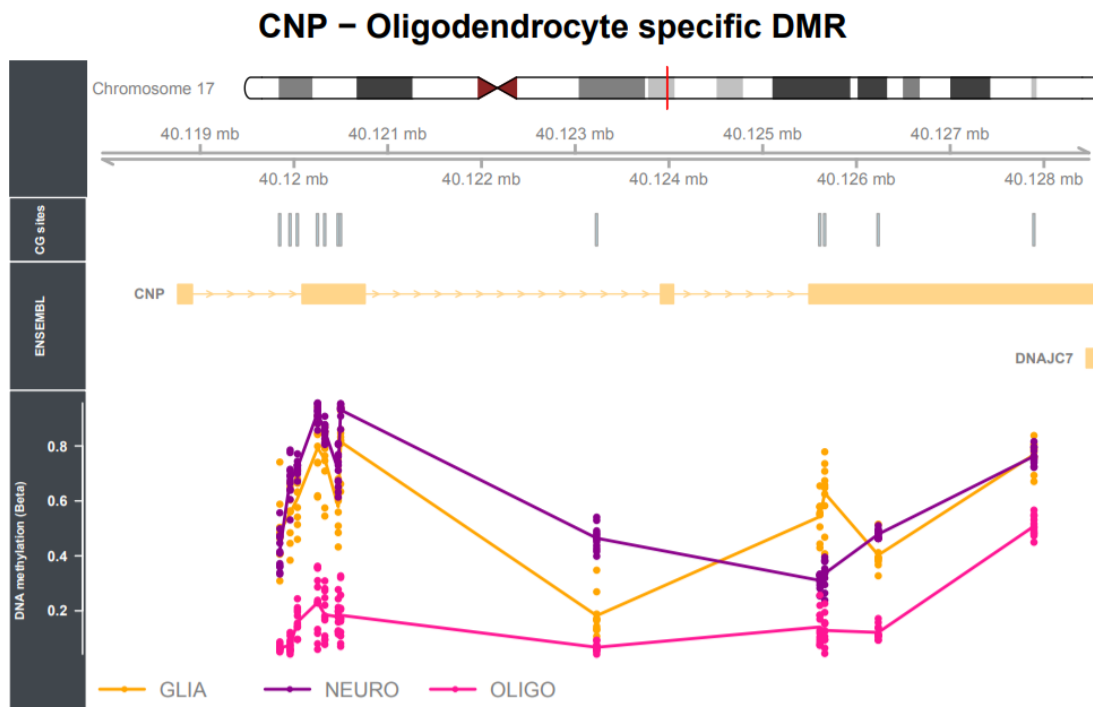

Figure 5.31 Oligodendrocyte-specific differentially methylated region (DMR) in FANS sorted nuclei from human prefrontal cortex.
This DMR, spanning 12 CpG sites and localised along the gene body of the oligodendrocytic marker CNP gene (P <9E-08), was found consistently hypomethylated in the oligo fraction (deep pink line) compared to neuronal (darkmagenta) and glial (orange)-enriched fractions. The solid line is for illustration purposes and not indicative that the CpG sites between sites are also methylated.

Iron plays many important roles in the brain, including involvement in myelination, neurotransmission and electron transfer in the respiratory chain and its transporter **Transferrin (Tf),** although mainly biosynthesized in the liver, can also be biosynthesized in the brain by oligodendrocytes predominantly (de Arriba Zerpa et al., 2000, Murakami et al., 2019). The brain-type Tf produced by oligodendrocytes reside in the cytosol and is not secreted (de Arriba Zerpa et al., 2000). The main function of oligodendrocytes is to produce myelin; on the other hand, oligodendrocytes require iron for myelination and store large amounts of ferritin-bound iron maintaining the iron homeostasis in the CNS (Koeppen, 1995). First experimental evidence indicating that *TF* gene expression correlates with

the postnatal development of oligodendrocytes in the mouse CNS dates back to the late 80's when the transient expression of Tf in oligodendrocytes which become MBP+, suggested a role for Tf in the early stages of myelinogenesis (Espinosa de los Monteros and de Vellis, 1988) later confirmed by an independent study reporting correlation of Tf expression with postnatal development of oligodendrocytes in the mouse CNS (Cassia et al., 1997). More recently, a strong body of evidence proposed Tf, together with thyroid hormones, as factors capable of favoring myelination due to the positive effects on oligodendroglial cell differentiation (Marziali et al., 2015, Marziali et al., 2016) and re-myelination in *in vitro* assays (Rosato-Siri et al., 2021). The first notion of a combined effect of apotransferrin and thyroid hormones emerged from experiments conducted in young hyperthyroid animals, which showed a seven-fold increase in the expression of Tf mRNA and precocious myelination when compared with control animals (Marziali et al., 2015). Altogether these findings provide a strong foundation to the assumption that *TF* could be a robust oligodendrocytic marker in the CNS.
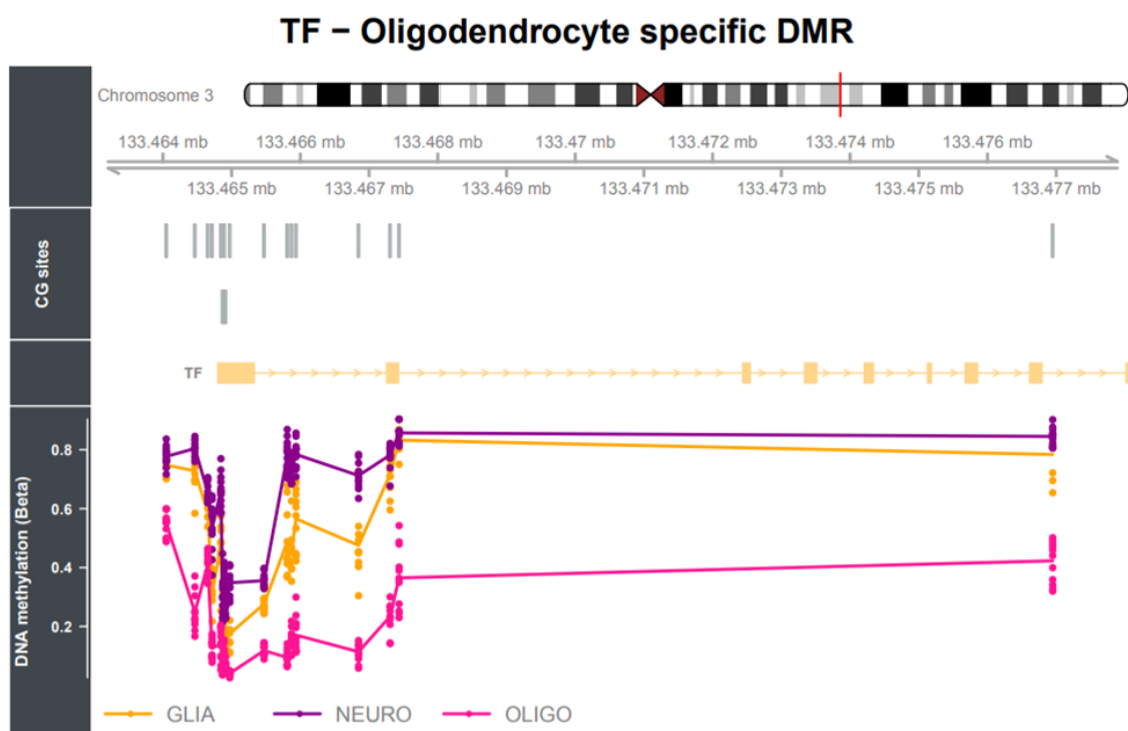
Figure 5.32 Oligodendrocyte-specific differentially methylated region (DMR) in FANS sorted nuclei from human prefrontal cortex.
This DMR, spanning 17 CpG sites and of distributed across the gene body the oligodendrocytic marker TF gene (P <9E-08), was found consistently hypomethylated in the oligo fraction (deep pink line) compared to neuronal (darkmagenta) and glial (orange)-enriched fractions. The solid line is for illustration purposes and not indicative that the CpG sites between sites are also methylated.

To summarize, the vast majority of genomic regions within genes that were known or predicted to be neuronal (e.g. *RBFOX3, ENO2, UCHL1*) oligodendrocytic (e.g. *SOX10, MBP,OLIG2*) or glial-related (e.g. *SOX9, GFAP, TMEM119*) confirmed the fractions identity based on their EPIC array DNA methylation profiles (hypomethylated hence presumably highly expressed in the cell type of election). Moreover, for the larger part of regions identified, consistency in the direction of DNA methylation levels was observed across the CpG sites constituting each ct-DMR. However, a substantial minority of known cell-type–specific genes displayed no obvious methylation preference or even showed methylation levels opposite to the expected.

5.4.4   Cell type specific DMPs in the human PFC feature in keybiological pathways

A pathway analysis was performed using the genes annotated to DMPs enriched for distinct brain cell types and that reached the EPIC significance threshold ($P <$ 9.0E-08). This stringent P value threshold was chosen to limit the number of associated genes included in the analysis in the attempt to prevent the identification of false positive pathways (refer to **Appendix G - Chapter 5, Supplementary material** for full details, only GO terms with FDR corrected P <9E-08 are reported. N<500 for neuronal-enriched pathways, N<200 for oligodendrocytes and other glia-enriched pathways). Relevant pathways of interest included 'Neuron differentiation', 'synaptic signalling' and 'neuron projection development', all of which were enriched for neuronal specific DMPs (GO:0030182, *FDR*= 3.88E-21; GO:0099536, *FDR* = 2.52E-18; GO:0031175, *FDR*=1.77E-17). Whereas, 'positive regulation of developmental process', 'axongenesis' and 'axon guidance' (GO:0051094, FDR= 4.06E-14; GO:0030424, FDR=3.81E-10; GO:0007411, FDR= 2.47E-06) were significant pathways enriched for oligodendrocyte-specific DMPs. In the double negative nuclei fraction (other glia cells), biological processes such as 'immune response', 'regulation of cell communication' and 'regulated exocytosis' (GO:0006955, FDR=7.57E-28; GO:0010646, FDR=6.72E-21; GO:0045055, FDR=1.85E-13) were the most represented in line with the biological roles played by microglia and astrocyte in the brain.

In order to summarise and facilitate the interpretation of the pathway analysis results, each cell type specific GO terms list was submitted separately to the web server Revigo (see Methods for details) which by using a simple clustering algorithm allowed to 1) investigate the relationship and interdependency among significant pathways within each cell type, 2) remove redundant GO terms and 3) find a representative subset of the terms. **Figure 5.33, Figure 5.34** and **Figure 5.35** report the output figures (network plots) generated by the web tool for neuronal, oligodendrocyte and other glia specific biological pathways respectively. Once again, the results aligned with the known functions of the predicted cell type further confirming the cellular identity of each sorted fraction. While '*signalling'*, '*cell communication'* and 'neurogenesis' were the most representative GO terms in the neuronal nuclei population, '*regulation of signalling*' and '*developmental processes*' distinguished the oligodendrocyte fraction. '*Regulation of response to stimulus'*, '*immune response*' and '*cell activation*' were instead the cluster representatives for the other glial cells (nuclei fraction which is presumed to be primarily constituted of astrocyte and microglia).
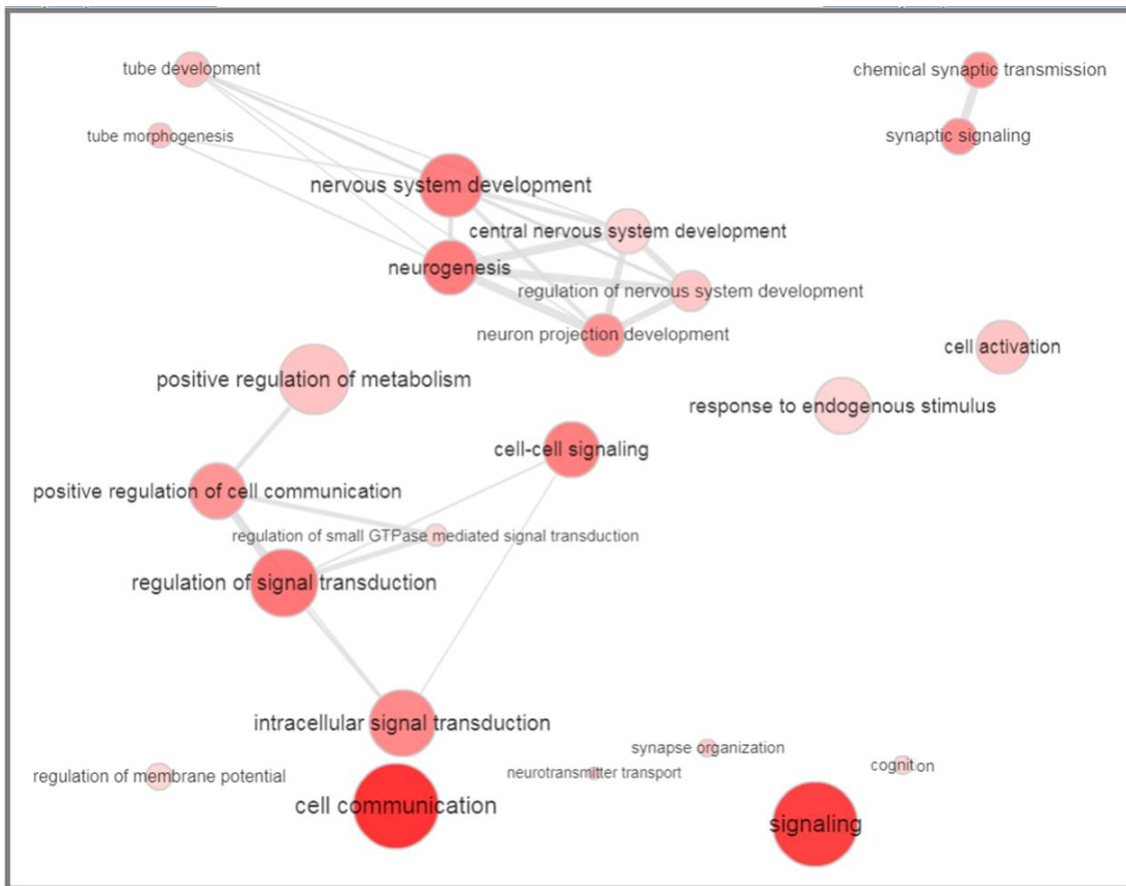
Figure 5.33 Pathways enrichment in neuronal-enriched nuclei fractions.
Significant biological pathways (P≤9.E-08) from GO enrichment analysis were selected and uploaded into the REVIGO algorithm (http://revigo.irb.hr/) in order to identify network of pathways, their representation levels (recurrence) and their relation to one another. Highly similar GO terms are linked by edges in the graph, where the line width indicates the degree of similarity. The initial placement of the nodes is determined by a 'force-directed' layout algorithm that aims to keep the more similar nodes closer together.
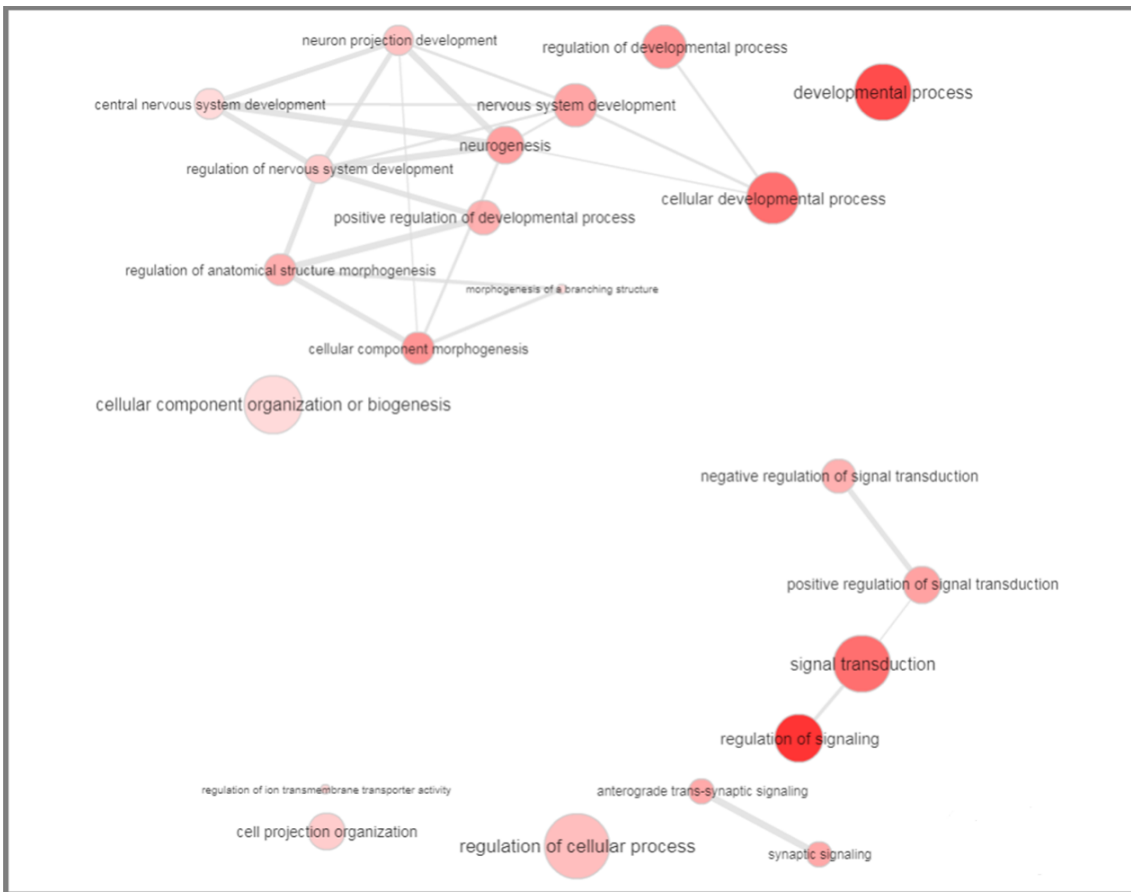
Figure 5.34 Pathway analysis results oligodendrocyte-enriched nuclei fractions.
Highly similar GO terms are linked by edges in the graph, where the line width indicates the degree of similarity. The initial placement of the nodes is determined by a 'force-directed' layout algorithm that aims to keep the more similar nodes closer together. Interactive plot obtained using the REVIGO algorithm (http://revigo.irb.hr/)
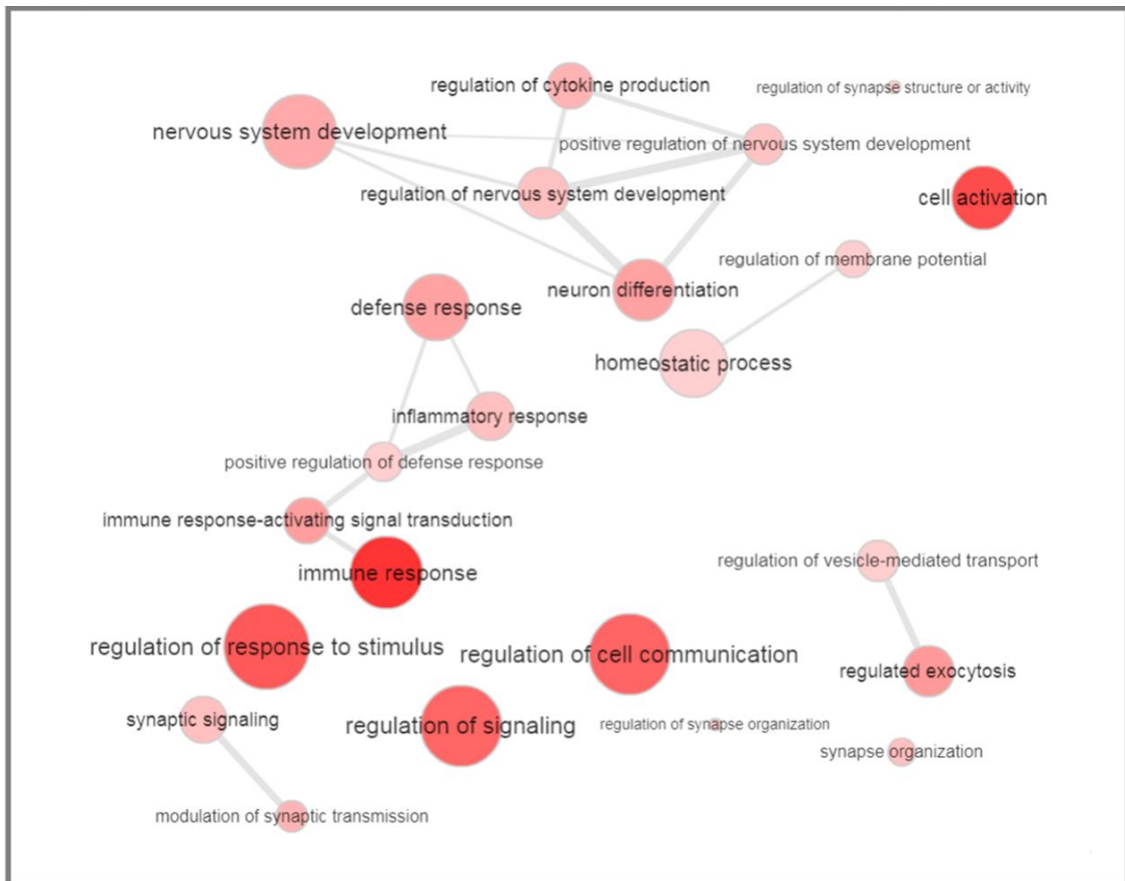
Figure 5.35 Pathway analysis results for other glia-enriched nuclei fractions.
Highly similar GO terms are linked by edges in the graph, where the line width indicates the degree of similarity. The initial placement of the nodes is determined by a 'force-directed' layout algorithm that aims to keep the more similar nodes closer together. Interactive plot obtained using the REVIGO algorithm (http://revigo.irb.hr/)

372

5.4.5 Cell-type specific differences in DNA methylation are seen across genomic features

Next, using a Fisher's exact test, the genomic location of the most significant ct-DMPs ($P < 5 \times 10^{-8}$) was compared to all nominally-significant DMPs ($P < 0.05$), in relation to genomic features that have been described by Illumina gene annotations (Homo sapiens UCSC hg19 and Hg38). Across all three cell types, most of the ct-DMPs significantly associated with cell type (t-test P<9E-08) were located at gene body (OR >1.38) and 3' UTR regions (OR> 1.12) as well as CpG shores (~2Kb from the CGI) and CpG shelves (~4Kb from the CGI) (OR> 1.50) while only very few were located at the 1st exon (OR≤ 0.57), TSS200 (OR≤ 0.57) or CpG Island (OR≤ 0.30). Also, intergenic regions were enriched in both neuronal- and oligodendrocyte- specific DMPs   (OR= 1.23 and OR=1.17 respectively) but not in other glia-specific DMPs (refer to **Table 5.6** and **Figure 5.36 and Figure 5.37** for full details).

Genomic Feature		Neuro DMPs	Oligo DMPs	Other Glia DMPs
1st Exon	OR	0.45	0.37	0.57
	P-value	0	3.82E-276	1.39E-59
3' UTR	OR	1.31	1.17	1.12
	P-value	3.85E-51	4.13E-11	4.83E-04
5' UTR	OR	1.01	1.11	1.11
	P-value	0.267	3.99E-14	5.29E-09
Gene Body	OR	1.48	1.74	1.38
	P-value	0	0	4.66E-162
ExonBnd	OR	0.89	0.97	0.88
	P-value	0.003	0.547	0.058
Intergenic regions	OR	1.23	1.17	0.99
	P-value	1.49E-225	2.26E-91	0.38
TSS1500	OR	0.87	0.66	0.80
	P-value	4.47E-49	5.58E-232	4.40E-43
TSS200	OR	0.43	0.35	0.55
	P-value	0	0	1.10E-157
CpG Island	OR	0.27	0.24	0.30
	P-value	0	0	0
N-shelf	OR	1.63	1.90	1.56
	P-value	5.92E-205	3.02E-203	2.07E-57
N-shore	OR	1.70	1.59	1.53
	P-value	0	2.21E-202	4.20E-105
S-shelf	OR	1.64	1.89	1.51
	P-value	5.75E-209	1.15E-198	9.72E-49
S-shore	OR	1.68	1.55	1.68
	P-value	0	4.77E-172	1.97E-153

Table 5.6 Fisher's Exact test results for cell-type specific DMPs enrichment in genomic features.
The Illumina EPIC manifest was used to annotate individual ct-DMPs and a P-value≤ 9E-08 was chosen as threshold to identify DMPs strongly associated with cell type relative to all tested probes. P-value is reported as 0 for those features where the P-value is extremely small. When odds ratio (OR) is 1 there is no association between the ct-DMPs and the genomic feature. If OR < 1 the genomic feature is under-represented, if OR >1 is over-represented. Comparison of the OR reveals that 1st Exon and CpG islands are under-represented across all cell types while gene body and non-CGIgenomic features are equally over-represented across all three cell types.
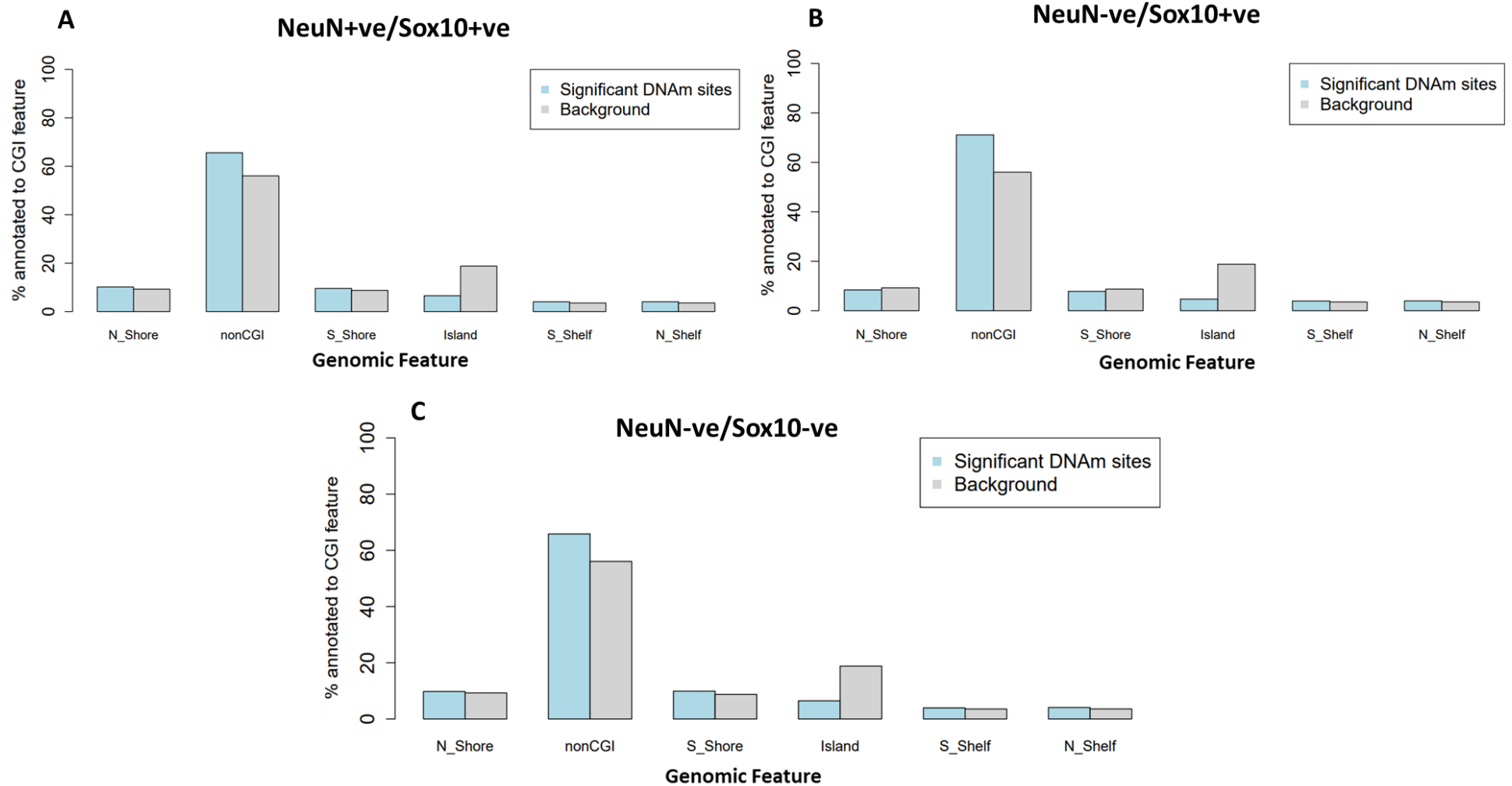
Figure 5.36 Barplot showing the distribution of significant DMPs (P<9E-08) compared to the background (all DMPs, significant and not) across CGI features while comparing the three cell types using a Fisher' Exact test.
An enrichment can be observed in non-CGI genomic features when compared to the background across all three cell types A) NeuN+ve/Sox10+ve (neuronal enriched nuclei), B) NeuN-ve/Sox10+ve oligodendrocytes enriched nuclei and C) NeuN-ve/Sox10-ve (other glia enriched nuclei). CGI, CpG-island, DNAm, DNA methylation.
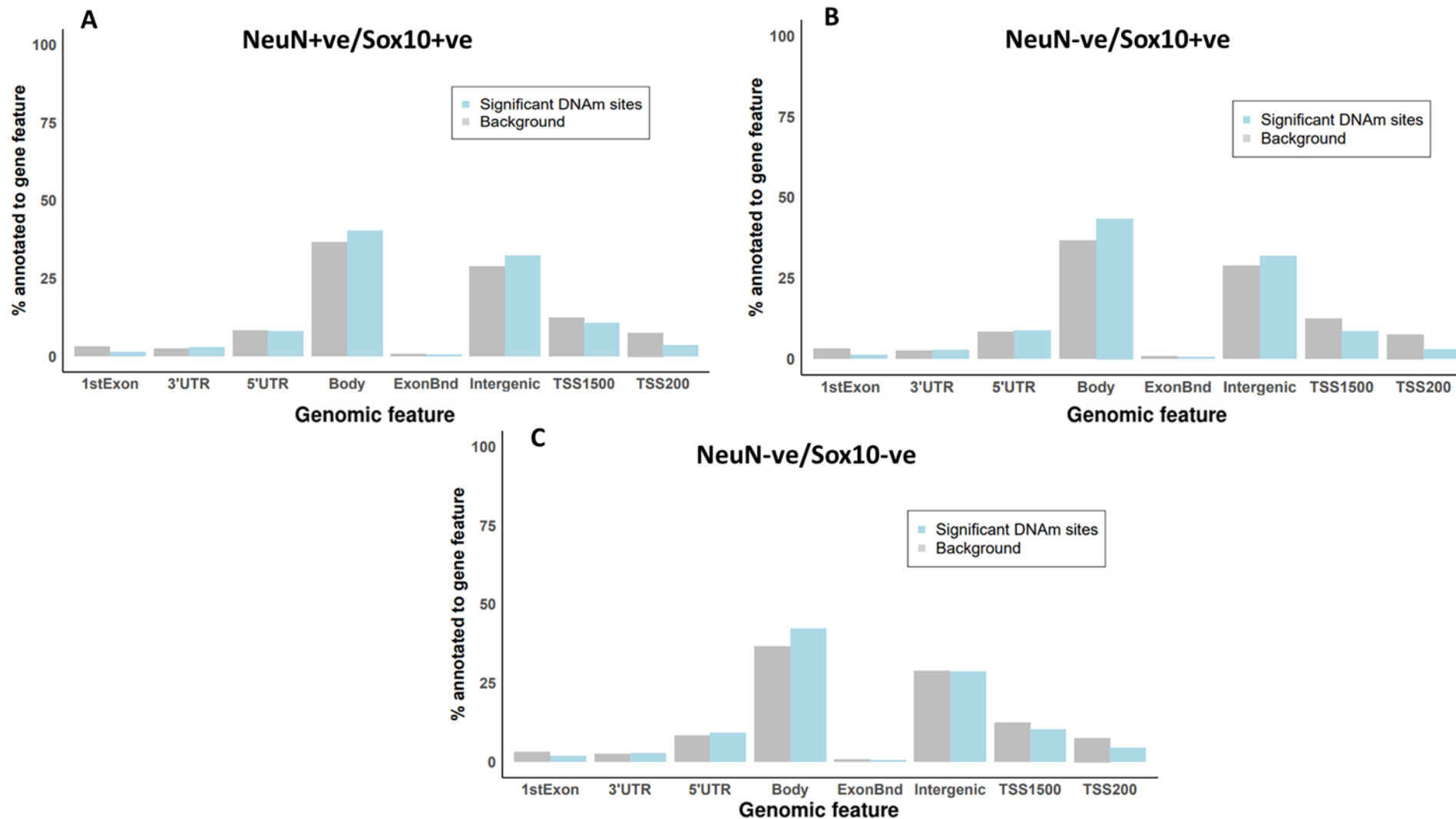
Figure 5.37 Barplot showing the distribution of significant DMPs (P<9E-08) compared to the background (all DMPs, significant and not) across non CGI genomic features while comparing the three cell types using a Fisher' Exact test.

An enrichment can be observed at gene body when compared to the background across all three cell types (A-C), while Intergenic regions are more represented in the NeuN+ve/Sox10+ve (A) and NeuN-ve/Sox10+ve populations (B) only. A) NeuN+ve/Sox10+ve (neuronal enriched nuclei), B) NeuN-ve/Sox10+ve oligodendrocytes enriched nuclei and C) NeuN-ve/Sox10-ve (other glia enriched nuclei). CGI, CpG-island, DNAm, DNA methylation.

The distribution of the genomic annotations was also investigated in relation to ct-DMRs using the Chipseeker package which annotates the location of each given DMR in terms of genomic features. **Figure 5.38** displays the distribution of ct-DMRs across genomic features. Results showed how ct-DMRsare predominately distributed in close promixity of promoter regions (≤ 1Kb) more so for the double negative population (microglia and astrocytes predominantly) (51.99%)   followed by i) 'distal intergenic regions' which was slightly more represented in neuronal specific DMRs (12.96% NeuN+ve/Sox10+ve vs 9.87% NeuN-ve/Sox10+ve) and ii) 'other introns' sligthly more represented in the oligodendrocyte-specific DMRs (14.3% NeuN-ve/Sox10+ve vs 12.35% NeuN+ve/Sox10+ve and 11.26% NeuN-ve/Sox10-ve).

A *NeuN+ve/Sox10+ve* specific DMRs

- Promoter (1−2kb) (8.29%)
- Promoter (2−3kb) (4.17%)
- Promoter (<=1kb) (46.5%)
- 5' UTR (0.38%)
- 3' UTR (2.99%)
- 1st Exon (1.58%)
- Other Exon (3.5%)
- 1st Intron (6.61%)
- Other Intron (12.35%)
- Downstream (<=300) (0.68%)
- Distal Intergenic (12.96%)

B *NeuN-ve/Sox10+ve* specific DMRs

- Promoter (1−2kb) (8.43%)
- Promoter (2−3kb) (4.34%)
- Promoter (<=1kb) (46.72%)
- 5' UTR (0.46%)
- 3' UTR (3.19%)
- 1st Exon (1.56%)
- Other Exon (2.74%)
- 1st Intron (7.88%)
- Other Intron (14.3%)
- Downstream (<=300) (0.52%)
- Distal Intergenic (9.87%)

C *NeuN-ve/Sox10-ve* specific DMRs

- Promoter (1−2kb) (7.79%)
- Promoter (2−3kb) (4.12%)
- Promoter (<=1kb) (51.99%)
- 5' UTR (0.2%)
- 3' UTR (2.75%)
- 1st Exon (1.54%)
- Other Exon (2.97%)
- 1st Intron (6.25%)
- Other Intron (11.26%)
- Downstream (<=300) (0.53%)
- Distal Intergenic (10.62%)

Figure 5.38 Distribution of ct-DMRs across genomic features.
The 'TxDb.Hsapiens.UCSC.hg38.knownGene' package (made from resources at UCSC and based on the hg38 genome based on the knownGene table) was used to annotate the ct-DMRs. Hence genomic features differs from those investigated for ct-DMPs enrichment. The ct-DMRs distribution across the genome were examined and the majority of the features were identified within the promoter region (≤ 1Kb) across all three cell types, consistent with the regulatory role of DNA methylation in cell-type specific gene regulation. DMR, differentially methylated regions; Kb. Kilobase.

5.5 Discussion

This data chapter is the product of the direct application of the improved FANS protocol profusely described in **Chapter 4** of this thesis proving its utility and efficacy for studies in cryopreserved bulk brain.

Post-mortem human prefrontal cortex specimens (N=12) were processed by fluorescence-assisted isolation of immunolabelled nuclei using a combined staining of NeuN-(RBFOX3-) and SOX10-specific antibodies to profile DNA methylation in purified neuronal, oligodendrocyte and other glial nuclei populations. NeuN has been considered a reliable marker of mature neurons for the past two decades despite the presence of distinct neuronal cell-types (such as cerebellar Purkinje cells, olfactory bulb mitral cells and retinal photoreceptor cells) which do not express NeuN and it has been extensively used for FANS applications in more recent years (Price et al., 2019, Yu et al., 2015b, Tansey and Hill, 2018, Kozlenkov et al., 2017, Gasparoni et al., 2018). SOX10 was reported in a recent study investigating the link between child abuse and suicide where it was employed to successfully enable the isolation of mature oligodendrocytes by FANS (Lutz et al., 2017b). The implementation of this method provided accurate separation of multiple neural cell types, allowing us to capture additional molecular features.

Recent data have highlighted the complex interplay between disease, age and cell-type-specific methylation levels (Gasparoni et al., 2018, Kozlenkov et al., 2014, Montano et al., 2013, Lutz et al., 2017b), reinforcing the relevance of this approach in offering new perspectives for the validation and interpretation of large EWAS results. A conventional whole tissue-based screen of unsorted cortical tissue comes with a low detection power and consequently a minimal number of epigenetic markers which mostly do not overlap with other large EWAS studies. Furthermore, diametric methylation changes in the major cell-types of the brain could not be detected in bulk brain tissue screens but rather were interpreted as changes in cell proportions. Hence confounding results due to cellular heterogeneity represents one of the foremost challenges EWASs are currently facing. Statistical methods leveraging the tissue-specificity of DNA methylation for the deconvolution of the cellular mixture in heterogeneous biospecimens offer a promising solution (Zeng et al., 2019, Koestler et al., 2016, Guintivano et al.,

2013), however the performance of such methods is variable and their accuracy is an ongoing debate (Titus et al., 2017).

This systematic cell-type-specific DNA methylation profiling on a pilot cohort of human post-mortem brain samples across three cell types has proved that cell sorting strongly enhances the detection of DNA methylation markers and allows a deep insight into cell-type-specific dynamics. In line with recently published data (Guintivano et al., 2013, Kozlenkov et al., 2014, Gasparoni et al., 2018, Lutz et al., 2017b) thousands of robust methylation differences were found between the neuronal, oligodendrocytic and glial fractions. Furthermore, the sets of neuron-specific and non–neuron-specific genes derived from differential methylation data showed excellent agreement with the available direct measurements of gene expression in human and mouse (Lutz et al., 2017b, Kozlenkov et al., 2014, Krishnaswami et al., 2016, Ruzicka B.W. et al., 2020), suggesting that differential methylation is a robust predictor of cell-type–specific gene expression. These findings are expected to be important in guiding future research aiming to investigate the role of DNA methylation in shaping specific cellular identities.

5.5.1 Samples quality control

Sample quality control was an essential step of the data pre-processing. It allowed to verify the performance of the nuclei sorting procedure confirming the sorting purity as well as revealing technical issues or the significant inter-individual variability in terms of abundancy/scarcity of cell types which otherwise could be interpreted as failure of the experimental set up. Not surprisingly, some differences were detected across tested variables and DNA methylation between female and male samples (e.g. miAge) which is in line with the body of evidence suggesting variability associated with sex (Grimm et al., 2019, Iurato et al., 2017, Conradt et al., 2019, Davegardh et al., 2019) .

5.5.2 FANS –purified nuclei fractions differ in DNA methylation profiles

Profiling of DNA methylation at the resolution of individual CpG sites in purified cell types enabled the detection of unexplored intra-individual variability inevitably overlooked when using bulk tissue. However, the accuracy of the screening remains limited to the probe coverage offered the by the pre-customised EPIC array which might explain the discordance between cell type marker genes and

DNA methylation status observed at given DMPs (see results section 5.4.2) . The profiling at CpG sites level across the purified fractions, also revealed similarities in DNA methylation patterns between cell types which offered insights to speculate about the function and role played simultaneously by different cell populations. Furthermore, the inclusion of the unsorted nuclei ("total" fraction) in the comparison for every specimen included in the analysis operated as proof of concept by a) confirming that changes occurring in individual cell type are likely to be masked in bulk tissue analysis b) providing evidence for cell type differential abundance across individuals (in those brain specimens where the total nuclei population was composed of neuronal cells predominately or lacked of the double negative fraction, the unsorted fraction showed a DNA methylation profile similar to the most represented cell type in that given sample). In regard to the analysis of the ct-DMRs, some of the genes explored showed no consistent pattern of differential methylation across the gene locus, suggesting that cell-specific gene expression of these markers might be determined by a combination of regulatory elements localized beyond the profiled genomic region. Additionally, the limited distribution of probes provided by the EPIC array might, once again, have played a role in this apparent lack of consistency observed in the regional analysis results.

5.5.3 Cell type specific DMPs in the human PFC feature in key biological pathways

The pathway analysis performed in each cell type separately revealed some degree of overlap in highly significant biological functions/ GO terms recurring in more than one cell type. This should not be surprising since, as previously discussed, even those cell populations identified through antibody immuno-tagging are likely to be heterogeneous and comprehensive of various cell subtypes and minor contamination from other purified nuclei fractions cannot be excluded. Furthermore, it is well documented the functional redundancy of different cell types in the brain which often complement each other in executing complex regulatory functions during CNS development as well as neuropathology of a diverse array of disorders (Hammond et al., 2018, Kessaris et al., 2006, Solga et al., 2015).

5.5.4 Modest enrichment of cell type-specific differences in DNA methylation is seen across gene features

The gene features distribution analysis revealed the absence of remarkable cell type-specific differences rather, an enrichment of similar extent was detected for some gene features (e.g. gene body and non-CGI features) across all three cell types investigated. Similarly, a prevalence of ct-DMRs in promoter regions was measured in each of the three fractions profiled (see Results section 5.4.5). This should not surprise since epigenetic changes at promoter regions are known to be regulatory in nature and therefore not expected to be different across cell types rather, different genes are likely to be epigenetically regulated in a similar manner in different cell types according to their biological function.

5.5.5 Study caveats

There are several limitations that comes with this work. Firstly, the modest number of samples processed and considered in the analysis which causes this study to be underpowered for the detection of subtle DNA methylation differences (<5%) between cell types. Secondly, only two nuclear markers, specific for neurons and oligodendrocytes, were adopted for the cell sorting, hence the actual cellular composition of the double negative fraction cannot be ruled out. Even within the immunolabelled populations, heterogeneity due to diverse cell subtypes cannot be excluded as well as minor contamination of other cell types within the purified fractions. Third, only one epigenetic marker, DNA methylation, has been the focus of this pilot study although it is well known the interplay between different epigenetic modifications which could ultimately counteract the effect of DNA methylation on gene expression. Additionally, classic bisulfite conversion chemistry that is known to be masked for 5mC and 5hmC was used to enable the quantification of DNA methylation across the genome. 5hmC has been shown to be enriched in the brain, particularly in synaptic genes (Khare et al., 2012) suggesting its preferential impact on the neuronal component of the brain. 5hmC is found at different levels across different brain regions (Lunnon et al., 2016), and is altered during brain development (Spiers et al., 2017). Recent studies have also demonstrated that 5hmC and 5mC have opposing effects on gene expression (Sherwani and Khan, 2015). The classic bisulfite chemistry converts unmodified cytosines to uracil whilst both 5mC (DNA methylation) and 5hmC (DNA hydroxymethylation) are protected from the conversion.

This approach cannot differentiate between DNA methylation and hydroxymethylation (Kernaleguen et al., 2018) and given the relatively high abundance of 5hmC in the brain this may represent a major confounder in DNA methylation analyses. Oxidative bisulfite treatment is one effective method enabling the quantitative mapping of 5mC in the absence of confounding by 5hmC in genomic DNA at single-nucleotide resolution (Slynko and Benner, 2019). Aside from that, post-mortem specimen obtained from two distinct brain collection (BDR and KCL) were included in the study and individuals were not matched for age and sex which inevitably introduced unwanted variability into the dataset. However, I did control for these confounding factors during the QC analyses and they did not seem to significantly impact the results. Studies have shown that cell-type-specific DMPs can emerge or vanish over a lifetime (Gasparoni et al., 2018) suggesting that besides cell composition, age represents a complex confounding parameter in tissues-based EWAS. Such phenomena require strong attention particularly when using cell-type-specific data as references for calculation of cell-type proportions and adjustments. As highlighted elsewhere, this procedure could be problematic if the reference and samples have a different age distribution since the tool could potentially select discriminative markers that have diverse aging dynamics (Gasparoni et al., 2018).

5.5.6 Future directions

Future work should aim to apply this same pipeline on a much wider cohort of post-mortem brain samples in order to burst the power of detection. Ideally, comparing matched cohorts of psychiatric cases and controls would provide valuable insights into the molecular changes characterising the brain in health and disease. By adopting this same experimental protocol, ongoing work in my group aims to profile genomic variation across multiple epigenetic signatures (DNA methylation, DNA hydroxymethylation, chromatin accessibility) in a broad cohort (N>100) of SCZ samples and healthy controls sourced from multiple US and UK brain collections. Additional sorting of neuronal fractions into subpopulations such as dopaminergic, glutamatergic and GABAergic neurons or glial subtypes (astrocytes and microglia) could further enhance the sensitivity of such screens. Indeed combined FACS separation with NeuN and Sox6

antibodies has been shown to effectively separate glutamatergic and GABAergic neurons from mice brains and allowed to identify additional neuronal epigenetic differences (Kozlenkov et al., 2016). However, to date, no other studies have replicated these findings in mice and Sox6 has not been validated for post-mortem human tissues probes. An alternative approach is to dissect the nature of heterogeneity by single nuclei analyses (Welch et al., 2019, Del-Aguila et al., 2019, Gaublomme et al., 2019) as well as RNA imaging using fluorescent in situ hybridization (RNA-FISH) which can provide quantitative information on mRNA abundance and localization at both the single cell and subcellular levels (Soler et al., 2017, Nguyen et al., 2016, Arrigucci et al., 2017). Such promising approaches are still not in a robust state for large-scale comparative studies on challenging post-mortem material. However, the speed at which the field is growing and gaining attention suggests rapid improvements of these platforms will be possible in a very near future.

5.6 Conclusion

The work described in this chapter demonstrates that it is possible to maximise the amount of data obtained from valuable specimens that have often undergone long and complex handling procedures and the tissue quality of each is therefore often compromised. Substantial differences in DNA methylation were detected at both genome-wide level and in cell-type specific markers proving the need for cell separation in methylomic screens of disease tissue. Here I showed that cell sorting strongly enhances the robust detection of cell type-related DNA methylation differences even in a relatively small cohort. Numerous genes with cell-type-specific methylation signatures and documenting differential methylation dynamics associated with cellular phenotype were identified. A comparison of FANS-based EWAS studies with previous tissue-based EWAS could help validating disease associated DNA methylation signals and additionally specifies their cell type origin. Even a relatively small cohort has the potential to allow the identification of novel differences in DNA methylation between cases and controls and assign known disease-associated epigenetic signals to specific cell populations. Deciphering the epigenome in normal cell types is essential to improve our understanding of the epigenetic basis of human

brain functioning. In comparison to their diseased counterparts, cells in physiological state contribute to our understanding of the mechanisms involved during disease development, and can reveal the particular cell type/s driving psychiatric and/or brain-related diseases which are still often unknown. A deep understanding of the heterogeneity present in the human CNS in both health and disease is key to enhance the development of therapeutic approaches for psychiatric diseases. The data and findings presented in this thesis are expected to serve as valuable resource for further study of cell-type–specific epigenetic marks and to enable new discoveries about the role of brain epigenetics in health and disease opening new promising avenues for basic and clinical research into mental illness. Lastly, sorting for major cell-types could enable systematic EWAS with the need of less samples compared to common tissue-based screens reducing time, costs and manual labour. This pilot study highlights cell-type composition as one of the major confounding factors in complex tissue analyses and strongly recommends to conduct EWAS on sorted cell types.

Chapter 6 - Differential microRNA expression in the prefrontal cortex of suicide completers

6.1 Introduction

Mental disorders such as schizophrenia (SCZ) and major depressive disorder (MDD) are associated with a reduced life expectancy and constitute a major risk factor for suicide, a leading cause of mortality among young people in developed countries. The risk for suicidal acts is multifactorial, including a range of biological, psychiatric, psychosocial and cultural risk factors (Murphy et al., 2017). Despite the associated costs and burden for the public health, the aetiology of mental health disorders leading to suicide as well as the molecular pathology of suicidality itself remain poorly understood. The increasing understanding about the complexity of the genome has led to recognise the crucial role for epigenetic variation in human health and disease (Consortium, 2012). By acting through heritable, but potentially reversible changes, epigenetic processes have shown to mediate associations between genetic risk burden, environmental risk exposure and phenotype (Siegmund et al., 2007, Viana et al., 2017).

Genes can be regulated at the transcriptional and post-transcriptional level through the activity of many non-coding RNA (ncRNA) transcripts that act to fine-tune gene expression patterns (Esteller, 2011). Small ncRNAs, among which the best characterised are miRNAs, regulate the transcription of mRNAs and participate in alternative splicing and epigenetic modifications such as chromatin remodelling and RNA editing (Mehler and Mattick, 2007, Taft et al., 2010). These regulatory functions can target either neighbouring transcripts ('cis') or loci that are distant from their own transcription site ('trans'). Collectively, ncRNAs constitute a unique layer of gene regulation where they function as key intermediate regulators in conveying the message from genotype to phenotype states (Sumazin et al., 2011).

Since several of their biological functions have been revealed, another class of epigenetic modifiers, long noncoding RNAs (lncRNAs), has been gaining attention in the study of psychiatric disorders (Kocerha et al., 2015). LncRNAs participate in chromatin modifications (Bohmdorfer and Wierzbicki, 2015, Han and Chang, 2015); act as 'sponges' that prevent miRNA functions (Du et al., 2016); act as scaffolds that provide docking sites for proteins (Guttman and Rinn, 2012); serve as activators and suppressors of mRNA transcription and act as regulators of splicing patterns (Gong and Maquat, 2011). In terms of functions in the brain, lncRNAs have been strongly related to brain development (Shi et al.,

2017) and found to participate in spatiotemporal regulation of proliferation and differentiation of pluripotent stem cells (Ng et al., 2012, Belgard et al., 2011). High-resolution and high-throughput technologies, such as microarray and RNA-sequencing, have helped in examining the number and patterns of lncRNA expression in the brain. Clustering analysis revealed that lncRNAs have a tissue-specific expression pattern (Cabili et al., 2011, Derrien et al., 2012). Additionally, a study using microarray analysis, investigated differential lncRNA expression in the temporal cortex ranging from infancy to adulthood and concluded that the expression pattern of lncRNA changes with age (Lipovich et al., 2014). Four studies have shown a relationship between SB and changes in lncRNA expression levels. Of them, three explored lncRNA expression in the brain (Zhou et al., 2018, Punzi et al., 2014, Punzi et al., 2019) suggesting suicide-associated altered expression of lncRNA targeting genes functionally related to purinergic signalling (Punzi et al., 2019) and interferon signalling (Zhou et al., 2018), the latter known for playing a key role in CNS homeostasis and in psychiatric disorders (Mostafavi et al., 2014). Thus, by understanding the full spectrum of epigenetic modifications across the genome, we can advance our knowledge of the molecular pathology of suicidality and ultimately elucidate early biomarkers and therapeutic targets of action.

The variety and vast gene-regulatory capacity of miRNAs are particularly valuable in the brain, being a very complex organ with functional specialisation of diverse neural cells highly adaptable to environmental stimuli. Literature reveals that 70% of known miRNAs are expressed in the brain (Fineberg et al., 2009, Kadakkuzha et al., 2015) and their expression has been found to be brain region- and cell type-specific (Lau et al., 2008, Mercer et al., 2010, Natera-Naranjo et al., 2010, Ponjavic et al., 2009). By expressing more distinct miRNAs than any other tissues (Adlakha and Saini, 2014) and with the increasing variety of miRNAs being identified in the brain, a clear connection between the biogenesis, dynamics of action and regulatory potential of miRNAs and the complexity of the brain becomes apparent (Fineberg et al., 2009). A plethora of evidence suggest that the ability of miRNAs to regulate several genes within a pathway or even multiple cross-talking pathways has a significant impact on complex regulatory networks and ultimately physiological processes and diseases (Wright et al., 2018, Yoshino and Dwivedi, 2020).

Several studies have shown the role of ncRNAs in brain evolution, development, homeostasis, stress response, and neuroplasticity and miRNA-mediated, brain functional changes are evident in cognition, inflammation, neuroprotection, lipid metabolism, mitochondrial function and lifespan (Mercer et al., 2010, Bernard et al., 2010, Bond et al., 2009, Ng et al., 2012, Qureshi and Mehler, 2013, Rani et al., 2016). Dysregulation of brain-enriched miRNAs contributes to accelerated cognitive decline and increased neurological disorders (Danka Mohammed et al., 2017). The importance of miRNA in brain development and neuroplasticity has been well-established (Xin et al., 2017, Nowakowski et al., 2018, Ma et al., 2019, Gizak et al., 2020). Abnormal expression and dysfunction of miRNAs are known to be involved in neurodegenerative phenotype of AD, PD and ALS (Ferrante and Conti, 2017, Kocerha et al., 2015, Sartor et al., 2012) as well as in the pathophysiology of many neuropsychiatric diseases including SCZ, MDD, and BPD (Cao and Zhen, 2018, Salta and De Strooper, 2012, Briggs et al., 2015, Qureshi and Mehler, 2013).

More recently, the role of miRNAs in suicidality has been postulated (Punzi et al., 2019, Wang et al., 2018a, Cui et al., 2017) suggesting the potential of studying miRNAs to better understand molecular processes associated with SB and provide valuable information for the development of diagnostic tools and successful therapeutic interventions for suicide prevention. Population-based studies have explored the expression changes of lncRNA and miRNA among psychiatric patients who have history of SI (Belzeaux et al., 2019, Kuang et al., 2018). Some post-mortem brain studies have also explored suicide-associated ncRNAs and interestingly, both lncRNAs and miRNAs were specifically changed in psychiatric patients who died by suicide even though the sample size and number of these studies are limited (Yoshino and Dwivedi, 2020). Although the role of miRNAs remains not well understood in its link to MDD leading to SB (Pompili et al., 2013), post-mortem brain studies have provided critical information regarding completed suicide, which may help explaining the molecular changes happening in the brain under such conditions (Roy et al., 2020). Using the TaqMan Array miRNA card which profiles 384 miRNAs in one assay, miRNA expression levels were examined in BA9 of 18 MDD suicide cases and 17 non-psychiatric control subjects (Smalheiser et al., 2012). The authors reported a global downregulation of miRNAs in MDD subjects and significant downregulation was detected in 21 miRNAs many of which had overlapping

mRNAs targets e.g. included ubiquitin ligases, *CAMK2G,* splicing factor *NOVA1*, and the GABA-A receptor subunit *GABRA4*. DNMT3b was another protein that was found to be targeted and further validated (Smalheiser et al., 2012). *DNMT3B* is a key gene in epigenetic modifications and has been found involved in MDD pathophysiology (Higuchi et al., 2011). A different study assessed miRNA expression in the synaptosome of BA10 from a cohort of 18 suicide subjects across SCZ, MDD, BPD, and control subjects (Smalheiser et al., 2014). Based on significance values, miR-152 was found to be strongly associated with suicide (Smalheiser et al., 2014). Maussion et al. examined differences in miRNA expression levels in BA10 from 38 suicide subjects across SCZ, MDD, BPD, and control subjects. miR-185 and miR-491-3p were found to be upregulated in suicide subjects compared to control subjects (Maussion et al., 2012). In the attempt to assess the regulation of pro-inflammatory cytokine genes in SB, the relationship between TNF-α and its regulatory miRNAs was examined in a more recent study (Wang et al., 2018a). The authors found an increased expression of miR-19a-3p in BA46 of MDD individuals who had died by suicide and suggested that miR-19a-3p may be involved in cytokine dysregulation in suicidal individuals. Recently, changes in miRNA expression levels were also explored in the locus coeruleus (LC) of MDD suicide subjects (Roy et al., 2017b). A total of 10 upregulated and 3 downregulated miRNAs were detected in these subjects (Roy et al., 2017b). Lastly, Maheu et al. examined glial cell line-derived neurotrophic factor in MDD suicide subjects and found an isoform-specific decrease in GDNF family receptor alpha 1 (*GFRA1*) mRNA, which was associated with lower GFRα1a protein levels in basolateral amygdala. They found upregulation in several miRNAs that may target *GFRA1* gene one of which was miR-511 (Maheu et al., 2015). Under the condition of miR-511 overexpression in NPCs, the authours observed that protein expression of GFRα1 was significantly decreased and concluded that GFRα1 is regulated by miR-511 and may be associated with suicidality (Maheu et al., 2015). Altogether, the results are encouraging and need further exploration in order to understand the precise role of miRNA in regulatory mechanisms that can be involved in the pathogenesis of suicidality.

Over the past few years, early life stress (ELS) has been established as a major risk factor for MDD and SB along with other psychiatric illnesses in adulthood (Syed and Nemeroff, 2017). Indeed, early life is a sensitive time period for brain development and childhood environment can have a profound impact on brain

structure and function. Epigenetic mechanisms have been shown to play a critical role in adaptive and maladaptive processes by regulating gene expression without changing the genome (Allen and Dwivedi, 2020). In a broader context, stress triggers a host of biological responses including neurochemical cascades in HPA axis (Whitnall, 1993) and immune reactions (Fagundes et al., 2013), which can subsequently alter neuronal connectivity and signalling (Arnsten, 2015) as well as brain matter density (Ansell et al., 2012). In resilient adults, chronic stress promotes adaptation over time through dendritic remodelling in the hippocampus, amygdala, and PFC (McEwen et al., 2015), yet in the case of susceptible individuals, these adaptive changes may not be reversible after stress is removed (McEwen et al., 2016). In order to execute these changes, the environment interacts with gene function through epigenetic modifications without directly affecting the genome itself (Burns et al., 2018). These changes have all been identified in patients with MDD and suicide completers (see (Roy and Dwivedi, 2018, Nestler, 2014) for comprehensive a review). Due to the role in neuronal development and brain physiology (Serafini et al., 2012) miRNAs have become strong candidates for the study of psychiatric disorders affected by ELS (Bai et al., 2012, O'Connor et al., 2013, Kocerha et al., 2015, Roy et al., 2017a). Several studies have shown changes in miRNA expression in the brain of depressed-suicide individuals (Roy et al., 2017a, Smalheiser et al., 2012, Lopez et al., 2017). Specifically, miR-497 (Smalheiser et al., 2012), 146b-5p (Lopez et al., 2017), and 330-3p (Roy et al., 2017b) have all been reported in both depressed-suicide victims and healthy individuals with ELS history (Cattane et al., 2019). Further studies will be necessary to concretely link miRNA expression changes to both ELS experience and suicide or SI. **Figure 6.1** offer a schematic overview of one of the postulated mechanisms through which ncRNAs might impact on mental illness and related phenotypes. Risk factors for mental illnesses include ELS, current or recurrent life events that along with gene-environment interaction can lead to epigenetic modifications mediated by ncRNAs. These modifications give rise to changes at cellular and/or molecular levels, which can subsequently alter neural circuitry culminating in neuropathology. Phenotypic changes can also arise from circuitry changes that can mediate the development of psychiatric illnesses and SB which could be a manifestation of psychiatric illnesses or may be independent from them (Yoshino and Dwivedi, 2020).
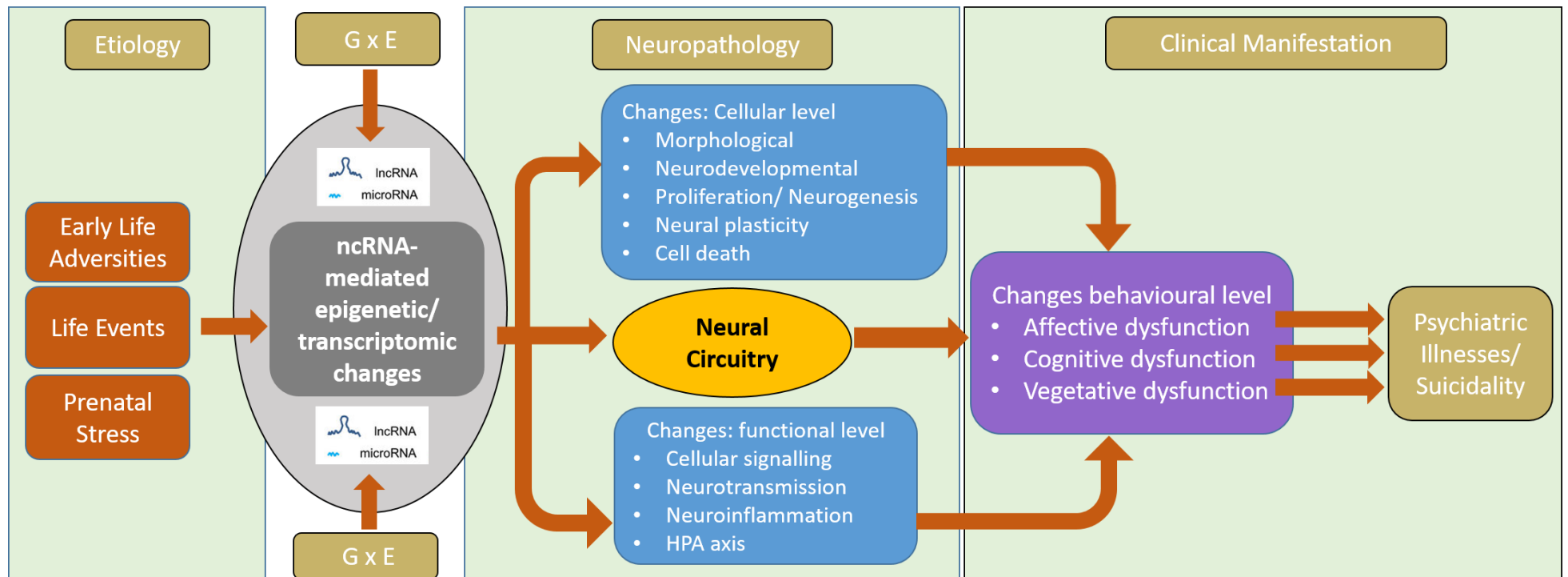
Figure 6.1 Schematic diagram of the hypothesised ncRNAs' impact on psychiatric illnesses and suicidality.
Abbreviations: ncRNA, non-coding RNA. GxE, gene-environment interaction; HPA, hypothalamic-pituitary-adrenal axis Figure taken from review (Yoshino and Dwivedi, 2020).

Although miRNAs have been diversely implicated in suicide, still very few studies have taken an unbiased, systematic screen of differential miRNA expression in post-mortem brain from suicide completers. With the purpose of further investigating the relationship between suicidality and miRNA regulation, I have quantified the abundance of >470 human miRNAs in post-mortem PFC tissue dissected from a collection of suicide cases and controls obtained from the Douglas Bell-Canada Brain Bank and already extensively characterised for genetic and epigenetic (DNAm) variations.

6.2 Aims

The aims of this chapter were to:

i)   Identify differences in miRNA expression levels between MDD suicide cases and non-psychiatric controls using the Taqman Open Array platform.

ii)   Perform an integrated omics analysis leveraging upon the availability of methylomic data from the same set of brain samples to identify suicide-associated changes in DNA methylation proximal to miRNA genes which are having a functional effect on mRNA expression levels.

6.3   Material and Methods

6.3.1 Study design and cohort description

Clinically and neuropathologically well-characterised PFC tissue dissected from donors with MDD suicide (n=32) and matched non-psychiatric controls (n=39) were collected from two distinct brain regions, BA11 and BA25 obtained from the Douglas Bell-Canada Brain Bank (https://douglasbrainbank.ca/) (**Table 6.1** provides details of the cohorts' demographics). All tissue donations were consented to, collected and stored following strict legal and ethical guidelines. Total RNA was extracted from the frozen PFC tissue using the miRNeasy Mini Qiagen Kit (Qiagen, UK, Cat No 217004). RNA integrity (RIN) was assessed using the Agilent Bionanalyzer 2100 and cDNA was prepared from the best-quality RNA samples (RIN>5) using the TaqMan Advanced miRNA cDNA Synthesis Kit (Applied Biosystems, UK). Prior profiling, all cDNA samples underwent a preliminary QC to establish the success rate of the reverse transcription by performing qPCR to assay the expression signal detection of two brain-enriched miRNAs, miR-101-3p and miR-9-5p (Catts et al., 2005, Montijn et al., 2016, Llorens et al., 2013) across all samples. Final number of samples loaded on the Open Array platform was 69 (MDD-suicide= 32 and CTR= 37; BA11= 38; BA25=31). Samples excluded during the QC were samples for which insufficient starting material was available at the RNA extraction stage or samples with good yield but low RIN values. Samples were profiled using TaqMan™ OpenArray Human Advanced MicroRNA Panel (Applied Biosystems, UK) on the QuantStudio-12K Flex Real-Time PCR platform as per the manufacturer's instructions. Each TaqMan™ OpenArray Panel contains 754 well-characterised and functionally validated human miRNA sequences from the Sanger miRBase-v21.

Group ID		CASE	CONTROL
N		17	22
Brain Region available	Both (BA11 & BA25)	N=15	N=17
	BA11 only	N =2	N=4
	BA25 only	N=0	N=1
Age	Mean (SD)	41 (20)	47.1 (20)
Sex	M	13	17
	F	4	5
pH	Mean (SD)	6.5 (0.2)	6.6 (0.4)
PMI	Mean (SD)	23.8 (17.5)	20.3 (15.7)

Table 6.1 Cohort Demographics.
Post-mortem tissue and data were available for 71 brain specimens dissected from 39 individuals. CASE are individuals with diagnosed MDD which died by suicide, CONTROL are non-psychiatric individuals died for accidental causes. PMI, post-mortem interval; BA, brodmann area; SD, standard deviation.

6.3.2 Data Analysis

miRNA expression values from 69 PFC samples assayed on RT-qPCR OpenArray plates were analysed by importing the raw data (from .eds file) in R version 3.6 using the publicly available miRoar v0.01 R package (Gorrie-Stone, 2019). Briefly, the *miRoar* pipeline uses Crt values - calculated using a predetermined internal reference efficiency to identify the fractional cycle at the point the reference efficiency reaches a specific value. Non-expressed miRNAs –e.g. those which had a Ct value >= 40 or did not amplify (amplification status =`-1`) – were removed for each individual and miRNAs that were detected in <20 samples were removed from subsequent analysis. Following these filtering steps, the final dataset included a total of 470 miRNAs quantified in 69 samples (32 suicide cases and 37 controls). Crt values were then converted to relative expression values (ΔCrt) using the NormFinder/Global Normalisation method which is the manufacturers default approach. The NormFinder method seeks to find the most stable miRNA between experimental groups (e.g. different brain areas) to find a robust miRNA that can be safely subtracted from the Ct values to

yield the relative delta Ct values. The NormFinder algorithm implementation is described in the NormqPCR R package (Perkins et al., 2012). The global normalisation method subtracts the median Ct value (for each sample) from all ubiquitously expressed miRNAs in a given dataset and aims to correct for different amounts of starting material of RNA (Mestdagh et al., 2009). The ΔCrts thus obtained for each miRNA were then statistically tested for association with suicide. ΔCrt values also underwent low-level processing to remove Crt values that were >1.5 IQRs away from the upper or lower quantile for each miRNAs to remove any obvious outliers (if any). Firstly, the differential expression analysis was conducted in each brain region separately using a linear regression model with age, sex, pH, PMI and slide as additional covariates. For this analysis the model used was as follows:

miR-ΔCrt ~ suicide + age +sex + pH + PMI + slide

The effect sizes were correlated highlighting all nominally significant *P*-values (p < 0.05). P-values were adjust using the *p.adjust* function and were considered significant if adj p < 0.05. Mixed effect linear regression model was also fitted by combining the ΔCrt matrices (processed using the pipeline above described) and data were analysed using the Cran package lme4. For the Mixed effect analysis the adopted model is reported below:

lmer (x ~ diag + age +sex + pH + PMI + (1|region) + (1|sample) + (1|slide)

6.4 Results

6.4.1 Expression Data quality control

First the internal controls that were included on the array were examined. These internal controls consisted of three miRNAs (cel-miR-39-3p, ath-miR-159a and has-miR-16-5p) which are assayed 16 times per each sample to check for contamination, to inspect whether the platform is working correctly and to assess for sufficient starting material. After this preliminary check, samples went through quality control. The method adopted here for the data QC refers to Crts which is based on the Ct method and by using the amplification curve trajectories calculates Cts according to the baseline threshold set by the machine itself (Applied Biosystems, Application Note). Upon assessing the amplification curves, miRNAs were considered as expressed if fulfilling two criteria:1) Crt value < 40 and 2) Amplification Status = -1. The logic behind these criteria are purely based on observational assessment of the raw dataset. Firstly a Crt greater than 40 is outside the number of cycles the qPCR machine performs so including any numbers beyond that is of dubious interpretation. Additionally, ThermoFisher appears to encode various error numbers at Crt values >= 40. Secondly, by making the assumption that all miRNAs which have been designed on the platform properly amplify, allows to make use of those qPCR reactions that have been determined as 'inconclusive' but otherwise amplified correctly.

The number of miRNAs ubiquitously expressed in BA11 and BA25 were 280 and 292 respectively. When Principal Component Analysis (PCA) on dCrt values was performed, the results did not provide many insights and almost all variance was found to be explained in PC1 (data not shown). With DNA methylation data it is usually extremely clear that tissue and sex drive a significant part of the variation and this is demonstrably shown when performing a PCA, however, for the miRNA analysis the variation appeared to be driven by sample level variation. As a result samples obtained from the same individual did not cluster (like we should expect) and additionally, samples from the same brain area also did not cluster. This could be due to the fact that only 127 miRs are used to generate the PCA and there simply isn't enough data to estimate the variance we should expect from using other -omics data.

In both brain regions 5 miRNAs (hsa-miR-100-3p, hsa-miR-595, hsa-miR-325, hsa-miR-501-3p, hsa-miR-593-5p) were found to have a mean Crt value < 10 (see **Figure 6.2** for reference). Three of these miRNAs (hsa-miR-595, hsa-miR-325 and hsa-miR-593-5p) were mostly unamplified in 70-90% of all samples while the remaining two miRs (miR-100-3p and miR -501-3p) were amplified (according to the machine report) in more than 50% of samples. Therefore, miR-100-3p and miR-501-3p only, since having a sufficient number of observations to be tested, were considered for downstream analysis whereas the other miRNAs with low Crts were discarded at this stage.
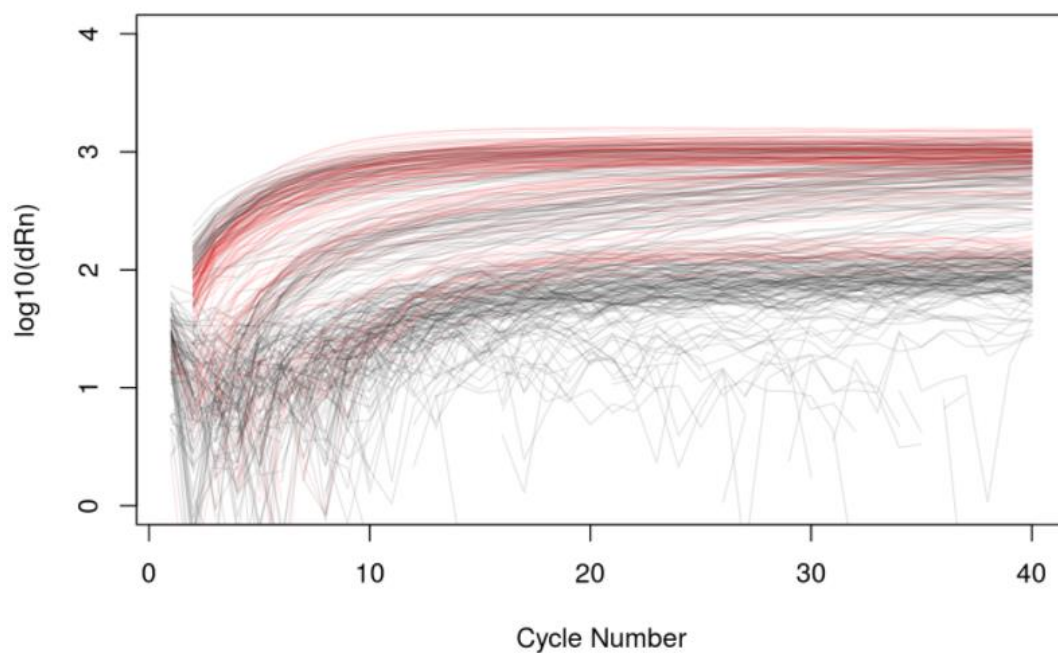
Figure 6.2 Amplification curves of miRs when mean Crt <10.

The following plots show the frequency distribution of expressed miRNAs per sample in each brain region separately (**Figure 6.3**) and the cross-region correlation (**Figure 6.4**). Correlation of number of miRNAs expressed between BA11 and BA25 was explored and found to be low (R = 0.345).
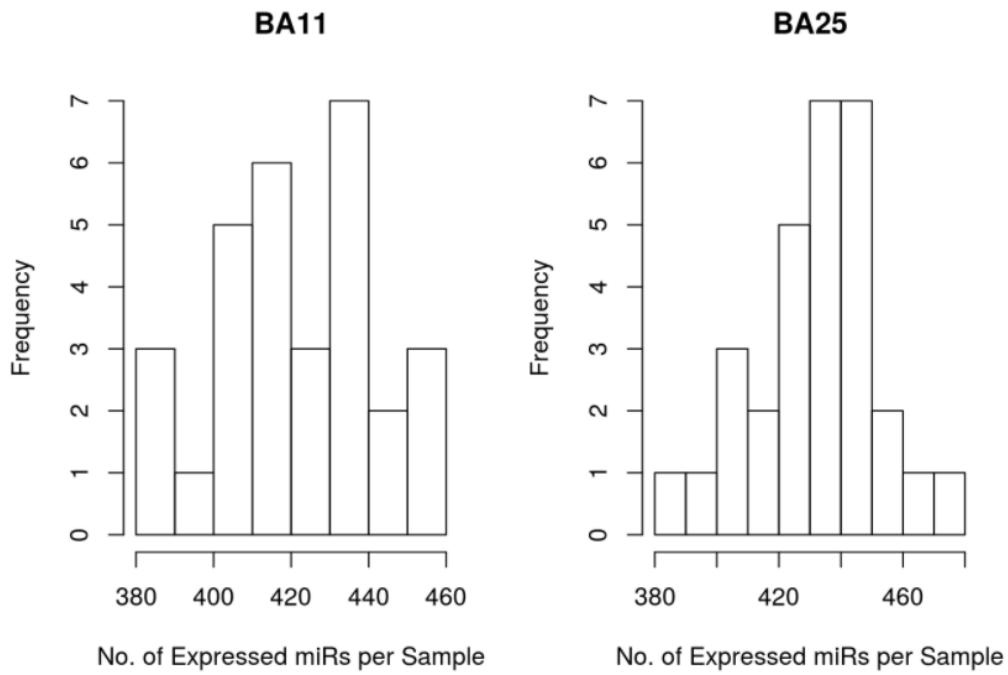
BA11

BA25

Figure 6.3 Histogram of the number of expressed miRNAs per sample.
The number of expressed miRNAs per sample was independently investigated in each profiled brain region (BA11, Brodmann area 11; BA25, Brodmann area 25; miRs; microRNAs).
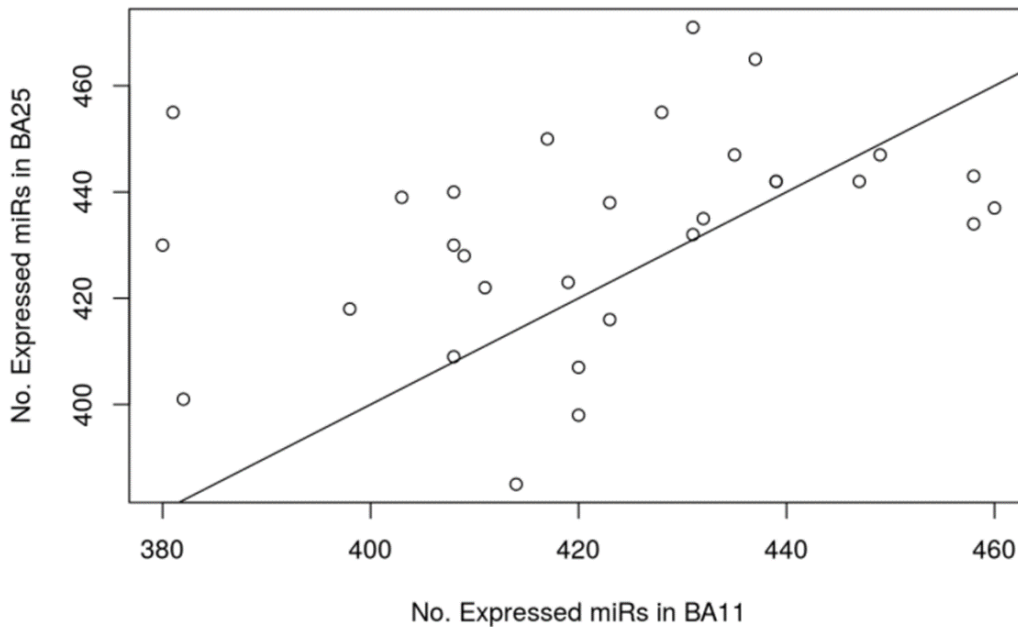
Figure 6.4 Cross-tissue correlation of number of expressed miRNAs across samples.
When comparing the number of miRNAs which are expressed (non-NAs) between the two brain regions from the same individual (each point represent a sample), we can see that samples from BA25 have slightly more miRNAs expressed compared to BA11, however the correlation between the number of expressed miRNAs for sample is quite low (R = 0.345). BA11, Brodmann area 11; BA25, Brodmann area 25; miRs; microRNAs.

399

Additionally, data were assessed for any technical and experimental artefacts as well as batch effect. Since samples were loaded in batches of 12, the number of miRNAs expressed according to slide was examined and two slides (BGH77 and BGH66) were found to have nominally fewer miRNAs expressed (**Figure 6.5**) and interestingly all of the samples with the number of expressed miRNAs < 390 were found to be from the same slide BGH77 suggesting a potential technical issue affecting this specific slide during the experimental procedure. Given the evidence, slide was included as a variable in the downstream statistical analyses. Overall, the median Crt for samples on each slide appeared to vary of 1 Crt unit around a crt value of 23 (**Figure 6.6**).
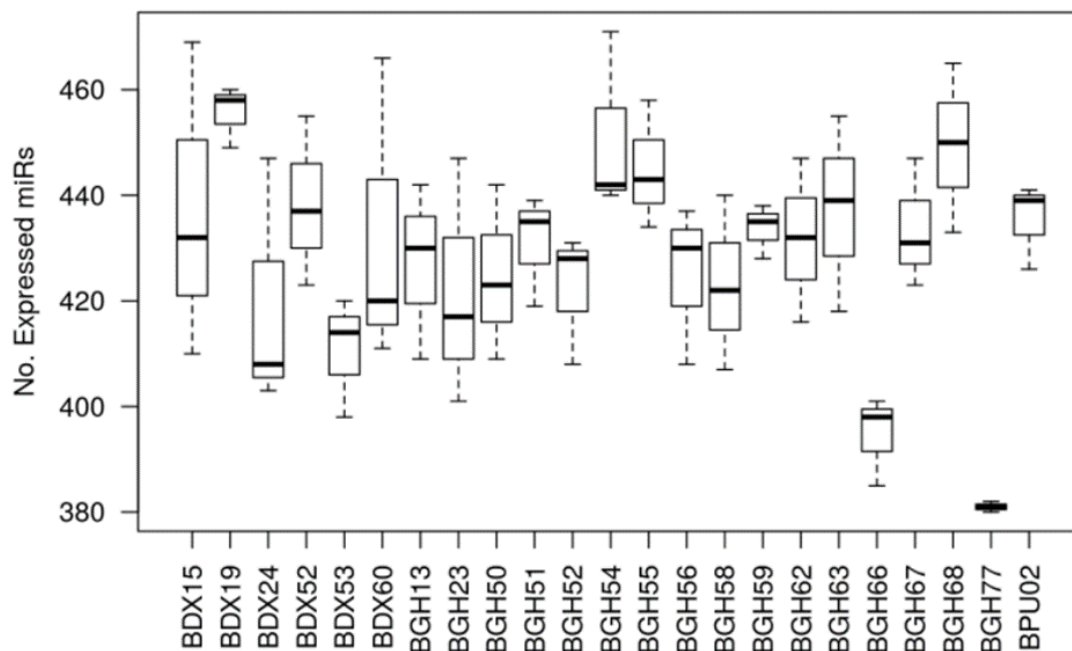
Figure 6.5 Boxplot reporting the number of expressed miRNAs across all slides.
X-axis is slide ID Y-axis is the number of expressed miRNAs. Two slides (BGH77 and BGH66) in particular showed nominally fewer miRs expressed compared to the general trend observed for the other slides. Boxplots are a standardized way of displaying the distribution of data based on a five number summary: minimum, maximum, median, first quartile, and third quartile. Each box extends from the first quartile to the third quartile (IQR). A line goes through the box at the median (mid-point of the data and is shown by the line that divides the box into two parts). The whisker lines go from each quartile to the minimum (1st quartile – 1.5 x IQR) or maximum (3rd quartile + 1.5 x IQR).
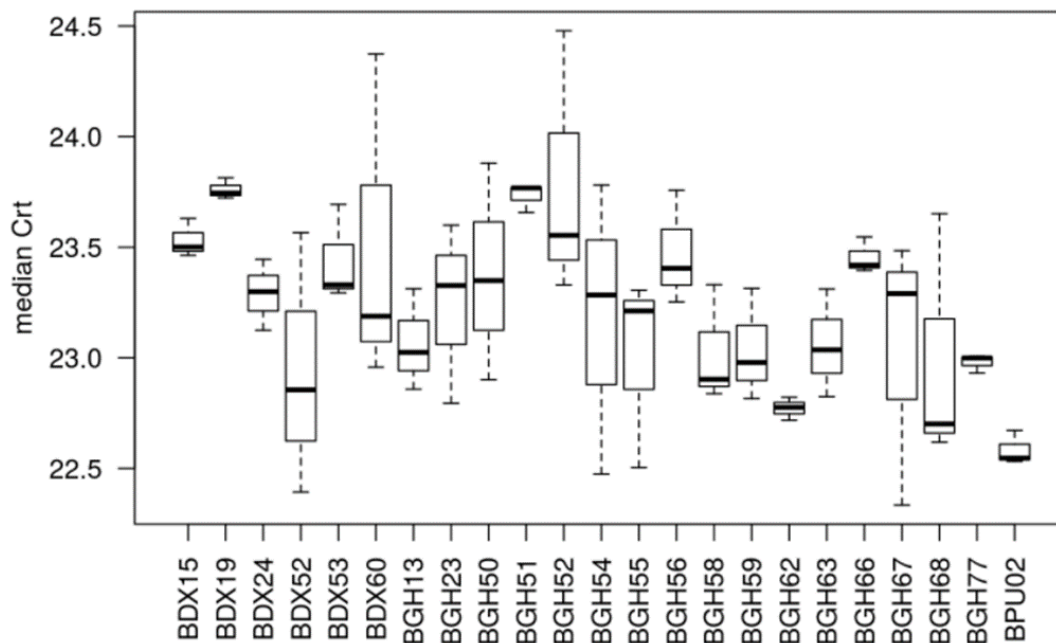
Figure 6.6 Boxplot of the median Crt across slide.
The X-axis represents slide ID, Y-axis reports the median Crt values. The median Crt for samples on each slide appeared to vary of 1 Crt unit around a crt values of 23 and 24. Boxplots are a standardized way of displaying the distribution of data based on a five number summary: minimum, maximum, median, first quartile, and third quartile. Each box extends from the first quartile to the third quartile (IQR). A line goes through the box at the median (mid-point of the data and is shown by the line that divides the box into two parts). The whisker lines go from each quartile to the minimum (1ˢᵗ quartile – 1.5 x IQR) or maximum (3ʳᵈ quartile + 1.5 x IQR).

Global normalisation was adopted for data normalisation since it is the method recommended by ThermoFisher and the most frequently adopted in other publications using this same profiling platform (Farr et al., 2015, McCall et al., 2016, Hernandez-Santana et al., 2016). Moreover, for the most part global normalisation and normFinder have been proved to be quite comparable when comparing the global normalisation factors vs the crt values of the selected normFinder miRNA: the global normalisation method correlated highly (R=0.81, $p < 0.01$) with the miRNA selected by normFinder (miR-421). The global normalisation revealed that the number of miRs ubiquitously expressed was comparable in the two brain regions assessed: 280 and 292 in BA11 and BA25 respectively (**Figure 6.7A**) Furthermore, no miRNA was found to be distinctly expressed in one region compared to the other (**Figure 6.7B**).
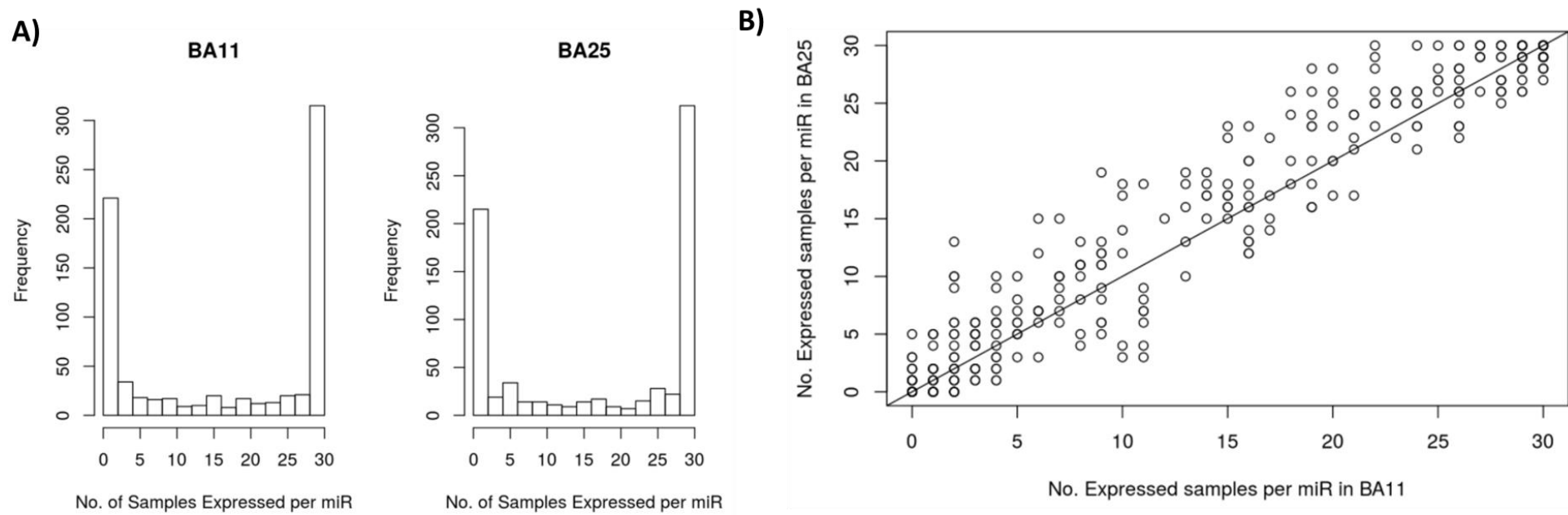
Figure 6.7 A) Histogram showing of number of detected (expressed) miRs across samples estimated for each brain region separately.
The distribution of frequency reveals that in both brain regions assessed, the majority of the observations is concentrated at the extremity of the distribution, with the majority of the brain samples expressing > 300 miRNAs ; B) Correlation between brain regions BA11 (Y-axis) and BA25 (X-axis). Notably no miRNA is distinctly expressed in one region compared to the other. BA11, Brodmann area 11; BA25, Brodmann area 25; miRs; microRNAs.

6.4.2 Identification of differentially-expressed miRNA transcripts in the cortex of suicide completers

All effect sizes described in this differential expression analysis were essentially Log2 fold change values (2^-ΔΔCrt) between non-psychiatric controls and MDD-suicide cases where a negative effect size would indicate an increase in miRNA expression in MDD suicide cases while a positive effect size a decreased expression levels for a given miRNA in MDD suicide cases relative to the control group. Two exploratory analyses were performed on these data. The linear regression analysis performed in each brain region separately aimed to identify the presence of brin region- specific differences in miRNA expression associated with suicidality whereas the mixed model was designed to determine cross region suicide-associated differences in miRNA expression taking into account the structure of the dataset (the two brain regions available for profiling were dissected from the same individuals). **Table 6.2** and **Table 6.3** reports the top 10-ranked differentially expressed (up-/down-regulated) miRNA in BA11 and BA25 respectively. Although the effect sizes suggest differential regulation of expression level between MDD-suicide cases and non-psychiatric controls, the corresponding p-values did not survive correction for multiple testing (corrected P-value >0.05). Furthermore, the distribution of differentially expressed miRNAs appeared to be comparable between the two brain regions although BA11 showed a slightly higher number of significant findings (see **Figure 6.8** for details). Correlation of effect sizes across the two brain regions, BA11 and BA25, of suicide-associated differentially expressed (nominally significant P-values) miRNAs was also investigated and no apparent correlation was observed between brain regions (**Figure 6.9**). Lastly, a similar trend was observed in the findings from the mixed model with effect size values suggesting differential expression for a few miRNAs with nominally significant (P<0.05) *P*-values however these differences did not survive correction for multiple testing (see **Table 6.4** and **Figure 6.10** for details). Although the results presented are not statistically robust to draw definitive conclusions, they suggest a potential dysregulation of miRNA levels in the brain of suicide completers.

Table 6.2 Top 10 miRNAs for suicide linear model using Crts from BA11 samples only							
	Effect Size	Standard Error	T Stat	P-value	Adj. P-value (FDR)	Nobs CASE	CTR
hsa-miR-219a-2-3p	1.434	0.393	3.649	0.002	0.571	32	34
hsa-miR-301a-3p	-0.657	0.197	-3.322	0.004	0.571	34	33
hsa-miR-338-5p	0.912	0.289	3.149	0.006	0.571	33	35
hsa-let-7b-5p	0.621	0.207	3.003	0.008	0.571	31	33
hsa-miR-590-3p	1.436	0.481	2.983	0.009	0.571	33	33
hsa-miR-504-5p	-1.142	0.398	-2.868	0.010	0.571	34	35
hsa-miR-17-3p	-1.585	0.518	-3.059	0.010	0.571	30	32
hsa-let-7i-3p	1.085	0.380	2.847	0.011	0.571	35	33
hsa-miR-1270	2.159	0.559	3.856	0.012	0.571	20	26
hsa-miR-503-5p	-1.3115	0.471	-2.781	0.016	0.670	33	31
Abbreviations: has-miR, human miRNA; FDR, false discovery rate; Nobs, number of observations, it reports in how many samples each miRNA was detected in (i.e. non-NA values).							

Table 6.2 Top 10 miRNAs for suicide linear model using Crts from BA11 samples only.
The differential expression analysis was conducted in each brain region separately using a linear regression model with age, sex, pH, PMI and slide as additional covariates.

Table 6.3. Top 10 miRNAs for suicide linear model using Crts from BA25 samples only

	Effect Size	Standard Error	T Stat	P-value	Adj. P-value (FDR)	Nobs CASE	CTR
hsa-miR-367-3p	-0.535	0.016	-33.255	0.0009	0.391	19	18
hsa-miR-431-3p	0.271	0.073	3.663	0.003	0.703	34	35
hsa-miR-515-5p	3.662	0.046	78.904	0.008	0.704	19	21
hsa-miR-340-3p	1.231	0.413	2.977	0.011	0.704	34	35
hsa-miR-29b-1-5p	0.996	0.345	2.882	0.014	0.704	34	33
hsa-miR-628-3p	-1.508	0.533	-2.827	0.015	0.704	33	33
hsa-miR-330-5p	0.607	0.216	2.806	0.017	0.704	33	35
hsa-miR-577	-1.242	0.168	-7.408	0.018	0.704	17	21
hsa-miR-381-3p	1.323	0.483	2.739	0.018	0.704	34	35
hsa-miR-370-3p	0.399	0.148	2.704	0.019	0.704	34	35

Abbreviations: has-miR, human miRNA; FDR, false discovery rate; Nobs, number of observations, it reports in how many samples each miRNA was detected in (i.e. non-NA values).

Table 6.3 Top 10 miRNAs for suicide linear model using Crts from BA25 samples only.
The differential expression analysis was conducted in each brain region separately using a linear regression model with age, sex, pH, PMI and slide as additional covariates.

A — −log 10 p−value vs Effect size BA11

B — −log 10 p−value vs Effect size BA25
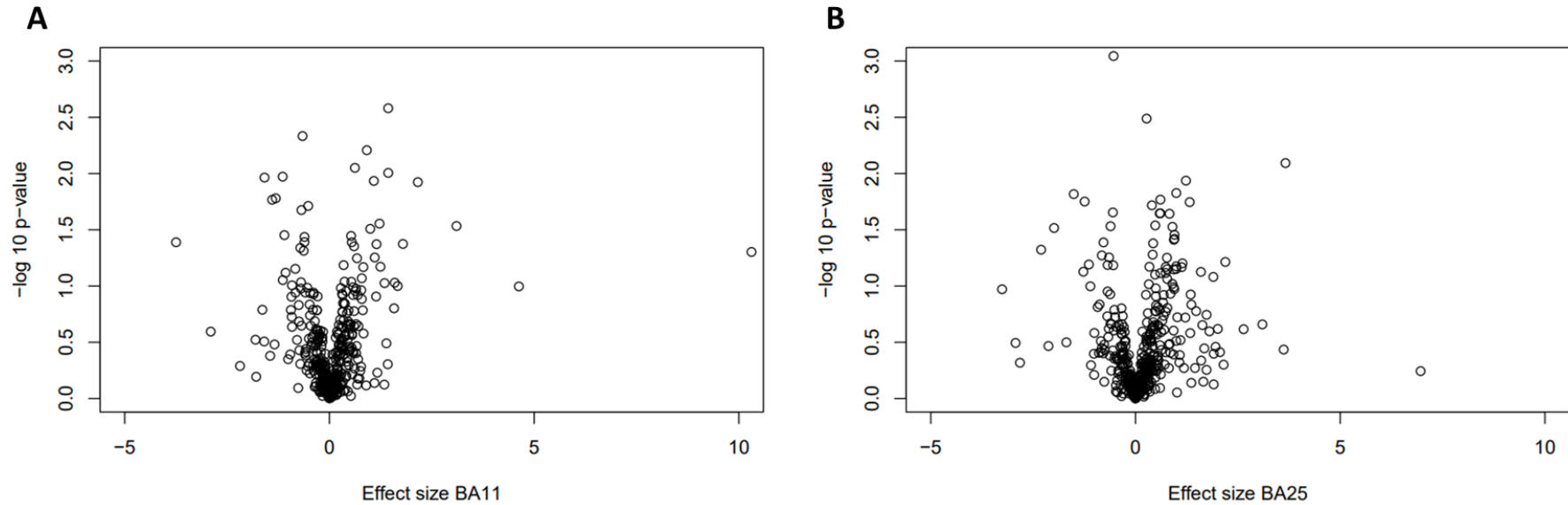
Figure 6.8 Scatterplot (volcano plot) showing the significance of differentially expressed miRNAs between MDD-suicide cases and non-psychiatric controls in each brain region separately*.*
Volcano plot is a type of scatterplot that shows statistical significance (P-value) versus magnitude of change (effect size) in BA11 (A) and BA25 (B). In a volcano plot, the most upregulated miRNAs are towards the right, the most downregulated ones are towards the left, and the most statistically significant miRNAs are distributed towards the top. The distribution of differentially expressed miRNAs appeared to be comparable between the two brain regions. MDD, Major Depressive Disorder; BA11, Brodmann Area 11; BA25, Brodmann Area 25.

BA11 Significant miRs p < 0.05

BA25 Significant miRs p < 0.05
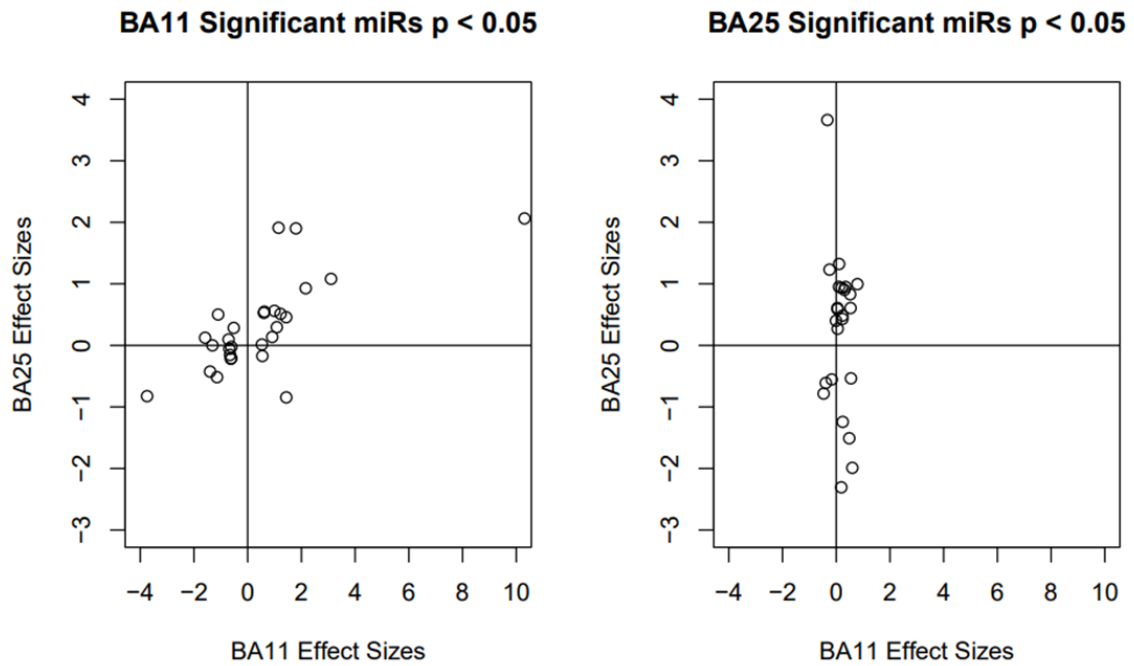
Figure 6.9 miRNAs differential expression cross-tissue correlations.
Correlation of effect sizes across the two brain regions, BA11 and BA25, of suicide-associated differentially expressed (nominally significant P-values before adjustment) miRNAs. No apparent correlation can be observed between brain regions when looking at differentially expressed (P-value<0.05) miRNAs between MDD suicide cases and non-psychiatric, sudden death controls. MDD, Major Depressive Disorder; BA11, Brodmann Area 11; BA25, Brodmann Area 25; miRs, microRNAs.

Table 6.4 Top 10 miRs from linear mixed effect model.

	Effect Size	Standard Error	DF	T-Stat	P-value	adj P-value (FDR)	Nobs CASE	CTR
hsa-miR-92a-1-5p	2.355	0.164	11.071	14.371	1.6E-08	8.3E-06	11	13
hsa-miR-149-3p	1.729	0.466	22.019	3.712	0.001	0.3232972	23	16
hsa-miR-504-5p	-0.761	0.222	46.677	-3.424	0.001	0.3232972	34	35
hsa-miR-539-5p	0.844	0.256	45.546	3.292	0.002	0.3232972	34	35
hsa-miR-27a-5p	2.068	0.598	13.358	3.461	0.004	0.3938060	24	12
hsa-let-7g-3p	0.327	0.110	46.630	2.955	0.005	0.3938060	33	35
hsa-miR-10b-5p	-4.738	1.609	31.000	-2.943	0.006	0.3938060	18	19
hsa-miR-423-3p	-0.385	0.135	48.824	-2.842	0.006	0.3938060	34	35
hsa-miR-758-3p	0.753	0.255	26.022	2.945	0.007	0.3938060	34	34
hsa-let-7i-3p	0.884	0.302	25.864	2.927	0.007	0.3938060	33	35
hsa-miR-130b-3p	0.481	0.175	48.208	2.748	0.008	0.4071293	34	35

Abbreviations: has-miR, human miRNA; FDR, false discovery rate; Nobs, number of observations, it reports how many samples each miRNA was detected in (i.e. non-NA values).

Table 6.4 Top 10 miRs from mixed-effect model.
The differential expression analysis between cases and control group was conducted by fitting a linear mixed-effect model using the lme4 R package whereby, brain region and sample ID were included in the model as random effects ('within participants' factors) together with slide while diagnosis, age, sex, PH and PMI were included in the model as fixed effects.
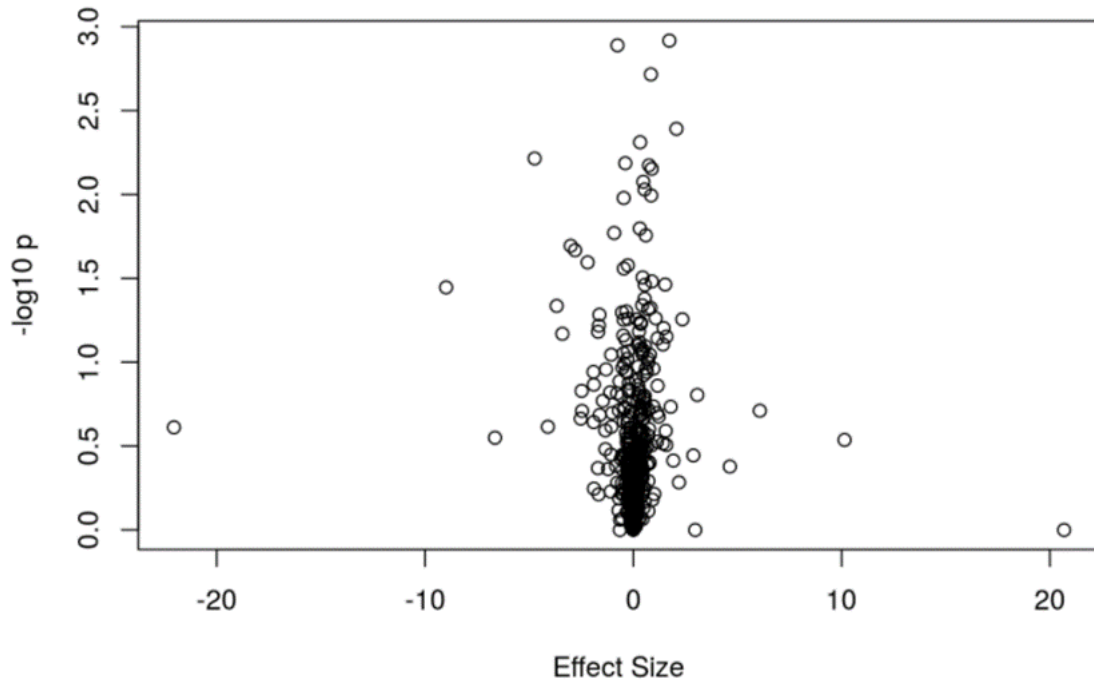
Figure 6.10 Scatterplot (volcano plot) showing the significance of differentially expressed miRNAs between MDD-suicide cases and non-psychiatric controls across both brain regions when running the mixed effect model.

For the majority of the detected miRNAs, no substantial differences in expression were be detected in MDD suicide cases vs non-psychiatric controls. For negative effect size values miRNAs are over-expressed in MDD suicide cases. For positive effect size values miRNAs are under-expressed in MDD suicide cases.

6.5 Discussion

In this chapter post-mortem PFC specimens dissected from donors with suicide history (n=32) and matched non-psychiatric controls (n=37) were profiled using the TaqMan™ OpenArray Human Advanced MicroRNA Panel (Applied Biosystems, UK) which quantifies the abundance of 754 well-characterised and functionally validated human miRNAs from miRBase-v21. Following stringent quality control and filtering of the raw data, the final dataset included a total of 470 miRNAs found to be reliably detected in PFC tissue quantified in 69 samples (32 MDD-suicide cases and 39 non-psychiatric controls). Differentially expressed miRNA associated with SB were subsequently identified using a linear regression model including age, sex, pH, PMI and slide as additional covariates. The differential expression analysis was performed on each brain region separately and the effect sizes were correlated highlighting all nominally significant P-values (p < 0.05). A number of miRNAs showing suggestive evidence of differential expression in MDD-suicide patients compared to non-psychiatric controls were identified in both brain regions (29 in BA11, 26 in BA25) although the detected differences did not survive the multiple testing adjustment (FDR). **Table 6.1** and **Table 6.2** report the top10-ranked differentially expressed miRNAs in BA11 and BA25 respectively.

Among the top 10 transcripts detected in BA11, four miRNAs showed increased expression while three reduced expression levels in the MDD-suicide cases but not in the control group. Similarly, in the 10 top-ranked miRNAs in BA25, three miRNA reported increased expression levels while three were downregulated in MDD-suicide cases relative to controls. As expected, the mixed model showed some overlap with the regression analysis performed in the two brain regions separately (e.g. miR-504-5p and let-7i-3p). Although in most cases the direction of change was maintained, the effect size was smaller in the mixed model.

Not surprisingly, many of the differentially expressed miRNAs in both regions have been previously reported in studies of psychiatric conditions such as MDD and SCZ as well as neurodegenerative disorders like PD and AD. Of particular interest, the top-ranked transcripts in BA11, miR-219a-2-3p, which showed reduced expression in the MDD-suicide group (effect size=1.44, unadj. *P=0.003, FDR=0.57*) was reported for its significant (FDR corrected; p < 0.05) differential regulation in the PFC of MDD subjects (Yoshino et al., 2020). miR-301a-3p, which

showed increased expression in the MDD-suicide group (effect size= -0.65, unadj. *P*=0.005) in a different study has been associated with treatment resistance in SCZ (Alacam et al., 2016) while miR-338-5p (effect size= 0.91, unadj. *P*=0.006) overexpression has been found to functionally prevent impairments in long-term synaptic plasticity, learning ability, and memory retention in transgenic mice and its under-expression to play an important role in the development of AD (Qian et al., 2019, Li et al., 2020a). In BA25, miR-369-3p, identified among the top 15 findings in this region (see **Appendix H**- Chapter 6 Supplementary Material) was previously reported in literature for being related to SI (significantly lower expression levels in plasma from patients with SI) (Sun et al., 2016). Furthermore, one of the top-ranked miRNA, miR-370-3p (effect size= 0.39, unadj. *P*= 0.019), has been implicated in the response to treatment in patients with MDD (Zastrozhin et al., 2020). miR-29b (effect size= 0.99, unadj. *P*=0.015, in BA25) is a brain-specific miRNA that plays an important role in brain development and neuronal maturation and has been found dysregulated in autistic patients (Sarachana et al., 2010).

In regards to the top findings from the cross region mixed-effect analysis (refer to **Table 6.4** for details), one of the miRNAs, miR-27a-5p, which revealed increased expression levels in the MDD-suicide group (effect size= 2.06, unadj. P=*0.004*) was found to have decreased expression in the CSF of patients with AD (Sala Frigerio et al., 2013). miR-539-5p (Effect size= 0.85, unadj. *P*=0.002) decreases amyloid beta-protein production and memory impairment in APP/PS1 double transgenic mice (Jiang et al., 2020) and its overexpressed inhibits inflammatory response of neurons to impede the progression of cerebral ischemic injury (Xue et al., 2020). miR-423-3p (Effect size= -0.39, *unadj. P*=0.007) levels were found significantly increased in rats with chronic temporal lobe epilepsy and correlated with the activity of caspase-3, an apoptosis indicator (Li et al., 2014a).

In spite of these evidence suggesting a clear relationship between the altered miRNAs and brain disorders, for many other miRNAs nominally significant (*P*=0.05) before adjustment no previous mention could be found in literature in the context of neuropsychiatric disorders or, more broadly, in brain research. Furthermore, no overlap was found between nominally significant differentially expressed miRNAs here reported and previous suicide studies looking at miRNA

expression. However, many of the established suicide–associated miRNAs elsewhere reported were detected by the Open Array miRNA panel.

Although replication and validation of selected miRNAs was not performed since this analysis did not yield statistically robust findings, these data ultimately support previous evidence of the applicability of this method to robustly detect miRNA expression in post-mortem brain tissue.

6.5.1 Study Limitations

This work is not exempt from limitations. Firstly, the modest sample size of this study meant we were underpowered to detect small differences in miRNA expression. An increased sample size is needed to robustly detect signals of differential miRNA expression. The lack of significant differential expression of miRNAs has been observed in a few published studies that used the same miRNA arrays (Grigorenko et al., 2011, Broccanello et al., 2020), however the top hits in other miRNA studies were biologically meaningful in most of the cases just not significant after adjustment.

Secondly, the differential expression analysis performed in this study did not attempt to correct for cell heterogeneity partly due to the low number of miRNA assayed which it may have further contributed to the lack of significance. Further analysis could include the CETS neuronal estimates predicted from the methylation data.

Given the subtle variation in median Crt values (i.e. 1 Crt unit, see **Figure 6.6**) and the low number of miRNAs ubiquitously expressed detected during the preliminary QC as well as two slides (BGH66, BGH77) with nominally fewer expressed miRNAs compared to the rest of the slides, all analyses did consider slide as a covariate (random effect in the cross-region analysis, fixed effect in the individual brain region regressions). Additionally, any possible added variation due to pH and PMI was ruled out by accounting for these two confounding factors in both models. The influence of pH variations on gene expression has been studied in different model systems, but only for a limited number of genes. Acidosis has been previously demonstrated to influence cellular responses, such as stimulating autophagy (Wojtkowiak et al., 2012), and to effect gene expression (Chen et al., 2008, Sorensen et al., 2007, Sorensen et al., 2005). In a study investigating the effect of changes in pH on gene expression in human dermal

fibroblasts, a modulated pattern of expression was displayed by numerous genes included, among others, cell cycle regulators and relevant extracellular matrix components (Bumke et al., 2003). Furthermore, human carcinoma cell lines treated in conditions of acidosis (pH 6.3) showed upregulation of several genes involved in the translation process (e.g. the translation initiation factor *EIF4A2*, and the ribosomal protein *RPL37*) as well as suppression of ATP turnover and *de novo* protein synthesis by 50% (Sorensen et al., 2015) highlighting the importance of considering pH to understand its impact on disease-associated changes in gene expression particularly so in *in vivo* studies. Similarly, studies have confirmed that RNA in tissues degrades with a delay in PMI (Ma et al., 2015, Li et al., 2014b, Lv et al., 2016). The effect of PMI on the expression of standard reference mRNA genes and miRNA was also investigated in four post-mortem human tissues among which brain (Zhang et al., 2013b) and the authors advised not to choose miRNAs for endogenous control genes due to their low stability (Zhang et al., 2013b). On the other hand, a recent study found miRNAs to be more stable than normal reference genes and considered to be less susceptible to PMI and environmental conditions in mouse post-mortem tissues (Tu et al., 2018). miRNAs have been found to be a consistent, stable, and well-preserved molecular target detectable even from formalin-fixed paraffin-embedded tissue proving their suitability for gene expression studies (Muciaccia et al., 2015). Between different classes of RNA molecules, miRNAs are less conditioned by post-mortem decay, thanks to their tiny size (about 22 nt) and close association with large protein complexes that makes mature miRNAs much more stable than mRNAs and less prone to degradation (Liu et al., 2009).

So far, miRNA-related research in the neuropsychiatric field has advanced our understanding of the clinical significance of miRNA in disease pathogenesis. However, their potential value as a biomarker to predict disease outcome is yet to be thoroughly tested under clinical settings. It has been a little over a decade since the first study of miRNAs in psychiatric disorders was published (Perkins et al., 2007); however, we are still in the early phases to best utilize miRNAs as biomarkers for diagnosis or treatment response. Several biomarkers have been tested for their prognostic value in predicting behavioural outcomes (e.g. suicide attempts); however, only a handful of them have proved to be reliable in clinical studies. There is a significant caveat in implying the preclinical concept of biomarker testing in the psychiatric field.

This is largely because of the complex nature of psychiatric conditions characterised by multi-dimensional psychopathological syndromes with multifactorial causation (Venkatasubramanian and Keshavan, 2016). However, preclinical studies could be translated into clinical settings. For example, several preclinical studies have focused on examining the functional relevance of miRNAs in behaviour (Issler and Chen, 2015).

Despite some shortcomings and challenges, the premise of miRNA research is strong and has significant potential in developing biomarkers in the field of neuropsychiatric disorders. Most important among their properties is their ability to cross the blood brain barrier due to their small size and to remain stable in a biofluid, particularly in blood. Besides, once established as validated biomarkers, their monitoring through repetitive assays will be much faster and less complex under clinical laboratory settings. Moreover, their detection as non-invasive markers is relatively cost-effective since the collection, processing, and storage of biofluid samples are relatively straightforward and less invasive in standard laboratory conditions (Roser et al., 2018). The similarity of changes in miRNA expression between the brain and peripheral tissues have been explored in a recent review which compared all the miRNA-related findings to date and a relatively large numbers of overlapping miRNA expression changes were found to be common between brain and blood across multiple psychiatric disorders (SCZ, MDD, BPD) (Roy et al., 2020) further supporting the exciting potential of miRNA for prevention in mental health research.

6.5.2 Future work

Future work should be aiming at replicating this study in a much larger cohort of post-mortem brain samples in order to increase the detection power as well as guarantee the robustness of the findings. Ideally, in the presence of robust associations (based on effect size and *P*-value), top hits identified in the discovery cohort would need replication in a larger dataset and validation using standard qPCR by selecting as normaliser the miRNA found to be the most stable and highly correlated with the global normalisation factor in the discovery dataset. In order to detect the contribution of the MDD comorbidity to the detectable changes in miRNA expression and distinguish it from the suicide-driven signal, the study

design should include in the investigation a third group of MDD non-suicide individuals. Almost all brain enriched miRNAs are co-expressed at varying levels across different brain regions presumably according to a region's functional needs (Ludwig et al., 2016). There is also evidence for cell-type (neuron vs glia) specific miRNAs in the CNS (Jovicic et al., 2013), which play a role in functions like neuronal differentiation and synaptic plasticity. Future replication is greatly needed in relevant regions like the PFC, but also amygdala, and hypothalamus, which have also been shown to play a major role in the overall stress response as well as depression symptoms and suicide risk (Allen and Dwivedi, 2020) since it will be interesting to know how these brain areas co-ordinately regulate miRNA expression. In addition, it would be compelling to disentangle how different cell types modulate miRNA expression patterns. Cataloguing the expression of miRNAs and additional small RNAs in healthy human brain as well as in major neuropsychiatric diseases and suicide has the potential to lead to new therapeutic targets and insight into disease aetiology.

Although several promising avenues for future research are constantly emerging, additional studies are needed to further elucidate the role of the most robust miRNA candidates in suicidality. For miRNAs identified to be differentially expressed between suicide cases and controls through hypothesis-free studies, their gene targets and neurobiological significance need further investigation. Future functional and genomic explorations of brain-expressed miRNAs, and other types of ncRNAs may identify additional candidate genes and pathways for common psychiatric disorders. Therefore implementing additional strategies to further elucidate the role of miRNAs in the etiology of common psychiatric disorders and related phenotypes is of great importance (Forero et al., 2010). Moreover, the biological significance of epigenetic associations remains unclear. For example, studies linking epigenetic modifications with gene expression in cellular models are needed to clarify the role of specific miRNAs and CpG sites. These studies could lead to the discovery of novel drug targets and biomarkers of suicide treatment outcome. Future studies should also investigate the combined and coordinated roles of DNA methylation, miRNAs, and histone modifications in gene regulation and risk of suicide. Lastly, since the contribution of early life stressful experiences to depression and suicide vulnerability has recently received tremendous attention, it would be valuable to explore differences in functions of miRNAs as a result of variation in conditions and stress

factors. Lentiviral injections have been used to selectively augment and reduce individual miRNAs in living rodent brain (Bahi et al., 2014, Higuchi et al., 2016), including one ELS study (Bahi, 2016). Knockout mice have also been extensively used to study the importance of individual and clusters of miRNAs (Park et al., 2010a) and more recent technological advances have proposed non-invasive means of delivering brain-specific anti-miRs to investigate miRNA knockdown (Suryawanshi et al., 2015). In combination with genome-wide expression and in-vitro studies, these techniques can help elucidate the importance of miRNAs in stress-induced suicide susceptibility and aid in designing more personalized treatment plans for those having depression or suicidal tendencies.

Chapter 7 - General Discussion

7.1 Introduction

The primary scope of this thesis was to expand on the existing knowledge about the epigenetic landscape in mental illness with a particular focus on DNA methylation and miRNA expression differences associated to with suicidality in the post-mortem brain. Furthermore, this work was orientated to address one of the main confounders in brain research, cellular heterogeneity, by optimising a method to investigate epigenetic variation in cryopreserved brain tissue at the resolution of individual cell types to disentangle the complexity of its regulatory machinery in health and disease.

This discussion will summarise the key findings from each chapter of this thesis and the limitations present within each study and the attempts undertaken to tackle some of the issues faced when studying epigenetic mechanisms in the human brain in health and in disease. Future perspectives for the research field aiming to address the issues uncovered by this work will also be discussed.

7.2   Summary of results and key findings

In **Chapter 3** I meta-analysed publicly available and unpublished methylomic datasets generated from post-mortem brain samples of individuals affected by various psychiatric conditions, but all sharing suicide as reported cause of death, to determine whether a distinctive signal associated to suicide could have been detected across multiple independent cohorts and brain regions. I identified numerous differentially methylated positions (DMPs) as well as genomic regions (DMRs) associated with suicide. These differences were primarily brain-region specific and enriched among functional pathways relevant to neuropsychiatric phenotypes and suicidality, including nervous system development (PFC) and regulation of long-term synaptic depression (CER). I have further explored these findings by investigating potential correlations between the two brain regions and by attempting to rule out the contribution of underlying psychiatric conditions to the epigenetic signature of suicide. Furthermore, I have attempted to validate one of the top findings from the CER suicide meta-analysis (*CERC2*-associated DMR) using pyrosequencing. Lastly I have investigated the functional consequences of variable DNA methylation within a PFC suicide-associated DMR (*PSORS1C3*-

associated DMR) previously reported in a suicide methylomic study (Murphy et al., 2017) by examining the expression of nearby genes using qPCR.

In **Chapter 4** I describe the optimisation of existing methods to construct a protocol suitable for genomic and epigenomic interrogation of multiple cell type populations in the human adult brain compatible with frozen samples obtained from post-mortem tissue. This one-day procedure consists of tissue homogenization without fixation, nuclei extraction and antibody staining followed by fluorescence-activated nuclei sorting (FANS). The characterisation of the obtained fractions (neurons, oligodendrocytes and other glia) showed that the contamination by debris is very low and that most nuclei are isolated (as singlets), not attached to other nuclei (multiplets). I have also validated the robustness of the method and confirmed the correct cell type enrichment of each fraction by measuring the expression levels of cell-type specific marker genes in each of the three sorted nuclei populations using qPCR. By using immunocytochemistry on human derived cell lines, I have explored nuclear microglia candidate markers to be incorporated in the nuclei isolation protocol in order to further dissect the composition of the 'other glial cells' fraction. I have thus identified *IRF8* as nuclear marker of human microglia which has now been stably integrated in the staining process for ongoing projects conducted within my group using my optimised method. The current FANS protocol allows cell-type specific profiling of neurons, oligodendrocytes, microglia and other glial cells (presumably astrocyte-enriched). These cell-type-specific nuclei populations can be used for downstream omics-scale sequencing applications with an emphasis on epigenomic interrogation such as DNA modifications (methylation and hydroxymethylation) histone modifications and chromatin accessibility.

In **Chapter 5** I have applied the protocol outlined in Chapter 4 to characterise cell type-specific genome-wide pattern of DNA methylation in purified nuclei populations obtained from a small cohort (N=12) of post-mortem brain samples from healthy individuals. By performing an Anova test, I have detected numerous individual sites and genomic regions where differences in DNA methylation levels were strongly associated to cell type identity. Only for a minority of DMPs, the methylation status was similar across all neural cell types examined. A similar pattern has been observed when performing enrichment and pathway analyses using cell-type specific *P*-values therefore proving the necessity of reinterpreting

findings from previous bulk studies as likely to be confounded by cellular heterogeneity.

In **Chapter 6,** I endeavoured to capture transcriptomic signatures of suicide in the human brain and the additional layer of epigenetic regulation exerted by ncRNA. By using the Open Array platform, I have profiled the expression levels of over 700 miRNAs in a pre-characterized cohort of human post-mortem samples (N=69). Using two different statistical models I have detected evidence of differential expression for several brain-enriched miRNAs when comparing suicide completers and non-psychiatric controls.

Taking a global view of my results, three common themes are revealed across the adopted experimental approaches: i) the challenge in distinguishing the epigenetics of suicidality from the contribution of psychiatric illnesses related to suicide ii) the extraordinary cellular complexity of the brain tissue and the distinct regulation profile to which each individual cell type is subjected to, making extremely difficult to pinpoint any causality for the observed epigenetic differences when using bulk tissue iii) the need for future studies to perform multi-omics assays on the same sample set to integrate more consistent data which can further our understanding of the interplay between different regulatory signatures and its role in determining disease phenotypes, and to maximise the omics information gathered from a precious finite resource as post-mortem brain tissue.

7.3   Discussion

When it comes to psychiatry, the brain is thought to be the most directly involved organ in the pathophysiology of disease. Owing to its functions in cognition, emotional processing and memory, the brain is poised to be the primary organ underlying the symptoms and diagnostic characteristics associated with psychiatric illnesses. Thus, the use of post-mortem brain for the study of psychiatric diseases has been crucial to our understanding of suicide as well as the impact of social stress on brain dysfunction (McCullumsmith and Meador-Woodruff, 2011). It has allowed scientists to carry out investigations of the neurobiological processes of suicide in specific brain regions (van Heeringen and Mann, 2014). With the latest developments in cell type-specific and single cell

isolation techniques, the exploration of the molecular mechanisms carried out by distinct cell populations is possible using post-mortem tissues (Hu et al., 2016b, Lutz et al., 2017a). Studies using these techniques have begun to reveal distinct molecular profiles from specific cell types and populations (Byne et al., 2008, Ruzicka et al., 2007), which could even be used to distinguish between certain psychiatric illnesses (Arion et al., 2017). As we uncover more of the complex nature of the brain, post-mortem brain tissues will continue to be an invaluable resource for the study of psychiatric illnesses (de Lange, 2017). Some of these molecular findings can then be investigated, at least in part, in living patients using brain imaging techniques (Oquendo et al., 2014) or studied in animal and *in vitro* models to provide further insight into the molecular mechanisms underlying brain dysfunction (McGowan et al., 2009). While post-mortem brain tissue offers many advantages for the study of psychiatric phenotypes, there are also unique challenges and limitations associated with its use. Since post-mortem tissues provides a snapshot of the subject's state at a specific time, they are usually used only in cross-sectional study designs that may not able to confirm the cause-and-effect relationship and may have no predictive value. Several factors affecting tissue quality have varying effects on the biomolecules used for the study, including DNA, RNA and proteins (Ferrer et al., 2008, Kretzschmar, 2009). The period of time in between the moment of death and the retrieval of brain tissue is called the post-mortem interval (PMI) and has been shown to have varying effects on different classes of RNA and other biomolecules (Nagy et al., 2015a) with longer PMI generally associating with higher RNA degradation (Birdsill et al., 2011).

Beyond the caveats related to the use of post-mortem tissue in brain research, there are a number of important limitations associated with each study of this thesis that should be considered when interpreting the results described in each of the data chapters. Firstly, the challenge posed by the limited sample size available for each study performed which has inevitably limited the power of detection for significant associations, especially given the small effect sizes expected in complex diseases (Dempster et al., 2013). Increased public sharing of data and active recruitment of more brain specimens through brain-banking is therefore essential to maximise the number of samples available for well-powered studies in molecular epidemiology.

Another intrinsic limitation of the analyses presented in this thesis is the unaccounted variation due to lack of phenotypic data. Although I have controlled for age, sex, pH, PMI, neuronal composition (where possible) and brain collection, it is plausible that other factors such as ethnicity, smoking, medication, influenced the results of my analyses. Although ethnicity and smoking status can both be estimated from methylation data in peripheral tissue like whole blood or placenta (Elliott et al., 2014, Bollepalli et al., 2019, Yuan et al., 2019), similar predictor tool have not been developed yet for brain tissue. Post-mortem samples are a precious resource and, when available, are often poorly characterised in terms of lifestyle habits such as smoking or medication intake as the majority of psychiatric patients are usually prescribed some type of medication during their lifetime. More efforts should be made to ensure that, when available, pre-mortem exposure and phenotypic data are systematically recorded in a standardised manner when recruiting samples for bio-banking.

7.4 Current challenges and future directions

7.4.1 Cellular heterogeneity

Epigenetic modifications are in their nature cell specific, with individual cell populations having a distinct epigenetic profile; therefore it is likely that disease-related epigenetic changes could be affecting just one or two cellular populations, rather than every cell type in a tissue. However, the majority of the studies reported in this thesis have utilised bulk tissue (**Chapter 3** and **Chapter 6**). Therefore epigenetic changes that have been reported in those chapters are representative of the cumulative contribution of all cellular populations, potentially masking biologically relevant cell type unique differences in the pathological brain. In **Chapter 3** I attempted to address this issue using the bioinformatic CETS correction method, which calculates the neuron/glia proportion in a given sample (Guintivano et al., 2013). Adding this estimate as a covariate in the analytical models partially altered the level of significance of the findings, but did not dramatically change the ranking of the top loci. However, one caveat of this approach is that the algorithm was developed using 5mC profiles generated from fluorescence activated cell sorted (FACS) neuronal and non-neuronal cells from cortical brain tissue, using the antibody NeuN. However, it is well known in the

literature that NeuN is not expressed by cerebellar Purkinje neurones (Guintivano et al., 2013, Mullen et al., 1992). As such, this method may is not appropriate for determining neuron/glia proportions in cerebellar tissue, preventing its application to the meta-analysis conducted in the cerebellum or in comparisons performed across multiple brain regions. Furthermore, the algorithm does not allow us to further dissect the composition of the non-neuronal fraction of the brain tissue therefore it cannot inform about disease relevant DNA methylation changes specific to individual glial cell types.

In order to address this specific issue I have optimised the existing FANS methods to incorporate multiple cell-type specific markers for the purification and characterization of the non-neuronal fraction. In particular by distinguishing the oligodendrocyte signature from the one of other glial origin cells. The improved protocol also allows to simultaneously assay multiple genomic markers (DNA modification analysis (5mC and 5hmC), histone modification analysis, open chromatin analysis, and RNA sequencing) maximising the amount of data generated from the same cryopreserved brain specimen. Furthermore, the FANS method has enabled the construction of an improved brain cellular deconvolution algorithm (trained on experimental FANS data) for DNA methylation data which partially compensate for the limitations of the CETS tool (neurons vs non-neurons only) (Guintivano et al., 2013) by offering cell proportion estimates for four distinct neural cell types: neurons, oligodendrocytes, microglia and other glial origin cells (unpublished). This enhanced bioinformatics tool is greatly valuable for the reinterpretation of previous studies conducted in bulk tissue in which findings are inevitably confounded by tissue heterogeneity. Future work indeed, aims to re-run the suicide meta-analysis (described in Chapter 3) including adjustment for cell estimates calculated applying the improved brain deconvolution algorithm to those PFC EWASs which were originally performed in bulk brain (2 out of 4 studies). The application of my FANS pipeline to post-mortem brain tissue from suicide completers would allow future studies to explore differences in DNA methylation (as well as other epigenetic markers) across individual cell types in parallel, partially overcoming the issue of controlling for tissue heterogeneity in the PFC. Since my method does rely on the NeuN marker, it is currently unsuitable for nuclei sorting in the CER as Purkinje cells for example do not express this marker (Mullen et al., 1992, Guintivano et al., 2013). So far, neurons have been defined as nuclei (confirmed by compatible size, shape, and presence

of DAPI-stained DNA) that express NeuN (Herculano-Houzel and Lent, 2005), and non-neuronal cells as all remaining nuclei, by exclusion of the NeuN-expressing fraction. This procedure stems from the assumption that the sum of NeuN-positive and NeuN-negative nuclei is the total number of nuclei, and therefore of cells, in the tissue of origin. Therefore this approach inevitably leaves unaccounted all those neuronal cell subtypes known to not express NeuN. Future work should endeavour to identify among others, a suitable nuclear marker unique to Purkinje cells in order to expand the application of the FANS method to the CER region enabling the characterization of suicide-associated cell type-specific DNA methylation differences in this region of the brain.

Alternative protocols for the separation of additional cellular subtypes from post-mortem brain tissue are now under development to allow this analysis in the future (Mastroeni et al., 2017, Li et al., 2019, Lake et al., 2016). These methods either take advantage of single-cell technologies or LCM. Laser capture allows microdissection of specific cell types, including, in principle, their nuclei (Cheng et al., 2013), but generally yields low amounts of material and is labour intensive (Martin et al., 2017). With the recent advances in single-cell gene expression profiling technologies, it is now possible to undertake the enormous task of disentangling brain cellular heterogeneity. High-throughput single-cell RNA sequencing (scRNA-seq) and multiplexed quantitative RT-PCR have become more accessible, and these technologies enable systematic categorization of individual cells into groups with similar molecular properties (Poulin et al., 2016). Given that a cell's function is rooted in its molecular composition, defining neural cell types on the basis of gene expression is one reasonable approach (Fishell and Heintz, 2013). Clustering of cells, based on their gene expression profiles, reveals a cell-type map that can be used to assess the composition of the tissue including the identification of new cell types or subtypes. The identity of these cell groups is assigned post hoc on the basis of previously known or newly discovered markers (Poulin et al., 2016). These rich data can be used to address many questions of gene expression and regulation within or between cell types and between tissues (Sandberg, 2014). Although technical noise confounds precise measurements of low-abundance transcripts, modern protocols have progressed to the point that single-cell measurements are rich in biological information. Moreover, the power to detect biological differences from single-cell data is demonstrated by the identification of hundreds to thousands of genes with

differences in abundances between cell types (Frishberg et al., 2019). Recent refinements will improve the signal-to-noise ratio even further by enhancing the efficiencies of reverse transcription and PCR (Lein et al., 2007) or applying molecular barcoding strategies that control for amplification bias (Gong et al., 2003).

7.4.2 Causality

Epigenetic changes in disease provide promises for intervention and treatments due to their modifiable state. Compounds that can target these modifications might potentially help reverse abnormal gene expression typical of disease. However due to the dynamic and temporal nature of epigenetic modifications, the interpretation of epigenetic findings is challenging; changes in cytosine or histone modifications could be, in fact, a result of the disease process, rather than a cause. The issue of causality is especially challenging in the context of psychiatric and neurological disorders, where longitudinal EWAS analyses in the tissue of primary pathology (brain) are not possible. Therefore, addressing whether loci nominated from epigenome studies are causal in the disease process has been difficult, with two-step Mendelian randomisation studies representing the only potentially feasible method for establishing causality to date (Relton and Davey Smith, 2012, Amaral et al., 2020, Caramaschi et al., 2017). Recent developments in CRISPR-cas9 genome editing technology, have allowed researchers to specifically target the DNA methylation machinery making it applicable to manipulating epigenetic modifications (Sander and Joung, 2014), providing a much more efficient method for causality determination although this can only be achieved in model systems which may not be representative of the complexity characterising the human brain.

7.4.3 Beyond DNA methylation - other cytosine modifications

One limitation of DNA methylation profiling (5mC) studies, included those presented in this thesis (**Chapter 3** and **Chapter 5**) is the confounding effect of other cytosine modifications, such as hydroxymethylation (5hmC). 5hmC in particular has been found to be expressed at greater levels in the brain and during development (Kriaucionis and Heintz, 2009, Wang et al., 2012), suggesting that

this previously overlooked modification does have functional relevance. Due to the chemistry of traditional BS conversion methods, the majority of EWAS could not distinguish between 5mC and 5hmC. Thanks to a recent adaptation to the BS conversion protocol, more recent studies address this issue by oxidising the DNA prior to BS conversion. The profiling of matched BS and OxBS treated samples simultaneously enabled the detection of both modifications throughout the genome and provides a measure of 'true' DNA methylation (5mC) (Lunnon et al., 2016, Hernandez Mora et al., 2018). However this methodology too has some drawbacks, for example the limited number of CpG sites profiled, and technical variation inherent in the profile resulting in some samples having a negative 5hmC level as well as the higher amount of DNA input required and the higher costs associated with having to run each sample twice on the array.

The adoption of hydroxymethylated DNA immunoprecipitation sequencing (hMeDIP-seq) would overcome this issue, however hMeDIP-seq has a relatively low resolution and cannot quantitatively determine 5hmC abundance at a single-base resolution (Skvortsova et al., 2017). Further studies are also needed to interrogate whether other cytosine modifications present in the human genome (5-fC and 5-caC) are relevant in the study of psychiatric phenotypes.

7.4.4 Array-based assays

Many of the existing epigenomic studies of psychiatric and neurological conditions have utilised microarray-based technologies. Although microarrays are a cost-effective method for analysing the epigenome, especially when profiling large numbers of samples, their content is relatively constrained, and they only cover a small proportion of DNA modification sites. As such, pathology-associated genomic variation in uncovered regions of the genome will not be detected. Sequencing-based technologies could offer a better approach for uncovering disease-associated genomic variation. For example, whole genome bisulfite sequencing (WGBS-Seq), allows the identification of DNA methylation changes at single nucleotide resolution across the entire genome, including at non-CpG sites (Yong et al., 2016); however, the depth of sequencing required to accurately profile DNA methylation using this approach is still associated with prohibitively high costs to enable a large number of samples to be profiled (Ziller

et al., 2015). A valid compromise to enable affordable profiling of DNA methylation at single base resolution is offered by RRBS (Gu et al., 2011a, Chatterjee et al., 2017). Furthermore, SMRT sequencing technologies, currently under active development, will soon enable the simultaneous identification of both genetic and epigenetic variation in the same sample (Hirst and Marra, 2010). Our understanding of the role of altered gene regulation in brain pathology has expanded considerably in the last decade thanks to the novel technological advances and the reduction in the cost of genomic sequencing. The increase in multi-omics analyses, including the integration of different data types, will require extensive collaboration between multidisciplinary teams and the development of novel analytical strategies. Although these studies are still in their infancy, the integration of genetic, epigenetic, transcriptomic, proteomic and clinical data from the same individuals, will enable a fully comprehensive analysis of dysfunctional mechanisms and pathways involved in suicide and, more broadly, complex psychiatric phenotypes.

7.4.5 NcRNA studies

There are a several limitations to ncRNA studies in neuropsychiatric disorders and related phenotypes: 1) several studies show changes in expression of lncRNAs and miRNAs; however, these are inconsistent even when studied in the same brain region from individuals with the same diagnosis (Yoshino and Dwivedi, 2020). This could be attributed to several factors. For example, confounding variables such as environmental factors (modality of death, age, sex) and the storage conditions (PMI, brain pH, freeze–thaw cycle) vary between studies. In addition, most of the studies use whole tissue. As mentioned in **Chapter 6**, the expression of lncRNAs and miRNAs are brain region- and cell-type specific. This cellular heterogeneity may affect ncRNA expression. Thus, studying their expression patterns in neurons and glial cells (i.e. oligodendrocytes, astrocytes, and microglia) could help delineate these discrepancies. Even within neurons, specific neuronal populations need to be studied. In this regard, single cell study will be helpful. Furthermore, new emerging technologies like nanopore sequencing and structure prediction algorithms can be helpful for the correct identification of new small ncRNAs and

their epigenetic roles even though new ncRNAs are being discovered regularly, the functions of these novel ncRNAs are not well understood. More *in vivo* functional studies followed by high-throughput sequencing after cross-linking and immunoprecipitation will be effective in probing the functional roles of novel ncRNAs at the cellular level (Huttenhofer and Vogel, 2006). These assays can be also performed in human post-mortem brain samples, with the advantage of minimising the loss of tissue integrity and maximising the likelihood of capturing the interaction at the molecular level. Furthermore, most of the studies have shown temporal changes in ncRNA expression. Although it is impossible to measure ncRNA expression at different time points in post-mortem samples, it is relatively easy to measure them in peripheral tissue (e.g. blood, CSF) which has been shown to share a relatively large numbers of overlapping changes in miRNA expression with the brain tissue across multiple psychiatric disorders (SZ, MDD, BPD) (Roy et al., 2020). Longitudinal studies, could allow to explore the diagnosis/therapeutic/disease state biomarkers for suicide and psychiatric illnesses.

7.5 Conclusion

This thesis has provided further evidence that epigenetic dysfunction is present in post mortem brains of suicide completers. I have confirmed previous associations (e.g. *PSORS1C3*) and identified new candidate genes that require further investigation and could provide crucial insights in the neurobiology of suicidality as an independent psychiatric phenotype. Hence, these data provide a strong foundation for follow-up investigation of epigenomic and genomic regulation involved in the molecular pathology associated with suicide. On the other hand, the improved FANS method described in **Chapter 4** represents the first attempt to further characterise the non-neuronal component of the brain while extending the molecular investigation of each processed sample to multiple epigenetic signatures in parallel. This nuclei isolation protocol enables examination of healthy and diseased brain specimens through utilization of archived specimens, including banked disease biopsies that had previously been difficult to analyse. Beyond the epigenomic investigation, cell type-specific nuclei populations can be also used for *in vitro* experiments (e.g. co-culture assay and organoids), proteomic, metabolomic, and single-cell analysis resulting of utmost importance not only for in-depth characterization of pathological processes in psychiatric and neurodegenerative diseases but also for preclinical assessment of cell-targeting treatments.

Nevertheless, many questions remain to be answered regarding the actual contribution of other mental disorders to the behavioural outcome of suicide and new efforts are required to further characterise the cell type variety of the human brain for too long overlooked in its contribution to the regulatory genomic landscape. Looking to the future, improved study designs together with the latest advances in single cell technologies and cutting-edge genome manipulation tools will ultimately allow these unsolved questions to be answered.

Bibliography

ABDELRAHMAN, H. A., AL-SHAMSI, A. M., ALI, B. R. & AL-GAZALI, L. 2018. A null variant in PUS3 confirms its involvement in intellectual disability and further delineates the associated neurodevelopmental disease. *Clin Genet,* 94**,** 586-587.

ABDOLMALEKY, H. M., ZHOU, J. R. & THIAGALINGAM, S. 2015. An update on the epigenetics of psychotic diseases and autism. *Epigenomics,* 7**,** 427-49.

ABDOLMALEKY, H. M., ZHOU, J. R., THIAGALINGAM, S. & SMITH, C. L. 2008. Epigenetic and pharmacoepigenomic studies of major psychoses and potentials for therapeutics. *Pharmacogenomics,* 9**,** 1809-23.

ABDUL, Q. A., YU, B. P., CHUNG, H. Y., JUNG, H. A. & CHOI, J. S. 2017. Epigenetic modifications of gene expression by lifestyle and environment. *Arch Pharm Res,* 40**,** 1219-1237.

ABERG, K., SAETRE, P., JAREBORG, N. & JAZIN, E. 2006. Human QKI, a potential regulator of mRNA expression of human oligodendrocyte-related genes involved in schizophrenia. *Proc Natl Acad Sci U S A,* 103**,** 7482-7.

ADAM, S. A., SCHNELL, O., POSCHL, J., EIGENBROD, S., KRETZSCHMAR, H. A., TONN, J. C. & SCHULLER, U. 2012. ALDH1A1 is a marker of astrocytic differentiation during brain development and correlates with better survival in glioblastoma patients. *Brain Pathol,* 22**,** 788-97.

ADAN, A., ALIZADA, G., KIRAZ, Y., BARAN, Y. & NALBANT, A. 2017. Flow cytometry: basic principles and applications. *Crit Rev Biotechnol,* 37**,** 163-176.

ADLAKHA, Y. K. & SAINI, N. 2014. Brain microRNAs and insights into biological functions and therapeutic potential of brain enriched miRNA-128. *Mol Cancer,* 13**,** 33.

AGERBO, E., NORDENTOFT, M. & MORTENSEN, P. B. 2002. Familial, psychiatric, and socioeconomic risk factors for suicide in young people: nested case-control study. *BMJ,* 325**,** 74.

AGILENT TECHNOLOGIES Standardization of RNA Quality Control. https://www.agilent.com/cs/library/applications/5989-1165EN.pdf.

AGUZZI, A., BARRES, B. A. & BENNETT, M. L. 2013. Microglia: scapegoat, saboteur, or something else? *Science,* 339**,** 156-61.

AHMED, S., GULL, A., KHUROO, T., AQIL, M. & SULTANA, Y. 2017. Glial Cell: A Potential Target for Cellular and Drug Based Therapy in Various CNS Diseases. *Curr Pharm Des,* 23**,** 2389-2399.

AJAMI, B., BENNETT, J. L., KRIEGER, C., TETZLAFF, W. & ROSSI, F. M. 2007. Local self-renewal can sustain CNS microglia maintenance and function throughout adult life. *Nat Neurosci,* 10**,** 1538-43.

AJDACIC-GROSS, V., WEISS, M. G., RING, M., HEPP, U., BOPP, M., GUTZWILLER, F. & ROSSLER, W. 2008. Methods of suicide: international suicide patterns derived from the WHO mortality database. *Bull World Health Organ,* 86**,** 726-32.

AKAMATSU, W., FUJIHARA, H., MITSUHASHI, T., YANO, M., SHIBATA, S., HAYAKAWA, Y., OKANO, H. J., SAKAKIBARA, S., TAKANO, H., TAKANO, T., TAKAHASHI, T., NODA, T. & OKANO, H. 2005. The RNA-binding protein HuD regulates neuronal cell identity and maturation. *Proc Natl Acad Sci U S A,* 102**,** 4625-30.

ALACAM, H., AKGUN, S., AKCA, H., OZTURK, O., KABUKCU, B. B. & HERKEN, H. 2016. miR-181b-5p, miR-195-5p and miR-301a-3p are related with treatment resistance in schizophrenia. *Psychiatry Res,* 245**,** 200-206.

ALAM, R., ABDOLMALEKY, H. M. & ZHOU, J. R. 2017. Microbiome, inflammation, epigenetic alterations, and mental diseases. *Am J Med Genet B Neuropsychiatr Genet,* 174**,** 651-660.

ALDERMAN, C. 1988. Apply within. *Nurs Stand,* 2**,** 24-5.

ALLEN, L. & DWIVEDI, Y. 2020. MicroRNA mediators of early life stress vulnerability to depression and suicidal behavior. *Mol Psychiatry,* 25**,** 308-320.

ALLEN, N. J. & BARRES, B. A. 2005. Signaling between glia and neurons: focus on synaptic plasticity. *Curr Opin Neurobiol,* 15**,** 542-8.

ALLEN, N. J. & BARRES, B. A. 2009. Neuroscience: Glia - more than just brain glue. *Nature,* 457**,** 675-7.

AMARAL, A. F. S., IMBODEN, M., WIELSCHER, M., REZWAN, F. I., MINELLI, C., GARCIA-AYMERICH, J., PERALTA, G. P., AUVINEN, J., JEONG, A., SCHAFFNER, E., BECKMEYER-BOROWKO, A., HOLLOWAY, J. W., JARVELIN, M. R., PROBST-HENSCH, N. M., JARVIS, D. L. & CONSORTIUM, A. 2020. Role of DNA methylation in the association of lung function with body mass index: a two-step epigenetic Mendelian randomisation study. *BMC Pulm Med,* 20**,** 171.

AMEN, D. G., PRUNELLA, J. R., FALLON, J. H., AMEN, B. & HANKS, C. 2009. A comparative analysis of completed suicide using high resolution brain SPECT imaging. *J Neuropsychiatry Clin Neurosci,* 21**,** 430-9.

AMERICAN PSYCHIATRIC ASSOCIATION 2000. Diagnostic and Statistical Manual of Mental Disorders 4th edn, text revision.

ANDRADE-MORAES, C. H., OLIVEIRA-PINTO, A. V., CASTRO-FONSECA, E., DA SILVA, C. G., GUIMARAES, D. M., SZCZUPAK, D., PARENTE-BRUNO, D. R., CARVALHO, L. R., POLICHISO, L., GOMES, B. V., OLIVEIRA, L. M., RODRIGUEZ, R. D., LEITE, R. E., FERRETTI-REBUSTINI, R. E., JACOB-FILHO, W., PASQUALUCCI, C. A., GRINBERG, L. T. & LENT, R. 2013. Cell number changes in Alzheimer's disease relate to dementia, not to plaques and tangles. *Brain,* 136**,** 3738-52.

ANGUELOVA, M., BENKELFAT, C. & TURECKI, G. 2003. A systematic review of association studies investigating genes coding for serotonin receptors and the serotonin transporter: II. Suicidal behavior. *Mol Psychiatry,* 8**,** 646-53.

ANSELL, E. B., RANDO, K., TUIT, K., GUARNACCIA, J. & SINHA, R. 2012. Cumulative adversity and smaller gray matter volume in medial prefrontal, anterior cingulate, and insula regions. *Biol Psychiatry,* 72**,** 57-64.

ANTHONY, T. E. & HEINTZ, N. 2007. The folate metabolic enzyme ALDH1L1 is restricted to the midline of the early CNS, suggesting a role in human neural tube defects. *J Comp Neurol,* 500**,** 368-83.

APPLIED BIOSYSTEMS Application Note. Crt, a relative threshold method for qPCR data analysis on the QuantStudio 12K Flex system with OpenArray technology.

APPLIED BIOSYSTEMS OPENARRAY® USER GUIDE https://assets.thermofisher.com/TFS-Assets/LSG/manuals/cms_088717.pdf.

APREA, J., PRENNINGER, S., DORI, M., GHOSH, T., MONASOR, L. S., WESSENDORF, E., ZOCHER, S., MASSALINI, S., ALEXOPOULOU, D., LESCHE, M., DAHL, A., GROSZER, M., HILLER, M. & CALEGARI, F. 2013. Transcriptome sequencing during mouse brain development identifies long non-coding RNAs functionally involved in neurogenic commitment. *EMBO J,* 32**,** 3145-60.

ARDUI, S., AMEUR, A., VERMEESCH, J. R. & HESTAND, M. S. 2018. Single molecule real-time (SMRT) sequencing comes of age: applications and utilities for medical diagnostics. *Nucleic Acids Res,* 46**,** 2159-2168.

ARENDT, D. 2008. The evolution of cell types in animals: emerging principles from molecular studies. *Nat Rev Genet,* 9**,** 868-82.

ARION, D., HUO, Z., ENWRIGHT, J. F., CORRADI, J. P., TSENG, G. & LEWIS, D. A. 2017. Transcriptome Alterations in Prefrontal Pyramidal Cells Distinguish Schizophrenia From Bipolar and Major Depressive Disorders. *Biol Psychiatry,* 82**,** 594-600.

ARION, D., SABATINI, M., UNGER, T., PASTOR, J., ALONSO-NANCLARES, L., BALLESTEROS-YANEZ, I., GARCIA SOLA, R., MUNOZ, A., MIRNICS, K. & DEFELIPE, J. 2006. Correlation of transcriptome profile with electrical activity in temporal lobe epilepsy. *Neurobiol Dis,* 22**,** 374-87.

ARNSTEN, A. F. 2015. Stress weakens prefrontal networks: molecular insults to higher cognition. *Nat Neurosci,* 18**,** 1376-85.

ARRIGUCCI, R., BUSHKIN, Y., RADFORD, F., LAKEHAL, K., VIR, P., PINE, R., MARTIN, D., SUGARMAN, J., ZHAO, Y., YAP, G. S., LARDIZABAL, A. A., TYAGI, S. & GENNARO, M. L. 2017. FISH-Flow, a protocol for the concurrent detection of mRNA and protein in single cells using fluorescence in situ hybridization and flow cytometry. *Nat Protoc,* 12**,** 1245-1260.

ARUGA, J., YOSHIKAWA, F., NOZAKI, Y., SAKAKI, Y., TOYODA, A. & FURUICHI, T. 2007. An oligodendrocyte enhancer in a phylogenetically conserved intron region of the mammalian myelin gene Opalin. *J Neurochem,* 102**,** 1533-1547.

ARYEE, M. J., JAFFE, A. E., CORRADA-BRAVO, H., LADD-ACOSTA, C., FEINBERG, A. P., HANSEN, K. D. & IRIZARRY, R. A. 2014. Minfi: a flexible and comprehensive Bioconductor package for the analysis of Infinium DNA methylation microarrays. *Bioinformatics,* 30**,** 1363-9.

ASTON, C., JIANG, L. & SOKOLOV, B. P. 2005. Transcriptional profiling reveals evidence for signaling and oligodendroglial abnormalities in the temporal cortex from patients with major depressive disorder. *Mol Psychiatry,* 10**,** 309-22.

AUTRY, A. E. & MONTEGGIA, L. M. 2009. Epigenetics in suicide and depression. *Biol Psychiatry,* 66**,** 812-3.

AVNER, P. & HEARD, E. 2001. X-chromosome inactivation: counting, choice and initiation. *Nat Rev Genet,* 2**,** 59-67.

BACHMAN, K. E., ROUNTREE, M. R. & BAYLIN, S. B. 2001. Dnmt3a and Dnmt3b are transcriptional repressors that exhibit unique localization properties to heterochromatin. *J Biol Chem,* 276**,** 32282-7.

BACHMAN, M., URIBE-LEWIS, S., YANG, X., BURGESS, H. E., IURLARO, M., REIK, W., MURRELL, A. & BALASUBRAMANIAN, S. 2015. 5-Formylcytosine can be a stable DNA modification in mammals. *Nat Chem Biol,* 11**,** 555-7.

BACHMAN, M., URIBE-LEWIS, S., YANG, X., WILLIAMS, M., MURRELL, A. & BALASUBRAMANIAN, S. 2014. 5-Hydroxymethylcytosine is a predominantly stable DNA modification. *Nat Chem,* 6**,** 1049-55.

BACHMANN, S. 2018. Epidemiology of Suicide and the Psychiatric Perspective. *Int J Environ Res Public Health,* 15.

BACON, C., SCHNEIDER, M., LE MAGUERESSE, C., FROEHLICH, H., STICHT, C., GLUCH, C., MONYER, H. & RAPPOLD, G. A. 2015. Brain-specific Foxp1 deletion impairs neuronal development and causes autistic-like behaviour. *Mol Psychiatry,* 20**,** 632-9.

BAHI, A. 2016. Sustained lentiviral-mediated overexpression of microRNA124a in the dentate gyrus exacerbates anxiety- and autism-like behaviors associated with neonatal isolation in rats. *Behav Brain Res,* 311**,** 298-308.

BAHI, A., CHANDRASEKAR, V. & DREYER, J. L. 2014. Selective lentiviral-mediated suppression of microRNA124a in the hippocampus evokes antidepressants-like effects in rats. *Psychoneuroendocrinology,* 46**,** 78-87.

BAHNEY, J. & VON BARTHELD, C. S. 2018. The Cellular Composition and Glia-Neuron Ratio in the Spinal Cord of a Human and a Nonhuman Primate: Comparison With Other Species and Brain Regions. *Anat Rec (Hoboken),* 301**,** 697-710.

BAI, M., ZHU, X., ZHANG, Y., ZHANG, S., ZHANG, L., XUE, L., YI, J., YAO, S. & ZHANG, X. 2012. Abnormal hippocampal BDNF and miR-16 expression is associated with depression-like behaviors induced by stress during early life. *PLoS One,* 7**,** e46921.

BALDESSARINI, R. J. & HENNEN, J. 2004. Genetics of suicide: an overview. *Harv Rev Psychiatry,* 12**,** 1-13.

BALMACEDA, C., GAYNOR, J. J., SUN, M., GLUCK, J. T. & DEANGELIS, L. M. 1995. Leptomeningeal tumor in primary central nervous system lymphoma: recognition, significance, and implications. *Ann Neurol,* 38**,** 202-9.

BANI-FATEMI, A., JEREMIAN, R., WANG, K. Z., SILVEIRA, J., ZAI, C., KOLLA, N. J., GRAFF, A., GERRETSEN, P., STRAUSS, J. & DE LUCA, V. 2018. Epigenome-wide association study of suicide attempt in schizophrenia. *J Psychiatr Res,* 104**,** 192-197.

BAPTISTE, D. C. & FEHLINGS, M. G. 2006. Pharmacological approaches to repair the injured spinal cord. *J Neurotrauma,* 23**,** 318-34.

BARATEIRO, A., BRITES, D. & FERNANDES, A. 2016. Oligodendrocyte Development and Myelination in Neurodevelopment: Molecular Mechanisms in Health and Disease. *Curr Pharm Des,* 22**,** 656-79.

BARDE, S., RUEGG, J., PRUD'HOMME, J., EKSTROM, T. J., PALKOVITS, M., TURECKI, G., BAGDY, G., IHNATKO, R., THEODORSSON, E., JUHASZ, G., DIAZ-HEIJTZ, R., MECHAWAR, N. & HOKFELT, T. G. 2016. Alterations in the neuropeptide galanin system in major depressive disorder involve levels of transcripts, methylation, and peptide. *Proc Natl Acad Sci U S A,* 113**,** E8472-E8481.

BARLEY, K., DRACHEVA, S. & BYNE, W. 2009. Subcortical oligodendrocyte- and astrocyte-associated gene expression in subjects with schizophrenia, major depression and bipolar disorder. *Schizophr Res,* 112**,** 54-64.

BARNABE-HEIDER, F., GORITZ, C., SABELSTROM, H., TAKEBAYASHI, H., PFRIEGER, F. W., MELETIS, K. & FRISEN, J. 2010. Origin of new glial cells in intact and injured adult spinal cord. *Cell Stem Cell,* 7**,** 470-82.

BAROZZI, I., SIMONATTO, M., BONIFACIO, S., YANG, L., ROHS, R., GHISLETTI, S. & NATOLI, G. 2014. Coregulation of transcription factor binding and nucleosome occupancy through DNA features of mammalian enhancers. *Mol Cell,* 54**,** 844-857.

BARROS, L. F., BROWN, A. & SWANSON, R. A. 2018. Glia in brain energy metabolism: A perspective. *Glia,* 66**,** 1134-1137.

BARRY, G. 2014. Integrating the roles of long and small non-coding RNA in brain function and disease. *Mol Psychiatry,* 19**,** 410-6.

BARTON, S. J., MELTON, P. E., TITCOMBE, P., MURRAY, R., RAUSCHERT, S., LILLYCROP, K. A., HUANG, R. C., HOLBROOK, J. D. & GODFREY, K. M. 2019. In Epigenomic Studies, Including Cell-Type Adjustments in Regression Models Can Introduce Multicollinearity, Resulting in Apparent Reversal of Direction of Association. *Front Genet,* 10**,** 816.

BASU, S., CAMPBELL, H. M., DITTEL, B. N. & RAY, A. 2010. Purification of specific cell population by fluorescence activated cell sorting (FACS). *J Vis Exp*.

BAUMANN, N. & PHAM-DINH, D. 2001. Biology of oligodendrocyte and myelin in the mammalian central nervous system. *Physiol Rev,* 81**,** 871-927.

BAUMGARTH, N. & ROEDERER, M. 2000. A practical approach to multicolor flow cytometry for immunophenotyping. *J Immunol Methods,* 243**,** 77-97.

BD FACSAria III User Guide. https://www.flowcytometry.bmc.med.uni-muenchen.de/best-practice-faq/acquisition/facsaria_user_guide.pdf.

BEERS, D. R., HENKEL, J. S., XIAO, Q., ZHAO, W., WANG, J., YEN, A. A., SIKLOS, L., MCKERCHER, S. R. & APPEL, S. H. 2006. Wild-type microglia extend survival in PU.1 knockout mice with familial amyotrophic lateral sclerosis. *Proc Natl Acad Sci U S A,* 103**,** 16021-6.

BEHAR, T. N. 2001. Analysis of fractal dimension of O2A glial cells differentiating in vitro. *Methods,* 24**,** 331-9.

BELGARD, T. G., MARQUES, A. C., OLIVER, P. L., ABAAN, H. O., SIREY, T. M., HOERDER-SUABEDISSEN, A., GARCIA-MORENO, F., MOLNAR, Z., MARGULIES, E. H. & PONTING, C. P. 2011. A transcriptomic atlas of mouse neocortical layers. *Neuron,* 71**,** 605-16.

BELL, J. T., TSAI, P. C., YANG, T. P., PIDSLEY, R., NISBET, J., GLASS, D., MANGINO, M., ZHAI, G., ZHANG, F., VALDES, A., SHIN, S. Y., DEMPSTER, E. L., MURRAY, R. M., GRUNDBERG, E., HEDMAN, A. K., NICA, A., SMALL, K. S., MU, T. C., DERMITZAKIS, E. T., MCCARTHY, M. I., MILL, J., SPECTOR, T. D. & DELOUKAS, P. 2012. Epigenome-wide scans identify differentially methylated regions for age and age-related phenotypes in a healthy ageing population. *PLoS Genet,* 8**,** e1002629.

BELL, S., MAUSSION, G., JEFRI, M., PENG, H., THEROUX, J. F., SILVEIRA, H., SOUBANNIER, V., WU, H., HU, P., GALAT, E., TORRES-PLATAS, S. G., BOUDREAU-PINSONNEAULT, C., O'LEARY, L. A., GALAT, V., TURECKI, G., DURCAN, T. M., FON, E. A., MECHAWAR, N. & ERNST, C.

2018. Disruption of GRIN2B Impairs Differentiation in Human Neurons. *Stem Cell Reports,* 11**,** 183-196.

BELZEAUX, R., FIORI, L. M., LOPEZ, J. P., BOUCEKINE, M., BOYER, L., BLIER, P., FARZAN, F., FREY, B. N., GIACOBBE, P., LAM, R. W., LERI, F., MACQUEEN, G. M., MILEV, R., MULLER, D. J., PARIKH, S. V., ROTZINGER, S., SOARES, C. N., UHER, R., FOSTER, J. A., KENNEDY, S. H. & TURECKI, G. 2019. Predicting Worsening Suicidal Ideation With Clinical Features and Peripheral Expression of Messenger RNA and MicroRNA During Antidepressant Treatment. *J Clin Psychiatry,* 80.

BENETTI, R., GONZALO, S., JACO, I., MUNOZ, P., GONZALEZ, S., SCHOEFTNER, S., MURCHISON, E., ANDL, T., CHEN, T., KLATT, P., LI, E., SERRANO, M., MILLAR, S., HANNON, G. & BLASCO, M. A. 2008. A mammalian microRNA cluster controls DNA methylation and telomere recombination via Rbl2-dependent regulation of DNA methyltransferases. *Nat Struct Mol Biol,* 15**,** 998.

BENNETT, M. L., BENNETT, F. C., LIDDELOW, S. A., AJAMI, B., ZAMANIAN, J. L., FERNHOFF, N. B., MULINYAWE, S. B., BOHLEN, C. J., ADIL, A., TUCKER, A., WEISSMAN, I. L., CHANG, E. F., LI, G., GRANT, G. A., HAYDEN GEPHART, M. G. & BARRES, B. A. 2016. New tools for studying microglia in the mouse and human CNS. *Proc Natl Acad Sci U S A,* 113**,** E1738-46.

BENNETT, M. R. 2011. The prefrontal-limbic network in depression: Modulation by hypothalamus, basal ganglia and midbrain. *Prog Neurobiol,* 93**,** 468-87.

BERGER, S. L. 2007. The complex language of chromatin regulation during transcription. *Nature,* 447**,** 407-12.

BERGMANN, M., SCHUSTER, T., GRABS, D., MARQUEZE-POUEY, B., BETZ, H., TRAURIG, H., MAYERHOFER, A. & GRATZL, M. 1993. Synaptophysin and synaptoporin expression in the developing rat olfactory system. *Brain Res Dev Brain Res,* 74**,** 235-44.

BERNAL, M., HARO, J. M., BERNERT, S., BRUGHA, T., DE GRAAF, R., BRUFFAERTS, R., LEPINE, J. P., DE GIROLAMO, G., VILAGUT, G., GASQUET, I., TORRES, J. V., KOVESS, V., HEIDER, D., NEELEMAN, J., KESSLER, R., ALONSO, J. & INVESTIGATORS, E. M. 2007. Risk factors for suicidality in Europe: results from the ESEMED study. *J Affect Disord,* 101**,** 27-34.

BERNARD, A., LUBBERS, L. S., TANIS, K. Q., LUO, R., PODTELEZHNIKOV, A. A., FINNEY, E. M., MCWHORTER, M. M., SERIKAWA, K., LEMON, T., MORGAN, R., COPELAND, C., SMITH, K., CULLEN, V., DAVIS-TURAK, J., LEE, C. K., SUNKIN, S. M., LOBODA, A. P., LEVINE, D. M., STONE, D. J., HAWRYLYCZ, M. J., ROBERTS, C. J., JONES, A. R., GESCHWIND, D. H. & LEIN, E. S. 2012. Transcriptional architecture of the primate neocortex. *Neuron,* 73**,** 1083-99.

BERNARD, D., PRASANTH, K. V., TRIPATHI, V., COLASSE, S., NAKAMURA, T., XUAN, Z., ZHANG, M. Q., SEDEL, F., JOURDREN, L., COULPIER, F., TRILLER, A., SPECTOR, D. L. & BESSIS, A. 2010. A long nuclear-retained non-coding RNA regulates synaptogenesis by modulating gene expression. *EMBO J,* 29**,** 3082-93.

BERNARD, R., KERMAN, I. A., THOMPSON, R. C., JONES, E. G., BUNNEY, W. E., BARCHAS, J. D., SCHATZBERG, A. F., MYERS, R. M., AKIL, H. & WATSON, S. J. 2011. Altered expression of glutamate signaling, growth factor, and glia genes in the locus coeruleus of patients with major depression. *Mol Psychiatry,* 16**,** 634-46.

BERNSTEIN, B. E., STAMATOYANNOPOULOS, J. A., COSTELLO, J. F., REN, B., MILOSAVLJEVIC, A., MEISSNER, A., KELLIS, M., MARRA, M. A., BEAUDET, A. L., ECKER, J. R., FARNHAM, P. J., HIRST, M., LANDER, E. S., MIKKELSEN, T. S. & THOMSON, J. A. 2010. The NIH Roadmap Epigenomics Mapping Consortium. *Nat Biotechnol,* 28**,** 1045-8.

BERNSTEIN, H. G., BAUMANN, B., DANOS, P., DIEKMANN, S., BOGERTS, B., GUNDELFINGER, E. D. & BRAUNEWELL, K. H. 1999. Regional and cellular distribution of neural visinin-like protein immunoreactivities (VILIP-1 and VILIP-3) in human brain. *J Neurocytol,* 28**,** 655-62.

BERNSTEIN, H. G., KEILHOFF, G., DOBROWOLNY, H., GUEST, P. C. & STEINER, J. 2019. Perineuronal oligodendrocytes in health and disease: the journey so far. *Rev Neurosci,* 31**,** 89-99.

BERNSTEIN, H. G., STEINER, J. & BOGERTS, B. 2009. Glial cells in schizophrenia: pathophysiological significance and possible consequences for therapy. *Expert Rev Neurother,* 9**,** 1059-71.

BERRY, K., WANG, J. & LU, Q. R. 2020. Epigenetic regulation of oligodendrocyte myelination in developmental disorders and neurodegenerative diseases. *F1000Res,* 9.

BERTO, S., USUI, N., KONOPKA, G. & FOGEL, B. L. 2016. ELAVL2-regulated transcriptional and splicing networks in human neurons link neurodevelopment and autism. *Hum Mol Genet,* 25**,** 2451-2464.

BERTOLOTE, J. M., FLEISCHMANN, A., DE LEO, D., BOLHARI, J., BOTEGA, N., DE SILVA, D., TRAN THI THANH, H., PHILLIPS, M., SCHLEBUSCH, L., VARNIK, A., VIJAYAKUMAR, L. & WASSERMAN, D. 2005. Suicide attempts, plans, and ideation in culturally diverse sites: the WHO SUPRE-MISS community survey. *Psychol Med,* 35**,** 1457-65.

BERTOLOTE, J. M., FLEISCHMANN, A., DE LEO, D., PHILLIPS, M. R., BOTEGA, N. J., VIJAYAKUMAR, L., DE SILVA, D., SCHLEBUSCH, L., NGUYEN, V. T., SISASK, M., BOLHARI, J. & WASSERMAN, D. 2010. Repetition of suicide attempts: data from emergency care settings in five culturally different low- and middle-income countries participating in the WHO SUPRE-MISS Study. *Crisis,* 31**,** 194-201.

BERTOLOTE, J. M., FLEISCHMANN, A., DE LEO, D. & WASSERMAN, D. 2003. Suicide and mental disorders: do we know enough? *Br J Psychiatry,* 183**,** 382-3.

BERTOLOTE, J. M., FLEISCHMANN, A., DE LEO, D. & WASSERMAN, D. 2004. Psychiatric diagnoses and suicide: revisiting the evidence. *Crisis,* 25**,** 147-55.

BETTENCOURT, C., FOTI, S. C., MIKI, Y., BOTIA, J., CHATTERJEE, A., WARNER, T. T., REVESZ, T., LASHLEY, T., BALAZS, R., VIRE, E. & HOLTON, J. L. 2020. White matter DNA methylation profiling reveals deregulation of HIP1, LMAN2, MOBP, and other loci in multiple system atrophy. *Acta Neuropathol,* 139**,** 135-156.

BEVERIDGE, N. J., TOONEY, P. A., CARROLL, A. P., GARDINER, E., BOWDEN, N., SCOTT, R. J., TRAN, N., DEDOVA, I. & CAIRNS, M. J. 2008. Dysregulation of miRNA 181b in the temporal cortex in schizophrenia. *Hum Mol Genet,* 17**,** 1156-68.

BHEDA, A., GULLAPALLI, A., CAPLOW, M., PAGANO, J. S. & SHACKELFORD, J. 2010. Ubiquitin editing enzyme UCH L1 and microtubule dynamics: implication in mitosis. *Cell Cycle,* 9**,** 980-94.

BIFULCO, M., LAEZZA, C., STINGO, S. & WOLFF, J. 2002. 2',3'-Cyclic nucleotide 3'-phosphodiesterase: a membrane-bound, microtubule-associated protein and membrane anchor for tubulin. *Proc Natl Acad Sci U S A,* 99**,** 1807-12.

BILGUVAR, K., TYAGI, N. K., OZKARA, C., TUYSUZ, B., BAKIRCIOGLU, M., CHOI, M., DELIL, S., CAGLAYAN, A. O., BARANOSKI, J. F., ERTURK, O., YALCINKAYA, C., KARACORLU, M., DINCER, A., JOHNSON, M. H., MANE, S., CHANDRA, S. S., LOUVI, A., BOGGON, T. J., LIFTON, R. P., HORWICH, A. L. & GUNEL, M. 2013. Recessive loss of function of the neuronal ubiquitin hydrolase UCHL1 leads to early-onset progressive neurodegeneration. *Proc Natl Acad Sci U S A,* 110**,** 3489-94.

BILSLAND, J. G., HALDON, C., GODDARD, J., OLIVER, K., MURRAY, F., WHEELDON, A., CUMBERBATCH, J., MCALLISTER, G. & MUNOZ-SANJUAN, I. 2006. A rapid method for the quantification of mouse hippocampal neurogenesis in vivo by flow cytometry. Validation with conventional and enhanced immunohistochemical methods. *J Neurosci Methods,* 157**,** 54-63.

BIRD, A. 2007. Perceptions of epigenetics. *Nature,* 447**,** 396-8.

BIRDSILL, A. C., WALKER, D. G., LUE, L., SUE, L. I. & BEACH, T. G. 2011. Postmortem interval effect on RNA and gene expression in human brain tissue. *Cell Tissue Bank,* 12**,** 311-8.

BLUEPRINT CONSORTIUM 2016. Quantitative comparison of DNA methylation assays for biomarker development and clinical applications. *Nat Biotechnol,* 34**,** 726-37.

BODDAERT, N., ZILBOVICIUS, M., PHILIPE, A., ROBEL, L., BOURGEOIS, M., BARTHELEMY, C., SEIDENWURM, D., MERESSE, I., LAURIER, L., DESGUERRE, I., BAHI-BUISSON, N.,

BRUNELLE, F., MUNNICH, A., SAMSON, Y., MOUREN, M. C. & CHABANE, N. 2009. MRI findings in 77 children with non-syndromic autistic disorder. *PLoS One,* 4**,** e4415.

BOHMDORFER, G. & WIERZBICKI, A. T. 2015. Control of Chromatin Structure by Long Noncoding RNA. *Trends Cell Biol,* 25**,** 623-632.

BOKS, M. P., RUTTEN, B. P., GEUZE, E., HOUTEPEN, L. C., VERMETTEN, E., KAMINSKY, Z. & VINKERS, C. H. 2016. SKA2 Methylation is Involved in Cortisol Stress Reactivity and Predicts the Development of Post-Traumatic Stress Disorder (PTSD) After Military Deployment. *Neuropsychopharmacology,* 41**,** 1350-6.

BOLLEPALLI, S., KORHONEN, T., KAPRIO, J., ANDERS, S. & OLLIKAINEN, M. 2019. EpiSmokEr: a robust classifier to determine smoking status from DNA methylation data. *Epigenomics,* 11**,** 1469-1486.

BOND, A. M., VANGOMPEL, M. J., SAMETSKY, E. A., CLARK, M. F., SAVAGE, J. C., DISTERHOFT, J. F. & KOHTZ, J. D. 2009. Balanced gene regulation by an embryonic brain ncRNA is critical for adult hippocampal GABA circuitry. *Nat Neurosci,* 12**,** 1020-7.

BOOR, P. K., DE GROOT, K., WAISFISZ, Q., KAMPHORST, W., OUDEJANS, C. B., POWERS, J. M., PRONK, J. C., SCHEPER, G. C. & VAN DER KNAAP, M. S. 2005. MLC1: a novel protein in distal astroglial processes. *J Neuropathol Exp Neurol,* 64**,** 412-9.

BOOTH, M. J., BRANCO, M. R., FICZ, G., OXLEY, D., KRUEGER, F., REIK, W. & BALASUBRAMANIAN, S. 2012. Quantitative sequencing of 5-methylcytosine and 5-hydroxymethylcytosine at single-base resolution. *Science,* 336**,** 934-7.

BOOTH, M. J., MARSICO, G., BACHMAN, M., BERALDI, D. & BALASUBRAMANIAN, S. 2014. Quantitative sequencing of 5-formylcytosine in DNA at single-base resolution. *Nat Chem,* 6**,** 435-40.

BOOTH, M. J., OST, T. W., BERALDI, D., BELL, N. M., BRANCO, M. R., REIK, W. & BALASUBRAMANIAN, S. 2013. Oxidative bisulfite sequencing of 5-methylcytosine and 5-hydroxymethylcytosine. *Nat Protoc,* 8**,** 1841-51.

BORRELLI, E., NESTLER, E. J., ALLIS, C. D. & SASSONE-CORSI, P. 2008. Decoding the epigenetic language of neuronal plasticity. *Neuron,* 60**,** 961-74.

BOSIO, A., BINCZEK, E., LE BEAU, M. M., FERNALD, A. A. & STOFFEL, W. 1996. The human gene CGT encoding the UDP-galactose ceramide galactosyl transferase (cerebroside synthase): cloning, characterization, and assignment to human chromosome 4, band q26. *Genomics,* 34**,** 69-75.

BOSKOVIC, A. & RANDO, O. J. 2018. Transgenerational Epigenetic Inheritance. *Annu Rev Genet,* 52**,** 21-41.

BOTA, M. & SWANSON, L. W. 2007. The neuron classification problem. *Brain Res Rev,* 56**,** 79-88.

BOULANGER, J. J. & MESSIER, C. 2014. From precursors to myelinating oligodendrocytes: contribution of intrinsic and extrinsic factors to white matter plasticity in the adult brain. *Neuroscience,* 269**,** 343-66.

BOZZOLA, M., LOCATELLI, F., CISTERNINO, M., GAMBARANA, D., GIORGIANI, G., BONETTI, F., VALTORTA, A., MORETTA, A., LORINI, R. & SEVERI, F. 1991. Growth in pubertal children after bone marrow transplantation. *Bone Marrow Transplant,* 8 Suppl 1**,** 60.

BRAAK, H. & DEL TREDICI, K. 2015. The preclinical phase of the pathological process underlying sporadic Alzheimer's disease. *Brain,* 138**,** 2814-33.

BRADLEY, K. A., CASE, J. A., KHAN, O., RICART, T., HANNA, A., ALONSO, C. M. & GABBAY, V. 2015. The role of the kynurenine pathway in suicidality in adolescent major depressive disorder. *Psychiatry Res,* 227**,** 206-12.

BRADVIK, L. 2018. Suicide Risk and Mental Disorders. *Int J Environ Res Public Health,* 15.

BRANCO, M. R., FICZ, G. & REIK, W. 2011. Uncovering the role of 5-hydroxymethylcytosine in the epigenome. *Nat Rev Genet,* 13**,** 7-13.

BRAUNEWELL, K. H. 2005. The darker side of Ca2+ signaling by neuronal Ca2+-sensor proteins: from Alzheimer's disease to cancer. *Trends Pharmacol Sci,* 26**,** 345-51.

BRAUNEWELL, K. H. 2012. The visinin-like proteins VILIP-1 and VILIP-3 in Alzheimer's disease-old wine in new bottles. *Front Mol Neurosci,* 5**,** 20.

BRAUNEWELL, K. H., BRACKMANN, M. & MANAHAN-VAUGHAN, D. 2003. Group I mGlu receptors regulate the expression of the neuronal calcium sensor protein VILIP-1 in vitro and in vivo: implications for mGlu receptor-dependent hippocampal plasticity? *Neuropharmacology,* 44**,** 707-15.

BRAUNEWELL, K. H., DWARY, A. D., RICHTER, F., TRAPPE, K., ZHAO, C., GIEGLING, I., SCHONRATH, K. & RUJESCU, D. 2011. Association of VSNL1 with schizophrenia, frontal cortical function, and biological significance for its gene product as a modulator of cAMP levels and neuronal morphology. *Transl Psychiatry,* 1**,** e22.

BREILING, A. & LYKO, F. 2015. Epigenetic regulatory functions of DNA modifications: 5-methylcytosine and beyond. *Epigenetics Chromatin,* 8**,** 24.

BRENT, D. A., BRIDGE, J., JOHNSON, B. A. & CONNOLLY, J. 1996. Suicidal behavior runs in families. A controlled family study of adolescent suicide victims. *Arch Gen Psychiatry,* 53**,** 1145-52.

BRENT, D. A., OQUENDO, M., BIRMAHER, B., GREENHILL, L., KOLKO, D., STANLEY, B., ZELAZNY, J., BRODSKY, B., MELHEM, N., ELLIS, S. P. & MANN, J. J. 2004. Familial transmission of mood disorders: convergence and divergence with transmission of suicidal behavior. *J Am Acad Child Adolesc Psychiatry,* 43**,** 1259-66.

BREZO, J., BUREAU, A., MERETTE, C., JOMPHE, V., BARKER, E. D., VITARO, F., HEBERT, M., CARBONNEAU, R., TREMBLAY, R. E. & TURECKI, G. 2010. Differences and similarities in the serotonergic diathesis for suicide attempts and mood disorders: a 22-year longitudinal gene-environment study. *Mol Psychiatry,* 15**,** 831-43.

BREZO, J., KLEMPAN, T. & TURECKI, G. 2008. The genetics of suicide: a critical review of molecular studies. *Psychiatr Clin North Am,* 31**,** 179-203.

BRIESE, T., PALACIOS, G., KOKORIS, M., JABADO, O., LIU, Z., RENWICK, N., KAPOOR, V., CASAS, I., POZO, F., LIMBERGER, R., PEREZ-BRENA, P., JU, J. & LIPKIN, W. I. 2005. Diagnostic system for rapid and sensitive differential detection of pathogens. *Emerg Infect Dis,* 11**,** 310-3.

BRIGGS, J. A., WOLVETANG, E. J., MATTICK, J. S., RINN, J. L. & BARRY, G. 2015. Mechanisms of Long Non-coding RNAs in Mammalian Nervous System Development, Plasticity, Disease, and Evolution. *Neuron,* 88**,** 861-877.

BRISCH, R., STEINER, J., MAWRIN, C., KRZYZANOWSKA, M., JANKOWSKI, Z. & GOS, T. 2017. Microglia in the dorsal raphe nucleus plays a potential role in both suicide facilitation and prevention in affective disorders. *Eur Arch Psychiatry Clin Neurosci,* 267**,** 403-415.

BROCCANELLO, C., GERACE, L. & STEVANATO, P. 2020. QuantStudio() 12K Flex OpenArray((R)) System as a Tool for High-Throughput Genotyping and Gene Expression Analysis. *Methods Mol Biol,* 2065**,** 199-208.

BUMKE, M. A., NERI, D. & ELIA, G. 2003. Modulation of gene expression by extracellular pH variations in human fibroblasts: a transcriptomic and proteomic study. *Proteomics,* 3**,** 675-88.

BURGOYNE, R. D. 2007. Neuronal calcium sensor proteins: generating diversity in neuronal Ca2+ signalling. *Nat Rev Neurosci,* 8**,** 182-93.

BURNS, S. B., SZYSZKOWICZ, J. K., LUHESHI, G. N., LUTZ, P. E. & TURECKI, G. 2018. Plasticity of the epigenome during early-life stress. *Semin Cell Dev Biol,* 77**,** 115-132.

BUSSE, M., BUSSE, S., MYINT, A. M., GOS, T., DOBROWOLNY, H., MULLER, U. J., BOGERTS, B., BERNSTEIN, H. G. & STEINER, J. 2015. Decreased quinolinic acid in the hippocampus of depressive patients: evidence for local anti-inflammatory and neuroprotective responses? *Eur Arch Psychiatry Clin Neurosci,* 265**,** 321-9.

BUTOVSKY, O., JEDRYCHOWSKI, M. P., MOORE, C. S., CIALIC, R., LANSER, A. J., GABRIELY, G., KOEGLSPERGER, T., DAKE, B., WU, P. M., DOYKAN, C. E., FANEK, Z., LIU, L., CHEN, Z., ROTHSTEIN, J. D., RANSOHOFF, R. M., GYGI, S. P., ANTEL, J. P. & WEINER, H. L. 2014. Identification of a unique TGF-beta-dependent molecular and functional signature in microglia. *Nat Neurosci,* 17**,** 131-43.

BUTTGEREIT, A., LELIOS, I., YU, X., VROHLINGS, M., KRAKOSKI, N. R., GAUTIER, E. L., NISHINAKAMURA, R., BECHER, B. & GRETER, M. 2016. Sall1 is a transcriptional regulator defining microglia identity and function. *Nat Immunol,* 17**,** 1397-1406.

BYNE, W., DRACHEVA, S., CHIN, B., SCHMEIDLER, J. M., DAVIS, K. L. & HAROUTUNIAN, V. 2008. Schizophrenia and sex associated differences in the expression of neuronal and oligodendrocyte-specific genes in individual thalamic nuclei. *Schizophr Res,* 98**,** 118-28.

BYRNES, K. R., GARAY, J., DI GIOVANNI, S., DE BIASE, A., KNOBLACH, S. M., HOFFMAN, E. P., MOVSESYAN, V. & FADEN, A. I. 2006. Expression of two temporally distinct microglia-related gene clusters after spinal cord injury. *Glia,* 53**,** 420-33.

BYUN, H. M., SIEGMUND, K. D., PAN, F., WEISENBERGER, D. J., KANEL, G., LAIRD, P. W. & YANG, A. S. 2009. Epigenetic profiling of somatic tissues from human autopsy specimens identifies tissue- and individual-specific DNA methylation patterns. *Hum Mol Genet,* 18**,** 4808-17.

CABILI, M. N., TRAPNELL, C., GOFF, L., KOZIOL, M., TAZON-VEGA, B., REGEV, A. & RINN, J. L. 2011. Integrative annotation of human large intergenic noncoding RNAs reveals global properties and specific subclasses. *Genes Dev,* 25**,** 1915-27.

CAHOY, J. D., EMERY, B., KAUSHAL, A., FOO, L. C., ZAMANIAN, J. L., CHRISTOPHERSON, K. S., XING, Y., LUBISCHER, J. L., KRIEG, P. A., KRUPENKO, S. A., THOMPSON, W. J. & BARRES, B. A. 2008. A transcriptome database for astrocytes, neurons, and oligodendrocytes: a new resource for understanding brain development and function. *J Neurosci,* 28**,** 264-78.

CAI, D., QIU, J., CAO, Z., MCATEE, M., BREGMAN, B. S. & FILBIN, M. T. 2001. Neuronal cyclic AMP controls the developmental loss in ability of axons to regenerate. *J Neurosci,* 21**,** 4731-9.

CAI, Z. & XIAO, M. 2016. Oligodendrocytes and Alzheimer's disease. *Int J Neurosci,* 126**,** 97-104.

CALDERO, J., BRUNET, N., CIUTAT, D., HEREU, M. & ESQUERDA, J. E. 2009. Development of microglia in the chick embryo spinal cord: implications in the regulation of motoneuronal survival and death. *J Neurosci Res,* 87**,** 2447-66.

CAMPBELL, R. R. & WOOD, M. A. 2019. How the epigenome integrates information and reshapes the synapse. *Nat Rev Neurosci,* 20**,** 133-147.

CANETTO, S. S. 2008. Women and suicidal behavior: a cultural analysis. *Am J Orthopsychiatry,* 78**,** 259-66.

CAO, T. & ZHEN, X. C. 2018. Dysregulation of miRNA and its potential therapeutic application in schizophrenia. *CNS Neurosci Ther,* 24**,** 586-597.

CARAMASCHI, D., SHARP, G. C., NOHR, E. A., BERRYMAN, K., LEWIS, S. J., DAVEY SMITH, G. & RELTON, C. L. 2017. Exploring a causal role of DNA methylation in the relationship between maternal vitamin B12 during pregnancy and child's IQ at age 8, cognitive performance and educational attainment: a two-step Mendelian randomization study. *Hum Mol Genet,* 26**,** 3001-3013.

CARDOZO, P. L., DE LIMA, I. B. Q., MACIEL, E. M. A., SILVA, N. C., DOBRANSKY, T. & RIBEIRO, F. M. 2019. Synaptic Elimination in Neurological Disorders. *Curr Neuropharmacol,* 17**,** 1071-1095.

CARIAGA-MARTINEZ, A. & ALELU-PAZ, R. 2017. Rethinking the Epigenetic Framework to Unravel the Molecular Pathology of Schizophrenia. *Int J Mol Sci,* 18.

CASANO, A. M. & PERI, F. 2015. Microglia: multitasking specialists of the brain. *Dev Cell,* 32**,** 469-77.

CASANOVA, M. F. 2006. Neuropathological and genetic findings in autism: the significance of a putative minicolumnopathy. *Neuroscientist,* 12**,** 435-41.

CASSIA, R., BESNARD, L., FIETTE, L., ESPINOSA DE LOS MONTEROS, A., AVE, P., PY, M. C., HUERRE, M., DE VELLIS, J., ZAKIN, M. M. & GUILLOU, F. 1997. Transferrin is an early marker of hepatic differentiation, and its expression correlates with the postnatal development of oligodendrocytes in mice. *J Neurosci Res,* 50**,** 421-32.

CATTANE, N., MORA, C., LOPIZZO, N., BORSINI, A., MAJ, C., PEDRINI, L., ROSSI, R., RIVA, M. A., PARIANTE, C. M. & CATTANEO, A. 2019. Identification of a miRNAs signature associated with exposure to stress early in life and enhanced vulnerability for schizophrenia: New insights for the key role of miR-125b-1-3p in neurodevelopmental processes. *Schizophr Res,* 205**,** 63-75.

CATTS, V. S., CATTS, S. V., FERNANDEZ, H. R., TAYLOR, J. M., COULSON, E. J. & LUTZE-MANN, L. H. 2005. A microarray study of post-mortem mRNA degradation in mouse brain tissue. *Brain Res Mol Brain Res,* 138**,** 164-77.

CAZALY, E., SAAD, J., WANG, W., HECKMAN, C., OLLIKAINEN, M. & TANG, J. 2019. Making Sense of the Epigenome Using Data Integration Approaches. *Front Pharmacol,* 10**,** 126.

CDC HEALTH REPORT. 2017. *CDC* [Online]. Available: https://www.cdc.gov/ [Accessed].

CERMINARA, N. L., LANG, E. J., SILLITOE, R. V. & APPS, R. 2015. Redefining the cerebellar cortex as an assembly of non-uniform Purkinje cell microcircuits. *Nat Rev Neurosci,* 16**,** 79-93.

CHANG, Y. T., CHOU, C. T., SHIAO, Y. M., LIN, M. W., YU, C. W., CHEN, C. C., HUANG, C. H., LEE, D. D., LIU, H. N., WANG, W. J. & TSAI, S. F. 2006. Psoriasis vulgaris in Chinese individuals is associated with PSORS1C3 and CDSN genes. *Br J Dermatol,* 155**,** 663-9.

CHANOUMIDOU, K., MOZAFARI, S., BARON-VAN EVERCOOREN, A. & KUHLMANN, T. 2020. Stem cell derived oligodendrocytes to study myelin diseases. *Glia,* 68**,** 705-720.

CHATTERJEE, A., RODGER, E. J., MORISON, I. M., ECCLES, M. R. & STOCKWELL, P. A. 2017. Tools and Strategies for Analysis of Genome-Wide and Gene-Specific DNA Methylation Patterns. *Methods Mol Biol,* 1537**,** 249-277.

CHATTOPADHYAY, P. K. & ROEDERER, M. 2012. Cytometry: today's technology and tomorrow's horizons. *Methods,* 57**,** 251-8.

CHEN, A., AKINYEMI, R. O., HASE, Y., FIRBANK, M. J., NDUNG'U, M. N., FOSTER, V., CRAGGS, L. J., WASHIDA, K., OKAMOTO, Y., THOMAS, A. J., POLVIKOSKI, T. M., ALLAN, L. M., OAKLEY, A. E., O'BRIEN, J. T., HORSBURGH, K., IHARA, M. & KALARIA, R. N. 2016. Frontal white matter hyperintensities, clasmatodendrosis and gliovascular abnormalities in ageing and post-stroke dementia. *Brain,* 139**,** 242-58.

CHEN, J. L., LUCAS, J. E., SCHROEDER, T., MORI, S., WU, J., NEVINS, J., DEWHIRST, M., WEST, M. & CHI, J. T. 2008. The genomic analysis of lactic acidosis and acidosis response in human cancers. *PLoS Genet,* 4**,** e1000293.

CHEN, K. H., BOETTIGER, A. N., MOFFITT, J. R., WANG, S. & ZHUANG, X. 2015. RNA imaging. Spatially resolved, highly multiplexed RNA profiling in single cells. *Science,* 348**,** aaa6090.

CHEN, T., UEDA, Y., DODGE, J. E., WANG, Z. & LI, E. 2003. Establishment and maintenance of genomic methylation patterns in mouse embryonic stem cells by Dnmt3a and Dnmt3b. *Mol Cell Biol,* 23**,** 5594-605.

CHEN, Y. A., LEMIRE, M., CHOUFANI, S., BUTCHER, D. T., GRAFODATSKAYA, D., ZANKE, B. W., GALLINGER, S., HUDSON, T. J. & WEKSBERG, R. 2013. Discovery of cross-reactive probes and polymorphic CpGs in the Illumina Infinium HumanMethylation450 microarray. *Epigenetics,* 8**,** 203-9.

CHENG, L., ZHANG, S., MACLENNAN, G. T., WILLIAMSON, S. R., DAVIDSON, D. D., WANG, M., JONES, T. D., LOPEZ-BELTRAN, A. & MONTIRONI, R. 2013. Laser-assisted microdissection in translational research: theory, technical considerations, and future applications. *Appl Immunohistochem Mol Morphol,* 21**,** 31-47.

CHENG, Y., LI, Z., MANUPIPATPONG, S., LIN, L., LI, X., XU, T., JIANG, Y. H., SHU, Q., WU, H. & JIN, P. 2018. 5-Hydroxymethylcytosine alterations in the human postmortem brains of autism spectrum disorder. *Hum Mol Genet,* 27**,** 2955-2964.

CHOI, J., LEVEY, A. I., WEINTRAUB, S. T., REES, H. D., GEARING, M., CHIN, L. S. & LI, L. 2004. Oxidative modifications and down-regulation of ubiquitin carboxyl-terminal hydrolase L1 associated with idiopathic Parkinson's and Alzheimer's diseases. *J Biol Chem,* 279**,** 13256-64.

CHOUDARY, P. V., MOLNAR, M., EVANS, S. J., TOMITA, H., LI, J. Z., VAWTER, M. P., MYERS, R. M., BUNNEY, W. E., JR., AKIL, H., WATSON, S. J. & JONES, E. G. 2005. Altered cortical

glutamatergic and GABAergic signal transmission with glial involvement in depression. *Proc Natl Acad Sci U S A,* 102**,** 15653-8.

CHOUDHERY, M. S., BADOWSKI, M., MUISE, A. & HARRIS, D. T. 2013. Comparison of human mesenchymal stem cells derived from adipose and cord tissue. *Cytotherapy,* 15**,** 330-43.

CHRISTOPHERSON, K. S., ULLIAN, E. M., STOKES, C. C., MULLOWNEY, C. E., HELL, J. W., AGAH, A., LAWLER, J., MOSHER, D. F., BORNSTEIN, P. & BARRES, B. A. 2005. Thrombospondins are astrocyte-secreted proteins that promote CNS synaptogenesis. *Cell,* 120**,** 421-33.

CHUNG, W. S., CLARKE, L. E., WANG, G. X., STAFFORD, B. K., SHER, A., CHAKRABORTY, C., JOUNG, J., FOO, L. C., THOMPSON, A., CHEN, C., SMITH, S. J. & BARRES, B. A. 2013. Astrocytes mediate synapse elimination through MEGF10 and MERTK pathways. *Nature,* 504**,** 394-400.

CLARK, S. M., POCIVAVSEK, A., NICHOLSON, J. D., NOTARANGELO, F. M., LANGENBERG, P., MCMAHON, R. P., KLEINMAN, J. E., HYDE, T. M., STILLER, J., POSTOLACHE, T. T., SCHWARCZ, R. & TONELLI, L. H. 2016. Reduced kynurenine pathway metabolism and cytokine expression in the prefrontal cortex of depressed individuals. *J Psychiatry Neurosci,* 41**,** 386-394.

CLARKE, J., WU, H. C., JAYASINGHE, L., PATEL, A., REID, S. & BAYLEY, H. 2009. Continuous base identification for single-molecule nanopore DNA sequencing. *Nat Nanotechnol,* 4**,** 265-70.

CLIVE, M. L., BOKS, M. P., VINKERS, C. H., OSBORNE, L. M., PAYNE, J. L., RESSLER, K. J., SMITH, A. K., WILCOX, H. C. & KAMINSKY, Z. 2016. Discovery and replication of a peripheral tissue DNA methylation biosignature to augment a suicide prediction model. *Clin Epigenetics,* 8**,** 113.

COLQUITT, B. M., ALLEN, W. E., BARNEA, G. & LOMVARDAS, S. 2013. Alteration of genic 5-hydroxymethylcytosine patterning in olfactory neurons correlates with changes in gene expression and cell identity. *Proc Natl Acad Sci U S A,* 110**,** 14682-7.

CONDLIFFE, D., WONG, A., TROAKES, C., PROITSI, P., PATEL, Y., CHOULIARAS, L., FERNANDES, C., COOPER, J., LOVESTONE, S., SCHALKWYK, L., MILL, J. & LUNNON, K. 2014. Cross-region reduction in 5-hydroxymethylcytosine in Alzheimer's disease brain. *Neurobiol Aging,* 35**,** 1850-4.

CONRADT, E., OSTLUND, B., GUERIN, D., ARMSTRONG, D. A., MARSIT, C. J., TRONICK, E., LAGASSE, L. & LESTER, B. M. 2019. DNA methylation of NR3c1 in infancy: Associations between maternal caregiving and infant sex. *Infant Ment Health J,* 40**,** 513-522.

CONSORTIUM, E. P. 2012. An integrated encyclopedia of DNA elements in the human genome. *Nature,* 489**,** 57-74.

CONSORTIUM, G. T. 2013. The Genotype-Tissue Expression (GTEx) project. *Nat Genet,* 45**,** 580-5.

COON, H., DARLINGTON, T. M., DIBLASI, E., CALLOR, W. B., FERRIS, E., FRASER, A., YU, Z., WILLIAM, N., DAS, S. C., CROWELL, S. E., CHEN, D., ANDERSON, J. S., KLEIN, M., JEROMINSKI, L., CANNON, D., SHABALIN, A., DOCHERTY, A., WILLIAMS, M., SMITH, K. R., KEESHIN, B., BAKIAN, A. V., CHRISTENSEN, E., LI, Q. S., CAMP, N. J. & GRAY, D. 2020. Genome-wide significant regions in 43 Utah high-risk families implicate multiple genes involved in risk for completed suicide. *Mol Psychiatry,* 25**,** 3077-3090.

CORDONE, I., MASI, S., CAROSI, M., VIDIRI, A., MARCHESI, F., MARINO, M., TELERA, S., PASQUALE, A., MENGARELLI, A., CONTI, L., PESCARMONA, E., PACE, A. & CARAPELLA, C. M. 2016. Brain stereotactic biopsy flow cytometry for central nervous system lymphoma characterization: advantages and pitfalls. *J Exp Clin Cancer Res,* 35**,** 128.

COSSARIZZA, A., CHANG, H. D., RADBRUCH, A., ACS, A., ADAM, D., ADAM-KLAGES, S., AGACE, W. W., AGHAEEPOUR, N., AKDIS, M., ALLEZ, M., ALMEIDA, L. N., ALVISI, G., ANDERSON, G., ANDRA, I., ANNUNZIATO, F., ANSELMO, A., BACHER, P., BALDARI, C. T., BARI, S., BARNABA, V., BARROS-MARTINS, J., BATTISTINI, L., BAUER, W., BAUMGART, S., BAUMGARTH, N., BAUMJOHANN, D., BAYING, B., BEBAWY, M., BECHER, B., BEISKER, W., BENES, V., BEYAERT, R., BLANCO, A., BOARDMAN, D. A., BOGDAN, C., BORGER, J. G.,

BORSELLINO, G., BOULAIS, P. E., BRADFORD, J. A., BRENNER, D., BRINKMAN, R. R., BROOKS, A. E. S., BUSCH, D. H., BUSCHER, M., BUSHNELL, T. P., CALZETTI, F., CAMERON, G., CAMMARATA, I., CAO, X., CARDELL, S. L., CASOLA, S., CASSATELLA, M. A., CAVANI, A., CELADA, A., CHATENOUD, L., CHATTOPADHYAY, P. K., CHOW, S., CHRISTAKOU, E., CICIN-SAIN, L., CLERICI, M., COLOMBO, F. S., COOK, L., COOKE, A., COOPER, A. M., CORBETT, A. J., COSMA, A., COSMI, L., COULIE, P. G., CUMANO, A., CVETKOVIC, L., DANG, V. D., DANG-HEINE, C., DAVEY, M. S., DAVIES, D., DE BIASI, S., DEL ZOTTO, G., DELA CRUZ, G. V., DELACHER, M., DELLA BELLA, S., DELLABONA, P., DENIZ, G., DESSING, M., DI SANTO, J. P., DIEFENBACH, A., DIELI, F., DOLF, A., DORNER, T., DRESS, R. J., DUDZIAK, D., DUSTIN, M., DUTERTRE, C. A., EBNER, F., ECKLE, S. B. G., EDINGER, M., EEDE, P., EHRHARDT, G. R. A., EICH, M., ENGEL, P., ENGELHARDT, B., ERDEI, A., et al. 2019. Guidelines for the use of flow cytometry and cell sorting in immunological studies (second edition). *Eur J Immunol,* 49**,** 1457-1973.

COTTER, D. R., PARIANTE, C. M. & EVERALL, I. P. 2001. Glial cell abnormalities in major psychiatric disorders: the evidence and implications. *Brain Res Bull,* 55**,** 585-95.

COUGHLIN, J. M., WANG, Y., AMBINDER, E. B., WARD, R. E., MINN, I., VRANESIC, M., KIM, P. K., FORD, C. N., HIGGS, C., HAYES, L. N., SCHRETLEN, D. J., DANNALS, R. F., KASSIOU, M., SAWA, A. & POMPER, M. G. 2016. In vivo markers of inflammatory response in recent-onset schizophrenia: a combined study using [(11)C]DPA-713 PET and analysis of CSF and plasma. *Transl Psychiatry,* 6**,** e777.

CRAWFORD, B., CRAIG, Z., MANSELL, G., WHITE, I., SMITH, A., SPAULL, S., IMM, J., HANNON, E., WOOD, A., YAGHOOTKAR, H., JI, Y., MAJOR DEPRESSIVE DISORDER WORKING GROUP OF THE PSYCHIATRIC GENOMICS, C., MULLINS, N., LEWIS, C. M., MILL, J. & MURPHY, T. M. 2018. DNA methylation and inflammation marker profiles associated with a history of depression. *Hum Mol Genet,* 27**,** 2840-2850.

CRIDER, A., FENG, T., PANDYA, C. D., DAVIS, T., NAIR, A., AHMED, A. O., BABAN, B., TURECKI, G. & PILLAI, A. 2018. Complement component 3a receptor deficiency attenuates chronic stress-induced monocyte infiltration and depressive-like behavior. *Brain Behav Immun,* 70**,** 246-256.

CROSETTO, N., BIENKO, M. & VAN OUDENAARDEN, A. 2015. Spatially resolved transcriptomics and beyond. *Nat Rev Genet,* 16**,** 57-66.

CROSS-DISORDER GROUP OF THE PSYCHIATRIC GENOMICS, C. 2013. Identification of risk loci with shared effects on five major psychiatric disorders: a genome-wide analysis. *Lancet,* 381**,** 1371-1379.

CRUCEANU, C., ALDA, M., NAGY, C., FREEMANTLE, E., ROULEAU, G. A. & TURECKI, G. 2013. H3K4 tri-methylation in synapsin genes leads to different expression patterns in bipolar disorder and major depression. *Int J Neuropsychopharmacol,* 16**,** 289-99.

CUI, X., NIU, W., KONG, L., HE, M., JIANG, K., CHEN, S., ZHONG, A., LI, W., LU, J. & ZHANG, L. 2017. Long noncoding RNA expression in peripheral blood mononuclear cells and suicide risk in Chinese patients with major depressive disorder. *Brain Behav,* 7**,** e00711.

CZOPKA, T., VON HOLST, A., SCHMIDT, G., FFRENCH-CONSTANT, C. & FAISSNER, A. 2009. Tenascin C and tenascin R similarly prevent the formation of myelin membranes in a RhoA-dependent manner, but antagonistically regulate the expression of myelin basic protein via a separate pathway. *Glia,* 57**,** 1790-801.

DACA-ROSZAK, P., PFEIFER, A., ZEBRACKA-GALA, J., RUSINEK, D., SZYBINSKA, A., JARZAB, B., WITT, M. & ZIETKIEWICZ, E. 2015. Impact of SNPs on methylation readouts by Illumina Infinium HumanMethylation450 BeadChip Array: implications for comparative population studies. *BMC Genomics,* 16**,** 1003.

DAINIAK, M. B., KUMAR, A., GALAEV, I. Y. & MATTIASSON, B. 2007. Methods in cell separations. *Adv Biochem Eng Biotechnol,* 106**,** 1-18.

DAMMER, E. B., DUONG, D. M., DINER, I., GEARING, M., FENG, Y., LAH, J. J., LEVEY, A. I. & SEYFRIED, N. T. 2013. Neuron enriched nuclear proteome isolated from human brain. *J Proteome Res,* 12**,** 3193-206.

DANG, T. C., ISHII, Y., NGUYEN, V., YAMAMOTO, S., HAMASHIMA, T., OKUNO, N., NGUYEN, Q. L., SANG, Y., OHKAWA, N., SAITOH, Y., SHEHATA, M., TAKAKURA, N., FUJIMORI, T., INOKUCHI, K., MORI, H., ANDRAE, J., BETSHOLTZ, C. & SASAHARA, M. 2019. Powerful Homeostatic Control of Oligodendroglial Lineage by PDGFRalpha in Adult Brain. *Cell Rep,* 27**,** 1073-1089 e5.

DANIELE, L. L., EMRAN, F., LOBO, G. P., GAIVIN, R. J. & PERKINS, B. D. 2016. Mutation of wrb, a Component of the Guided Entry of Tail-Anchored Protein Pathway, Disrupts Photoreceptor Synapse Structure and Function. *Invest Ophthalmol Vis Sci,* 57**,** 2942-54.

DANINO, Y. M., EVEN, D., IDESES, D. & JUVEN-GERSHON, T. 2015. The core promoter: At the heart of gene expression. *Biochim Biophys Acta,* 1849**,** 1116-31.

DANKA MOHAMMED, C. P., PARK, J. S., NAM, H. G. & KIM, K. 2017. MicroRNAs in brain aging. *Mech Ageing Dev,* 168**,** 3-9.

DANTZER, R., O'CONNOR, J. C., LAWSON, M. A. & KELLEY, K. W. 2011. Inflammation-associated depression: from serotonin to kynurenine. *Psychoneuroendocrinology,* 36**,** 426-36.

DAVEGARDH, C., HALL WEDIN, E., BROHOLM, C., HENRIKSEN, T. I., PEDERSEN, M., PEDERSEN, B. K., SCHEELE, C. & LING, C. 2019. Sex influences DNA methylation and gene expression in human skeletal muscle myoblasts and myotubes. *Stem Cell Res Ther,* 10**,** 26.

DAVIES, M. N., KRAUSE, L., BELL, J. T., GAO, F., WARD, K. J., WU, H., LU, H., LIU, Y., TSAI, P. C., COLLIER, D. A., MURPHY, T., DEMPSTER, E., MILL, J., CONSORTIUM, U. K. B. E., BATTLE, A., MOSTAFAVI, S., ZHU, X., HENDERS, A., BYRNE, E., WRAY, N. R., MARTIN, N. G., SPECTOR, T. D. & WANG, J. 2014. Hypermethylation in the ZBTB20 gene is associated with major depressive disorder. *Genome Biol,* 15**,** R56.

DAVIES, M. N., VOLTA, M., PIDSLEY, R., LUNNON, K., DIXIT, A., LOVESTONE, S., COARFA, C., HARRIS, R. A., MILOSAVLJEVIC, A., TROAKES, C., AL-SARRAJ, S., DOBSON, R., SCHALKWYK, L. C. & MILL, J. 2012. Functional annotation of the human brain methylome identifies tissue-specific epigenetic variation across brain and blood. *Genome Biol,* 13**,** R43.

DAVIES, W., ISLES, A. R. & WILKINSON, L. S. 2005. Imprinted gene expression in the brain. *Neurosci Biobehav Rev,* 29**,** 421-30.

DAVIS S, , D. P., , B. S., , T. T. & , B. M. 2014. methylumi: Handle illumina methylation data. R Package version 2.0.

DAWLATY, M. M., BREILING, A., LE, T., RADDATZ, G., BARRASA, M. I., CHENG, A. W., GAO, Q., POWELL, B. E., LI, Z., XU, M., FAULL, K. F., LYKO, F. & JAENISCH, R. 2013. Combined deficiency of Tet1 and Tet2 causes epigenetic abnormalities but is compatible with postnatal development. *Dev Cell,* 24**,** 310-23.

DAWSON, M. R., POLITO, A., LEVINE, J. M. & REYNOLDS, R. 2003. NG2-expressing glial progenitor cells: an abundant and widespread population of cycling cells in the adult rat CNS. *Mol Cell Neurosci,* 24**,** 476-88.

DAY, I. N. & THOMPSON, R. J. 2010. UCHL1 (PGP 9.5): neuronal biomarker and ubiquitin system protein. *Prog Neurobiol,* 90**,** 327-62.

DE ARRIBA ZERPA, G. A., SALEH, M. C., FERNANDEZ, P. M., GUILLOU, F., ESPINOSA DE LOS MONTEROS, A., DE VELLIS, J., ZAKIN, M. M. & BARON, B. 2000. Alternative splicing prevents transferrin secretion during differentiation of a human oligodendrocyte cell line. *J Neurosci Res,* 61**,** 388-95.

DE LANGE, G. M. 2017. Understanding the cellular and molecular alterations in PTSD brains: The necessity of post-mortem brain tissue. *Eur J Psychotraumatol,* 8**,** 1341824.

DE PAIVA, A. R. B., LYNCH, D. S., MELO, U. S., LUCATO, L. T., FREUA, F., DE ASSIS, B. D. R., BARCELOS, I., LISTIK, C., DE CASTRO DOS SANTOS, D., MACEDO-SOUZA, L. I., HOULDEN, H. & KOK, F. 2019. PUS3 mutations are associated with intellectual disability, leukoencephalopathy, and nephropathy. *Neurol Genet,* 5**,** e306.

DEAL, R. B. & HENIKOFF, S. 2010. A simple method for gene expression and chromatin profiling of individual cell types within a tissue. *Dev Cell,* 18**,** 1030-40.

DEAMER, D., AKESON, M. & BRANTON, D. 2016. Three decades of nanopore sequencing. *Nat Biotechnol,* 34**,** 518-24.

DEATON, A. M. & BIRD, A. 2011. CpG islands and the regulation of transcription. *Genes Dev,* 25**,** 1010-22.

DECZKOWSKA, A., MATCOVITCH-NATAN, O., TSITSOU-KAMPELI, A., BEN-HAMO, S., DVIR-SZTERNFELD, R., SPINRAD, A., SINGER, O., DAVID, E., WINTER, D. R., SMITH, L. K., KERTSER, A., BARUCH, K., ROSENZWEIG, N., TEREM, A., PRINZ, M., VILLEDA, S., CITRI, A., AMIT, I. & SCHWARTZ, M. 2017. Mef2C restrains microglial inflammatory response and is lost in brain ageing in an IFN-I-dependent manner. *Nat Commun,* 8**,** 717.

DEDEURWAERDER, S., DEFRANCE, M., CALONNE, E., DENIS, H., SOTIRIOU, C. & FUKS, F. 2011. Evaluation of the Infinium Methylation 450K technology. *Epigenomics,* 3**,** 771-84.

DEL-AGUILA, J. L., LI, Z., DUBE, U., MIHINDUKULASURIYA, K. A., BUDDE, J. P., FERNANDEZ, M. V., IBANEZ, L., BRADLEY, J., WANG, F., BERGMANN, K., DAVENPORT, R., MORRIS, J. C., HOLTZMAN, D. M., PERRIN, R. J., BENITEZ, B. A., DOUGHERTY, J., CRUCHAGA, C. & HARARI, O. 2019. A single-nuclei RNA sequencing study of Mendelian and sporadic AD in the human brain. *Alzheimers Res Ther,* 11**,** 71.

DEMPSTER, E., VIANA, J., PIDSLEY, R. & MILL, J. 2013. Epigenetic studies of schizophrenia: progress, predicaments, and promises for the future. *Schizophr Bull,* 39**,** 11-6.

DEMPSTER, E. L., WONG, C. C., LESTER, K. J., BURRAGE, J., GREGORY, A. M., MILL, J. & ELEY, T. C. 2014. Genome-wide methylomic analysis of monozygotic twins discordant for adolescent depression. *Biol Psychiatry,* 76**,** 977-83.

DENERIS, E. S. & HOBERT, O. 2014. Maintenance of postmitotic neuronal cell identity. *Nat Neurosci,* 17**,** 899-907.

DENIS, H., NDLOVU, M. N. & FUKS, F. 2011. Regulation of mammalian DNA methyltransferases: a route to new mechanisms. *EMBO Rep,* 12**,** 647-56.

DEONI, S. C., ZINKSTOK, J. R., DALY, E., ECKER, C., CONSORTIUM, M. A., WILLIAMS, S. C. & MURPHY, D. G. 2015. White-matter relaxation time and myelin water fraction differences in young adults with autism. *Psychol Med,* 45**,** 795-805.

DERRIEN, T., JOHNSON, R., BUSSOTTI, G., TANZER, A., DJEBALI, S., TILGNER, H., GUERNEC, G., MARTIN, D., MERKEL, A., KNOWLES, D. G., LAGARDE, J., VEERAVALLI, L., RUAN, X., RUAN, Y., LASSMANN, T., CARNINCI, P., BROWN, J. B., LIPOVICH, L., GONZALEZ, J. M., THOMAS, M., DAVIS, C. A., SHIEKHATTAR, R., GINGERAS, T. R., HUBBARD, T. J., NOTREDAME, C., HARROW, J. & GUIGO, R. 2012. The GENCODE v7 catalog of human long noncoding RNAs: analysis of their gene structure, evolution, and expression. *Genome Res,* 22**,** 1775-89.

DIETZ, K. C., POLANCO, J. J., POL, S. U. & SIM, F. J. 2016. Targeting human oligodendrocyte progenitors for myelin repair. *Exp Neurol,* 283**,** 489-500.

DIETZSCHOLD, B., SCHWAEBLE, W., SCHAFER, M. K., HOOPER, D. C., ZEHNG, Y. M., PETRY, F., SHENG, H., FINK, T., LOOS, M., KOPROWSKI, H. & WEIHE, E. 1995. Expression of C1q, a subcomponent of the rat complement system, is dramatically enhanced in brains of rats with either Borna disease or experimental allergic encephalomyelitis. *J Neurol Sci,* 130**,** 11-6.

DINGER, M. E., AMARAL, P. P., MERCER, T. R., PANG, K. C., BRUCE, S. J., GARDINER, B. B., ASKARIAN-AMIRI, M. E., RU, K., SOLDA, G., SIMONS, C., SUNKIN, S. M., CROWE, M. L., GRIMMOND, S. M., PERKINS, A. C. & MATTICK, J. S. 2008. Long noncoding RNAs in mouse embryonic stem cell pluripotency and differentiation. *Genome Res,* 18**,** 1433-45.

DOCHERTY, A. R., SHABALIN, A. A., DIBLASI, E., MONSON, E., MULLINS, N., ADKINS, D. E., BACANU, S. A., BAKIAN, A. V., CROWELL, S., CHEN, D., DARLINGTON, T. M., CALLOR, W. B., CHRISTENSEN, E. D., GRAY, D., KEESHIN, B., KLEIN, M., ANDERSON, J. S., JEROMINSKI, L., HAYWARD, C., PORTEOUS, D. J., MCINTOSH, A., LI, Q. & COON, H. 2020. Genome-Wide Association Study of Suicide Death and Polygenic Prediction of Clinical Antecedents. *Am J Psychiatry,* 177**,** 917-927.

DOMINGUEZ, S. R., BRIESE, T., PALACIOS, G., HUI, J., VILLARI, J., KAPOOR, V., TOKARZ, R., GLODE, M. P., ANDERSON, M. S., ROBINSON, C. C., HOLMES, K. V. & LIPKIN, W. I. 2008. Multiplex MassTag-PCR for respiratory pathogens in pediatric nasopharyngeal washes negative by conventional diagnostic testing shows a high prevalence of viruses belonging to a newly recognized rhinovirus clade. *J Clin Virol,* 43**,** 219-22.

DOUVARAS, P. & FOSSATI, V. 2015. Generation and isolation of oligodendrocyte progenitor cells from human pluripotent stem cells. *Nat Protoc,* 10**,** 1143-54.

DOYLE, J. P., DOUGHERTY, J. D., HEIMAN, M., SCHMIDT, E. F., STEVENS, T. R., MA, G., BUPP, S., SHRESTHA, P., SHAH, R. D., DOUGHTY, M. L., GONG, S., GREENGARD, P. & HEINTZ, N. 2008. Application of a translational profiling approach for the comparative analysis of CNS cell types. *Cell,* 135**,** 749-62.

DREW, P. D., FRANZOSO, G., CARLSON, L. M., BIDDISON, W. E., SIEBENLIST, U. & OZATO, K. 1995. Interferon regulatory factor-2 physically interacts with NF-kappa B in vitro and inhibits NF-kappa B induction of major histocompatibility class I and beta 2-microglobulin gene expression in transfected human neuroblastoma cells. *J Neuroimmunol,* 63**,** 157-62.

DU, P., ZHANG, X., HUANG, C. C., JAFARI, N., KIBBE, W. A., HOU, L. & LIN, S. M. 2010. Comparison of Beta-value and M-value methods for quantifying methylation levels by microarray analysis. *BMC Bioinformatics,* 11**,** 587.

DU, Z., SUN, T., HACISULEYMAN, E., FEI, T., WANG, X., BROWN, M., RINN, J. L., LEE, M. G., CHEN, Y., KANTOFF, P. W. & LIU, X. S. 2016. Integrative analyses reveal a long noncoding RNA-mediated sponge regulatory network in prostate cancer. *Nat Commun,* 7**,** 10982.

DUARTE, J. M., GASPAR, R., CAETANO, L., PATRICIO, P., SOARES-CUNHA, C., MATEUS-PINHEIRO, A., ALVES, N. D., SANTOS, A. R., FERREIRA, S. G., SARDINHA, V., OLIVEIRA, J. F., FONTES-RIBEIRO, C., SOUSA, N., CUNHA, R. A., AMBROSIO, A. F., PINTO, L., RODRIGUES, A. J. & GOMES, C. A. 2019. Region-specific control of microglia by adenosine A2A receptors: uncoupling anxiety and associated cognitive deficits in female rats. *Glia,* 67**,** 182-192.

DUGAS, J. C., TAI, Y. C., SPEED, T. P., NGAI, J. & BARRES, B. A. 2006. Functional genomic analysis of oligodendrocyte differentiation. *J Neurosci,* 26**,** 10967-83.

DWIVEDI, Y. 2010. Brain-derived neurotrophic factor and suicide pathogenesis. *Ann Med,* 42**,** 87-96.

EASLEY-NEAL, C., FOREMAN, O., SHARMA, N., ZARRIN, A. A. & WEIMER, R. M. 2019. CSF1R Ligands IL-34 and CSF1 Are Differentially Required for Microglia Development and Maintenance in White and Gray Matter Brain Regions. *Front Immunol,* 10**,** 2199.

EBERWINE, J., YEH, H., MIYASHIRO, K., CAO, Y., NAIR, S., FINNELL, R., ZETTEL, M. & COLEMAN, P. 1992. Analysis of gene expression in single live neurons. *Proc Natl Acad Sci U S A,* 89**,** 3010-4.

EDGAR, R. D., JONES, M. J., MEANEY, M. J., TURECKI, G. & KOBOR, M. S. 2017. BECon: a tool for interpreting DNA methylation findings from blood in the context of brain. *Transl Psychiatry,* 7**,** e1187.

EDISON, P., ARCHER, H. A., GERHARD, A., HINZ, R., PAVESE, N., TURKHEIMER, F. E., HAMMERS, A., TAI, Y. F., FOX, N., KENNEDY, A., ROSSOR, M. & BROOKS, D. J. 2008. Microglia, amyloid, and cognition in Alzheimer's disease: An [11C](R)PK11195-PET and [11C]PIB-PET study. *Neurobiol Dis,* 32**,** 412-9.

EDWARDS, J. R., YARYCHKIVSKA, O., BOULARD, M. & BESTOR, T. H. 2017. DNA methylation and DNA methyltransferases. *Epigenetics Chromatin,* 10**,** 23.

EHRICH, M., ZOLL, S., SUR, S. & VAN DEN BOOM, D. 2007. A new method for accurate assessment of DNA quality after bisulfite treatment. *Nucleic Acids Res,* 35**,** e29.

EHRLICH, M., MOZAFARI, S., GLATZA, M., STAROST, L., VELYCHKO, S., HALLMANN, A. L., CUI, Q. L., SCHAMBACH, A., KIM, K. P., BACHELIN, C., MARTEYN, A., HARGUS, G., JOHNSON, R. M., ANTEL, J., STERNECKERT, J., ZAEHRES, H., SCHOLER, H. R., BARON-VAN EVERCOOREN, A. & KUHLMANN, T. 2017. Rapid and efficient generation of oligodendrocytes from human induced pluripotent stem cells using transcription factors. *Proc Natl Acad Sci U S A,* 114**,** E2243-E2252.

EID, J., FEHR, A., GRAY, J., LUONG, K., LYLE, J., OTTO, G., PELUSO, P., RANK, D., BAYBAYAN, P., BETTMAN, B., BIBILLO, A., BJORNSON, K., CHAUDHURI, B., CHRISTIANS, F., CICERO, R., CLARK, S., DALAL, R., DEWINTER, A., DIXON, J., FOQUET, M., GAERTNER, A., HARDENBOL, P., HEINER, C., HESTER, K., HOLDEN, D., KEARNS, G., KONG, X., KUSE, R., LACROIX, Y., LIN, S., LUNDQUIST, P., MA, C., MARKS, P., MAXHAM, M., MURPHY, D., PARK, I., PHAM, T., PHILLIPS, M., ROY, J., SEBRA, R., SHEN, G., SORENSON, J., TOMANEY, A., TRAVERS, K., TRULSON, M., VIECELI, J., WEGENER, J., WU, D., YANG, A., ZACCARIN, D., ZHAO, P., ZHONG, F., KORLACH, J. & TURNER, S. 2009. Real-time DNA sequencing from single polymerase molecules. *Science,* 323**,** 133-8.

EIKELENBOOM, P. & VEERHUIS, R. 1996. The role of complement and activated microglia in the pathogenesis of Alzheimer's disease. *Neurobiol Aging,* 17**,** 673-80.

EKDAHL, C. T., KOKAIA, Z. & LINDVALL, O. 2009. Brain inflammation and adult neurogenesis: the dual role of microglia. *Neuroscience,* 158**,** 1021-9.

ELLIOTT, H. R., TILLIN, T., MCARDLE, W. L., HO, K., DUGGIRALA, A., FRAYLING, T. M., DAVEY SMITH, G., HUGHES, A. D., CHATURVEDI, N. & RELTON, C. L. 2014. Differences in smoking associated DNA methylation patterns in South Asians and Europeans. *Clin Epigenetics,* 6**,** 4.

ELMORE, M. R., NAJAFI, A. R., KOIKE, M. A., DAGHER, N. N., SPANGENBERG, E. E., RICE, R. A., KITAZAWA, M., MATUSOW, B., NGUYEN, H., WEST, B. L. & GREEN, K. N. 2014. Colony-stimulating factor 1 receptor signaling is necessary for microglia viability, unmasking a microglia progenitor cell in the adult brain. *Neuron,* 82**,** 380-97.

EMERY, B. 2010. Transcriptional and post-transcriptional control of CNS myelination. *Curr Opin Neurobiol,* 20**,** 601-7.

ERLANGSEN, A., APPADURAI, V., WANG, Y., TURECKI, G., MORS, O., WERGE, T., MORTENSEN, P. B., STARNAWSKA, A., BORGLUM, A. D., SCHORK, A., NUDEL, R., BAEKVAD-HANSEN, M., BYBJERG-GRAUHOLM, J., HOUGAARD, D. M., THOMPSON, W. K., NORDENTOFT, M. & AGERBO, E. 2020. Genetics of suicide attempts in individuals with and without mental disorders: a population-based genome-wide association study. *Mol Psychiatry,* 25**,** 2410-2421.

ERNST, C., CHEN, E. S. & TURECKI, G. 2009a. Histone methylation and decreased expression of TrkB.T1 in orbital frontal cortex of suicide completers. *Mol Psychiatry,* 14**,** 830-2.

ERNST, C., DELEVA, V., DENG, X., SEQUEIRA, A., POMARENSKI, A., KLEMPAN, T., ERNST, N., QUIRION, R., GRATTON, A., SZYF, M. & TURECKI, G. 2009b. Alternative splicing, methylation state, and expression profile of tropomyosin-related kinase B in the frontal cortex of suicide completers. *Arch Gen Psychiatry,* 66**,** 22-32.

ERNST, C., NAGY, C., KIM, S., YANG, J. P., DENG, X., HELLSTROM, I. C., CHOI, K. H., GERSHENFELD, H., MEANEY, M. J. & TURECKI, G. 2011. Dysfunction of astrocyte connexins 30 and 43 in dorsal lateral prefrontal cortex of suicide completers. *Biol Psychiatry,* 70**,** 312-9.

ESPINOSA DE LOS MONTEROS, A. & DE VELLIS, J. 1988. Myelin basic protein and transferrin characterize different subpopulations of oligodendrocytes in rat primary glial cultures. *J Neurosci Res,* 21**,** 181-7.

ESPOSITO, C., SCRIMA, M., CAROTENUTO, A., TEDESCHI, A., ROVERO, P., D'ERRICO, G., MALFITANO, A. M., BIFULCO, M. & D'URSI, A. M. 2008. Structures and micelle locations of the nonlipidated and lipidated C-terminal membrane anchor of 2',3'-cyclic nucleotide-3'-phosphodiesterase. *Biochemistry,* 47**,** 308-19.

ESTELLER, M. 2011. Non-coding RNAs in human disease. *Nat Rev Genet,* 12**,** 861-74.

EZ-96 DNA METHYLATION-GOLD™ KIT MANUAL http://www.zymoresearch.com/downloads/dl/file/id/59/d5007i.pdf.

FAGAN, A. M. & GAGE, F. H. 1990. Cholinergic sprouting in the hippocampus: a proposed role for IL-1. *Exp Neurol,* 110**,** 105-20.

FAGUNDES, C. P., GLASER, R. & KIECOLT-GLASER, J. K. 2013. Stressful early life experiences and immune dysregulation across the lifespan. *Brain Behav Immun,* 27**,** 8-12.

FAISSNER, A., PYKA, M., GEISSLER, M., SOBIK, T., FRISCHKNECHT, R., GUNDELFINGER, E. D. & SEIDENBECHER, C. 2010. Contributions of astrocytes to synapse formation and maturation - Potential functions of the perisynaptic extracellular matrix. *Brain Res Rev,* 63**,** 26-38.

FAKHOURY, M. 2018. Microglia and Astrocytes in Alzheimer's Disease: Implications for Therapy. *Curr Neuropharmacol,* 16**,** 508-518.

FARMER, W. T., ABRAHAMSSON, T., CHIERZI, S., LUI, C., ZAELZER, C., JONES, E. V., BALLY, B. P., CHEN, G. G., THEROUX, J. F., PENG, J., BOURQUE, C. W., CHARRON, F., ERNST, C., SJOSTROM, P. J. & MURAI, K. K. 2016. Neurons diversify astrocytes in the adult brain through sonic hedgehog signaling. *Science,* 351**,** 849-54.

FARR, R. J., JANUSZEWSKI, A. S., JOGLEKAR, M. V., LIANG, H., MCAULLEY, A. K., HEWITT, A. W., THOMAS, H. E., LOUDOVARIS, T., KAY, T. W., JENKINS, A. & HARDIKAR, A. A. 2015. A comparative analysis of high-throughput platforms for validation of a circulating microRNA signature in diabetic retinopathy. *Sci Rep,* 5**,** 10375.

FAZEL, S. & RUNESON, B. 2020. Suicide. *N Engl J Med,* 382**,** 266-274.

FEIL, R. & FRAGA, M. F. 2012. Epigenetics and the environment: emerging patterns and implications. *Nat Rev Genet,* 13**,** 97-109.

FENG, J., ZHOU, Y., CAMPBELL, S. L., LE, T., LI, E., SWEATT, J. D., SILVA, A. J. & FAN, G. 2010. Dnmt1 and Dnmt3a maintain DNA methylation and regulate synaptic function in adult forebrain neurons. *Nat Neurosci,* 13**,** 423-30.

FERRANTE, M. & CONTI, G. O. 2017. Environment and Neurodegenerative Diseases: An Update on miRNA Role. *Microrna,* 6**,** 157-165.

FERRARI, A. J., NORMAN, R. E., FREEDMAN, G., BAXTER, A. J., PIRKIS, J. E., HARRIS, M. G., PAGE, A., CARNAHAN, E., DEGENHARDT, L., VOS, T. & WHITEFORD, H. A. 2014. The burden attributable to mental and substance use disorders as risk factors for suicide: findings from the Global Burden of Disease Study 2010. *PLoS One,* 9**,** e91936.

FERREIRA, H. J. & ESTELLER, M. 2018. Non-coding RNAs, epigenetics, and cancer: tying it all together. *Cancer Metastasis Rev,* 37**,** 55-73.

FERRER, I., MARTINEZ, A., BOLUDA, S., PARCHI, P. & BARRACHINA, M. 2008. Brain banks: benefits, limitations and cautions concerning the use of post-mortem brain tissue for molecular studies. *Cell Tissue Bank,* 9**,** 181-94.

FICZ, G., BRANCO, M. R., SEISENBERGER, S., SANTOS, F., KRUEGER, F., HORE, T. A., MARQUES, C. J., ANDREWS, S. & REIK, W. 2011. Dynamic regulation of 5-hydroxymethylcytosine in mouse ES cells and during differentiation. *Nature,* 473**,** 398-402.

FINE, H. A. & MAYER, R. J. 1993. Primary central nervous system lymphoma. *Ann Intern Med,* 119**,** 1093-104.

FINEBERG, S. K., KOSIK, K. S. & DAVIDSON, B. L. 2009. MicroRNAs potentiate neural development. *Neuron,* 64**,** 303-9.

FINEGERSH, A. & HOMANICS, G. E. 2016. Chromatin immunoprecipitation and gene expression analysis of neuronal subtypes after fluorescence activated cell sorting. *J Neurosci Methods,* 263**,** 81-8.

FINGERMAN, I. M., MCDANIEL, L., ZHANG, X., RATZAT, W., HASSAN, T., JIANG, Z., COHEN, R. F. & SCHULER, G. D. 2011. NCBI Epigenomics: a new public resource for exploring epigenomic data sets. *Nucleic Acids Res,* 39**,** D908-12.

FINGERMAN, I. M., ZHANG, X., RATZAT, W., HUSAIN, N., COHEN, R. F. & SCHULER, G. D. 2013. NCBI Epigenomics: what's new for 2013. *Nucleic Acids Res,* 41**,** D221-5.

FINNEGAN, E. J. & MATZKE, M. A. 2003. The small RNA world. *J Cell Sci,* 116**,** 4689-93.

FIORI, L. M., BUREAU, A., LABBE, A., CROTEAU, J., NOEL, S., MERETTE, C. & TURECKI, G. 2011. Global gene expression profiling of the polyamine system in suicide completers. *Int J Neuropsychopharmacol,* 14**,** 595-605.

FIORI, L. M., GROSS, J. A. & TURECKI, G. 2012. Effects of histone modifications on increased expression of polyamine biosynthetic genes in suicide. *Int J Neuropsychopharmacol,* 15**,** 1161-6.

FIORI, L. M., MECHAWAR, N. & TURECKI, G. 2009. Identification and characterization of spermidine/spermine N1-acetyltransferase promoter variants in suicide completers. *Biol Psychiatry,* 66**,** 460-7.

FIORI, L. M. & TURECKI, G. 2010. Genetic and epigenetic influences on expression of spermine synthase and spermine oxidase in suicide completers. *Int J Neuropsychopharmacol,* 13**,** 725-36.

FIORI, L. M. & TURECKI, G. 2011. Epigenetic regulation of spermidine/spermine N1-acetyltransferase (SAT1) in suicide. *J Psychiatr Res,* 45**,** 1229-35.

FISHELL, G. & HEINTZ, N. 2013. The neuron identity problem: form meets function. *Neuron,* 80**,** 602-12.

FISHER, H. L., MURPHY, T. M., ARSENEAULT, L., CASPI, A., MOFFITT, T. E., VIANA, J., HANNON, E., PIDSLEY, R., BURRAGE, J., DEMPSTER, E. L., WONG, C. C., PARIANTE, C. M. & MILL, J. 2015. Methylomic analysis of monozygotic twins discordant for childhood psychotic symptoms. *Epigenetics,* 10**,** 1014-23.

FLEIGE, S., WALF, V., HUCH, S., PRGOMET, C., SEHM, J. & PFAFFL, M. W. 2006. Comparison of relative mRNA quantification models and the impact of RNA integrity in quantitative real-time RT-PCR. *Biotechnol Lett,* 28**,** 1601-13.

FLUGGE, G., ARAYA-CALLIS, C., GAREA-RODRIGUEZ, E., STADELMANN-NESSLER, C. & FUCHS, E. 2014. NDRG2 as a marker protein for brain astrocytes. *Cell Tissue Res,* 357**,** 31-41.

FLUSBERG, B. A., WEBSTER, D. R., LEE, J. H., TRAVERS, K. J., OLIVARES, E. C., CLARK, T. A., KORLACH, J. & TURNER, S. W. 2010. Direct detection of DNA methylation during single-molecule, real-time sequencing. *Nat Methods,* 7**,** 461-5.

FORERO, D. A., VAN DER VEN, K., CALLAERTS, P. & DEL-FAVERO, J. 2010. miRNA genes and the brain: implications for psychiatric disorders. *Hum Mutat,* 31**,** 1195-204.

FORTIN, J. P., TRICHE, T. J., JR. & HANSEN, K. D. 2017. Preprocessing, normalization and integration of the Illumina HumanMethylationEPIC array with minfi. *Bioinformatics,* 33**,** 558-560.

FOUSE, S. D., NAGARAJAN, R. O. & COSTELLO, J. F. 2010. Genome-scale DNA methylation analysis. *Epigenomics,* 2**,** 105-17.

FRANKLIN, R. J., FFRENCH-CONSTANT, C., EDGAR, J. M. & SMITH, K. J. 2012. Neuroprotection and repair in multiple sclerosis. *Nat Rev Neurol,* 8**,** 624-34.

FRISHBERG, A., PESHES-YALOZ, N., COHN, O., ROSENTUL, D., STEUERMAN, Y., VALADARSKY, L., YANKOVITZ, G., MANDELBOIM, M., IRAQI, F. A., AMIT, I., MAYO, L., BACHARACH, E. & GAT-VIKS, I. 2019. Cell composition analysis of bulk genomics using single-cell data. *Nat Methods,* 16**,** 327-332.

FU, H., LIU, B., FROST, J. L., HONG, S., JIN, M., OSTASZEWSKI, B., SHANKAR, G. M., COSTANTINO, I. M., CARROLL, M. C., MAYADAS, T. N. & LEMERE, C. A. 2012. Complement component C3 and complement receptor type 3 contribute to the phagocytosis and clearance of fibrillar Abeta by microglia. *Glia,* 60**,** 993-1003.

FU, J., ZHANG, J., JIN, F., PATCHEFSKY, J., BRAUNEWELL, K. H. & KLEIN-SZANTO, A. J. 2009. Promoter regulation of the visinin-like subfamily of neuronal calcium sensor proteins by nuclear respiratory factor-1. *J Biol Chem,* 284**,** 27577-86.

FU, Q., HEATH, A. C., BUCHOLZ, K. K., NELSON, E. C., GLOWINSKI, A. L., GOLDBERG, J., LYONS, M. J., TSUANG, M. T., JACOB, T., TRUE, M. R. & EISEN, S. A. 2002. A twin study of genetic and environmental influences on suicidality in men. *Psychol Med,* 32**,** 11-24.

FUKS, F., BURGERS, W. A., GODIN, N., KASAI, M. & KOUZARIDES, T. 2001. Dnmt3a binds deacetylases and is recruited by a sequence-specific repressor to silence transcription. *EMBO J,* 20**,** 2536-44.

FULLARD, J. F., HALENE, T. B., GIAMBARTOLOMEI, C., HAROUTUNIAN, V., AKBARIAN, S. & ROUSSOS, P. 2016. Understanding the genetic liability to schizophrenia through the neuroepigenome. *Schizophr Res,* 177**,** 115-124.

GALATRO, T. F., HOLTMAN, I. R., LERARIO, A. M., VAINCHTEIN, I. D., BROUWER, N., SOLA, P. R., VERAS, M. M., PEREIRA, T. F., LEITE, R. E. P., MOLLER, T., WES, P. D., SOGAYAR, M. C.,

LAMAN, J. D., DEN DUNNEN, W., PASQUALUCCI, C. A., OBA-SHINJO, S. M., BODDEKE, E., MARIE, S. K. N. & EGGEN, B. J. L. 2017. Transcriptomic analysis of purified human cortical microglia reveals age-associated changes. *Nat Neurosci,* 20**,** 1162-1171.

GALFALVY, H., ZALSMAN, G., HUANG, Y. Y., MURPHY, L., ROSOKLIJA, G., DWORK, A. J., HAGHIGHI, F., ARANGO, V. & MANN, J. J. 2013. A pilot genome wide association and gene expression array study of suicide with and without major depression. *World J Biol Psychiatry,* 14**,** 574-82.

GARCIA-LEON, J. A., KUMAR, M., BOON, R., CHAU, D., ONE, J., WOLFS, E., EGGERMONT, K., BERCKMANS, P., GUNHANLAR, N., DE VRIJ, F., LENDEMEIJER, B., PAVIE, B., CORTHOUT, N., KUSHNER, S. A., DAVILA, J. C., LAMBRICHTS, I., HU, W. S. & VERFAILLIE, C. M. 2018. SOX10 Single Transcription Factor-Based Fast and Efficient Generation of Oligodendrocytes from Human Pluripotent Stem Cells. *Stem Cell Reports,* 10**,** 655-672.

GASPARONI, G., BULTMANN, S., LUTSIK, P., KRAUS, T. F. J., SORDON, S., VLCEK, J., DIETINGER, V., STEINMAURER, M., HAIDER, M., MULHOLLAND, C. B., ARZBERGER, T., ROEBER, S., RIEMENSCHNEIDER, M., KRETZSCHMAR, H. A., GIESE, A., LEONHARDT, H. & WALTER, J. 2018. DNA methylation analysis on purified neurons and glia dissects age and Alzheimer's disease-specific changes in the human cortex. *Epigenetics Chromatin,* 11**,** 41.

GAUBLOMME, J. T., LI, B., MCCABE, C., KNECHT, A., YANG, Y., DROKHLYANSKY, E., VAN WITTENBERGHE, N., WALDMAN, J., DIONNE, D., NGUYEN, L., DE JAGER, P. L., YEUNG, B., ZHAO, X., HABIB, N., ROZENBLATT-ROSEN, O. & REGEV, A. 2019. Nuclei multiplexing with barcoded antibodies for single-nucleus genomics. *Nat Commun,* 10**,** 2907.

GAUTIER, E. L., SHAY, T., MILLER, J., GRETER, M., JAKUBZICK, C., IVANOV, S., HELFT, J., CHOW, A., ELPEK, K. G., GORDONOV, S., MAZLOOM, A. R., MA'AYAN, A., CHUA, W. J., HANSEN, T. H., TURLEY, S. J., MERAD, M., RANDOLPH, G. J. & IMMUNOLOGICAL GENOME, C. 2012. Gene-expression profiles and transcriptional regulatory pathways that underlie the identity and diversity of mouse tissue macrophages. *Nat Immunol,* 13**,** 1118-28.

GEISSMANN, F., MANZ, M. G., JUNG, S., SIEWEKE, M. H., MERAD, M. & LEY, K. 2010. Development of monocytes, macrophages, and dendritic cells. *Science,* 327**,** 656-61.

GENTLEMAN, R. C., CAREY, V. J., BATES, D. M., BOLSTAD, B., DETTLING, M., DUDOIT, S., ELLIS, B., GAUTIER, L., GE, Y., GENTRY, J., HORNIK, K., HOTHORN, T., HUBER, W., IACUS, S., IRIZARRY, R., LEISCH, F., LI, C., MAECHLER, M., ROSSINI, A. J., SAWITZKI, G., SMITH, C., SMYTH, G., TIERNEY, L., YANG, J. Y. & ZHANG, J. 2004. Bioconductor: open software development for computational biology and bioinformatics. *Genome Biol,* 5**,** R80.

GERRING, Z. F., MCRAE, A. F., MONTGOMERY, G. W. & NYHOLT, D. R. 2018. Genome-wide DNA methylation profiling in whole blood reveals epigenetic signatures associated with migraine. *BMC Genomics,* 19**,** 69.

GHILDIYAL, M. & ZAMORE, P. D. 2009. Small silencing RNAs: an expanding universe. *Nat Rev Genet,* 10**,** 94-108.

GHOSH, S., YATES, A. J., FRUHWALD, M. C., MIECZNIKOWSKI, J. C., PLASS, C. & SMIRAGLIA, D. 2010. Tissue specific DNA methylation of CpG islands in normal human adult somatic tissues distinguishes neural from non-neural tissues. *Epigenetics,* 5**,** 527-38.

GIBBS, J. R., VAN DER BRUG, M. P., HERNANDEZ, D. G., TRAYNOR, B. J., NALLS, M. A., LAI, S. L., AREPALLI, S., DILLMAN, A., RAFFERTY, I. P., TRONCOSO, J., JOHNSON, R., ZIELKE, H. R., FERRUCCI, L., LONGO, D. L., COOKSON, M. R. & SINGLETON, A. B. 2010. Abundant quantitative trait loci exist for DNA methylation and gene expression in human brain. *PLoS Genet,* 6**,** e1000952.

GIERKE, P., ZHAO, C., BRACKMANN, M., LINKE, B., HEINEMANN, U. & BRAUNEWELL, K. H. 2004. Expression analysis of members of the neuronal calcium sensor protein family: combining bioinformatics and Western blot analysis. *Biochem Biophys Res Commun,* 323**,** 38-43.

GILAD, G. M. & GILAD, V. H. 2003. Overview of the brain polyamine-stress-response: regulation, development, and modulation by lithium and role in cell survival. *Cell Mol Neurobiol,* 23**,** 637-49.

GINHOUX, F., GRETER, M., LEBOEUF, M., NANDI, S., SEE, P., GOKHAN, S., MEHLER, M. F., CONWAY, S. J., NG, L. G., STANLEY, E. R., SAMOKHVALOV, I. M. & MERAD, M. 2010. Fate mapping analysis reveals that adult microglia derive from primitive macrophages. *Science,* 330**,** 841-5.

GIVAN, A. L. 2011. Flow cytometry: an introduction. *Methods Mol Biol,* 699**,** 1-29.

GIZAK, A., DUDA, P., PIELKA, E., MCCUBREY, J. A. & RAKUS, D. 2020. GSK3 and miRNA in neural tissue: From brain development to neurodegenerative diseases. *Biochim Biophys Acta Mol Cell Res,* 1867**,** 118696.

GLOBISCH, D., MUNZEL, M., MULLER, M., MICHALAKIS, S., WAGNER, M., KOCH, S., BRUCKL, T., BIEL, M. & CARELL, T. 2010. Tissue distribution of 5-hydroxymethylcytosine and search for active demethylation intermediates. *PLoS One,* 5**,** e15367.

GOMEZ PERDIGUERO, E., KLAPPROTH, K., SCHULZ, C., BUSCH, K., AZZONI, E., CROZET, L., GARNER, H., TROUILLET, C., DE BRUIJN, M. F., GEISSMANN, F. & RODEWALD, H. R. 2015. Tissue-resident macrophages originate from yolk-sac-derived erythro-myeloid progenitors. *Nature,* 518**,** 547-51.

GOMEZ RAVETTI, M., ROSSO, O. A., BERRETTA, R. & MOSCATO, P. 2010. Uncovering molecular biomarkers that correlate cognitive decline with the changes of hippocampus' gene expression profiles in Alzheimer's disease. *PLoS One,* 5**,** e10153.

GONG, B., CAO, Z., ZHENG, P., VITOLO, O. V., LIU, S., STANISZEWSKI, A., MOOLMAN, D., ZHANG, H., SHELANSKI, M. & ARANCIO, O. 2006. Ubiquitin hydrolase Uch-L1 rescues beta-amyloid-induced decreases in synaptic function and contextual memory. *Cell,* 126**,** 775-88.

GONG, C. & MAQUAT, L. E. 2011. lncRNAs transactivate STAU1-mediated mRNA decay by duplexing with 3' UTRs via Alu elements. *Nature,* 470**,** 284-8.

GONG, S., ZHENG, C., DOUGHTY, M. L., LOSOS, K., DIDKOVSKY, N., SCHAMBRA, U. B., NOWAK, N. J., JOYNER, A., LEBLANC, G., HATTEN, M. E. & HEINTZ, N. 2003. A gene expression atlas of the central nervous system based on bacterial artificial chromosomes. *Nature,* 425**,** 917-25.

GORRIE-STONE, T. 2019. miRoar v0.01 R package

GORRIE-STONE, T. J., SMART, M. C., SAFFARI, A., MALKI, K., HANNON, E., BURRAGE, J., MILL, J., KUMARI, M. & SCHALKWYK, L. C. 2019. Bigmelon: tools for analysing large DNA methylation datasets. *Bioinformatics,* 35**,** 981-986.

GOSSELIN, D., LINK, V. M., ROMANOSKI, C. E., FONSECA, G. J., EICHENFIELD, D. Z., SPANN, N. J., STENDER, J. D., CHUN, H. B., GARNER, H., GEISSMANN, F. & GLASS, C. K. 2014. Environment drives selection and function of enhancers controlling tissue-specific macrophage identities. *Cell,* 159**,** 1327-40.

GOUDRIAAN, A., DE LEEUW, C., RIPKE, S., HULTMAN, C. M., SKLAR, P., SULLIVAN, P. F., SMIT, A. B., POSTHUMA, D. & VERHEIJEN, M. H. 2014. Specific glial functions contribute to schizophrenia susceptibility. *Schizophr Bull,* 40**,** 925-35.

GRAU-EXPOSITO, J., SERRA-PEINADO, C., MIGUEL, L., NAVARRO, J., CURRAN, A., BURGOS, J., OCANA, I., RIBERA, E., TORRELLA, A., PLANAS, B., BADIA, R., CASTELLVI, J., FALCO, V., CRESPO, M. & BUZON, M. J. 2017. A Novel Single-Cell FISH-Flow Assay Identifies Effector Memory CD4(+) T cells as a Major Niche for HIV-1 Transcription in HIV-Infected Patients. *mBio,* 8.

GRAYSON, D. R., JIA, X., CHEN, Y., SHARMA, R. P., MITCHELL, C. P., GUIDOTTI, A. & COSTA, E. 2005. Reelin promoter hypermethylation in schizophrenia. *Proc Natl Acad Sci U S A,* 102**,** 9341-6.

GRIGORENKO, E. V., ORTENBERG, E., HURLEY, J., BOND, A. & MUNNELLY, K. 2011. miRNA profiling on high-throughput OpenArray system. *Methods Mol Biol,* 676**,** 101-10.

GRIMM, C. M., AKSAMAZ, S., SCHULZ, S., TEUTSCH, J., SICINSKI, P., LISS, B. & KATZEL, D. 2018. Schizophrenia-related cognitive dysfunction in the Cyclin-D2 knockout mouse model of ventral hippocampal hyperactivity. *Transl Psychiatry,* 8**,** 212.

GRIMM, S. A., SHIMBO, T., TAKAKU, M., THOMAS, J. W., AUERBACH, S., BENNETT, B. D., BUCHER, J. R., BURKHOLDER, A. B., DAY, F., DU, Y., DUNCAN, C. G., FRENCH, J. E., FOLEY, J. F., LI, J., MERRICK, B. A., TICE, R. R., WANG, T., XU, X., PROGRAM, N. C. S., BUSHEL, P. R., FARGO, D. C., MULLIKIN, J. C. & WADE, P. A. 2019. DNA methylation in mice is influenced by genetics as well as sex and life experience. *Nat Commun,* 10**,** 305.

GRINDBERG, R. V., YEE-GREENBAUM, J. L., MCCONNELL, M. J., NOVOTNY, M., O'SHAUGHNESSY, A. L., LAMBERT, G. M., ARAUZO-BRAVO, M. J., LEE, J., FISHMAN, M., ROBBINS, G. E., LIN, X., VENEPALLY, P., BADGER, J. H., GALBRAITH, D. W., GAGE, F. H. & LASKEN, R. S. 2013. RNA-sequencing from single nuclei. *Proc Natl Acad Sci U S A,* 110**,** 19802-7.

GROSS, J. A., FIORI, L. M., LABONTE, B., LOPEZ, J. P. & TURECKI, G. 2013. Effects of promoter methylation on increased expression of polyamine biosynthetic genes in suicide. *J Psychiatr Res,* 47**,** 513-9.

GROSS, J. A., NAGY, C., LIN, L., BONNEIL, E., MAHEU, M., THIBAULT, P., MECHAWAR, N., JIN, P. & TURECKI, G. 2016. Global and Site-Specific Changes in 5-Methylcytosine and 5-Hydroxymethylcytosine after Extended Post-mortem Interval. *Front Genet,* 7**,** 120.

GRUBMAN, A., CHEW, G., OUYANG, J. F., SUN, G., CHOO, X. Y., MCLEAN, C., SIMMONS, R. K., BUCKBERRY, S., VARGAS-LANDIN, D. B., POPPE, D., PFLUEGER, J., LISTER, R., RACKHAM, O. J. L., PETRETTO, E. & POLO, J. M. 2019. A single-cell atlas of entorhinal cortex from individuals with Alzheimer's disease reveals cell-type-specific gene expression regulation. *Nat Neurosci,* 22**,** 2087-2097.

GU, H., SMITH, Z. D., BOCK, C., BOYLE, P., GNIRKE, A. & MEISSNER, A. 2011a. Preparation of reduced representation bisulfite sequencing libraries for genome-scale DNA methylation profiling. *Nat Protoc,* 6**,** 468-81.

GU, T. P., GUO, F., YANG, H., WU, H. P., XU, G. F., LIU, W., XIE, Z. G., SHI, L., HE, X., JIN, S. G., IQBAL, K., SHI, Y. G., DENG, Z., SZABO, P. E., PFEIFER, G. P., LI, J. & XU, G. L. 2011b. The role of Tet3 DNA dioxygenase in epigenetic reprogramming by oocytes. *Nature,* 477**,** 606-10.

GU, W., SANDER, T., BECKER, T. & STEINLEIN, O. K. 2004. Genotypic association of exonic LGI4 polymorphisms and childhood absence epilepsy. *Neurogenetics,* 5**,** 41-4.

GUEZ-BARBER, D., FANOUS, S., HARVEY, B. K., ZHANG, Y., LEHRMANN, E., BECKER, K. G., PICCIOTTO, M. R. & HOPE, B. T. 2012. FACS purification of immunolabeled cell types from adult rat brain. *J Neurosci Methods,* 203**,** 10-8.

GUINTIVANO, J., ARYEE, M. J. & KAMINSKY, Z. A. 2013. A cell epigenotype specific model for the correction of brain cellular heterogeneity bias and its application to age, brain region and major depression. *Epigenetics,* 8**,** 290-302.

GUINTIVANO, J., BROWN, T., NEWCOMER, A., JONES, M., COX, O., MAHER, B. S., EATON, W. W., PAYNE, J. L., WILCOX, H. C. & KAMINSKY, Z. A. 2014. Identification and replication of a combined epigenetic and genetic biomarker predicting suicide and suicidal behaviors. *Am J Psychiatry,* 171**,** 1287-96.

GUIPPONI, M., DEUTSCH, S., KOHLER, K., PERROUD, N., LE GAL, F., VESSAZ, M., LAFORGE, T., PETIT, B., JOLLANT, F., GUILLAUME, S., BAUD, P., COURTET, P., LA HARPE, R. & MALAFOSSE, A. 2009. Genetic and epigenetic analysis of SSAT gene dysregulation in suicidal behavior. *Am J Med Genet B Neuropsychiatr Genet,* 150B**,** 799-807.

GUJAR, H., LIANG, J. W., WONG, N. C. & MOZHUI, K. 2018. Profiling DNA methylation differences between inbred mouse strains on the Illumina Human Infinium MethylationEPIC microarray. *PLoS One,* 13**,** e0193496.

GUSEL'NIKOVA, V. V. & KORZHEVSKIY, D. E. 2015. NeuN As a Neuronal Nuclear Antigen and Neuron Differentiation Marker. *Acta Naturae,* 7**,** 42-7.

GUTTMAN, M. & RINN, J. L. 2012. Modular regulatory principles of large non-coding RNAs. *Nature,* 482**,** 339-46.

GYONEVA, S., HOSUR, R., GOSSELIN, D., ZHANG, B., OUYANG, Z., COTLEUR, A. C., PETERSON, M., ALLAIRE, N., CHALLA, R., CULLEN, P., ROBERTS, C., MIAO, K., REYNOLDS, T. L., GLASS, C. K., BURKLY, L. & RANSOHOFF, R. M. 2019. Cx3cr1-deficient microglia exhibit a premature aging transcriptome. *Life Sci Alliance,* 2.

HACKLER, L., JR., MASUDA, T., OLIVER, V. F., MERBS, S. L. & ZACK, D. J. 2012. Use of laser capture microdissection for analysis of retinal mRNA/miRNA expression and DNA methylation. *Methods Mol Biol,* 884**,** 289-304.

HAGA, S., AIZAWA, T., ISHII, T. & IKEDA, K. 1996. Complement gene expression in mouse microglia and astrocytes in culture: comparisons with mouse peritoneal macrophages. *Neurosci Lett,* 216**,** 191-4.

HAGA, S., IKEDA, K., SATO, M. & ISHII, T. 1993. Synthetic Alzheimer amyloid beta/A4 peptides enhance production of complement C3 component by cultured microglial cells. *Brain Res,* 601**,** 88-94.

HAGHIGHI, F., GALFALVY, H., CHEN, S., HUANG, Y. Y., COOPER, T. B., BURKE, A. K., OQUENDO, M. A., MANN, J. J. & SUBLETTE, M. E. 2015. DNA methylation perturbations in genes involved in polyunsaturated Fatty Acid biosynthesis associated with depression and suicide risk. *Front Neurol,* 6**,** 92.

HAGHIGHI, F., XIN, Y., CHANRION, B., O'DONNELL, A. H., GE, Y., DWORK, A. J., ARANGO, V. & MANN, J. J. 2014. Increased DNA methylation in the suicide brain. *Dialogues Clin Neurosci,* 16**,** 430-8.

HALFORD, J., SHEN, S., ITAMURA, K., LEVINE, J., CHONG, A. C., CZERWIENIEC, G., GLENN, T. C., HOVDA, D. A., VESPA, P., BULLOCK, R., DIETRICH, W. D., MONDELLO, S., LOO, J. A. & WANNER, I. B. 2017. New astroglial injury-defined biomarkers for neurotrauma assessment. *J Cereb Blood Flow Metab,* 37**,** 3278-3299.

HALL, J. S., TAYLOR, J., VALENTINE, H. R., IRLAM, J. J., EUSTACE, A., HOSKIN, P. J., MILLER, C. J. & WEST, C. M. 2012. Enhanced stability of microRNA expression facilitates classification of FFPE tumour samples exhibiting near total mRNA degradation. *Br J Cancer,* 107**,** 684-94.

HAMDAN, F. F., SROUR, M., CAPO-CHICHI, J. M., DAOUD, H., NASSIF, C., PATRY, L., MASSICOTTE, C., AMBALAVANAN, A., SPIEGELMAN, D., DIALLO, O., HENRION, E., DIONNE-LAPORTE, A., FOUGERAT, A., PSHEZHETSKY, A. V., VENKATESWARAN, S., ROULEAU, G. A. & MICHAUD, J. L. 2014. De novo mutations in moderate or severe intellectual disability. *PLoS Genet,* 10**,** e1004772.

HAMDAN, H., KOCKARA, N. T., JOLLY, L. A., HAUN, S. & WIGHT, P. A. 2015. Control of human PLP1 expression through transcriptional regulatory elements and alternatively spliced exons in intron 1. *ASN Neuro,* 7.

HAMMOND, T. R., ROBINTON, D. & STEVENS, B. 2018. Microglia and the Brain: Complementary Partners in Development and Disease. *Annu Rev Cell Dev Biol,* 34**,** 523-544.

HAN, P. & CHANG, C. P. 2015. Long non-coding RNA and chromatin remodeling. *RNA Biol,* 12**,** 1094-8.

HANNESTAD, J., GALLEZOT, J. D., SCHAFBAUER, T., LIM, K., KLOCZYNSKI, T., MORRIS, E. D., CARSON, R. E., DING, Y. S. & COSGROVE, K. P. 2012. Endotoxin-induced systemic inflammation activates microglia: [(1)(1)C]PBR28 positron emission tomography in nonhuman primates. *Neuroimage,* 63**,** 232-9.

HANNON, E., DEMPSTER, E., VIANA, J., BURRAGE, J., SMITH, A. R., MACDONALD, R., ST CLAIR, D., MUSTARD, C., BREEN, G., THERMAN, S., KAPRIO, J., TOULOPOULOU, T., HULSHOFF POL, H. E., BOHLKEN, M. M., KAHN, R. S., NENADIC, I., HULTMAN, C. M., MURRAY, R. M., COLLIER, D. A., BASS, N., GURLING, H., MCQUILLIN, A., SCHALKWYK, L. & MILL, J. 2016. An integrated genetic-epigenetic analysis of schizophrenia: evidence for co-localization of genetic associations and differential DNA methylation. *Genome Biol,* 17**,** 176.

HANNON, E., SCHENDEL, D., LADD-ACOSTA, C., GROVE, J., I, P.-B. A. S. D. G., HANSEN, C. S., ANDREWS, S. V., HOUGAARD, D. M., BRESNAHAN, M., MORS, O., HOLLEGAARD, M. V., BAEKVAD-HANSEN, M., HORNIG, M., MORTENSEN, P. B., BORGLUM, A. D., WERGE, T., PEDERSEN, M. G., NORDENTOFT, M., BUXBAUM, J., DANIELE FALLIN, M., BYBJERG-

GRAUHOLM, J., REICHENBERG, A. & MILL, J. 2018. Elevated polygenic burden for autism is associated with differential DNA methylation at birth. *Genome Med,* 10**,** 19.

HARTMANN, K., SEPULVEDA-FALLA, D., ROSE, I. V. L., MADORE, C., MUTH, C., MATSCHKE, J., BUTOVSKY, O., LIDDELOW, S., GLATZEL, M. & KRASEMANN, S. 2019. Complement 3(+)-astrocytes are highly abundant in prion diseases, but their abolishment led to an accelerated disease course and early dysregulation of microglia. *Acta Neuropathol Commun,* 7**,** 83.

HASIN, Y., SELDIN, M. & LUSIS, A. 2017. Multi-omics approaches to disease. *Genome Biol,* 18**,** 83.

HAWLEY, T. S., HAWLEY, R. G. & TELFORD, W. G. 2017. Fluorescent Proteins for Flow Cytometry. *Curr Protoc Cytom,* 80**,** 9 12 1-9 12 20.

HAWTON, K. & VAN HEERINGEN, K. 2009. Suicide. *Lancet,* 373**,** 1372-81.

HE, Y. F., LI, B. Z., LI, Z., LIU, P., WANG, Y., TANG, Q., DING, J., JIA, Y., CHEN, Z., LI, L., SUN, Y., LI, X., DAI, Q., SONG, C. X., ZHANG, K., HE, C. & XU, G. L. 2011. Tet-mediated formation of 5-carboxylcytosine and its excision by TDG in mammalian DNA. *Science,* 333**,** 1303-7.

HEIMAN, M., SCHAEFER, A., GONG, S., PETERSON, J. D., DAY, M., RAMSEY, K. E., SUAREZ-FARINAS, M., SCHWARZ, C., STEPHAN, D. A., SURMEIER, D. J., GREENGARD, P. & HEINTZ, N. 2008. A translational profiling approach for the molecular characterization of CNS cell types. *Cell,* 135**,** 738-48.

HEINZ, S., BENNER, C., SPANN, N., BERTOLINO, E., LIN, Y. C., LASLO, P., CHENG, J. X., MURRE, C., SINGH, H. & GLASS, C. K. 2010. Simple combinations of lineage-determining transcription factors prime cis-regulatory elements required for macrophage and B cell identities. *Mol Cell,* 38**,** 576-89.

HERCULANO-HOUZEL, S. 2014. The glia/neuron ratio: how it varies uniformly across brain structures and species and what that means for brain physiology and evolution. *Glia,* 62**,** 1377-91.

HERCULANO-HOUZEL, S. & DOS SANTOS, S. E. 2018. You Do Not Mess with the Glia. *Neuroglia*.

HERCULANO-HOUZEL, S. & LENT, R. 2005. Isotropic fractionator: a simple, rapid method for the quantification of total cell and neuron numbers in the brain. *J Neurosci,* 25**,** 2518-21.

HERMAN, J. P., MCKLVEEN, J. M., GHOSAL, S., KOPP, B., WULSIN, A., MAKINSON, R., SCHEIMANN, J. & MYERS, B. 2016. Regulation of the Hypothalamic-Pituitary-Adrenocortical Stress Response. *Compr Physiol,* 6**,** 603-21.

HERNANDEZ-SANTANA, Y. E., ONTORIA, E., GONZALEZ-GARCIA, A. C., QUISPE-RICALDE, M. A., LARRAGA, V., VALLADARES, B. & CARMELO, E. 2016. The Challenge of Stability in High-Throughput Gene Expression Analysis: Comprehensive Selection and Evaluation of Reference Genes for BALB/c Mice Spleen Samples in the Leishmania infantum Infection Model. *PLoS One,* 11**,** e0163219.

HERNANDEZ MORA, J. R., SANCHEZ-DELGADO, M., PETAZZI, P., MORAN, S., ESTELLER, M., IGLESIAS-PLATAS, I. & MONK, D. 2018. Profiling of oxBS-450K 5-hydroxymethylcytosine in human placenta and brain reveals enrichment at imprinted loci. *Epigenetics,* 13**,** 182-191.

HERTZ, L. 2004. Intercellular metabolic compartmentation in the brain: past, present and future. *Neurochem Int,* 45**,** 285-96.

HICKMAN, S. E., KINGERY, N. D., OHSUMI, T. K., BOROWSKY, M. L., WANG, L. C., MEANS, T. K. & EL KHOURY, J. 2013. The microglial sensome revealed by direct RNA sequencing. *Nat Neurosci,* 16**,** 1896-905.

HIGUCHI, F., UCHIDA, S., YAMAGATA, H., ABE-HIGUCHI, N., HOBARA, T., HARA, K., KOBAYASHI, A., SHINTAKU, T., ITOH, Y., SUZUKI, T. & WATANABE, Y. 2016. Hippocampal MicroRNA-124 Enhances Chronic Stress Resilience in Mice. *J Neurosci,* 36**,** 7253-67.

HIGUCHI, F., UCHIDA, S., YAMAGATA, H., OTSUKI, K., HOBARA, T., ABE, N., SHIBATA, T. & WATANABE, Y. 2011. State-dependent changes in the expression of DNA methyltransferases in mood disorder patients. *J Psychiatr Res,* 45**,** 1295-300.

HIRST, M. & MARRA, M. A. 2010. Next generation sequencing based approaches to epigenomics. *Brief Funct Genomics,* 9**,** 455-65.

HOL, E. M. & PEKNY, M. 2015. Glial fibrillary acidic protein (GFAP) and the astrocyte intermediate filament system in diseases of the central nervous system. *Curr Opin Cell Biol,* 32**,** 121-30.

HOLMBERG, J. & PERLMANN, T. 2012. Maintaining differentiated cellular identity. *Nat Rev Genet,* 13**,** 429-39.

HOLMES, E. E., JUNG, M., MELLER, S., LEISSE, A., SAILER, V., ZECH, J., MENGDEHL, M., GARBE, L. A., UHL, B., KRISTIANSEN, G. & DIETRICH, D. 2014. Performance evaluation of kits for bisulfite-conversion of DNA from tissues, cell lines, FFPE tissues, aspirates, lavages, effusions, plasma, serum, and urine. *PLoS One,* 9**,** e93933.

HOLMES, S. E., HINZ, R., CONEN, S., GREGORY, C. J., MATTHEWS, J. C., ANTON-RODRIGUEZ, J. M., GERHARD, A. & TALBOT, P. S. 2018. Elevated Translocator Protein in Anterior Cingulate in Major Depression and a Role for Inflammation in Suicidal Thinking: A Positron Emission Tomography Study. *Biol Psychiatry,* 83**,** 61-69.

HOLTMAN, I. R., SKOLA, D. & GLASS, C. K. 2017. Transcriptional control of microglia phenotypes in health and disease. *J Clin Invest,* 127**,** 3220-3229.

HORVATH, S. 2013. DNA methylation age of human tissues and cell types. *Genome Biol,* 14**,** R115.

HORVATH, S. 2015. Erratum to: DNA methylation age of human tissues and cell types. *Genome Biol,* 16**,** 96.

HOUSEMAN, E. A., ACCOMANDO, W. P., KOESTLER, D. C., CHRISTENSEN, B. C., MARSIT, C. J., NELSON, H. H., WIENCKE, J. K. & KELSEY, K. T. 2012. DNA methylation arrays as surrogate measures of cell mixture distribution. *BMC Bioinformatics,* 13**,** 86.

HOUSEMAN, E. A., KELSEY, K. T., WIENCKE, J. K. & MARSIT, C. J. 2015. Cell-composition effects in the analysis of DNA methylation array data: a mathematical perspective. *BMC Bioinformatics,* 16**,** 95.

HOUSEMAN, E. A., KILE, M. L., CHRISTIANI, D. C., INCE, T. A., KELSEY, K. T. & MARSIT, C. J. 2016. Reference-free deconvolution of DNA methylation data and mediation by cell composition effects. *BMC Bioinformatics,* 17**,** 259.

HOUSEMAN, E. A., MOLITOR, J. & MARSIT, C. J. 2014. Reference-free cell mixture adjustments in analysis of DNA methylation data. *Bioinformatics,* 30**,** 1431-9.

HU, C., CHEN, W., MYERS, S. J., YUAN, H. & TRAYNELIS, S. F. 2016a. Human GRIN2B variants in neurodevelopmental disorders. *J Pharmacol Sci,* 132**,** 115-121.

HU, P., ZHANG, W., XIN, H. & DENG, G. 2016b. Single Cell Isolation and Analysis. *Front Cell Dev Biol,* 4**,** 116.

HUANG, H. L., HSING, H. W., LAI, T. C., CHEN, Y. W., LEE, T. R., CHAN, H. T., LYU, P. C., WU, C. L., LU, Y. C., LIN, S. T., LIN, C. W., LAI, C. H., CHANG, H. T., CHOU, H. C. & CHAN, H. L. 2010. Trypsin-induced proteome alteration during cell subculture in mammalian cells. *J Biomed Sci,* 17**,** 36.

HULSPAS, R., DOMBKOWSKI, D., PREFFER, F., DOUGLAS, D., KILDEW-SHAH, B. & GILBERT, J. 2009a. Flow cytometry and the stability of phycoerythrin-tandem dye conjugates. *Cytometry A,* 75**,** 966-72.

HULSPAS, R., O'GORMAN, M. R., WOOD, B. L., GRATAMA, J. W. & SUTHERLAND, D. R. 2009b. Considerations for the control of background fluorescence in clinical flow cytometry. *Cytometry B Clin Cytom,* 76**,** 355-64.

HUSE, J. T. & HOLLAND, E. C. 2010. Targeting brain cancer: advances in the molecular pathology of malignant glioma and medulloblastoma. *Nat Rev Cancer,* 10**,** 319-31.

HUTTENHOFER, A. & VOGEL, J. 2006. Experimental approaches to identify non-coding RNAs. *Nucleic Acids Res,* 34**,** 635-46.

HWANG, J. P., LEE, T. W., TSAI, S. J., CHEN, T. J., YANG, C. H., LIRNG, J. F. & TSAI, C. F. 2010. Cortical and subcortical abnormalities in late-onset depression with history of suicide attempts investigated with MRI and voxel-based morphometry. *J Geriatr Psychiatry Neurol,* 23**,** 171-84.

IBRAHIM, S. F. & VAN DEN ENGH, G. 2007. Flow cytometry and cell sorting. *Adv Biochem Eng Biotechnol,* 106**,** 19-39.

ILLUMINA 2016.

IMBEAUD, S., GRAUDENS, E., BOULANGER, V., BARLET, X., ZABORSKI, P., EVENO, E., MUELLER, O., SCHROEDER, A. & AUFFRAY, C. 2005. Towards standardization of RNA quality assessment using user-independent classifiers of microcapillary electrophoresis traces. *Nucleic Acids Res,* 33**,** e56.

INCE-DUNN, G., OKANO, H. J., JENSEN, K. B., PARK, W. Y., ZHONG, R., ULE, J., MELE, A., FAK, J. J., YANG, C., ZHANG, C., YOO, J., HERRE, M., OKANO, H., NOEBELS, J. L. & DARNELL, R. B. 2012. Neuronal Elav-like (Hu) proteins regulate RNA splicing and abundance to control glutamate levels and neuronal excitability. *Neuron,* 75**,** 1067-80.

INFINIUM METHYLATIONEPIC KIT https://www.illumina.com/products/by-type/microarray-kits/infinium-methylation-epic.html.

INFNIUM® HD ASSAY METHYLATION PROTOCOL GUIDE https://support.illumina.com/content/dam/illumina-support/documents/documentation/chemistry_documentation/infinium_assays/infinium_hd_methylation/infinium-hd-methylation-guide-15019519-01.pdf.

INGELSSON, M., FUKUMOTO, H., NEWELL, K. L., GROWDON, J. H., HEDLEY-WHYTE, E. T., FROSCH, M. P., ALBERT, M. S., HYMAN, B. T. & IRIZARRY, M. C. 2004. Early Abeta accumulation and progressive synaptic loss, gliosis, and tangle formation in AD brain. *Neurology,* 62**,** 925-31.

INOUE, A., SHEN, L., DAI, Q., HE, C. & ZHANG, Y. 2011. Generation and replication-dependent dilution of 5fC and 5caC during mouse preimplantation development. *Cell Res,* 21**,** 1670-6.

INTA, D., LANG, U. E., BORGWARDT, S., MEYER-LINDENBERG, A. & GASS, P. 2017. Microglia Activation and Schizophrenia: Lessons From the Effects of Minocycline on Postnatal Neurogenesis, Neuronal Survival and Synaptic Pruning. *Schizophr Bull,* 43**,** 493-496.

IRSHAD, M., GUPTA, P., MANKOTIA, D. S. & ANSARI, M. A. 2016. Multiplex qPCR for serodetection and serotyping of hepatitis viruses: A brief review. *World J Gastroenterol,* 22**,** 4824-34.

ISSLER, O. & CHEN, A. 2015. Determining the role of microRNAs in psychiatric disorders. *Nat Rev Neurosci,* 16**,** 201-12.

ITO, S., SHEN, L., DAI, Q., WU, S. C., COLLINS, L. B., SWENBERG, J. A., HE, C. & ZHANG, Y. 2011. Tet proteins can convert 5-methylcytosine to 5-formylcytosine and 5-carboxylcytosine. *Science,* 333**,** 1300-3.

IURATO, S., CARRILLO-ROA, T., ARLOTH, J., CZAMARA, D., DIENER-HOLZL, L., LANGE, J., MULLER-MYHSOK, B., BINDER, E. B. & ERHARDT, A. 2017. "DNA Methylation signatures in panic disorder". *Transl Psychiatry,* 7**,** 1287.

IWAMOTO, K., BUNDO, M., UEDA, J., OLDHAM, M. C., UKAI, W., HASHIMOTO, E., SAITO, T., GESCHWIND, D. H. & KATO, T. 2011. Neurons show distinctive DNA methylation profile and higher interindividual variations compared with non-neurons. *Genome Res,* 21**,** 688-96.

JAFFE, A. E., GAO, Y., DEEP-SOBOSLAY, A., TAO, R., HYDE, T. M., WEINBERGER, D. R. & KLEINMAN, J. E. 2016. Mapping DNA methylation across development, genotype and schizophrenia in the human frontal cortex. *Nat Neurosci,* 19**,** 40-7.

JAFFE, A. E. & IRIZARRY, R. A. 2014. Accounting for cellular heterogeneity is critical in epigenome-wide association studies. *Genome Biol,* 15**,** R31.

JAIN, M., OLSEN, H. E., PATEN, B. & AKESON, M. 2016. The Oxford Nanopore MinION: delivery of nanopore sequencing to the genomics community. *Genome Biol,* 17**,** 239.

JAKOBSSON, J., STRIDSBERG, M., ZETTERBERG, H., BLENNOW, K., EKMAN, C. J., JOHANSSON, A. G., SELLGREN, C. & LANDEN, M. 2013. Decreased cerebrospinal fluid secretogranin II concentrations in severe forms of bipolar disorder. *J Psychiatry Neurosci,* 38**,** E21-6.

JAKOVCEVSKI, M. & AKBARIAN, S. 2012. Epigenetic mechanisms in neurological disease. *Nat Med,* 18**,** 1194-204.

JANOVA, H., ARINRAD, S., BALMUTH, E., MITJANS, M., HERTEL, J., HABES, M., BITTNER, R. A., PAN, H., GOEBBELS, S., BEGEMANN, M., GERWIG, U. C., LANGNER, S., WERNER, H. B., KITTEL-SCHNEIDER, S., HOMUTH, G., DAVATZIKOS, C., VOLZKE, H., WEST, B. L., REIF, A., GRABE, H. J., BORETIUS, S., EHRENREICH, H. & NAVE, K. A. 2018. Microglia ablation alleviates myelin-associated catatonic signs in mice. *J Clin Invest,* 128**,** 734-745.

JEREMIAN, R., CHEN, Y. A., DE LUCA, V., VINCENT, J. B., KENNEDY, J. L., ZAI, C. C. & STRAUSS, J. 2017. Investigation of correlations between DNA methylation, suicidal behavior and aging. *Bipolar Disord,* 19**,** 32-40.

JHUN, M. A., SMITH, J. A., WARE, E. B., KARDIA, S. L. R., MOSLEY, T. H., JR., TURNER, S. T., PEYSER, P. A. & PARK, S. K. 2017. Modeling the Causal Role of DNA Methylation in the Association Between Cigarette Smoking and Inflammation in African Americans: A 2-Step Epigenetic Mendelian Randomization Study. *Am J Epidemiol,* 186**,** 1149-1158.

JIANG, Y., MATEVOSSIAN, A., HUANG, H. S., STRAUBHAAR, J. & AKBARIAN, S. 2008. Isolation of neuronal chromatin from brain tissue. *BMC Neurosci,* 9**,** 42.

JIANG, Y., ZHANG, Y. & SU, L. 2020. MiR-539-5p Decreases amyloid beta-protein production, hyperphosphorylation of Tau and Memory Impairment by Regulating PI3K/Akt/GSK-3beta Pathways in APP/PS1 Double Transgenic Mice. *Neurotox Res,* 38**,** 524-535.

JIN, W. N., SHI, S. X., LI, Z., LI, M., WOOD, K., GONZALES, R. J. & LIU, Q. 2017. Depletion of microglia exacerbates postischemic inflammation and brain injury. *J Cereb Blood Flow Metab,* 37**,** 2224-2236.

JOHNSON, K. W., DOONER, M. & QUESENBERRY, P. J. 2007. Fluorescence activated cell sorting: a window on the stem cell. *Curr Pharm Biotechnol,* 8**,** 133-9.

JOHNSON, M. B. & WALSH, C. A. 2017. Cerebral cortical neuron diversity and development at single-cell resolution. *Curr Opin Neurobiol,* 42**,** 9-16.

JOHNSON, S. A., LAMPERT-ETCHELLS, M., PASINETTI, G. M., ROZOVSKY, I. & FINCH, C. E. 1992. Complement mRNA in the mammalian brain: responses to Alzheimer's disease and experimental brain lesioning. *Neurobiol Aging,* 13**,** 641-8.

JOHNSTON-WILSON, N. L., SIMS, C. D., HOFMANN, J. P., ANDERSON, L., SHORE, A. D., TORREY, E. F. & YOLKEN, R. H. 2000. Disease-specific alterations in frontal cortex brain proteins in schizophrenia, bipolar disorder, and major depressive disorder. The Stanley Neuropathology Consortium. *Mol Psychiatry,* 5**,** 142-9.

JOKINEN, J., BOSTROM, A. E., DADFAR, A., CIUCULETE, D. M., CHATZITTOFIS, A., ASBERG, M. & SCHIOTH, H. B. 2018. Epigenetic Changes in the CRH Gene are Related to Severity of Suicide Attempt and a General Psychiatric Risk Score in Adolescents. *EBioMedicine,* 27**,** 123-133.

JOVICIC, A., ROSHAN, R., MOISOI, N., PRADERVAND, S., MOSER, R., PILLAI, B. & LUTHI-CARTER, R. 2013. Comprehensive expression analyses of neural cell-type-specific miRNAs identify new determinants of the specification and maintenance of neuronal phenotypes. *J Neurosci,* 33**,** 5127-37.

JUNG, J., CHOI, S., HAN, K. M., KIM, A., KANG, W., PAIK, J. W., LEE, H. W. & HAM, B. J. 2019. Alterations in functional brain networks in depressed patients with a suicide attempt history. *Neuropsychopharmacology*.

JUNG, M., SCHAEFER, A., STEINER, I., KEMPKENSTEFFEN, C., STEPHAN, C., ERBERSDOBLER, A. & JUNG, K. 2010. Robust microRNA stability in degraded RNA preparations from human tissue and cell samples. *Clin Chem,* 56**,** 998-1006.

KADAKKUZHA, B. M., LIU, X. A., MCCRATE, J., SHANKAR, G., RIZZO, V., AFINOGENOVA, A., YOUNG, B., FALLAHI, M., CARVALLOZA, A. C., RAVEENDRA, B. & PUTHANVEETTIL, S. V. 2015. Transcriptome analyses of adult mouse brain reveal enrichment of lncRNAs in specific brain regions and neuronal populations. *Front Cell Neurosci,* 9**,** 63.

KAISER, T. & FENG, G. 2019. Tmem119-EGFP and Tmem119-CreERT2 Transgenic Mice for Labeling and Manipulating Microglia. *eNeuro,* 6.

KAMINSKY, Z., WILCOX, H. C., EATON, W. W., VAN ECK, K., KILARU, V., JOVANOVIC, T., KLENGEL, T., BRADLEY, B., BINDER, E. B., RESSLER, K. J. & SMITH, A. K. 2015. Epigenetic and genetic variation at SKA2 predict suicidal behavior and post-traumatic stress disorder. *Transl Psychiatry,* 5**,** e627.

KAMME, F., SALUNGA, R., YU, J., TRAN, D. T., ZHU, J., LUO, L., BITTNER, A., GUO, H. Q., MILLER, N., WAN, J. & ERLANDER, M. 2003. Single-cell microarray analysis in hippocampus CA1: demonstration and validation of cellular heterogeneity. *J Neurosci,* 23**,** 3607-15.

KANG, H. J., KIM, J. M., LEE, J. Y., KIM, S. Y., BAE, K. Y., KIM, S. W., SHIN, I. S., KIM, H. R., SHIN, M. G. & YOON, J. S. 2013. BDNF promoter methylation and suicidal behavior in depressive patients. *J Affect Disord,* 151**,** 679-85.

KAPRANOV, P., CHENG, J., DIKE, S., NIX, D. A., DUTTAGUPTA, R., WILLINGHAM, A. T., STADLER, P. F., HERTEL, J., HACKERMULLER, J., HOFACKER, I. L., BELL, I., CHEUNG, E., DRENKOW, J., DUMAIS, E., PATEL, S., HELT, G., GANESH, M., GHOSH, S., PICCOLBONI, A., SEMENTCHENKO, V., TAMMANA, H. & GINGERAS, T. R. 2007. RNA maps reveal new RNA classes and a possible function for pervasive transcription. *Science,* 316**,** 1484-8.

KASHON, M. L., ROSS, G. W., O'CALLAGHAN, J. P., MILLER, D. B., PETROVITCH, H., BURCHFIEL, C. M., SHARP, D. S., MARKESBERY, W. R., DAVIS, D. G., HARDMAN, J., NELSON, J. & WHITE, L. R. 2004. Associations of cortical astrogliosis with cognitive performance and dementia status. *J Alzheimers Dis,* 6**,** 595-604; discussion 673-81.

KAWAGUCHI, A., MIYATA, T., SAWAMOTO, K., TAKASHITA, N., MURAYAMA, A., AKAMATSU, W., OGAWA, M., OKABE, M., TANO, Y., GOLDMAN, S. A. & OKANO, H. 2001. Nestin-EGFP transgenic mice: visualization of the self-renewal and multipotency of CNS stem cells. *Mol Cell Neurosci,* 17**,** 259-73.

KE, R., MIGNARDI, M., PACUREANU, A., SVEDLUND, J., BOTLING, J., WAHLBY, C. & NILSSON, M. 2013. In situ sequencing for RNA analysis in preserved tissue and cells. *Nat Methods,* 10**,** 857-60.

KEENEY, M., GRATAMA, J. W., CHIN-YEE, I. H. & SUTHERLAND, D. R. 1998. Isotype controls in the analysis of lymphocytes and CD34+ stem and progenitor cells by flow cytometry--time to let go! *Cytometry,* 34**,** 280-3.

KEIL, K. P. & LEIN, P. J. 2016. DNA methylation: a mechanism linking environmental chemical exposures to risk of autism spectrum disorders? *Environ Epigenet,* 2.

KELLER, S., SARCHIAPONE, M., ZARRILLI, F., TOMAIUOLO, R., CARLI, V., ANGRISANO, T., VIDETIC, A., AMATO, F., PERO, R., DI GIANNANTONIO, M., IOSUE, M., LEMBO, F., CASTALDO, G. & CHIARIOTTI, L. 2011. TrkB gene expression and DNA methylation state in Wernicke area does not associate with suicidal behavior. *J Affect Disord,* 135**,** 400-4.

KELLER, S., SARCHIAPONE, M., ZARRILLI, F., VIDETIC, A., FERRARO, A., CARLI, V., SACCHETTI, S., LEMBO, F., ANGIOLILLO, A., JOVANOVIC, N., PISANTI, F., TOMAIUOLO, R., MONTICELLI, A., BALAZIC, J., ROY, A., MARUSIC, A., COCOZZA, S., FUSCO, A., BRUNI, C. B., CASTALDO, G. & CHIARIOTTI, L. 2010. Increased BDNF promoter methylation in the Wernicke area of suicide subjects. *Arch Gen Psychiatry,* 67**,** 258-67.

KEPECS, A. & FISHELL, G. 2014. Interneuron cell types are fit to function. *Nature,* 505**,** 318-26.

KEREN-SHAUL, H., SPINRAD, A., WEINER, A., MATCOVITCH-NATAN, O., DVIR-SZTERNFELD, R., ULLAND, T. K., DAVID, E., BARUCH, K., LARA-ASTAISO, D., TOTH, B., ITZKOVITZ, S., COLONNA, M., SCHWARTZ, M. & AMIT, I. 2017. A Unique Microglia Type Associated with Restricting Development of Alzheimer's Disease. *Cell,* 169**,** 1276-1290 e17.

KERNALEGUEN, M., DAVIAUD, C., SHEN, Y., BONNET, E., RENAULT, V., DELEUZE, J. F., MAUGER, F. & TOST, J. 2018. Whole-Genome Bisulfite Sequencing for the Analysis of Genome-Wide DNA Methylation and Hydroxymethylation Patterns at Single-Nucleotide Resolution. *Methods Mol Biol,* 1767**,** 311-349.

KESSARIS, N., FOGARTY, M., IANNARELLI, P., GRIST, M., WEGNER, M. & RICHARDSON, W. D. 2006. Competing waves of oligodendrocytes in the forebrain and postnatal elimination of an embryonic lineage. *Nat Neurosci,* 9**,** 173-9.

KHARE, T., PAI, S., KONCEVICIUS, K., PAL, M., KRIUKIENE, E., LIUTKEVICIUTE, Z., IRIMIA, M., JIA, P., PTAK, C., XIA, M., TICE, R., TOCHIGI, M., MORERA, S., NAZARIANS, A., BELSHAM, D., WONG, A. H., BLENCOWE, B. J., WANG, S. C., KAPRANOV, P., KUSTRA, R., LABRIE, V., KLIMASAUSKAS, S. & PETRONIS, A. 2012. 5-hmC in the brain is abundant in synaptic genes and shows differences at the exon-intron boundary. *Nat Struct Mol Biol,* 19**,** 1037-43.

KIERDORF, K., ERNY, D., GOLDMANN, T., SANDER, V., SCHULZ, C., PERDIGUERO, E. G., WIEGHOFER, P., HEINRICH, A., RIEMKE, P., HOLSCHER, C., MULLER, D. N., LUCKOW, B., BROCKER, T., DEBOWSKI, K., FRITZ, G., OPDENAKKER, G., DIEFENBACH, A., BIBER, K., HEIKENWALDER, M., GEISSMANN, F., ROSENBAUER, F. & PRINZ, M. 2013. Microglia emerge from erythromyeloid precursors via Pu.1- and Irf8-dependent pathways. *Nat Neurosci,* 16**,** 273-80.

KIM, C. D., SEGUIN, M., THERRIEN, N., RIOPEL, G., CHAWKY, N., LESAGE, A. D. & TURECKI, G. 2005. Familial aggregation of suicidal behavior: a family study of male suicide completers from the general population. *Am J Psychiatry,* 162**,** 1017-9.

KIM, J. M., KANG, H. J., BAE, K. Y., KIM, S. W., SHIN, I. S., KIM, H. R., SHIN, M. G. & YOON, J. S. 2014. Association of BDNF promoter methylation and genotype with suicidal ideation in elderly Koreans. *Am J Geriatr Psychiatry,* 22**,** 989-96.

KIM, J. M., KANG, H. J., KIM, S. Y., KIM, S. W., SHIN, I. S., KIM, H. R., PARK, M. H., SHIN, M. G., YOON, J. H. & YOON, J. S. 2015a. BDNF promoter methylation associated with suicidal ideation in patients with breast cancer. *Int J Psychiatry Med,* 49**,** 75-94.

KIM, K. K., ADELSTEIN, R. S. & KAWAMOTO, S. 2009. Identification of neuronal nuclei (NeuN) as Fox-3, a new member of the Fox-1 gene family of splicing factors. *J Biol Chem,* 284**,** 31052-61.

KIM, R., HEALEY, K. L., SEPULVEDA-ORENGO, M. T. & REISSNER, K. J. 2018. Astroglial correlates of neuropsychiatric disease: From astrocytopathy to astrogliosis. *Prog Neuropsychopharmacol Biol Psychiatry,* 87**,** 126-146.

KIM, S. & WEBSTER, M. J. 2011. Integrative genome-wide association analysis of cytoarchitectural abnormalities in the prefrontal cortex of psychiatric disorders. *Mol Psychiatry,* 16**,** 452-61.

KIM, T., LIM, C. S. & KAANG, B. K. 2015b. Cell type-specific gene expression profiling in brain tissue: comparison between TRAP, LCM and RNA-seq. *BMB Rep,* 48**,** 388-94.

KIM, T. K., HEMBERG, M., GRAY, J. M., COSTA, A. M., BEAR, D. M., WU, J., HARMIN, D. A., LAPTEWICZ, M., BARBARA-HALEY, K., KUERSTEN, S., MARKENSCOFF-PAPADIMITRIOU, E., KUHL, D., BITO, H., WORLEY, P. F., KREIMAN, G. & GREENBERG, M. E. 2010. Widespread transcription at neuronal activity-regulated enhancers. *Nature,* 465**,** 182-7.

KIMBREL, N. A., GARRETT, M. E., DENNIS, M. F., VA MID-ATLANTIC MENTAL ILLNESS RESEARCH, E., CLINICAL CENTER, W., HAUSER, M. A., ASHLEY-KOCH, A. E. & BECKHAM, J. C. 2018. A genome-wide association study of suicide attempts and suicidal ideation in U.S. military veterans. *Psychiatry Res,* 269**,** 64-69.

KLEIN, R. S. & FRICKER, L. D. 1993. Differential effects of a phorbol ester on carboxypeptidase E in cultured astrocytes and AtT-20 cells, a neuroendocrine cell line. *J Neurochem,* 60**,** 1615-25.

KLEMM, S. L., SHIPONY, Z. & GREENLEAF, W. J. 2019. Chromatin accessibility and the regulatory epigenome. *Nat Rev Genet,* 20**,** 207-220.

KOCERHA, J., DWIVEDI, Y. & BRENNAND, K. J. 2015. Noncoding RNAs and neurobehavioral mechanisms in psychiatric disease. *Mol Psychiatry,* 20**,** 677-684.

KODANI, M., YANG, G., CONKLIN, L. M., TRAVIS, T. C., WHITNEY, C. G., ANDERSON, L. J., SCHRAG, S. J., TAYLOR, T. H., JR., BEALL, B. W., BREIMAN, R. F., FEIKIN, D. R., NJENGA, M. K., MAYER, L. W., OBERSTE, M. S., TONDELLA, M. L., WINCHELL, J. M., LINDSTROM, S. L., ERDMAN, D. D. & FIELDS, B. S. 2011. Application of TaqMan low-density arrays for simultaneous detection of multiple respiratory pathogens. *J Clin Microbiol,* 49**,** 2175-82.

KOEPPEN, A. H. 1995. The history of iron in the brain. *J Neurol Sci,* 134 Suppl**,** 1-9.

KOESTER, S. K. & BOLTON, W. E. 2000. Intracellular markers. *J Immunol Methods,* 243**,** 99-106.

KOESTLER, D. C., JONES, M. J., USSET, J., CHRISTENSEN, B. C., BUTLER, R. A., KOBOR, M. S., WIENCKE, J. K. & KELSEY, K. T. 2016. Improving cell mixture deconvolution by identifying optimal DNA methylation libraries (IDOL). *BMC Bioinformatics,* 17**,** 120.

KOH, K. P. & RAO, A. 2013. DNA methylation and methylcytosine oxidation in cell fate decisions. *Curr Opin Cell Biol,* 25**,** 152-61.

KOHYAMA, M., ISE, W., EDELSON, B. T., WILKER, P. R., HILDNER, K., MEJIA, C., FRAZIER, W. A., MURPHY, T. L. & MURPHY, K. M. 2009. Role for Spi-C in the development of red pulp macrophages and splenic iron homeostasis. *Nature,* 457**,** 318-21.

KONNO, T., KASANUKI, K., IKEUCHI, T., DICKSON, D. W. & WSZOLEK, Z. K. 2018. CSF1R-related leukoencephalopathy: A major player in primary microgliopathies. *Neurology,* 91**,** 1092-1104.

KOPP, F. & MENDELL, J. T. 2018. Functional Classification and Experimental Dissection of Long Noncoding RNAs. *Cell,* 172**,** 393-407.

KOSO, H., TSUHAKO, A., LAI, C. Y., BABA, Y., OTSU, M., UENO, K., NAGASAKI, M., SUZUKI, Y. & WATANABE, S. 2016. Conditional rod photoreceptor ablation reveals Sall1 as a microglial marker and regulator of microglial morphology in the retina. *Glia,* 64**,** 2005-24.

KOUTER, K., ZUPANC, T. & VIDETIC PASKA, A. 2019. Genome-wide DNA methylation in suicide victims revealing impact on gene expression. *J Affect Disord,* 253**,** 419-425.

KOZLENKOV, A., JAFFE, A. E., TIMASHPOLSKY, A., APONTES, P., RUDCHENKO, S., BARBU, M., BYNE, W., HURD, Y. L., HORVATH, S. & DRACHEVA, S. 2017. DNA Methylation Profiling of Human Prefrontal Cortex Neurons in Heroin Users Shows Significant Difference between Genomic Contexts of Hyper- and Hypomethylation and a Younger Epigenetic Age. *Genes (Basel),* 8.

KOZLENKOV, A., LI, J., APONTES, P., HURD, Y. L., BYNE, W. M., KOONIN, E. V., WEGNER, M., MUKAMEL, E. A. & DRACHEVA, S. 2018. A unique role for DNA (hydroxy)methylation in epigenetic regulation of human inhibitory neurons. *Sci Adv,* 4**,** eaau6190.

KOZLENKOV, A., ROUSSOS, P., TIMASHPOLSKY, A., BARBU, M., RUDCHENKO, S., BIBIKOVA, M., KLOTZLE, B., BYNE, W., LYDDON, R., DI NARZO, A. F., HURD, Y. L., KOONIN, E. V. & DRACHEVA, S. 2014. Differences in DNA methylation between human neuronal and glial cells are concentrated in enhancers and non-CpG sites. *Nucleic Acids Res,* 42**,** 109-27.

KOZLENKOV, A., WANG, M., ROUSSOS, P., RUDCHENKO, S., BARBU, M., BIBIKOVA, M., KLOTZLE, B., DWORK, A. J., ZHANG, B., HURD, Y. L., KOONIN, E. V., WEGNER, M. & DRACHEVA, S. 2016. Substantial DNA methylation differences between two major neuronal subtypes in human brain. *Nucleic Acids Res,* 44**,** 2593-612.

KRETZSCHMAR, H. 2009. Brain banking: opportunities, challenges and meaning for the future. *Nat Rev Neurosci,* 10**,** 70-8.

KRIAUCIONIS, S. & HEINTZ, N. 2009. The nuclear DNA base 5-hydroxymethylcytosine is present in Purkinje neurons and the brain. *Science,* 324**,** 929-30.

KRISHNASWAMI, S. R., GRINDBERG, R. V., NOVOTNY, M., VENEPALLY, P., LACAR, B., BHUTANI, K., LINKER, S. B., PHAM, S., ERWIN, J. A., MILLER, J. A., HODGE, R., MCCARTHY, J. K., KELDER, M., MCCORRISON, J., AEVERMANN, B. D., FUERTES, F. D., SCHEUERMANN, R. H., LEE, J., LEIN, E. S., SCHORK, N., MCCONNELL, M. J., GAGE, F. H. & LASKEN, R. S. 2016. Using single nuclei for RNA-seq to capture the transcriptome of postmortem neurons. *Nat Protoc,* 11**,** 499-524.

KRISTENSEN, L. S. & HANSEN, L. L. 2009. PCR-based methods for detecting single-locus DNA methylation biomarkers in cancer diagnostics, prognostics, and response to treatment. *Clin Chem,* 55**,** 1471-83.

KRUPENKO, S. A. 2009. FDH: an aldehyde dehydrogenase fusion enzyme in folate metabolism. *Chem Biol Interact,* 178**,** 84-93.

KUANG, W. H., DONG, Z. Q., TIAN, L. T. & LI, J. 2018. MicroRNA-451a, microRNA-34a-5p, and microRNA-221-3p as predictors of response to antidepressant treatment. *Braz J Med Biol Res,* 51**,** e7212.

KUMAR, S., CHINNUSAMY, V. & MOHAPATRA, T. 2018. Epigenetics of Modified DNA Bases: 5-Methylcytosine and Beyond. *Front Genet,* 9**,** 640.

KUNDAKOVIC, M., JIANG, Y., KAVANAGH, D. H., DINCER, A., BROWN, L., POTHULA, V., ZHAROVSKY, E., PARK, R., JACOBOV, R., MAGRO, I., KASSIM, B., WISEMAN, J., DANG, K., SIEBERTS, S. K., ROUSSOS, P., FROMER, M., HARRIS, B., LIPSKA, B. K., PETERS, M. A., SKLAR, P. & AKBARIAN, S. 2017. Practical Guidelines for High-Resolution Epigenomic Profiling of Nucleosomal Histones in Postmortem Human Brain Tissue. *Biol Psychiatry,* 81**,** 162-170.

KUNG, J. T., COLOGNORI, D. & LEE, J. T. 2013. Long noncoding RNAs: past, present, and future. *Genetics,* 193**,** 651-69.

LABONTE, B., SUDERMAN, M., MAUSSION, G., LOPEZ, J. P., NAVARRO-SANCHEZ, L., YERKO, V., MECHAWAR, N., SZYF, M., MEANEY, M. J. & TURECKI, G. 2013. Genome-wide methylation changes in the brains of suicide completers. *Am J Psychiatry,* 170**,** 511-20.

LABONTE, B., SUDERMAN, M., MAUSSION, G., NAVARO, L., YERKO, V., MAHAR, I., BUREAU, A., MECHAWAR, N., SZYF, M., MEANEY, M. J. & TURECKI, G. 2012a. Genome-wide epigenetic regulation by early-life trauma. *Arch Gen Psychiatry,* 69**,** 722-31.

LABONTE, B. & TURECKI, G. 2010. The epigenetics of suicide: explaining the biological effects of early life environmental adversity. *Arch Suicide Res,* 14**,** 291-310.

LABONTE, B., YERKO, V., GROSS, J., MECHAWAR, N., MEANEY, M. J., SZYF, M. & TURECKI, G. 2012b. Differential glucocorticoid receptor exon 1(B), 1(C), and 1(H) expression and methylation in suicide completers with a history of childhood abuse. *Biol Psychiatry,* 72**,** 41-8.

LADD-ACOSTA, C., HANSEN, K. D., BRIEM, E., FALLIN, M. D., KAUFMANN, W. E. & FEINBERG, A. P. 2014. Common DNA methylation alterations in multiple brain regions in autism. *Mol Psychiatry,* 19**,** 862-71.

LADD-ACOSTA, C., PEVSNER, J., SABUNCIYAN, S., YOLKEN, R. H., WEBSTER, M. J., DINKINS, T., CALLINAN, P. A., FAN, J. B., POTASH, J. B. & FEINBERG, A. P. 2007. DNA methylation signatures within the human brain. *Am J Hum Genet,* 81**,** 1304-15.

LAKE, B. B., AI, R., KAESER, G. E., SALATHIA, N. S., YUNG, Y. C., LIU, R., WILDBERG, A., GAO, D., FUNG, H. L., CHEN, S., VIJAYARAGHAVAN, R., WONG, J., CHEN, A., SHENG, X., KAPER, F., SHEN, R., RONAGHI, M., FAN, J. B., WANG, W., CHUN, J. & ZHANG, K. 2016. Neuronal subtypes and diversity revealed by single-nucleus RNA sequencing of the human brain. *Science,* 352**,** 1586-90.

LANDAY, A. L. & MUIRHEAD, K. A. 1989. Procedural guidelines for performing immunophenotyping by flow cytometry. *Clin Immunol Immunopathol,* 52**,** 48-60.

LAPLANT, Q., VIALOU, V., COVINGTON, H. E., 3RD, DUMITRIU, D., FENG, J., WARREN, B. L., MAZE, I., DIETZ, D. M., WATTS, E. L., INIGUEZ, S. D., KOO, J. W., MOUZON, E., RENTHAL, W., HOLLIS, F., WANG, H., NOONAN, M. A., REN, Y., EISCH, A. J., BOLANOS, C. A., KABBAJ, M., XIAO, G., NEVE, R. L., HURD, Y. L., OOSTING, R. S., FAN, G., MORRISON, J. H. & NESTLER, E. J. 2010. Dnmt3a regulates emotional behavior and spine plasticity in the nucleus accumbens. *Nat Neurosci,* 13**,** 1137-43.

LARSEN, C. N., PRICE, J. S. & WILKINSON, K. D. 1996. Substrate binding and catalysis by ubiquitin C-terminal hydrolases: identification of two active site residues. *Biochemistry,* 35**,** 6735-44.

LASKARIS, L. E., DI BIASE, M. A., EVERALL, I., CHANA, G., CHRISTOPOULOS, A., SKAFIDAS, E., CROPLEY, V. L. & PANTELIS, C. 2016. Microglial activation and progressive brain changes in schizophrenia. *Br J Pharmacol,* 173**,** 666-80.

LASZLO, A. H., DERRINGTON, I. M., BRINKERHOFF, H., LANGFORD, K. W., NOVA, I. C., SAMSON, J. M., BARTLETT, J. J., PAVLENOK, M. & GUNDLACH, J. H. 2013. Detection and mapping of 5-methylcytosine and 5-hydroxymethylcytosine with nanopore MspA. *Proc Natl Acad Sci U S A,* 110**,** 18904-9.

LATTICE, S. D. 2008. *Multivariate Data Visualization with R* [Online]. Springer: New York, NY, USA,. Available: http://lmdvrr-forger-projectorg, 2008. [Accessed].

LAU, P., VERRIER, J. D., NIELSEN, J. A., JOHNSON, K. R., NOTTERPEK, L. & HUDSON, L. D. 2008. Identification of dynamically regulated microRNA and mRNA networks in developing oligodendrocytes. *J Neurosci,* 28**,** 11720-30.

LAURENCE, J. A. & FATEMI, S. H. 2005. Glial fibrillary acidic protein is elevated in superior frontal, parietal and cerebellar cortices of autistic subjects. *Cerebellum,* 4**,** 206-10.

LAVIN, Y., WINTER, D., BLECHER-GONEN, R., DAVID, E., KEREN-SHAUL, H., MERAD, M., JUNG, S. & AMIT, I. 2014. Tissue-resident macrophage enhancer landscapes are shaped by the local microenvironment. *Cell,* 159**,** 1312-26.

LE-NICULESCU, H., KURIAN, S. M., YEHYAWI, N., DIKE, C., PATEL, S. D., EDENBERG, H. J., TSUANG, M. T., SALOMON, D. R., NURNBERGER, J. I., JR. & NICULESCU, A. B. 2009. Identifying blood biomarkers for mood disorders using convergent functional genomics. *Mol Psychiatry,* 14**,** 156-74.

LE-NICULESCU, H., LEVEY, D. F., AYALEW, M., PALMER, L., GAVRIN, L. M., JAIN, N., WINIGER, E., BHOSREKAR, S., SHANKAR, G., RADEL, M., BELLANGER, E., DUCKWORTH, H., OLESEK, K., VERGO, J., SCHWEITZER, R., YARD, M., BALLEW, A., SHEKHAR, A., SANDUSKY, G. E., SCHORK, N. J., KURIAN, S. M., SALOMON, D. R. & NICULESCU, A. B., 3RD 2013. Discovery and validation of blood biomarkers for suicidality. *Mol Psychiatry,* 18**,** 1249-64.

LEAVESLEY, S. J., BRITAIN, A. L., CICHON, L. K., NIKOLAEV, V. O. & RICH, T. C. 2013. Assessing FRET using spectral techniques. *Cytometry A,* 83**,** 898-912.

LECCA, D., JANDA, E., MULAS, G., DIANA, A., MARTINO, C., ANGIUS, F., SPOLITU, S., CASU, M. A., SIMBULA, G., BOI, L., BATETTA, B., SPIGA, S. & CARTA, A. R. 2018. Boosting phagocytosis and anti-inflammatory phenotype in microglia mediates neuroprotection by PPARgamma agonist MDG548 in Parkinson's disease models. *Br J Pharmacol,* 175**,** 3298-3314.

LEE, J. H., DAUGHARTHY, E. R., SCHEIMAN, J., KALHOR, R., YANG, J. L., FERRANTE, T. C., TERRY, R., JEANTY, S. S., LI, C., AMAMOTO, R., PETERS, D. T., TURCZYK, B. M., MARBLESTONE, A. H., INVERSO, S. A., BERNARD, A., MALI, P., RIOS, X., AACH, J. & CHURCH, G. M. 2014. Highly multiplexed subcellular RNA sequencing in situ. *Science,* 343**,** 1360-3.

LEE, J. M., BLENNOW, K., ANDREASEN, N., LATERZA, O., MODUR, V., OLANDER, J., GAO, F., OHLENDORF, M. & LADENSON, J. H. 2008. The brain injury biomarker VLP-1 is increased in the cerebrospinal fluid of Alzheimer disease patients. *Clin Chem,* 54**,** 1617-23.

LEE, Y. J., KIM, S., GWAK, A. R., KIM, S. J., KANG, S. G., NA, K. S., SON, Y. D. & PARK, J. 2016. Decreased regional gray matter volume in suicide attempters compared to suicide non-attempters with major depressive disorders. *Compr Psychiatry,* 67**,** 59-65.

LEGROUX, L., PITTET, C. L., BEAUSEIGLE, D., DEBLOIS, G., PRAT, A. & ARBOUR, N. 2015. An optimized method to process mouse CNS to simultaneously analyze neural cells and leukocytes by flow cytometry. *J Neurosci Methods,* 247**,** 23-31.

LEHNARDT, S. 2010. Innate immunity and neuroinflammation in the CNS: the role of microglia in Toll-like receptor-mediated neuronal injury. *Glia,* 58**,** 253-63.

LEIN, E. S., HAWRYLYCZ, M. J., AO, N., AYRES, M., BENSINGER, A., BERNARD, A., BOE, A. F., BOGUSKI, M. S., BROCKWAY, K. S., BYRNES, E. J., CHEN, L., CHEN, L., CHEN, T. M., CHIN, M. C., CHONG, J., CROOK, B. E., CZAPLINSKA, A., DANG, C. N., DATTA, S., DEE, N. R., DESAKI, A. L., DESTA, T., DIEP, E., DOLBEARE, T. A., DONELAN, M. J., DONG, H. W., DOUGHERTY, J. G., DUNCAN, B. J., EBBERT, A. J., EICHELE, G., ESTIN, L. K., FABER, C., FACER, B. A., FIELDS, R., FISCHER, S. R., FLISS, T. P., FRENSLEY, C., GATES, S. N., GLATTFELDER, K. J., HALVERSON, K. R., HART, M. R., HOHMANN, J. G., HOWELL, M. P., JEUNG, D. P., JOHNSON, R. A., KARR, P. T., KAWAL, R., KIDNEY, J. M., KNAPIK, R. H., KUAN, C. L., LAKE, J. H., LARAMEE, A. R., LARSEN, K. D., LAU, C., LEMON, T. A., LIANG, A. J., LIU, Y., LUONG, L. T., MICHAELS, J., MORGAN, J. J., MORGAN, R. J., MORTRUD, M. T., MOSQUEDA, N. F., NG, L. L., NG, R., ORTA, G. J., OVERLY, C. C., PAK, T. H., PARRY, S. E., PATHAK, S. D., PEARSON, O. C., PUCHALSKI, R. B., RILEY, Z. L., ROCKETT, H. R., ROWLAND, S. A., ROYALL, J. J., RUIZ, M. J., SARNO, N. R., SCHAFFNIT, K., SHAPOVALOVA, N. V., SIVISAY, T., SLAUGHTERBECK, C. R., SMITH, S. C., SMITH, K. A., SMITH, B. I., SODT, A. J.,

STEWART, N. N., STUMPF, K. R., SUNKIN, S. M., SUTRAM, M., TAM, A., TEEMER, C. D., THALLER, C., THOMPSON, C. L., VARNAM, L. R., VISEL, A., WHITLOCK, R. M., WOHNOUTKA, P. E., WOLKEY, C. K., WONG, V. Y., et al. 2007. Genome-wide atlas of gene expression in the adult mouse brain. *Nature,* 445**,** 168-76.

LETI, F., LLACI, L., MALENICA, I. & DISTEFANO, J. K. 2018. Methods for CpG Methylation Array Profiling Via Bisulfite Conversion. *Methods Mol Biol,* 1706**,** 233-254.

LEVEY, D. F., POLIMANTI, R., CHENG, Z., ZHOU, H., NUNEZ, Y. Z., JAIN, S., HE, F., SUN, X., URSANO, R. J., KESSLER, R. C., SMOLLER, J. W., STEIN, M. B., KRANZLER, H. R. & GELERNTER, J. 2019. Genetic associations with suicide attempt severity and genetic overlap with major depression. *Transl Psychiatry,* 9**,** 22.

LI, J., CHAI, A., WANG, L., MA, Y., WU, Z., YU, H., MEI, L., LU, L., ZHANG, C., YUE, W., XU, L., RAO, Y. & ZHANG, D. 2015. Synaptic P-Rex1 signaling regulates hippocampal long-term depression and autism-like social behavior. *Proc Natl Acad Sci U S A,* 112**,** E6964-72.

LI, J., LI, D., ZHOU, H., WU, G., HE, Z., LIAO, W., LI, Y. & ZHI, Y. 2020a. MicroRNA-338-5p alleviates neuronal apoptosis via directly targeting BCL2L11 in APP/PS1 mice. *Aging (Albany NY),* 12**,** 20728-20742.

LI, J., YOSHIKAWA, A. & MELTZER, H. Y. 2017. Replication of rs300774, a genetic biomarker near ACP1, associated with suicide attempts in patients with schizophrenia: Relation to brain cholesterol biosynthesis. *J Psychiatr Res,* 94**,** 54-61.

LI, L., HUNG, A. C. & PORTER, A. G. 2008a. Secretogranin II: a key AP-1-regulated protein that mediates neuronal differentiation and protection from nitric oxide-induced apoptosis of neuroblastoma cells. *Cell Death Differ,* 15**,** 879-88.

LI, M. M., JIANG, T., SUN, Z., ZHANG, Q., TAN, C. C., YU, J. T. & TAN, L. 2014a. Genome-wide microRNA expression profiles in hippocampus of rats with chronic temporal lobe epilepsy. *Sci Rep,* 4**,** 4734.

LI, Q., CHENG, Z., ZHOU, L., DARMANIS, S., NEFF, N. F., OKAMOTO, J., GULATI, G., BENNETT, M. L., SUN, L. O., CLARKE, L. E., MARSCHALLINGER, J., YU, G., QUAKE, S. R., WYSS-CORAY, T. & BARRES, B. A. 2019. Developmental Heterogeneity of Microglia and Brain Myeloid Cells Revealed by Deep Single-Cell RNA Sequencing. *Neuron,* 101**,** 207-223 e10.

LI, Q., LAN, X., HAN, X. & WANG, J. 2018. Expression of Tmem119/Sall1 and Ccr2/CD69 in FACS-Sorted Microglia- and Monocyte/Macrophage-Enriched Cell Populations After Intracerebral Hemorrhage. *Front Cell Neurosci,* 12**,** 520.

LI, W. C., MA, K. J., LV, Y. H., ZHANG, P., PAN, H., ZHANG, H., WANG, H. J., MA, D. & CHEN, L. 2014b. Postmortem interval determination using 18S-rRNA and microRNA. *Sci Justice,* 54**,** 307-10.

LI, W. W., GONG, L. & BAYLEY, H. 2013. Single-molecule detection of 5-hydroxymethylcytosine in DNA through chemical modification and nanopore analysis. *Angew Chem Int Ed Engl,* 52**,** 4350-5.

LI, X., ITO, M., ZHOU, F., YOUNGSON, N., ZUO, X., LEDER, P. & FERGUSON-SMITH, A. C. 2008b. A maternal-zygotic effect gene, Zfp57, maintains both maternal and paternal imprints. *Dev Cell,* 15**,** 547-57.

LI, X., WU, X., LUO, P. & XIONG, L. 2020b. Astrocyte-specific NDRG2 gene: functions in the brain and neurological diseases. *Cell Mol Life Sci,* 77**,** 2461-2472.

LI, Z. & WU, H. 2019. TOAST: improving reference-free cell composition estimation by cross-cell type differential analysis. *Genome Biol,* 20**,** 190.

LIM, L., MI, D., LLORCA, A. & MARIN, O. 2018. Development and Functional Diversification of Cortical Interneurons. *Neuron,* 100**,** 294-313.

LIMON, A., MAMDANI, F., HJELM, B. E., VAWTER, M. P. & SEQUEIRA, A. 2016. Targets of polyamine dysregulation in major depression and suicide: Activity-dependent feedback, excitability, and neurotransmission. *Neurosci Biobehav Rev,* 66**,** 80-91.

LIN, R. & TURECKI, G. 2017. Noncoding RNAs in Depression. *Adv Exp Med Biol,* 978**,** 197-210.

LINDQVIST, D., JANELIDZE, S., HAGELL, P., ERHARDT, S., SAMUELSSON, M., MINTHON, L., HANSSON, O., BJORKQVIST, M., TRASKMAN-BENDZ, L. & BRUNDIN, L. 2009. Interleukin-

6 is elevated in the cerebrospinal fluid of suicide attempters and related to symptom severity. *Biol Psychiatry,* 66**,** 287-92.

LING, K. H., HEWITT, C. A., TAN, K. L., CHEAH, P. S., VIDYADARAN, S., LAI, M. I., LEE, H. C., SIMPSON, K., HYDE, L., PRITCHARD, M. A., SMYTH, G. K., THOMAS, T. & SCOTT, H. S. 2014. Functional transcriptome analysis of the postnatal brain of the Ts1Cje mouse model for Down syndrome reveals global disruption of interferon-related molecular networks. *BMC Genomics,* 15**,** 624.

LIPOVICH, L., TARCA, A. L., CAI, J., JIA, H., CHUGANI, H. T., STERNER, K. N., GROSSMAN, L. I., UDDIN, M., HOF, P. R., SHERWOOD, C. C., KUZAWA, C. W., GOODMAN, M. & WILDMAN, D. E. 2014. Developmental changes in the transcriptome of human cerebral cortex tissue: long noncoding RNA transcripts. *Cereb Cortex,* 24**,** 1451-9.

LISTER, R., MUKAMEL, E. A., NERY, J. R., URICH, M., PUDDIFOOT, C. A., JOHNSON, N. D., LUCERO, J., HUANG, Y., DWORK, A. J., SCHULTZ, M. D., YU, M., TONTI-FILIPPINI, J., HEYN, H., HU, S., WU, J. C., RAO, A., ESTELLER, M., HE, C., HAGHIGHI, F. G., SEJNOWSKI, T. J., BEHRENS, M. M. & ECKER, J. R. 2013. Global epigenomic reconfiguration during mammalian brain development. *Science,* 341**,** 1237905.

LIU, A., TETZLAFF, M. T., VANBELLE, P., ELDER, D., FELDMAN, M., TOBIAS, J. W., SEPULVEDA, A. R. & XU, X. 2009. MicroRNA expression profiling outperforms mRNA expression profiling in formalin-fixed paraffin-embedded tissues. *Int J Clin Exp Pathol,* 2**,** 519-27.

LIU, D., DIORIO, J., TANNENBAUM, B., CALDJI, C., FRANCIS, D., FREEDMAN, A., SHARMA, S., PEARSON, D., PLOTSKY, P. M. & MEANEY, M. J. 1997. Maternal care, hippocampal glucocorticoid receptors, and hypothalamic-pituitary-adrenal responses to stress. *Science,* 277**,** 1659-62.

LIU, G. J., MIDDLETON, R. J., KAM, W. W., CHIN, D. Y., HATTY, C. R., CHAN, R. H. & BANATI, R. B. 2017. Functional gains in energy and cell metabolism after TSPO gene insertion. *Cell Cycle,* 16**,** 436-447.

LIU, H., LI, W., ROSE, M. E., HICKEY, R. W., CHEN, J., UECHI, G. T., BALASUBRAMANI, M., DAY, B. W., PATEL, K. V. & GRAHAM, S. H. 2015. The point mutation UCH-L1 C152A protects primary neurons against cyclopentenone prostaglandin-induced cytotoxicity: implications for post-ischemic neuronal injury. *Cell Death Dis,* 6**,** e1966.

LIU, H., POVYSHEVA, N., ROSE, M. E., MI, Z., BANTON, J. S., LI, W., CHEN, F., REAY, D. P., BARRIONUEVO, G., ZHANG, F. & GRAHAM, S. H. 2019a. Role of UCHL1 in axonal injury and functional recovery after cerebral ischemia. *Proc Natl Acad Sci U S A,* 116**,** 4643-4650.

LIU, J., DIETZ, K., DELOYHT, J. M., PEDRE, X., KELKAR, D., KAUR, J., VIALOU, V., LOBO, M. K., DIETZ, D. M., NESTLER, E. J., DUPREE, J. & CASACCIA, P. 2012. Impaired adult myelination in the prefrontal cortex of socially isolated mice. *Nat Neurosci,* 15**,** 1621-3.

LIU, Y., FALLON, L., LASHUEL, H. A., LIU, Z. & LANSBURY, P. T., JR. 2002. The UCH-L1 gene encodes two opposing enzymatic activities that affect alpha-synuclein degradation and Parkinson's disease susceptibility. *Cell,* 111**,** 209-18.

LIU, Y., WANG, M., MARCORA, E. M., ZHANG, B. & GOATE, A. M. 2019b. Promoter DNA hypermethylation - Implications for Alzheimer's disease. *Neurosci Lett,* 711**,** 134403.

LIU, Z., HU, X., CAI, J., LIU, B., PENG, X., WEGNER, M. & QIU, M. 2007. Induction of oligodendrocyte differentiation by Olig2 and Sox10: evidence for reciprocal interactions and dosage-dependent mechanisms. *Dev Biol,* 302**,** 683-93.

LLORENS, F., BANEZ-CORONEL, M., PANTANO, L., DEL RIO, J. A., FERRER, I., ESTIVILL, X. & MARTI, E. 2013. A highly expressed miR-101 isomiR is a functional silencing small RNA. *BMC Genomics,* 14**,** 104.

LO, F. S., ZHAO, S. & ERZURUMLU, R. S. 2011. Astrocytes promote peripheral nerve injury-induced reactive synaptogenesis in the neonatal CNS. *J Neurophysiol,* 106**,** 2876-87.

LOBO, M. K., KARSTEN, S. L., GRAY, M., GESCHWIND, D. H. & YANG, X. W. 2006. FACS-array profiling of striatal projection neuron subtypes in juvenile and adult mouse brains. *Nat Neurosci,* 9**,** 443-52.

LOCKWOOD, L. E., SU, S. & YOUSSEF, N. A. 2015. The role of epigenetics in depression and suicide: A platform for gene-environment interactions. *Psychiatry Res,* 228**,** 235-42.

LODATO, S., SHETTY, A. S. & ARLOTTA, P. 2015. Cerebral cortex assembly: generating and reprogramming projection neuron diversity. *Trends Neurosci,* 38**,** 117-25.

LOMBARDINO, A. J., LI, X. C., HERTEL, M. & NOTTEBOHM, F. 2005. Replaceable neurons and neurodegenerative disease share depressed UCHL1 levels. *Proc Natl Acad Sci U S A,* 102**,** 8036-41.

LOPEZ-ANIDO, C., SUN, G., KOENNING, M., SRINIVASAN, R., HUNG, H. A., EMERY, B., KELES, S. & SVAREN, J. 2015. Differential Sox10 genomic occupancy in myelinating glia. *Glia,* 63**,** 1897-1914.

LOPEZ-ATALAYA, J. P., ASKEW, K. E., SIERRA, A. & GOMEZ-NICOLA, D. 2018. Development and maintenance of the brain's immune toolkit: Microglia and non-parenchymal brain macrophages. *Dev Neurobiol,* 78**,** 561-579.

LOPEZ-URRUTIA, E., BUSTAMANTE MONTES, L. P., LADRON DE GUEVARA CERVANTES, D., PEREZ-PLASENCIA, C. & CAMPOS-PARRA, A. D. 2019. Crosstalk Between Long Non-coding RNAs, Micro-RNAs and mRNAs: Deciphering Molecular Mechanisms of Master Regulators in Cancer. *Front Oncol,* 9**,** 669.

LOPEZ, J. P., FIORI, L. M., CRUCEANU, C., LIN, R., LABONTE, B., CATES, H. M., HELLER, E. A., VIALOU, V., KU, S. M., GERALD, C., HAN, M. H., FOSTER, J., FREY, B. N., SOARES, C. N., MULLER, D. J., FARZAN, F., LERI, F., MACQUEEN, G. M., FEILOTTER, H., TYRYSHKIN, K., EVANS, K. R., GIACOBBE, P., BLIER, P., LAM, R. W., MILEV, R., PARIKH, S. V., ROTZINGER, S., STROTHER, S. C., LEWIS, C. M., AITCHISON, K. J., WITTENBERG, G. M., MECHAWAR, N., NESTLER, E. J., UHER, R., KENNEDY, S. H. & TURECKI, G. 2017. MicroRNAs 146a/b-5 and 425-3p and 24-3p are markers of antidepressant response and regulate MAPK/Wnt-system genes. *Nat Commun,* 8**,** 15497.

LOPEZ, J. P., FIORI, L. M., GROSS, J. A., LABONTE, B., YERKO, V., MECHAWAR, N. & TURECKI, G. 2014. Regulatory role of miRNAs in polyamine gene expression in the prefrontal cortex of depressed suicide completers. *Int J Neuropsychopharmacol,* 17**,** 23-32.

LOVATT, D., SONNEWALD, U., WAAGEPETERSEN, H. S., SCHOUSBOE, A., HE, W., LIN, J. H., HAN, X., TAKANO, T., WANG, S., SIM, F. J., GOLDMAN, S. A. & NEDERGAARD, M. 2007. The transcriptome and metabolic gene signature of protoplasmic astrocytes in the adult murine cortex. *J Neurosci,* 27**,** 12255-66.

LUBECK, E., COSKUN, A. F., ZHIYENTAYEV, T., AHMAD, M. & CAI, L. 2014. Single-cell in situ RNA profiling by sequential hybridization. *Nat Methods,* 11**,** 360-1.

LUDWIG, N., LEIDINGER, P., BECKER, K., BACKES, C., FEHLMANN, T., PALLASCH, C., RHEINHEIMER, S., MEDER, B., STAHLER, C., MEESE, E. & KELLER, A. 2016. Distribution of miRNA expression across human tissues. *Nucleic Acids Res,* 44**,** 3865-77.

LUNNON, K., HANNON, E., SMITH, R. G., DEMPSTER, E., WONG, C., BURRAGE, J., TROAKES, C., AL-SARRAJ, S., KEPA, A., SCHALKWYK, L. & MILL, J. 2016. Variation in 5-hydroxymethylcytosine across human cortex and cerebellum. *Genome Biol,* 17**,** 27.

LUNNON, K., SMITH, R., HANNON, E., DE JAGER, P. L., SRIVASTAVA, G., VOLTA, M., TROAKES, C., AL-SARRAJ, S., BURRAGE, J., MACDONALD, R., CONDLIFFE, D., HARRIES, L. W., KATSEL, P., HAROUTUNIAN, V., KAMINSKY, Z., JOACHIM, C., POWELL, J., LOVESTONE, S., BENNETT, D. A., SCHALKWYK, L. C. & MILL, J. 2014. Methylomic profiling implicates cortical deregulation of ANK1 in Alzheimer's disease. *Nat Neurosci,* 17**,** 1164-70.

LUTZ, P. E., MECHAWAR, N. & TURECKI, G. 2017a. Neuropathology of suicide: recent findings and future directions. *Mol Psychiatry,* 22**,** 1395-1412.

LUTZ, P. E., TANTI, A., GASECKA, A., BARNETT-BURNS, S., KIM, J. J., ZHOU, Y., CHEN, G. G., WAKID, M., SHAW, M., ALMEIDA, D., CHAY, M. A., YANG, J., LARIVIERE, V., M'BOUTCHOU, M. N., VAN KEMPEN, L. C., YERKO, V., PRUD'HOMME, J., DAVOLI, M. A., VAILLANCOURT, K., THEROUX, J. F., BRAMOULLE, A., ZHANG, T. Y., MEANEY, M. J., ERNST, C., COTE, D., MECHAWAR, N. & TURECKI, G. 2017b. Association of a History of Child Abuse With

Impaired Myelination in the Anterior Cingulate Cortex: Convergent Epigenetic, Transcriptional, and Morphological Evidence. *Am J Psychiatry,* 174**,** 1185-1194.

LV, J., LIU, H., YU, S., LIU, H., CUI, W., GAO, Y., ZHENG, T., QIN, G., GUO, J., ZENG, T., HAN, Z., ZHANG, Y. & WU, Q. 2015. Identification of 4438 novel lincRNAs involved in mouse pre-implantation embryonic development. *Mol Genet Genomics,* 290**,** 685-97.

LV, Y. H., MA, J. L., PAN, H., ZHANG, H., LI, W. C., XUE, A. M., WANG, H. J., MA, K. J. & CHEN, L. 2016. RNA degradation as described by a mathematical model for postmortem interval determination. *J Forensic Leg Med,* 44**,** 43-52.

MA, C., GU, C., HUO, Y., LI, X. & LUO, X. J. 2018. The integrated landscape of causal genes and pathways in schizophrenia. *Transl Psychiatry,* 8**,** 67.

MA, J., PAN, H., ZENG, Y., LV, Y., ZHANG, H., XUE, A., JIANG, J., MA, K. & CHEN, L. 2015. Exploration of the R code-based mathematical model for PMI estimation using profiling of RNA degradation in rat brain tissue at different temperatures. *Forensic Sci Med Pathol,* 11**,** 530-7.

MA, Q., ZHANG, L. & PEARCE, W. J. 2019. MicroRNAs in brain development and cerebrovascular pathophysiology. *Am J Physiol Cell Physiol,* 317**,** C3-C19.

MACIOROWSKI, Z., CHATTOPADHYAY, P. K. & JAIN, P. 2017. Basic Multicolor Flow Cytometry. *Curr Protoc Immunol,* 117**,** 5 4 1-5 4 38.

MADDOX, S. A., SCHAFE, G. E. & RESSLER, K. J. 2013. Exploring epigenetic regulation of fear memory and biomarkers associated with post-traumatic stress disorder. *Front Psychiatry,* 4**,** 62.

MAECKER, H. T., FREY, T., NOMURA, L. E. & TROTTER, J. 2004. Selecting fluorochrome conjugates for maximum sensitivity. *Cytometry A,* 62**,** 169-73.

MAECKER, H. T. & TROTTER, J. 2006. Flow cytometry controls, instrument setup, and the determination of positivity. *Cytometry A,* 69**,** 1037-42.

MAGES, B., ALEITHE, S., BLIETZ, A., KRUEGER, M., HARTIG, W. & MICHALSKI, D. 2019. Simultaneous alterations of oligodendrocyte-specific CNP, astrocyte-specific AQP4 and neuronal NF-L demarcate ischemic tissue after experimental stroke in mice. *Neurosci Lett,* 711**,** 134405.

MAGISTRETTI, P. J. 2006. Neuron-glia metabolic coupling and plasticity. *J Exp Biol,* 209**,** 2304-11.

MAHEU, M., LOPEZ, J. P., CRAPPER, L., DAVOLI, M. A., TURECKI, G. & MECHAWAR, N. 2015. MicroRNA regulation of central glial cell line-derived neurotrophic factor (GDNF) signalling in depression. *Transl Psychiatry,* 5**,** e511.

MAKINODAN, M., ROSEN, K. M., ITO, S. & CORFAS, G. 2012. A critical period for social experience-dependent oligodendrocyte maturation and myelination. *Science,* 337**,** 1357-60.

MAKSIMOVIC, J., GORDON, L. & OSHLACK, A. 2012. SWAN: Subset-quantile within array normalization for illumina infinium HumanMethylation450 BeadChips. *Genome Biol,* 13**,** R44.

MALLYA, A. P. & DEUTCH, A. Y. 2018. (Micro)Glia as Effectors of Cortical Volume Loss in Schizophrenia. *Schizophr Bull,* 44**,** 948-957.

MANCUSO, R., FRYATT, G., CLEAL, M., OBST, J., PIPI, E., MONZON-SANDOVAL, J., RIBE, E., WINCHESTER, L., WEBBER, C., NEVADO, A., JACOBS, T., AUSTIN, N., THEUNIS, C., GRAUWEN, K., DANIELA RUIZ, E., MUDHER, A., VICENTE-RODRIGUEZ, M., PARKER, C. A., SIMMONS, C., CASH, D., RICHARDSON, J., CONSORTIUM, N., JONES, D. N. C., LOVESTONE, S., GOMEZ-NICOLA, D. & PERRY, V. H. 2019. CSF1R inhibitor JNJ-40346527 attenuates microglial proliferation and neurodegeneration in P301S mice. *Brain,* 142**,** 3243-3264.

MANDAL, C., HALDER, D., JUNG, K. H. & CHAI, Y. G. 2017. Gestational Alcohol Exposure Altered DNA Methylation Status in the Developing Fetus. *Int J Mol Sci,* 18.

MANN, J. J. 2013. The serotonergic system in mood disorders and suicidal behaviour. *Philos Trans R Soc Lond B Biol Sci,* 368**,** 20120537.

MANN, J. J. & CURRIER, D. M. 2010. Stress, genetics and epigenetic effects on the neurobiology of suicidal behavior and depression. *Eur Psychiatry,* 25**,** 268-71.

MANSELL, G., GORRIE-STONE, T. J., BAO, Y., KUMARI, M., SCHALKWYK, L. S., MILL, J. & HANNON, E. 2019. Guidance for DNA methylation studies: statistical insights from the Illumina EPIC array. *BMC Genomics,* 20**,** 366.

MARION-POLL, L., MONTALBAN, E., MUNIER, A., HERVE, D. & GIRAULT, J. A. 2014. Fluorescence-activated sorting of fixed nuclei: a general method for studying nuclei from specific cell populations that preserves post-translational modifications. *Eur J Neurosci,* 39**,** 1234-44.

MARQUES, S., ZEISEL, A., CODELUPPI, S., VAN BRUGGEN, D., MENDANHA FALCAO, A., XIAO, L., LI, H., HARING, M., HOCHGERNER, H., ROMANOV, R. A., GYLLBORG, D., MUNOZ MANCHADO, A., LA MANNO, G., LONNERBERG, P., FLORIDDIA, E. M., REZAYEE, F., ERNFORS, P., ARENAS, E., HJERLING-LEFFLER, J., HARKANY, T., RICHARDSON, W. D., LINNARSSON, S. & CASTELO-BRANCO, G. 2016. Oligodendrocyte heterogeneity in the mouse juvenile and adult central nervous system. *Science,* 352**,** 1326-1329.

MARTIN, D., XU, J., PORRETTA, C. & NICHOLS, C. D. 2017. Neurocytometry: Flow Cytometric Sorting of Specific Neuronal Populations from Human and Rodent Brain. *ACS Chem Neurosci,* 8**,** 356-367.

MARZI, S. J., LEUNG, S. K., RIBARSKA, T., HANNON, E., SMITH, A. R., PISHVA, E., POSCHMANN, J., MOORE, K., TROAKES, C., AL-SARRAJ, S., BECK, S., NEWMAN, S., LUNNON, K., SCHALKWYK, L. C. & MILL, J. 2018. A histone acetylome-wide association study of Alzheimer's disease identifies disease-associated H3K27ac differences in the entorhinal cortex. *Nat Neurosci,* 21**,** 1618-1627.

MARZIALI, L. N., CORREALE, J., GARCIA, C. I. & PASQUINI, J. M. 2016. Combined effects of transferrin and thyroid hormone during oligodendrogenesis In vitro. *Glia,* 64**,** 1879-91.

MARZIALI, L. N., GARCIA, C. I. & PASQUINI, J. M. 2015. Transferrin and thyroid hormone converge in the control of myelinogenesis. *Exp Neurol,* 265**,** 129-41.

MASLAND, R. H. 2004. Neuronal cell types. *Curr Biol,* 14**,** R497-500.

MASSER, D. R., STANFORD, D. R. & FREEMAN, W. M. 2015. Targeted DNA methylation analysis by next-generation sequencing. *J Vis Exp*.

MASTROENI, D., SEKAR, S., NOLZ, J., DELVAUX, E., LUNNON, K., MILL, J., LIANG, W. S. & COLEMAN, P. D. 2017. ANK1 is up-regulated in laser captured microglia in Alzheimer's brain; the importance of addressing cellular heterogeneity. *PLoS One,* 12**,** e0177814.

MASUDA, T., TSUDA, M., YOSHINAGA, R., TOZAKI-SAITOH, H., OZATO, K., TAMURA, T. & INOUE, K. 2012. IRF8 is a critical transcription factor for transforming microglia into a reactive phenotype. *Cell Rep,* 1**,** 334-340.

MATEVOSSIAN, A. & AKBARIAN, S. 2008. Neuronal nuclei isolation from human postmortem brain tissue. *J Vis Exp*.

MATHYS, H., ADAIKKAN, C., GAO, F., YOUNG, J. Z., MANET, E., HEMBERG, M., DE JAGER, P. L., RANSOHOFF, R. M., REGEV, A. & TSAI, L. H. 2017. Temporal Tracking of Microglia Activation in Neurodegeneration at Single-Cell Resolution. *Cell Rep,* 21**,** 366-380.

MATHYS, H., DAVILA-VELDERRAIN, J., PENG, Z., GAO, F., MOHAMMADI, S., YOUNG, J. Z., MENON, M., HE, L., ABDURROB, F., JIANG, X., MARTORELL, A. J., RANSOHOFF, R. M., HAFLER, B. P., BENNETT, D. A., KELLIS, M. & TSAI, L. H. 2019. Single-cell transcriptomic analysis of Alzheimer's disease. *Nature,* 570**,** 332-337.

MATTEI, D., IVANOV, A., VAN OOSTRUM, M., PANTELYUSHIN, S., RICHETTO, J., MUELLER, F., BEFFINGER, M., SCHELLHAMMER, L., VOM BERG, J., WOLLSCHEID, B., BEULE, D., PAOLICELLI, R. C. & MEYER, U. 2020. Enzymatic Dissociation Induces Transcriptional and Proteotype Bias in Brain Cell Populations. *Int J Mol Sci,* 21.

MATTICK, J. S., AMARAL, P. P., DINGER, M. E., MERCER, T. R. & MEHLER, M. F. 2009. RNA regulation of epigenetic processes. *Bioessays,* 31**,** 51-9.

MATTICK, J. S. & MAKUNIN, I. V. 2006. Non-coding RNA. *Hum Mol Genet,* 15 Spec No 1**,** R17-29.

MAUSSION, G., YANG, J., SUDERMAN, M., DIALLO, A., NAGY, C., ARNOVITZ, M., MECHAWAR, N. & TURECKI, G. 2014. Functional DNA methylation in a transcript specific 3'UTR region of TrkB associates with suicide. *Epigenetics,* 9**,** 1061-70.

MAUSSION, G., YANG, J., YERKO, V., BARKER, P., MECHAWAR, N., ERNST, C. & TURECKI, G. 2012. Regulation of a truncated form of tropomyosin-related kinase B (TrkB) by Hsa-miR-185* in frontal cortex of suicide completers. *PLoS One,* 7**,** e39301.

MCCALL, M. N., BARAS, A. S., CRITS-CHRISTOPH, A., INGERSOLL, R., MCALEXANDER, M. A., WITWER, K. W. & HALUSHKA, M. K. 2016. A benchmark for microRNA quantification algorithms using the OpenArray platform. *BMC Bioinformatics,* 17**,** 138.

MCCARTNEY, D. L., WALKER, R. M., MORRIS, S. W., MCINTOSH, A. M., PORTEOUS, D. J. & EVANS, K. L. 2016. Identification of polymorphic and off-target probe binding sites on the Illumina Infinium MethylationEPIC BeadChip. *Genom Data,* 9**,** 22-4.

MCCOY, J. P., JR., CAREY, J. L. & KRAUSE, J. R. 1990. Quality control in flow cytometry for diagnostic pathology. I. Cell surface phenotyping and general laboratory procedures. *Am J Clin Pathol,* 93**,** S27-37.

MCCULLUMSMITH, R. E. & MEADOR-WOODRUFF, J. H. 2011. Novel approaches to the study of postmortem brain in psychiatric illness: old limitations and new challenges. *Biol Psychiatry,* 69**,** 127-33.

MCEWEN, B. S., GRAY, J. D. & NASCA, C. 2015. 60 YEARS OF NEUROENDOCRINOLOGY: Redefining neuroendocrinology: stress, sex and cognitive and emotional regulation. *J Endocrinol,* 226**,** T67-83.

MCEWEN, B. S., NASCA, C. & GRAY, J. D. 2016. Stress Effects on Neuronal Structure: Hippocampus, Amygdala, and Prefrontal Cortex. *Neuropsychopharmacology,* 41**,** 3-23.

MCGIRR, A., ALDA, M., SEGUIN, M., CABOT, S., LESAGE, A. & TURECKI, G. 2009. Familial aggregation of suicide explained by cluster B traits: a three-group family study of suicide controlling for major depressive disorder. *Am J Psychiatry,* 166**,** 1124-34.

MCGOWAN, P. O., SASAKI, A., D'ALESSIO, A. C., DYMOV, S., LABONTE, B., SZYF, M., TURECKI, G. & MEANEY, M. J. 2009. Epigenetic regulation of the glucocorticoid receptor in human brain associates with childhood abuse. *Nat Neurosci,* 12**,** 342-8.

MCGOWAN, P. O., SASAKI, A., HUANG, T. C., UNTERBERGER, A., SUDERMAN, M., ERNST, C., MEANEY, M. J., TURECKI, G. & SZYF, M. 2008. Promoter-wide hypermethylation of the ribosomal RNA gene promoter in the suicide brain. *PLoS One,* 3**,** e2085.

MCGOWAN, P. O. & SZYF, M. 2010. The epigenetics of social adversity in early life: implications for mental health outcomes. *Neurobiol Dis,* 39**,** 66-72.

MCGUFFIN, P., PERROUD, N., UHER, R., BUTLER, A., AITCHISON, K. J., CRAIG, I., LEWIS, C. & FARMER, A. 2010. The genetics of affective disorder and suicide. *Eur Psychiatry,* 25**,** 275-7.

MCKENNA, N. J. & O'MALLEY, B. W. 2002. Combinatorial control of gene expression by nuclear receptors and coregulators. *Cell,* 108**,** 465-74.

MCKENZIE, A. T., MOYON, S., WANG, M., KATSYV, I., SONG, W. M., ZHOU, X., DAMMER, E. B., DUONG, D. M., AAKER, J., ZHAO, Y., BECKMANN, N., WANG, P., ZHU, J., LAH, J. J., SEYFRIED, N. T., LEVEY, A. I., KATSEL, P., HAROUTUNIAN, V., SCHADT, E. E., POPKO, B., CASACCIA, P. & ZHANG, B. 2017. Multiscale network modeling of oligodendrocytes reveals molecular components of myelin dysregulation in Alzheimer's disease. *Mol Neurodegener,* 12**,** 82.

MCKENZIE, A. T., WANG, M., HAUBERG, M. E., FULLARD, J. F., KOZLENKOV, A., KEENAN, A., HURD, Y. L., DRACHEVA, S., CASACCIA, P., ROUSSOS, P. & ZHANG, B. 2018. Brain Cell Type Specific Gene Expression and Co-expression Network Architectures. *Sci Rep,* 8**,** 8868.

MEANEY, M. J. 2001. Maternal care, gene expression, and the transmission of individual differences in stress reactivity across generations. *Annu Rev Neurosci,* 24**,** 1161-92.

MEANEY, M. J. & FERGUSON-SMITH, A. C. 2010. Epigenetic regulation of the neural transcriptome: the meaning of the marks. *Nat Neurosci,* 13**,** 1313-8.

MEHLER, M. F. & MATTICK, J. S. 2007. Noncoding RNAs and RNA editing in brain development, functional diversification, and neurological disease. *Physiol Rev,* 87**,** 799-823.

MEIER, K. & RECILLAS-TARGA, F. 2017. New insights on the role of DNA methylation from a global view. *Front Biosci (Landmark Ed),* 22**,** 644-668.

MELIEF, J., SNEEBOER, M. A., LITJENS, M., ORMEL, P. R., PALMEN, S. J., HUITINGA, I., KAHN, R. S., HOL, E. M. & DE WITTE, L. D. 2016. Characterizing primary human microglia: A comparative study with myeloid subsets and culture models. *Glia,* 64**,** 1857-68.

MELLIOS, N., HUANG, H. S., GRIGORENKO, A., ROGAEV, E. & AKBARIAN, S. 2008. A set of differentially expressed miRNAs, including miR-30a-5p, act as post-transcriptional inhibitors of BDNF in prefrontal cortex. *Hum Mol Genet,* 17**,** 3030-42.

MENDIZABAL, I., BERTO, S., USUI, N., TORIUMI, K., CHATTERJEE, P., DOUGLAS, C., HUH, I., JEONG, H., LAYMAN, T., TAMMINGA, C. A., PREUSS, T. M., KONOPKA, G. & YI, S. V. 2019. Cell type-specific epigenetic links to schizophrenia risk in the brain. *Genome Biol,* 20**,** 135.

MERBS, S. L., KHAN, M. A., HACKLER, L., JR., OLIVER, V. F., WAN, J., QIAN, J. & ZACK, D. J. 2012. Cell-specific DNA methylation patterns of retina-specific genes. *PLoS One,* 7**,** e32602.

MERCER, T. R., QURESHI, I. A., GOKHAN, S., DINGER, M. E., LI, G., MATTICK, J. S. & MEHLER, M. F. 2010. Long noncoding RNAs in neuronal-glial fate specification and oligodendrocyte lineage maturation. *BMC Neurosci,* 11**,** 14.

MESTDAGH, P., VAN VLIERBERGHE, P., DE WEER, A., MUTH, D., WESTERMANN, F., SPELEMAN, F. & VANDESOMPELE, J. 2009. A novel and universal method for microRNA RT-qPCR data normalization. *Genome Biol,* 10**,** R64.

MICHELS, K. B. & BINDER, A. M. 2018. Considerations for Design and Analysis of DNA Methylation Studies. *Methods Mol Biol,* 1708**,** 31-46.

MIDDELDORP, J. & HOL, E. M. 2011. GFAP in health and disease. *Prog Neurobiol,* 93**,** 421-43.

MIDHA, M. K., WU, M. & CHIU, K. P. 2019. Long-read sequencing in deciphering human genetics to a greater depth. *Hum Genet,* 138**,** 1201-1215.

MIKLOS, G. L. & MALESZKA, R. 2004. Microarray reality checks in the context of a complex disease. *Nat Biotechnol,* 22**,** 615-21.

MILL, J. & HEIJMANS, B. T. 2013. From promises to practical strategies in epigenetic epidemiology. *Nat Rev Genet,* 14**,** 585-94.

MILL, J. & PETRONIS, A. 2009. Profiling DNA methylation from small amounts of genomic DNA starting material: efficient sodium bisulfite conversion and subsequent whole-genome amplification. *Methods Mol Biol,* 507**,** 371-81.

MILLER, B. H. & WAHLESTEDT, C. 2010. MicroRNA dysregulation in psychiatric disease. *Brain Res,* 1338**,** 89-99.

MIRKOVIC, B., LAURENT, C., PODLIPSKI, M. A., FREBOURG, T., COHEN, D. & GERARDIN, P. 2016. Genetic Association Studies of Suicidal Behavior: A Review of the Past 10 Years, Progress, Limitations, and Future Directions. *Front Psychiatry,* 7**,** 158.

MOCHIDA, G. H. 2005. Cortical malformation and pediatric epilepsy: a molecular genetic approach. *J Child Neurol,* 20**,** 300-3.

MOLINA ESTEVEZ, F. J., MATHEWS, T. D., BIFFI, A. & PEVIANI, M. 2019. Simultaneous Flow Cytometric Characterization of Multiple Cell Types Retrieved from Mouse Brain/Spinal Cord Through Different Homogenization Methods. *J Vis Exp.*

MOLNAR, Z., CLOWRY, G. J., SESTAN, N., ALZU'BI, A., BAKKEN, T., HEVNER, R. F., HUPPI, P. S., KOSTOVIC, I., RAKIC, P., ANTON, E. S., EDWARDS, D., GARCEZ, P., HOERDER-SUABEDISSEN, A. & KRIEGSTEIN, A. 2019. New insights into the development of the human cerebral cortex. *J Anat,* 235**,** 432-451.

MOLOFSKY, A. V., GLASGOW, S. M., CHABOUB, L. S., TSAI, H. H., MURNEN, A. T., KELLEY, K. W., FANCY, S. P., YUEN, T. J., MADIREDDY, L., BARANZINI, S., DENEEN, B., ROWITCH, D. H. & OLDHAM, M. C. 2013. Expression profiling of Aldh1l1-precursors in the developing spinal cord reveals glial lineage-specific genes and direct Sox9-Nfe2l1 interactions. *Glia,* 61**,** 1518-32.

MOLYNEAUX, B. J., ARLOTTA, P., FAME, R. M., MACDONALD, J. L., MACQUARRIE, K. L. & MACKLIS, J. D. 2009. Novel subtype-specific genes identify distinct subpopulations of callosal projection neurons. *J Neurosci,* 29**,** 12343-54.

MOLYNEAUX, B. J., ARLOTTA, P., MENEZES, J. R. & MACKLIS, J. D. 2007. Neuronal subtype specification in the cerebral cortex. *Nat Rev Neurosci,* 8**,** 427-37.

MONACO, M. C., MARIC, D., BANDEIAN, A., LEIBOVITCH, E., YANG, W. & MAJOR, E. O. 2012. Progenitor-derived oligodendrocyte culture system from human fetal brain. *J Vis Exp*.

MONDELLI, V., VERNON, A. C., TURKHEIMER, F., DAZZAN, P. & PARIANTE, C. M. 2017. Brain microglia in psychiatric disorders. *Lancet Psychiatry,* 4**,** 563-572.

MONFRIM, X., GAZAL, M., DE LEON, P. B., QUEVEDO, L., SOUZA, L. D., JANSEN, K., OSES, J. P., PINHEIRO, R. T., SILVA, R. A., LARA, D. R., GHISLENI, G., SPESSATO, B. & KASTER, M. P. 2014. Immune dysfunction in bipolar disorder and suicide risk: is there an association between peripheral corticotropin-releasing hormone and interleukin-1beta? *Bipolar Disord,* 16**,** 741-7.

MONJE, M. 2018. Myelin Plasticity and Nervous System Function. *Annu Rev Neurosci,* 41**,** 61-76.

MONTANO, C. M., IRIZARRY, R. A., KAUFMANN, W. E., TALBOT, K., GUR, R. E., FEINBERG, A. P. & TAUB, M. A. 2013. Measuring cell-type specific differential methylation in human brain tissue. *Genome Biol,* 14**,** R94.

MONTIJN, J. S., OLCESE, U. & PENNARTZ, C. M. 2016. Visual Stimulus Detection Correlates with the Consistency of Temporal Sequences within Stereotyped Events of V1 Neuronal Population Activity. *J Neurosci,* 36**,** 8624-40.

MOORE, L. D., LE, T. & FAN, G. 2013. DNA methylation and its basic function. *Neuropsychopharmacology,* 38**,** 23-38.

MORAN, S., ARRIBAS, C. & ESTELLER, M. 2016. Validation of a DNA methylation microarray for 850,000 CpG sites of the human genome enriched in enhancer sequences. *Epigenomics,* 8**,** 389-99.

MOREL, L., CHIANG, M. S. R., HIGASHIMORI, H., SHONEYE, T., IYER, L. K., YELICK, J., TAI, A. & YANG, Y. 2017. Molecular and Functional Properties of Regional Astrocytes in the Adult Brain. *J Neurosci,* 37**,** 8706-8717.

MORGAN, T. E., ROZOVSKY, I., SARKAR, D. K., YOUNG-CHAN, C. S., NICHOLS, N. R., LAPING, N. J. & FINCH, C. E. 2000. Transforming growth factor-beta1 induces transforming growth factor-beta1 and transforming growth factor-beta receptor messenger RNAs and reduces complement C1qB messenger RNA in rat brain microglia. *Neuroscience,* 101**,** 313-21.

MORGAN, T. E., XIE, Z., GOLDSMITH, S., YOSHIDA, T., LANZREIN, A. S., STONE, D., ROZOVSKY, I., PERRY, G., SMITH, M. A. & FINCH, C. E. 1999. The mosaic of brain glial hyperactivity during normal ageing and its attenuation by food restriction. *Neuroscience,* 89**,** 687-99.

MORISON, I. M., RAMSAY, J. P. & SPENCER, H. G. 2005. A census of mammalian imprinting. *Trends Genet,* 21**,** 457-65.

MOSTAFAVI, S., BATTLE, A., ZHU, X., POTASH, J. B., WEISSMAN, M. M., SHI, J., BECKMAN, K., HAUDENSCHILD, C., MCCORMICK, C., MEI, R., GAMEROFF, M. J., GINDES, H., ADAMS, P., GOES, F. S., MONDIMORE, F. M., MACKINNON, D. F., NOTES, L., SCHWEIZER, B., FURMAN, D., MONTGOMERY, S. B., URBAN, A. E., KOLLER, D. & LEVINSON, D. F. 2014. Type I interferon signaling genes in recurrent major depression: increased expression detected by whole-blood RNA sequencing. *Mol Psychiatry,* 19**,** 1267-74.

MUCIACCIA, B., VICO, C., AROMATARIO, M., FAZI, F. & CECCHI, R. 2015. Molecular analysis of different classes of RNA molecules from formalin-fixed paraffin-embedded autoptic tissues: a pilot study. *Int J Legal Med,* 129**,** 11-21.

MULLEN, R. J., BUCK, C. R. & SMITH, A. M. 1992. NeuN, a neuronal specific nuclear protein in vertebrates. *Development,* 116**,** 201-11.

MULLINS, N., BIGDELI, T. B., BORGLUM, A. D., COLEMAN, J. R. I., DEMONTIS, D., MEHTA, D., POWER, R. A., RIPKE, S., STAHL, E. A., STARNAWSKA, A., ANJORIN, A., M.R.C.PSYCH, CORVIN, A., SANDERS, A. R., FORSTNER, A. J., REIF, A., KOLLER, A. C., SWIATKOWSKA, B.,

BAUNE, B. T., MULLER-MYHSOK, B., PENNINX, B., PATO, C., ZAI, C., RUJESCU, D., HOUGAARD, D. M., QUESTED, D., LEVINSON, D. F., BINDER, E. B., BYRNE, E. M., AGERBO, E., DR.MED.SC, STREIT, F., MAYORAL, F., BELLIVIER, F., DEGENHARDT, F., BREEN, G., MORKEN, G., TURECKI, G., ROULEAU, G. A., GRABE, H. J., VOLZKE, H., JONES, I., GIEGLING, I., AGARTZ, I., MELLE, I., LAWRENCE, J., M.R.C.PSYCH, WALTERS, J. T. R., STROHMAIER, J., SHI, J., HAUSER, J., BIERNACKA, J. M., VINCENT, J. B., KELSOE, J., STRAUSS, J. S., LISSOWSKA, J., PIMM, J., M.R.C.PSYCH, SMOLLER, J. W., GUZMAN-PARRA, J., BERGER, K., SCOTT, L. J., JONES, L. A., AZEVEDO, M. H., TRZASKOWSKI, M., KOGEVINAS, M., RIETSCHEL, M., BOKS, M., ISING, M., GRIGOROIU-SERBANESCU, M., HAMSHERE, M. L., LEBOYER, M., FRYE, M., NOTHEN, M. M., ALDA, M., PREISIG, M., NORDENTOFT, M., BOEHNKE, M., O'DONOVAN, M. C., OWEN, M. J., PATO, M. T., RENTERIA, M. E., BUDDE, M., DIPL, P., WEISSMAN, M. M., WRAY, N. R., BASS, N., M.R.C.PSYCH, CRADDOCK, N., SMELAND, O. B., ANDREASSEN, O. A., MORS, O., GEJMAN, P. V., SKLAR, P., MCGRATH, P., HOFFMANN, P., MCGUFFIN, P., LEE, P. H., MORTENSEN, P. B., KAHN, R. S., et al. 2019. GWAS of Suicide Attempt in Psychiatric Disorders and Association With Major Depression Polygenic Risk Scores. *Am J Psychiatry,* appiajp201918080957.

MULLINS, N., PERROUD, N., UHER, R., BUTLER, A. W., COHEN-WOODS, S., RIVERA, M., MALKI, K., EUESDEN, J., POWER, R. A., TANSEY, K. E., JONES, L., JONES, I., CRADDOCK, N., OWEN, M. J., KORSZUN, A., GILL, M., MORS, O., PREISIG, M., MAIER, W., RIETSCHEL, M., RICE, J. P., MULLER-MYHSOK, B., BINDER, E. B., LUCAE, S., ISING, M., CRAIG, I. W., FARMER, A. E., MCGUFFIN, P., BREEN, G. & LEWIS, C. M. 2014. Genetic relationships between suicide attempts, suicidal ideation and major psychiatric disorders: a genome-wide association and polygenic scoring study. *Am J Med Genet B Neuropsychiatr Genet,* 165B**,** 428-37.

MUNDEL, P., HEID, H. W., MUNDEL, T. M., KRUGER, M., REISER, J. & KRIZ, W. 1997. Synaptopodin: an actin-associated protein in telencephalic dendrites and renal podocytes. *J Cell Biol,* 139**,** 193-204.

MURAKAMI, Y., SAITO, K., ITO, H. & HASHIMOTO, Y. 2019. Transferrin isoforms in cerebrospinal fluid and their relation to neurological diseases. *Proc Jpn Acad Ser B Phys Biol Sci,* 95**,** 198-210.

MURPHY, T. M., CRAWFORD, B., DEMPSTER, E. L., HANNON, E., BURRAGE, J., TURECKI, G., KAMINSKY, Z. & MILL, J. 2017. Methylomic profiling of cortex samples from completed suicide cases implicates a role for PSORS1C3 in major depression and suicide. *Transl Psychiatry,* 7**,** e989.

MURPHY, T. M., MULLINS, N., RYAN, M., FOSTER, T., KELLY, C., MCCLELLAND, R., O'GRADY, J., CORCORAN, E., BRADY, J., REILLY, M., JEFFERS, A., BROWN, K., MAHER, A., BANNAN, N., CASEMENT, A., LYNCH, D., BOLGER, S., BUCKLEY, A., QUINLIVAN, L., DALY, L., KELLEHER, C. & MALONE, K. M. 2013. Genetic variation in DNMT3B and increased global DNA methylation is associated with suicide attempts in psychiatric patients. *Genes Brain Behav,* 12**,** 125-32.

MURPHY, T. M., O'DONOVAN, A., MULLINS, N., O'FARRELLY, C., MCCANN, A. & MALONE, K. 2015. Anxiety is associated with higher levels of global DNA methylation and altered expression of epigenetic and interleukin-6 genes. *Psychiatr Genet,* 25**,** 71-8.

MYERS, B., MCKLVEEN, J. M. & HERMAN, J. P. 2014. Glucocorticoid actions on synapses, circuits, and behavior: implications for the energetics of stress. *Front Neuroendocrinol,* 35**,** 180-196.

MYINT, A. M. 2012. Kynurenines: from the perspective of major psychiatric disorders. *FEBS J,* 279**,** 1375-85.

NAGHAVI, M. & GLOBAL BURDEN OF DISEASE SELF-HARM, C. 2019. Global, regional, and national burden of suicide mortality 1990 to 2016: systematic analysis for the Global Burden of Disease Study 2016. *BMJ,* 364**,** l94.

NAGY, C., MAHEU, M., LOPEZ, J. P., VAILLANCOURT, K., CRUCEANU, C., GROSS, J. A., ARNOVITZ, M., MECHAWAR, N. & TURECKI, G. 2015a. Effects of postmortem interval on biomolecule integrity in the brain. *J Neuropathol Exp Neurol,* 74**,** 459-69.

NAGY, C., SUDERMAN, M., YANG, J., SZYF, M., MECHAWAR, N., ERNST, C. & TURECKI, G. 2015b. Astrocytic abnormalities and global DNA methylation patterns in depression and suicide. *Mol Psychiatry,* 20**,** 320-8.

NAGY, C., TORRES-PLATAS, S. G., MECHAWAR, N. & TURECKI, G. 2017. Repression of Astrocytic Connexins in Cortical and Subcortical Brain Regions and Prefrontal Enrichment of H3K9me3 in Depression and Suicide. *Int J Neuropsychopharmacol,* 20**,** 50-57.

NAGY, J. I., PATEL, D., OCHALSKI, P. A. & STELMACK, G. L. 1999. Connexin30 in rodent, cat and human brain: selective expression in gray matter astrocytes, co-localization with connexin43 at gap junctions and late developmental appearance. *Neuroscience,* 88**,** 447-68.

NAIR, R. P., STUART, P. E., NISTOR, I., HIREMAGALORE, R., CHIA, N. V. C., JENISCH, S., WEICHENTHAL, M., ABECASIS, G. R., LIM, H. W., CHRISTOPHERS, E., VOORHEES, J. J. & ELDER, J. T. 2006. Sequence and haplotype analysis supports HLA-C as the psoriasis susceptibility 1 gene. *Am J Hum Genet,* 78**,** 827-851.

NAJM, F. J., LAGER, A. M., ZAREMBA, A., WYATT, K., CAPRARIELLO, A. V., FACTOR, D. C., KARL, R. T., MAEDA, T., MILLER, R. H. & TESAR, P. J. 2013. Transcription factor-mediated reprogramming of fibroblasts to expandable, myelinogenic oligodendrocyte progenitor cells. *Nat Biotechnol,* 31**,** 426-33.

NAKANO, K., SHIROMA, A., SHIMOJI, M., TAMOTSU, H., ASHIMINE, N., OHKI, S., SHINZATO, M., MINAMI, M., NAKANISHI, T., TERUYA, K., SATOU, K. & HIRANO, T. 2017. Advantages of genome sequencing by long-read sequencer using SMRT technology in medical area. *Hum Cell,* 30**,** 149-161.

NANDI, S., GOKHAN, S., DAI, X. M., WEI, S., ENIKOLOPOV, G., LIN, H., MEHLER, M. F. & STANLEY, E. R. 2012. The CSF-1 receptor ligands IL-34 and CSF-1 exhibit distinct developmental brain expression patterns and regulate neural progenitor cell maintenance and maturation. *Dev Biol,* 367**,** 100-13.

NARAYAN, S., HEAD, S. R., GILMARTIN, T. J., DEAN, B. & THOMAS, E. A. 2009. Evidence for disruption of sphingolipid metabolism in schizophrenia. *J Neurosci Res,* 87**,** 278-88.

NARDON, E., DONADA, M., BONIN, S., DOTTI, I. & STANTA, G. 2009. Higher random oligo concentration improves reverse transcription yield of cDNA from bioptic tissues and quantitative RT-PCR reliability. *Exp Mol Pathol,* 87**,** 146-51.

NASRABADY, S. E., RIZVI, B., GOLDMAN, J. E. & BRICKMAN, A. M. 2018. White matter changes in Alzheimer's disease: a focus on myelin and oligodendrocytes. *Acta Neuropathol Commun,* 6**,** 22.

NATERA-NARANJO, O., ASCHRAFI, A., GIOIO, A. E. & KAPLAN, B. B. 2010. Identification and quantitative analyses of microRNAs located in the distal axons of sympathetic neurons. *RNA,* 16**,** 1516-29.

NATION, D. A., SWEENEY, M. D., MONTAGNE, A., SAGARE, A. P., D'ORAZIO, L. M., PACHICANO, M., SEPEHRBAND, F., NELSON, A. R., BUENNAGEL, D. P., HARRINGTON, M. G., BENZINGER, T. L. S., FAGAN, A. M., RINGMAN, J. M., SCHNEIDER, L. S., MORRIS, J. C., CHUI, H. C., LAW, M., TOGA, A. W. & ZLOKOVIC, B. V. 2019. Blood-brain barrier breakdown is an early biomarker of human cognitive dysfunction. *Nat Med,* 25**,** 270-276.

NAZE, P., VUILLAUME, I., DESTEE, A., PASQUIER, F. & SABLONNIERE, B. 2002. Mutation analysis and association studies of the ubiquitin carboxy-terminal hydrolase L1 gene in Huntington's disease. *Neurosci Lett,* 328**,** 1-4.

NEEDHAMSEN, M., EWING, E., LUND, H., GOMEZ-CABRERO, D., HARRIS, R. A., KULAR, L. & JAGODIC, M. 2017. Usability of human Infinium MethylationEPIC BeadChip for mouse DNA methylation studies. *BMC Bioinformatics,* 18**,** 486.

NELSON, L. H. & LENZ, K. M. 2017. Microglia depletion in early life programs persistent changes in social, mood-related, and locomotor behavior in male and female rats. *Behav Brain Res,* 316**,** 279-293.

NELSON, S. B., SUGINO, K. & HEMPEL, C. M. 2006. The problem of neuronal cell types: a physiological genomics approach. *Trends Neurosci,* 29**,** 339-45.

NENISKYTE, U., VILALTA, A. & BROWN, G. C. 2014. Tumour necrosis factor alpha-induced neuronal loss is mediated by microglial phagocytosis. *FEBS Lett,* 588**,** 2952-6.

NESTLER, E. J. 2014. Epigenetic mechanisms of depression. *JAMA Psychiatry,* 71**,** 454-6.

NESTOR, C. E., LENTINI, A., HAGG NILSSON, C., GAWEL, D. R., GUSTAFSSON, M., MATTSON, L., WANG, H., RUNDQUIST, O., MEEHAN, R. R., KLOCKE, B., SEIFERT, M., HAUCK, S. M., LAUMEN, H., ZHANG, H. & BENSON, M. 2016. 5-Hydroxymethylcytosine Remodeling Precedes Lineage Specification during Differentiation of Human CD4(+) T Cells. *Cell Rep,* 16**,** 559-570.

NEWMAN, A. M., LIU, C. L., GREEN, M. R., GENTLES, A. J., FENG, W., XU, Y., HOANG, C. D., DIEHN, M. & ALIZADEH, A. A. 2015. Robust enumeration of cell subsets from tissue expression profiles. *Nat Methods,* 12**,** 453-7.

NG, S. Y., JOHNSON, R. & STANTON, L. W. 2012. Human long non-coding RNAs promote pluripotency and neuronal differentiation by association with chromatin modifiers and transcription factors. *EMBO J,* 31**,** 522-33.

NG, S. Y. & STANTON, L. W. 2013. Long non-coding RNAs in stem cell pluripotency. *Wiley Interdiscip Rev RNA,* 4**,** 121-8.

NGUYEN, T. C., CAO, X., YU, P., XIAO, S., LU, J., BIASE, F. H., SRIDHAR, B., HUANG, N., ZHANG, K. & ZHONG, S. 2016. Mapping RNA-RNA interactome and RNA structure in vivo by MARIO. *Nat Commun,* 7**,** 12023.

NGUYEN, T. T., DAMMER, E. B., OWINO, S. A., GIDDENS, M. M., MADARAS, N. S., DUONG, D. M., SEYFRIED, N. T. & HALL, R. A. 2020. Quantitative Proteomics Reveal an Altered Pattern of Protein Expression in Brain Tissue from Mice Lacking GPR37 and GPR37L1. *J Proteome Res,* 19**,** 744-755.

NICHOLS, N. R., DAY, J. R., LAPING, N. J., JOHNSON, S. A. & FINCH, C. E. 1993. GFAP mRNA increases with age in rat and human brain. *Neurobiol Aging,* 14**,** 421-9.

NICULESCU, A. B., LEVEY, D., LE-NICULESCU, H., NICULESCU, E., KURIAN, S. M. & SALOMON, D. 2015a. Psychiatric blood biomarkers: avoiding jumping to premature negative or positive conclusions. *Mol Psychiatry,* 20**,** 286-8.

NICULESCU, A. B., LEVEY, D. F., PHALEN, P. L., LE-NICULESCU, H., DAINTON, H. D., JAIN, N., BELANGER, E., JAMES, A., GEORGE, S., WEBER, H., GRAHAM, D. L., SCHWEITZER, R., LADD, T. B., LEARMAN, R., NICULESCU, E. M., VANIPENTA, N. P., KHAN, F. N., MULLEN, J., SHANKAR, G., COOK, S., HUMBERT, C., BALLEW, A., YARD, M., GELBART, T., SHEKHAR, A., SCHORK, N. J., KURIAN, S. M., SANDUSKY, G. E. & SALOMON, D. R. 2015b. Understanding and predicting suicidality using a combined genomic and clinical risk assessment approach. *Mol Psychiatry,* 20**,** 1266-85.

NISHIYAMA, A., SUZUKI, R. & ZHU, X. 2014. NG2 cells (polydendrocytes) in brain physiology and repair. *Front Neurosci,* 8**,** 133.

NIZON, M., LAUGEL, V., FLANIGAN, K. M., PASTORE, M., WALDROP, M. A., ROSENFELD, J. A., MAROM, R., XIAO, R., GERARD, A., PICHON, O., LE CAIGNEC, C., GERARD, M., DIETERICH, K., TRUITT CHO, M., MCWALTER, K., HIATT, S., THOMPSON, M. L., BEZIEAU, S., WADLEY, A., WIERENGA, K. J., EGLY, J. M. & ISIDOR, B. 2019. Variants in MED12L, encoding a subunit of the mediator kinase module, are responsible for intellectual disability associated with transcriptional defect. *Genet Med*.

NOCH, E. K., YIM, I., MILNER, T. A. & CANTLEY, L. C. 2020. Distribution and localization of phosphatidylinositol 5-phosphate, 4-kinase alpha and beta in the brain. *J Comp Neurol*.

NOCK, M. K., GREEN, J. G., HWANG, I., MCLAUGHLIN, K. A., SAMPSON, N. A., ZASLAVSKY, A. M. & KESSLER, R. C. 2013. Prevalence, correlates, and treatment of lifetime suicidal

behavior among adolescents: results from the National Comorbidity Survey Replication Adolescent Supplement. *JAMA Psychiatry,* 70**,** 300-10.

NOLAN, T., HANDS, R. E. & BUSTIN, S. A. 2006. Quantification of mRNA using real-time RT-PCR. *Nat Protoc,* 1**,** 1559-82.

NOLTE, C., MATYASH, M., PIVNEVA, T., SCHIPKE, C. G., OHLEMEYER, C., HANISCH, U. K., KIRCHHOFF, F. & KETTENMANN, H. 2001. GFAP promoter-controlled EGFP-expressing transgenic mice: a tool to visualize astrocytes and astrogliosis in living brain tissue. *Glia,* 33**,** 72-86.

NORDENTOFT, M., MORTENSEN, P. B. & PEDERSEN, C. B. 2011. Absolute risk of suicide after first hospital contact in mental disorder. *Arch Gen Psychiatry,* 68**,** 1058-64.

NOTT, A., SCHLACHETZKI, J. C. M., FIXSEN, B. R. & GLASS, C. K. 2021. Nuclei isolation of multiple brain cell types for omics interrogation. *Nat Protoc,* 16**,** 1629-1646.

NOTTER, T. & MEYER, U. 2017. Microglia and schizophrenia: where next? *Mol Psychiatry,* 22**,** 788-789.

NOWAKOWSKI, T. J., RANI, N., GOLKARAM, M., ZHOU, H. R., ALVARADO, B., HUCH, K., WEST, J. A., LEYRAT, A., POLLEN, A. A., KRIEGSTEIN, A. R., PETZOLD, L. R. & KOSIK, K. S. 2018. Regulation of cell-type-specific transcriptomes by microRNA networks during human brain development. *Nat Neurosci,* 21**,** 1784-1792.

NUMATA, S., YE, T., HYDE, T. M., GUITART-NAVARRO, X., TAO, R., WININGER, M., COLANTUONI, C., WEINBERGER, D. R., KLEINMAN, J. E. & LIPSKA, B. K. 2012. DNA methylation signatures in development and aging of the human prefrontal cortex. *Am J Hum Genet,* 90**,** 260-72.

O'CARROLL, D. & SCHAEFER, A. 2013. General principals of miRNA biogenesis and regulation in the brain. *Neuropsychopharmacology,* 38**,** 39-54.

O'CONNOR, R. M., GRENHAM, S., DINAN, T. G. & CRYAN, J. F. 2013. microRNAs as novel antidepressant targets: converging effects of ketamine and electroconvulsive shock therapy in the rat hippocampus. *Int J Neuropsychopharmacol,* 16**,** 1885-92.

O'GORMAN, M. R. & THOMAS, J. 1999. Isotype controls--time to let go? *Cytometry,* 38**,** 78-80.

O'LEARY, L. A., DAVOLI, M. A., BELLIVEAU, C., TANTI, A., MA, J. C., FARMER, W. T., TURECKI, G., MURAI, K. K. & MECHAWAR, N. 2020. Characterization of Vimentin-Immunoreactive Astrocytes in the Human Brain. *Front Neuroanat,* 14**,** 31.

OBERHEIM, N. A., GOLDMAN, S. A. & NEDERGAARD, M. 2012. Heterogeneity of astrocytic form and function. *Methods Mol Biol,* 814**,** 23-45.

OKADA, S., SAIWAI, H., KUMAMARU, H., KUBOTA, K., HARADA, A., YAMAGUCHI, M., IWAMOTO, Y. & OHKAWA, Y. 2011. Flow cytometric sorting of neuronal and glial nuclei from central nervous system tissue. *J Cell Physiol,* 226**,** 552-8.

OOSTERHOF, N., CHANG, I. J., KARIMIANI, E. G., KUIL, L. E., JENSEN, D. M., DAZA, R., YOUNG, E., ASTLE, L., VAN DER LINDE, H. C., SHIVARAM, G. M., DEMMERS, J., LATIMER, C. S., KEENE, C. D., LOTER, E., MAROOFIAN, R., VAN HAM, T. J., HEVNER, R. F. & BENNETT, J. T. 2019. Homozygous Mutations in CSF1R Cause a Pediatric-Onset Leukoencephalopathy and Can Result in Congenital Absence of Microglia. *Am J Hum Genet,* 104**,** 936-947.

OQUENDO, M. A., SULLIVAN, G. M., SUDOL, K., BACA-GARCIA, E., STANLEY, B. H., SUBLETTE, M. E. & MANN, J. J. 2014. Toward a biosignature for suicide. *Am J Psychiatry,* 171**,** 1259-77.

OTHMAN, A., FRIM, D. M., POLAK, P., VUJICIC, S., ARNASON, B. G. & BOULLERNE, A. I. 2011. Olig1 is expressed in human oligodendrocytes during maturation and regeneration. *Glia,* 59**,** 914-26.

OVSYANNIKOVA, I. G., SALK, H. M., LARRABEE, B. R., PANKRATZ, V. S. & POLAND, G. A. 2015. Single nucleotide polymorphisms/haplotypes associated with multiple rubella-specific immune response outcomes post-MMR immunization in healthy children. *Immunogenetics,* 67**,** 547-61.

PADEN, C. M., BERGLUND, D. L., HAPNER, S. J. & WELSH, C. J. 1986. A flow cytometric method for intracellular labeling and purification of rare neuronal populations: isolation of fixed neurophysin neurons. *Brain Res,* 376**,** 310-9.

PAN, Y., CHEN, X. Y., ZHANG, Q. Y. & KONG, L. D. 2014. Microglial NLRP3 inflammasome activation mediates IL-1beta-related inflammation in prefrontal cortex of depressive rats. *Brain Behav Immun,* 41**,** 90-100.

PANDEY, G. N., RIZAVI, H. S., REN, X., FAREED, J., HOPPENSTEADT, D. A., ROBERTS, R. C., CONLEY, R. R. & DWIVEDI, Y. 2012. Proinflammatory cytokines in the prefrontal cortex of teenage suicide victims. *J Psychiatr Res,* 46**,** 57-63.

PANDEY, G. N., RIZAVI, H. S., ZHANG, H., BHAUMIK, R. & REN, X. 2018. Abnormal protein and mRNA expression of inflammatory cytokines in the prefrontal cortex of depressed individuals who died by suicide. *J Psychiatry Neurosci,* 43**,** 376-385.

PANTAZATOS, S. P., ANDREWS, S. J., DUNNING-BROADBENT, J., PANG, J., HUANG, Y. Y., ARANGO, V., NAGY, P. L. & JOHN MANN, J. 2015. Isoform-level brain expression profiling of the spermidine/spermine N1-Acetyltransferase1 (SAT1) gene in major depression and suicide. *Neurobiol Dis,* 79**,** 123-34.

PANTAZATOS, S. P., HUANG, Y. Y., ROSOKLIJA, G. B., DWORK, A. J., ARANGO, V. & MANN, J. J. 2017. Whole-transcriptome brain expression and exon-usage profiling in major depression and suicide: evidence for altered glial, endothelial and ATPase activity. *Mol Psychiatry,* 22**,** 760-773.

PAOLICELLI, R. C., BOLASCO, G., PAGANI, F., MAGGI, L., SCIANNI, M., PANZANELLI, P., GIUSTETTO, M., FERREIRA, T. A., GUIDUCCI, E., DUMAS, L., RAGOZZINO, D. & GROSS, C. T. 2011. Synaptic pruning by microglia is necessary for normal brain development. *Science,* 333**,** 1456-8.

PARK, C. Y., CHOI, Y. S. & MCMANUS, M. T. 2010a. Analysis of microRNA knockouts in mice. *Hum Mol Genet,* 19**,** R169-75.

PARK, H., HAYNES, C. A., NAIRN, A. V., KULIK, M., DALTON, S., MOREMEN, K. & MERRILL, A. H., JR. 2010b. Transcript profiling and lipidomic analysis of ceramide subspecies in mouse embryonic stem cells and embryoid bodies. *J Lipid Res,* 51**,** 480-9.

PEDERSEN, B. S., SCHWARTZ, D. A., YANG, I. V. & KECHRIS, K. J. 2012. Comb-p: software for combining, analyzing, grouping and correcting spatially correlated P-values. *Bioinformatics,* 28**,** 2986-8.

PEFEROEN, L. A., VOGEL, D. Y., UMMENTHUM, K., BREUR, M., HEIJNEN, P. D., GERRITSEN, W. H., PEFEROEN-BAERT, R. M., VAN DER VALK, P., DIJKSTRA, C. D. & AMOR, S. 2015. Activation status of human microglia is dependent on lesion formation stage and remyelination in multiple sclerosis. *J Neuropathol Exp Neurol,* 74**,** 48-63.

PELVIG, D. P., PAKKENBERG, H., STARK, A. K. & PAKKENBERG, B. 2008. Neocortical glial cell numbers in human brains. *Neurobiol Aging,* 29**,** 1754-62.

PERKINS, D. O., JEFFRIES, C. D., JARSKOG, L. F., THOMSON, J. M., WOODS, K., NEWMAN, M. A., PARKER, J. S., JIN, J. & HAMMOND, S. M. 2007. microRNA expression in the prefrontal cortex of individuals with schizophrenia and schizoaffective disorder. *Genome Biol,* 8**,** R27.

PERKINS, J. R., DAWES, J. M., MCMAHON, S. B., BENNETT, D. L., ORENGO, C. & KOHL, M. 2012. ReadqPCR and NormqPCR: R packages for the reading, quality checking and normalisation of RT-qPCR quantification cycle (Cq) data. *BMC Genomics,* 13**,** 296.

PERLIS, R. H., HUANG, J., PURCELL, S., FAVA, M., RUSH, A. J., SULLIVAN, P. F., HAMILTON, S. P., MCMAHON, F. J., SCHULZE, T. G., POTASH, J. B., ZANDI, P. P., WILLOUR, V. L., PENNINX, B. W., BOOMSMA, D. I., VOGELZANGS, N., MIDDELDORP, C. M., RIETSCHEL, M., NOTHEN, M., CICHON, S., GURLING, H., BASS, N., MCQUILLIN, A., HAMSHERE, M., WELLCOME TRUST CASE CONTROL CONSORTIUM BIPOLAR DISORDER, G., CRADDOCK, N., SKLAR, P. & SMOLLER, J. W. 2010. Genome-wide association study of suicide attempts in mood disorder patients. *Am J Psychiatry,* 167**,** 1499-507.

PESCHL, P., BRADL, M., HOFTBERGER, R., BERGER, T. & REINDL, M. 2017. Myelin Oligodendrocyte Glycoprotein: Deciphering a Target in Inflammatory Demyelinating Diseases. *Front Immunol,* 8**,** 529.

PESHEVA, P., GLOOR, S., SCHACHNER, M. & PROBSTMEIER, R. 1997. Tenascin-R is an intrinsic autocrine factor for oligodendrocyte differentiation and promotes cell adhesion by a sulfatide-mediated mechanism. *J Neurosci,* 17**,** 4642-51.

PETER, C. J. & AKBARIAN, S. 2011. Balancing histone methylation activities in psychiatric disorders. *Trends Mol Med,* 17**,** 372-9.

PETROSINO, J. F., HIGHLANDER, S., LUNA, R. A., GIBBS, R. A. & VERSALOVIC, J. 2009. Metagenomic pyrosequencing and microbial identification. *Clin Chem,* 55**,** 856-66.

PFAFFL, M. W. 2001. A new mathematical model for relative quantification in real-time RT-PCR. *Nucleic Acids Res,* 29**,** e45.

PFLEGER, C. M. 2017. The Hippo Pathway: A Master Regulatory Network Important in Development and Dysregulated in Disease. *Curr Top Dev Biol,* 123**,** 181-228.

PHILLIPS, C. 2017. Brain-Derived Neurotrophic Factor, Depression, and Physical Activity: Making the Neuroplastic Connection. *Neural Plast,* 2017**,** 7260130.

PHILLIPS, J. R., HEWEDI, D. H., EISSA, A. M. & MOUSTAFA, A. A. 2015. The cerebellum and psychiatric disorders. *Front Public Health,* 3**,** 66.

PHIPSON, B., MAKSIMOVIC, J. & OSHLACK, A. 2016. missMethyl: an R package for analyzing data from Illumina's HumanMethylation450 platform. *Bioinformatics,* 32**,** 286-8.

PIDSLEY, R., CC, Y. W., VOLTA, M., LUNNON, K., MILL, J. & SCHALKWYK, L. C. 2013. A data-driven approach to preprocessing Illumina 450K methylation array data. *BMC Genomics,* 14**,** 293.

PIDSLEY, R. & MILL, J. 2011. Epigenetic studies of psychosis: current findings, methodological approaches, and implications for postmortem research. *Biol Psychiatry,* 69**,** 146-56.

PIDSLEY, R., VIANA, J., HANNON, E., SPIERS, H., TROAKES, C., AL-SARAJ, S., MECHAWAR, N., TURECKI, G., SCHALKWYK, L. C., BRAY, N. J. & MILL, J. 2014. Methylomic profiling of human brain tissue supports a neurodevelopmental origin for schizophrenia. *Genome Biol,* 15**,** 483.

PIDSLEY, R., ZOTENKO, E., PETERS, T. J., LAWRENCE, M. G., RISBRIDGER, G. P., MOLLOY, P., VAN DJIK, S., MUHLHAUSLER, B., STIRZAKER, C. & CLARK, S. J. 2016. Critical evaluation of the Illumina MethylationEPIC BeadChip microarray for whole-genome DNA methylation profiling. *Genome Biol,* 17**,** 208.

PIEPER, A. A., WU, X., HAN, T. W., ESTILL, S. J., DANG, Q., WU, L. C., REECE-FINCANON, S., DUDLEY, C. A., RICHARDSON, J. A., BRAT, D. J. & MCKNIGHT, S. L. 2005. The neuronal PAS domain protein 3 transcription factor controls FGF-mediated adult hippocampal neurogenesis in mice. *Proc Natl Acad Sci U S A,* 102**,** 14052-7.

PLANT, K., FAIRFAX, B. P., MAKINO, S., VANDIEDONCK, C., RADHAKRISHNAN, J. & KNIGHT, J. C. 2014. Fine mapping genetic determinants of the highly variably expressed MHC gene ZFP57. *Eur J Hum Genet,* 22**,** 568-71.

PLOTSKY, P. M., THRIVIKRAMAN, K. V., NEMEROFF, C. B., CALDJI, C., SHARMA, S. & MEANEY, M. J. 2005. Long-term consequences of neonatal rearing on central corticotropin-releasing factor systems in adult male rat offspring. *Neuropsychopharmacology,* 30**,** 2192-204.

POLANOWSKA, J., FABBRIZIO, E., LE CAM, L., TROUCHE, D., EMILIANI, S., HERRERA, R. & SARDET, C. 2001. The periodic down regulation of Cyclin E gene expression from exit of mitosis to end of G(1) is controlled by a deacetylase- and E2F-associated bipartite repressor element. *Oncogene,* 20**,** 4115-27.

POLICICCHIO S ET AL, S, W., , V. J., , I. A., , B. J., , H. E., , T. G., , K. Z., , M. J., , D. E. L. & TM, M. 2020. Genome-wide DNA methylation meta-analysis in the brains of suicide completers. *Translational Psychiatry*.

POLICICCHIO S ET AL., D., E.L., MURPHY, T.M. 2018. Deciphering the Epigenetic Landscape of Suicidal Behaviour: A Review of Current Findings, Caveats and Future Directions. *OBM Genetics*.

POLICICCHIO S. ET AL 2021. Fluorescence-activated nuclei sorting (FANS) enables the parallel assessment of regulatory genomic variation across major cell-types in the human cortex. *Nucleic Acids Research*

POMPILI, M., SHRIVASTAVA, A., SERAFINI, G., INNAMORATI, M., MILELLI, M., ERBUTO, D., RICCI, F., LAMIS, D. A., SCOCCO, P., AMORE, M., LESTER, D. & GIRARDI, P. 2013. Bereavement after the suicide of a significant other. *Indian J Psychiatry,* 55**,** 256-63.

PONJAVIC, J., OLIVER, P. L., LUNTER, G. & PONTING, C. P. 2009. Genomic and transcriptional co-localization of protein-coding and long non-coding RNA pairs in the developing brain. *PLoS Genet,* 5**,** e1000617.

POULIN, J. F., TASIC, B., HJERLING-LEFFLER, J., TRIMARCHI, J. M. & AWATRAMANI, R. 2016. Disentangling neural cell diversity using single-cell transcriptomics. *Nat Neurosci,* 19**,** 1131-41.

POULTER, M. O., DU, L., WEAVER, I. C., PALKOVITS, M., FALUDI, G., MERALI, Z., SZYF, M. & ANISMAN, H. 2008. GABAA receptor promoter hypermethylation in suicide brain: implications for the involvement of epigenetic processes. *Biol Psychiatry,* 64**,** 645-52.

PRASAD, K. M., BURGESS, A. M., KESHAVAN, M. S., NIMGAONKAR, V. L. & STANLEY, J. A. 2016. Neuropil pruning in Early-Course Schizophrenia: Immunological, Clinical, and Neurocognitive Correlates. *Biol Psychiatry Cogn Neurosci Neuroimaging,* 1**,** 528-538.

PRETI, A. 2011. Animal model and neurobiology of suicide. *Prog Neuropsychopharmacol Biol Psychiatry,* 35**,** 818-30.

PRICE, A. J., COLLADO-TORRES, L., IVANOV, N. A., XIA, W., BURKE, E. E., SHIN, J. H., TAO, R., MA, L., JIA, Y., HYDE, T. M., KLEINMAN, J. E., WEINBERGER, D. R. & JAFFE, A. E. 2019. Divergent neuronal DNA methylation patterns across human cortical development reveal critical periods and a unique role of CpH methylation. *Genome Biol,* 20**,** 196.

PRICE, M. E., COTTON, A. M., LAM, L. L., FARRE, P., EMBERLY, E., BROWN, C. J., ROBINSON, W. P. & KOBOR, M. S. 2013. Additional annotation enhances potential for biologically-relevant analysis of the Illumina Infinium HumanMethylation450 BeadChip array. *Epigenetics Chromatin,* 6**,** 4.

PRIDANS, C., RAPER, A., DAVIS, G. M., ALVES, J., SAUTER, K. A., LEFEVRE, L., REGAN, T., MEEK, S., SUTHERLAND, L., THOMSON, A. J., CLOHISEY, S., BUSH, S. J., ROJO, R., LISOWSKI, Z. M., WALLACE, R., GRABERT, K., UPTON, K. R., TSAI, Y. T., BROWN, D., SMITH, L. B., SUMMERS, K. M., MABBOTT, N. A., PICCARDO, P., CHEESEMAN, M. T., BURDON, T. & HUME, D. A. 2018. Pleiotropic Impacts of Macrophage and Microglial Deficiency on Development in Rats with Targeted Mutation of the Csf1r Locus. *J Immunol,* 201**,** 2683-2699.

PRIMER3PLUS https://primer3plus.com/cgi-bin/dev/primer3plus.cgi.

PRINZ, M., JUNG, S. & PRILLER, J. 2019. Microglia Biology: One Century of Evolving Concepts. *Cell,* 179**,** 292-311.

PRINZ, M. & MILDNER, A. 2011. Microglia in the CNS: immigrants from another world. *Glia,* 59**,** 177-87.

PUKASS, K. & RICHTER-LANDSBERG, C. 2015. Inhibition of UCH-L1 in oligodendroglial cells results in microtubule stabilization and prevents alpha-synuclein aggregate formation by activating the autophagic pathway: implications for multiple system atrophy. *Front Cell Neurosci,* 9**,** 163.

PULAY, A. J. & RETHELYI, J. M. 2016. Multimarker analysis suggests the involvement of BDNF signaling and microRNA biosynthesis in suicidal behavior. *Am J Med Genet B Neuropsychiatr Genet,* 171**,** 763-76.

PUNZI, G., URSINI, G., SHIN, J. H., KLEINMAN, J. E., HYDE, T. M. & WEINBERGER, D. R. 2014. Increased expression of MARCKS in post-mortem brain of violent suicide completers is related to transcription of a long, noncoding, antisense RNA. *Mol Psychiatry,* 19**,** 1057-9.

PUNZI, G., URSINI, G., VISCANTI, G., RADULESCU, E., SHIN, J. H., QUARTO, T., CATANESI, R., BLASI, G., JAFFE, A. E., DEEP-SOBOSLAY, A., HYDE, T. M., KLEINMAN, J. E., BERTOLINO, A. & WEINBERGER, D. R. 2019. Association of a Noncoding RNA Postmortem With Suicide by Violent Means and In Vivo With Aggressive Phenotypes. *Biol Psychiatry,* 85**,** 417-424.

PURGER, D., GIBSON, E. M. & MONJE, M. 2016. Myelin plasticity in the central nervous system. *Neuropharmacology,* 110**,** 563-573.

PYROMARK Q24 USER MANUAL HB-0240-005-1100448-UM-PyroMarkQ24-0116-WW.pdf.

QIAGEN 2005. AllPrep DNA/RNA Mini Handbook. EN-AllPrep-DNARNA-Mini-Handbook.pdf.

QIAGEN 2020. miRNeasy_Mini_Handbook.pdf.

QIAN, Q., ZHANG, J., HE, F. P., BAO, W. X., ZHENG, T. T., ZHOU, D. M., PAN, H. Y., ZHANG, H., ZHANG, X. Q., HE, X., SUN, B. G., LUO, B. Y., CHEN, C. & PENG, G. P. 2019. Down-regulated expression of microRNA-338-5p contributes to neuropathology in Alzheimer's disease. *FASEB J,* 33**,** 4404-4417.

QIN, P. 2011. The impact of psychiatric illness on suicide: differences by diagnosis of disorders and by sex and age of subjects. *J Psychiatr Res,* 45**,** 1445-52.

QUANTABIO 2007. Manual Phase Lock Gel™ (PLG). https://www.genetargetsolutions.com.au/wp-content/uploads/2016/05/5-Prime-Phase-Lock-Gel-Manual.pdf

QUENNEVILLE, S., VERDE, G., CORSINOTTI, A., KAPOPOULOU, A., JAKOBSSON, J., OFFNER, S., BAGLIVO, I., PEDONE, P. V., GRIMALDI, G., RICCIO, A. & TRONO, D. 2011. In embryonic stem cells, ZFP57/KAP1 recognize a methylated hexanucleotide to affect chromatin and DNA methylation of imprinting control regions. *Mol Cell,* 44**,** 361-72.

QUINODOZ, M., GOBET, C., NAEF, F. & GUSTAFSON, K. B. 2014. Characteristic bimodal profiles of RNA polymerase II at thousands of active mammalian promoters. *Genome Biol,* 15**,** R85.

QURESHI, I. A. & MEHLER, M. F. 2012. Emerging roles of non-coding RNAs in brain evolution, development, plasticity and disease. *Nat Rev Neurosci,* 13**,** 528-41.

QURESHI, I. A. & MEHLER, M. F. 2013. Long non-coding RNAs: novel targets for nervous system disease diagnosis and therapy. *Neurotherapeutics,* 10**,** 632-46.

RABIONET, M., VAN DER SPOEL, A. C., CHUANG, C. C., VON TUMPLING-RADOSTA, B., LITJENS, M., BOUWMEESTER, D., HELLBUSCH, C. C., KORNER, C., WIEGANDT, H., GORGAS, K., PLATT, F. M., GRONE, H. J. & SANDHOFF, R. 2008. Male germ cells require polyenoic sphingolipids with complex glycosylation for completion of meiosis: a link to ceramide synthase-3. *J Biol Chem,* 283**,** 13357-69.

RAHMANI, E., ZAITLEN, N., BARAN, Y., ENG, C., HU, D., GALANTER, J., OH, S., BURCHARD, E. G., ESKIN, E., ZOU, J. & HALPERIN, E. 2016. Sparse PCA corrects for cell type heterogeneity in epigenome-wide association studies. *Nat Methods,* 13**,** 443-5.

RAHMANI, E., ZAITLEN, N., BARAN, Y., ENG, C., HU, D., GALANTER, J., OH, S., BURCHARD, E. G., ESKIN, E., ZOU, J. & HALPERIN, E. 2017. Correcting for cell-type heterogeneity in DNA methylation: a comprehensive evaluation. *Nat Methods,* 14**,** 218-219.

RAHMANIAN, N., BOZORGMEHR, M., TORABI, M., AKBARI, A. & ZARNANI, A. H. 2017. Cell separation: Potentials and pitfalls. *Prep Biochem Biotechnol,* 47**,** 38-51.

RAISON, C. L. & MILLER, A. H. 2003. When not enough is too much: the role of insufficient glucocorticoid signaling in the pathophysiology of stress-related disorders. *Am J Psychiatry,* 160**,** 1554-65.

RAJKOWSKA, G. & MIGUEL-HIDALGO, J. J. 2007. Gliogenesis and glial pathology in depression. *CNS Neurol Disord Drug Targets,* 6**,** 219-33.

RAJKOWSKA, G. & STOCKMEIER, C. A. 2013. Astrocyte pathology in major depressive disorder: insights from human postmortem brain tissue. *Curr Drug Targets,* 14**,** 1225-36.

RAMANATHAN, S., DALE, R. C. & BRILOT, F. 2016. Anti-MOG antibody: The history, clinical phenotype, and pathogenicity of a serum biomarker for demyelination. *Autoimmun Rev,* 15**,** 307-24.

RANI, N., NOWAKOWSKI, T. J., ZHOU, H., GODSHALK, S. E., LISI, V., KRIEGSTEIN, A. R. & KOSIK, K. S. 2016. A Primate lncRNA Mediates Notch Signaling during Neuronal Development by Sequestering miRNA. *Neuron,* 90**,** 1174-1188.

RAO, M. S., HATTIANGADY, B. & SHETTY, A. K. 2006. The window and mechanisms of major age-related decline in the production of new neurons within the dentate gyrus of the hippocampus. *Aging Cell,* 5**,** 545-58.

RAYAPROLU, S., GAO, T., XIAO, H., RAMESHA, S., WEINSTOCK, L. D., SHAH, J., DUONG, D. M., DAMMER, E. B., WEBSTER, J. A., JR., LAH, J. J., WOOD, L. B., BETARBET, R., LEVEY, A. I., SEYFRIED, N. T. & RANGARAJU, S. 2020. Flow-cytometric microglial sorting coupled with quantitative proteomics identifies moesin as a highly-abundant microglial protein with relevance to Alzheimer's disease. *Mol Neurodegener,* 15**,** 28.

REGGETI, F. & BIENZLE, D. 2011. Flow cytometry in veterinary oncology. *Vet Pathol,* 48**,** 223-35.

REINIUS, L. E., ACEVEDO, N., JOERINK, M., PERSHAGEN, G., DAHLEN, S. E., GRECO, D., SODERHALL, C., SCHEYNIUS, A. & KERE, J. 2012. Differential DNA methylation in purified human blood cells: implications for cell lineage and studies on disease susceptibility. *PLoS One,* 7**,** e41361.

RELTON, C. L. & DAVEY SMITH, G. 2012. Two-step epigenetic Mendelian randomization: a strategy for establishing the causal role of epigenetic processes in pathways to disease. *Int J Epidemiol,* 41**,** 161-76.

RICE, L., WATERS, C. E., ECCLES, J., GARSIDE, H., SOMMER, P., KAY, P., BLACKHALL, F. H., ZEEF, L., TELFER, B., STRATFORD, I., CLARKE, R., SINGH, D., STEVENS, A., WHITE, A. & RAY, D. W. 2008. Identification and functional analysis of SKA2 interaction with the glucocorticoid receptor. *J Endocrinol,* 198**,** 499-509.

RIVERA, C. M. & REN, B. 2013. Mapping human epigenomes. *Cell,* 155**,** 39-55.

RIVOLLIER, F., CHAUMETTE, B., BENDJEMAA, N., CHAYET, M., MILLET, B., JAAFARI, N., BARHDADI, A., LEMIEUX PERREAULT, L. P., PROVOST, S., DUBE, M. P., GAILLARD, R., KREBS, M. O. & KEBIR, O. 2017. Methylomic changes in individuals with psychosis, prenatally exposed to endocrine disrupting compounds: Lessons from diethylstilbestrol. *PLoS One,* 12**,** e0174783.

ROADMAP EPIGENOMICS, C., KUNDAJE, A., MEULEMAN, W., ERNST, J., BILENKY, M., YEN, A., HERAVI-MOUSSAVI, A., KHERADPOUR, P., ZHANG, Z., WANG, J., ZILLER, M. J., AMIN, V., WHITAKER, J. W., SCHULTZ, M. D., WARD, L. D., SARKAR, A., QUON, G., SANDSTROM, R. S., EATON, M. L., WU, Y. C., PFENNING, A. R., WANG, X., CLAUSSNITZER, M., LIU, Y., COARFA, C., HARRIS, R. A., SHORESH, N., EPSTEIN, C. B., GJONESKA, E., LEUNG, D., XIE, W., HAWKINS, R. D., LISTER, R., HONG, C., GASCARD, P., MUNGALL, A. J., MOORE, R., CHUAH, E., TAM, A., CANFIELD, T. K., HANSEN, R. S., KAUL, R., SABO, P. J., BANSAL, M. S., CARLES, A., DIXON, J. R., FARH, K. H., FEIZI, S., KARLIC, R., KIM, A. R., KULKARNI, A., LI, D., LOWDON, R., ELLIOTT, G., MERCER, T. R., NEPH, S. J., ONUCHIC, V., POLAK, P., RAJAGOPAL, N., RAY, P., SALLARI, R. C., SIEBENTHALL, K. T., SINNOTT-ARMSTRONG, N. A., STEVENS, M., THURMAN, R. E., WU, J., ZHANG, B., ZHOU, X., BEAUDET, A. E., BOYER, L. A., DE JAGER, P. L., FARNHAM, P. J., FISHER, S. J., HAUSSLER, D., JONES, S. J., LI, W., MARRA, M. A., MCMANUS, M. T., SUNYAEV, S., THOMSON, J. A., TLSTY, T. D., TSAI, L. H., WANG, W., WATERLAND, R. A., ZHANG, M. Q., CHADWICK, L. H., BERNSTEIN, B. E., COSTELLO, J. F., ECKER, J. R., HIRST, M., MEISSNER, A., MILOSAVLJEVIC, A., REN, B., STAMATOYANNOPOULOS, J. A., WANG, T. & KELLIS, M. 2015. Integrative analysis of 111 reference human epigenomes. *Nature,* 518**,** 317-30.

ROEDERER, M. 2001. Spectral compensation for flow cytometry: visualization artifacts, limitations, and caveats. *Cytometry,* 45**,** 194-205.

ROGERS, J. T., MORGANTI, J. M., BACHSTETTER, A. D., HUDSON, C. E., PETERS, M. M., GRIMMIG, B. A., WEEBER, E. J., BICKFORD, P. C. & GEMMA, C. 2011. CX3CR1 deficiency leads to impairment of hippocampal cognitive function and synaptic plasticity. *J Neurosci,* 31**,** 16241-50.

ROJO, R., RAPER, A., OZDEMIR, D. D., LEFEVRE, L., GRABERT, K., WOLLSCHEID-LENGELING, E., BRADFORD, B., CARUSO, M., GAZOVA, I., SANCHEZ, A., LISOWSKI, Z. M., ALVES, J., MOLINA-GONZALEZ, I., DAVTYAN, H., LODGE, R. J., GLOVER, J. D., WALLACE, R., MUNRO, D. A. D., DAVID, E., AMIT, I., MIRON, V. E., PRILLER, J., JENKINS, S. J., HARDINGHAM, G.

E., BLURTON-JONES, M., MABBOTT, N. A., SUMMERS, K. M., HOHENSTEIN, P., HUME, D. A. & PRIDANS, C. 2019. Deletion of a Csf1r enhancer selectively impacts CSF1R expression and development of tissue macrophage populations. *Nat Commun,* 10**,** 3215.

ROMANI, A., PETRACHI, R. & COSI, V. 1988. Somatosensory evoked potentials by median nerve stimulation in rabbits. II. Normative data of surface recordings. *Boll Soc Ital Biol Sper,* 64**,** 55-60.

ROMANO, G., VENEZIANO, D., NIGITA, G. & NANA-SINKAM, S. P. 2018. RNA Methylation in ncRNA: Classes, Detection, and Molecular Associations. *Front Genet,* 9**,** 243.

ROSATO-SIRI, M. V., MARZIALI, L. N., MATTERA, V., CORREALE, J. & PASQUINI, J. M. 2021. Combination therapy of apo-transferrin and thyroid hormones enhances remyelination. *Glia,* 69**,** 151-164.

ROSENBAUER, F. & TENEN, D. G. 2007. Transcription factors in myeloid development: balancing differentiation with transformation. *Nat Rev Immunol,* 7**,** 105-17.

ROSER, A. E., CALDI GOMES, L., SCHUNEMANN, J., MAASS, F. & LINGOR, P. 2018. Circulating miRNAs as Diagnostic Biomarkers for Parkinson's Disease. *Front Neurosci,* 12**,** 625.

ROSS, D. M., WATKINS, D. B., HUGHES, T. P. & BRANFORD, S. 2008. Reverse transcription with random pentadecamer primers improves the detection limit of a quantitative PCR assay for BCR-ABL transcripts in chronic myeloid leukemia: implications for defining sensitivity in minimal residual disease. *Clin Chem,* 54**,** 1568-71.

ROTHSTEIN, J. D., MARTIN, L., LEVEY, A. I., DYKES-HOBERG, M., JIN, L., WU, D., NASH, N. & KUNCL, R. W. 1994. Localization of neuronal and glial glutamate transporters. *Neuron,* 13**,** 713-25.

ROY, A., HODGKINSON, C. A., DELUCA, V., GOLDMAN, D. & ENOCH, M. A. 2012. Two HPA axis genes, CRHBP and FKBP5, interact with childhood trauma to increase the risk for suicidal behavior. *J Psychiatr Res,* 46**,** 72-9.

ROY, A. & SEGAL, N. L. 2001. Suicidal behavior in twins: a replication. *J Affect Disord,* 66**,** 71-4.

ROY, B., DUNBAR, M., SHELTON, R. C. & DWIVEDI, Y. 2017a. Identification of MicroRNA-124-3p as a Putative Epigenetic Signature of Major Depressive Disorder. *Neuropsychopharmacology,* 42**,** 864-875.

ROY, B. & DWIVEDI, Y. 2018. Understanding the Neuroepigenetic Constituents of Suicide Brain. *Prog Mol Biol Transl Sci,* 157**,** 233-262.

ROY, B., WANG, Q., PALKOVITS, M., FALUDI, G. & DWIVEDI, Y. 2017b. Altered miRNA expression network in locus coeruleus of depressed suicide subjects. *Sci Rep,* 7**,** 4387.

ROY, B., YOSHINO, Y., ALLEN, L., PRALL, K., SCHELL, G. & DWIVEDI, Y. 2020. Exploiting Circulating MicroRNAs as Biomarkers in Psychiatric Disorders. *Mol Diagn Ther,* 24**,** 279-298.

RUNESON, B. & ASBERG, M. 2003. Family history of suicide among suicide victims. *Am J Psychiatry,* 160**,** 1525-6.

RUSTAD, S. R., PAPALE, L. A. & ALISCH, R. S. 2019. DNA Methylation and Hydroxymethylation and Behavior. *Curr Top Behav Neurosci,* 42**,** 51-82.

RUSTENHOVEN, J., PARK, T. I., SCHWEDER, P., SCOTTER, J., CORREIA, J., SMITH, A. M., GIBBONS, H. M., OLDFIELD, R. L., BERGIN, P. S., MEE, E. W., FAULL, R. L., CURTIS, M. A., SCOTT GRAHAM, E. & DRAGUNOW, M. 2016. Isolation of highly enriched primary human microglia for functional studies. *Sci Rep,* 6**,** 19371.

RUTTEN, B. P. F., VERMETTEN, E., VINKERS, C. H., URSINI, G., DASKALAKIS, N. P., PISHVA, E., DE NIJS, L., HOUTEPEN, L. C., EIJSSEN, L., JAFFE, A. E., KENIS, G., VIECHTBAUER, W., VAN DEN HOVE, D., SCHRAUT, K. G., LESCH, K. P., KLEINMAN, J. E., HYDE, T. M., WEINBERGER, D. R., SCHALKWYK, L., LUNNON, K., MILL, J., COHEN, H., YEHUDA, R., BAKER, D. G., MAIHOFER, A. X., NIEVERGELT, C. M., GEUZE, E. & BOKS, M. P. M. 2018. Longitudinal analyses of the DNA methylome in deployed military servicemen identify susceptibility loci for post-traumatic stress disorder. *Mol Psychiatry,* 23**,** 1145-1156.

RUZICKA B.W., MOHAMMADI S., DAVILA-VELDERRAIN J., SUBBURAJU S., TSO D.R., HOURIHAN M. & KELLIS M. 2020. Single-cell dissection of schizophrenia reveals neurodevelopmental-synaptic axis and transcriptional resilience.

RUZICKA, W. B., ZHUBI, A., VELDIC, M., GRAYSON, D. R., COSTA, E. & GUIDOTTI, A. 2007. Selective epigenetic alteration of layer I GABAergic neurons isolated from prefrontal cortex of schizophrenia patients using laser-assisted microdissection. *Mol Psychiatry,* 12**,** 385-97.

RYDBIRK, R., FOLKE, J., WINGE, K., AZNAR, S., PAKKENBERG, B. & BRUDEK, T. 2016. Assessment of brain reference genes for RT-qPCR studies in neurodegenerative diseases. *Sci Rep,* 6**,** 37116.

SADEH, N., WOLF, E. J., LOGUE, M. W., HAYES, J. P., STONE, A., GRIFFIN, L. M., SCHICHMAN, S. A. & MILLER, M. W. 2016. Epigenetic Variation at Ska2 Predicts Suicide Phenotypes and Internalizing Psychopathology. *Depress Anxiety,* 33**,** 308-15.

SAHA, R. N. & PAHAN, K. 2006. HATs and HDACs in neurodegeneration: a tale of disconcerted acetylation homeostasis. *Cell Death Differ,* 13**,** 539-50.

SAKAI, J. 2020. Core Concept: How synaptic pruning shapes neural wiring during development and, possibly, in disease. *Proc Natl Acad Sci U S A,* 117**,** 16096-16099.

SAKRY, D., YIGIT, H., DIMOU, L. & TROTTER, J. 2015. Oligodendrocyte precursor cells synthesize neuromodulatory factors. *PLoS One,* 10**,** e0127222.

SAKURAI, K. & OSUMI, N. 2008. The neurogenesis-controlling factor, Pax6, inhibits proliferation and promotes maturation in murine astrocytes. *J Neurosci,* 28**,** 4604-12.

SAKURAI, M., SEKIGUCHI, M., ZUSHIDA, K., YAMADA, K., NAGAMINE, S., KABUTA, T. & WADA, K. 2008. Reduction in memory in passive avoidance learning, exploratory behaviour and synaptic plasticity in mice with a spontaneous deletion in the ubiquitin C-terminal hydrolase L1 gene. *Eur J Neurosci,* 27**,** 691-701.

SALA FRIGERIO, C., LAU, P., SALTA, E., TOURNOY, J., BOSSERS, K., VANDENBERGHE, R., WALLIN, A., BJERKE, M., ZETTERBERG, H., BLENNOW, K. & DE STROOPER, B. 2013. Reduced expression of hsa-miR-27a-3p in CSF of patients with Alzheimer disease. *Neurology,* 81**,** 2103-6.

SALTA, E. & DE STROOPER, B. 2012. Non-coding RNAs with essential roles in neurodegenerative disorders. *Lancet Neurol,* 11**,** 189-200.

SALTER, M. W. & STEVENS, B. 2017. Microglia emerge as central players in brain disease. *Nat Med,* 23**,** 1018-1027.

SAMUDYATA, CASTELO-BRANCO, G. & LIU, J. 2020. Epigenetic regulation of oligodendrocyte differentiation: From development to demyelinating disorders. *Glia,* 68**,** 1619-1630.

SANDBERG, R. 2014. Entering the era of single-cell transcriptomics in biology and medicine. *Nat Methods,* 11**,** 22-4.

SANDER, J. D. & JOUNG, J. K. 2014. CRISPR-Cas systems for editing, regulating and targeting genomes. *Nat Biotechnol,* 32**,** 347-55.

SANZ, E., YANG, L., SU, T., MORRIS, D. R., MCKNIGHT, G. S. & AMIEUX, P. S. 2009. Cell-type-specific isolation of ribosome-associated mRNA from complex tissues. *Proc Natl Acad Sci U S A,* 106**,** 13939-44.

SARACHANA, T., ZHOU, R., CHEN, G., MANJI, H. K. & HU, V. W. 2010. Investigation of post-transcriptional gene regulatory networks associated with autism spectrum disorders by microRNA expression profiling of lymphoblastoid cell lines. *Genome Med,* 2**,** 23.

SARTOR, G. C., ST LAURENT, G., 3RD & WAHLESTEDT, C. 2012. The Emerging Role of Non-Coding RNAs in Drug Addiction. *Front Genet,* 3**,** 106.

SATOH, J., KINO, Y., ASAHINA, N., TAKITANI, M., MIYOSHI, J., ISHIDA, T. & SAITO, Y. 2016. TMEM119 marks a subset of microglia in the human brain. *Neuropathology,* 36**,** 39-49.

SAXENA, A., WAGATSUMA, A., NORO, Y., KUJI, T., ASAKA-OBA, A., WATAHIKI, A., GURNOT, C., FAGIOLINI, M., HENSCH, T. K. & CARNINCI, P. 2012. Trehalose-enhanced isolation of neuronal sub-types from adult mouse brain. *Biotechniques,* 52**,** 381-5.

SCHNEIDER, E., EL HAJJ, N., MULLER, F., NAVARRO, B. & HAAF, T. 2015. Epigenetic Dysregulation in the Prefrontal Cortex of Suicide Completers. *Cytogenet Genome Res,* 146**,** 19-27.

SCHNIEDER, T. P. & DWORK, A. J. 2011. Searching for neuropathology: gliosis in schizophrenia. *Biol Psychiatry,* 69**,** 134-9.

SCHNIEDER, T. P., TRENCEVSKA, I., ROSOKLIJA, G., STANKOV, A., MANN, J. J., SMILEY, J. & DWORK, A. J. 2014. Microglia of prefrontal white matter in suicide. *J Neuropathol Exp Neurol,* 73**,** 880-90.

SCHOSSER, A., BUTLER, A. W., ISING, M., PERROUD, N., UHER, R., NG, M. Y., COHEN-WOODS, S., CRADDOCK, N., OWEN, M. J., KORSZUN, A., JONES, L., JONES, I., GILL, M., RICE, J. P., MAIER, W., MORS, O., RIETSCHEL, M., LUCAE, S., BINDER, E. B., PREISIG, M., PERRY, J., TOZZI, F., MUGLIA, P., AITCHISON, K. J., BREEN, G., CRAIG, I. W., FARMER, A. E., MULLER-MYHSOK, B., MCGUFFIN, P. & LEWIS, C. M. 2011. Genomewide association scan of suicidal thoughts and behaviour in major depression. *PLoS One,* 6**,** e20690.

SCHOUSBOE, A., SCAFIDI, S., BAK, L. K., WAAGEPETERSEN, H. S. & MCKENNA, M. C. 2014. Glutamate metabolism in the brain focusing on astrocytes. *Adv Neurobiol,* 11**,** 13-30.

SCHULTE, U., THUMFART, J. O., KLOCKER, N., SAILER, C. A., BILDL, W., BINIOSSEK, M., DEHN, D., DELLER, T., EBLE, S., ABBASS, K., WANGLER, T., KNAUS, H. G. & FAKLER, B. 2006. The epilepsy-linked Lgi1 protein assembles into presynaptic Kv1 channels and inhibits inactivation by Kvbeta1. *Neuron,* 49**,** 697-706.

SCHULZ, C., GOMEZ PERDIGUERO, E., CHORRO, L., SZABO-ROGERS, H., CAGNARD, N., KIERDORF, K., PRINZ, M., WU, B., JACOBSEN, S. E., POLLARD, J. W., FRAMPTON, J., LIU, K. J. & GEISSMANN, F. 2012. A lineage of myeloid cells independent of Myb and hematopoietic stem cells. *Science,* 336**,** 86-90.

SCHWARZER G, , C. J. & , R. G. 2015. Meta-Analysis with R. *Springer International Publishing*.

SELLGREN, C. M., GRACIAS, J., WATMUFF, B., BIAG, J. D., THANOS, J. M., WHITTREDGE, P. B., FU, T., WORRINGER, K., BROWN, H. E., WANG, J., KAYKAS, A., KARMACHARYA, R., GOOLD, C. P., SHERIDAN, S. D. & PERLIS, R. H. 2019. Increased synapse elimination by microglia in schizophrenia patient-derived models of synaptic pruning. *Nat Neurosci,* 22**,** 374-385.

SELLGREN, C. M., SHERIDAN, S. D., GRACIAS, J., XUAN, D., FU, T. & PERLIS, R. H. 2017. Patient-specific models of microglia-mediated engulfment of synapses and neural progenitors. *Mol Psychiatry,* 22**,** 170-177.

SEQUEIRA, A., GWADRY, F. G., FFRENCH-MULLEN, J. M., CANETTI, L., GINGRAS, Y., CASERO, R. A., JR., ROULEAU, G., BENKELFAT, C. & TURECKI, G. 2006. Implication of SSAT by gene expression and genetic variation in suicide and major depression. *Arch Gen Psychiatry,* 63**,** 35-48.

SEQUEIRA, A., KLEMPAN, T., CANETTI, L., FFRENCH-MULLEN, J., BENKELFAT, C., ROULEAU, G. A. & TURECKI, G. 2007. Patterns of gene expression in the limbic system of suicides with and without major depression. *Mol Psychiatry,* 12**,** 640-55.

SERAFINI, G., POMPILI, M., HANSEN, K. F., OBRIETAN, K., DWIVEDI, Y., SHOMRON, N. & GIRARDI, P. 2014. The involvement of microRNAs in major depression, suicidal behavior, and related disorders: a focus on miR-185 and miR-491-3p. *Cell Mol Neurobiol,* 34**,** 17-30.

SERAFINI, G., POMPILI, M., INNAMORATI, M., GIORDANO, G., MONTEBOVI, F., SHER, L., DWIVEDI, Y. & GIRARDI, P. 2012. The role of microRNAs in synaptic plasticity, major affective disorders and suicidal behavior. *Neurosci Res,* 73**,** 179-90.

SHAPIRO, H. M. 2003. Practical Flow ctyometry. *Wiley-Liss*.

SHAPIRO, H. M. 2004. Lasers for flow cytometry. *Curr Protoc Cytom,* Chapter 1**,** Unit 1 9.

SHERWANI, S. I. & KHAN, H. A. 2015. Role of 5-hydroxymethylcytosine in neurodegeneration. *Gene,* 570**,** 17-24.

SHI, C., ZHANG, L. & QIN, C. 2017. Long non-coding RNAs in brain development, synaptic biology, and Alzheimer's disease. *Brain Res Bull,* 132**,** 160-169.

SHIGEMOTO-MOGAMI, Y., HOSHIKAWA, K., GOLDMAN, J. E., SEKINO, Y. & SATO, K. 2014. Microglia enhance neurogenesis and oligodendrogenesis in the early postnatal subventricular zone. *J Neurosci,* 34**,** 2231-43.

SHIREBY G.L., J. P. D., PAUL T FRANCIS, JOE BURRAGE, EMMA M WALKER, GRANT W A NEILSON, AISHA DAHIR, ALAN J THOMAS, SETH LOVE, REBECCA G SMITH, KATIE LUNNON, MEENA KUMARI, LEONARD C SCHALKWYK, KEVIN MORGAN, KEELEY BROOKES, EILIS J HANNON,

JONATHAN MILL, 2020. Recalibrating the Epigenetic Clock: Implications for Assessing Biological Age in the Human Cortex. *Brain*

SHIREBY, G. L., DAVIES, J. P., FRANCIS, P. T., BURRAGE, J., WALKER, E. M., NEILSON, G. W. A., DAHIR, A., THOMAS, A. J., LOVE, S., SMITH, R. G., LUNNON, K., KUMARI, M., SCHALKWYK, L. C., MORGAN, K., BROOKES, K., HANNON, E. & MILL, J. 2020. Recalibrating the epigenetic clock: implications for assessing biological age in the human cortex. *Brain,* 143**,** 3763-3775.

SHUKLA, A., SEHGAL, M. & SINGH, T. R. 2015. Hydroxymethylation and its potential implication in DNA repair system: A review and future perspectives. *Gene,* 564**,** 109-18.

SHYU, W. C., LIN, S. Z., CHIANG, M. F., CHEN, D. C., SU, C. Y., WANG, H. J., LIU, R. S., TSAI, C. H. & LI, H. 2008. Secretoneurin promotes neuroprotection and neuronal plasticity via the Jak2/Stat3 pathway in murine models of stroke. *J Clin Invest,* 118**,** 133-48.

SI, X., MIGUEL-HIDALGO, J. J., O'DWYER, G., STOCKMEIER, C. A. & RAJKOWSKA, G. 2004. Age-dependent reductions in the level of glial fibrillary acidic protein in the prefrontal cortex in major depression. *Neuropsychopharmacology,* 29**,** 2088-96.

ŠIDÁK, Z. 1967. Rectangular Confidence Regions for the Means of Multivariate Normal Distributions. *Journal of the American Statistical Association,* 62:318**,** 626-633.

SIDORYK-WEGRZYNOWICZ, M., WEGRZYNOWICZ, M., LEE, E., BOWMAN, A. B. & ASCHNER, M. 2011. Role of astrocytes in brain function and disease. *Toxicol Pathol,* 39**,** 115-23.

SIEGMUND, K. D., CONNOR, C. M., CAMPAN, M., LONG, T. I., WEISENBERGER, D. J., BINISZKIEWICZ, D., JAENISCH, R., LAIRD, P. W. & AKBARIAN, S. 2007. DNA methylation in the human cerebral cortex is dynamically regulated throughout the life span and involves differentiated neurons. *PLoS One,* 2**,** e895.

SIERRA, A., ENCINAS, J. M., DEUDERO, J. J., CHANCEY, J. H., ENIKOLOPOV, G., OVERSTREET-WADICHE, L. S., TSIRKA, S. E. & MALETIC-SAVATIC, M. 2010. Microglia shape adult hippocampal neurogenesis through apoptosis-coupled phagocytosis. *Cell Stem Cell,* 7**,** 483-95.

SIMONS, M. & NAVE, K. A. 2015. Oligodendrocytes: Myelination and Axonal Support. *Cold Spring Harb Perspect Biol,* 8**,** a020479.

SIMPSON, J. E., INCE, P. G., LACE, G., FORSTER, G., SHAW, P. J., MATTHEWS, F., SAVVA, G., BRAYNE, C., WHARTON, S. B., FUNCTION, M. R. C. C. & AGEING NEUROPATHOLOGY STUDY, G. 2010. Astrocyte phenotype in relation to Alzheimer-type pathology in the ageing brain. *Neurobiol Aging,* 31**,** 578-90.

SINGEC, I., KNOTH, R., DITTER, M., HAGEMEYER, C. E., ROSENBROCK, H., FROTSCHER, M. & VOLK, B. 2002. Synaptic vesicle protein synaptoporin is differently expressed by subpopulations of mouse hippocampal neurons. *J Comp Neurol,* 452**,** 139-53.

SKVORTSOVA, K., ZOTENKO, E., LUU, P. L., GOULD, C. M., NAIR, S. S., CLARK, S. J. & STIRZAKER, C. 2017. Comprehensive evaluation of genome-wide 5-hydroxymethylcytosine profiling approaches in human DNA. *Epigenetics Chromatin,* 10**,** 16.

SLYNKO, A. & BENNER, A. 2019. Statistical methods for classification of 5hmC levels based on the Illumina Inifinium HumanMethylation450 (450k) array data, under the paired bisulfite (BS) and oxidative bisulfite (oxBS) treatment. *PLoS One,* 14**,** e0218103.

SMALHEISER, N. R., LUGLI, G., RIZAVI, H. S., TORVIK, V. I., TURECKI, G. & DWIVEDI, Y. 2012. MicroRNA expression is down-regulated and reorganized in prefrontal cortex of depressed suicide subjects. *PLoS One,* 7**,** e33201.

SMALHEISER, N. R., LUGLI, G., ZHANG, H., RIZAVI, H., COOK, E. H. & DWIVEDI, Y. 2014. Expression of microRNAs and other small RNAs in prefrontal cortex in schizophrenia, bipolar disorder and depressed subjects. *PLoS One,* 9**,** e86469.

SMITH, A. M., GIBBONS, H. M., OLDFIELD, R. L., BERGIN, P. M., MEE, E. W., CURTIS, M. A., FAULL, R. L. & DRAGUNOW, M. 2013. M-CSF increases proliferation and phagocytosis while modulating receptor and transcription factor expression in adult human microglia. *J Neuroinflammation,* 10**,** 85.

SMITH, A. R., WHEILDON, G. & LUNNON, K. 2020. Invited Review - A 5-year update on epigenome-wide association studies of DNA modifications in Alzheimer's disease: progress, practicalities and promise. *Neuropathol Appl Neurobiol,* 46**,** 641-653.

SMITH, S. M. 2017. Strategies for the Purification of Membrane Proteins. *Methods Mol Biol,* 1485**,** 389-400.

SOKOLOWSKI, M., WASSERMAN, J. & WASSERMAN, D. 2014. Genome-wide association studies of suicidal behaviors: a review. *Eur Neuropsychopharmacol,* 24**,** 1567-77.

SOKOLOWSKI, M., WASSERMAN, J. & WASSERMAN, D. 2015. An overview of the neurobiology of suicidal behaviors as one meta-system. *Mol Psychiatry,* 20**,** 56-71.

SOLER, M., BOQUE-SASTRE, R. & GUIL, S. 2017. RNA-FISH to Study Regulatory RNA at the Site of Transcription. *Methods Mol Biol,* 1543**,** 221-229.

SOLGA, A. C., PONG, W. W., WALKER, J., WYLIE, T., MAGRINI, V., APICELLI, A. J., GRIFFITH, M., GRIFFITH, O. L., KOHSAKA, S., WU, G. F., BRODY, D. L., MARDIS, E. R. & GUTMANN, D. H. 2015. RNA-sequencing reveals oligodendrocyte and neuronal transcripts in microglia relevant to central nervous system disease. *Glia,* 63**,** 531-548.

SORENSEN, B. S., ALSNER, J., OVERGAARD, J. & HORSMAN, M. R. 2007. Hypoxia induced expression of endogenous markers in vitro is highly influenced by pH. *Radiother Oncol,* 83**,** 362-6.

SORENSEN, B. S., BUSK, M., OVERGAARD, J., HORSMAN, M. R. & ALSNER, J. 2015. Simultaneous Hypoxia and Low Extracellular pH Suppress Overall Metabolic Rate and Protein Synthesis In Vitro. *PLoS One,* 10**,** e0134955.

SORENSEN, B. S., HAO, J., OVERGAARD, J., VORUM, H., HONORE, B., ALSNER, J. & HORSMAN, M. R. 2005. Influence of oxygen concentration and pH on expression of hypoxia induced genes. *Radiother Oncol,* 76**,** 187-93.

SOSNA, J., PHILIPP, S., ALBAY, R., 3RD, REYES-RUIZ, J. M., BAGLIETTO-VARGAS, D., LAFERLA, F. M. & GLABE, C. G. 2018. Early long-term administration of the CSF1R inhibitor PLX3397 ablates microglia and reduces accumulation of intraneuronal amyloid, neuritic plaque deposition and pre-fibrillar oligomers in 5XFAD mouse model of Alzheimer's disease. *Mol Neurodegener,* 13**,** 11.

SPADARO, P. A., FLAVELL, C. R., WIDAGDO, J., RATNU, V. S., TROUP, M., RAGAN, C., MATTICK, J. S. & BREDY, T. W. 2015. Long Noncoding RNA-Directed Epigenetic Regulation of Gene Expression Is Associated With Anxiety-like Behavior in Mice. *Biol Psychiatry,* 78**,** 848-59.

SPIERS, H., HANNON, E., SCHALKWYK, L. C., BRAY, N. J. & MILL, J. 2017. 5-hydroxymethylcytosine is highly dynamic across human fetal brain development. *BMC Genomics,* 18**,** 738.

SPILKER, C., GUNDELFINGER, E. D. & BRAUNEWELL, K. H. 2002. Evidence for different functional properties of the neuronal calcium sensor proteins VILIP-1 and VILIP-3: from subcellular localization to cellular function. *Biochim Biophys Acta,* 1600**,** 118-27.

SQUARZONI, P., OLLER, G., HOEFFEL, G., PONT-LEZICA, L., ROSTAING, P., LOW, D., BESSIS, A., GINHOUX, F. & GAREL, S. 2014. Microglia modulate wiring of the embryonic forebrain. *Cell Rep,* 8**,** 1271-9.

STANGEGAARD, M., DUFVA, I. H. & DUFVA, M. 2006. Reverse transcription using random pentadecamer primers increases yield and quality of resulting cDNA. *Biotechniques,* 40**,** 649-57.

STAWSKI, R., PIASKOWSKI, S., STOCZYNSKA-FIDELUS, E., WOZNIAK, K., BIENKOWSKI, M., ZAKRZEWSKA, M., WITUSIK-PERKOWSKA, M., JASKOLSKI, D. J., OCH, W., PAPIERZ, W., SIKORSKA, B., RIESKE, P. & LIBERSKI, P. P. 2013. Reduced expression of ELAVL4 in male meningioma patients. *Brain Tumor Pathol,* 30**,** 160-6.

STEINER, F. A., TALBERT, P. B., KASINATHAN, S., DEAL, R. B. & HENIKOFF, S. 2012. Cell-type-specific nuclei purification from whole animals for genome-wide expression and chromatin profiling. *Genome Res,* 22**,** 766-77.

STEINER, J., BIELAU, H., BRISCH, R., DANOS, P., ULLRICH, O., MAWRIN, C., BERNSTEIN, H. G. & BOGERTS, B. 2008. Immunological aspects in the neurobiology of suicide: elevated

microglial density in schizophrenia and depression is associated with suicide. *J Psychiatr Res,* 42**,** 151-7.

STEINER, J., MAWRIN, C., ZIEGELER, A., BIELAU, H., ULLRICH, O., BERNSTEIN, H. G. & BOGERTS, B. 2006. Distribution of HLA-DR-positive microglia in schizophrenia reflects impaired cerebral lateralization. *Acta Neuropathol,* 112**,** 305-16.

STEINER, J., WALTER, M., GOS, T., GUILLEMIN, G. J., BERNSTEIN, H. G., SARNYAI, Z., MAWRIN, C., BRISCH, R., BIELAU, H., MEYER ZU SCHWABEDISSEN, L., BOGERTS, B. & MYINT, A. M. 2011. Severe depression is associated with increased microglial quinolinic acid in subregions of the anterior cingulate gyrus: evidence for an immune-modulated glutamatergic neurotransmission? *J Neuroinflammation,* 8**,** 94.

STEVENS, B., ALLEN, N. J., VAZQUEZ, L. E., HOWELL, G. R., CHRISTOPHERSON, K. S., NOURI, N., MICHEVA, K. D., MEHALOW, A. K., HUBERMAN, A. D., STAFFORD, B., SHER, A., LITKE, A. M., LAMBRIS, J. D., SMITH, S. J., JOHN, S. W. & BARRES, B. A. 2007. The classical complement cascade mediates CNS synapse elimination. *Cell,* 131**,** 1164-78.

STOGSDILL, J. A. & EROGLU, C. 2017. The interplay between neurons and glia in synapse development and plasticity. *Curr Opin Neurobiol,* 42**,** 1-8.

STOLT, C. C., REHBERG, S., ADER, M., LOMMES, P., RIETHMACHER, D., SCHACHNER, M., BARTSCH, U. & WEGNER, M. 2002. Terminal differentiation of myelin-forming oligodendrocytes depends on the transcription factor Sox10. *Genes Dev,* 16**,** 165-70.

STOLTZNER, S. E., GRENFELL, T. J., MORI, C., WISNIEWSKI, K. E., WISNIEWSKI, T. M., SELKOE, D. J. & LEMERE, C. A. 2000. Temporal accrual of complement proteins in amyloid plaques in Down's syndrome with Alzheimer's disease. *Am J Pathol,* 156**,** 489-99.

STUART, T., BUTLER, A., HOFFMAN, P., HAFEMEISTER, C., PAPALEXI, E., MAUCK, W. M., 3RD, HAO, Y., STOECKIUS, M., SMIBERT, P. & SATIJA, R. 2019. Comprehensive Integration of Single-Cell Data. *Cell,* 177**,** 1888-1902 e21.

SUBRAMANIAN, L., SARKAR, A., SHETTY, A. S., MURALIDHARAN, B., PADMANABHAN, H., PIPER, M., MONUKI, E. S., BACH, I., GRONOSTAJSKI, R. M., RICHARDS, L. J. & TOLE, S. 2011. Transcription factor Lhx2 is necessary and sufficient to suppress astrogliogenesis and promote neurogenesis in the developing hippocampus. *Proc Natl Acad Sci U S A,* 108**,** E265-74.

SUDERMAN, M., MCGOWAN, P. O., SASAKI, A., HUANG, T. C., HALLETT, M. T., MEANEY, M. J., TURECKI, G. & SZYF, M. 2012. Conserved epigenetic sensitivity to early life experience in the rat and human hippocampus. *Proc Natl Acad Sci U S A,* 109 Suppl 2**,** 17266-72.

SULLIVAN, P. F., NEALE, M. C. & KENDLER, K. S. 2000. Genetic epidemiology of major depression: review and meta-analysis. *Am J Psychiatry,* 157**,** 1552-62.

SUMAZIN, P., YANG, X., CHIU, H. S., CHUNG, W. J., IYER, A., LLOBET-NAVAS, D., RAJBHANDARI, P., BANSAL, M., GUARNIERI, P., SILVA, J. & CALIFANO, A. 2011. An extensive microRNA-mediated network of RNA-RNA interactions regulates established oncogenic pathways in glioblastoma. *Cell,* 147**,** 370-81.

SUN, H., WANG, J., GONG, Z., YAO, J., WANG, Y., XU, J., YUAN, G. C., ZHANG, Y. & SHAO, Z. 2018a. Quantitative integration of epigenomic variation and transcription factor binding using MAmotif toolkit identifies an important role of IRF2 as transcription activator at gene promoters. *Cell Discov,* 4**,** 38.

SUN, N., LEI, L., WANG, Y., YANG, C., LIU, Z., LI, X. & ZHANG, K. 2016. Preliminary comparison of plasma notch-associated microRNA-34b and -34c levels in drug naive, first episode depressed patients and healthy controls. *J Affect Disord,* 194**,** 109-14.

SUN, R., WANG, Z., CLAUS HENN, B., SU, L., LU, Q., LIN, X., WRIGHT, R. O., BELLINGER, D. C., KILE, M., MAZUMDAR, M., TELLEZ-ROJO, M. M., SCHNAAS, L. & CHRISTIANI, D. C. 2018b. Identification of novel loci associated with infant cognitive ability. *Mol Psychiatry*.

SUN, T., XIAO, H. S., ZHOU, P. B., LU, Y. J., BAO, L. & ZHANG, X. 2006. Differential expression of synaptoporin and synaptophysin in primary sensory neurons and up-regulation of synaptoporin after peripheral nerve injury. *Neuroscience,* 141**,** 1233-45.

SUN, W., CORNWELL, A., LI, J., PENG, S., OSORIO, M. J., AALLING, N., WANG, S., BENRAISS, A., LOU, N., GOLDMAN, S. A. & NEDERGAARD, M. 2017. SOX9 Is an Astrocyte-Specific Nuclear Marker in the Adult Brain Outside the Neurogenic Regions. *J Neurosci,* 37**,** 4493-4507.

SUPEK, F., BOSNJAK, M., SKUNCA, N. & SMUC, T. 2011. REVIGO summarizes and visualizes long lists of gene ontology terms. *PLoS One,* 6**,** e21800.

SURYAWANSHI, H., SARANGDHAR, M. A., VIJ, M., ROSHAN, R., SINGH, V. P., GANGULI, M. & PILLAI, B. 2015. A Simple Alternative to Stereotactic Injection for Brain Specific Knockdown of miRNA. *J Vis Exp***,** e53307.

SUTPHEN, C. L., MCCUE, L., HERRIES, E. M., XIONG, C., LADENSON, J. H., HOLTZMAN, D. M., FAGAN, A. M. & ADNI 2018. Longitudinal decreases in multiple cerebrospinal fluid biomarkers of neuronal injury in symptomatic late onset Alzheimer's disease. *Alzheimers Dement,* 14**,** 869-879.

SUZUKI, H., OHGIDANI, M., KUWANO, N., CHRETIEN, F., LORIN DE LA GRANDMAISON, G., ONAYA, M., TOMINAGA, I., SETOYAMA, D., KANG, D., MIMURA, M., KANBA, S. & KATO, T. A. 2019. Suicide and Microglia: Recent Findings and Future Perspectives Based on Human Studies. *Front Cell Neurosci,* 13**,** 31.

SUZUKI, R., WATANABE, J., ARATA, S., FUNAHASHI, H., KIKUYAMA, S. & SHIODA, S. 2003. A transgenic mouse model for the detailed morphological study of astrocytes. *Neurosci Res,* 47**,** 451-4.

SWEENEY, M. D., ZHAO, Z., MONTAGNE, A., NELSON, A. R. & ZLOKOVIC, B. V. 2019. Blood-Brain Barrier: From Physiology to Disease and Back. *Physiol Rev,* 99**,** 21-78.

SYED, S. A. & NEMEROFF, C. B. 2017. Early Life Stress, Mood, and Anxiety Disorders. *Chronic Stress (Thousand Oaks),* 1.

SYKORA, M. M. & RESCHKE, M. 2019. Immunophenotyping of Tissue Samples Using Multicolor Flow Cytometry. *Methods Mol Biol,* 1953**,** 253-268.

SZULWACH, K. E., LI, X., LI, Y., SONG, C. X., WU, H., DAI, Q., IRIER, H., UPADHYAY, A. K., GEARING, M., LEVEY, A. I., VASANTHAKUMAR, A., GODLEY, L. A., CHANG, Q., CHENG, X., HE, C. & JIN, P. 2011. 5-hmC-mediated epigenetic dynamics during postnatal neurodevelopment and aging. *Nat Neurosci,* 14**,** 1607-16.

SZWAGIERCZAK, A., BULTMANN, S., SCHMIDT, C. S., SPADA, F. & LEONHARDT, H. 2010. Sensitive enzymatic quantification of 5-hydroxymethylcytosine in genomic DNA. *Nucleic Acids Res,* 38**,** e181.

TAFT, R. J., SIMONS, C., NAHKURI, S., OEY, H., KORBIE, D. J., MERCER, T. R., HOLST, J., RITCHIE, W., WONG, J. J., RASKO, J. E., ROKHSAR, D. S., DEGNAN, B. M. & MATTICK, J. S. 2010. Nuclear-localized tiny RNAs are associated with transcription initiation and splice sites in metazoans. *Nat Struct Mol Biol,* 17**,** 1030-4.

TAHILIANI, M., KOH, K. P., SHEN, Y., PASTOR, W. A., BANDUKWALA, H., BRUDNO, Y., AGARWAL, S., IYER, L. M., LIU, D. R., ARAVIND, L. & RAO, A. 2009. Conversion of 5-methylcytosine to 5-hydroxymethylcytosine in mammalian DNA by MLL partner TET1. *Science,* 324**,** 930-5.

TAKAGI, Y., AOKI, T., TAKAHASHI, J. C., YOSHIDA, K., ISHII, A., ARAKAWA, Y., KIKUCHI, T., FUNAKI, T. & MIYAMOTO, S. 2014. Differential gene expression in relation to the clinical characteristics of human brain arteriovenous malformations. *Neurol Med Chir (Tokyo),* 54**,** 163-75.

TAKIZAWA, T., NAKASHIMA, K., NAMIHIRA, M., OCHIAI, W., UEMURA, A., YANAGISAWA, M., FUJITA, N., NAKAO, M. & TAGA, T. 2001. DNA methylation is a critical cell-intrinsic determinant of astrocyte differentiation in the fetal brain. *Dev Cell,* 1**,** 749-58.

TALMAN, V., PASCALE, A., JANTTI, M., AMADIO, M. & TUOMINEN, R. K. 2016. Protein Kinase C Activation as a Potential Therapeutic Strategy in Alzheimer's Disease: Is there a Role for Embryonic Lethal Abnormal Vision-like Proteins? *Basic Clin Pharmacol Toxicol,* 119**,** 149-60.

TAMURA, S., MORIKAWA, Y., IWANISHI, H., HISAOKA, T. & SENBA, E. 2003. Expression pattern of the winged-helix/forkhead transcription factor Foxp1 in the developing central nervous system. *Gene Expr Patterns,* 3**,** 193-7.

TAMURA, Y., KUNUGI, H., OHASHI, J. & HOHJOH, H. 2007. Epigenetic aberration of the human REELIN gene in psychiatric disorders. *Mol Psychiatry,* 12**,** 519, 593-600.

TANAKA, K. & OKAMOTO, A. 2007. Degradation of DNA by bisulfite treatment. *Bioorg Med Chem Lett,* 17**,** 1912-5.

TANSEY, K. E. & HILL, M. J. 2018. Enrichment of schizophrenia heritability in both neuronal and glia cell regulatory elements. *Transl Psychiatry,* 8**,** 7.

TAQMAN ARRAY MICRO FLUIDIC CARDS USER GUIDE http://tools.thermofisher.com/content/sfs/manuals/cms_062836.pdf.

TAQMAN® ADVANCED MIRNA ASSAYS USER GUIDE https://assets.thermofisher.com/TFS-Assets/LSG/manuals/MAN0016122_TaqManAdvmiRNAArrayCards_UG.pdf.

TAQMAN® OPENARRAY® MICRORNA PANEL https://assets.thermofisher.com/TFS-Assets/LSG/manuals/4461306B.pdf.

TARASOV, V. V., SVISTUNOV, A. A., CHUBAREV, V. N., SOLOGOVA, S. S., MUKHORTOVA, P., LEVUSHKIN, D., SOMASUNDARAM, S. G., KIRKLAND, C. E., BACHURIN, S. O. & ALIEV, G. 2019. Alterations of Astrocytes in the Context of Schizophrenic Dementia. *Front Pharmacol,* 10**,** 1612.

TASDEMIR-YILMAZ, O. E. & FREEMAN, M. R. 2014. Astrocytes engage unique molecular programs to engulf pruned neuronal debris from distinct subsets of neurons. *Genes Dev,* 28**,** 20-33.

TAUPENOT, L., HARPER, K. L. & O'CONNOR, D. T. 2003. The chromogranin-secretogranin family. *N Engl J Med,* 348**,** 1134-49.

TELFORD, W. G. 2018. Overview of Lasers for Flow Cytometry. *Methods Mol Biol,* 1678**,** 447-479.

TELFORD, W. G., BABIN, S. A., KHOREV, S. V. & ROWE, S. H. 2009. Green fiber lasers: an alternative to traditional DPSS green lasers for flow cytometry. *Cytometry A,* 75**,** 1031-9.

TELFORD, W. G., SHCHERBAKOVA, D. M., BUSCHKE, D., HAWLEY, T. S. & VERKHUSHA, V. V. 2015. Multiparametric flow cytometry using near-infrared fluorescent proteins engineered from bacterial phytochromes. *PLoS One,* 10**,** e0122342.

TENNER, A. J. 2001. Complement in Alzheimer's disease: opportunities for modulating protective and pathogenic events. *Neurobiol Aging,* 22**,** 849-61.

THION, M. S., GINHOUX, F. & GAREL, S. 2018. Microglia and early brain development: An intimate journey. *Science,* 362**,** 185-189.

THRUPP, N., SALA FRIGERIO, C., WOLFS, L., SKENE, N. G., FATTORELLI, N., POOVATHINGAL, S., FOURNE, Y., MATTHEWS, P. M., THEYS, T., MANCUSO, R., DE STROOPER, B. & FIERS, M. 2020. Single-Nucleus RNA-Seq Is Not Suitable for Detection of Microglial Activation Genes in Humans. *Cell Rep,* 32**,** 108189.

TIAN, T., WANG, J. & ZHOU, X. 2015. A review: microRNA detection methods. *Org Biomol Chem,* 13**,** 2226-38.

TIMMERMAN, R., BURM, S. M. & BAJRAMOVIC, J. J. 2018. An Overview of in vitro Methods to Study Microglia. *Front Cell Neurosci,* 12**,** 242.

TITUS, A. J., GALLIMORE, R. M., SALAS, L. A. & CHRISTENSEN, B. C. 2017. Cell-type deconvolution from DNA methylation: a review of recent applications. *Hum Mol Genet,* 26**,** R216-R224.

TOLLEFSEN, I. M., HEM, E. & EKEBERG, O. 2012. The reliability of suicide statistics: a systematic review. *BMC Psychiatry,* 12**,** 9.

TORRES-PLATAS, S. G., CRUCEANU, C., CHEN, G. G., TURECKI, G. & MECHAWAR, N. 2014. Evidence for increased microglial priming and macrophage recruitment in the dorsal anterior cingulate white matter of depressed suicides. *Brain Behav Immun,* 42**,** 50-9.

TORRES-PLATAS, S. G., HERCHER, C., DAVOLI, M. A., MAUSSION, G., LABONTE, B., TURECKI, G. & MECHAWAR, N. 2011. Astrocytic hypertrophy in anterior cingulate white matter of depressed suicides. *Neuropsychopharmacology,* 36**,** 2650-8.

TORRES, L., DANVER, J., JI, K., MIYAUCHI, J. T., CHEN, D., ANDERSON, M. E., WEST, B. L., ROBINSON, J. K. & TSIRKA, S. E. 2016. Dynamic microglial modulation of spatial learning and social behavior. *Brain Behav Immun,* 55**,** 6-16.

TOST, J. & GUT, I. G. 2007. DNA methylation analysis by pyrosequencing. *Nat Protoc,* 2**,** 2265-75.

TRAPNELL, C. 2015. Defining cell types and states with single-cell genomics. *Genome Res,* 25**,** 1491-8.

TRUMMER, A., DE ROP, C., TIEDE, A., GANSER, A. & EISERT, R. 2008. Isotype controls in phenotyping and quantification of microparticles: a major source of error and how to evade it. *Thromb Res,* 122**,** 691-700.

TSAGARATOU, A., AIJO, T., LIO, C. W., YUE, X., HUANG, Y., JACOBSEN, S. E., LAHDESMAKI, H. & RAO, A. 2014. Dissecting the dynamic changes of 5-hydroxymethylcytosine in T-cell development and differentiation. *Proc Natl Acad Sci U S A,* 111**,** E3306-15.

TSAI, M. C., MANOR, O., WAN, Y., MOSAMMAPARAST, N., WANG, J. K., LAN, F., SHI, Y., SEGAL, E. & CHANG, H. Y. 2010. Long noncoding RNA as modular scaffold of histone modification complexes. *Science,* 329**,** 689-93.

TSAI, S. J., HONG, C. J. & LIOU, Y. J. 2011. Recent molecular genetic studies and methodological issues in suicide research. *Prog Neuropsychopharmacol Biol Psychiatry,* 35**,** 809-17.

TSE, K. H., CHENG, A., MA, F. & HERRUP, K. 2018. DNA damage-associated oligodendrocyte degeneration precedes amyloid pathology and contributes to Alzheimer's disease and dementia. *Alzheimers Dement,* 14**,** 664-679.

TU, C., DU, T., SHAO, C., LIU, Z., LI, L. & SHEN, Y. 2018. Evaluating the potential of housekeeping genes, rRNAs, snRNAs, microRNAs and circRNAs as reference genes for the estimation of PMI. *Forensic Sci Med Pathol,* 14**,** 194-201.

TUCKER, K. L. 2001. Methylated cytosine and the brain: a new base for neuroscience. *Neuron,* 30**,** 649-52.

TULLOCH, J., LEONG, L., THOMSON, Z., CHEN, S., LEE, E. G., KEENE, C. D., MILLARD, S. P. & YU, C. E. 2018. Glia-specific APOE epigenetic changes in the Alzheimer's disease brain. *Brain Res,* 1698**,** 179-186.

TUNG, J. W., PARKS, D. R., MOORE, W. A., HERZENBERG, L. A. & HERZENBERG, L. A. 2004. New approaches to fluorescence compensation and visualization of FACS data. *Clin Immunol,* 110**,** 277-83.

TURECKI, G. 2014. The molecular bases of the suicidal brain. *Nat Rev Neurosci,* 15**,** 802-16.

TURECKI, G. & BRENT, D. A. 2016. Suicide and suicidal behaviour. *Lancet,* 387**,** 1227-39.

TYAGI, S. 2009. Imaging intracellular RNA distribution and dynamics in living cells. *Nat Methods,* 6**,** 331-8.

UDDIN, M., AIELLO, A. E., WILDMAN, D. E., KOENEN, K. C., PAWELEC, G., DE LOS SANTOS, R., GOLDMANN, E. & GALEA, S. 2010. Epigenetic and immune function profiles associated with posttraumatic stress disorder. *Proc Natl Acad Sci U S A,* 107**,** 9470-5.

UDDIN, M., KOENEN, K. C., AIELLO, A. E., WILDMAN, D. E., DE LOS SANTOS, R. & GALEA, S. 2011. Epigenetic and inflammatory marker profiles associated with depression in a community-based epidemiologic sample. *Psychol Med,* 41**,** 997-1007.

UENO, M., FUJITA, Y., TANAKA, T., NAKAMURA, Y., KIKUTA, J., ISHII, M. & YAMASHITA, T. 2013. Layer V cortical neurons require microglial support for survival during postnatal development. *Nat Neurosci,* 16**,** 543-51.

URDINGUIO, R. G., SANCHEZ-MUT, J. V. & ESTELLER, M. 2009. Epigenetic mechanisms in neurological diseases: genes, syndromes, and therapies. *Lancet Neurol,* 8**,** 1056-72.

VALLES, S. L., IRADI, A., ALDASORO, M., VILA, J. M., ALDASORO, C., DE LA TORRE, J., CAMPOS-CAMPOS, J. & JORDA, A. 2019. Function of Glia in Aging and the Brain Diseases. *Int J Med Sci,* 16**,** 1473-1479.

VAN DER MEULEN, M., BROMBERG, J. E. C., LAM, K. H., DAMMERS, R., LANGERAK, A. W., DOORDUIJN, J. K., KROS, J. M., VAN DEN BENT, M. J. & VAN DER VELDEN, V. H. J. 2018. Flow cytometry shows added value in diagnosing lymphoma in brain biopsies. *Cytometry B Clin Cytom,* 94**,** 928-934.

VAN DER POEL, M., ULAS, T., MIZEE, M. R., HSIAO, C. C., MIEDEMA, S. S. M., ADELIA, SCHUURMAN, K. G., HELDER, B., TAS, S. W., SCHULTZE, J. L., HAMANN, J. & HUITINGA, I. 2019. Transcriptional profiling of human microglia reveals grey-white matter heterogeneity and multiple sclerosis-associated changes. *Nat Commun,* 10**,** 1139.

VAN HEERINGEN, K. & MANN, J. J. 2014. The neurobiology of suicide. *Lancet Psychiatry,* 1**,** 63-72.

VANGUILDER STARKEY, H. D., VAN KIRK, C. A., BIXLER, G. V., IMPERIO, C. G., KALE, V. P., SERFASS, J. M., FARLEY, J. A., YAN, H., WARRINGTON, J. P., HAN, S., MITSCHELEN, M., SONNTAG, W. E. & FREEMAN, W. M. 2012. Neuroglial expression of the MHCI pathway and PirB receptor is upregulated in the hippocampus with advanced aging. *J Mol Neurosci,* 48**,** 111-26.

VARLEY, K. E., GERTZ, J., BOWLING, K. M., PARKER, S. L., REDDY, T. E., PAULI-BEHN, F., CROSS, M. K., WILLIAMS, B. A., STAMATOYANNOPOULOS, J. A., CRAWFORD, G. E., ABSHER, D. M., WOLD, B. J. & MYERS, R. M. 2013. Dynamic DNA methylation across diverse human cell lines and tissues. *Genome Res,* 23**,** 555-67.

VELMESHEV, D., SCHIRMER, L., JUNG, D., HAEUSSLER, M., PEREZ, Y., MAYER, S., BHADURI, A., GOYAL, N., ROWITCH, D. H. & KRIEGSTEIN, A. R. 2019. Single-cell genomics identifies cell type-specific molecular changes in autism. *Science,* 364**,** 685-689.

VENKATASUBRAMANIAN, G. & KESHAVAN, M. S. 2016. Biomarkers in Psychiatry - A Critique. *Ann Neurosci,* 23**,** 3-5.

VERCAUTEREN, F. G., FLORES, G., MA, W., CHABOT, J. G., GEENEN, L., CLERENS, S., FAZEL, A., BERGERON, J. J., SRIVASTAVA, L. K., ARCKENS, L. & QUIRION, R. 2007. An organelle proteomic method to study neurotransmission-related proteins, applied to a neurodevelopmental model of schizophrenia. *Proteomics,* 7**,** 3569-79.

VIANA, J., HANNON, E., DEMPSTER, E., PIDSLEY, R., MACDONALD, R., KNOX, O., SPIERS, H., TROAKES, C., AL-SARAJ, S., TURECKI, G., SCHALKWYK, L. C. & MILL, J. 2017. Schizophrenia-associated methylomic variation: molecular signatures of disease and polygenic risk burden across multiple brain regions. *Hum Mol Genet,* 26**,** 210-225.

VISONE, R., BACALINI, M. G., DI FRANCO, S., FERRACIN, M., COLORITO, M. L., PAGOTTO, S., LAPROVITERA, N., LICASTRO, D., DI MARCO, M., SCAVO, E., BASSI, C., SACCENTI, E., NICOTRA, A., GRZES, M., GARAGNANI, P., DE LAURENZI, V., VALERI, N., MARIANI-COSTANTINI, R., NEGRINI, M., STASSI, G. & VERONESE, A. 2019. DNA methylation of shelf, shore and open sea CpG positions distinguish high microsatellite instability from low or stable microsatellite status colon cancer stem cells. *Epigenomics,* 11**,** 587-604.

VITUCCI, D., DI GIORGIO, A., NAPOLITANO, F., PELOSI, B., BLASI, G., ERRICO, F., ATTROTTO, M. T., GELAO, B., FAZIO, L., TAURISANO, P., DI MAIO, A., MARSILI, V., PASQUALETTI, M., BERTOLINO, A. & USIELLO, A. 2016. Rasd2 Modulates Prefronto-Striatal Phenotypes in Humans and 'Schizophrenia-Like Behaviors' in Mice. *Neuropsychopharmacology,* 41**,** 916-27.

VOGL, M. R., REIPRICH, S., KUSPERT, M., KOSIAN, T., SCHREWE, H., NAVE, K. A. & WEGNER, M. 2013. Sox10 cooperates with the mediator subunit 12 during terminal differentiation of myelinating glia. *J Neurosci,* 33**,** 6679-90.

VOLOVITZ, I., SHAPIRA, N., EZER, H., GAFNI, A., LUSTGARTEN, M., ALTER, T., BEN-HORIN, I., BARZILAI, O., SHAHAR, T., KANNER, A., FRIED, I., VESHCHEV, I., GROSSMAN, R. & RAM, Z. 2016. A non-aggressive, highly efficient, enzymatic method for dissociation of human brain-tumors and brain-tissues to viable single-cells. *BMC Neurosci,* 17**,** 30.

VOLTERRA, A. & MELDOLESI, J. 2005. Astrocytes, from brain glue to communication elements: the revolution continues. *Nat Rev Neurosci,* 6**,** 626-40.

VON BARTHELD, C. S. 2018. Myths and truths about the cellular composition of the human brain: A review of influential concepts. *J Chem Neuroanat,* 93**,** 2-15.

VON BARTHELD, C. S., BAHNEY, J. & HERCULANO-HOUZEL, S. 2016. The search for true numbers of neurons and glial cells in the human brain: A review of 150 years of cell counting. *J Comp Neurol,* 524**,** 3865-3895.

VOSKUIL, J. L. 2017. The challenges with the validation of research antibodies. *F1000Res,* 6**,** 161.

VOSTRIKOV, V. M. & URANOVA, N. A. 2018. [Deficit of oligodendrocytes in the frontal cortex in schizophrenia]. *Zh Nevrol Psikhiatr Im S S Korsakova,* 118**,** 100-103.

WAKE, H., MOORHOUSE, A. J., JINNO, S., KOHSAKA, S. & NABEKURA, J. 2009. Resting microglia directly monitor the functional state of synapses in vivo and determine the fate of ischemic terminals. *J Neurosci,* 29**,** 3974-80.

WALKER, D. G., KIM, S. U. & MCGEER, P. L. 1995. Complement and cytokine gene expression in cultured microglial derived from postmortem human brains. *J Neurosci Res,* 40**,** 478-93.

WALTON, E., HASS, J., LIU, J., ROFFMAN, J. L., BERNARDONI, F., ROESSNER, V., KIRSCH, M., SCHACKERT, G., CALHOUN, V. & EHRLICH, S. 2016. Correspondence of DNA Methylation Between Blood and Brain Tissue and Its Application to Schizophrenia Research. *Schizophr Bull,* 42**,** 406-14.

WANG, J., POL, S. U., HABERMAN, A. K., WANG, C., O'BARA, M. A. & SIM, F. J. 2014. Transcription factor induction of human oligodendrocyte progenitor fate and differentiation. *Proc Natl Acad Sci U S A,* 111**,** E2885-94.

WANG, J., ZHANG, K. X., LU, G. Z. & ZHAO, X. H. 2017. Research progress on 5hmC and TET dioxygenases in neurodevelopment and neurological diseases. *Yi Chuan,* 39**,** 1138-1149.

WANG, Q., ROY, B., TURECKI, G., SHELTON, R. C. & DWIVEDI, Y. 2018a. Role of Complex Epigenetic Switching in Tumor Necrosis Factor-alpha Upregulation in the Prefrontal Cortex of Suicide Subjects. *Am J Psychiatry,* 175**,** 262-274.

WANG, T., GUAN, W., LIN, J., BOUTAOUI, N., CANINO, G., LUO, J., CELEDON, J. C. & CHEN, W. 2015. A systematic study of normalization methods for Infinium 450K methylation data using whole-genome bisulfite sequencing data. *Epigenetics,* 10**,** 662-9.

WANG, T., PAN, Q., LIN, L., SZULWACH, K. E., SONG, C. X., HE, C., WU, H., WARREN, S. T., JIN, P., DUAN, R. & LI, X. 2012. Genome-wide DNA hydroxymethylation changes are associated with neurodevelopmental genes in the developing human cerebellum. *Hum Mol Genet,* 21**,** 5500-10.

WANG, Z., WU, X. & WANG, Y. 2018b. A framework for analyzing DNA methylation data from Illumina Infinium HumanMethylation450 BeadChip. *BMC Bioinformatics,* 19**,** 115.

WANNER, B., VITARO, F., TREMBLAY, R. E. & TURECKI, G. 2012. Childhood trajectories of anxiousness and disruptiveness explain the association between early-life adversity and attempted suicide. *Psychol Med,* 42**,** 2373-82.

WARD, M. S. 1999. The use of flow cytometry in the diagnosis and monitoring of malignant hematological disorders. *Pathology,* 31**,** 382-92.

WATSON, C. T., ROUSSOS, P., GARG, P., HO, D. J., AZAM, N., KATSEL, P. L., HAROUTUNIAN, V. & SHARP, A. J. 2016. Genome-wide DNA methylation profiling in the superior temporal gyrus reveals epigenetic signatures associated with Alzheimer's disease. *Genome Med,* 8**,** 5.

WEAVER, I. C., CERVONI, N., CHAMPAGNE, F. A., D'ALESSIO, A. C., SHARMA, S., SECKL, J. R., DYMOV, S., SZYF, M. & MEANEY, M. J. 2004. Epigenetic programming by maternal behavior. *Nat Neurosci,* 7**,** 847-54.

WEAVER, I. C., CHAMPAGNE, F. A., BROWN, S. E., DYMOV, S., SHARMA, S., MEANEY, M. J. & SZYF, M. 2005. Reversal of maternal programming of stress responses in adult offspring through methyl supplementation: altering epigenetic marking later in life. *J Neurosci,* 25**,** 11045-54.

WEGNER, M. 2008. A matter of identity: transcriptional control in oligodendrocytes. *J Mol Neurosci,* 35**,** 3-12.

WEIDER, M., REIPRICH, S. & WEGNER, M. 2013. Sox appeal - Sox10 attracts epigenetic and transcriptional regulators in myelinating glia. *Biol Chem,* 394**,** 1583-93.

WEIGHTMAN POTTER, P. G., VLACHAKI WALKER, J. M., ROBB, J. L., CHILTON, J. K., WILLIAMSON, R., RANDALL, A. D., ELLACOTT, K. L. J. & BEALL, C. 2019. Basal fatty acid oxidation increases after recurrent low glucose in human primary astrocytes. *Diabetologia,* 62**,** 187-198.

WELCH, J. D., KOZAREVA, V., FERREIRA, A., VANDERBURG, C., MARTIN, C. & MACOSKO, E. Z. 2019. Single-Cell Multi-omic Integration Compares and Contrasts Features of Brain Cell Identity. *Cell,* 177**,** 1873-1887 e17.

WERNER, H. B., KUHLMANN, K., SHEN, S., UECKER, M., SCHARDT, A., DIMOVA, K., ORFANIOTOU, F., DHAUNCHAK, A., BRINKMANN, B. G., MOBIUS, W., GUARENTE, L., CASACCIA-BONNEFIL, P., JAHN, O. & NAVE, K. A. 2007. Proteolipid protein is required for transport of sirtuin 2 into CNS myelin. *J Neurosci,* 27**,** 7717-30.

WES, P. D., HOLTMAN, I. R., BODDEKE, E. W., MOLLER, T. & EGGEN, B. J. 2016. Next generation transcriptomics and genomics elucidate biological complexity of microglia in health and disease. *Glia,* 64**,** 197-213.

WHITNALL, M. H. 1993. Regulation of the hypothalamic corticotropin-releasing hormone neurosecretory system. *Prog Neurobiol,* 40**,** 573-629.

WIEDERMANN, C. J. 2000. Secretoneurin: a functional neuropeptide in health and disease. *Peptides,* 21**,** 1289-98.

WILCOX, J. T., LAI, J. K., SEMPLE, E., BRISSON, B. A., GARTLEY, C., ARMSTRONG, J. N. & BETTS, D. H. 2011. Synaptically-competent neurons derived from canine embryonic stem cells by lineage selection with EGF and Noggin. *PLoS One,* 6**,** e19768.

WILHELM-BENARTZI, C. S., KOESTLER, D. C., KARAGAS, M. R., FLANAGAN, J. M., CHRISTENSEN, B. C., KELSEY, K. T., MARSIT, C. J., HOUSEMAN, E. A. & BROWN, R. 2013. Review of processing and analysis methods for DNA methylation array data. *Br J Cancer,* 109**,** 1394-402.

WILKERSON, M. J. 2012. Principles and applications of flow cytometry and cell sorting in companion animal medicine. *Vet Clin North Am Small Anim Pract,* 42**,** 53-71.

WILLOUR, V. L., SEIFUDDIN, F., MAHON, P. B., JANCIC, D., PIROOZNIA, M., STEELE, J., SCHWEIZER, B., GOES, F. S., MONDIMORE, F. M., MACKINNON, D. F., BIPOLAR GENOME STUDY, C., PERLIS, R. H., LEE, P. H., HUANG, J., KELSOE, J. R., SHILLING, P. D., RIETSCHEL, M., NOTHEN, M., CICHON, S., GURLING, H., PURCELL, S., SMOLLER, J. W., CRADDOCK, N., DEPAULO, J. R., JR., SCHULZE, T. G., MCMAHON, F. J., ZANDI, P. P. & POTASH, J. B. 2012. A genome-wide association study of attempted suicide. *Mol Psychiatry,* 17**,** 433-44.

WISNIEWSKI, A., MATUSIAK, L., SZCZERKOWSKA-DOBOSZ, A., NOWAK, I. & KUSNIERCZYK, P. 2018. HLA-C*06:02-independent, gender-related association of PSORS1C3 and PSORS1C1/CDSN single-nucleotide polymorphisms with risk and severity of psoriasis. *Mol Genet Genomics,* 293**,** 957-966.

WOCKNER, L. F., MORRIS, C. P., NOBLE, E. P., LAWFORD, B. R., WHITEHALL, V. L., YOUNG, R. M. & VOISEY, J. 2015. Brain-specific epigenetic markers of schizophrenia. *Transl Psychiatry,* 5**,** e680.

WOJTKOWIAK, J. W., ROTHBERG, J. M., KUMAR, V., SCHRAMM, K. J., HALLER, E., PROEMSEY, J. B., LLOYD, M. C., SLOANE, B. F. & GILLIES, R. J. 2012. Chronic autophagy is a cellular adaptation to tumor acidic pH microenvironments. *Cancer Res,* 72**,** 3938-47.

WOLF, S. A., BODDEKE, H. W. & KETTENMANN, H. 2017. Microglia in Physiology and Disease. *Annu Rev Physiol,* 79**,** 619-643.

WONG, C. C., MEABURN, E. L., RONALD, A., PRICE, T. S., JEFFRIES, A. R., SCHALKWYK, L. C., PLOMIN, R. & MILL, J. 2014. Methylomic analysis of monozygotic twins discordant for autism spectrum disorder and related behavioural traits. *Mol Psychiatry,* 19**,** 495-503.

WORLD HEALTH ORGANIZATION. 2017. Available: http://www.who.int/news-room/fact-sheets/detail/suicide [Accessed].

WRIGHT, C., ROSS, D. A. & WEINBERGER, D. R. 2018. Small RNAs May Answer Big Questions in Mental Illness. *Biol Psychiatry,* 83**,** e1-e3.

WU, A. R., NEFF, N. F., KALISKY, T., DALERBA, P., TREUTLEIN, B., ROTHENBERG, M. E., MBURU, F. M., MANTALAS, G. L., SIM, S., CLARKE, M. F. & QUAKE, S. R. 2014. Quantitative assessment of single-cell RNA-sequencing methods. *Nat Methods,* 11**,** 41-6.

WU, S. C. & ZHANG, Y. 2010. Active DNA demethylation: many roads lead to Rome. *Nat Rev Mol Cell Biol,* 11**,** 607-20.

XIE, Y., HUANG, D., WEI, L. & LUO, X. J. 2018. Further evidence for the genetic association between CACNA1I and schizophrenia. *Hereditas,* 155**,** 16.

XIN, H., KATAKOWSKI, M., WANG, F., QIAN, J. Y., LIU, X. S., ALI, M. M., BULLER, B., ZHANG, Z. G. & CHOPP, M. 2017. MicroRNA cluster miR-17-92 Cluster in Exosomes Enhance Neuroplasticity and Functional Recovery After Stroke in Rats. *Stroke,* 48**,** 747-753.

XIN, Y., O'DONNELL, A. H., GE, Y., CHANRION, B., MILEKIC, M., ROSOKLIJA, G., STANKOV, A., ARANGO, V., DWORK, A. J., GINGRICH, J. A. & HAGHIGHI, F. G. 2011. Role of CpG context and content in evolutionary signatures of brain DNA methylation. *Epigenetics,* 6**,** 1308-18.

XU, B., KARAYIORGOU, M. & GOGOS, J. A. 2010. MicroRNAs in psychiatric and neurodevelopmental disorders. *Brain Res,* 1338**,** 78-88.

XUE, H., LIU, J., SHI, L. & YANG, H. 2020. Overexpressed microRNA-539-5p inhibits inflammatory response of neurons to impede the progression of cerebral ischemic injury by histone deacetylase 1. *Am J Physiol Cell Physiol,* 319**,** C381-C391.

YAMADA, K., HATTORI, E., IWAYAMA, Y., TOYOTA, T., IWATA, Y., SUZUKI, K., KIKUCHI, M., HASHIMOTO, T., KANAHARA, N., MORI, N. & YOSHIKAWA, T. 2015. Population-dependent contribution of the major histocompatibility complex region to schizophrenia susceptibility. *Schizophr Res,* 168**,** 444-9.

YAMADA, K., IWAYAMA, Y., HATTORI, E., IWAMOTO, K., TOYOTA, T., OHNISHI, T., OHBA, H., MAEKAWA, M., KATO, T. & YOSHIKAWA, T. 2011. Genome-wide association study of schizophrenia in Japanese population. *PLoS One,* 6**,** e20468.

YAMAGUCHI, S., HONG, K., LIU, R., SHEN, L., INOUE, A., DIEP, D., ZHANG, K. & ZHANG, Y. 2012. Tet1 controls meiosis by regulating meiotic gene expression. *Nature,* 492**,** 443-7.

YANG, C. P., LI, X., WU, Y., SHEN, Q., ZENG, Y., XIONG, Q., WEI, M., CHEN, C., LIU, J., HUO, Y., LI, K., XUE, G., YAO, Y. G., ZHANG, C., LI, M., CHEN, Y. & LUO, X. J. 2018. Comprehensive integrative analyses identify GLT8D1 and CSNK2B as schizophrenia risk genes. *Nat Commun,* 9**,** 838.

YANG, F., GUAN, Y., FENG, X., ROLFS, A., SCHLUTER, H. & LUO, J. 2019. Proteomics of the corpus callosum to identify novel factors involved in hypomyelinated Niemann-Pick Type C disease mice. *Mol Brain,* 12**,** 17.

YANG, N., ZUCHERO, J. B., AHLENIUS, H., MARRO, S., NG, Y. H., VIERBUCHEN, T., HAWKINS, J. S., GEISSLER, R., BARRES, B. A. & WERNIG, M. 2013. Generation of oligodendroglial cells by direct lineage conversion. *Nat Biotechnol,* 31**,** 434-9.

YANG, Y., VIDENSKY, S., JIN, L., JIE, C., LORENZINI, I., FRANKL, M. & ROTHSTEIN, J. D. 2011. Molecular comparison of GLT1+ and ALDH1L1+ astrocytes in vivo in astroglial reporter mice. *Glia,* 59**,** 200-7.

YI, S., LONG, F., CHENG, J. & HUANG, D. 2017. An optimized rapid bisulfite conversion method with high recovery of cell-free DNA. *BMC Mol Biol,* 18**,** 24.

YILDIZ, M., ORAK, U., WALKER, M. H. & SOLAKOGLU, O. 2019. Suicide contagion, gender, and suicide attempts among adolescents. *Death Stud,* 43**,** 365-371.

YODER, J. A., WALSH, C. P. & BESTOR, T. H. 1997. Cytosine methylation and the ecology of intragenomic parasites. *Trends Genet,* 13**,** 335-40.

YOKOTA, N., ARUGA, J., TAKAI, S., YAMADA, K., HAMAZAKI, M., IWASE, T., SUGIMURA, H. & MIKOSHIBA, K. 1996. Predominant expression of human zic in cerebellar granule cell lineage and medulloblastoma. *Cancer Res,* 56**,** 377-83.

YONG, W. S., HSU, F. M. & CHEN, P. Y. 2016. Profiling genome-wide DNA methylation. *Epigenetics Chromatin,* 9**,** 26.

YOSHIKAWA, F., SATO, Y., TOHYAMA, K., AKAGI, T., HASHIKAWA, T., NAGAKURA-TAKAGI, Y., SEKINE, Y., MORITA, N., BABA, H., SUZUKI, Y., SUGANO, S., SATO, A. & FURUICHI, T. 2008. Opalin, a transmembrane sialylglycoprotein located in the central nervous system myelin paranodal loop membrane. *J Biol Chem,* 283**,** 20830-40.

YOSHINO, Y. & DWIVEDI, Y. 2020. Non-Coding RNAs in Psychiatric Disorders and Suicidal Behavior. *Front Psychiatry,* 11**,** 543893.

YOSHINO, Y., ROY, B. & DWIVEDI, Y. 2020. Differential and unique patterns of synaptic miRNA expression in dorsolateral prefrontal cortex of depressed subjects. *Neuropsychopharmacology*.

YOUN, A. & WANG, S. 2018. The MiAge Calculator: a DNA methylation-based mitotic age calculator of human tissue types. *Epigenetics,* 13**,** 192-206.

YU, G., WANG, L. G. & HE, Q. Y. 2015a. ChIPseeker: an R/Bioconductor package for ChIP peak annotation, comparison and visualization. *Bioinformatics,* 31**,** 2382-3.

YU, M., HON, G. C., SZULWACH, K. E., SONG, C. X., ZHANG, L., KIM, A., LI, X., DAI, Q., SHEN, Y., PARK, B., MIN, J. H., JIN, P., REN, B. & HE, C. 2012. Base-resolution analysis of 5-hydroxymethylcytosine in the mammalian genome. *Cell,* 149**,** 1368-80.

YU, P., MCKINNEY, E. C., KANDASAMY, M. M., ALBERT, A. L. & MEAGHER, R. B. 2015b. Characterization of brain cell nuclei with decondensed chromatin. *Dev Neurobiol,* 75**,** 738-56.

YUAN, J. H., YANG, F., CHEN, B. F., LU, Z., HUO, X. S., ZHOU, W. P., WANG, F. & SUN, S. H. 2011. The histone deacetylase 4/SP1/microrna-200a regulatory network contributes to aberrant histone acetylation in hepatocellular carcinoma. *Hepatology,* 54**,** 2025-35.

YUAN, V., PRICE, E. M., DEL GOBBO, G., MOSTAFAVI, S., COX, B., BINDER, A. M., MICHELS, K. B., MARSIT, C. & ROBINSON, W. P. 2019. Accurate ethnicity prediction from placental DNA methylation data. *Epigenetics Chromatin,* 12**,** 51.

ZARATIEGUI, M., IRVINE, D. V. & MARTIENSSEN, R. A. 2007. Noncoding RNAs and gene silencing. *Cell,* 128**,** 763-76.

ZASTROZHIN, SMIRNOV, PETUKHOV, PANKRATENKO, ZASTROZHINA, GRISHINA, RYZHIKOVA, BURE, SKRYABIN, VLASOVSKIH, BRYUN & SYCHEV 2020. The Influence of Concentration of Micro-RNA hsa-miR-370-3p and CYP2D6*4 on Equilibrium Concentration of Mirtazapine in Patients With Major Depressive Disorder. *Psychopharmacol Bull,* 50**,** 58-75.

ZENG, W., CHEN, X., DUREN, Z., WANG, Y., JIANG, R. & WONG, W. H. 2019. DC3 is a method for deconvolution and coupled clustering from bulk and single-cell genomics data. *Nat Commun,* 10**,** 4613.

ZHAN, Y., PAOLICELLI, R. C., SFORAZZINI, F., WEINHARD, L., BOLASCO, G., PAGANI, F., VYSSOTSKI, A. L., BIFONE, A., GOZZI, A., RAGOZZINO, D. & GROSS, C. T. 2014. Deficient neuron-microglia signaling results in impaired functional brain connectivity and social behavior. *Nat Neurosci,* 17**,** 400-6.

ZHANG, B., GAITERI, C., BODEA, L. G., WANG, Z., MCELWEE, J., PODTELEZHNIKOV, A. A., ZHANG, C., XIE, T., TRAN, L., DOBRIN, R., FLUDER, E., CLURMAN, B., MELQUIST, S., NARAYANAN, M., SUVER, C., SHAH, H., MAHAJAN, M., GILLIS, T., MYSORE, J., MACDONALD, M. E., LAMB, J. R., BENNETT, D. A., MOLONY, C., STONE, D. J., GUDNASON, V., MYERS, A. J., SCHADT, E. E., NEUMANN, H., ZHU, J. & EMILSSON, V. 2013a. Integrated systems approach identifies genetic nodes and networks in late-onset Alzheimer's disease. *Cell,* 153**,** 707-20.

ZHANG, D., CHENG, L., BADNER, J. A., CHEN, C., CHEN, Q., LUO, W., CRAIG, D. W., REDMAN, M., GERSHON, E. S. & LIU, C. 2010. Genetic control of individual differences in gene-specific methylation in human brain. *Am J Hum Genet,* 86**,** 411-9.

ZHANG, H., ZHANG, P., MA, K. J., LV, Y. H., LI, W. C., LUO, C. L., LI, L. L., SHEN, Y. W., HE, M., JIANG, J. Q. & CHEN, L. 2013b. The selection of endogenous genes in human postmortem tissues. *Sci Justice,* 53**,** 115-20.

ZHANG, L., LU, X., LU, J., LIANG, H., DAI, Q., XU, G. L., LUO, C., JIANG, H. & HE, C. 2012. Thymine DNA glycosylase specifically recognizes 5-carboxylcytosine-modified DNA. *Nat Chem Biol,* 8**,** 328-30.

ZHANG, L., VERWER, R. W. H., LUCASSEN, P. J., HUITINGA, I. & SWAAB, D. F. 2020. Prefrontal cortex alterations in glia gene expression in schizophrenia with and without suicide. *J Psychiatr Res,* 121**,** 31-38.

ZHANG, T. Y. & MEANEY, M. J. 2010. Epigenetics and the environmental regulation of the genome and its function. *Annu Rev Psychol,* 61**,** 439-66, C1-3.

ZHANG, Y., CHEN, K., SLOAN, S. A., BENNETT, M. L., SCHOLZE, A. R., O'KEEFFE, S., PHATNANI, H. P., GUARNIERI, P., CANEDA, C., RUDERISCH, N., DENG, S., LIDDELOW, S. A., ZHANG, C., DANEMAN, R., MANIATIS, T., BARRES, B. A. & WU, J. Q. 2014. An RNA-sequencing transcriptome and splicing database of glia, neurons, and vascular cells of the cerebral cortex. *J Neurosci,* 34**,** 11929-47.

ZHANG, Y., SLOAN, S. A., CLARKE, L. E., CANEDA, C., PLAZA, C. A., BLUMENTHAL, P. D., VOGEL, H., STEINBERG, G. K., EDWARDS, M. S., LI, G., DUNCAN, J. A., 3RD, CHESHIER, S. H., SHUER, L. M., CHANG, E. F., GRANT, G. A., GEPHART, M. G. & BARRES, B. A. 2016. Purification and Characterization of Progenitor and Mature Human Astrocytes Reveals Transcriptional and Functional Differences with Mouse. *Neuron,* 89**,** 37-53.

ZHENG, S. C., BECK, S., JAFFE, A. E., KOESTLER, D. C., HANSEN, K. D., HOUSEMAN, A. E., IRIZARRY, R. A. & TESCHENDORFF, A. E. 2017. Correcting for cell-type heterogeneity in epigenome-wide association studies: revisiting previous analyses. *Nat Methods,* 14**,** 216-217.

ZHOU, B., ZUO, Y. X. & JIANG, R. T. 2019a. Astrocyte morphology: Diversity, plasticity, and role in neurological diseases. *CNS Neurosci Ther,* 25**,** 665-673.

ZHOU, K., GAULLIER, G. & LUGER, K. 2019b. Nucleosome structure and dynamics are coming of age. *Nat Struct Mol Biol,* 26**,** 3-13.

ZHOU, N., LIU, K., SUN, Y., CAO, Y. & YANG, J. 2019c. Transcriptional mechanism of IRF8 and PU.1 governs microglial activation in neurodegenerative condition. *Protein Cell,* 10**,** 87-103.

ZHOU, W., LAIRD, P. W. & SHEN, H. 2017. Comprehensive characterization, annotation and innovative use of Infinium DNA methylation BeadChip probes. *Nucleic Acids Res,* 45**,** e22.

ZHOU, Y., LUTZ, P. E., WANG, Y. C., RAGOUSSIS, J. & TURECKI, G. 2018. Global long non-coding RNA expression in the rostral anterior cingulate cortex of depressed suicides. *Transl Psychiatry,* 8**,** 224.

ZHU, J., ADLI, M., ZOU, J. Y., VERSTAPPEN, G., COYNE, M., ZHANG, X., DURHAM, T., MIRI, M., DESHPANDE, V., DE JAGER, P. L., BENNETT, D. A., HOUMARD, J. A., MUOIO, D. M., ONDER, T. T., CAMAHORT, R., COWAN, C. A., MEISSNER, A., EPSTEIN, C. B., SHORESH, N. & BERNSTEIN, B. E. 2013. Genome-wide chromatin state transitions associated with developmental and environmental cues. *Cell,* 152**,** 642-54.

ZILLER, M. J., HANSEN, K. D., MEISSNER, A. & ARYEE, M. J. 2015. Coverage recommendations for methylation analysis by whole-genome bisulfite sequencing. *Nat Methods,* 12**,** 230-2, 1 p following 232.

ZRZAVY, T., HAMETNER, S., WIMMER, I., BUTOVSKY, O., WEINER, H. L. & LASSMANN, H. 2017. Loss of 'homeostatic' microglia and patterns of their activation in active multiple sclerosis. *Brain,* 140**,** 1900-1913.

ZUCHERO, J. B. & BARRES, B. A. 2013. Intrinsic and extrinsic control of oligodendrocyte development. *Curr Opin Neurobiol,* 23**,** 914-20.

ZUO, X., SHENG, J., LAU, H. T., MCDONALD, C. M., ANDRADE, M., CULLEN, D. E., BELL, F. T., IACOVINO, M., KYBA, M., XU, G. & LI, X. 2012. Zinc finger protein ZFP57 requires its co-factor to recruit DNA methyltransferases and maintains DNA methylation imprint in embryonic stem cells via its transcriptional repression domain. *J Biol Chem,* 287**,** 2107-18.

ZYMO RESEARCH Direct-zol™ RNA Microprep User Guide. https://files.zymoresearch.com/protocols/_r2060_r2061_r2062_r2063_direct-zol_rna_microprep.pdf.

Appendix A

Deciphering the Epigenetic Landscape of Suicidal Behaviour: A Review of Current Findings, Caveats and Future Directions

Review

Deciphering the Epigenetic Landscape of Suicidal Behaviour: A Review of Current Findings, Caveats and Future Directions

Stefania Policicchio [1, *], Emma L Dempster [1, †], Therese M Murphy [1, †]

1. University of Exeter Medical School, Barrack Road, EX2 5DW, Exeter, UK; E-Mails: S.policicchio@exeter.ac.uk; E.L.Dempster@exeter.ac.uk; T.Murphy@exeter.ac.uk

† These authors contributed equally to this work.

* **Correspondence:** Stefania Policicchio; E-Mail: S.policicchio@exeter.ac.uk

Abstract

Suicide is the second leading cause of death globally among young people and the tenth leading cause of death across all ages. Approximately 800,000 people die by suicide every year representing a significant global health burden. Despite this burden, the molecular pathology of suicide remains poorly understood. A number of recent studies have shown that epigenetic alterations are associated with suicidal behaviour. These epigenetic mechanisms, which act to regulate gene expression via modifications to DNA, histone proteins and chromatin, change with age and in response to specific environmental and psychosocial factors —providing a mechanism for the interaction between genotype and the environment. The present review briefly outlines the main epigenetic mechanisms involved in gene regulation and discusses recent findings of epigenetic alterations in suicidal behaviour, their caveats and the future direction of this emerging field of research.

1. Introduction

Suicide is a serious public health problem that can have lasting harmful effects on individuals, families, and communities [1]. Suicide is the second leading cause of death among 15–29 year olds worldwide and ranks amongst the 20th leading causes of death across all ages [2]. Approximately 800,000 people die by suicide every year [2] representing a significant global health burden. Suicidal behaviour (SB) spans a spectrum ranging from suicidal ideation (SI) to suicide attempt (SA) and completed suicide [3, 4]. Up to one-third of individuals with SI have a SA within 1 year; individuals who have had a SA have 1.6% risk of suicide within the year [5]. Despite its economic and social burden, the underlying aetiology of SB remains poorly understood. Genetic epidemiological studies have found evidence of family clustering of SB and have highlighted a clear genetic susceptibility to SB [6, 7] with heritability estimates ranging from 30-50% [8-10]. A significant proportion of the heritability for SB and SA appears to be independent of psychiatric diseases as when the heritability of SA is corrected for transmission of psychiatric disorders, specific heritability is between 17% and 36% [8, 11-15].

Pre-existing knowledge of biological systems likely to be associated with SB, such as serotonergic neurotransmission and neurotrophic factors, resulted in several candidate-gene association studies [7, 14-17] which have largely yielded inconsistent results. Similarly, large-scale genome-wide association studies (GWAS) [18-20] have failed to identify robust associations suggesting that the risk of SB is highly polygenic in nature and that individual gene variants are likely to account only for a very small proportion of the total phenotypic variability. Other factors, such as the environment, behavioural traits, lifestyle and coping mechanisms, are essential regulators of suicide risk and likely to account for more sizeable effects [21]. Recently, increased understanding of epigenetic processes that occur in the brain has opened promising avenues in suicide research. The epigenome is potentially malleable—changing with age [22] and in response to specific environmental [23] and psychosocial factors [24] —providing a mechanism for the interaction between genotype and the environment [25]. Epigenetic processes, including DNA methylation, have recently been implicated in the aetiology of numerous mental health disorders [26-33] and SB [34, 35]. The present review will briefly introduce epigenetic mechanisms, focussing primarily on DNA methylation, histone modifications and non-coding RNAs and explore their relevance to suicide and SB, before discussing future directions and caveats of this emerging field of research and its potential to further our understanding of SB.

1.1 Beyond Genome-Wide Association Studies: a Role for Epigenetic Variation in Suicide and SB

The term epigenetics, literally meaning 'above' genetics, was originally coined to refer to the study of any potentially stable and heritable changes in gene expression or cellular phenotype that occurs without changes in Watson–Crick base-pairing of DNA [36]. However, the epigenome, which is the chemical structure surrounding our genome, can alter the function of our genes in response to the environment [37], and remains dynamic throughout life [37-39].

Epigenetic variation is regulated in a tissue-specific manner by stochastic, genetic and environmental factors [40]. In the brain, epigenetic variation is thought to influence the gene

expression profile of neurons and glial cells [41, 42]. Therefore it is possible that alterations of epigenetic profiles in the brain may induce long-term behavioural consequences. As such they have the potential to play a crucial role in determining predisposition to SB [43]. The most commonly studied epigenetic mechanisms that can influence gene expression are: molecular modifications of the DNA sequence, post-translational histone modifications and non-coding RNA gene silencing [44].
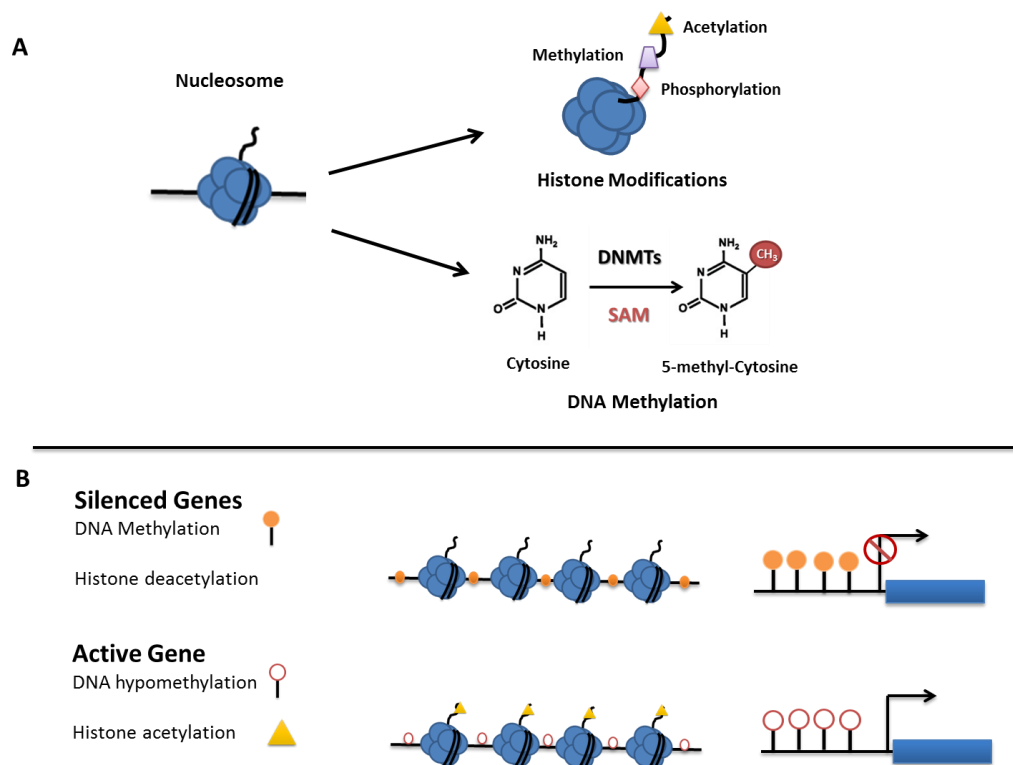
1.2 DNA Modifications

DNA methylation is the covalent modification at the C5 carbon of cytosine residues, occurring mainly at CG dinucleotides (CpG) (See Figure 1). In somatic cells, approximately 80% of CpGs are methylated [45]; the remaining unmethylated CpGs tend to be concentrated around gene promoters (CpG islands) [37]. A Recent study has reported 5-methyl cytosine (5mC) to be central to the establishment of tissue-specific gene expression, cell differentiation, genomic imprinting, and X-inactivation [46]. When found in promoter regions of genes, CpG methylation is generally associated with transcriptional repression or downregulation of RNA transcription [47]. However, DNA methylation has also been described in other regions of the genome and the transcriptional effect in those areas is not consistent [24]. Previous research has suggested a role for global DNA methylation as a potential marker of suicide risk. A significantly higher level of global methylation (5mC %) has been reported in peripheral blood of psychiatric patients with a history of SA when compared with psychiatric controls [35]. Similarly, an increase in DNA methylation in the brain region BA47 was found to be 8 times greater in the group who died by suicide relative to controls [44]. Taken together these findings, although requiring further replication, suggest that global DNA methylation may be a biomarker of suicide risk in psychiatric patients and support the idea that blood tissue may be reasonably considered a valid proxy to monitor brain changes.

Although DNA methylation has been considered as a stable epigenetic mark, studies in the past decade have revealed that this modification is not as static as once thought. Recently, research has provided evidence that 5mC can be oxidized to 5-hydroxymethylcytosine (5hmC) in a reaction catalysed by the ten–eleven translocation (TET) enzymes [48-50] along with two other oxidative products: 5-formylcytosine (5fC) and 5-carboxylcytosine (5caC). Growing evidence suggests that these demethylation states may play an important biological role [51, 52].

1.3 Histone Modifications

Chromatin exists as two functional structures: euchromatin which is the ''opened'' state associated with gene transcription and heterochromatin which is the ''closed'' state associated with gene silencing. Proteins forming this complex structure are called histones (H2A, H2B, H3, and H4). These globular proteins, with a tail of amino-acids, can be covalently modified by the addition or the removal of chemical groups at specific residues on their N-terminus tails (See Figure 1) [37]. Histone modifications are able to alter the access of transcriptional machinery to the DNA by modifying the condensation of chromatin [37]. Although there are several molecular modifications histone acetylation/deacetylation and methylation are the two most commonly studied.

Studies examining the role of histone modifications in SB are limited to the study of candidate genes [53, 54], thus genome-wide approaches have not yet been undertaken.

Figure 1 Epigenetic modifications and transcriptional regulation. (A) Figure illustrates common modifications that occur on the tails of histone proteins and the conversion of Cytosine to 5-methyl-Cytosine by a group of enzymes called DNA methyltransferases (DNMTs) and S-Adenosyl-L-methionine (SAM). (B) Transcriptionally inactive genes are generally characterised by DNA Methylation at CpG dinucleotides in the promoter region of genes and histone deacetylation. In contrast, transcriptionally active genes are generally characterised by absence of DNA methylation (DNA hypomethylation) and histone acetylation.

1.4 Non-Coding RNAs

Another mechanism of epigenetic regulation of gene expression is mediated by non-coding RNAs (ncRNAs), functional RNA molecules that are transcribed from DNA but not translated into proteins. These regulatory RNAs function to regulate gene expression at the transcriptional and post-transcriptional level. Several classes of ncRNAs exist, including microRNAs (miRNAs), short interfering RNAs (siRNAs), and piwi-interacting RNAs (piRNAs) also referred to as short ncRNAs (<30 nts) to distinguish them from the long non-coding RNAs (lncRNAs) (>200 nts). Both major groups are shown to play a role in heterochromatin formation, histone modification, DNA methylation targeting and gene silencing [55]. To date, miRNAs are the best characterised ncRNA group. They act as regulators of gene expression and protein translation in many tissues, including brain, by binding to the target mRNA and contributing to its degradation through the RNA-induced silencing complex (RISC) complex or by directly inhibiting translation [56]. MiRNAs are known to play a critical role in developmental processes, including neurodevelopment and synaptic plasticity and they have been implicated in the pathogenesis of various neuropsychiatric disorders like schizophrenia, major depression and bipolar disorders [55-58]. The specific dysregulation of miRNA function in suicide is just beginning to be appreciated, as recently reviewed [56].

Cataloguing the expression of miRNAs and additional small RNAs in healthy human brain as well as in major neuropsychiatric diseases and suicide may lead to new therapeutic targets and insight into disease aetiology [55].

LncRNAs represent another interesting class as they are enriched for expression in the brain [59] and are developmentally regulated [60] but less evolutionarily conserved than other RNA species. Although preclinical studies have begun to unravel how lncRNAs may contribute to emotional control [61], their role in SB is currently unknown.

2. Common Neurobiological Pathways Epigenetically Dysregulated in Suicide

In the last decade, understanding the role of epigenetic mechanisms in SB has implicated the role of key biological pathways, including hypothalamic pituitary adrenal (HPA) axis, stress response, polyamine system, neurotrophic signalling and lipid metabolism. A comprehensive overview of genes epigenetically dysregulated in suicide and SB is reported in Table 1 and Table 2. Common pathways frequently targeted by epigenetic and miRNA dysregulation are illustrated in Figure 2 and discussed in detail below.
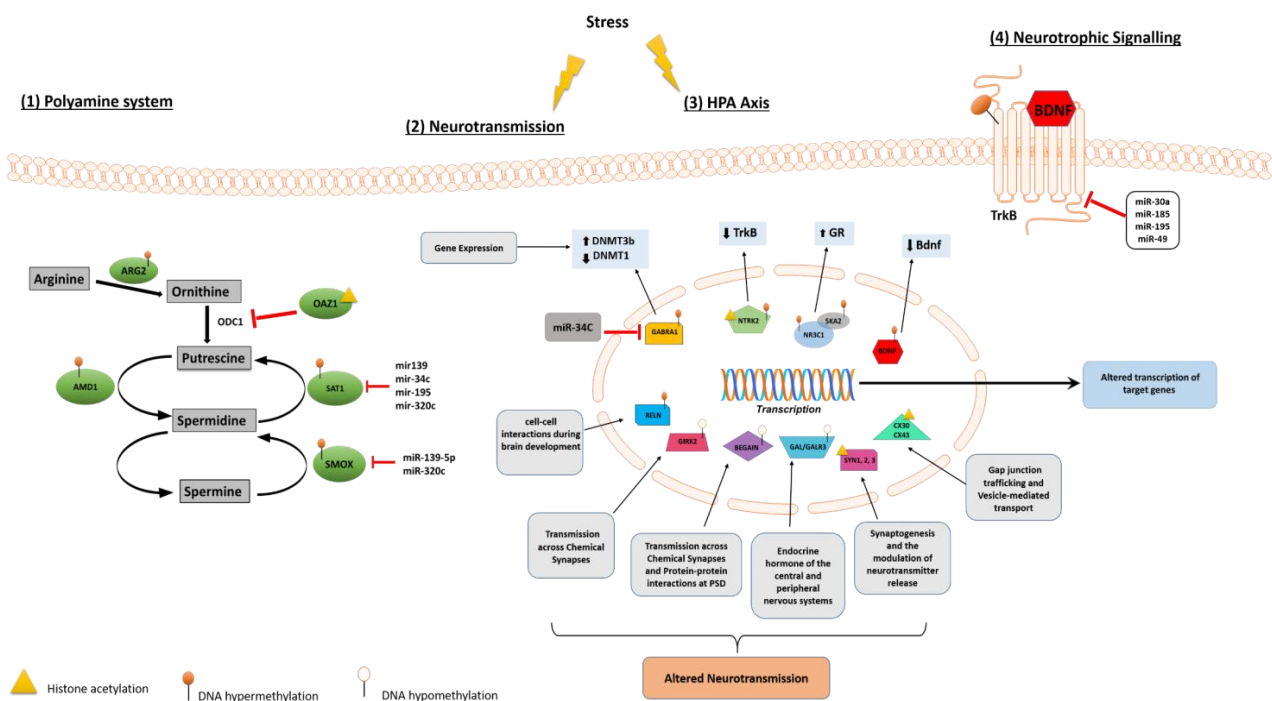
Figure 2 Molecular pathways involved in suicide behaviour. (1) Polyamine system: several enzymes involved in the regulation of polyamine intracellular concentration exhibit epigenetic regulatory mechanisms in suicide through DNA methylation (*AMD1, ARG2*), histone methylation (*OAZ1*) and/or post-translational mechanisms (*SAT1, SMOX*) as miRNAs regulation. (2) Neurotransmission: many genes known to play a key role at chemical and/or electrical synapses have been reported as hypomethylated (*BEGAIN, GIRK2, GALR3*), hypermethylated (*RELN*) or histone methylated (*SYN1-3, CX30, CX43*) in suicide cases compared to healthy controls suggesting that neurotransmission may be compromised in suicide. (3) HPA axis: two genes differentially involved in cortisol release following stress (*NR3C1, SKA2*) have been

found to be both significantly hypermethylated in suicide cases relative to controls supporting the hypothesis of suicide-associated HPA axis dysregulation. (4) Neurotrophic Signalling: several studies examining *BDNF* and *TrkB* in post-mortem suicide brains revealed distinct epigenetic regulation pattern for these two genes: the receptor TrkB seems to be regulated via miRNAs (miR-30a, miR-185, miR-195 and miR-49) and histone acetylation while the expression levels of the neurotrophin Bdnf correlate with DNA hypermethylation in the promoter region of the gene.

2.1 HPA Stress Axis

It is well established that perturbations in the HPA axis are associated with the pathophysiology of suicide [62]. The HPA axis is a neuroendocrine system, key regulator of cortisol release and the stress response [63]. Research has shown that the HPA axis may be epigenetically programmed by the early-life environment [64]. Several HPA-axis coupled genes have been identified over the years: corticotropin releasing hormone (*CRH*), corticotropin releasing hormone binding protein (*CRHBP*), corticotropin releasing hormone receptor 1 (*CRHR1*), corticotropin releasing hormone receptor 2 (*CRHR2*), FK506-binding protein 51 (*FKBP5*) and the glucocorticoid receptor (*NR3C1*)[65].

More recently, a study aiming to identify DNA methylation shifts linked to severity of the SA in HPA-axis coupled genes was conducted in whole blood derived DNA. The authors reported reduced levels of DNA methylation at two loci within the *CRH* promoter in serious suicide attempters. Interestingly, significant blood-brain correlations in DNA methylation were also found suggesting that these alterations may impact on expression profile of *CRH* in the brain [65].

Glucocorticoids. Glucocorticoids play a crucial role in the maintenance and survival of neurons and in synaptic plasticity. A study examining the DNA methylation status of *GR* exon 1F variant in individuals who died by suicide and were severely abused during childhood observed increased DNA methylation at the *GR* promoter compared to suicide victims with no childhood abuse or controls [66]. Moreover, *GR* methylation status appears to regulate the binding of the *NGFI-A* transcription factor associated with the *GR* expression [66, 67]. The disrupted GR function may result in inadequate control of the HPA axis, possibly leading to hyperactive cortisol secretion and development of anxiety traits. In turn, anxiety mediates the relationship between the exposure to early life adversity (ELA) and SB [64],[68]. More recently, a study has suggested a role for dietary deficiencies in mediating the interaction between an altered GR system and SB. DNA methyltransferases catalyse the transfer of a methyl group from the methyl donor, s-adenoslymethionine (SAM), onto the 5C position of the dinucleotide sequence CG. However, the synthesis of SAM is dependent on the availability of dietary foliates, vitamin B12 and choline, suggesting an alternative mechanism to altering the expression of the *GRII* exon 17 promoter [69].

SKA2 - Altered microtubule binding. An exciting new candidate in the relationship between cortisol regulation and suicide is the spindle and kinetochore associated protein 2 (*SKA2*), a gene that has been implicated in GR signalling [70]. This microtubule binding protein is thought to interact with the HPA axis by chaperoning the GR from the cytoplasm to the nucleus upon cortisol binding [70]. Once in the nucleus, the GR can interact with genomic DNA and influence gene expression involved in negative feedback regulation of the HPA axis response. In 2014, a study identified site and allele-specific DNA methylation patterns in the *SKA2* gene, in particular

increased *SKA2* 3' untranslated region methylation and concomitantly decreased *SKA2* mRNA levels, were detected in the frontal cortex of suicide completers [71]. Further research found that *SKA2* DNA methylation predicted lifetime SA in saliva and blood in individuals suffering from post-traumatic stress disorder (PTSD) [72]. Higher DNA methylation at the same site and allele was also found to predict lower levels of miR-301a in the cortex of depressed suicide completers [73]. Since the expression of this miRNA is tied to *SKA2* expression, it was suggested as a proxy of suicide-associated *SKA2* decreases [55, 72]. Further support to these preliminary findings has been provided by more recent studies suggesting the influence of trauma exposure on *SKA2* DNA methylation as well as DNA methylation of the *SKA2* gene as a biomarker of suicide risk and stress-related psychopathology [74, 75].

2.2 Polyamine System and SAT1

The polyamine system is another stress response pathway which has been extensively characterized in relation to suicide risk. Polyamines, aliphatic compounds with multiple amine groups, have been implicated in regulation of gene expression at transcriptional and posttranscriptional levels, regulating the function of several neuromodulators and acting as neurotransmitters themselves [76, 77]. Involvement of epigenetic modifications in the regulation of genes associated with polyamine biosynthesis has been implicated in SB [78].

SAT1 is an enzyme involved in polyamine catabolism and is arguably one of the most consistently downregulated gene in depressed suicide completers [79-85]. A potential mechanism for *SAT1* downregulation is through epigenetic control, as studies have identified that *SAT1* promoter DNA methylation is inversely correlated with *SAT1* expression. Moreover, there is evidence for histone modifications affecting *SAT1* expression along with other key enzymes in polyamine synthesis [54, 78, 82] and that miRNAs can target polyamine transcripts, including *SAT1* [86]. *SAT1* has therefore emerged as a potential biomarker for suicide, topping the lists of candidate genes in several studies [84, 87, 88]. However, it is still unknown whether this gene is involved in major depressive disorder (MDD) independently of suicide, which isoforms are dysregulated and whether the gene undergoes differential splicing in suicide and depression [89].

The expression of several other polyamine-associated enzymes were found altered in the cortex of post-mortem suicide cases. The spermine oxidase (*SMOX*) gene, encoding for a catabolic enzyme, was found hypermethylated in the promoter region in the prefrontal cortex (PFC) of suicide subjects. However, there was no correlation between aberrant promoter DNA hypermethylation and gene expression changes [83]. Two studies have identified DNA hypomethylation at the promoter region of the arginase 2 (*ARG2*) and adenosylmethionine decarboxylase1 (*AMD1*) genes, which correlated with increased gene expression in suicide completers compared to controls [54, 78]. A different epigenetic modification showed to regulate the Ornithine Decarboxylase Antizyme 1 (*OAZ1*) gene, also involved in the intracellular regulation of the polyamine levels. Increased H3K4me3 levels in the promoter region of *OAZ1* were found in suicide completers and appeared to correlate with the expression of *OAZ1* and *ARG2* in Brodmann area 44 [54]. Taken together this research provides support for the involvement of epigenetic modifications in the regulation of genes associated with polyamine biosynthesis, which may play an important role in SB.

2.3 Neurotrophic Pathways - BDNF and NTRK2

Genome-wide DNA methylation studies in the brains of suicide completers indicates that suicide is associated with widespread changes in DNA methylation patterns of neurotrophic and neuroprotective factors in the hippocampus and PFC [40, 90]. Brain derived neurotrophic factor (BDNF) is a well-known receptor binding factor with growth factor activity; it is essential for the survival and plasticity of cortical and striatal neurons and it has been implicated in both stress response [17] and mood disorders [91]. Increased *BDNF* promoter/exon 4 DNA methylation has been reported in suicide brains [92], a finding that is consistent with those observed in depressed patients with a history of SA, or with SI during treatment with antidepressants [93]. Similarly, another study focusing on the Wernicke area of suicide subjects, reported a remarkable increase of DNA methylation at the *BDNF* promoter IV in suicide subjects with respect to controls [43]. Taken together this evidence suggest that *BDNF* DNA methylation status maybe a proxy marker for previous suicidal attempts and a clinical biomarker for poor treatment outcomes of SI in depression. However, larger studies are required to confirm these findings.

Interestingly, TrkB, main receptor of BDNF and encoded by the *NTRK2* gene, is also regulated through epigenetic changes that appear to have an impact on suicide risk. In brain tissue from individuals who died by suicide, mRNA expression of *Trk-BT1,* the astrocyte-enriched TrkB truncated variant, was found significantly decreased and correlated with increased DNA methylation at the *TrkB-T1* promoter suggesting that astrocytic dysfunction may occur in individuals who die by suicide [53, 94, 95].

3. Non-Coding RNAs and Their Role in SB

Recently, a number of studies have implicated a role for miRNA dysregulation in the pathogenesis of SB (see Table 2 for full list of suicide-associated miRNAs). Interestingly, some of the suicide-associated genes previously discussed as showing altered DNA methylation and/or histone modifications were found to be targets of differentially expressed miRNAs. For example, the expression levels of two genes involved in the polyamine metabolism (*SAT1* and *SMOX*) were found to be downregulated by overexpression of miRNAs (e.g. miR-139, miR-34c, miR-195, miR-320c) [86, 89] in suicide cases compared to controls. Similarly, miR-185, which is thought to regulate the *NTRK2* gene (TrkB receptor) is differentially expressed in the frontal cortex of suicide completers [96]. Furthermore, miR-185, together with miR-195 and miR-30a have been implicated in regulating the BDNF signalling pathway [56, 96, 97], a pathway widely reported as involved in SB. Taken together, these findings suggest a co-ordinated epigenetic and miRNA regulation of pathways relevant to SB.

Sun *et al*, implicated a role for notch signalling in SI in a study of miRNAs from peripheral blood leukocytes of Chinese MDD patients [98].The expression levels of two notch-associated miRNAs, miR-34b–5p and miR-369–3p, were found to be significantly lower in patients with SI relative to patients without SI [98]. Consistent with these results, expression levels of these miRNAs have been previously shown to be reduced in PFC of depressive suicidal patients compared to normal controls [73], highlighting the potential utility in examining changes in miRNA expression in blood in individuals with SB.

In addition to miRNAs, expression levels of lncRNAs have also been implicated in suicide. Recently, our group implicated a role for differential DNA methylation at the *PSORS1C3* locus, a

non-coding RNA, in the brains of suicide completers. Although the function of the *PSORS1C3* gene product remains unknown, it is thought to potentially regulate nearby genes (for example, *POU5F1* and *HLA-C*), suggesting a role in immune system regulation. Moreover, *PSORS1C3* is a known psoriasis susceptibility gene further supporting a role in immune system regulation [34]. Futhermore, a recent study identified six lncRNAs (see Table 2) whose expression was downregulated in peripheral blood samples of MDD patients with SI [99] . Finally, Punzi *et al* showed that the expression of an uncharacterized lncRNA, *LOC285758*, is significantly increased in violent suicide cases compared to non-violent suicide cases [100]. Interestingly, DNA methylation of an intragenic CpG island in the myristoylated alanine-rich protein kinase C substrate (*MARCKS*) gene, a gene previously reported [84] as potential blood biomarker for suicidality, was found to be associated with the expression of this lncRNA, suggesting that the previously reported *MARCKS* association with violent suicide involves regulation by LOC285758 expression. In conclusion, profiling ncRNAs can substantially contribute to our understanding of how gene expression networks are reorganized in suicide.

4. Current Methodological Caveats in Suicide Epigenetic Research

4.1 Phenotype Assessment

The wide range of phenotypes that may be considered in studies investigating SB further complicate identification of clear biological markers by hampering the comparability of studies, even among studies adopting similar approaches. SI and SA may at times be studied concurrently. These phenotypes are often considered to exist on a spectrum and, as a result, are frequently studied and reported on together in genetic and epigenetic studies. A genetic component has been demonstrated for SA and completed suicide but the role of genetics in SI is currently unclear [11]. Thus, it has been suggested to exclude SI from future SB epigenetic studies [3]. SA ranges from highly lethal, to low lethality for failed SA, and could be divided according to impulsive characteristics or chronic SA. However these two phenotypes, completed suicide and SA, are likely to only partly share underlying etiological and neurobiological mechanisms [101] suggesting therefore the need for a revised and more accurate definition of SA phenotype, which includes lethality, in order to ensure inter-study comparability. Finally, SB is generally a complication of a psychiatric disorders like MDD, schizophrenia and/or bipolar disorder. How to distinguish suicide diathesis-related epigenetic changes from those associated with mood disorders and other suicide-associated psychiatric diseases is a crucial issue. Future epigenetic studies need to examine potential SB-related epigenetic modification in a suicidal population with and without psychiatric disorder comorbidity.

4.2 Tissue Heterogeneity

Compared with genetic studies, epigenetics studies are constrained by several additional biological and methodological design issues. A major challenge that distinguishes epigenetic and genetic studies is the choice of tissue type [25]. In contrast to genetic studies, epigenetic marks are by definition tissue and cell type specific, thus tissue choice for epigenetic studies of complex traits, requires careful consideration [25]. As almost all tissues consist of multiple epigenetically distinct cell types, a major concern in epigenetic epidemiology studies is that any apparent

disease-associated epigenetic differences may simply reflect differences in cellular composition [25]. Furthermore, failure to account for this cellular heterogeneity could limit the power of epigenetic studies in complex phenotypes. For whole blood, routine cell counts [102] or the use of algorithms that can infer cellular composition from epigenomic data [103] can be applied to control for this variation statistically, and similar approaches have been developed for other heterogeneous tissues, such as the brain [104]. Approaches such as laser capture microdissection (LCM) or using fluorescence-activated cell sorting (FACS) have been recruited to detect disease-associated changes that are manifest in only a small subset of cells, which may not be detectable in analyses of whole tissue. However, manual sorting [105] and LCM [106] are useful for isolating small numbers of cells but do not provide enough material for epigenomic studies. FACS can isolate larger numbers of cells but may be challenging in tissues such as the adult brain, where cells are morphologically complex and densely interconnected. To overcome these challenges nuclei can be isolated from post-mortem tissue and then sorted using FACS for cell type specific epigenomic /transcriptomic studies [107-110]. However, FACS-sorted nuclei are fragile and difficult to concentrate into the small volumes that are optimal for chromatin assays or to keep intact for DNA methylation assays. Another major challenge is selecting nuclear expressed cell-type specific markers for sorting. Although several cell-specific markers have been identified and validated over the years, most of them are expressed in the cytoplasm or on the cellular membrane making them unsuitable for nuclei sorting. Neuronal nuclear antigen (NeuN) is commonly used as a robust marker of neurons and its application in flow cytometry analyses have been widely validated by several recent studies in mouse and human post-mortem brain samples [104, 111-114]. Although NeuN is specific to neurons, not all neurons express NeuN (e.g. cerebellar Purkinje neurons, olfactory bulb mitral cells, cortical Cajal-Retzius neurons, neurons of the inferior olive and dentate nuclei) [115, 116]. Moreover, no robust nuclear markers suitable for FACS are available to date for mature oligodendrocytes, astrocytes and microglia isolation from human brain tissue.

Further research aiming to identify new markers for nuclei labelling is needed to separate nuclei from different brain regions as well as different cell-types and neuronal sub-types unique to different cortical layers. This would empower research discoveries on nuclear changes occurring during disease progression, especially in rare but important populations, such as immune cell types present in the brain, which are thought to be critical in neuroprotective and neuroinflammatory processes [117].

4.3 True Methylation Assessment

5hmC plays a key role in the brain, where it is particularly abundant and dynamic during development [118, 119]. Current molecular approaches used to measure levels of DNA methylation (including sodium bisulphite conversion methods) do not distinguish between 5mC and 5hmC [120] suggesting that densely hydroxymethylated regions of DNA may be underrepresented in quantitative methylation analyses. However, several methodologies have now been developed to address this issue (including oxBS-Seq [121], mTAB-Seq [122] or Aba-Seq [123]). 5mC and 5hmC seem to have opposite relationships with transcriptional activity, with 5mC negatively correlating with gene expression [124] and 5hmC positively correlating with gene expression in the rodent [125] and human brains [118]. Although many studies showed that 5hmC

is linked with neurological disorders such as Alzheimer's and Huntington's diseases [126, 127] and psychiatric disorders disorder [128-130] its potential implication in SB remains unknown.

4.4 Caveats of miRNA Profiling

Expression profiling of miRNAs have increased our understanding of which miRNAs are present in specific tissues and how they may change under pathological conditions [131]. However, once identified, linking a miRNA to its mRNA targets can be a challenging task, and the mRNA target pairs should be validated. As reviewed elsewhere [132], a very small fraction of software-predicted miRNA targets are validated *in vivo* and many databases for miRNA target prediction are being developed in order to address this issue [132]. However, those databases can provide a surprising level of divergent results when we take into account degrees of sequence similarity, conservation, site accessibility, and variation in the targeted regions of the mRNA. Similarly, there are a number of conflicting studies with regard to the magnitude and direction of biologically-relevant miRNA expression changes in psychiatric disorders [133, 134]. This could be due to tissue-specific variation in expression levels as well as heterogeneity in quantification and normalization procedures [135]. Furthermore, some studies on miRNAs and depression were conducted in peripheral blood despite uncertainties regarding how closely changes in peripheral miRNA expression reflect modifications in the central nervous system (e.g., [136]). Finally, it should be also considered that "control" RNAs commonly used to normalize miRNA data (U6, U44, and U48) are very sensitive to post-mortem decay [132].

4.5 Sample Size and Peripheral Tissue Profiling

The abundance and availability of brain samples is a big challenge and many studies are relying on a limited number of brain samples reducing the power of epigenome-wide association studies [40]. Only genes that have been replicated in independent methylation studies should be considered further as primary candidate genes. Although it is desirable to increase sample sizes in the next few years, it is unfeasible to reach the numbers of samples currently being analysed in GWASs using human brain [40]. The small sample size of most of the current studies also represents a limitation when it comes to identifying gender-specific epigenetic changes associated to SB. Studies are looking towards the use of peripheral tissues (e.g. whole blood, saliva, cerebrospinal fluid (CSF)) to model a brain-related phenotype. Given the tissue-specific nature of the epigenome, the assessment of disease-relevant tissue is an important consideration for EWASs. Although some studies suggest that peripheral samples (e.g. CSF) would adequately model brain gene expression changes, little is known about whether easily accessible tissues, such as whole blood, can be used to address questions about inter-individual epigenomic variation in inaccessible tissues, such as the brain [137]. Epigenetic marks are more variable between different tissues of the same individual than between the same tissue of different individuals. There is however evidence of within-individual epigenetic variation correlation across tissues [138]. A recent study explored co-variation between tissues and the extent to which methylomic variation in blood is predictive of inter-individual variation identified in the brain. Their data suggest that for the majority of the genome, a blood-based EWAS for disorders where brain is presumed to be the primary tissue of interest will give limited information relating to underlying pathological

processes [137]. However, the authors do not discount the utility of using a blood-based EWASs to identify biomarkers of disease phenotypes manifest in the brain [137].

4.6 Animal Models

To date no convincing animal models of suicide have been produced [4]. Suicidal behaviour is challenging to detail in a non-human model as the underlying pathophysiology is poorly known and the risk for suicidal acts is multi-factorial, consisting of a range of biological (e.g. genetics), psychiatric, psychosocial, interpersonal and cultural risk factors. The most promising endophenotypes worth investigating in animals are the cortisol social-stress response and the aggression/impulsivity trait, involving the serotonergic system as well as neurotrophic factors and neurotrophins which have been implicated in suicide previously [4]. Future animal studies could focus on elucidating the effect of suicide-associated epigenetic changes on gene function and how this might impact known suicide-associated endophenotypes and biological pathways.

4.7 Causality

Currently it remains unclear whether the epigenetic changes observed cause SB and suicidal acts or if these phenotypes (or underlying psychiatric conditions/medication) cause the detected epigenetic changes. In the attempt to answer this question, Mendelian randomization (MR) is proving to be a promising approach. MR posits that if a biomarker is causally related to a disease or phenotype, genetic variant(s) controlling activity of that biomarker should also be associated with the outcome [139, 140]. Using genetic variants as proxy for exposure overcomes confounding because genetic variants are inherited at random during meiosis, so they are unrelated to potential confounders (measured or unmeasured). Therefore, following the principles of MR may represent a valid method for revealing the role of specific genes as modifiers/risk factors of SB, leading to a possible association between suicidality and a given biomarker. Future studies examining epigenetic alterations in SB should be undertaken by applying these novel approaches in order to investigate the direction of effect. For instance, the 2-step epigenetic MR approach, which is an extension of MR assumptions, allows researchers to investigate the causal role of DNA methylation in the association between an environmental exposure and SB [141, 142].

None of the studies outlined in this review have attempted to examine the causal pathways between epigenetics changes and SB, either statistically or experimentally. Recent advances in CRISPR-Cas9 based systems enable researchers to direct epigenetic machinery to specific locations with possibly greater ease and at a lower cost. Once the major drawbacks with dCas9 have been solved (such as the inefficiency of precise base editing and off-target activities), *in vivo* epigenome editing methods will potentially allow for more labs to investigate the behavioural outcomes of specific epigenetic patterns in cell or animal models. Although most of the excitement around CRISPR to date has been focused on the ability of genome editing to cure disease, epigenome editing methods might enable more subtle and reversible modulatory control [24]. Future studies will greatly benefit from these new tools and allow for a precise investigation of the direct molecular and behavioural outcomes of suicide -induced epigenetic patterns in the brain.

4.8 Other Considerations

Typically, post-mortem studies report post-mortem interval (PMI), which represents the amount of time between a subject's death and collection and processing of the brain. It has previously been shown that DNA, miRNAs and some histone modifications are stable across extended PMIs [143-146]. Moreover, a recent study has reported that neither global nor site-specific levels of 5mC and 5hmC are affected by the post-mortem intervals [46].

A further complication stems from the emergence of SI during antidepressant treatment. There is indeed a longstanding belief that antidepressants might have an early "triggering effect" that induce depressed patients to pursue suicidal impulses before the treatment-induced mood improvement [147]. Some patients being treated for depression and other psychiatric illnesses experience suicidal thoughts and actions (suicidality) as previously reported in a small proportion of patients receiving selective serotonin reuptake inhibitors [147]. Therefore, when medication data are not available for all individuals included in a study, the possibility that the observed epigenetic changes are confounded by medication cannot be ruled out.

5. Future Perspectives

A multi-omics approach to disentangle the molecular basis underlying SB is warranted to further our understanding of suicidality and SB. Genome-wide investigations have demonstrated that the genetic predisposition to complex traits is highly polygenic. The common variants detected by polygenic risk score analyses may help to predict the extent to which the genetic predisposition for suicidal acts has influence on the risk of suicide attempts. By integrating polygenic risk scores for SA, DNA modifications, chromatin modifications and miRNA expression profiling together would allow the research community to gain a broader and deeper understanding of the pathways primarily involved in the neurobiology of suicide and their potential co-ordinated interaction. For the same reason, future studies should also examine the transcriptional consequences of the observed suicide-related DNA methylation changes. System biology methods, such as weighted correlation network analysis (WGCNA), could be applied to identify suicide-associated gene pathways and networks that could be further targeted as biomarkers or therapeutic targets for suicide prevention.

Author Contributions

All authors conceived the topic of the review. SP prepared the first draft of the review and ELD and TMM edited subsequent versions of the draft. SP and TMM prepared and conceived Figure 1 and Figure 2.

Competing Interests

The authors have declared that no competing interests exist.

References

1. Report CH. CDC 2017 [Available from: https://www.cdc.gov/.

2. Organization WH. 2017 [Available from: http://www.who.int/news-room/fact-sheets/detail/suicide.

3. Tsai SJ, Hong CJ, Liou YJ. Recent molecular genetic studies and methodological issues in suicide research. Prog Neuropsychopharmacol Biol Psychiatry. 2011; 35: 809-817.

4. Preti A. Animal model and neurobiology of suicide. Prog Neuropsychopharmacol Biol Psychiatry. 2011; 35: 818-830.

5. Nock MK, Green JG, Hwang I, McLaughlin KA, Sampson NA, Zaslavsky AM, et al. Prevalence, correlates, and treatment of lifetime suicidal behavior among adolescents: results from the National Comorbidity Survey Replication Adolescent Supplement. JAMA Psychiatry. 2013; 70: 300-310.

6. Roy A, Segal NL. Suicidal behavior in twins: a replication. J Affect Disord. 2001; 66: 71-74.

7. Mullins N, Perroud N, Uher R, Butler AW, Cohen-Woods S, Rivera M, et al. Genetic relationships between suicide attempts, suicidal ideation and major psychiatric disorders: a genome-wide association and polygenic scoring study. Am J Med Genet B Neuropsychiatr Genet. 2014; 165B: 428-437.

8. Fu Q, Heath AC, Bucholz KK, Nelson EC, Glowinski AL, Goldberg J, et al. A twin study of genetic and environmental influences on suicidality in men. Psychol Med. 2002; 32: 11-24.

9. Statham DJ, Heath AC, Madden PA, Bucholz KK, Bierut L, Dinwiddie SH, et al. Suicidal behaviour: an epidemiological and genetic study. Psychol Med. 1998; 28: 839-855.

10. Pedersen NL, Fiske A. Genetic influences on suicide and nonfatal suicidal behavior: twin study findings. Eur Psychiatry. 2010; 25: 264-267.

11. Brent DA, Bridge J, Johnson BA, Connolly J. Suicidal behavior runs in families. A controlled family study of adolescent suicide victims. Arch Gen Psychiatry. 1996; 53: 1145-1152.

12. Brent DA, Oquendo M, Birmaher B, Greenhill L, Kolko D, Stanley B, et al. Familial transmission of mood disorders: convergence and divergence with transmission of suicidal behavior. J Am Acad Child Adolesc Psychiatry. 2004; 43: 1259-1266.

13. Kim CD, Seguin M, Therrien N, Riopel G, Chawky N, Lesage AD, et al. Familial aggregation of suicidal behavior: a family study of male suicide completers from the general population. Am J Psychiatry. 2005; 162: 1017-1019.

14. Anguelova M, Benkelfat C, Turecki G. A systematic review of association studies investigating genes coding for serotonin receptors and the serotonin transporter: II. Suicidal behavior. Mol Psychiatry. 2003; 8: 646-653.

15. Brezo J, Klempan T, Turecki G. The genetics of suicide: a critical review of molecular studies. Psychiatr Clin North Am. 2008; 31: 179-203.

16. Mann JJ. The serotonergic system in mood disorders and suicidal behaviour. Philos Trans R Soc Lond B Biol Sci. 2013; 368: 20120537.

17. Dwivedi Y. Brain-derived neurotrophic factor and suicide pathogenesis. Ann Med. 2010; 42: 87-96.

18. Schosser A, Butler AW, Ising M, Perroud N, Uher R, Ng MY, et al. Genomewide association scan of suicidal thoughts and behaviour in major depression. PLoS One. 2011; 6: e20690.

19. Willour VL, Seifuddin F, Mahon PB, Jancic D, Pirooznia M, Steele J, et al. A genome-wide association study of attempted suicide. Mol Psychiatry. 2012; 17: 433-444.

20. Galfalvy H, Zalsman G, Huang YY, Murphy L, Rosoklija G, Dwork AJ, et al. A pilot genome wide association and gene expression array study of suicide with and without major depression. World J Biol Psychiatry. 2013; 14: 574-582.

21. Turecki G, Brent DA. Suicide and suicidal behaviour. Lancet. 2016; 387: 1227-1239.

22. Bell JT, Tsai PC, Yang TP, Pidsley R, Nisbet J, Glass D, et al. Epigenome-wide scans identify differentially methylated regions for age and age-related phenotypes in a healthy ageing population. PLoS Genet. 2012; 8: e1002629.

23. Feil R, Fraga MF. Epigenetics and the environment: emerging patterns and implications. Nat Rev Genet. 2012; 13: 97-109.

24. Burns SB, Szyszkowicz JK, Luheshi GN, Lutz PE, Turecki G. Plasticity of the epigenome during early-life stress. Semin Cell Dev Biol. 2018; 77: 115-132.

25. Mill J, Heijmans BT. From promises to practical strategies in epigenetic epidemiology. Nat Rev Genet. 2013; 14: 585-594.

26. Wong CC, Meaburn EL, Ronald A, Price TS, Jeffries AR, Schalkwyk LC, et al. Methylomic analysis of monozygotic twins discordant for autism spectrum disorder and related behavioural traits. Mol Psychiatry. 2014; 19: 495-503.

27. Pidsley R, Viana J, Hannon E, Spiers H, Troakes C, Al-Saraj S, et al. Methylomic profiling of human brain tissue supports a neurodevelopmental origin for schizophrenia. Genome Biol. 2014; 15: 483.

28. Uddin M, Aiello AE, Wildman DE, Koenen KC, Pawelec G, de Los Santos R, et al. Epigenetic and immune function profiles associated with posttraumatic stress disorder. Proc Natl Acad Sci U S A. 2010; 107: 9470-9475.

29. Fisher HL, Murphy TM, Arseneault L, Caspi A, Moffitt TE, Viana J, et al. Methylomic analysis of monozygotic twins discordant for childhood psychotic symptoms. Epigenetics. 2015; 10: 1014-1023.

30. Murphy TM, O'Donovan A, Mullins N, O'Farrelly C, McCann A, Malone K. Anxiety is associated with higher levels of global DNA methylation and altered expression of epigenetic and interleukin-6 genes. Psychiatr Genet. 2015; 25: 71-78.

31. Dempster EL, Wong CC, Lester KJ, Burrage J, Gregory AM, Mill J, et al. Genome-wide methylomic analysis of monozygotic twins discordant for adolescent depression. Biol Psychiatry. 2014; 76: 977-983.

32. Davies MN, Krause L, Bell JT, Gao F, Ward KJ, Wu H, et al. Hypermethylation in the ZBTB20 gene is associated with major depressive disorder. Genome Biol. 2014; 15: R56.

33. Uddin M, Koenen KC, Aiello AE, Wildman DE, de los Santos R, Galea S. Epigenetic and inflammatory marker profiles associated with depression in a community-based epidemiologic sample. Psychol Med. 2011; 41: 997-1007.

34. Murphy TM, Crawford B, Dempster EL, Hannon E, Burrage J, Turecki G, et al. Methylomic profiling of cortex samples from completed suicide cases implicates a role for PSORS1C3 in major depression and suicide. Transl Psychiatry. 2017; 7: e989.

35. Murphy TM, Mullins N, Ryan M, Foster T, Kelly C, McClelland R, et al. Genetic variation in DNMT3B and increased global DNA methylation is associated with suicide attempts in psychiatric patients. Genes Brain Behav. 2013; 12: 125-132.

36. Goldberg AD, Allis CD, Bernstein E. Epigenetics: a landscape takes shape. Cell. 2007; 128: 635-638.

37. Labonte B, Turecki G. The epigenetics of suicide: explaining the biological effects of early life environmental adversity. Arch Suicide Res. 2010; 14: 291-310.
38. Autry AE, Monteggia LM. Epigenetics in suicide and depression. Biol Psychiatry. 2009; 66: 812-813.
39. McGowan PO, Szyf M. The epigenetics of social adversity in early life: implications for mental health outcomes. Neurobiol Dis. 2010; 39: 66-72.
40. Schneider E, El Hajj N, Muller F, Navarro B, Haaf T. Epigenetic Dysregulation in the Prefrontal Cortex of Suicide Completers. Cytogenet Genome Res. 2015; 146: 19-27.
41. He Y, Ecker JR. Non-CG Methylation in the Human Genome. Annu Rev Genomics Hum Genet. 2015; 16: 55-77.
42. Lister R, Mukamel EA, Nery JR, Urich M, Puddifoot CA, Johnson ND, et al. Global epigenomic reconfiguration during mammalian brain development. Science. 2013; 341: 1237905.
43. Keller S, Sarchiapone M, Zarrilli F, Tomaiuolo R, Carli V, Angrisano T, et al. TrkB gene expression and DNA methylation state in Wernicke area does not associate with suicidal behavior. J Affect Disord. 2011; 135: 400-404.
44. Haghighi F, Xin Y, Chanrion B, O'Donnell AH, Ge Y, Dwork AJ, et al. Increased DNA methylation in the suicide brain. Dialogues Clin Neurosci. 2014; 16: 430-438.
45. Tucker KL. Methylated cytosine and the brain: a new base for neuroscience. Neuron. 2001; 30: 649-652.
46. Gross JA, Nagy C, Lin L, Bonneil E, Maheu M, Thibault P, et al. Global and Site-Specific Changes in 5-Methylcytosine and 5-Hydroxymethylcytosine after Extended Post-mortem Interval. Front Genet. 2016; 7: 120.
47. Berger SL. The complex language of chromatin regulation during transcription. Nature. 2007; 447: 407-412.
48. Kriaucionis S, Heintz N. The nuclear DNA base 5-hydroxymethylcytosine is present in Purkinje neurons and the brain. Science. 2009; 324: 929-930.
49. Tahiliani M, Koh KP, Shen Y, Pastor WA, Bandukwala H, Brudno Y, et al. Conversion of 5-methylcytosine to 5-hydroxymethylcytosine in mammalian DNA by MLL partner TET1. Science. 2009; 324: 930-935.
50. Ito S, Shen L, Dai Q, Wu SC, Collins LB, Swenberg JA, et al. Tet proteins can convert 5-methylcytosine to 5-formylcytosine and 5-carboxylcytosine. Science. 2011; 333: 1300-1303.
51. Szulwach KE, Li X, Li Y, Song CX, Wu H, Dai Q, et al. 5-hmC-mediated epigenetic dynamics during postnatal neurodevelopment and aging. Nat Neurosci. 2011; 14: 1607-1616.
52. Hahn MA, Qiu R, Wu X, Li AX, Zhang H, Wang J, et al. Dynamics of 5-hydroxymethylcytosine and chromatin marks in Mammalian neurogenesis. Cell Rep. 2013; 3: 291-300.
53. Ernst C, Chen ES, Turecki G. Histone methylation and decreased expression of TrkB.T1 in orbital frontal cortex of suicide completers. Mol Psychiatry. 2009; 14: 830-832.
54. Fiori LM, Gross JA, Turecki G. Effects of histone modifications on increased expression of polyamine biosynthetic genes in suicide. Int J Neuropsychopharmacol. 2012; 15: 1161-1166.
55. Smalheiser NR, Lugli G, Zhang H, Rizavi H, Cook EH, Dwivedi Y. Expression of microRNAs and other small RNAs in prefrontal cortex in schizophrenia, bipolar disorder and depressed subjects. PLoS One. 2014; 9: e86469.

56. Serafini G, Pompili M, Hansen KF, Obrietan K, Dwivedi Y, Shomron N, et al. The involvement of microRNAs in major depression, suicidal behavior, and related disorders: a focus on miR-185 and miR-491-3p. Cell Mol Neurobiol. 2014; 34: 17-30.

57. Xu B, Karayiorgou M, Gogos JA. MicroRNAs in psychiatric and neurodevelopmental disorders. Brain Res. 2010; 1338: 78-88.

58. Miller BH, Wahlestedt C. MicroRNA dysregulation in psychiatric disease. Brain Res. 2010; 1338: 89-99.

59. Derrien T, Johnson R, Bussotti G, Tanzer A, Djebali S, Tilgner H, et al. The GENCODE v7 catalog of human long noncoding RNAs: analysis of their gene structure, evolution, and expression. Genome Res. 2012; 22: 1775-1789.

60. Aprea J, Prenninger S, Dori M, Ghosh T, Monasor LS, Wessendorf E, et al. Transcriptome sequencing during mouse brain development identifies long non-coding RNAs functionally involved in neurogenic commitment. EMBO J. 2013; 32: 3145-3160.

61. Spadaro PA, Flavell CR, Widagdo J, Ratnu VS, Troup M, Ragan C, et al. Long Noncoding RNA-Directed Epigenetic Regulation of Gene Expression Is Associated With Anxiety-like Behavior in Mice. Biol Psychiatry. 2015; 78: 848-859.

62. Mann JJ, Currier DM. Stress, genetics and epigenetic effects on the neurobiology of suicidal behavior and depression. Eur Psychiatry. 2010; 25: 268-271.

63. Raison CL, Miller AH. When not enough is too much: the role of insufficient glucocorticoid signaling in the pathophysiology of stress-related disorders. Am J Psychiatry. 2003; 160: 1554-1565.

64. Turecki G. The molecular bases of the suicidal brain. Nat Rev Neurosci. 2014; 15: 802-816.

65. Jokinen J, Bostrom AE, Dadfar A, Ciuculete DM, Chatzittofis A, Asberg M, et al. Epigenetic Changes in the CRH Gene are Related to Severity of Suicide Attempt and a General Psychiatric Risk Score in Adolescents. EBioMedicine. 2018; 27: 123-133.

66. McGowan PO, Sasaki A, D'Alessio AC, Dymov S, Labonte B, Szyf M, et al. Epigenetic regulation of the glucocorticoid receptor in human brain associates with childhood abuse. Nat Neurosci. 2009; 12: 342-348.

67. Weaver IC, Cervoni N, Champagne FA, D'Alessio AC, Sharma S, Seckl JR, et al. Epigenetic programming by maternal behavior. Nat Neurosci. 2004; 7: 847-854.

68. Wanner B, Vitaro F, Tremblay RE, Turecki G. Childhood trajectories of anxiousness and disruptiveness explain the association between early-life adversity and attempted suicide. Psychol Med. 2012; 42: 2373-2382.

69. Bennett MR. The prefrontal-limbic network in depression: Modulation by hypothalamus, basal ganglia and midbrain. Prog Neurobiol. 2011; 93: 468-487.

70. Rice L, Waters CE, Eccles J, Garside H, Sommer P, Kay P, et al. Identification and functional analysis of SKA2 interaction with the glucocorticoid receptor. J Endocrinol. 2008; 198: 499-509.

71. Guintivano J, Brown T, Newcomer A, Jones M, Cox O, Maher BS, et al. Identification and replication of a combined epigenetic and genetic biomarker predicting suicide and suicidal behaviors. Am J Psychiatry. 2014; 171: 1287-1296.

72. Kaminsky Z, Wilcox HC, Eaton WW, Van Eck K, Kilaru V, Jovanovic T, et al. Epigenetic and genetic variation at SKA2 predict suicidal behavior and post-traumatic stress disorder. Transl Psychiatry. 2015 ;5: e627.

73. Smalheiser NR, Lugli G, Rizavi HS, Torvik VI, Turecki G, Dwivedi Y. MicroRNA expression is down-regulated and reorganized in prefrontal cortex of depressed suicide subjects. PLoS One. 2012; 7: e33201.

74. Boks MP, Rutten BP, Geuze E, Houtepen LC, Vermetten E, Kaminsky Z, et al. SKA2 Methylation is Involved in Cortisol Stress Reactivity and Predicts the Development of Post-Traumatic Stress Disorder (PTSD) After Military Deployment. Neuropsychopharmacology. 2016; 41: 1350-1356.

75. Sadeh N, Wolf EJ, Logue MW, Hayes JP, Stone A, Griffin LM, et al. Epigenetic Variation at Ska2 Predicts Suicide Phenotypes and Internalizing Psychopathology. Depress Anxiety. 2016; 33: 308-315.

76. Limon A, Mamdani F, Hjelm BE, Vawter MP, Sequeira A. Targets of polyamine dysregulation in major depression and suicide: Activity-dependent feedback, excitability, and neurotransmission. Neurosci Biobehav Rev. 2016; 66: 80-91.

77. Gilad GM, Gilad VH. Overview of the brain polyamine-stress-response: regulation, development, and modulation by lithium and role in cell survival. Cell Mol Neurobiol. 2003; 23: 637-649.

78. Gross JA, Fiori LM, Labonte B, Lopez JP, Turecki G. Effects of promoter methylation on increased expression of polyamine biosynthetic genes in suicide. J Psychiatr Res. 2013; 47: 513-519.

79. Sequeira A, Gwadry FG, Ffrench-Mullen JM, Canetti L, Gingras Y, Casero RA, Jr., et al. Implication of SSAT by gene expression and genetic variation in suicide and major depression. Arch Gen Psychiatry. 2006; 63: 35-48.

80. Fiori LM, Mechawar N, Turecki G. Identification and characterization of spermidine/spermine N1-acetyltransferase promoter variants in suicide completers. Biol Psychiatry. 2009; 66: 460-467.

81. Guipponi M, Deutsch S, Kohler K, Perroud N, Le Gal F, Vessaz M, et al. Genetic and epigenetic analysis of SSAT gene dysregulation in suicidal behavior. Am J Med Genet B Neuropsychiatr Genet. 2009; 150B: 799-807.

82. Fiori LM, Turecki G. Epigenetic regulation of spermidine/spermine N1-acetyltransferase (SAT1) in suicide. J Psychiatr Res. 2011; 45: 1229-1235.

83. Fiori LM, Turecki G. Genetic and epigenetic influences on expression of spermine synthase and spermine oxidase in suicide completers. Int J Neuropsychopharmacol. 2010; 13: 725-736.

84. Le-Niculescu H, Levey DF, Ayalew M, Palmer L, Gavrin LM, Jain N, et al. Discovery and validation of blood biomarkers for suicidality. Mol Psychiatry. 2013; 18: 1249-1264.

85. Sequeira A, Klempan T, Canetti L, ffrench-Mullen J, Benkelfat C, Rouleau GA, et al. Patterns of gene expression in the limbic system of suicides with and without major depression. Mol Psychiatry. 2007; 12: 640-655.

86. Lopez JP, Fiori LM, Gross JA, Labonte B, Yerko V, Mechawar N, et al. Regulatory role of miRNAs in polyamine gene expression in the prefrontal cortex of depressed suicide completers. Int J Neuropsychopharmacol. 2014; 17: 23-32.

87. Niculescu AB, Levey D, Le-Niculescu H, Niculescu E, Kurian SM, Salomon D. Psychiatric blood biomarkers: avoiding jumping to premature negative or positive conclusions. Mol Psychiatry. 2015; 20: 286-288.

88. Niculescu AB, Levey DF, Phalen PL, Le-Niculescu H, Dainton HD, Jain N, et al. Understanding and predicting suicidality using a combined genomic and clinical risk assessment approach. Mol Psychiatry. 2015; 20: 1266-1285.

89. Pantazatos SP, Andrews SJ, Dunning-Broadbent J, Pang J, Huang YY, Arango V, et al. Isoform-level brain expression profiling of the spermidine/spermine N1-Acetyltransferase1 (SAT1) gene in major depression and suicide. Neurobiol Dis. 2015; 79: 123-134.

90. Labonte B, Suderman M, Maussion G, Lopez JP, Navarro-Sanchez L, Yerko V, et al. Genome-wide methylation changes in the brains of suicide completers. Am J Psychiatry. 2013; 170: 511-520.

91. Phillips C. Brain-Derived Neurotrophic Factor, Depression, and Physical Activity: Making the Neuroplastic Connection. Neural Plast. 2017; 2017: 7260130.

92. Keller S, Sarchiapone M, Zarrilli F, Videtic A, Ferraro A, Carli V, et al. Increased BDNF promoter methylation in the Wernicke area of suicide subjects. Arch Gen Psychiatry. 2010; 67: 258-267.

93. Kang HJ, Kim JM, Lee JY, Kim SY, Bae KY, Kim SW, et al. BDNF promoter methylation and suicidal behavior in depressive patients. J Affect Disord. 2013; 151: 679-685.

94. Ernst C, Deleva V, Deng X, Sequeira A, Pomarenski A, Klempan T, et al. Alternative splicing, methylation state, and expression profile of tropomyosin-related kinase B in the frontal cortex of suicide completers. Arch Gen Psychiatry. 2009; 66: 22-32.

95. Maussion G, Yang J, Suderman M, Diallo A, Nagy C, Arnovitz M, et al. Functional DNA methylation in a transcript specific 3'UTR region of TrkB associates with suicide. Epigenetics. 2014; 9: 1061-1070.

96. Maussion G, Yang J, Yerko V, Barker P, Mechawar N, Ernst C, et al. Regulation of a truncated form of tropomyosin-related kinase B (TrkB) by Hsa-miR-185* in frontal cortex of suicide completers. PLoS One. 2012; 7: e39301.

97. Mellios N, Huang HS, Grigorenko A, Rogaev E, Akbarian S. A set of differentially expressed miRNAs, including miR-30a-5p, act as post-transcriptional inhibitors of BDNF in prefrontal cortex. Hum Mol Genet. 2008; 17: 3030-3042.

98. Sun N, Lei L, Wang Y, Yang C, Liu Z, Li X, et al. Preliminary comparison of plasma notch-associated microRNA-34b and -34c levels in drug naive, first episode depressed patients and healthy controls. J Affect Disord. 2016; 194: 109-114.

99. Cui X, Niu W, Kong L, He M, Jiang K, Chen S, et al. Long noncoding RNA expression in peripheral blood mononuclear cells and suicide risk in Chinese patients with major depressive disorder. Brain Behav. 2017; 7: e00711.

100. Punzi G, Ursini G, Shin JH, Kleinman JE, Hyde TM, Weinberger DR. Increased expression of MARCKS in post-mortem brain of violent suicide completers is related to transcription of a long, noncoding, antisense RNA. Mol Psychiatry. 2014; 19: 1057-1059.

101. Turecki G, Ernst C, Jollant F, Labonte B, Mechawar N. The neurodevelopmental origins of suicidal behavior. Trends Neurosci. 2012; 35: 14-23.

102. Heijmans BT, Mill J. Commentary: The seven plagues of epigenetic epidemiology. Int J Epidemiol. 2012; 41: 74-78.

103. Houseman EA, Accomando WP, Koestler DC, Christensen BC, Marsit CJ, Nelson HH, et al. DNA methylation arrays as surrogate measures of cell mixture distribution. BMC Bioinformatics. 2012; 13: 86.

104. Guintivano J, Aryee MJ, Kaminsky ZA. A cell epigenotype specific model for the correction of brain cellular heterogeneity bias and its application to age, brain region and major depression. Epigenetics. 2013; 8: 290-302.

105. Sugino K, Hempel CM, Miller MN, Hattox AM, Shapiro P, Wu C, et al. Molecular taxonomy of major neuronal classes in the adult mouse forebrain. Nat Neurosci. 2006; 9: 99-107.

106. Emmert-Buck MR, Bonner RF, Smith PD, Chuaqui RF, Zhuang Z, Goldstein SR, et al. Laser capture microdissection. Science. 1996; 274: 998-1001.

107. Kepecs A, Fishell G. Interneuron cell types are fit to function. Nature. 2014; 505: 318-326.

108. Amin NM, Greco TM, Kuchenbrod LM, Rigney MM, Chung MI, Wallingford JB, et al. Proteomic profiling of cardiac tissue by isolation of nuclei tagged in specific cell types (INTACT). Development. 2014; 141: 962-973.

109. Henry GL, Davis FP, Picard S, Eddy SR. Cell type-specific genomics of Drosophila neurons. Nucleic Acids Res. 2012; 40: 9691-9704.

110. Steiner FA, Talbert PB, Kasinathan S, Deal RB, Henikoff S. Cell-type-specific nuclei purification from whole animals for genome-wide expression and chromatin profiling. Genome Res. 2012; 22: 766-777.

111. Kozlenkov A, Roussos P, Timashpolsky A, Barbu M, Rudchenko S, Bibikova M, et al. Differences in DNA methylation between human neuronal and glial cells are concentrated in enhancers and non-CpG sites. Nucleic Acids Res. 2014; 42: 109-127.

112. Kozlenkov A, Wang M, Roussos P, Rudchenko S, Barbu M, Bibikova M, et al. Substantial DNA methylation differences between two major neuronal subtypes in human brain. Nucleic Acids Res. 2016; 44: 2593-2612.

113. Krishnaswami SR, Grindberg RV, Novotny M, Venepally P, Lacar B, Bhutani K, et al. Using single nuclei for RNA-seq to capture the transcriptome of postmortem neurons. Nat Protoc. 2016; 11: 499-524.

114. Kundakovic M, Jiang Y, Kavanagh DH, Dincer A, Brown L, Pothula V, et al. Practical Guidelines for High-Resolution Epigenomic Profiling of Nucleosomal Histones in Postmortem Human Brain Tissue. Biol Psychiatry. 2017; 81: 162-170.

115. Sarnat HB, Nochlin D, Born DE. Neuronal nuclear antigen (NeuN): a marker of neuronal maturation in early human fetal nervous system. Brain Dev. 1998; 20: 88-94.

116. Mullen RJ, Buck CR, Smith AM. NeuN, a neuronal specific nuclear protein in vertebrates. Development. 1992; 116: 201-211.

117. Ransohoff RM, Brown MA. Innate immunity in the central nervous system. J Clin Invest. 2012; 122: 1164-1171.

118. Gross JA, Pacis A, Chen GG, Barreiro LB, Ernst C, Turecki G. Characterizing 5-hydroxymethylcytosine in human prefrontal cortex at single base resolution. BMC Genomics. 2015; 16: 672.

119. Shi DQ, Ali I, Tang J, Yang WC. New Insights into 5hmC DNA Modification: Generation, Distribution and Function. Front Genet. 2017; 8: 100.

120. Huang Y, Pastor WA, Shen Y, Tahiliani M, Liu DR, Rao A. The behaviour of 5-hydroxymethylcytosine in bisulfite sequencing. PLoS One. 2010; 5: e8888.

121. Booth MJ, Branco MR, Ficz G, Oxley D, Krueger F, Reik W, et al. Quantitative sequencing of 5-methylcytosine and 5-hydroxymethylcytosine at single-base resolution. Science. 2012; 336: 934-937.

122. Yu M, Hon GC, Szulwach KE, Song CX, Zhang L, Kim A, et al. Base-resolution analysis of 5-hydroxymethylcytosine in the mammalian genome. Cell. 2012; 149: 1368-1380.

123. Sun Z, Terragni J, Borgaro JG, Liu Y, Yu L, Guan S, et al. High-resolution enzymatic mapping of genomic 5-hydroxymethylcytosine in mouse embryonic stem cells. Cell Rep. 2013; 3: 567-576.

124. Jones PA. Functions of DNA methylation: islands, start sites, gene bodies and beyond. Nat Rev Genet. 2012; 13: 484-492.

125. Mellen M, Ayata P, Dewell S, Kriaucionis S, Heintz N. MeCP2 binds to 5hmC enriched within active genes and accessible chromatin in the nervous system. Cell. 2012; 151: 1417-1430.

126. Coppieters N, Dieriks BV, Lill C, Faull RL, Curtis MA, Dragunow M. Global changes in DNA methylation and hydroxymethylation in Alzheimer's disease human brain. Neurobiol Aging. 2014; 35: 1334-1344.

127. Villar-Menendez I, Blanch M, Tyebji S, Pereira-Veiga T, Albasanz JL, Martin M, et al. Increased 5-methylcytosine and decreased 5-hydroxymethylcytosine levels are associated with reduced striatal A2AR levels in Huntington's disease. Neuromolecular Med. 2013; 15: 295-309.

128. Dong E, Gavin DP, Chen Y, Davis J. Upregulation of TET1 and downregulation of APOBEC3A and APOBEC3C in the parietal cortex of psychotic patients. Transl Psychiatry. 2012; 2: e159.

129. Matrisciano F, Tueting P, Dalal I, Kadriu B, Grayson DR, Davis JM, et al. Epigenetic modifications of GABAergic interneurons are associated with the schizophrenia-like phenotype induced by prenatal stress in mice. Neuropharmacology. 2013; 68: 184-194.

130. Tseng PT, Lin PY, Lee Y, Hung CF, Lung FW, Chen CS, et al. Age-associated decrease in global DNA methylation in patients with major depression. Neuropsychiatr Dis Treat. 2014; 10: 2105-2114.

131. Oved K, Morag A, Pasmanik-Chor M, Oron-Karni V, Shomron N, Rehavi M, et al. Genome-wide miRNA expression profiling of human lymphoblastoid cell lines identifies tentative SSRI antidepressant response biomarkers. Pharmacogenomics. 2012; 13: 1129-1139.

132. Serafini G, Pompili M, Hansen KF, Obrietan K, Dwivedi Y, Amore M, et al. MicroRNAs: fundamental regulators of gene expression in major affective disorders and suicidal behavior? Front Cell Neurosci. 2013; 7: 208.

133. Perkins DO, Jeffries CD, Jarskog LF, Thomson JM, Woods K, Newman MA, et al. microRNA expression in the prefrontal cortex of individuals with schizophrenia and schizoaffective disorder. Genome Biol. 2007; 8: R27.

134. Beveridge NJ, Gardiner E, Carroll AP, Tooney PA, Cairns MJ. Schizophrenia is associated with an increase in cortical microRNA biogenesis. Mol Psychiatry. 2010; 15: 1176-1189.

135. Belzeaux R, Bergon A, Jeanjean V, Loriod B, Formisano-Treziny C, Verrier L, et al. Responder and nonresponder patients exhibit different peripheral transcriptional signatures during major depressive episode. Transl Psychiatry. 2012; 2: e185.

136. Bocchio-Chiavetto L, Maffioletti E, Bettinsoli P, Giovannini C, Bignotti S, Tardito D, et al. Blood microRNA changes in depressed patients during antidepressant treatment. Eur Neuropsychopharmacol. 2013; 23: 602-611.

137. Hannon E, Lunnon K, Schalkwyk L, Mill J. Interindividual methylomic variation across blood, cortex, and cerebellum: implications for epigenetic studies of neurological and neuropsychiatric phenotypes. Epigenetics. 2015; 10: 1024-1032.

138. Davies MN, Volta M, Pidsley R, Lunnon K, Dixit A, Lovestone S, et al. Functional annotation of the human brain methylome identifies tissue-specific epigenetic variation across brain and blood. Genome Biol. 2012; 13: R43.

139. Burgess S, Timpson NJ, Ebrahim S, Davey Smith G. Mendelian randomization: where are we now and where are we going? Int J Epidemiol. 2015; 44: 379-388.

140. Smith GD, Ebrahim S. 'Mendelian randomization': can genetic epidemiology contribute to understanding environmental determinants of disease? Int J Epidemiol. 2003; 32: 1-22.

141. Relton CL, Davey Smith G. Two-step epigenetic Mendelian randomization: a strategy for establishing the causal role of epigenetic processes in pathways to disease. Int J Epidemiol. 2012; 41: 161-176.

142. Jhun MA, Smith JA, Ware EB, Kardia SLR, Mosley TH, Jr., Turner ST, et al. Modeling the Causal Role of DNA Methylation in the Association Between Cigarette Smoking and Inflammation in African Americans: A 2-Step Epigenetic Mendelian Randomization Study. Am J Epidemiol. 2017; 186: 1149-1158.

143. Hynd MR, Lewohl JM, Scott HL, Dodd PR. Biochemical and molecular studies using human autopsy brain tissue. J Neurochem. 2003; 85: 543-562.

144. Huang HS, Matevossian A, Jiang Y, Akbarian S. Chromatin immunoprecipitation in postmortem brain. J Neurosci Methods. 2006; 156: 284-292.

145. Stan AD, Ghose S, Gao XM, Roberts RC, Lewis-Amezcua K, Hatanpaa KJ, et al. Human postmortem tissue: what quality markers matter? Brain Res. 2006; 1123: 1-11.

146. Nagy C, Maheu M, Lopez JP, Vaillancourt K, Cruceanu C, Gross JA, et al. Effects of postmortem interval on biomolecule integrity in the brain. J Neuropathol Exp Neurol. 2015; 74: 459-469.

147. Stone M, Laughren T, Jones ML, Levenson M, Holland PC, Hughes A, et al. Risk of suicidality in clinical trials of antidepressants in adults: analysis of proprietary data submitted to US Food and Drug Administration. BMJ. 2009; 339: b2880.

Enjoy *OBM Genetics* by:

1. Submitting a manuscript
2. Joining in volunteer reviewer bank
3. Joining Editorial Board
4. Guest editing a special issue

For more details, please visit:
http://www.lidsen.com/journals/genetics

Table 1 Aberrant epigenetic changes associated with suicidal behavior

GENE SYMBOL	PROTEIN ENCODED	GENE FUNCTION (NCBI)	MOLECULAR FUNCTION (UniProt)	TISSUE	KEY FINDINGS	REFERENCES (PMID)
DNA methylation						
Global DNA methylation	NA	NA	NA	BA47	8-fold increased DNA methylation in suicide group compared to controls	25364291*
Global DNA methylation	NA	NA	NA	Peripheral blood	Psychiatric patients with a history of SA had significantly higher levels of global DNA methylation compared with controls	23025623*§
NR3C1	Glucocorticoid receptor	Maintenance and survival of neurons and in synaptic plasticity	Affects inflammatory responses, cellular proliferation and differentiation in target tissues. Involved in chromatin remodelling. Plays a role in	Hippocampus	Significant DNA hypermethylation at *GR* promoter in the hippocampus of suicide completers with history of abuse compared to controls	19234457*§
				Hippocampus	DNA hypermethylation in the exon 1F of the *GR* gene in abused individuals who died by suicide compared to non-abused individuals	22752237*
RNR1	ribosomal RNA	Critical functions in the ribosome that allow protein synthesis to occur	NA	Hippocampus	Overall DNA hypermethylation of rRNA promoter in the hippocampus of suicide completers with history of abuse/childhood adversity	18461137*

Gene	Protein	Function	Activity	Brain Region	Findings	PMID
NTRK2	TrkB-T1 (astrocytic variant)	Receptors of neurotrophins. Role in neurotransmission, calcium release, synaptic plasticity, and cell survival. High affinity receptor of BDNF associated with mood disorders and SB	Development and the maturation of the central and the peripheral nervous system	PFC (BA 8/9)	Increased DNA methylation in two CpG sites within the promoter of TrkB-T1 accompanied by decreased mRNA expression in the PFC of suicide completers compared to controls	19124685
				PFC (BA 8 / 9)	DNA hypermethylation at four CpG sites in the TrkB-T1 3' UTR region in suicide cases compared to controls. Correlation between DNA methylation levels at these sites and TrkB-T1 expression	24802768*
GABRA1	GABAA α1	Stabilizing or hyperpolarising the resting potential Inhibitory effect, reducing the activity of the neurons	Drug binding,GABA-A receptor activity, GABA-gated chloride ion channel activity	FPC	Increased DNA methylation detected in the *GABRA1* gene and negatively correlated with *DNMT3B* protein expression but positively with *DNMT1* mRNA in the FPC of suicide cases	18639864
RELN	reelin, glutamic acid decarboxylase	Cell-cell interactions control, critical role in cell positioning and neuronal migration during brain development	Lipoprotein particle receptor binding, metal ion binding, protein kinase activity	Occipital cortex	DNA hypermethylation at the *RELN* promoter in SZ subjects who died by suicide compared to controls	15961543
				Forebrain	Hypermethylation at 3 CpG sites within *RELN* promoter in SZ suicide cases compared to controls. DNA hypermethylation negatively correlated with reelin expression	17310238

Gene	Name	Function	Activity	Tissue	Finding	Reference
SAT1	Diamine acetyltransferase 1	Enzyme in polyamine catabolism	Polyamine metabolism	PFC (BA 8/9)	DNA hypermethylation in suicide completers carrying the C allele at the rs6526342 SNP within the *SAT1* promoter region. CpG methylation at *SAT1* promoter negatively correlates with gene expression	21501848*
SMOX	spermine oxidase	Enzyme in polyamine catabolism	Role in the regulation of polyamine intracellular concentration	PFC	DNA hypermethylation in the promoter of *SMOX* in the brain of suicide subjects. No correlation with the gene expression levels	20059804[*]
BDNF	brain derived neurotrophic factor	Role in neuronal survival and plasticity, in the regulation of the stress response and in the biology of mood disorders	Growth factor activity, neurotrophin, TRKB receptor binding	Wernicke area	*BDNF* promoter IV hypermethylation in the suicide brains compared to controls. DNA hypermethylation levels correlates with significantly lower *BDNF* expression	20194826*[§]
				Peripheral blood	Increased *BDNF* methylation was significantly associated with SI and depression in female patients 1 year after breast surgery and this association was independent of previous depression, and *BDNF* genotype. No significant methylation–genotype interactions were found	25838322*
				Peripheral blood	Higher *BDNF* DNA methylation levels significantly associated with previous SA, SI during antidepressant treatment, and SI at the last treatment session	23992681*[§]
				Peripheral blood	Higher DNA methylation at *BDNF* promoter is significantly associated with SI at baseline in a geriatric Korean population	24731781*[§]

Gene	Name	Function	Role	Region	Finding	Reference
ARG2	arginase 2	Suggested role in nitric oxide and polyamine metabolism	Role in the regulation of extra-urea cycle, arginine metabolism and down-regulation of nitric oxide synthesis	BA 44	DNA methylation in the promoter region of *ARG2* showed a relationship to the respective levels of expression in suicides	22008221*
				BA 44	Increased expression of *ARG2* in suicide completers correlates with decreased DNA methylation levels of specific CpGs in the promoter region	23260169*
AMD1	S-adenosylmethionine decarboxylase	polyamine biosynthesis	Polyamines biosynthesis	BA 44	Site-specific DNA methylation in the promoter region of *ADM1* was associated with *ADM1* gene expression in suicide cases compared to controls	22008221*
				BA 44	Increases in gene expression of *AMD1* in suicide completers correlate with decreases in methylation of specific CpGs in the promoter of this gene	23260169*
GRIK2	glutamate receptor ionotropic kainate 2	Regulation of circuit activity in neuronal cells, through G-protein coupled receptor stimulation	Ion channel, receptor activity	PFC (BA 8/9, BA10)	*GRIK2* is hypomethylated in suicide cases compared to controls. *GRIK2* showed higher levels of expression in cases	24662927*[§]
BEGAIN	brain-enriched guanylate kinase associated protein	Structural role in the postsynaptic density	Transmission across chemical synapses and protein-protein interactions at synapses	PFC (BA 8/9, BA10)	*BEGAIN* is hypomethylated in suicide cases compared to controls. *BEGAIN* showed higher levels of expression in cases relative to controls	24662927*[§]

Gene	Name	Function	Process	Tissue	Finding	PMID
SKA2	spindle and kinetochore associated complex subunit 2	Structural role, microtubule organization. Potential role in suppressing cortisol following stress	microtubule binding (Cell cycle, Cell division, Mitosis)	FC	DNA hypermethylation at C allele of rs7208505 predicted lower *SKA2* expression in suicide completers	25073599*§
				Blood and saliva	DNA methylation variation at *SKA2* gene mediates vulnerability to SB and PTSD through dysregulation of the HPA axis in response to stress	26305478*§
ELOVL5	Elongation of very long chain fatty acids protein 5	Elongation of long-chain polyunsaturated fatty acids	Polyunsaturated fatty acid biosynthesis	Plasma	SA significantly associated with DNA methylation in *ELOVL5* gene regulatory regions	25972837*§
GAL, GALR3	amino acid neuropeptide galanin, galanin receptor 3	Mood regulation	Chemical synaptic transmission, inflammatory response, nervous system development	LC, DRN	Increased *GAL* and *GALR3* mRNA levels, in parallel with decreased DNA methylation suicide cases compared with controls	27940914*
				BA 8/9, BA 24	*GAL* and *GALR3* transcript levels were decreased, *GALR1* was increased, and DNA methylation was increased in the DLPFC of male suicide cases compared to controls	27940914*
TNF-A	Tumor necrosis factor alfa	Cell signalling protein (cytokine)	Pro-inflammatory cytokine involved in inflammatory and immune responses, mediating neuronal death in injured brain	DLPFC	*TNF-A* promoter significantly hypomethylated in the suicide cases compared with the control group	29361849
MARCKS	Protein Kinase C Substrate	Metabolism and Integration of energy metabolism	calmodulin binding and protein kinase C binding	DLPFC	DNA hypomethylation (cg24011531) in the *MARCKS* gene in violent suicide cases compared to controls	29361849

PSORS1C3	Long non-coding RNA	Long non-coding RNA with a postulated role in immune system regulation	not reported	PFC (BA 11 and 25)	Significantly hypomethylated DMRs upstream of the *PSORS1C3* gene in both cortical regions in depressed suicide cases compared to controls	28045465*[§]

Histone modifications

OAZ1	Ornithine antizym decarboxylase e 1	Role in cell growth and proliferation by regulating intracellular polyamine levels	intracellular polyamine biosynthesis and uptake	VLPFC (BA44)	Increased H3K4me3 levels in the promoter region of *OAZ1* in suicide completers correlated with the expression of *OAZ1* and *ARG2*	22008221*
NTRK2	Neurotrophic Tyrosine Kinase Receptor Type 2	Receptors of neurotrophins	Role in neurotransmission, calcium release, synaptic plasticity, and cell survival	PFC (BA10)	Increased methylation at H3 Lysine 27 in suicide brains compared to controls. Significant correlation between increased H3 lysine 27 methylation and TrkB.T1 expression level	19696771
SYN1, SYN2 and SYN3	Neuronal phosphoproteins	Synaptogenesis, synaptic transmission and synaptic plasticity	Regulation of axonogenesis and synaptogenesis	PFC (BA10)	H3K4me3 promoter enrichment in psychiatric suicide cases relative to controls	22571925*[§]
CX30, CX43	Connexin 30 and 43	Diffusion of ions and metabolites between the cytoplasm of adjacent cells	Gap junction channels	NEOCORTEX (BA4, BA17)	Enrichment of H3K9me3 for both *CX30* and *CX43* in the PFC of depressed suicide cases	27516431

Abbreviations: PFC, Prefrontal cortex; FPC, frontopolar cortex; DLPFC, Dorsolateral Prefrontal cortex; LC, Locus Coeruleus; DRN, dorsal raphe nucleus; SZ, Schizophrenia. *Study used age matched cases and controls and/or included age as a co-variate in their analysis. [§] Study used gender matched cases and controls and/or included gender as a co-variate in their analysis.

Table 2 Differentially expressed miRNAs associated with suicidal behavior

non-coding RNA	PUTATIVE / VALIDATED TARGET GENE	TARGET GENE FUNCTION (NCBI)	TISSUE	KEY FINDINGS	REFERENCES (PMID)
MicroRNAs					
miR-152 miR-181a miR-330-3p miR-34a	NA	NA	PFC (BA10)	8 miRNAs were significantly altered (2 up, 6 down) in psychiatric suicide subjects	24475125[¥§]
miR-34c-5p miR-320c	*SAT1*	Enzyme in polyamine catabolism	PFC (BA44)	miRNAs targeting the 3' UTR of *SAT1* upregulated in PFC of suicide cases and lower expression levels of *SAT1* gene in suicide cases vs controls	24025154[*§]
miR-139-5p miR-320c	*SMOX*	Enzyme in polyamine catabolism (Roles in neurotransmission through the regulation of cell-surface receptor activity, involvement in intracellular signalling pathways)	PFC (BA44)	miRNAs targeting the 3' UTR of *SMOX* upregulated in PFC associated to a lower expression levels of *SMOX* gene in suicide cases	24025154[*§]
miR-20b miR-20a miR-34a miR- 34b	*BCL2* *DNMT3B* *MYCN* *VEGFA*	cellular growth and differentiation	PFC (BA9)	Globally downregulated expression pattern of miRNAs in the PFC of depressed suicide subjects	22427989
miR-34b–5p miR-369–3p	*NOTCH*	neuronal plasticity (sequence-specific DNA binding transcriptional activator activity, RNA polymerase II transcription factor binding)	Peripheral blood	Expression levels of miR-34b–5p and miR-369–3p were significantly lower in leucocytes of Chinese MDD	26807671[*§]

miR-185	*NTRK2*	Receptors of neurotrophins Neurotransmission, calcium release, synaptic plasticity and cell survival	PFC (BA10)	The miRNA miR-185 found differentially expressed and inversely correlated with TrkB-T1 expression in the PFC of suicide completers	22802923
miR-185 miR-195 miR-30a miR-49	*DICER1* *NTRK2*	miRNA bio-synthesis (nucleic acid binding and hydrolase activity)	PFC	*DICER1* expression level associated with SB in both MDD and BD samples; Polygenic profile scores negatively predicted SB in the BP sample for only 4 miRNA genes	26921221
miR-19a-3p	*TNF-A*	mediating neuronal death in injured brain	DLPFC	Specifically upregulated in individuals who died by suicide compared to normal controls	29361849

Long non-coding RNAs

LOC285758	*MARCKS*	Metabolism and Integration of energy metabolism (calmodulin binding and protein kinase C binding)	DLPFC	*LOC285758* expression is significantly increased in violent suicides irrespective of *MARCKS* transcription levels but not the opposite	24821221*[§]
TCONS_00019174 ENST00000566208 NONHSAG045500 ENST00000517573	NA	Protein complex biogenesis	PMBCs	Expression of six down-regulated lncRNAs had a negative association with suicide risk in MDD patients	28638716

Abbreviations: PFC, Prefrontal cortex; DLPFC, Dorsolateral Prefrontal cortex; LC, Locus Coeruleus; DRN, dorsal raphe nucleus; PBMCs, peripheral blood mononuclear cells; MDD, major depressive disorder; BD, bipolar disorder. *Study used age matched cases and controls and/or included age as a co-variate in their analysis. [§] Study used gender matched cases and controls and/or included gender as a co-variate in their analysis.

Appendix B

Genome-wide DNA methylation meta-analysis in the brains of suicide completers

Genome-wide DNA methylation meta-analysis in the brains of suicide completers

Stefania Policicchio[1], Sam Washer[1], Joana Viana[1], Artemis Iatrou[2], Joe Burrage[1], Eilis Hannon [1], Gustavo Turecki [3], Zachary Kaminsky[4,5], Jonathan Mill [1], Emma L. Dempster[1] and Therese M. Murphy[1,6]

Abstract

Suicide is the second leading cause of death globally among young people representing a significant global health burden. Although the molecular correlates of suicide remains poorly understood, it has been hypothesised that epigenomic processes may play a role. The objective of this study was to identify suicide-associated DNA methylation changes in the human brain by utilising previously published and unpublished methylomic datasets. We analysed prefrontal cortex (PFC, $n = 211$) and cerebellum (CER, $n = 114$) DNA methylation profiles from suicide completers and non-psychiatric, sudden-death controls, meta-analysing data from independent cohorts for each brain region separately. We report evidence for altered DNA methylation at several genetic loci in suicide cases compared to controls in both brain regions with suicide-associated differentially methylated positions enriched among functional pathways relevant to psychiatric phenotypes and suicidality, including nervous system development (PFC) and regulation of long-term synaptic depression (CER). In addition, we examined the functional consequences of variable DNA methylation within a PFC suicide-associated differentially methylated region (*PSORS1C3 DMR*) using a dual luciferase assay and examined expression of nearby genes. DNA methylation within this region was associated with decreased expression of firefly luciferase but was not associated with expression of nearby genes, *PSORS1C3* and *POU5F1*. Our data suggest that suicide is associated with DNA methylation, offering novel insights into the molecular pathology associated with suicidality.

Introduction

Suicide represents a global public health problem, with approximately 800,000 people dying worldwide from suicide annually and suicide attempts up to 20 times more frequent than completed suicide[1]. Moreover, suicide is the second leading cause of death among young people worldwide and ranks among the 20th leading causes of death across all ages[2]. The risk for suicidal acts is multifactorial, and consists of a range of biological, psychiatric, psychosocial, and cultural risk factors[3]. Despite its economic and social burden, the underlying biological

aetiology of suicidal behaviour (SB) remains poorly understood.

To date, large-scale genome-wide association studies (GWAS)[4–7] have failed to identify robust associations suggesting that the risk of SB is highly polygenic in nature and that individual gene variants are likely to account only for a small proportion of the total phenotypic variability[8]. Other factors, such as the environment, behavioural traits, psychiatric diagnosis, lifestyle, and coping mechanisms, are essential regulators of suicide risk and likely to account for more sizeable effects[9]. Recently, increased understanding of epigenetic processes that occur in the brain has opened promising avenues in suicide research. The epigenome is potentially malleable—changing with age[10], in response to specific environmental[11] and psychosocial factors[12]—providing a mechanism for the interaction between genotype and the environment[13].

Correspondence: Therese M. Murphy (therese.murphy@TUDublin.ie)
[1]University of Exeter Medical School, University of Exeter, Exeter, UK
[2]Rush Alzheimer's Neurodisease Center, Rush University Medical Center, 600 South Paulina Street, Chicago, IL 60612, USA
Full list of author information is available at the end of the article.
These authors contributed equally: Emma L. Dempster, Therese M. Murphy

Epigenetic processes, including DNA methylation, have recently been implicated in the aetiology of numerous mental health disorders[14–21] and SB[22,23].

In the last decade, research aiming to understand the contribution of epigenetic mechanisms to SB has implicated the role for key biological pathways, including hypothalamic pituitary adrenal axis, stress response, polyamine system, neurotrophic signalling, and lipid metabolism[8]. However, studies examining DNA methylation differences associated with SB have primarily focussed on candidate genes[24–27] and few have examined genome-wide DNA methylation changes in the brains of suicide completers[22,28]. The availability of brain samples is a major challenge for psychiatric research and many previous studies examining DNA methylation variation in suicide are performed on a limited number of post-mortem brain samples[22,29,30]. Such small studies have reduced statistical power to detect small changes in DNA methylation. The objective of this study was to identify suicide-associated DNA methylation changes in the human brain by utilising previously published and unpublished methylomic datasets.

Genome-wide DNA methylation profiles were available from post-mortem brain samples of suicide completers and non-psychiatric, sudden-death controls for a total of seven cohorts. Methylomic data available for two different brain regions —prefrontal cortex (PFC) and cerebellum (CER) (PFC: 4 cohorts, $n = 211$; CER: 3 cohorts, $n = 114$) —were meta-analysed across the suicide cohorts for each brain region separately. We report evidence for altered DNA methylation in suicide cases compared to non-psychiatric controls in both the PFC and CER and examined the functional implications of a top-ranked PFC suicide-associated differentially methylated region (DMR) on gene expression levels in that region. Finally, gene ontology enrichment analysis was performed in each brain region separately to identify pathways of genes associated with suicide completion.

Materials and methods
Sample collection/data recruitment
For the PFC meta-analysis, we included four independent previously published studies[22,31–33] aimed at profiling DNA methylation in human PFC in individuals with a diagnosed axis-I psychiatric disorder and healthy non-psychiatric controls. Only data from individuals who died by suicide and non-psychiatric controls were included for the initial meta-analysis. In two of the four studies selected[31,32], DNA methylation was profiled from fluorescence-activated nuclei sorted neurones, with the remaining two studies performed in bulk tissue[22,33]. Raw DNA methylation data for all four studies are deposited in the Gene Expression Omnibus (GEO) database (accession number: GSE89707, GSE88890, GSE98203, GSE41826) and full details of the sample cohort

can be obtained from the original studies[22,31–33]. For the CER meta-analysis, three DNA methylation datasets were included two of which are currently unpublished (GSE137222 and GSE137223). Raw DNA methylation data for the CER published EWAS study[33] is deposited in GEO database (accession number: GSE89702). The unpublished studies were approved by the University of Exeter Medical School Research Ethics Board (REB). In all three CER cohort's DNA methylation profiles were derived from bulk brain tissue and cases were individuals who died by suicide (hanging, jumping from height, intentional poisoning, self-harm/bleeding). Cause and manner of death as well as joint presence of psychiatric diagnosis were determined by a forensic pathologist after evaluating autopsy results, circumstances of death, data from extensive toxicological testing, police reports, family interviews, and medical records. Controls were individuals who died suddenly (e.g. cardiac failure, viral infection, or accidents) and did not have evidence of axis-I disorders. See Supplementary Table S1 for a complete description of sample selection, numbers, and demographic characteristics of each cohort.

DNA methylation analysis
DNA methylation was measured using the Illumina HumanMethylation450K BeadChip ('Illumina 450K array') or Infinium MethylationEPIC BeadChip ('Illumina EPIC array', one CER cohort) platform (Illumina Inc., San Diego, CA, USA). To ensure consistency of the methodological approach, raw DNA methylation data (idat files) were recovered and each cohort was independently reanalysed, applying the same quality control (QC) and pre-processing pipelines. Briefly, QC checks, quantile normalisation, and separate background adjustment of methylated and unmethylated intensities of type I and II probes were employed using the wateRmelon package in R[34]. Probes on the X- and Y-chromosomes were used to confirm sample sex. Only samples which passed stringent QC measures (>1% of sites with a detection P value (P) >0.01) were included. Probes with a detection $P > 0.01$ in at least 1% of samples and/or a beadcount <3 in 5% of samples, non-specific probes, potentially cross-reactive probes, or probes near SNPs[35,36] were removed across all samples. Only probes common to both the 450k array and EPIC array were included in downstream analyses for the CER. For the annotation of probes, the University of California, Santa Cruz (UCSC) RefGene name from Illumina's annotation file and enhanced annotation to the UCSC Known Gene were used. All annotations used the human February 2009 (GRCh37/hg19) assembly.

Estimating differential neuronal proportions
The R package (available at www.cran.r-project.org), Cell EpigenoType Specific (CETS) mapper, designed for the quantification and normalisation of differing neuronal

proportions in genome-wide DNA methylation datasets was used as previously described[32] to estimate brain cellular heterogeneity in each of the four PFC cohorts. Similar estimates could not be obtained for the CER cohorts as the algorithm for the correction of brain cellular heterogeneity bias was developed using post-mortem frontal cortex data and NeuN is not expressed in CER purkinje neurons[32].

Data analysis

Statistical analyses were performed using R statistical package (version 3.4.3). The β-value is a ratio between methylated probe intensity and total probe intensities (sum of methylated and unmethylated probe intensities) and ranges from 0 to 1. Linear regression was used to examine differences in DNA methylation scores (reported as change in β-value ($\Delta\beta$)) between suicide cases and controls at each CpG site, controlling for potential confounders. Covariates included in all models were age, sex, and chip. We also included ethnicity or brain bank as covariates in the model for those cohorts where that information was available and represented a potential source of variation. In the PFC cohorts only, we also adjusted for estimated neuronal proportions. For one study[22], DNA methylation differences were investigated across individual-matched cortical regions (Brodmann area 11 (BA11), Brodmann area 25 (BA25)) by fitting a linear mixed-effect model (LMM) using the lme4 R package (available at https://cran.r-project.org[37]). Whereby, brain region and sample ID were included in the model as random effects ('within participants' factors) while diagnosis, age, sex, PH, and cellular composition were included in the model as fixed effects.

Meta-analyses
Suicide completers versus non-psychiatric controls

The results obtained from the linear regression were then meta-analysed for each brain region independently. A fixed-effect model, using the 'metagen' function in the R package 'meta', was applied by providing the regression coefficients and standard errors from each individual cohort to calculate weighted pooled estimates and to test for significance. Experiment-wide significance ($P < 1E-07$) (threshold estimated from permutation analysis in a larger dataset ($N = 675$ individuals) generated previously by our group[38]) was chosen as a multiple testing threshold to determine statistically significant DNA methylation changes.

Suicide completers versus non-suicide psychiatric controls

In order to assess whether the observed suicide-associated DNA methylation changes identified in our original meta-analysis were driven by the psychiatric disorder comorbidity rather than being suicide-specific

changes, a second exploratory analysis was performed in additional samples obtained from the CER datasets only, which had additional non-suicide psychiatric samples with DNA methylation data available (not included in the primary analysis report here). In the second meta-analysis, each CER cohort consisted of suicide cases (that were included in the original meta-analysis) and psychiatric controls, where individuals had a diagnosed axis-I disorders (major depressive disorders (MDD), schizophrenia (SZ), bipolar disorder (BD)) but had no documented evidence of SB. In total, the secondary meta-analysis included 130 samples (case group, $N = 50$; psychiatric control group, $N = 80$). Results obtained from the linear regression were then meta-analysed using a fixed-effect model as described previously.

Region-based analysis

The results obtained from both the PFC and CER meta-analyses were used to perform a regional-based analysis using the Python module Comb-p[39] to identify suicide-associated DMRs. The Comb-p software groups spatially correlated DMPs (seed $P < 1E-03$, minimum of three probes) at a maximum distance of 500 bp in each brain region. DMR P were corrected for multiple testing using Šidák correction[40].

Gene ontology term enrichment analysis

A previously described logistic regression approach[41] was used to test if genes (Illumina UCSC gene annotation) annotated to probes in our PFC and CER meta-analyses (DMPs with $P \leq 1E-04$) predicted pathway membership, while controlling for the number of probes annotated to each gene. Briefly, pathways were downloaded from the Gene Ontology (GO) website (http://geneontology.org/) and all genes annotated to parent terms were also included. Genes containing at least one Illumina probe and annotated to at least one GO pathway were considered. Pathways were filtered to those containing between 10 and 2000 genes and a list of significant (after correction for multiple testing—Bonferroni correction) pathways were identified as previously described[41].

Functional follow-up of significant DNA methylation findings

Tissue ($N = 71$) from two regions of the cortex, BA11 ($N = 38$) and BA25 ($N = 33$), collected from 20 MDD suicide cases and 20 non-psychiatric sudden-death controls was obtained from the Douglas Bell Canada Brain Bank (DBCBB) (http://douglasbrainbank.ca/), further details are available in ref.[22]. Previously, our group performed DNA methylation profiling in these samples[22] and the results of that study were included in this meta-analysis study. To examine whether our identified suicide-associated DMR (*PSORS1C3 DMR;* Chr6:31,148,370-31,148,553 (Hg19), 2694 bp downstream

the TSS of *PSORS1C3* gene) is associated with the expression of nearby genes, we measured expression levels of two nearby genes in these brain tissue samples. We tested for an association with gene expression firstly at the closest transcription start site (TSS) gene—the lncRNA gene, *PSORS1C3*—and then at the second closest gene, *POU5F1* (see Supplementary Fig. S1 for details).

Gene expression analysis

Thirty milligrams of frozen PFC tissue from each brain sample was homogenised with Qiazol Lysis Reagent (Qiagen, Valencia, CA, USA), as per the manufacturer's instructions, before running it through a QIAshredder (Qiagen, Valencia, CA, USA). Total RNA was extracted using the Qiagen miRNeasy Mini column-purification system and treated with DNase I as outlined by the manufacturer. The Agilent 2100 Bioanalyzer was used to check the quality and concentration of the extracted RNA samples. One microgram of total RNA was reverse transcribed into complementary DNA (cDNA) (20 µL reactions) according to the manufacturer's instructions using the Invitrogen VILO cDNA synthesis kit (Life Technologies Ltd, Paisley, UK). Three housekeeping genes Ubiquitin Conjugating Enzyme E2 D2 (*UBE2D2*), Cytochrome C1 (*CYC1*), and Ribosomal Protein L13 (*RPL13)* identified previously[42] as being among the most stably expressed in the brain were selected to normalise the target gene expression. Next, quantitative RT-PCR was performed in triplicate for each assay using the StepOnePlus Real-Time PCR machine (Applied Biosystems, Foster City, Calif) and pre-optimised Taqman gene expression assays (Applied Biosystems, Foster City, Calif). A full list of the qPCR assays used is given in Supplementary Table S2. PCR cycling conditions were as follows: 50 °C for 2 min, 95 °C for 20 s, and 40 cycles of 95 °C for 10 s, and 60 °C for 20 s. We undertook stringent QC of raw qPCR data, repeating samples where there was high variability between triplicates (Ct > 0.5). The abundance of each test gene was determined by the comparative Ct method[43], expressed relative to the geometric mean of the three housekeeping genes. Data were log2-transformed to ensure normal distribution and presented as a fold-difference in expression of suicide cases relative to controls using the $2-\Delta\Delta CT$ method. To assess whether *POU5F1* expression levels were associated with a history of suicide, we used a LMM using the lme4 R package (available at https://cran.r-project.org)[37] where ΔCt values of the target gene (*POU5F1*) was the response variable. Brain region and sample ID were included in the model as random effects ('within participants' factors) while diagnosis, age, sex, and neuronal proportion were included in the model as fixed effects. Finally, since 450K array data were available from the same individuals, we examined the correlation between gene expression levels and mean DNA methylation levels at the DMR.

Reporter constructs

The *PSORS1C3 DMR* sequence was inserted into the pCpGL-basic vector (see ref. [44] for details), which is devoid of CpG sites and was generously provided by the Rehli laboratory[44]. Briefly, the cleaned *PSORS1C3* PCR amplicon was inserted into a digested pCpGL-basic plasmid using T4 ligase and buffer (Invitrogen, California, USA). Ligated plasmids were transformed into One Shot PIR1 *E. coli* (ThermoFisher Scientific, Massachusetts, USA) to allow for monoclonal amplification of the recombinant plasmids. For the transformation, 50 µl of One Shot PIR1 *E. coli* was used, including a negative ligation control and a positive transformation control (pUC19) using standard procedures.

Clones were subsequently checked by clonal PCR, restriction digest using *Bgl*II and *Nco*I and Sanger sequencing (see Supplementary Fig. S2) to confirm the DMR had been inserted in the correct orientation. The pCpGL construct was methylated in vitro using M.sssI methyltransferase (New England Biolabs, Massachusetts, USA) in the presence of *S*-adenosylmethionine (SAM) following the manufacture's protocol. An empty pCpGL-basic vector was also methylated to act as a control. To confirm successful methylation, the plasmids underwent digestion with the methylation sensitive enzyme *Hpa*II (see Supplementary Fig. S3).

Cell culture and transfections in HEK293 cells were cultured in Dulbecco's modified Eagle's medium (þ4.5 g l_1 D-glucose, L-glutamate, pyruvate) (Gibco) with 10% foetal bovine serum (Gibco) at 37 °C and 5% CO_2. Briefly, 2×10^5 cells were seeded in six-well plates. The following day media was removed, the cells washed with PBS, and 1.5 ml of fresh growth media was added. Five hundred nanograms of PSORS1C3 or pCpGL plasmid and 100 ng of pGL4.74[hRluc/TK] reporter control vector (Promega, Wisconsin, USA) were diluted in 500 µl of Opti-MEM reduced serum media (Gibco, Massachusetts, USA) in an Eppendorf and left to equilibrate for 5 min at room temperature. In all, 4.5 µl of Lipofectamine LTX Reagent (ThermoFisher Scientific, Massachusetts, USA) was then added to each Eppendorf and incubated for 30 min at room temperature. Following incubation, 500 µl of LTX plasmid mix was added to the HEK293 cells in six-well plates. Cells were then incubated at 37 °C, 5% CO_2, for 24 h to allow expression of firefly and *Renilla* luciferases.

Dual-luciferase assay

Twenty-four hours following transfection a dual-luciferase reporter assay (Promega, Wisconsin, USA) was carried out to measure the expression of firefly luciferase and *Renilla* luciferase in the transfected cells as per the manufacturers' instructions. Each experiment contained three technical repeats and the experiment was repeated three times. The injections and light absorbance

were carried out automatically using the pherastar plate reader. The average firefly luciferase activity was calculated by averaging absorbance readings between 2 and 10 s. The average *Renilla* luciferase activity was calculated by averaging absorbance readings between 14 and 22 s. Data analysis was carried out as described in ref. [45]. All data are presented as a normalised firefly luciferase activity relative to *Renilla* luciferase. Fold change expression was calculated by dividing the unmethylated normalised firefly luciferase activity by the respective methylated normalised luciferase activity. A Student's *T*-test was used to compare the methylated versus unmethylated vectors.

Results

Suicide-associated DMPs in human cortex and cerebellum

An overview of the methodological approach used in this study is given in Supplementary Fig. S4. We identified one DMP (cg00963169) in the PFC, which reached experiment-wide significance ($P = 3.30E-08$ (Fig. 1a)). The effect size at this CpG site, located downstream of exon 1 of the neuron-specific protein coding gene, ELAV-like RNA binding protein 4 (*ELAVL4*), was largely consistent across all cohorts included (see Supplementary Fig. S5), showing hypomethylation in suicide cases relative to controls. Interestingly, the 20 most significant ($P < 5E-05$) suicide-associated differentially methylated loci identified in the PFC, listed in Supplementary Table S3, include probes in the vicinity of several

loci previously implicated in psychiatric phenotypes. In the CER, six probes (cg14392966, cg17855963, cg25590492, cg 12284382, cg10757978, cg04525580) passed the experiment-wide significance threshold ($P < 1E-07$) (Fig. 1b). Of interest the top-ranked DMP, cg14392966 ($P = 3.06E-11$), which is located within the coding region (exon 1) of the *PUS3* gene on Chr11, has been previously associated with severe neurodevelopmental disorders[46]. Supplementary Figure S6 shows that this DMP is hypomethylated in two of the three cohorts in suicide cases compared to healthy controls. A list of the top 20 DMPs in the CER is provided in Supplementary Table S4.

Region-based analysis of altered DNA methylation in suicide completers

We used the python module, Comb-p[39], to identify DMRs in suicide cases compared to controls in each brain region. The regional analysis identified three and eight significant (Sidak-corrected $P < 0.05$) DMRs in the PFC and CER, respectively (see Table 1 for details). In the PFC, the top-ranked DMR was found within the *WRB* gene (Sidak-corrected $P = 5.11E-06$) and was consistently hypomethylated across all five CpG sites in suicide cases relative to controls, in all four PFC methylomic studies (Fig. 2). Of interest, the second top-ranked suicide-associated DMR in the PFC (Sidak-corrected $P = 3.81E-05$) was located downstream of the promoter region of the *PSORS1C3* non-coding gene, a DMR previously
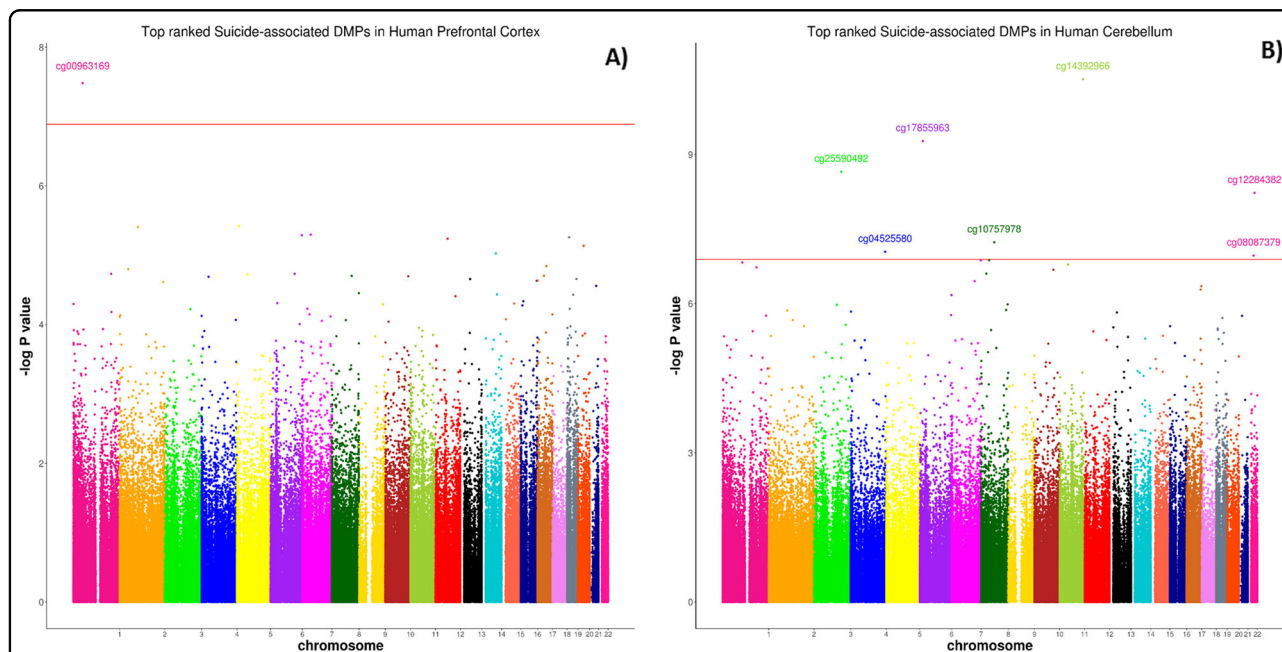
Fig. 1 Suicide-associated DMPs in human cortex and cerebellum. Manhattan plot showing site-specific genome-wide pattern of DNA methylation in **a** the human prefrontal cortex (PFC) and **b** the human xerebellum (CER). One CpG site was identified as differentially methylated between suicide cases and healthy controls at experiment-wide significant ($P = 1E-07$) in the PFC. Six CpG sites were identified as differentially methylated between suicide cases and healthy controls at experiment-wide significant ($P = 1E-07$) in the CER.

Table 1 Comb-p differentially methylated region (DMR) analysis.

Brain region	Hg19	Annotated gene (UCSC)	No. of probes	Slk *P* value	Sidak *P* value
PFC	chr21:40759534-40759695	*WRB*	5	2.02E-09	5.11E-06
	chr6:31148370-31148553	*PSORS1C3*	10	1.71E-08	3.81E-05
	chr22:38071168-38071189	*LGALS1*	3	3.37E-08	0.0006529
CER	chr22:17956453-17956561	*CECR2*	4	1.55E-10	5.68E-07
	chrX:79590789-79590956	*CHMP1B2P*	4	3.74E-09	8.84E-06
	chr13:99100506-99100587	*FARP1*	3	2.68E-09	1.31E-05
	chr6:31838402-31838529	*SLC44A4*	5	2.68E-08	8.32E-05
	chr3:149374761-149374915	*WWTR1*	3	7.56E-08	0.0001938
	chr12:116756805-116756949	*MED13L*	3	8.64E-08	0.0002369
	chr1:1846046-1846155	*CALML6*	3	9.40E-08	0.0003406
	chr11:2397486-2397686	*CD81-AS1*	4	2.10E-06	0.004138

CER cerebellum, *PFC* prefrontal cortex, *Hg19* human genome version 19, *UCSC* University of California, Santa Cruz Human Genome Browser. Stouffer-Liptak-Kechris correction (slk); one-step Siidak (1967) multiple testing correction.

reported by our group as associated with MDD suicide completers[22].

In the CER, the top-ranked suicide-associated DMR was identified on chromosome 22, distributed along the intronic region of the *CERC2* gene and spanning 4 CpG sites. The *CERC2*-associated DMR (Fig. 3) showed significant hypermethylation (Sidak-corrected P = 5.68E-07) across all 4 CpG sites within the region in suicide cases compared with controls. The direction of this change was found to be consistent across all 3 CER methylomic studies.

Pathway analysis

The biological relevance of our findings was investigated through gene ontology analysis on genes annotated to suicide-associated DMPs ($P \leq 1E-04$). Results revealed an enrichment of DNA methylation alterations in genes involved in cognitive processes such as long-term synaptic depression and brain development (See Supplementary Table S5 and S6).

### Suicide-associated DMPs identified in the CER are largely independent of comorbid psychiatric disorders

In order to disentangle the relative contribution of psychopathologies from DNA methylation changes specific to suicide, we performed an additional meta-analysis in the CER whereby all the non-psychiatric controls initially included in our meta-analysis were excluded and individuals with documented Axis-I psychiatric disorders (MDD, SZ, BD) and who died by suicide were compared to psychiatric cases without a documented history of SB/suicide fatalities (3 cohorts, $N = 130$, cases $N = 50$, controls $N = 80$). Comparison of the results (effect sizes at the top 500 ($P < 0.05$) DMPs) from our original CER meta-

analysis and the secondary analysis (Supplementary Fig. S7) revealed a strong positive correlation ($P = 2.2E-16$; $R = 0.89$). Moreover, 2 of the 6 CER-associated DMPs ($P < 1E-07$) were nominally significantly differentially methylated in our suicide cases versus psychiatric controls analysis (cg10757978, $P = 1.19E-04$; cg04525580, $P = 0.017$) (see Supplementary Table S7 for details) and a similar direction of effect was observed for both analyses for the remaining 4 CER-associated DMPs. We were unable to perform the same analysis in the PFC due to lack of samples from individuals with an axis-I diagnosis who did not die by suicide.

Functional validation and gene expression analysis of the PSORS1C3 DMR

Given our replication of a *PSORS1C3* DMR in suicide[22] we aimed to functionally evaluate its effect on the expression of nearby genes. First, we examined the effect of DNA methylation at the suicide-associated DMR on nearby gene expression using a CpG-Free Luciferase Reporter (pCpGL vector) gene assay[47]. Next, we examined gene expression levels of nearby annotated genes (*PSORS1C3* and *POU5F1*) in a subset of samples for which brain tissue was available (two brain regions (BA11 and BA25, $N = 70$; suicide cases ($N = 36$), non-psychiatric controls ($N = 34$)) and examined the correlation between expression levels of our selected target genes and mean DNA methylation at the suicide-associated DMR.

We found a marked increase in the relative expression of firefly luciferase activity normalised to *Renilla luciferase* in the unmethylated *PSORS1C3* cloned pCpGL vector compared to the methylated vector (Fig. 4) (fold change = 206, $P = 0.006$, $N = 3$). Next, we quantified gene expression levels of the *PSORS1C3* long non-coding gene
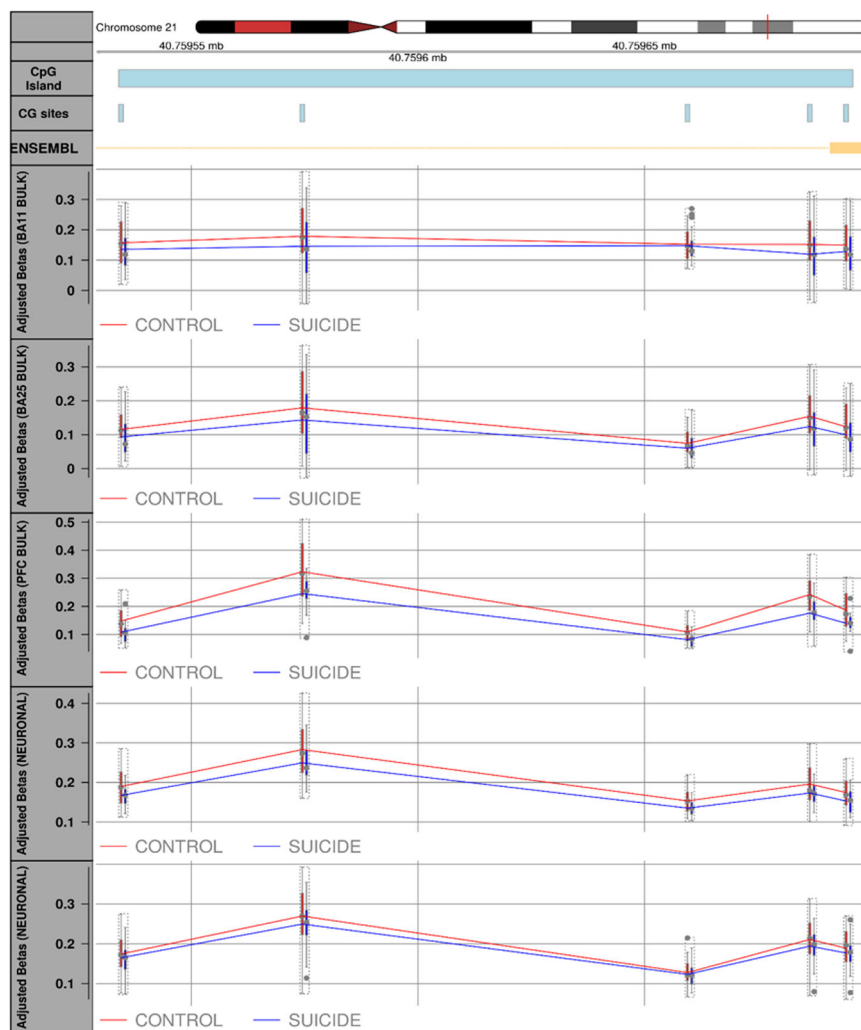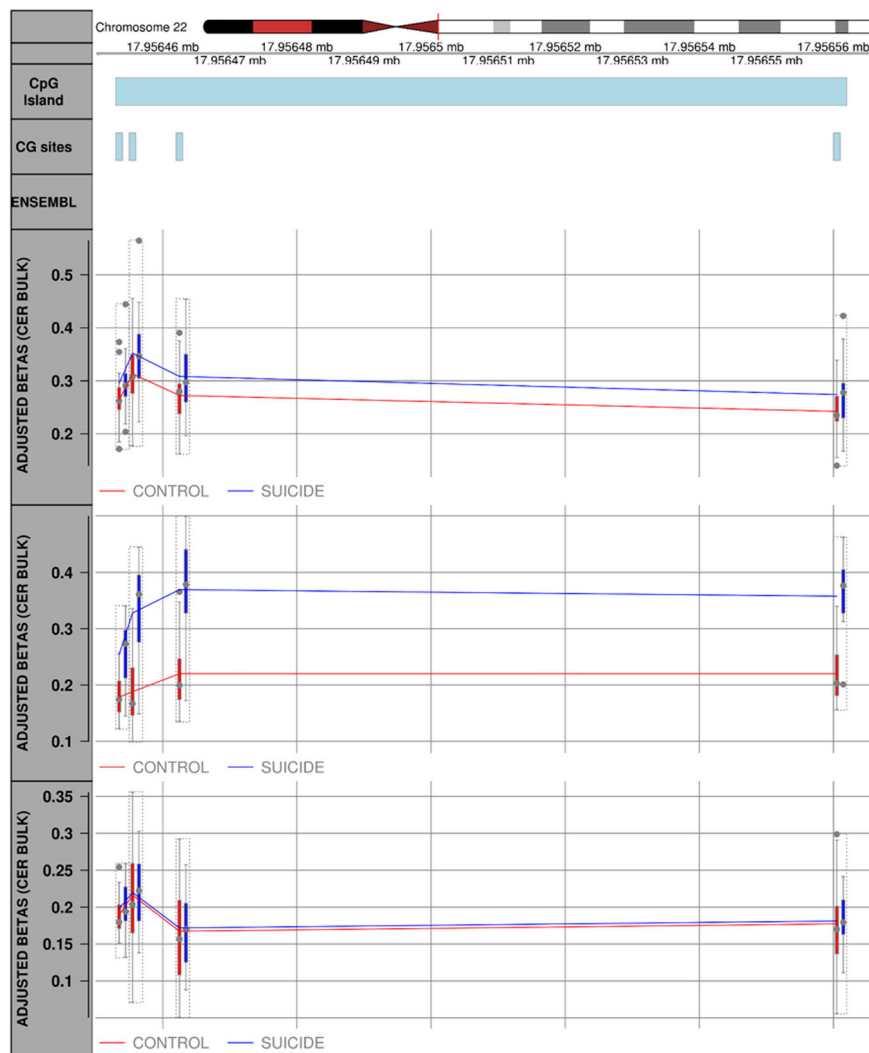
Fig. 2 Suicide-associated differentially methylated region (DMR) in human Prefrontal cortex (PFC). Plot showing the top-ranked DMR in the PFC. This DMR, spanning 5 CpG sites and located in the promoter region of the *WRB* gene (Sidak-corrected $P = 5.11\text{E-06}$), was found consistently hypomethylated in suicide cases compared to healthy controls, across all 4 suicide brain cohorts. The solid line is for illustration purposes and not indicative that the CpG sites between sites are also methylated.

in a cohort of 70 post-mortem brain samples (BA11, $N = 38$; BA25, $N = 32$, both regions obtained from the same individuals). Our analysis showed that in our sample set, *PSORS1C3* lncRNA was not expressed in the PFC (Ct Value >31 or undetermined). This result is consistent with findings in Genotype-Tissue Expression (GTEx) portal[48] (https://www.gtexportal.org/home/gene/PSORS1C3), which shows little to no expression for this gene in brain samples examined. Next, we examined expression levels of the second closest gene (*POU5F1*) to the suicide-associated DMR. An LMM was used to compare mean dCt values between suicide cases and non-psychiatric controls and the analysis showed no significant difference in gene expression levels between the two groups ($P = 0.598$; Supplementary Fig. S8A).

Furthermore, we found no significant correlation between mean DNA methylation at the suicide-associated region *PSORS1C3* DMR and *POU5F1* gene expression levels (Pearson's $R = -0.04$, $P = 0.67$; Supplementary Fig. S8B).

Discussion

In this study, we utilised previously published and unpublished methylomic datasets to perform a meta-analysis of variable DNA methylation in the brain of suicide completers. DNA methylation data were available for two different brain regions (PFC: 4 cohorts, $N = 211$; CER: 3 cohorts, $N = 114$) and data were meta-analysed across the suicide cohorts for each brain region separately. To our knowledge, this represents the most extensive

Fig. 3 Suicide-associated differentially methylated region (DMR) in human Cerebellum (CER). Plot showing the top-ranked DMR in the CER. This DMR, spanning 4 CpG sites and located within the coding region of the *CECR2* gene (Sidak-corrected $P = 5.68E\text{-}07$), was found consistently hypermethylated in suicide cases compared to healthy controls, across 3 suicide brain cohorts. The solid line is for illustration purposes and not indicative that the CpG sites between sites are also methylated.
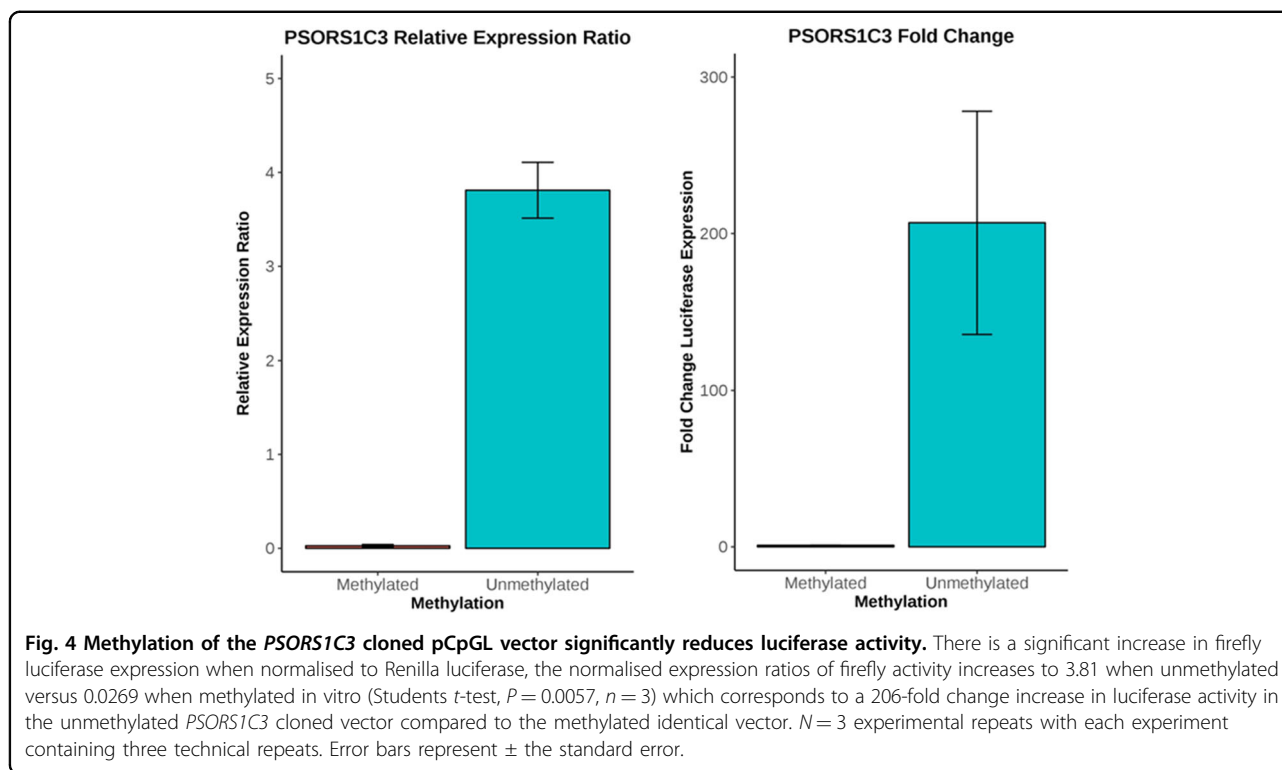
methylomic study of suicide completers using post-mortem brain tissue to date.

While several studies suggest the involvement of the PFC in SB[22,49–51], suicide-associated epigenetic changes in the CER have not been investigated. However, the CER is known to play an important role in motor control, cognition, and emotional processing and is involved in a variety of psychiatric disorders, including depression, bipolar disorder, and schizophrenia[52]. Suicidal behaviour in those with depression has been associated with a decreased cerebellar volume[53] and low regional cerebral blood flow in the cerebellum[54]. Moreover imaging studies have reported structural abnormalities associated to suicide attempt in MDD in cortical and subcortical regions, including cerebellum[55] and alterations in functional

cerebellum networks were found in depressed patients with a suicide attempt history[56]. Altogether these studies support the hypothesis of a potential involvement of CER in the psychopathology of attempted suicide in patients with MDD. We set out to further explore the role of DNA methylation and suicidality in this region as well as to determine if suicidality associated DNA methylation changes are brain region specific.

We first examined site-specific genome-wide patterns of DNA methylation in suicide cases compared with controls in the PFC and CER separately. We identified one DMP (*cg00963169*, $P = 3.30E\text{-}08$) in the PFC, which reached experiment-wide significance. This probe, located in the intronic region of the *ELAVL4* gene, shows consistent hypomethylation in suicide cases compared to controls.

Fig. 4 Methylation of the *PSORS1C3* cloned pCpGL vector significantly reduces luciferase activity. There is a significant increase in firefly luciferase expression when normalised to Renilla luciferase, the normalised expression ratios of firefly activity increases to 3.81 when unmethylated versus 0.0269 when methylated in vitro (Students *t*-test, $P = 0.0057$, $n = 3$) which corresponds to a 206-fold change increase in luciferase activity in the unmethylated *PSORS1C3* cloned vector compared to the methylated identical vector. $N = 3$ experimental repeats with each experiment containing three technical repeats. Error bars represent ± the standard error.

The *ELAVL4* gene has a known role in translation and stabilisation of mRNA, especially in the brain, and acts as a negative regulator of proliferation, activity, and differentiation in neural stem cells[57,58]. Through their mRNA stabilising activities, this family of proteins modulate neuronal development and maintenance, and their altered activity has been implicated in neurological conditions[59] and disorders including Alzheimer's disease[60], schizophrenia[61], and autism[62]. Of interest, the association with suicide at this site was found to be largely driven by PFC cohorts derived from neuronal nuclei (see Supplementary Fig. S5) and thus future replication of this finding in sorted neuronal cells may yield more significant associations with suicide.

In the CER, we identified six probes (cg14392966, cg17855963, cg25590492, cg12284382, cg10757978, cg 04525580) at experiment-wide significance threshold ($P <$ 1E-07). The top-ranked DMP, cg14392966 ($P = 3.06\text{E-}11$), is located in exon 1 of the *PUS3* gene. *PUS3* encodes a highly conserved enzyme responsible for post-transcriptional modification of tRNA and has previously been associated with intellectual disability[63] and severe neurodevelopmental disorders[46]. The remaining DMPs include probes in the vicinity of several loci previously implicated in pathways relevant to psychiatric phenotypes. For example, *ZIC1* is thought to play an important role in neurogenesis and cerebellum differentiation[64], whereas *RASD2* is known to modulate dopaminergic neurotransmission[65]. Furthermore,

the probe cg04525580 ($P = 9.08\text{E-}08$) is located at the 5′ UTR of the interferon regulatory factor 2 (*IRF2*) gene. This locus plays an important role in transcriptional activation at promoters[66] and regulates the expression of a variety of genes involved in immune responses in the brain[67], further supporting a role for immune-related pathways in suicide.

To increase the power of our study to identify changes in DNA methylation between cases and controls and given that DNA methylation at adjacent probes is often correlated, we employed the regional-based analysis, Comb-p, to identify DMRs. Our analysis identified three and eight significant (Sidak-corrected $P < 0.05$) DMRs in the PFC and CER, respectively. In the PFC, the top-ranked DMR, located in intron 1 of the *WRB* gene, is consistently hypomethylated across all five CpG sites in suicide cases relative to controls, in all cohorts. Recent studies suggest a role for Wrb in photoreceptor synaptic transmission in zebrafish[68] and the *WRB* locus was reported among the differentially expressed genes in a mouse model study looking at cognitive impairment and neuropathology in Down syndrome brain[69] further supporting the hypothesis of its involvement in the correct development and functioning of the CNS.

The second top-ranked suicide-associated DMR in the PFC (Sidak-corrected $P = 3.81\text{E-}05$) was located downstream the promoter region of the *PSORS1C3* non-coding gene, a DMR previously reported by our group as associated with MDD suicide completers[22]. Although the

function of this gene product remains unclear, it is thought to be a potential regulator of nearby immune-related genes[70] and is a known risk gene for psoriasis[71,72], supporting a role in immune system regulation. To gain further insight into the role of this suicide-associated *PSORS1C3 DMR* on nearby gene expression, we first used a dual-luciferase assay to determine if DNA methylation at this region decreases expression of firefly luciferase in a CpG-free vector. The methylated *PSORS1C3 DMR* construct was significantly associated with decreased expression of the reporter gene product, indicating that the methylation status of this DMR has the potential to modify promoter activity; however, the identity of the modified gene product is unknown. We found no evidence of suicide-associated differential gene expression of nearby genes, *PSORS1C3* and *POU5F1*, in the PFC. We hypothesise that DNA methylation changes at this suicide-associated DMR are associated with a different nearby gene or an unknown splice variant of either the *PSORS1C3* or *POU5F1* genes. Finally, an additional DMR was identified in the PFC, located on chromosome 22, in the promoter region of the *LGALS1* gene. This gene is thought to play a role in immune system functioning[65] and DNA methylation changes at this locus have previously been implicated in schizophrenia[33].

In the CER, the top-ranked suicide-associated DMR, located in the intronic region of the *CERC2* gene on chromosome 22, spans four CpG sites. This locus is known to be involved in the control of the periodic oscillation of cyclin E expression in proliferating cells likely through its histone deacetylase activity[73]. The *CERC2*-associated DMR showed significant hypermethylation (Sidak-corrected $P = 5.68E\text{-}07$) across all four CpG sites within the region in suicide cases compared with controls and the direction of this change was found to be consistent across all three independent CER methylomic studies. To the best of our knowledge, this gene has not been previously implicated in the pathology of SB. Seven additional suicide-associated DMRs were identified in the CER. Of interest is the DMR located in exon 10 of the *SLC44A4* gene; a gene recently implicated in a study looking at the role of the major histocompatibility complex region in schizophrenia susceptibility[74]. An additional suicide-associated DMR, worthy of further investigation, is located in exon 3 of the *WWTR1* gene, a transcriptional coactivator known for its role in preserving neuronal health[75]. Furthermore, a missense variant in this gene was recently associated with lower cognitive ability in a GWAS study for infant mental and motor ability[76]. Finally, we identified a suicide-associated DMR located downstream the promoter region of *MED13L* gene and genetic variants at this locus have been widely reported as associated with intellectual disability[77,78], suggesting that this gene may play an important role in neurological development.

Since SB is often a complication of a psychiatric disorder, distinguishing suicide diathesis-related DNA methylation changes from those associated with mood disorders and other psychiatric disorders has remained a challenge. In order to unravel the relative contribution of psychopathologies from DNA methylation changes specific to suicide, we performed an additional meta-analysis in the CER whereby individuals with documented Axis-I psychiatric disorders (MDD, SZ, BD) and who died by suicide were compared to psychiatric cases without a documented history of SB. Comparison of the results (effect size of the top 500 nominally significant ($P < 0.05$) DMPs) from our original CER meta-analysis and the secondary analysis revealed a strong positive correlation ($P = 2.2E\text{-}16$; $R = 0.89$). Moreover, we replicated our findings for two of the six CER-associated DMPs, which reached multiple testing threshold in our suicide cases versus psychiatric controls meta-analysis (cg10757978, $P = 1.19E\text{-}04$; cg04525580, $P = 0.017$) and we observed similar direction of effect for the remaining loci. Taken together these findings suggest that suicide-associated DMPs identified in the CER are largely independent of comorbid psychiatric disorders. Unfortunately, we were unable to perform the same analysis in the PFC due to the limited number of samples that did not die by suicide but had an Axis-I diagnosis.

Despite the power of the methodological approaches used in this study, there are several caveats. First, the modest number of studies included made this meta-analysis relatively underpowered to detect small changes in DNA methylation. Despite this we were able to identify several statistically significant DMPs and DMRs in both brain regions. Another major limitation is that bulk brain tissue was used in most of the studies included in our meta-analysis and cellular heterogeneity is a well-known confounder in DNA methylation studies. In order to bypass this issue, we used a previously reported in silico method to estimate the neuronal proportion in each sample in bulk PFC cohorts and included these estimates in the statistical models[32]. This method could not be applied to our analysis of the CER and thus it is plausible that cellular heterogeneity is confounding some of our CER results. Third, recent research has implicated the importance of other DNA modifications (i.e., 5-hydroxymethyl cytosine) in the brain[79]. Our measure of DNA methylation in this study cannot be distinguished from 5-hydroxymethyl cytosine (5hmC). Of interest, we examined the presence of detectable 5hmC levels at statistical significant DMPs identified in this study in their respective brain regions using the Hydroxymethylation Annotation in Brain Integrative Tool (HABIT) tool (http://epigenetics.iop.kcl.ac.uk/HMC/)[41]. This tool identified detectable levels of 5hmC at the following suicide-associated DMPs cg00963169 (PFC), and cg17855963 and

cg04525580 (CER), suggesting that the majority of DMPs identified in this study are not confounded by 5hmC. However, future studies should attempt to examine the role of 5hmC in SB. Fourth, medication data, smoking information, and method of suicide were not available for all individuals; thus, we cannot rule out the possibility that the observed DNA methylation changes are influenced by these potential confounders.

Fifth, we acknowledge the possibility that many of the associations reported (DMPs/DMRs) could be related to the severity and/or duration of the mental health disorder. From our secondary analysis in the cerebellum we show that for certain top-ranked DMPs the association appears to be suicide associated rather than associated with the underlying mental health disorder. Given the lack of information related to severity and/or duration of mental illness for samples included in this meta-analysis we cannot rule out the contribution of the above-mentioned confounders.

Finally, although our study presents evidence for novel DNA methylation changes associated with suicide, further replication using a larger sample size is required to support these results. In addition, future studies could also examine the transcriptional consequences of the observed DNA methylation changes at the *PSORS1C3 DMR* on additional nearby genes and/or novel splice variants in the region. There is considerable interest in using DNA methylation-based biomarkers as predictors for suicide risk and previous studies[30,80–84] have identified polymorphic CpGs that can act as a unique molecular signature for suicide prediction. The data from this study provide many more candidate regions as potential biomarkers for suicide risk and also identifies genes/networks potentially dysregulated in suicidal brain.

In summary, our data, which utilise several published and unpublished suicide cohorts, have identified DMPs and several DMRs associated with suicide in both the PFC and CER, including the previously identified DMR upstream of the *PSORS1C3* non-coding gene. We show that this DMR can influence gene expression using a dual-luciferase assay, but we have yet to identify its target gene.

Author details
[1]University of Exeter Medical School, University of Exeter, Exeter, UK. [2]Rush Alzheimer's Neurodisease Center, Rush University Medical Center, 600 South Paulina Street, Chicago, IL 60612, USA. [3]Douglas Institute, Department of Psychiatry, McGill University, Verdun, QC H4H 1R3, Canada. [4]Department of Psychiatry, School of Medicine, Johns Hopkins University, Baltimore, MD, USA. [5]Department of Mental Health, Johns Hopkins Bloomberg School of Public Health, Baltimore, MD, USA. [6]School of Biological and Health Sciences, Technological University Dublin, City Campus, Dublin 2, Ireland

References
1. CDC. *Suicide Mortality by State Report.* https://www.cdc.gov/nchs/pressroom/sosmap/suicide-mortality/suicide.htm (2017).
2. WHO. *Global Health Observatory (GHO) Data.* https://www.who.int/news-room/fact-sheets/detail/suicide (2018)
3. Malone, K. M. et al. Protective factors against suicidal acts in major depression: reasons for living. *Am. J. Psychiatry* **157**, 1084–1088 (2000).
4. Schosser, A. et al. Genomewide association scan of suicidal thoughts and behaviour in major depression. *PLoS ONE* **6**, e20690 (2011).
5. Willour, V. L. et al. A genome-wide association study of attempted suicide. *Mol. Psychiatry* **17**, 433–444 (2012).
6. Galfalvy, H. et al. A pilot genome wide association and gene expression array study of suicide with and without major depression. *World J. Biol. Psychiatry* **14**, 574–582 (2013).
7. Mullins, N. et al. GWAS of suicide attempt in psychiatric disorders and association with major depression polygenic risk scores. *Am. J. Psychiatry.* https://doi.org/10.1176/appiajp201918080957 (2019).
8. Policicchio, S., Dempster, E. L. & Murphy, T. M. Deciphering the epigenetic landscape of suicidal behaviour: a review of current findings, caveats and future directions. *OBM Genet.* **2**, 039 (2018).
9. Turecki, G. & Brent, D. A. Suicide and suicidal behaviour. *Lancet* **387**, 1227–1239 (2016).
10. Bell, J. T. et al. Epigenome-wide scans identify differentially methylated regions for age and age-related phenotypes in a healthy ageing population. *PLoS Genet.* **8**, e1002629 (2012).
11. Feil, R. & Fraga, M. F. Epigenetics and the environment: emerging patterns and implications. *Nat. Rev. Genet.* **13**, 97–109 (2012).
12. Burns, S. B., Szyszkowicz, J. K., Luheshi, G. N., Lutz, P. E. & Turecki, G. Plasticity of the epigenome during early-life stress. *Semin. Cell Dev. Biol.* **77**, 115–132 (2018).
13. Mill, J. & Heijmans, B. T. From promises to practical strategies in epigenetic epidemiology. *Nat. Rev. Genet.* **14**, 585–594 (2013).
14. Wong, C. C. et al. Methylomic analysis of monozygotic twins discordant for autism spectrum disorder and related behavioural traits. *Mol. Psychiatry* **19**, 495–503 (2014).
15. Pidsley, R. et al. Methylomic profiling of human brain tissue supports a neurodevelopmental origin for schizophrenia. *Genome Biol.* **15**, 483 (2014).
16. Uddin, M. et al. Epigenetic and immune function profiles associated with posttraumatic stress disorder. *Proc. Natl Acad. Sci. USA* **107**, 9470–9475 (2010).
17. Fisher, H. L. et al. Methylomic analysis of monozygotic twins discordant for childhood psychotic symptoms. *Epigenetics* **10**, 1014–1023 (2015).
18. Murphy, T. M. et al. Anxiety is associated with higher levels of global DNA methylation and altered expression of epigenetic and interleukin-6 genes. *Psychiatr. Genet.* **25**, 71–78 (2015).
19. Dempster, E. L. et al. Genome-wide methylomic analysis of monozygotic twins discordant for adolescent depression. *Biol. Psychiatry* **76**, 977–983 (2014).
20. Davies, M. N. et al. Hypermethylation in the ZBTB20 gene is associated with major depressive disorder. *Genome Biol.* **15**, R56 (2014).

21. Uddin, M. et al. Epigenetic and inflammatory marker profiles associated with depression in a community-based epidemiologic sample. *Psychol. Med.* **41**, 997–1007 (2011).

22. Murphy, T. M. et al. Methylomic profiling of cortex samples from completed suicide cases implicates a role for PSORS1C3 in major depression and suicide. *Transl. Psychiatry* **7**, e989 (2017).

23. Murphy, T. M. et al. Genetic variation in DNMT3B and increased global DNA methylation is associated with suicide attempts in psychiatric patients. *Genes Brain Behav.* **12**, 125–132 (2013).

24. Labonte, B. et al. Genome-wide epigenetic regulation by early-life trauma. *Arch. Gen. Psychiatry* **69**, 722–731 (2012).

25. Ernst, C. et al. Alternative splicing, methylation state, and expression profile of tropomyosin-related kinase B in the frontal cortex of suicide completers. *Arch. Gen. Psychiatry* **66**, 22–32 (2009).

26. Fiori, L. M. & Turecki, G. Epigenetic regulation of spermidine/spermine N1-acetyltransferase (SAT1) in suicide. *J. Psychiatr. Res* **45**, 1229–1235 (2011).

27. Keller, S. et al. Increased BDNF promoter methylation in the Wernicke area of suicide subjects. *Arch. Gen. Psychiatry* **67**, 258–267 (2010).

28. Haghighi, F. et al. Increased DNA methylation in the suicide brain. *Dialogues Clin. Neurosci.* **16**, 430–438 (2014).

29. Fiori, L. M., Gross, J. A. & Turecki, G. Effects of histone modifications on increased expression of polyamine biosynthetic genes in suicide. *Int. J. Neuropsychopharmacol.* **15**, 1161–1166 (2012).

30. Maussion, G. et al. Functional DNA methylation in a transcript specific 3′UTR region of TrkB associates with suicide. *Epigenetics* **9**, 1061–1070 (2014).

31. Kozlenkov, A. et al. DNA methylation profiling of human prefrontal cortex neurons in heroin users shows significant difference between genomic contexts of hyper- and hypomethylation and a younger epigenetic age. *Genes (Basel)* **8**, 152 (2017).

32. Guintivano, J., Aryee, M. J. & Kaminsky, Z. A. A cell epigenotype specific model for the correction of brain cellular heterogeneity bias and its application to age, brain region and major depression. *Epigenetics* **8**, 290–302 (2013).

33. Viana, J. et al. Schizophrenia-associated methylomic variation: molecular signatures of disease and polygenic risk burden across multiple brain regions. *Hum. Mol. Genet.* **26**, 210–225 (2017).

34. Pidsley, R. et al. A data-driven approach to preprocessing Illumina 450K methylation array data. *BMC Genomics* **14**, 293 (2013).

35. Price, M. E. et al. Additional annotation enhances potential for biologically-relevant analysis of the Illumina Infinium HumanMethylation450 BeadChip array. *Epigenet. Chromatin* **6**, 4 (2013).

36. Chen, Y. A. et al. Discovery of cross-reactive probes and polymorphic CpGs in the Illumina Infinium HumanMethylation450 microarray. *Epigenetics* **8**, 203–209 (2013).

37. Sarkar, D. Multivariate Data Visualization with R. http://lmdvr.r-forge.r-project.org. Accessed 2008 (2008).

38. Hannon, E. et al. An integrated genetic-epigenetic analysis of schizophrenia: evidence for co-localization of genetic associations and differential DNA methylation. *Genome Biol.* **17**, 176 (2016).

39. Pedersen, B. S., Schwartz, D. A., Yang, I. V. & Kechris, K. J. Comb-p: software for combining, analyzing, grouping and correcting spatially correlated P-values. *Bioinformatics* **28**, 2986–2988 (2012).

40. Šidák, Z. Rectangular confidence regions for the means of multivariate normal distributions. *J. Am. Stat. Assoc.* **62**, 626–633 (1967).

41. Lunnon, K. et al. Variation in 5-hydroxymethylcytosine across human cortex and cerebellum. *Genome Biol.* **17**, 27 (2016).

42. Rydbirk, R. et al. Assessment of brain reference genes for RT-qPCR studies in neurodegenerative diseases. *Sci. Rep.* **6**, 37116 (2016).

43. Pfaffl, M. W. A new mathematical model for relative quantification in real-time RT-PCR. *Nucleic Acids Res.* **29**, e45 (2001).

44. Rehli, M. K. M. Functional analysis of promoter CPG-methylation using a CpG-free luciferase reporter vector. *Epigenetics* **1**, 4 (2006).

45. Jacobs, J. L. & Dinman, J. D. Systematic analysis of bicistronic reporter assay data. *Nucleic Acids Res.* **32**, e160 (2004).

46. Abdelrahman, H. A., Al-Shamsi, A. M., Ali, B. R. & Al-Gazali, L. A null variant in PUS3 confirms its involvement in intellectual disability and further delineates the associated neurodevelopmental disease. *Clin. Genet.* **94**, 586–587 (2018).

47. Klug, M. & Rehli, M. Functional analysis of promoter CPGmethylation using a CpG-free luciferase reporter vector. *Epigenetics* **1**, 127–130 (2006).

48. Consortium, G. T. The Genotype-Tissue Expression (GTEx) project. *Nat. Genet.* **45**, 580–585 (2013).

49. Schneider, E., El Hajj, N., Muller, F., Navarro, B. & Haaf, T. Epigenetic dysregulation in the prefrontal cortex of suicide completers. *Cytogenet. Genome Res* **146**, 19–27 (2015).

50. Nagy, C. et al. Astrocytic abnormalities and global DNA methylation patterns in depression and suicide. *Mol. Psychiatry* **20**, 320–328 (2015).

51. Nagy, C., Torres-Platas, S. G., Mechawar, N. & Turecki, G. Repression of astrocytic connexins in cortical and subcortical brain regions and prefrontal enrichment of H3K9me3 in depression and suicide. *Int. J. Neuropsychopharmacol.* **20**, 50–57 (2017).

52. Phillips, J. R., Hewedi, D. H., Eissa, A. M. & Moustafa, A. A. The cerebellum and psychiatric disorders. *Front. Public Health* **3**, 66 (2015).

53. Hwang, J. P. et al. Cortical and subcortical abnormalities in late-onset depression with history of suicide attempts investigated with MRI and voxel-based morphometry. *J. Geriatr. Psychiatry Neurol.* **23**, 171–184 (2010).

54. Amen, D. G., Prunella, J. R., Fallon, J. H., Amen, B. & Hanks, C. A comparative analysis of completed suicide using high resolution brain SPECT imaging. *J. Neuropsychiatry Clin. Neurosci.* **21**, 430–439 (2009).

55. Lee, Y. J. et al. Decreased regional gray matter volume in suicide attempters compared to suicide non-attempters with major depressive disorders. *Compr. Psychiatry* **67**, 59–65 (2016).

56. Jung, J. et al. Alterations in functional brain networks in depressed patients with a suicide attempt history. *Neuropsychopharmacology*. https://doi.org/10.1038/s41386-019-0560-z (2019).

57. Stawski, R. et al. Reduced expression of ELAVL4 in male meningioma patients. *Brain Tumor Pathol.* **30**, 160–166 (2013).

58. Akamatsu, W. et al. The RNA-binding protein HuD regulates neuronal cell identity and maturation. *Proc. Natl Acad. Sci. USA* **102**, 4625–4630 (2005).

59. Ince-Dunn, G. et al. Neuronal Elav-like (Hu) proteins regulate RNA splicing and abundance to control glutamate levels and neuronal excitability. *Neuron* **75**, 1067–1080 (2012).

60. Talman, V., Pascale, A., Jantti, M., Amadio, M. & Tuominen, R. K. Protein kinase C activation as a potential therapeutic strategy in Alzheimer's disease: is there a role for embryonic lethal abnormal vision-like proteins? *Basic Clin. Pharm. Toxicol.* **119**, 149–160 (2016).

61. Yamada, K. et al. Genome-wide association study of schizophrenia in Japanese population. *PLoS ONE* **6**, e20468 (2011).

62. Berto, S., Usui, N., Konopka, G. & Fogel, B. L. ELAVL2-regulated transcriptional and splicing networks in human neurons link neurodevelopment and autism. *Hum. Mol. Genet.* **25**, 2451–2464 (2016).

63. de Paiva, A. R. B. et al. PUS3 mutations are associated with intellectual disability, leukoencephalopathy, and nephropathy. *Neurol. Genet.* **5**, e306 (2019).

64. Yokota, N. et al. Predominant expression of human zic in cerebellar granule cell lineage and medulloblastoma. *Cancer Res.* **56**, 377–383 (1996).

65. Vitucci, D. et al. Rasd2 modulates prefronto-striatal phenotypes in humans and 'schizophrenia-like behaviors' in mice. *Neuropsychopharmacology* **41**, 916–927 (2016).

66. Sun, H. et al. Quantitative integration of epigenomic variation and transcription factor binding using MAmotif toolkit identifies an important role of IRF2 as transcription activator at gene promoters. *Cell Discov.* **4**, 38 (2018).

67. Drew, P. D. et al. Interferon regulatory factor-2 physically interacts with NF-kappa B in vitro and inhibits NF-kappa B induction of major histocompatibility class I and beta 2-microglobulin gene expression in transfected human neuroblastoma cells. *J. Neuroimmunol.* **63**, 157–162 (1995).

68. Daniele, L. L., Emran, F., Lobo, G. P., Gaivin, R. J. & Perkins, B. D. Mutation of wrb, a component of the guided entry of tail-anchored protein pathway, disrupts photoreceptor synapse structure and function. *Invest. Ophthalmol. Vis. Sci.* **57**, 2942–2954 (2016).

69. Ling, K. H. et al. Functional transcriptome analysis of the postnatal brain of the Ts1Cje mouse model for Down syndrome reveals global disruption of interferon-related molecular networks. *BMC Genomics* **15**, 624 (2014).

70. Nair, R. P. et al. Sequence and haplotype analysis supports HLA-C as the psoriasis susceptibility 1 gene. *Am. J. Hum. Genet.* **78**, 827–851 (2006).

71. Chang, Y. T. et al. Psoriasis vulgaris in Chinese individuals is associated with PSORS1C3 and CDSN genes. *Br. J. Dermatol.* **155**, 663–669 (2006).

72. Wisniewski, A., Matusiak, L., Szczerkowska-Dobosz, A., Nowak, I. & Kusnierczyk, P. HLA-C*06:02-independent, gender-related association of PSORS1C3 and PSORS1C1/CDSN single-nucleotide polymorphisms with risk and severity of psoriasis. *Mol. Genet. Genomics* **293**, 957–966 (2018).

73. Polanowska, J. et al. The periodic down regulation of Cyclin E gene expression from exit of mitosis to end of G(1) is controlled by a deacetylase-

and E2F-associated bipartite repressor element. *Oncogene* **20**, 4115–4127 (2001).

74. Yamada, K. et al. Population-dependent contribution of the major histocompatibility complex region to schizophrenia susceptibility. *Schizophr. Res.* **168**, 444–449 (2015).

75. Pfleger, C. M. The Hippo pathway: a master regulatory network important in development and dysregulated in disease. *Curr. Top. Dev. Biol.* **123**, 181–228 (2017).

76. Sun, R. et al. Identification of novel loci associated with infant cognitive ability. *Mol. Psychiatry*. https://doi.org/10.1038/s41380-018-0205-3 (2018).

77. Hamdan, F. F. et al. De novo mutations in moderate or severe intellectual disability. *PLoS Genet.* **10**, e1004772 (2014).

78. Nizon, M. et al. Variants in MED12L, encoding a subunit of the mediator kinase module, are responsible for intellectual disability associated with transcriptional defect. *Genet. Med.* **21**, 2713–2722 (2019).

79. Branco, M. R., Ficz, G. & Reik, W. Uncovering the role of 5-hydroxymethylcytosine in the epigenome. *Nat. Rev. Genet.* **13**, 7–13 (2011).

80. Clive, M. L. et al. Discovery and replication of a peripheral tissue DNA methylation biosignature to augment a suicide prediction model. *Clin. Epigenet.* **8**, 113 (2016).

81. Sadeh, N. et al. Epigenetic Variation at Ska2 Predicts Suicide Phenotypes and Internalizing Psychopathology. *Depress Anxiety* **33**, 308–315 (2016).

82. Kaminsky, Z. et al. Epigenetic and genetic variation at SKA2 predict suicidal behavior and post-traumatic stress disorder. *Transl. Psychiatry* **5**, e627 (2015).

83. Lockwood, L. E., Su, S. & Youssef, N. A. The role of epigenetics in depression and suicide: a platform for gene-environment interactions. *Psychiatry Res* **228**, 235–242 (2015).

84. Guintivano, J. et al. Identification and replication of a combined epigenetic and genetic biomarker predicting suicide and suicidal behaviors. *Am. J. Psychiatry* **171**, 1287–1296 (2014).

Appendix C

Fluorescence-activated nuclei sorting (FANS) on human post-mortem cortex tissue enabling the isolation of distinct neural cell populations for multiple omic profiling

protocols.io
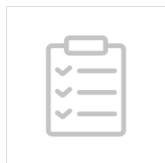
🌐 Fluorescence-activated nuclei sorting (FANS) on human post-mortem cortex tissue enabling the isolation of distinct neural cell populations for multiple omic profiling

Oct 06, 2020

Stefania S Policicchio[1], Jonathan P Davies[1], Barry Chioza[1], Joe Burrage[1], Jonathan Mill[1], Emma L Dempster[1]

[1]University of Exeter Medical School, Exeter, UK

2 Works for me   dx.doi.org/10.17504/protocols.io.bmh2k38e

Complex Disease Epigenetics Group

👤 Stefania Policicchio

ABSTRACT

Increased understanding of the functional complexity of the genome has led to growing recognition about the role of epigenetic/transcriptional variation in health and disease. Current analyses of the human brain, however, are limited by the use of "bulk" tissue, comprising a heterogeneous mix of different neural cell types. Because epigenetic processes play a critical role in determining cell type-specific patterns of gene regulation it is important to consider cellular composition in regulatory genomic studies of human post-mortem tissue, and there is a need for methods to purify populations of specific cell-types. Furthermore, the valuable nature of human post-mortem tissue means it is important to use methods that maximize the amount of genomic data generated on each sample. This protocol describes a method that uses fluorescence-activated nuclei sorting (FANS) to isolate and profile nuclei from multiple different human brain cell-types from frozen post-mortem tissue. This protocol can be used to robustly purify populations of neuronal (NeuN+ve), oligodendrocytes (SOX10+ve), microglia (IRF8+ve) and other glial origin nuclei (NeuN-ve/SOX10-ve/IRF8-ve) from adult post-mortem frozen brain, with each tissue sample yielding purified populations of nuclei amenable to simultaneous analysis of i) DNA modifications (via bisulfite sequencing / array), ii) histone modifications (via CUT&Run-seq), iii) open chromatin analysis (via ATAC-seq), and iv) gene expression (via RNA-seq).

DOI

dx.doi.org/10.17504/protocols.io.bmh2k38e

PROTOCOL CITATION

KEYWORDS

FANS, post-mortem brain, nuclei, flow cytometry, anti-SOX10, anti-IRF8, anti-NeuN, nuclei sorting

LICENSE

CREATED

Sep 18, 2020

LAST MODIFIED

Oct 06, 2020

MATERIALS TEXT

	Supplier	Catalogue No
BD FACSAria™ III Cell Sorter	BD Biosciences	648282-23
Sorvall WX 80+ Ultracentrifuge	Thermo Scientific™	75000080
7mL Dounce Tissue Grinder	DWK Life Sciences	357542
PA Thin-walled ultracentrifuge tubes	Thermo Scientific	03699

Table 1: Specifications of the equipment required for FANS protocol

Reagent name	Supplier	Catalogue No
D-Sucrose (Molecular Biology)	Fisher Scientific	10638403
Calcium chloride (CaCl2) anhydrous, granular	Sigma-Aldrich	C1016-100G
Magnesium acetate (Mg(Ace)2), 1M aq. soln	Alfa Aesar	J60041
UltraPure™ 0.5M EDTA, pH 8.0	Invitrogen	15575020
UltraPure™ 1M Tris-HCl Buffer, pH 8.0	Fisher Scientific	15568025
1,4-Dithiothreitol (DTT) - crystalline powder	Sigma-Aldrich	3483-12-3
Triton™ X-100	Sigma-Aldrich	T9284
UltraPure™ DNase/RNase-Free Distilled Water (ddH20)	Fisher Scientific	12060346
Bovine Serum Albumin (BSA)	Sigma-Aldrich	A9647-500G
PBS Phosphate-Buffered Saline (10X) pH 7.4	Fisher Scientific	10722497
RNasin® Plus RNase Inhibitor	Promega	PAN2615
TRIzol™ LS Reagent	Invitrogen™	11588616
BD FACSDiva CS&T Research Beads	BD biosciences	655051
BD FACS™ Accudrop Beads	BD biosciences	345249
BD FACSFlow™ Sheath Fluid 20L	BD Scientific	342003
BD FACS Clean Solution	BD Scientific	15875858
BD FACSRinse Solution	BD Scientific	340346

Table 2 : Specification of reagents required for FANS protocol

Lysis Buffer (LB)	
0.32M Sucrose	5.47 g
5mM CaCl2	250 µL
3mM Mg(Ace)2	150 µL
0.1mM EDTA	10 µL
10mM Tris-HCl, pH 8	500 µL
1mM DTT	17 µL
0.1% Triton X-100	50 µL
Adjust with ddH2O to	50 mL
1.8M Sucrose Solution (SS)	
1.8M Sucrose	30.78 g
3mM Mg(Ace)2	150 µL
1mM DTT	17 µL
10mM Tris-HCl, pH8	500 µL
Adjust with ddH2O to	50 mL
5% BSA Solution (BB)	
BSA	200 mg
Dissolve in 1x PBS	4 mL
Optional: RNasin® Plus RNase Inhibitor	2 µL / 1mL
Staining Buffer (SB)	
5% BSA	400 µL
10X PBS	400 µL
ddH2O	3.2 mL

Table 3 : Recipes for buffers and solutions required

Supplier	Thermo Scientific™
Model	Sorvall™ WX 80+
Rotor	TH-641
Speed	25,200 RPM / 108670.8 x g
Acceleration	9
Deceleration	5
Temperature	4°C

Table 4: *Ultracentrifuge specification and conditions*

Antibody	Preconjugated	Supplier	Cat No	Dilution
Hoechst 33342	--	Abcam	ab228551	1:500
Anti-SOX10	to NL577	R&D systems	NL2864R	1:10
Anti-NeuN	to Alexa Fluor488	Millipore	MAB377X	1:1000
Anti-IRF8	to APC	Invitrogen	17-9852-82	1:150

Table 5: List of antibodies required for FANS protocol
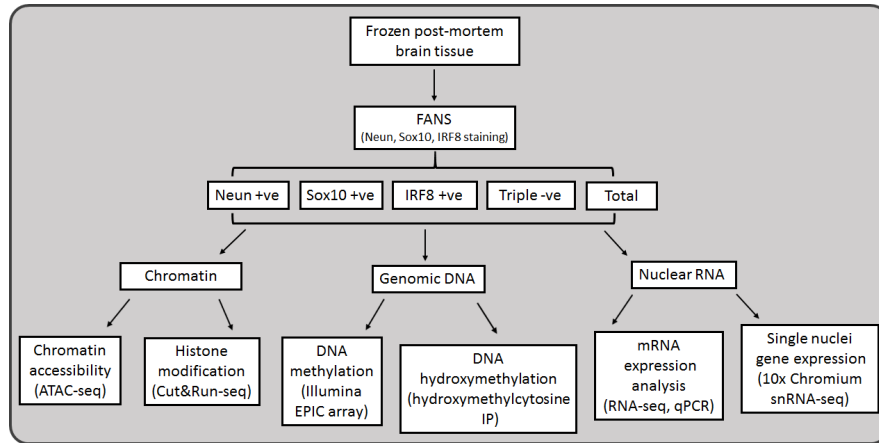
Figure S1. Schematic overview showing the array of downstream applications for which FANS-processed nuclei are suitable

ABSTRACT

Increased understanding of the functional complexity of the genome has led to growing recognition about the role of epigenetic/transcriptional variation in health and disease. Current analyses of the human brain, however, are limited by the use of "bulk" tissue, comprising a heterogeneous mix of different neural cell types. Because epigenetic processes play a critical role in determining cell type-specific patterns of gene regulation it is important to consider cellular composition in regulatory genomic studies of human post-mortem tissue, and there is a need for methods to purify populations of specific cell-types. Furthermore, the valuable nature of human post-mortem tissue means it is important to use methods that maximize the amount of genomic data generated on each sample. This protocol describes a method that uses fluorescence-activated nuclei sorting (FANS) to isolate and profile nuclei from multiple different human brain cell-types from frozen post-mortem tissue. This protocol can be used to robustly purify populations of neuronal (NeuN+ve), oligodendrocytes (SOX10+ve), microglia (IRF8+ve) and other glial origin nuclei (NeuN-ve/SOX10-ve/IRF8-ve) from adult post-mortem frozen brain, with each tissue sample yielding purified populations of nuclei amenable to simultaneous analysis of i) DNA modifications (via bisulfite sequencing / array), ii) histone modifications (via CUT&Run-seq), iii) open chromatin analysis (via ATAC-seq), and iv) gene expression (via RNA-seq).

Nuclear prep for FACS separation (using SOX10, IRF8, NeuN and Hoechst)

1   The protocol below yields at least 1,000,000 NeuN +ve, 1,000,000 SOX10 +ve, 400,000 IRF8 +ve (when the population is present) and 200,000 triple negative (NeuN-ve/SOX10-ve/IRF8-ve) nuclei per 🔲**500 mg** of frozen human post-mortem cortex tissue. Recovery might vary from sample to sample due to high inter-sample variability (brain collection, cortex sub-areas, fat content of tissue sectioned, and white to grey matter ratio)

Refer to Materials-***Table 1*** for details about the equipment required and to Materials-***Table 2*** for specifications of reagents required.

1.1   *Solution and buffer preps*

- *Lysis Buffer (LB)*
- *Sucrose Solution (SS)*
- *Staining Buffer (SB)*

Solutions should be kept at 🌡 **4 °C** or 🌡 **On ice** . Refer to Materials-*Table 3* for recipes of solutions and buffers.

> **NOTE 1** – LB and SS can be prepared a week in advance, with DTT added on the day of use. Solutions should be stored at 🌡 **4 °C** once made.

> **NOTE 2** – SB should be prepared fresh each day

> **NOTE 3**- Samples are homogenised as bulk tissue using a 🧪**6 mL** Dounce homogeniser and then equally divided into three ultracentrifuge tubes.

1.2 *Nuclei isolation*

1. Pre-cool the ultracentrifuge to 🌡 **4 °C** ⏱**00:30:00** before starting this stage of the protocol.
2. All buffers and the Dounce homogenisers should be pre-cooled on ice.
4. Add 1mM DTT to the SS and LB according to the recipe (i.e. 17µL per 50 mL of SS/LB)
5. Transfer 3 mL LB to the homogeniser per 500mg human brain tissue
6. Add the dissected tissue sample into the homogeniser
7. Wait 3-5 minutes before douncing the tissue to allow the sample to defrost

To reduce heat caused by friction, the Dounce homogenisation step should be performed on ice with gentle strokes, and care should be taken to avoid foaming.

> **NOTE 1** – Using the "TIGHT" pestle helps reduce the number of strokes required to reach full tissue disruption.

> **NOTE 2** - The number of strokes required to fully homogenise the tissue may vary between samples due to heterogeneity in cellular composition, lipid content, and the amount of connective tissue.
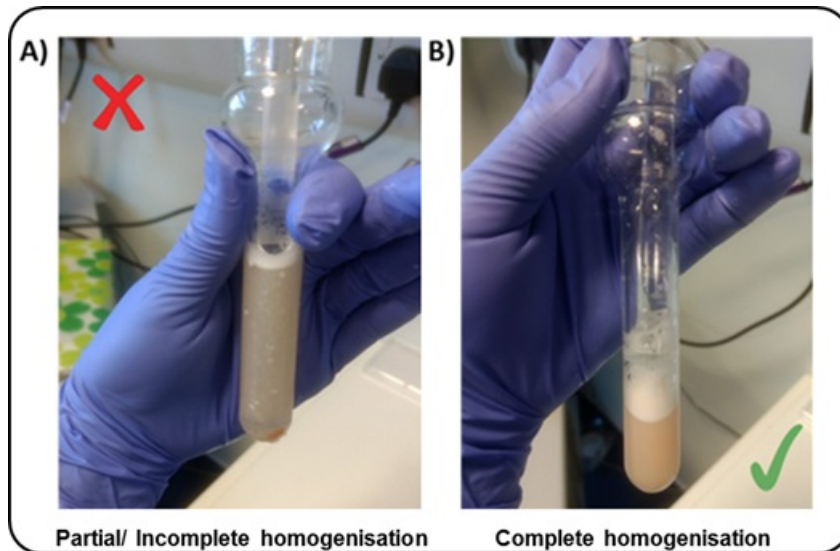
Figure 1 Example of brain tissue sample **A)** only partially homogenised **B)** complete homogenisation.

8.Transfer 8 mL SS (1.8M) to PA thin-walled ultracentrifuge tubes

9.Carefully overlay with tissue homogenate (1 mL per tube) - using a P1000 pipette, releasing slowly down the side of the tube

10.Overlay with another 1 mL LB – do not worry about disrupting the homogenate phase

11.Balance opposite tubes by weight with 1x PBS using a fine microbalance

12.Perform ultracentrifugation for ⏲ **00:45:00** (see **Table 4** for centrifuge specification and conditions)

1.3 *After Ultracentrifugation step*

1. Aspirate supernatant leaving 1-2 mL of the solution in the tube along with the pellet.
2. Pour off any remaining supernatant, taking care not to dislodge the pellet (90-degree inclination of the tube). If the pellet is hard to see, it is okay to leave 100-200 μL solution in the ultracentrifuge tube
3. Re-suspend pellet in SB (1 mL), gently pipette up and down
4. Let samples sit on ice for ⏲ **00:15:00 at least** (**Blocking step**)
5. Transfer volume into 2 mL tubes
6. Rinse out ultracentrifuge tubes in order to maximise nuclei collection by adding 1 extra mL of SB per tube, pipetting up and down several times, and transferring into the 2 mL tubes
7. **Washing step:** ◎**1.0 x g** for ⏲ **00:05:00** , ♨ **Room temperature**
8. Discard supernatant (pipetting off gently)
9. Re-suspend each nuclei pellet in fresh SB (500 μL)
10. If the sample was split then pool together pellets from the same sample (Final Volume = 1.5 mL)
11. Add DNA dye (Hoechst, 2 μL/1 mL) and mix thoroughly via inversion.
12. Pipette out 200 μL of nuclei solution for the Unstained Control (Hoechst dye only) and transfer to a new 2 mL tube
13. Bring the volume up to 1 mL for the Unstained tube with fresh SB
14. Replace the 200μL taken from the Stained" tube with 200μL of fresh SB (Final Volume = 1.5 mL)

1.4 *Immunostaining*

1.Add the following three antibodies (Ab) to Stained tube (1.5ml):

- SOX10 pre-conjugated antibody (1:10 dilution) – [150 μL Ab]
- NeuN Alexa488 (1:1000) – [2 μL Ab]
- IRF8 pre-conjugated antibody (1:150) - [10μL Ab]

Refer to *Table 5* for specifications of the antibodies used

2.Incubate tubes for ⏱ **01:30:00** on the rotor (speed=14 max) at 🌡 **4 °C** , keeping the tubes in the dark

3.Washing step: ⚙ **1.0 x g** for ⏱ **00:05:00** , 🌡 **Room temperature** (both "Stained" and "Unstained" tubes)

4.Discard supernatant (by pipetting off)

5.Re-suspend in fresh SB (1 mL for the Unstained tube, 1.5-2 mL for the Stained tube - depending on pellet size)

Fluorescence-Activated Nuclei Sorting (FANS)

2　For machine start-up, CST and Accudrop calibrations refer to [BD FACSAria III User's Guide](#) for guidance and troubleshooting. The following instructions describe FANS using BD FACSAria III. Other FACS platforms can be used but might require modifications to the protocol.

2.1　*General Gating Parameters*

For each sample, load stained and unstained tubes individually for data acquisition. A preliminary qualitative analysis of the data acquired is essential to select the appropriate gating strategy to maximize the nuclei capture while excluding unnecessary debris and to ensure optimal signal/noise ratio.

Gating Parameters (X-axis:Y-axis):

FSC-A:SSC-A (Size, cell granularity or internal complexity)
SSC-W:SSC-A (to gate out doublets)
FSC-A:DAPI-A (to gate the single nuclei population)
DAPI-A:FITC-A (to gate NeuN stained nuclei)
DAPI-A:PE-A (to gate SOX10 stained nuclei)
DAPI-A:APC-A (to gate IRF8 stained nuclei)
FITC-A: PE-A (to visualize the distribution of triple staining)

> The SOX10 +ve population is gated as a "daughter" population from the NeuN-ve fraction. The IRF8+ve population is gated as a "daughter" population of the SOX10-ve fraction. Refer to **Figure 2** for a visualization of the gating strategy.
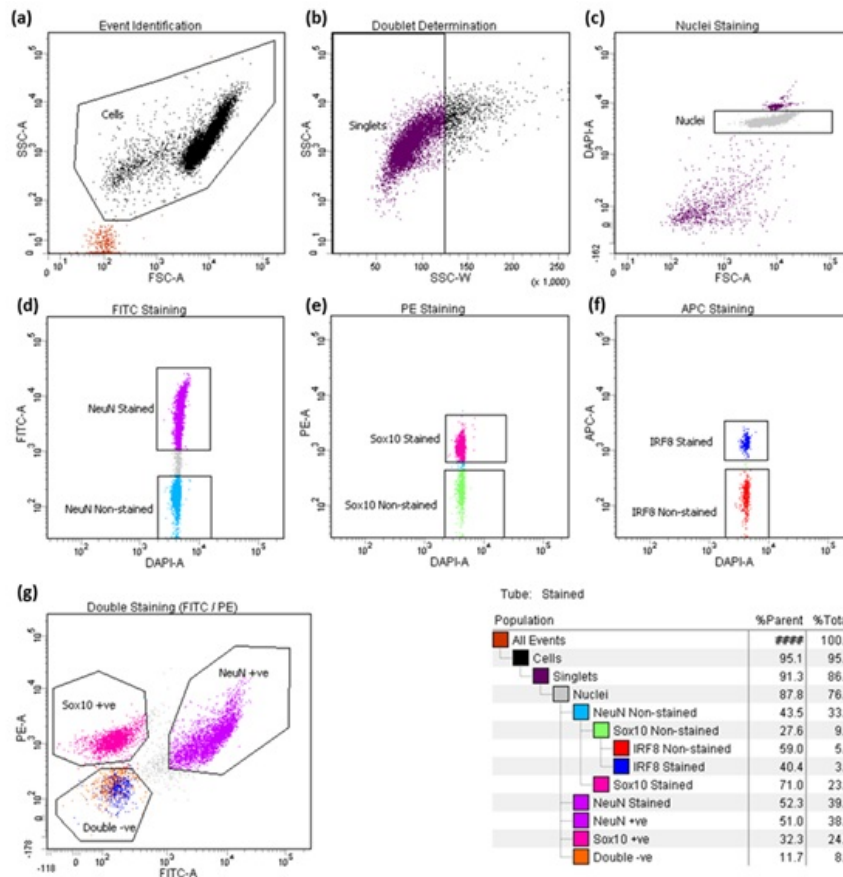
Figure 2. FANS gating strategy. **(a)** Particles smaller than nuclei (black dots) were eliminated with an area plot of forward-scatter (FSC-A) versus side-scatter (SSC-A), with gating for nuclei-sized particles inside the gate (box). **(b)** Plots of height versus width in the side scatter channel are used for doublet discrimination with gating to exclude aggregates of two or more nuclei. **(c)** Doublet discrimination gating was used to isolate nuclei determined by subgating on Hoechst 33342. (d, g) Subsequent scatterplots discerning **(d)** NeuN-Alexa Fluor488–conjugated antibody staining (purple) **(e)** Sox10 NL577-stained nuclei (darkpink) **(f)** IRF8-APC stained nuclei (darkblue) **(g)** the distribution of the three main nuclei subpopulations identified through triple staining strategy (NeuN +ve, neurons; Sox10+ve, oligodendrocytes; double−ve, glia). The resultant hierarchical colour key ensures that only nuclei that are positive or negative for staining with the NeuN and/or Sox10/Irf8 antibody are passed through each gating condition.

2.2 *Data recording settings*

In line with the experiment design, FSC, SSC, DAPI, FITC, APC and PE are the parameters for which voltage values may need to be slightly adjusted due to experiment/ inter-sample variability.
It is advisable to set the threshold value between 200 and 500 during data recording. Moreover, in the acquisition dashboard tab, we recommend setting **Events to Record** ≤3000, **Event to display** ≤1000 and **Flow Rate** = 1.0 (1,000 events per second) in order to increase the accuracy of signal detection.
The flow rate can be increased during sample collection to reduce the sort speed (ideally max events per second =1,500 for a 100-micron nozzle). However higher flow rates impact the data resolution and accuracy of events detection, and subsequent sorting of cellular fractions (see BD FACSAria III User's

for details).

During analysis, recorded data is displayed in plots, while gates are used to define populations of interest for selection. **Figure 3** shows a representative example of the two most common outcomes we often observe.
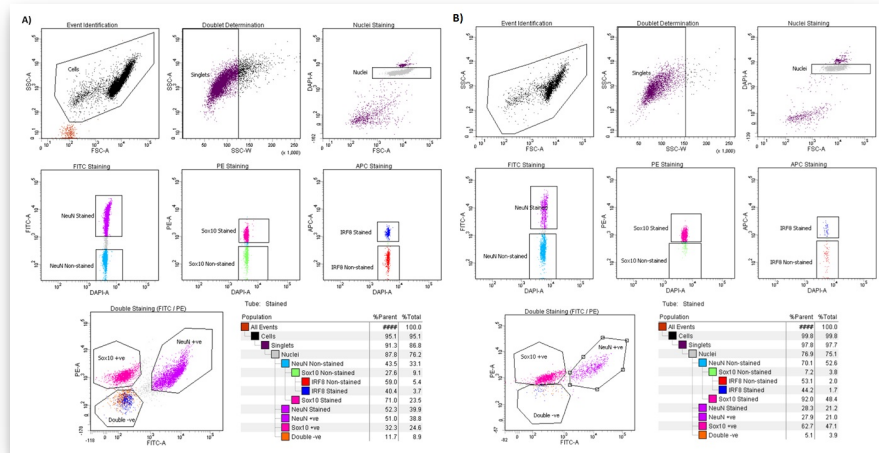
Figure 3. Representative example of inter-individual variability.
The data shown here are derived from two different control prefrontal cortex specimens of comparable age, gender, and brain collection which were processed in parallel following the same procedure. **A)** Optimal sample separation and abundant IRF8+ve fraction vs **B)** poor sample separation and completely missing a double negative population or an IRF8+ve population.

2.3 *Sample Collection*

1. LoBind Tubes (Eppendorf, Cat No:30108051) are required to collect nuclei (to maximize sample recovery of nucleic acids by significantly reducing sample−to−surface binding).

2. Collected fractions can be used directly for downstream applications (e.g. DNA/RNA extraction, chromatin shearing) or stored in ❄ **-80 °C freezer**

3. If you are collecting for DNA or RNA, as soon as the number of events desired (200,000 for DNA, 300,000 for RNA) is reached, transfer the tubes ❄ **On ice** , do not hold them at ❄ **Room temperature** .

> **NOTE** – During collection, it is crucial to regularly pause the sorting to mix the two phases in order to preserve the integrity of resulting RNA preparations.

> For RNA extraction, LoBind Tubes should each contain 500µL of pre-chilled TRIzol™ LS Reagent (Fisher Scientific, Cat No: 11578616) prior to sorting.

4. Keep samples ❄ **On ice** for the entire duration of the sorting

5. Lightly vortex sample tubes to make the mixture homogeneous (not clumped) before loading the tube into the FACS chamber

6. Load the **UNSTAINED** control tube into the chamber first and proceed with nuclei collection (for DNA, 200,000 events; for RNA, 300,000 events; for ATAC-seq 50,000 events). Refer to Materials -

Figure S1 for the full range of applications sorted nuclei can be used.

7. Proceed by collecting **STAINED** tube by simultaneously sorting for NeuN, SOX10 and IRF8 or Double Negative.

NOTE 1 - 1 µg of genomic DNA at least is expected from 500 mg tissue. For optimal recovery of high-quality genomic DNA from FANS sorted nuclei we recommend this extraction protocol

---

NOTE 2 – The IRF8+ve population may not be detectable in every brain sample processed (high inter-individual variability); when it is, it represents between 5-10% of the total sample, therefore yielding often insufficient material for multiple assays.

General Recommendations for the user

3

For every new experiment we recommend performing the following steps:

1. When loading your tube into the FACS machine, run the unstained / IgG control sample first as this aids in setting the baseline parameters
2. Check your **event rate** in the **Acquisition Dashboard** window. If it is greater than 1500 evt/s turn down the "**flow rate**" or unload and dilute the sample further. If less than 100 evt/s, turn up the "**flow rate**" (don't exceed a flow rate of 5.0 if possible, as the instrument is less focused and more inaccurate at higher flow rates)
3. In the **Acquisition Dashboard** window choose the appropriate "**stopping gate**" and "**storage gate**" (when working with nuclei, set as "Nuclei" and "All events" respectively)
4. Choose the range of "**events to record**" and "**events to display**" that best suits your purpose (≥ 5000 for both is advised)
5. Under the "**threshold**" tab in the Cytometer window, change the threshold (should be set for FSC) so that any small events in the bottom corner of the FSC vs SSC graph (caused by general cell debris and dust) are no longer shown. The threshold should not be set too high so that it causes an arbitrary, artificial cut-off through the left side of your population but not so low that small events caused by debris/dust are visible (ideally between a threshold 200-500).
6. Under the "**parameters**" tab in the Cytometer window, adjust the "**FSC**" and "**SSC**" values to get your population sitting in the centre of the FSC vs SSC graph (a re-adjustment of the "**threshold**" may be required at this point). It is essential to select "**restart**" each time any of the parameters are changed to update the events being displayed to ensure only events are recorded under the new settings.
7. Adjust or draw a new gate in the FSC vs SSC plot to encompass the population of interest.
8. Look in the scatter graph of SSC-A vs SSC-W (if you opened a blank experiment you will need to draw one). Right-click on the graph and check it is only displaying the events encompassed by your previous FSC vs SSC gate. Adjust or draw a gate for SSC A vs SSC W to encompass all of the main population to the left of the graph and exclude outliers to the right (these are doublets and other cell debris clumps)
9. Under the "**parameters**" tab in the Cytometer window adjust parameters for the fluorochromes selected so the unstained / IgG control sample sits close to 0 for the fluorochrome on a graph of FSC vs fluorochrome.
10. Load the stained samples and check the stained population has a clear increase in signal for the fluorochrome in comparison to the unstained (signal should not exceed 10^{x4}). Several minor re-adjustments of the fluorochrome's "**parameters**" may be necessary for the stained sample at this stage. If so, the unstained / IgG control has to be reset and re-recorded.

WARNING – Do not change parameter settings between samples you wish to compare, if you do you will need to re-record all samples using the changed parameters.

11. Select the correct option for the collection device in the **Sort Layout** window (we recommend "**4-Way Purity**" for general collection)

12. Regularly check your "**Efficiency**" in the **Sort Layout** window value. Between 80-100% is ideal, 70% is acceptable if less than 70% either the sample is too concentrated or you are sorting a rare population. Although the "**flow rate**" in the **Acquisition Dashboard** window can be increased to make the sort quicker, faster flow rates are less efficient.

13. Check the "**Electronic abort rate**" (N° errors /sec) and "**Electronic abort count**" (Tot N° of errors) at the bottom of the **Acquisition Dashboard** window. These parameters measure potential miss-sorts (different from efficiency as efficiency measures undetermined drops which are directed to the "**Waste**" and therefore lost but do not contaminate)."**Electronic abort rate**" should be <1% of total events per second.

14. For long sorts, gate positions should be regularly monitored, especially for stained populations as fluorochromes lose intensity over time and the population can shift towards the unstained. Gates can be moved during long sorts to compensate.